Tuning Reactivity of Platinum(II) Complexes

A Kinetic and Mechanistic Investigation into Substitution Behaviour of Mono- and Dinuclear Platinum(II) Complexes

Peter Olengo Ongoma

School of Chemistry and Physics

University of KwaZulu-Natal,

Pietermaritzburg

December 2012

Tuning Reactivity of platinum(II) complexes

A Kinetic and Mechanistic Investigation into Substitution Behaviour of Mono- and Dinuclear Platinum(II) Complexes

By

Peter Olengo Ongoma

B. Ed(Sc.) (Hons), Nairobi; MSc. (Hull, UK)

Submitted in Partial fulfilment of the academic requirements for the degree of

Doctor of Philosophy

in the College of Agriculture, Engineering and Science

School of Chemistry and Physics

University of KwaZulu-Natal, Pietermaritzburg

UNIVERSITY OF
KWAZULU-NATAL

Declaration

This thesis report is based on results from an original work carried out in the School of Chemistry and Physics, University of KwaZulu-Natal, Pietermaritzburg and has not been submitted for the award of a Degree or a Diploma at any University. Where use has been made of work of others, it is duly accredited in the text.

_____

P. O. Ongoma

I hereby certify that the statement is true.

_____

Professor D. Jaganyi

Supervisor

Pietermaritzburg

December 2012

Dedicated to my son Brian Olengo; Cosmas O. Mainga and Christopher O. Oboya (both Posthumous), with lots of love.

Abstract

Systematic kinetic and thermodynamic analyses of the substitution reactions of different Pt(II) complexes with a series of bio-relevant nucleophiles have been investigated as a function of concentration and temperature, using standard stopped-flow and UV–Vis Spectrophotometric methods. For this purpose, five different systems involving square-planar Pt(II) complexes, *viz*. (i) mononuclear Pt(II) complexes with tridentate nitrogen-donor ligands of varying degree of π-conjugation, and (ii) polynuclear Pt(II) complexes with azine, pyridyl units separated by S, S-S and CH_2CH_2 spacer groups, and α,ω-alkanediamine bridging ligands were synthesised and characterised by various spectroscopic methods. All substitution reactions of the Pt(II) chlorido complexes of the type $[Pt(terpy)Cl]^+$ were studied in the presence of 10 mM LiCl to prevent spontaneous parallel reaction due to hydrolysis or solvolysis. The substitution reactions of the coordinated water molecules in the dinuclear Pt(II) complexes by thiourea nucleophiles of varying steric hindrance were studied under acidic conditions. The concentration of the nucleophile solution was prepared in 0.1 M $NaClO_4$, at pH 2.0 and always at least 10-fold excess to provide *pseudo* first-order conditions. The pK_a values of the coordinated aqua ligands of the dinuclear Pt(II) complexes were determined by Spectrophotometric acid-base titrations. DFT calculations were also performed in an effort to account for the observed reactivity of homologous analogues in each series of complexes, in terms of NBO charges and energies of frontier molecular orbitals.

Substitution reactions of the Mononuclear Pt(II) complexes with tridentate ligands showed reactivity of the complexes is controlled by the π–acceptor characteristics of the chelate ligands. The fused rigid pyridyl system allows electronic interaction between the platinum centre and the pyridyl ligands, because of the extended conjugated π-system. This effect is controlled by how the fused ring system around the terpy moiety is structured. The isoquinoline moiety was found to reduce the effective π-backbonding and the lability of **CH_3PhisoqPtCl** complex compared to 1,10-phenanthroline and terpyridine systems, indicating that isoquinoline ligand is a net σ-donor.

The results obtained for the substitution reactions of the diaqua Pt(II) complexes with the thiourea and ionic (Br^-, I^- SCN^-) nucleophiles demonstrate that reactivity increases with decreasing pK_a values as well as decreasing distance between the Pt(II)centres. An increase in steric crowding at the Pt(II) centre imposed by the methyl groups on the

azine linker decelerates the lability of the aqua ligands. The ^{1}H and ^{195}Pt NMR spectroscopic results confirmed degradation of the aromatic-based bridging ligand from the metal centre. The final cleavage of the complex linkers was only achieved after addition of excessive amounts of thiourea and other strong nucleophiles. The negative activation entropies and second-order kinetics for all the substitution reactions support the Associative mode of substitution mechanism.

Table of contents

Chapter Two

Acknowledgements

First of all, I wish to thank Prof D. Jaganyi for the supervision of this work, his continuous support and trust in me, and for giving me the opportunity to come up with and fulfil some remarkable ideas. Thanks for everything!

I am grateful towards Dr Desigan Reddy for mentorship and untiring support during initial stages of this work. Dr Allen. Mambanda, room-mate and colleague at work, during the long times we spent in the laboratories. Our discussions were very encouraging and fruitful. I am grateful to Mr Craig Grimmer, for his guidance and technical support during the analysis of NMR spectra.

I would like to thank Prof. John S. Field and Dr. Anne Soares, for supporting my advancement by many constructive ideas and discussions. Special thanks to Prof. Orde Q. Munro for financial support and good working relationship we developed during CTEC practical demonstrations.

I would like to acknowledge the following people and Institutions:

Prof. Dr. Rudi van Eldik, Dr. Ralph Puchta and Ms Stephanie Hochreuther, at the Institute of Inorganic Chemistry, University of Erlangen-Nürnberg, Germany, for assistance with the CHN analysis.

The National Research Foundation of South Africa, University of KwaZulu-Natal, South Africa and Egerton University, Kenya, for financial assistance.

I extend many thanks to all the members of the Platinum Chemistry group. They just were like my family over the years. In particular, thanks to Isaac Wekesa, Grace K Kinunda, Aishath Shaira, Asman P. Wangoli, Dr. Mohammad Altaf, and Tshephiso (*terpy*) Papo. In these last years, our friendship soon grew far beyond working colleagues.

Special thanks to the entire Academic, technical and support staff in the School of Chemistry and Physics-Chemistry Division: Messers H. Desai and S Ball for the

procurements, Messers P. Forder and C. Mortlock for the glass blowing services, Mr B. Dlamini and Mrs I Ngubane for their warm friendship. Thanks to all my friends. To be able to rely on all of you anytime is a great gift.

Many thanks to Mr. Moses A. Ollengo, School of Chemistry and Physics, Westville Campus, University of KwaZulu-Natal, for organising the thesis into a readable manuscript.

Finally I am highly indebted to my spouse Jennipher and family–my mom and dad, dad-in-law, mother-in-law (posthumous) and my sons and daughters. I greatly appreciate your consistent support in every part of my life. I owe you so much.

List of Figures

List of Tables

List of Commonly used Abbreviations

Å	Angstrom (10^{-10} m)
T	temperature
K	Kelvin
C	Celsius
Pa	Pascal
kcal	kilocalorie
kJ	kilojoules
g	gram
L	litre
mL	millilitre
M	molar, mol L^{-1}
R	gas constant, 8.3145 J K^{-1} mol^{-1}
h	Planck constant, 6.6261 x 10^{-34} J s
k_b	Boltzmann constant, 1.3807 x 10^{-23} J K^{-1}
k_{obs}	observed rate constant for *pseudo* first-order reactions
k_1, k_2, k_{-1}, k_{-2}	rate constants
$\Delta H^{\#}$	activation enthalpy
$\Delta S^{\#}$	activation entropy
$\Delta V^{\#}$	activation volume
K	equilibrium constant
I	ionic strength
ts	transition state
DFT	density functional theory
s, m, h, d (time)	seconds, minutes, hours, days
NMR	nuclear magnetic resonance
s, d, t, m (NMR)	singlet, doublet, triplet, multiplet
δ	chemical shift
ppm (NMR)	parts per million
MS	mass spectrometry
UV–Vis	ultraviolet–visible
λ	wavelength

TU	thiourea
DMTU	1,3-dimethyl-2-thiourea
TMTU	1,1,3,3-tetramethyl-2-thiourea
IR	infrared

Publications and Conference Contributions

Publications

Parts of the work reported in Chapters 3 & 4 of the thesis have been published in *Dalton Transactions*, while the rest are ready for submission for publication.

1. **Peter Ongoma** and Deogratius Jaganyi, The π-Acceptor Effect in the Substitution Reactions of Tridentate N-Donor Ligand Complexes of Platinum(II): *A Detailed Kinetic and Mechanistic study, Dalton Trans.*, 2012**,** **41**, 10724-10730.
2. **Peter O. Ongoma** and Deogratius Jaganyi, Mechanistic Elucidation of Linker and Ancillary Ligand Substitution Reactions in Pt(II) Dinuclear Complexes, Dalton Trans**, DOI**: 10.1039/C2DT31956J.
3. **Peter O. Ongoma** and Deogratius Jaganyi, Substitution Reactions in Dinuclear Platinum(II) Complexes: *an Evaluation of the* i*nfluence of the Diazine-bridge on Reactivity* (Submitted to *Dalton Transactions*).
4. **Peter O. Ongoma** and Deogratius Jaganyi, Tuning Reactivity of Platinum (II) complexes with parametalated Pyridine Spacer groups: a *kinetic and Mechanistic Study* (Submitted to *International Journal of Chemical Kinetics*)
5. **Peter O. Ongoma** and Deogratius Jaganyi, The Influence of α,ω-diaminealkane Linker on Ligand Substitution of Pt(II) Dinuclear Complexes: *A Thermodynamic and Kinetic Stu*dy (Submitted to *Transition Metal Chemistry*)

Poster Presentation

39th Convention of South Africa Chemical Institute, University of Stellenbosch, South Africa, 30 November to 5 December 2008, entitled: *The Role of extended π-conjugation on Substitution Reactions of Pt(II) complexes with Tridentate N-donor ligands.*

Table of Contents-1

List of Figures

Chapter 1

1.0 Introduction

1.1 Cancer Disease

Cancer is a generic term for a group of more than 100 diseases that can affect any part of the body.[1] Other terms used to describe the different types of cancer are malignant tumours and neoplasm (new growth). It is caused when genetic damage to the cells prevents them from being responsive to normal tissue controls. Cancer is a leading cause of death in the human population worldwide.[1] From a total of 7.6 million deaths in 2008 from cancer,[2] it is estimated that 9 million people will die from this disease by 2015 and another 11.4 million in 2030.[3] The major cause of death from cancer is Metastasis,[4] which results from the ability of cancerous cells to stimulate cell division. This leads to rapid growth of abnormal cells beyond their usual boundaries. These changes enable cancer to invade adjoining tissues of the body and spread to other organs through the blood and the lymphatic systems.[5,6] Mutations and other genetic abnormalities observed in cancer cells can be caused by a combination of environmental factors such as chemical carcinogens or life style effects like use of alcohol, tobacco and drugs.[7] The most common types of cancer prevalent in men are: lung, stomach, liver, colorectal, oesophagus and prostate; while among women are: breast, lung stomach, colorectal and cervical.[4] Hence, from the above statistics there is need to develop new drugs, especially Pt(II) compounds as potential anti-tumour drugs to cure cancer, in addition to the existing ones.[8,9]

1.2 Cancer Treatment

Currently, cancer can be treated by; surgery, chemotherapy, radiotherapy alone or in a combination of the listed strategies,[10] with aim of killing all malignant cells or at least considerably reducing their numbers. From the 16th century, heavy metals like platinum, gold, and ruthenium have been used systemically to treat cancers, with the d^8 Pt(II) being the leading metal ion.[11] The prototype example is *cis*-diamminedichloridoplatinum(II), better known as *cisplatin*.

1.2.1 Chemotherapy

In cancer, a chemotherapeutic agent is one that kills the rapidly dividing cells, thus slowing and stopping the cancer from spreading. The anti-tumour agents include plant alkaloids, alkylating agents, hormones, and antibiotics (Figure 1.1).[12] Many of these chemotherapeutic agents target specific mechanisms within the body that control the progression of cancer. For instance, alkylating agents such as *cisplatin* interrupt replication of genetic material by cross-linking and strand-breaking DNA, leading to cell lysis; whereas hormones or hormone-like agents, such as estradiol (an oestrogenic hormone present in the ovaries) inhibit tumour growth by antagonizing naturally occurring ligands from their receptors and initiating tumour proliferation.[12] Antitumor antibiotics such as Doxorubicin prevent cell division by damaging the cell and interfering with DNA and RNA syntheses.

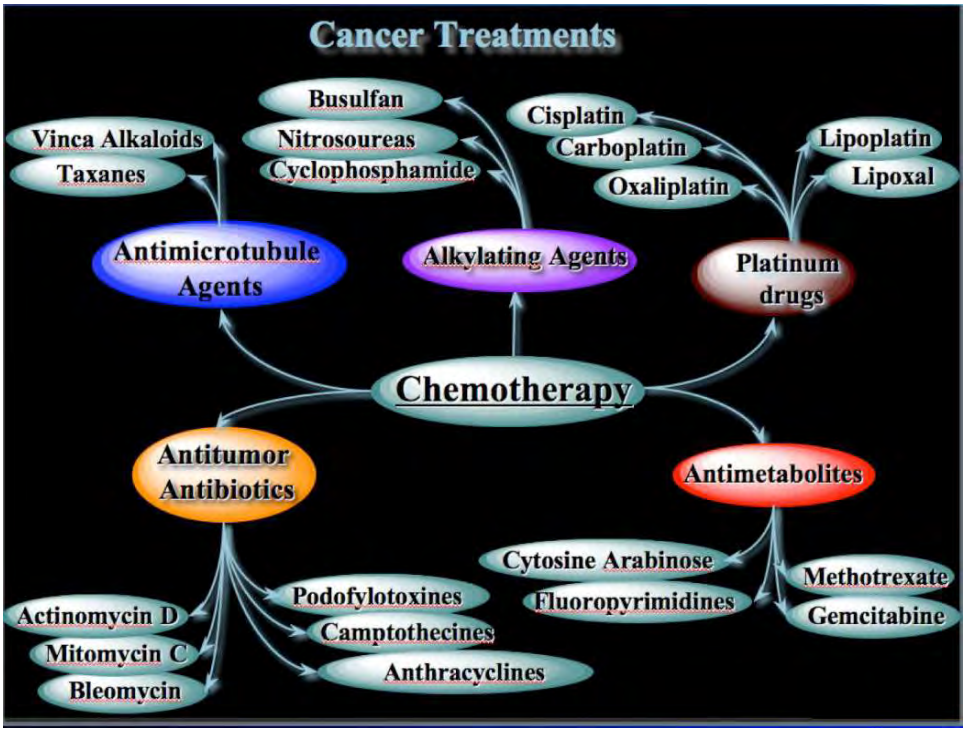

Figure 1.1: Classification of chemotherapy drugs[13]

1.3 Platinum Chemistry

Platinum is not an essential element, but due to its bioactivity, it is currently one of the most important therapeutic agents in cancer therapy[14] notwithstanding its well-known

toxic potential. The most well-known chemistry of platinum is in the oxidation states of 0, +2 and +4.[15] The higher oxidation states, +5 and +6 exist as fluorides and fluoro-complexes, but are quite rare due to their lower stability.[15,16]

The Pt(II) and Pt(IV) metal centres are positively charged and therefore , more favoured to bind negatively charged biomolecules such as proteins, nucleic acids and enzymes. The major boost into the Pt(II) chemistry occurred in the 1950s when chemists started to systematically investigate inorganic reaction mechanisms. Substitutions reactions at the square-planar sites were dominated by Pt(II) complexes due to their higher redox stability and moderately slower reactivity.[15,17–20] Also, studies in the early 1960's by Rosenberg *et al*. indicated that both bivalent Pt(II) and tetravalent Pt(IV) complexes exhibited antitumor activity.[21] The most well-known of the Pt(II) compounds is [*cis*-$PtCl_2(NH_3)_2$] (*cisplatin* in Figure 1.2).

In addition, Pt(II) prefers amine ligands, halogens, sulphides (*e.g*. R_2S) and π-acceptor ligands such as CN^-, C_2H_4, CO and tertiary phosphines. It has modest affinity for hard bases like F^- and oxygen ligands since the Pt(II) centre is a soft acid. It can react with bidentate ligands N–N, P–P, S–S, N–O, N–S and N–P to form mononuclear as well as bridged-dinuclear chelate complexes.[22] Its reaction with tridentate ligands such as N–N–N, N–P–N, N–C–N and N–S–N gives mononuclear four-coordinate square-planar complexes. The tetradentate ligands like As–As–As–As and P–P–P–P yield mainly five-coordinate complexes because the higher π-acceptor ability of the As- and P-based ligands stabilises the 18e trigonal–bipyramidal geometry.

1.3.1 Platinum-Based Anticancer Drugs

Cisplatin and *oxaliplatin* [oxalato-1,2-diaminocyclohexaneplatinum(II)]; and *satraplatin* [(OC-6-43)-bis(acetato(aminedichloro)cyclohexylamine)platinum(IV)] and *LA-12* [(OC-6-43)-bis(acetato)(1-adamantylamine)amminedichloroplatinum(IV)] (Figure 1.2) respectively are, some examples of Pt(II) and Pt(IV) complexes that are in use as anticancer drugs. In particular, Pt(II) complexes are suitable as antitumour agents because these compounds exhibit metal-ligand exchange kinetics in the same order of magnitude as the division of the cancerous cells, which makes them fit to suppress mitosis processes.[23] In addition, Pt(II) has the potential to form thermodynamically

stable bonds with N-donor ligands in the DNA helix, thus preventing DNA replication and promoting cell death.

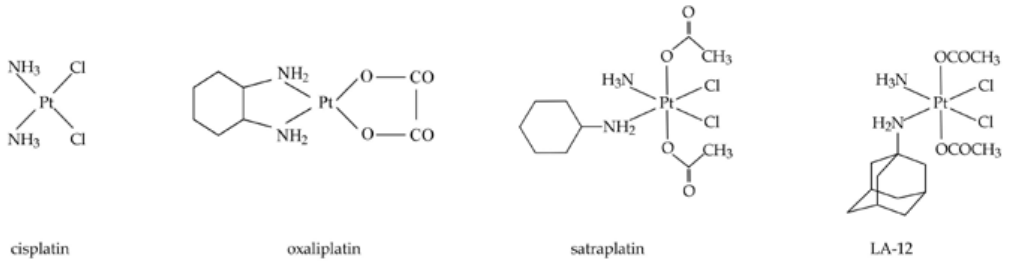

Figure 1.2: Chemical structures of selected platinum compounds

1.3.2 Cisplatin

Cisplatin is a very effective, but highly toxic antitumor drug. Its clinical use was initiated in the early 1970s, and is one of the most widely employed anticancer agents, useful in ovarian, testicular, small cell lung, and other cancers.[24] It is a square-planar complex, containing two labile chlorines and two relatively inert ammonia molecules coordinated to the central Pt(II) atom in a *cis* configuration (Figure 1.1).

1.3.2.1 Mechanism of Action

The mode of action of cisplatin and other Pt(II) complexes includes hydrolysis in the first step (Scheme 1.1) followed by preferential binding to the guanine N7 atom of DNA.[25] But the exact mechanism is not yet fully understood. The first two reactions to consider are sequential hydrolysis of the two chloro ligands to yield the chloro–aqua and diaqua complexes as illustrated in Scheme 1.1.

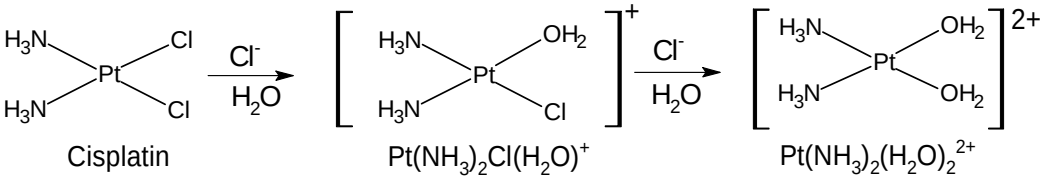

Scheme 1.1: Sequential hydrolysis of the cisplatin in the cytoplasm.

1.3.2.2 Cellular Uptake

Cisplatin is administered intravenously because of its poor water solubility and to protect it from hydrolysis reaction in the acidic medium of the digestion tract–in the stomach. In the blood plasma, chloride concentration (100 mM) is high to prevent hydrolysis reactions of chloride containing complexes. However, *cisplatin* enters the cells either by *passive diffusion* or *active transport mechanisms* that involve organic cation transporters and copper transporter proteins *viz.* CTR1.[26] It is probable that Pt(II) complexes enter the cells by a variety of mechanisms which depend on the charge of the complex and the hydrophilic or lipophilic nature of the ligands.[27] In a recent report, it was observed that increasing the positive charge and charge dispersion along the polynuclear species of the type [{*trans*-$PtCl(NH_3)_2$}$_2${μ-*trans*-$Pt(NH_3)_2$-$(NH_2(CH_2)_6NH_2)_2$}]$^{4+}$ (BBR3464), results in higher levels of cellular uptake and enhanced cytotoxicity of the drug.[28] These multinuclear (dinuclear) compounds form part of the research objectives as discussed in chapters 4–7.

1.3.2.3 Hydrolysis

Inside the cell, due to the lower chloride concentration (2–4 mM) present in the cytoplasm,[29] cisplatin and other chloride Pt(II) compounds undergo hydrolysis to yield the positively charged species (**1**) and (**2**) (Figure 1.3). These are the active species of the drug with the aqua-chloro species (**1**) considered as the more active form.[14,30] In contrast, species (**2**) is more reactive towards nucleophilic centres of biomolecules because the aqua ligand is a better leaving group than the chloride ligand.[31] In light of the pK_a value 6.4 for $[Pt(NH_3)_2(OH_2)Cl]^+$ and pK_{a1}/pK_{a2} of 5.4/7.2 for $[Pt(NH_3)_2(OH_2)_2]^{2+}$, both complexes are known to form, approximately 18% each, of the inert mono-hydroxo species, i.e. *cis*-$[Pt(NH_3)_2Cl(OH)]$ and *cis*-$[Pt(NH_3)_2(OH)(OH_2)]^+$, at the physiological pH.[32] To optimize the acid-based properties of the Pt(II) containing drugs, it is important to tune the stability of the reactive species, the diaqua form (**2**), at the desired pH by careful choice of the spectator ligands and leaving groups.

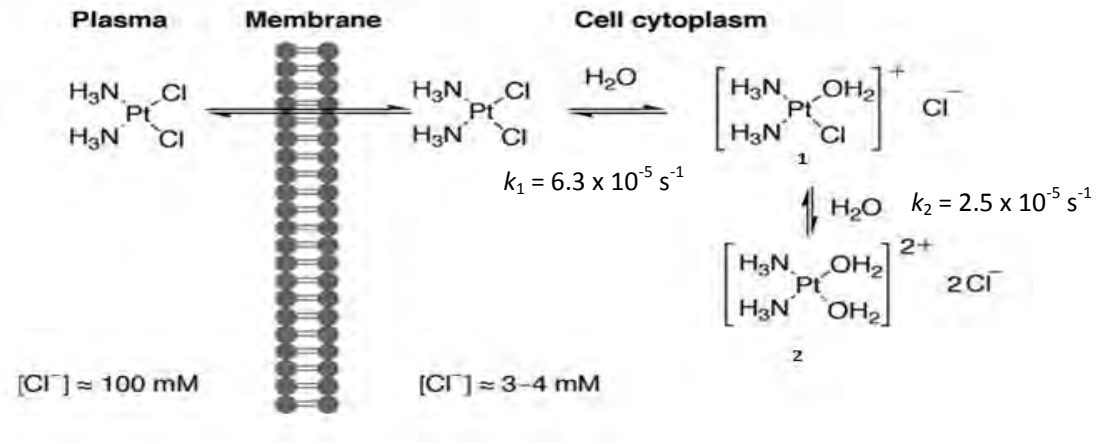

Figure 1.3: Intracellular hydrolysis and bio-activation of cisplatin in aqueous solution leading to binding at DNA in the cell nucleus.[33]

The reactivity of the 1:1 complexes bearing Cl^- or H_2O as the fourth ligand is, however, controlled by the lability of the aqua ligand, which dramatically decreases with increasing pH.[34] This study investigated the impact of the structure and chain-length of the bridging ligand of square-planar Pt(II) dinuclear complexes of general formula [{*cis*-$Pt(NH_3)_2(OH_2)\}_2$–μ–L]$^{+4}$ (L being α,ω-alkanediamine, diazine, and 4,4'-dipyridinesulphide linkers) on the acid-base properties of the two water molecules in the *cis*-position.

1.3.2.4 DNA Adducts and Cell Response

Once the active complex species enter the nucleus, they become attracted to the negatively charged DNA. The electrostatic interaction complexation with nitrogen atoms of purine bases, normally the N7 atoms of two vicinal guanine units, occurs via the displacement of the two water molecules; leading to intrastrand cross-linking that deforms the DNA tertiary conformation as shown Figure 1.4. This is key step in the mechanism of action.[29a]

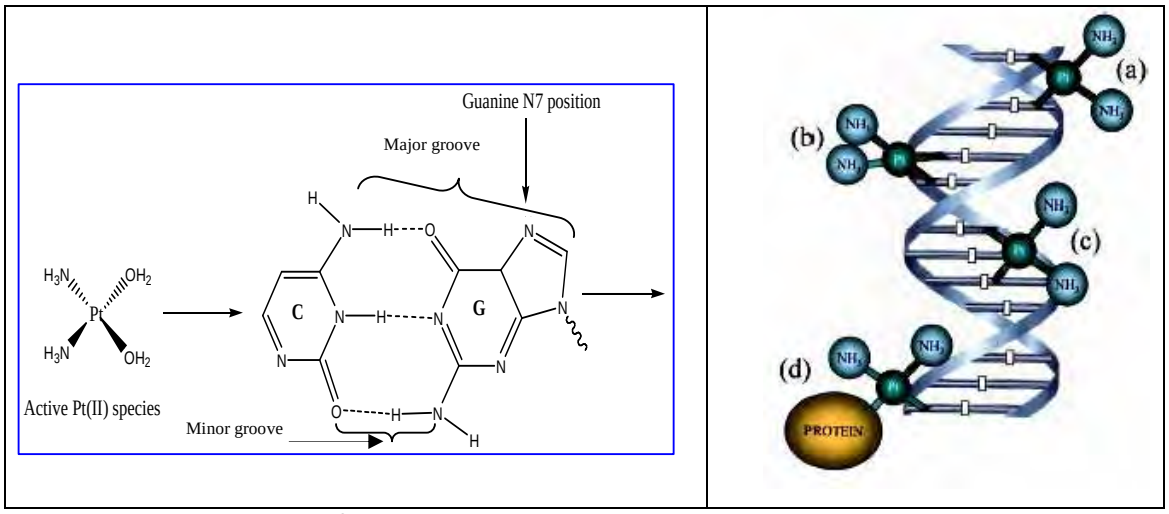

Figure 1.4: DNA-adduct formation with cisplatin leaving two amino groups coordinated on the platinum atom. The main adducts formed in the interaction cisplatin with DNA: (a) interstrand cross-link; (b) 1,2-intrastrand cross-link; (c) 1,3-intrastrand cross-link and; (d) protein-DNA cross-link.[35]

Approximately 90% of cisplatin-DNA adducts are 1,2 intrastrand cross-links, 65% of which are two adjacent N7 guanine-N7 guanine sites, while 25% are two adjacent N7 guanine-N7 adenine sites.[36] The N7 atoms of guanine and adenine are the most accessible and reactive nucleophilic sites of platinum to the DNA, and are located in the major groove of the double helix.[37] The larger amount of 1,2-intrastrand adducts are attributed to:

- The shortest distance existing between the two N7 atoms of guanine and the ability of the NH groups of cisplatin being involved in intramolecular hydrogen bonding interactions with guanine–O6 atom.[38]
- Guanine is the most nucleophilic base with a decreasing order of reactivity: guanine–N7 >> adenine–N7 > cytosine–N3.[39]
- The N7 atom of the guanine base is the most electronegative (more electron dense) and more "exposed site" than the corresponding N7 atom of the adenine, which results in the former acting as a stronger ligand towards Pt(II) than the latter.

As a consequence, the guanine N7 atom can replace a thioethereal sulphur atom bonded to platinum, whereas that of adenine cannot.[40] The remaining adducts comprise of interstrand cross-links and monofunctional cisplatin adducts.[41]

Coordination of the platinum complex to DNA distorts the normal double helix structure resulting in a significant bending of about 40° away from the site of attachment. [42] This propagates steric constraints that lead to a loss in helix stability. The kink in the DNA structure is recognized by repair cellular proteins like the high mobility group (HMG) proteins (*i.e.* an 80 amino acid sequence found in many proteins that bend DNA significantly)[43] These may successfully repair the damaged DNA by cutting out platinum–adducts and re-synthesise at the open sites, or fail to repair and thereby block DNA replication and transcription, ultimately inducing cell death by apoptosis ("programmed cell death").[44] This results in high rate of DNA repairs or higher tolerance to Pt-DNA adducts which can be one of the factors of drug resistance arising in the cause of treatment.

1.3.2.5 Cisplatin Resistance

Experimental evidence indicates that resistance may occur at any of the following three levels (Figure 1.5):[45,46] (a) decreased accumulation of platinum compounds due to either reduced influx or enhanced efflux at the plasma membrane; This reduced intake of the drug decreases the amount reaching the intracellular target, the DNA, due to changes in membrane properties and may result in intrinsic resistance; (b) detoxification of platinum compounds by S-donor reductants such as glutathione and methallothioneins; and (c) removal from DNA by evasion of apoptosis or high rate of DNA repairs.[47,48]

1.3.2.6 Competition between N– and S–Donor Nucleophiles

Pt is a 5d transition metal, which forms strong covalent bonds with N and S donor ligands. From the hard-soft acid-base theory (HSAB), S-donor biomolecules would readily bind to the soft Pt(II) centre[25,49] and generate stable platinum complexes. The formation of the Pt-S adducts is more preferred pathway kinetically since the reactions with S-donors are fast, while binding to the nucleobases (N-donors) occurs very slowly and is thermodynamically more stable under physiological conditions.[50]

The interaction of cisplatin with sulphur-containing enzymes is thought to be involved in the resistance of cells to cisplatin. This is closely related to the drug's bio-

transformational pathways that compete for the bioavailability of the drug at the target, DNA (Figure 1.5).

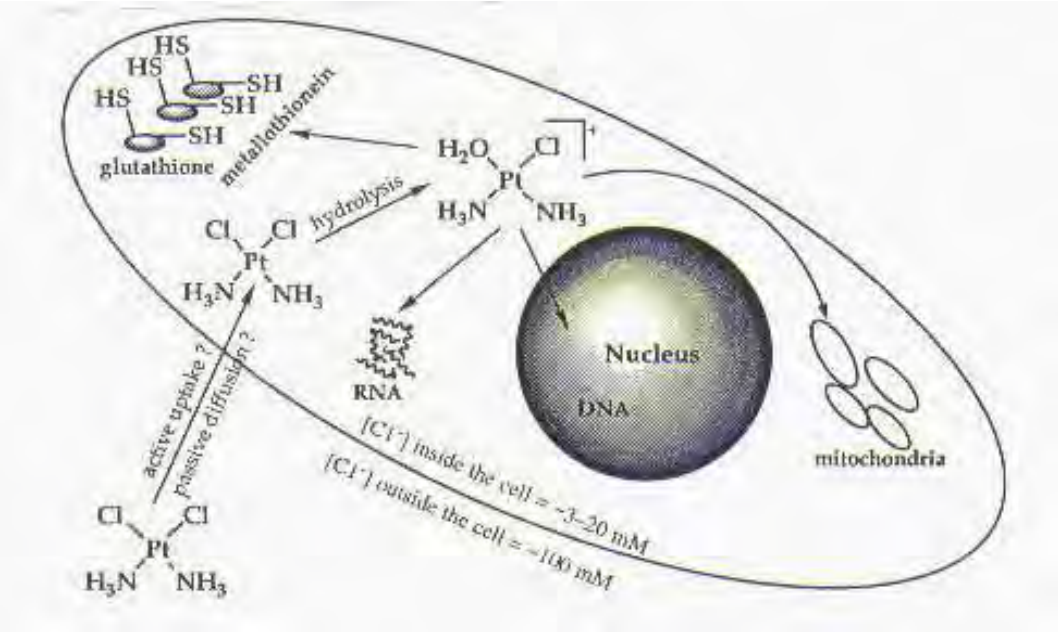

Figure 1.5: Schematic pathway of a platinum drug in cells showing how sulphur containing compounds are thought to act as potential drug reserving agents in platinum chemotherapy.[51]

Inside the cell, the active forms of the drug, *i.e.* Cl/H_2O (**1**) and H_2O/H_2O (**2**), do not only undergo DNA (N-donor) adduct formation, but also can be deactivated by S-donor biomolecules such as glutathione (0.5-10 mM GSH) and metallothioneins (MT) that are available in large amounts.[52] This results in accumulation of Pt-S intermediates *in vivo* that depletes intracellular concentration of the drug to levels insufficient to inhibit tumour growth and is responsible for the serious toxic side effects of cisplatin caused by binding of platinum to the proteins.[10,49,53,] The high affinity of sulphur for Pt(II) centre has led to the development of the so-called "rescue or protective agents" like thiourea (TU), 2-mercaptoethanesulfonate (mesna) and sodium thiosulphate (STS). These are co-administered with other drugs to suppress the coordination of platinum to S-containing proteins which is responsible for severe toxic side effects such as nephrotoxicity (reduced kidney function and damage), ototoxicity (hearing loss) and myelosuppression (reduction in bone marrow activity).[49,54] Their protective effect can be attributed to either prevention from causing unwanted toxic side effects[49,55] or reversals of the Pt-S

adducts in proteins and therefore act as platinum-reservoirs. Finally, the remaining platinum compounds probably are excreted from the cell via the Golgi apparatus, a process that also brings about cell detoxification.[56,57]

1.3.3 New and "Non-classical" Platinum Complexes

In an effort to overcome the resistance and reduce the toxicity of cisplatin, novel platinum complexes have been designed and synthesised. These include "second generation platinum drugs" with improved toxicological profiles and "third generation drugs" that have the advantages of overcoming cisplatin resistance and convenience of drug delivery and administration.

1.3.3.1 Second Generation Cisplatin Analogues

Carboplatin (*cis*-diammine-1,1'-cyclobutanedicarboxylatoplatinate(II)) was developed on the hypothesis that altering the leaving group could change the toxicity of the platinum drug. As an example of the second generation platinum anti-tumour compound, it still carries primary amines as the inert ligand and a more stable (1,1'-cyclobutanedicarboxylate) leaving group that slows down the hydrolytic activation. The cyclobutanedicarboxylate ligand confers a 17-fold increase in solubility in water and a moderate rate of hydrolysis (10^{-8} s^{-1}) compared to *cisplatin* (10^{-5} s^{-1}).[58,59] Such properties confer to the drug the following effects:

- longer circulation lifetime in the body due to its improved stability,
- reduced toxicity as a result of the decreased rate of competitive binding to plasma proteins, glutathione and other platinum deactivating biomolecules,
- due to lower reactivity, a higher dosage of up to 2000 mg d^{-1} can be administered.

Carboplatin is successful in the treatment of ovarian cancer, but is unable to overcome cisplatin-acquired resistance.

Oxaliplatin [oxalato-1,2-diaminocyclohexaneplatinum(II)] (figure 1.1) is most effective in the treatment of colon cancer, a type of cancer that is insensitive to cisplatin and carboplatin treatments. It was developed and first used as an anti-cancer drug in France in 1996. The oxalate leaving group enhances its aqueous solubility and also slows down

the hydrolysis of the complex, whereas the non-hydrolysable and sterically demanding lipophilic chelating amine (dach) ligand makes the complex less polar. This has been proposed to contribute to a better cellular uptake.[60] In addition, the dach ligand prevents the binding of the DNA repair proteins by pointing into the major DNA groove (Figure 1.6). These adducts shield the inhibition of DNA replication, resulting in apoptosis and cell death. Oxaliplatin and carboplatin both have bidentate leaving groups that reduce the severity of the side effects by slow ligand exchange reaction with plasma proteins.

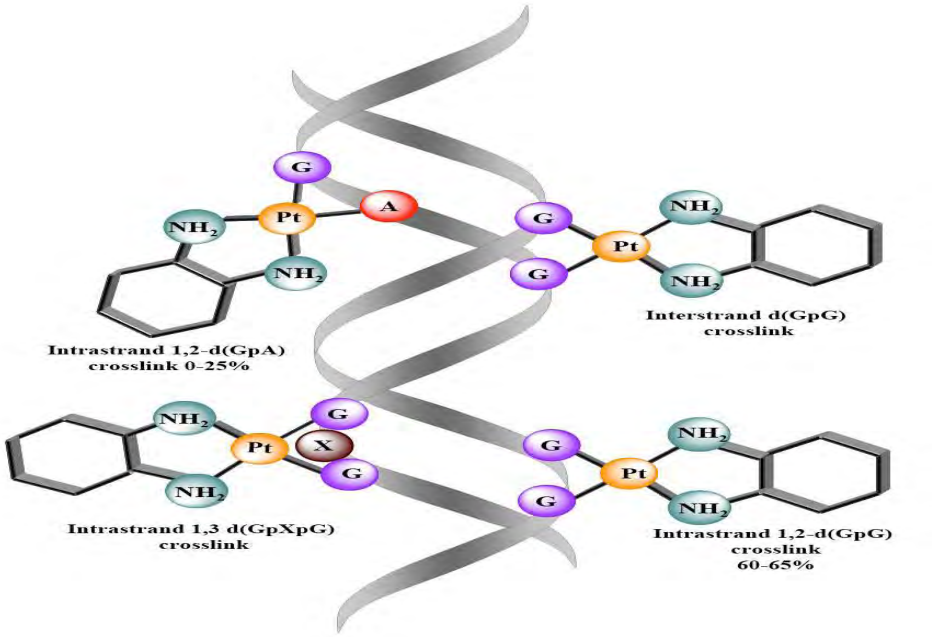

Figure 1.6: DNA adducts formed by oxaliplatin[13].

*Sterically Hindered Platinum(II) Complex (**ZD0473**)*

One of the main mechanisms of cisplatin-resistance is an increase in intracellular thiol-mediated detoxification by peptides and proteins such as glutathione and metallothionines (see section 1.3.2.5). *Cis*-ammninedichlorido(2-methylpyridine)Pt(II), (ZD0473) (Figure 1.7) is the first drug to be administered orally. It is sterically hindered platinum(II) complex and is in phase II clinical trials.[61] Crystal structures of the complex have shown that the pyridine ring is tilted at 102.7° with respect to the PtN_2Cl_2 coordination square-plane.[62] This introduces steric hindrance directly above the platinum coordination plane, limiting the axial attack by the incoming nucleophile to

one side of the coordination square-plane.[63] In addition; this steric hindrance makes it less susceptible to deactivation by the S-containing proteins than cisplatin. This is essential in retarding *in vivo* cellular detoxification reaction by ubiquitous deactivating scavengers like GSH and MT. This feature is also linked to its ability to overcome cisplatin/drug resistance mechanisms.

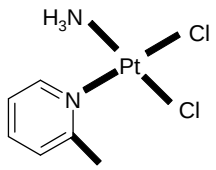

ZD0473

Figure 1.7: Structure of a sterically hindered platinum(II) complex (**ZD0473**) that circumvents cisplatin resistance.

1.3.3.2 Platinum(IV) Complexes

Platinum(II)-based complexes: cisplatin, carboplatin and oxaliplatin are associated with poor saline solubility, high reactivity and therefore, poor bioavailability and lower pharmaco-stability. In addition, these drugs can only be administered intravenously, making them expensive. An oral drug must be neutral, lipophylic, water soluble and stable to survive in the gastrointestinal media.[64] As a result, octahedral Pt(IV) complexes were developed. Notable examples are *satraplatin* (**JM216**) (see Figure 1.2), which has entered phase III of clinical trials for the treatment of ovarian and small lung cancers; and LA-12. These complexes display greater advantages that include

i. Greater stability to ligand substitution reactions and bioreductive activation which allows a greater proportion of the drug to arrive at its target the DNA.[65]
ii. Higher solubility in aqueous solution enables them to be administered orally.
iii. Moderate lipophilic properties due to the presence of bulky non-leaving groups enable them to circumvent resistance caused by decreased Pt accumulation.
iv. Exhibition of lower nephrotoxicity and neurotoxicity, besides better sensitivity in cisplatin resistant cell-lines than cisplatin.

1.3.4 Terpyridine Platinum(II) Complexes

Terpyridine-platinum(II) complexes are known to possess DNA intercalating activity and have been regarded as potential anti-tumour agents.[66] Some of the selected aromatic intercalators are listed in Figure 1.8.

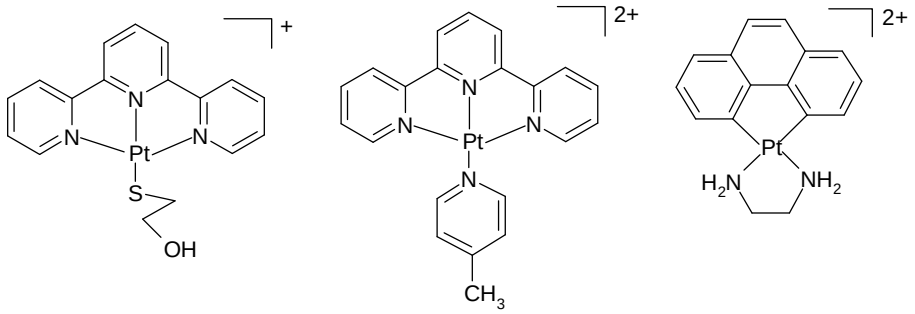

[Pt(terpy)(HET)]$^{+}$ [Pt(terpy)(4-picoline)]$^{2+}$ [Pt(phen)(en)]$^{2+}$

Figure 1.8: Selected Pt(II) metallo-intercalators: terpy = terpyridine, phen = phenanthroline, 4-picoline = 4-methylpyridine, en = 1,2-diaminoethane, and HET = 2-hydroxyethanethiolato ligand.

Intercalative binding, as most commonly studied, is the noncovalent stacking interaction resulting from the insertion of a planar heterocyclic aromatic ring between the base pairs of the DNA double helix. Intercalation stabilizes, lengthens, stiffens, and unwinds the DNA double helix.[67] Previous studies have demonstrated (2,2':6',2''–terpyridine)platinum(II) complexes to be cytotoxic to human ovarian cancer and that bis-[(2,2':6',2''–terpyridine)platinum(II)] complexes with short and rigid linkers are particularly effective.[68,69] The single charged complex {Pt(terpy)(HET)]$^{+}$ was found to intercalate into DNA with a binding constant of 8.3 × 10^{6} M^{-1}, whilst the [Pt(terpy)(4-picoline)]$^{+2}$ is a much stronger intercalator with a binding constant of 2.0 x 10^{7} M^{-1}, which translates to more than two orders of magnitude greater. [70] This is due to the double positive charge of the 4-picoline complex. However, their cytotoxic mechanism remains unclear. These Pt(II) terpy metal complexes can also be used as probes of the electronic and steric effects on the binding to DNA, as the ancillary ligand and nature of the metal can be sterically and electronically tuned.[70,71,72] The π-acceptor effects of terpyridine ligands have been shown to play an important role in the substitution behaviour of Pt(II) complexes.[73] Systematic variation of π-bonding character of the

spectator tridentates (N–donor chelates) on their thermodynamic and kinetic behaviour forms part of the investigation in chapter 3.

1.3.5. Multinuclear Platinum(II) Complexes

One of the most successful approaches in Pt antitumor drugs design is the synthesis of multinuclear Pt complexes with bridging linkers.[74] This class of Pt(II) complexes consist of two or three platinum centres that are linked through a bridging ligand.[75] The properties of the linker such as length, flexibility, hydrogen-bonding capacity and a high positive charge are the major factors that facilitate long-range interstrand cross-links, improved water solubility and cellular uptake that govern their anti-tumour activity.[76] Their success is based on the ability of such complexes to form DNA adducts that are structurally different from those of *cisplatin*. For instance, the length of the complex, which consists of two or more active platinum centres are able to bind to DNA, leading to long-range interstrand cross-links that are less susceptible to repair than the intrastrand cross-links formed by mononuclear platinum complexes. Hence, multinuclear complexes may help in terms of overcoming Pt–drug resistance.

Some of the multinuclear (mostly dinuclear) antitumor active Pt(II) complexes are described in literature (Figure 1.9).

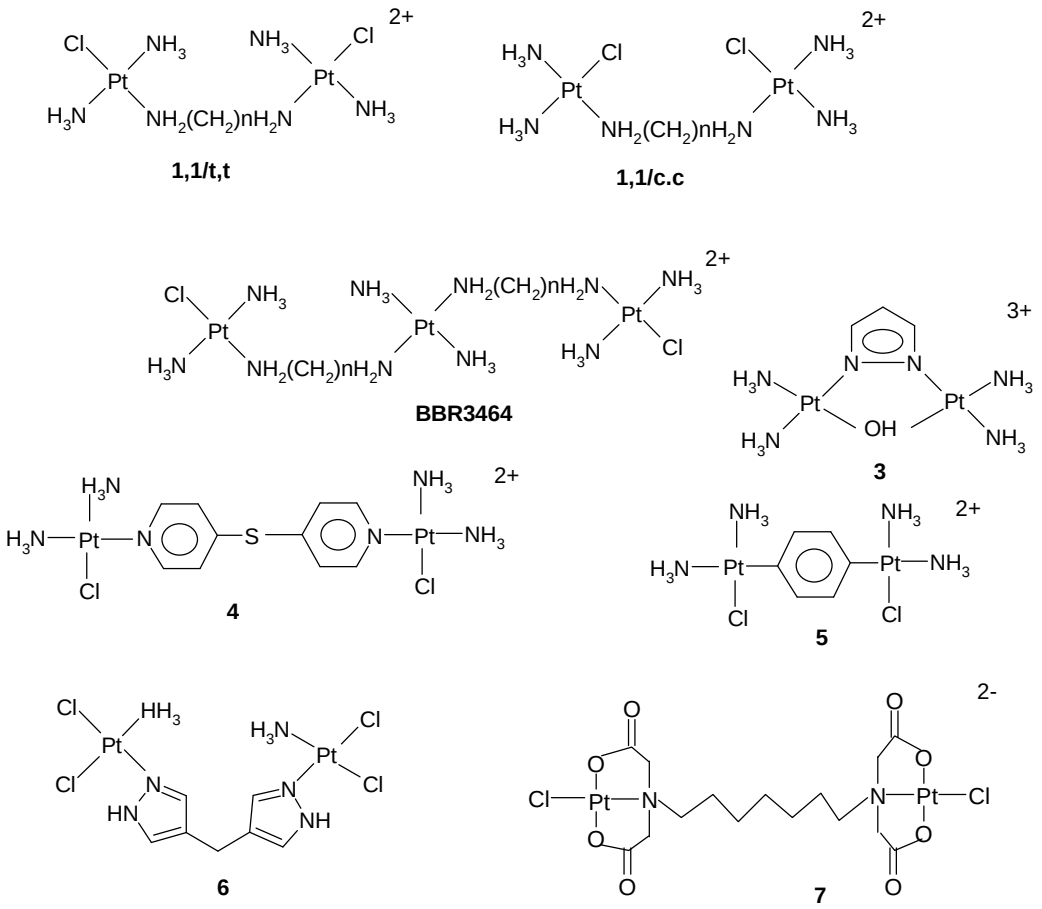

Figure 1.9: Selected multinuclear platinum(II) complexes with flexible amino- and rigid azine and azoles ligands. [77,78]

1.3.5.1 Amino Linkers

The complexes with flexible linkers, for instance, aliphatic diamines developed by Farrell and co-workers (**1,1/t,t** and **1,1/c,c** in Figure 1.9) were designed to form long-range cross-links to DNA.[79,80] In contrast with the mononuclear complexes, such as antitumor cisplatin and clinically ineffective transplatin, both the *cis* and *trans*-isomers in the dinuclear platinum complexes are antitumor active,[81] although their efficiencies are affected by geometry.[82,83] The dinuclear *cis* isomer [{*cis*-$PtCl(NH_3)_2$}$_2$(H_2N-$(CH_2)_6$-NH_2]$^{+2}$ (**1,1/c,c**) is kinetically more inert in its reactions with DNA and in double-stranded DNA produces more interstrand cross-links than its *trans* counterpart.[83] Also, for the **1,1/c,c** complex, the chloro ligand is less sterically accessible than the chloro ligand on the **1,1/t,t** complex, and this is reflected in slower reaction rates.[84] Similarly, a

comparison of the reactions between 1,1/*cis,cis* (alkanediamine, n = 6) and 1,1/*cis,cis* (4,4'-dipyridylsulfide) (**4**) with glutathione suggests that steric hindrance of the phenyl rings of the latter complex is likely to impede deactivation by strong sulphur containing molecules.[85] However, their cytotoxic activity in tumour cell lines exhibits an increasing trend with the increase of the carbon chain length when comparing complexes having 6, 8, 10 and 12 carbons in the alkyl moiety.[84,86] In contrast, complexes possessing rigid bridging ligands, such as hydrazine and azoles (**3**) are developed to minimize distortion of the DNA double helix in a 1,2-intrastrand cross-link.[87]

1.3.5.2 Aromatic Linkers

A new class of dinuclear Pt(II) complexes with azines as bridging ligands has been described in a study by Kalayda,[77,88] which exhibited considerable activity in vitro against several human tumour cell lines. In particular, the pyrazine-linked complex (**5**) displays the highest antitumour activity against cisplatin-resistant L1210 murine leukaemia cell lines. Unlike the dinuclear platinum complexes bridged by the 4,4'-dipyrazolymethane (dpzm) ligand(**6**)[89] where it was reported that the rigidity of the bridge would lead to their poor cytotoxicities, the isomeric azine-bridged complexes were found to exhibit good antitumour activity, more so in cisplatin resistance cells.[77,88] These complexes (diazines), unlike the trinuclear Pt complex **BBR3464** (see Figure 1.9) that was invented jointly by Novuspharma and Farrell[90,91] and other 1,1-*trans*,*trans* analogues, are expected due to their 1,1-*cis*,*cis* geometry to be resistant to decomposition by S-donor nucleophiles that hampers the clinical use of the *trans* Pt(II) complexes hitherto tested. **BBR3464** has entered phase II clinical trials, and shows activity against pancreatic, lung and melanoma cancers.[92] The diazine complexes form part of the research objectives and are further discussed in chapter 5.

Several dinuclear Pt(II) complexes based on EDTA-like ligands have been synthesised (**7**).[37] These complexes are anionic and have a decreasing affinity towards DNA due to the negative charge. Another reason for lack of anti-tumour activity of these compounds is the impossibility of the anionic complexes to penetrate through the cell system and the cytoplasmatic membranes as well as their rapid elimination from the system.[93]

1.4 Kinetic Interest

The platinum-based drugs represent a unique and important class of anti-tumour agents. The discovery of cisplatin in the 1970's revolutionized the chemotherapy in human cancer. Despite its unparalleled successes, the full therapeutic potential of cisplatin has not been realized due to its severe side effects and the emergence of cisplatin-resistant tumour cells. It is also clear from the increasing number of new platinum complexes that synthetic possibilities for more effective platinum-based anti-tumour agents are far from being exhausted. Hence there is need to investigate their kinetic and thermodynamic behaviour in order to obtain a detailed mechanism of action of these systems using appropriate biological nucleophiles. Information on the kinetic parameters and products for the reactions of Pt(II) compounds with the anions of bromides, iodides, thiocyanate and sulphur-donor nucleophiles such as thiourea and its derivatives is of significance to understanding the mechanism of chemo-protection and platinum metabolism in anticancer therapy.[94] This is of importance because the platinum complexes can be systematically tuned through electronic and steric effects. This is important for their application in drug design, C-H activation and homogeneous catalysis.[95]

1.5 Aim and Scope of This Study

Recent investigations by jaganyi *et al*. [73] have been limited to modification of the terpy ligand by either varying the number of pyridine rings, through direct substitution of a pyridine ring with electron-withdrawing or donating groups,[96] and by introducing an aromatic ring substituent in 4'-position of the central pyridine ring.[97,98] Therefore, the first case of this study was to look into the effect of changing the co-ligand on the tridendate N-donor ligand of mononuclear Pt(II) complexes. The second case was extended to new platinum anticancer drugs with cis geometry, similar to *cisplatin*, that have been developed with the aim of decreasing the severe side effects of *cisplatin* and exhibit enhanced stability to metabolic deactivation by coordinated S-donor nucleophiles.[99] Studies by Jaganyi and his group[100] and van Eldik's group[101] have been limited to *trans* Pt(II) dinuclear complexes and only one *cis*-Pt(II) dinuclear complex system was investigated by Van Eldik *et al*.[102] Which merits further studies on *cis*-platinum(II) complexes. The main aim is therefore to extend the study into the kinetics

and thermodynamic properties of mono- and dinuclear Pt(II) complexes. In this thesis the kinetic behaviour of mono- and dinuclear Pt(II) complexes have been explored with neutral ligands: thiourea, *N,N*-dimethylthiourea and *N,N,N,N*-tetramethylthiourea and/or anions, bromide, iodide and thiocyanate. To help explain the kinetic trends and determine how the structures of the complexes would influence reactivity of the Pt(II) centres, Chemical Quantum calculations of the optimised complexes were performed using DFT computation technique at the B3LYP/LACVP level of theory.

Specific Objectives of this study were:

1. To investigate the role of extended π-conjugation on substitution behaviour of tridentate N-donor Pt(II) complexes in which one or two of the outer pyridine rings of the terpy structure was converted into an isoquinoyl moiety (specifically 4'-(2"'-CH_3-phenyl)-6-(3''-isoquinoyl)-2,2'-bipyridine) or a phenanthroline moiety (2-(2'-pyridyl)-1,10-phenanthroline) as illustrated in Figure 1.10. The results obtained were compared with those of the [Pt(2,2'-terpyridine)Cl]$^+$ complex in literature.[103]

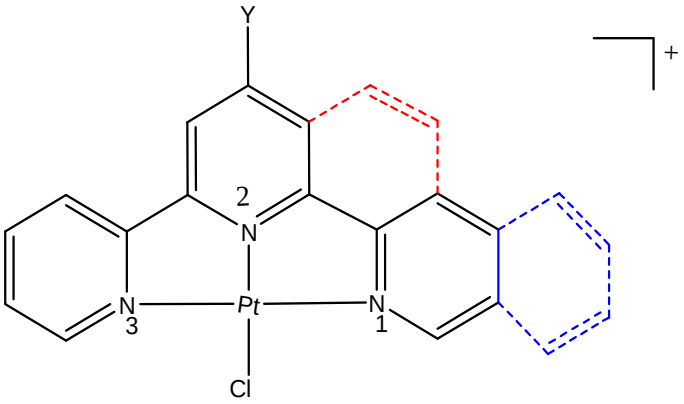

Figure 1.10: Structure of extended terpy Pt(II) complexes; blue ring for isoquinoline ring and red for phenanthroline ring system.

2. To investigate the influence of position of bulky methyl groups on the σ-donor and steric properties of pyrazine-bridged Pt(II) complexes; their effect on kinetic and thermodynamic behaviour.

3. The effect of varying the position of the N-donor atoms of the bridging-diazine ligand on the σ-donor and π-acceptor properties of the ligand and its influence S. Hochreuther, R. Puchta, and R. van Eldik, *Inorg. Chem*., 2011, **50**, 8984 on substitution reactivity of Pt(II) dinuclear complexes was investigated.

4. The kinetic and thermodynamic behaviour of Pt(II) complexes with Parametalated pyridine spacer groups. Density functional theory (DFT) calculations were used to explain the difference in lability of the complexes that could be dependent on structural and steric effects of the flexible linker.

5. The influence of α,ω-alkananediamine linker on ligand substitution of Pt(II) dinuclear complexes was investigated.

Chapter 8 presents a summary of the results obtained in this study including future prospects.

References

1 E. M. Walker and S. M. Walker, , *Annals of Clinical and Laboratory Science,* 1999, **29**, 263.

2 A. Jamal, F. Bray, M. M. Centre, M. E. Jacques Ferlay, E. Ward and D. Forman, *CA Cancer J. Clin.*, 2011, **61**, 69.

3. B. Kumar, P. R.Yadav, H. C. Goel, M. Moshahid, and A. Rizvi, *Digest J. Nanomaterials and Biostructure*s, 2009, **4**, 1.

4 Pan American Health Organization, Regional Office of the World Health Organisation (WHO), *Cancer* (WHO Fact Sheet No. **297**), 24/Oct/2006.

5 Y. Ho, S. F. Au-Yeung and K. W. To, *Med. Res. Rev.*, 2003, **23**, 633.

6 M. Pan and C. Ho, Chem. Soc. Rev., 2008, **37**, 2558

7 (a)R.A. Weinberg, *How cancer arises: Sci. Am.,* 2006, **275,** 62; (b) M. A. Jakubec, M. Galanski and B. K. Keppler, *Rev. Physiol. Biochem. Pharmacol.* 2003, **146**, 1-53.

8 P. C. A. Bruijnincx and P. J. Sadler, *Adv Inorg Chem.,* 2009, **61**:1–62.

9 M. A. Jakupec, M. Galanski, V. B. Arion, C. G. Hartinger and B. K. Keppler, *Dalton Trans*., 2008, 183–194.

10 M. Glanski, M. A. Jakupec and B. K. Keppler, *Curr*. *Med. Chem*., 2005, **12**, 225.

11 (a) M. J. Hannon, *Pure Appl. Chem*., 2007, **79**, 2243; (b) L. M. Pasetto, M. A. D'Andrea, A. A. Brandes, E. Rossi, S. Monfardini, *Critic. Rev. Onco. / Hemat.*, 2006, 59; (c) C. J. Jones and J. Thornback, *Medicinal Applications of Coordination Chemistry*, RSC Publishing, Cambridge, UK, 2007, pp. 218-257.

12 D. C. G. J, Baquiran. *Lippincott's Cancer Chemotherapy Handbook*, Lippincott. 1998.

13 T. Boulikas, A. Pantos, E. Bellis and P. Christofis, *Cancer Therapy*, 2007, **5**, 537.

14 B. E. Lippert, *Cisplatin: Chemistry and Biochemistry of a Leading Anticancer Drug*. Wiley-VCH: Zürich, 1999; p 183-221.

15 U. Belluco, Organometallic and Coordination Chemistry of Platinum, Academic Press, London, 1974, pp. v, vi, 1, 2, 19, 20.

16 F.A. Cotton, G. Wilkinson and P. L. Gaus, *Basic Inorganic Chemistry, 3rd* Ed. John Wiley & Sons, Inc., New York, 1995, pp. 229, 597-599, 605, 606.

17 R. A. Henderson, The Mechanism of Reactions oat Transition Metal Sites, Oxford University Press, Oxford, 1993, p. 1.

18 A. Sigel and H. Sigel, *Metal ions in biological systems*. Marcel Dekker Inc, New York, 1996, p 393.

19 M.L. Tobe and J. Burgess, *Inorganic reaction mechanisms*. Addison Wesley Longman Ltd., Essex, 1999, pp 30–43, 70–112.

20 J. D. Atwood, *Inorganic and Organometallic reaction mechanisms*, 2nd Ed., Wiley-VCH Inc, New York, 1997, pp 43–61.

21 B. Rosenberg, L. Van Camp, E.B. Grimley, *et al. J. Biol. Chem*., 1967, **25**, 1347–1352.

22 (a) S. Hochreuther, S. T. Nandibewoor, R. Puchta, and R. van Eldik, *Dalton Trans*., 2012, **41**, 512; (b) S. Hochreuther, R. Puchta, and R. van Eldik, *Inorg. Chem*., 2012, **51**, 3025; (c) S. Hochreuther, R. Puchta, and R. van Eldik, *Inorg. Chem*., 2012, **50**, 12747.

23 J. Reedijk, In: *How can platinum antitumor compounds reach the cellular DNA*? 226th ACS National Meeting, New York, NY, United states, September 7-11, 2003; New York, NY, United states, 2003.

24 (a) T. Soldatovic´, S. Jovanovic´, Z. D. Bugarcˇic´ and R. van Eldik**,** *Dalton Trans*., 2012, **41**, 876; (b) S.J. Lippard, In: *Progress in Inorganic Chemistry, Bioinorganic Chemistry, Vol. **48***; John Wiley and Sons: Sydney,1995.

25 B. E. Lippert, *Cisplatin: Chemistry and Biochemistry of a Leading anticancer Drug*, Wiley-VCH: Zürich, 1999; (b) X. J. Lin, T. Okudua, A. Holzer and S. B. Howell, *Mol. Pharmacol.*, 2002, **62**, 1154; (c) K. S. Lovejoy, and S. J. Lippard, *Dalton Trans*., 2009, **48**, 1065.

26 C. A. Puckett, R. J. Ernst and J. K. Barton, *Dalton Trans.* 2010, ***39***, 1159–1170.

27 C. W. Schwietert and J. P. McCue, *Coord. Chem. Rev*., 1990, **184**, 67.

28 A. L. Harris, X. Yang, A. Hegmans, L. Povirk, J. J. Ryan, L. Kelland and N. P. Farrell, *Inorg. Chem.*, 2005, **44**, 9598.

29 (a) J. Reedijk*, Chem. Commun*., 1996, 801; (b) G. McGowan, S. Parsons and P. J. Sadler, *Inorg. Chem*., 2005, **44**, 7459.

30 S. E. Miller and D. A. House, *Inorg. Chim. Acta*, 1989, **166**, 189.

31 M. Kotowski and R. Van Eldik, In: Van Eldik R (Ed) *Inorganic high pressure chemistry, kinetics and mechanism*, Elsevier, Amsterdam, 1986, Chapters 1, 3 and 4.

32 S. J. Berners-Price, T. A. Frenkiel, U. Frey, J. D. Ranford and P. J. Sadler, *J. Chem. Soc., Chem. Commun*., 1992, 789.

33 C. Avendaño and J. Carlos Menéndez, *Medicinal Chemistry of Anticancer Drugs,* 2008, p 170 (Access online via Elsevier on 24-07-2012).

34 M. Mikola, K. D. Klika, A. Hakala and J. Arpalahti, *Inorg. Chem.,* 1999, **38**, 571.

35 V. M. Gonzalez, M. A. Fuertes, C. Alonso and J. M. Perez, *Molecular Pharmacol.,* 2001, **59**: 657.

36 (a) M. Kartalou, J. and M Essigman, *Mutat. Res*., 2001, **478**, 1; (b) A. M. J. Fichtinger-Schepman, J. L. van der Veer, J. H. J. den Hartog, P. H. M. Lohnman and J. Reedijk, *Biochem.*, 1985, **24**, 707.

37 M. A. Fuertes, C. Alonso and J. M. Pérez, *Chem. Rev*., 2003, **103**, 645.

38 Z. Guo, P. J. Sadler, and E. Zang, *Chem. Commun*.,1997, **1**,27.

39 A. Pullman, B. *Q.* Pullman, *Rev. Biophys.* 1983, **14**, 289–298.

40 E. R. Jamieson and S. J. Lippard, *Chemistry Reviews* 1999, **99**, 2467-2498.

41 (http://bio.chem.niu.edu/Resources/fall2000 /Templates/DNA%20and%20cisplatin/adducts.htm; Siddik, 2003) accessed on 12/07/2012.

42 H. Sigel, (Ed.), *Metal ions in Biological Systems: Metal Complexes as Anticancer Agents*, Marcel Dekker, 1980, **11**, p. 9, 64-90, 134.

43 J. M. Teuben, M. Rodriguez, I. Zubiri and J. Reedijk, Dalton, 2000, 369-372.

44 (a) Y. W. Jung, S. J. Lippard, *Chem. Rev.* 2007, **107**, 1387–1407; (b) U. M. Ohndorf, M. A. Rould, Q. He, C. O. Pabo, S. J. Lippard, *Nature* 1999, **399**, 708–712; (c) Galanski, M.; Keppler, B. K. *Anticancer Agents Med. Chem*. 2007, **7**, 55.

45 L. M. Pasetto, M. A. D'Andrea, A. A. Brandes, E. Rossi, S. Monfardini, *Critic. Rev., Onco. / Hemat.*, 2006, 59.

46 (a) J. Reedijk, *Chem. Rev*., 1999, **99**, 2499; (b) J. Reedijk, *PNAS*., 2003, **100**, 3611. (c) J. H. J. den Hartog, C. Altona, J. H. van Boom, G. A. van der Marel, C. A. G. Haasnoot, J. Reedijk, *J. Biomol. Struct. Dyn*., 1985, **2**, 1137. (d) J. H. J. den Hartog, C.

Altona J. H. van Boom, G. A. van der Marel, C. A. G. Haasnoot, J. Reedijk, *J. Am. Chem., Soc.* 1984, **106**, 1528.

47 P. J. Morin, *Drug Resist Update,* 2003, **6**, 169.

48 (a) Z. H. Siddik, *Oncogene*, 2003, **22**, 7265; (b) D. J. Stewart, *Crit. Rev. Oncol. Hematol*., 2007, **63**, 12.

49 J. Reedijk, *Chem. Rev*., 1999, **99**, 2499-2510.

50 (a) S. S. G. E. van Boom and J. Reedijk, *J. Chem. Soc., Chem. Commun.* 1993, **18**, 1397–1398; (b) K.J. Barnham, Z. Guo, P. J. Sadler, *J. Chem. Soc., Dalton Trans.* 1996, **13**, 2867–2876; (c) J. M. Teuben, S. S.G. E. van Boom, J. Reedijk, *J. Chem. Soc., Dalton Trans.* 1997, **21**, 3979–3980 (d) Y. Chen, Z. Guo, P. del S. Murdoch, E. Zang, P. J. Sadler, *J. Chem. Soc, Dalton Trans.* 1998, **9**, 1503–1508.

51 D. Du Plessi-Stoman, *MSC. Thesis*, Nelson Mandela Metropolitan University, South Africa, 2006, p 15.

52 C. H. Versantvoort, H. J. Broxterman, T. R. Badrij, J. Scheper and P. R. Twentyman, *J. Cancer*, 1995, **72**, 82.

53 A. Pasini and C. Fiore, *Inorg. Chim. Acta*., 1999, **285**, 249.

54 (a) N. J. Wheate, S. Walker, G. E. Craig and R. Oun , *Dalton trans.,* 2010, **39**, 8113-8127; (b) J. Reedijk, *Chem. Rev.*, 1999, **99**, 2499.

55 E. Cvitkovic, *Cancer Treatment Reviews*, 1998, **24**, 265-281.

56 C. Molenaar, J.-M. Teuben, R. J. Heetebrij, H. J. Tanke and J. Reedijk, *J. Biol. Inorg. Chem.* 2000, **5**, 655–665.

57 G. Samimi, K. Katano, A. K. Holzer *et al., Mol. Pharmacol*., 2004, **66**, 25–32.

58 S. Neidle, I. M. Ismail and P. J.Sadler, *J. Inorg. Biochem,.* 1980, **13**, 205–212.

59 U. FREY, J. D. RANFORD AND P. J. SADLER, *INORG. CHEM.,* 1993, **32**, 1333–1340.

60. (a) T. Bolelikas and M. Vougiouka, *Oncol. Reports,* 2003, **10**, 1663; (b) J. M. Woynarowski, S. Faivre, M. C. S. Herzig, B. Arnett, W. G. Chapman, A. V. Trevino, E. Raymond, S. G. Chaney, A. Vaisman, M. Varchenko, P. E. Juniewicz, *Mol. Pharmacol*. 2000, **58**, 920.

61 (a) J. Holford, F. Raymond, B. A. Murrer, K. Grimaldi, J. A. Hartley, M. Abrams and L. R. Kelland, *Anticancer Drug Des*., 1998, **13**, 1; (b) M. Hay, *Curr. Opin. Oncol.,*

Endocr. Metab. Invest. Drugs, 1999, **4**, 443; (c) Anormed Product Profile: ***ZD0473***, June 2001.

62 Y. Chen, Z. Guo, S. Parsons and P.J. Sadler, *Chem. Eur. J.*, 1998, **4**, 672.

63 (a) T. W. Sorenson, M. Eastman, *Cancer Res*., 1988, **48**, 4484; (b) M. Eastman, *In Cisplatin: Chemistry and biochemistry of a leading anticancer drug,* 1999, B. Lippert, Ed. Wiley VCH, Weinheim, 111.

64 C. M. Giandomenico, M. J. Abrams, B. A. Murrer, J. F. Vollano, M. I. Rheinheimer, S. B. Wyer, G. E. Bossard, and J. D. Higgins, *Inorg. Chem.*, 1995, **34**, 1015.

65 V. Kvardova, R. Hrstka, D. Walerych, P. Muller, E. Matoulkova, V. Hruskova, D. Stelclova, P. Sova and B. Vojtesek, *Molecular Cancer* 2010, **9**:147.

66 Y.-C. Lo, T-P, Ko, W-C, Su, T-L, Su and A. H.-J. Wang, J*. Inorg. Biochem*., 2009, **103**, 1082.

67 H.-Ke. Liu and P. J. Sadler,*Acc. Chem. Research*, 2011, **44**, 349.and cited references therein.

68 G. Lowe, S. A. Ross, M. Probert and A. Cowley, *Chem. Commun.*, 2001, **14**, 1288.

69 G. Lowe, A.S. Droz, T. Vilaivan, G. W. Weaver, J. J. Park, J.M. Pratt, L. Tweedale and L. R. Kelland, *J. Med. Chem.*, 1999, **42**, 3167.

70 K. Jennette, S. J. Lippard, G. Vassiliades and W. Bauer, *Proc. Natl. Acad. Sci*. U.S.A, 1974, **71**, 3839.

71 M. Howe-Grant, K. C. Wu, W. R. Bauer and S. J. Lippard, *Biochemistry*, 1976, **15**, 4339.

72 M. Casamento, G. E Arena, C. Lo Passo, I. Pernice, A. Romeo and L. Monsú Scolaro, *Inorg. Chim. Acta*., 1998, **276**, 242.

73 (a) D. Jaganyi, A. Hofmann and R. van Eldik*, Angew. Chem., Int. Ed*. 2001, **40**, 1680; (b) A. Hofmann, D. Jaganyi, O. Q. Munro, G. Leihr and R. van Eldik, *Inorg. Chem*., 2003, **42**, 1688; (c) D. Jaganyi and F. Tiba, *Transition Met. Chem*., 2003, **28**, 803, D. Jaganyi, D. Reddy, J. A. Gertenbach, A. Hofmann and R. van Eldik, *J. Chem Soc., Dalton Trans*. 2004, 299.

74 J. Reedijk, *Proc. Natl. Acad. Sci. U.S.A*., 2003, 3611-3616.

75 N. J. Wheate, and J. D. Collins, *Curr. Med. Chem.-Anti-Cancer Agents*, 2005, **5**, 267.

76 (a)J. Kašpárková, J. Zehnulova, N. Farrell and V. Brabec, *J. Biol. Chem.*, 2001, **276**, 22191; (b) M. B. G. Kloster, J. C. Hannis, D. C. Muddiman and N. Farrell, *Biochemistry*, 1999, **38**, 14731;(c)V. Brabec and J. Kasparova, *Drug resist. Updates*, 2005, **8,** 131.

77 G. kalayda, S. Komeda, K. Ikeda, T. Sato, M. Chikuma, and J. Reedijk, *Eur. J. Inorg. Chem*., 2003, 4347-4355

78 (a) S. van Zutphen, M. Robillard, G. van der Marel, H. Overkleeft, H. den Dulk, J. Brouwer, and J.Reedijk, *Chem. Commun*., 2003, 634; (b) J. Zhu, M. Lin, D. Fan, Z. Wu, Y. Chen, J. Zhang, Y. Lu and Z. Guo, *Dalton Trans.*, 2009, 10889.

79 (a) V. Brabec, J. Kasparkova, O. Vrana, O. Novakova, J. Cox, Y. Qu and N. Farrell, Biochem., 1995,**9**, 6781; (b) H. Ertürk, R. Puchta and R. van Eldik, *Eur. J. Inorg. Chem.,* 2009, 1331.

80 N. Farrell, T. G. Appleton, Y.Qu, J. D. Roberts, A. P. Fontes, K. Skov, P. Wu and Y. Zou, Biochem., 1995,15480-15486.

81 N. Farrell, *Polynuclear platinum drugs.* In: Sigel A, Sigel H, editors. Metal ions in biological systems. New York, Basel: Marcel Dekker, Inc.; 2004, p. 251-96.

82 J. Kasparkova, N. Farrell and V. Brabec, *J. Biol. Chem*., 2000, **275**, 15789.

83 J. Kasparkova, O. Novakova, O. Vrana, N. Farrell, V. Brabec, *Biochemistry,* 1999, **38**, 10997.

84 K. J. Mellish, Y. Qu, N. Scarsdale, N. Farrell, *Nucl. Acids Res*., 1997, **25**, 1265.

85 G. Zhao, H. Lin, S. Zhu, H. Sun and Y. Chen, *Anti-Cancer Drug Des.*, 1998, **13**, 769.

86 H. Silva, C. V. Barra, F. V. Rocha, F. Frézard, M. T. P. Lopes and A. P. S. Fontes, *J. Braz. Chem. Soc.*, 2010, **21**, 1961.

87 S. Komeda, H. Ohishi, H. Yamane, M. Harikava, K. Sakaguchi, M. Chikuma, *J.Chem. Soc*., *Dalton Trans*., 1999, 2959-2962.

88 S. Komeda, G. V. Kalayda, M. Lutz, A. L. Spek, Y. Yamanaka, T. Sato, M. Chikuma and J.Reedijk, *J. Med. Chem*., 2003, **46**, 1210.

89 N. J. Wheate, C. Cullinane, L. K. Webster and J. G. Collins, *Anti-Cancer Drug Des.*, 2001, **16**, 91.

90 N. Farrel and S. Spinelli, *Dinuclear and trinuclear platinum anticancer Agents*, In: N. Farrell (Ed.), Uses of Inorganic Chemistry in Medicine, Royal Society of Chemistry, 1999, p.124.

91 G. Zhao, H. Lin, S. Zhu, H. Sun and Y. Chen, *Anti-Cancer Drug Des.*, 1998, **13**, 769.

92 I. Kostova, *Recent patents on Anti-Cancer Drug Discovery*, 2006, **1**, 1-22

93 B. Rosenberg, *Naturwissenschaften*, 1973, **9**,399.

94 K. Lemma, S. F. K. Elmroth and L. I. Elding, *J. Chem. Soc., Dalton Trans*., 2002, 1281.

95 A. Hofmann, L. Dahlenburg and R. van Eldik, *Inorg. Chem*., 2003, **42**, 6528.

96 D. Jaganyi, K-L, De Boer, J-A. Gertenbach and J. Perils, *Int. J. Chem. Kinet.,* 2008, **40**, 807.

97 D. Jaganyi, D. Reddy, J. A. Gertenbach, A. Hofmann and R. van Eldik, *J. Chem. Soc., Dalton Trans.*, 2004, 299.

98 D. Reddy, K. J. Akerman, M. P. Akerman and D. Jaganyi, Transition Met. Chem., 2011 **36**:593.

99 J. W. Williams, Y. Qu, H. Bulluss. E. Alvorado and N. Farrell, *Inorg. Chem.*, 2007, **46**, 5820.

100 (a) D. Jaganyi, V. M. Munisamy and D. Reddy, *Int. J. Chem. Kinet.,* 2006, **38**, 202;(b) D.Jaganyi, A. Mambanda, S. Hochreuther and R. van Eldik, *Dalton Trans.,* 2010, **39**, 3595; (c) D. Reddy and D. Jaganyi, *Int. J. Chem. Kinet.,* 2011, **43**, 161.

101 (a) N. Summa, J. Maigut, R. Puchta and R. van Eldik, *Inorg Chem.,* 2007) **46**: 2094; (b) H. Ertuerk, J. Maigut, R. Puchta, R. van Eldik (2008) *Dalton Trans* **20**: 2759; Hochreuther S.; Puchta R.; van Eldik R., *Inorg Chem* 2011, **50**, 12747; (c) Soldatović T.; Jovanović S.; Bugarčić Ž. D.; van Eldik R. *Dalton Trans* 2012, **41**, 876.

102 H. Ertuerk, R. Puchta and R. van Eldik, *Eur. J. Inorg. Chem.,* 2009, 1331.

103 R. J. Mureinik and M Bidani, *Inorg. Chim. Acta*, 1978, **29**, 37.

Table of Contents-2

List of Figures

List of Tables

Chapter Two

2.0 Ligand Substitution at Pt(II) Square-planar Centre

2.1 Introduction

In order to understand how a metal such as Pt achieves the desired anticancer activity, the kinetics underlying the interaction of the Pt-based drugs with their target, the DNA and S-donor ligands present in biological fluids is important.[1] The prime target of Pt is thiols (RS^-) like glutathione and cysteine. These are known to bind irreversibly to Pt(II) under the conditions obtained in the body fluids at a neutral pH. This renders the anticancer Pt(II) agent inert and ineffective.

These Pt(II) complexes in comparison to other d^8 square-planar complexes such as Pd(II), Rh(I), Ir(I) and Au(III) are characterised by similar in ionic radii due to the lanthanide contraction. However, the rate of metal-ligand exchange is slow in Pt(II) complexes. This gives it high kinetic stability and results in ligand-exchange reactions of a longer duration than the other metals. The Pt(II) compounds exhibit ligand-exchange kinetics in the same order of magnitude as the division of tumour cells,[2] which makes them suitable to stop mitosis and promote cell death before the Pt(II) centre could be inactivated by non-target binding sites like the soft S-donor ligands. Moreover, Pt(II) complexes containing N and S donor atom ligands are both kinetically stable (slow ligand exchange) and thermodynamically stable.[3] The analogous complexes of Au(III) are effective as anticancer drugs, but are thermodynamically unstable since they are readily reduced to Au(1) and Au(0).[4] Therefore, continued investigation into ligand-exchange kinetics of Pt(II) complexes remains an important area in contemporary drug design and synthesis. The varying of parameters such as steric and electronic effects to tune solubility, acidity and reactivity of these complexes may improve the therapeutic efficacy of the anticancer drugs as well as tune the reactivity of the complexes. In the last few decades, an appreciable amount of research has been done on the kinetic and the mechanistic behaviour of substitution reactions of Pt(II) complexes.[5,6,7,8] Due to the similarity in the reaction mechanisms of platinum(II) complexes with the other square planar complexes, the information collected on platinum(II) complexes can be applied to the other square planar complexes.

The mononuclear Pt(II) complexes **1**-**3** (Figure 2.1) do not adhere to the Cleare and Hoeschele structure-activity relationship principle.[9,10] Nevertheless, they exhibit cytotoxicity against tumour cell lines comparable to cisplatin.[11,12] Variations in their cytotoxic activity are related to the differences in lipophilicity of these complexes. The most lipophilic complex (**1**) is also the most cytotoxic,[11] since its higher lipophilicity can facilitate improved passive uptake rates of the drug molecules across the lipid cell membrane and affect the activity of the drug. In addition, the presence of bulky groups such as pyridine and flexible substituents significantly reduces the rate of deactivation by S-containing molecules like glutathione (GHS) as discussed for ZD0473 in Chapter 1 (section 1.3.5).[13,14] Complex **3** (Figure 2.1) hardly reacted with GHS as it is sterically hindered. This steric hindrance reduces *in vivo* reactions associated with competing S-nucleophiles like GHS and sulphur containing proteins. In summary, the lability of the Pt–Cl bond can contribute to the observed cytotoxicity.

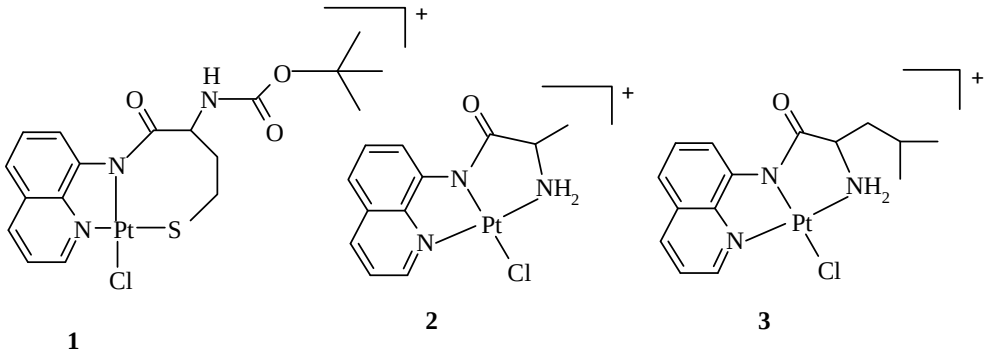

Figure 2.1: Structures of some monofunctional platinum(II) complexes active against human colon carcinoma cell line (HCT-116).[11]

Therefore besides controlling antitumor activity, the kinetics of ligand exchange reactions of the Pt(II) complexes is important in controlling other side reactions that could mediate toxicity. A brief summary of the relevant theoretical aspects of possible ligand substitution reaction mechanisms of d^8 square-planar Pt(II) complexes was undertaken.

2.2 Mechanism of Ligand Substitution Reactions for Square-planar Complexes

The study of ligand substitution reactions involving coordination compounds has become an integral part of Inorganic Chemistry. Ligand substitution reaction mechanisms for transition metal complexes have been categorised by Langford and Gray[5] into three simple pathways, namely:

i. A dissociative path (**D**) in which the leaving ligand is lost in the first step.

ii. An associative path (**A**) in which the entering ligand adds in the first step, producing an intermediate of increased coordination number.

iii. A concerted path called interchange (**I**) in which the leaving ligand is moving from the inner to the outer coordination sphere as the entering group is moving from outer to inner.

These reaction paths can be summarised according to *Equations 2.1–2.3*;

$$\text{D: } [L_nMX] \underset{+X}{\overset{-X}{\rightleftharpoons}} [L_nM] \underset{-Y}{\overset{+Y}{\rightleftharpoons}} [L_nMY] \qquad (2.1)$$

$$\text{A: } [L_nMX] \underset{-Y}{\overset{+Y}{\rightleftharpoons}} [L_nMXY] \underset{+X}{\overset{-X}{\rightleftharpoons}} [L_nMY] \qquad (2.2)$$

$$\text{I: } [L_nMX] + Y \longrightarrow [L_nMX]\text{---}Y \longrightarrow [L_nMY]\text{---}X \longrightarrow [L_nMY] + X \qquad (2.3)$$

where, Y = nucleophile or solvent molecule.

These reaction paths can also be illustrated as presented in Figure 2.2.

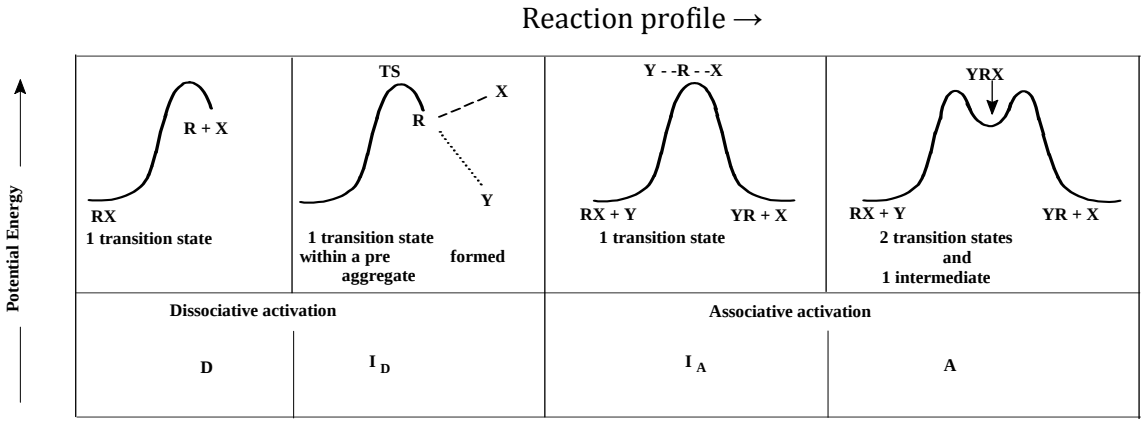

Figure 2.2: Potential energy profiles of different mechanisms occurring at a square planar Pt(II) centre as proposed by Langford-Gray.[5,15]

In a dissociative mechanism the activation energy is determined by the energy required to break the bond of the leaving group whereas bond making is the main factor determining the size of the activation energy for an associative mechanism.

2.2.1 The Dissociation Mechanism (D)

Although, dissociative mechanisms of square-planar complexes have been rare in the past, Tobe and Burgess[15] reported that the dissociative mechanism change over is favoured by; [5]

- A strong *trans* σ-donor ligand, *i.e*. the amount of negative charge that the ligand donates to the metal ion through the σ-bond will enhance the weakening of the metal-leaving group bond; thereby stabilizing the 14-electron transition state by increasing in electron charge density at metal centre. This prevents the facile approach of the entering nucleophile.
- A sterically hindered metal centre that possesses high electron density at the metal atom destabilizes the ground state of the complex by decreasing the electrophilicity of the metal centre and as a result prevents attack of nucleophile from the axial position, either from below or above the Pt(II) centre.
- A strong coordinating solvent will readily displace the leaving group; thereby enhancing the formation of the 14-electron coordinate intermediate.

In a dissociation mechanism the transition state consists of a 14-electron (T-shaped) intermediate of lower coordination number. The intermediate can last for a sufficiently long time, allowing it to equilibrate with its environment before capturing the incoming ligand. Accordingly, the rate of consumption of the incoming group is dependent on the nature of the leaving group but is independent of the nature and concentration of the incoming ligand.[7] Also, the consumption of the intermediate may occur when the leaving group is still in close proximity to the metal centre since the bond length between the metal centre and the leaving group (**M---X**) increases.[15] This reduces the ability of the metal complex to discriminate and enables the solvent (usually present in excess) to dominate the substitution process. In addition, contact times are long enough due to high stability of the three coordinate intermediate which leads to '*cis*-*trans* isomerisation', thereby resulting in non-stereo specific products on addition of the nucleophile.[5] For that reason, the dissociative mechanism is "non-stereo selective".

2.2.2 The Associative Mechanism (A)

The intermediate is formed via two transition states (Figure 2.2), in which the bond-making (**M---Y**) is more important than the bond-breaking (**M---X**) process as illustrated in Scheme 2.1 and by *Equation 2.2*.

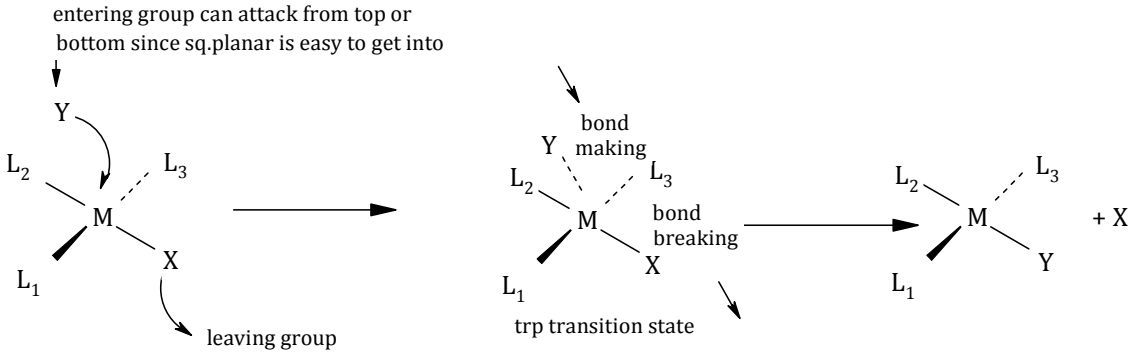

○ Stereospecific-leaving group (X) is *trans* to L_2 and so is Y (entering group)

Scheme 2.1: Reaction pathway for the associative substitution reaction showing direct nucleophilic attack

For the associative mechanism (**A**), the rate determining step is the making of the bond between the metal centre and the incoming group (Y). Hence, in a non-coordinating medium in the presence of excess of the concentration of Y, the rate of substitution reaction is strongly dependent on the nature of the incoming ligand, given that it participates in the early section of the transition state. Also, the stereochemistry of the complex is retained during the course of the substitution process.[15,16]

In an associative mode of substitution mechanism, all the ligands involved can influence the stability and activation energy of the five- coordinate activated complex (see Scheme2.1). As a result, all the groups (i.e. entering, leaving and co-ligands) will affect the magnitude of rate obtained from the substitution reaction of a d^8 square-planar Pt(II) complex. Because of this many studies have systematically been carried out by varying the character of the ligands.[17,19]

In previous studies,[20,21,22,23] Pt(II) complexes of the type *cis*-$[Pt(Me)_2R_2]$ and *cis*-$[Pt(Ph)_2R_2]$ (where R= DMSO or thioether) revealed that the two strong *cis* σ-donor atoms, *i.e*. carbene in the organo-ligands, S or P, display a strong preference for dissociative mechanism. As a result of the high *trans*-influence of the two strong σ-donor bonding ligands, the Pt-S bond of the thioether leaving groups are weakened by the increase in electron density at the metal centre. This prevents the facile attack by the incoming nucleophile, but there is stabilisation of the 14-electron intermediate by the two strong σ-bonded ligands. On the other hand, when one of the thioethers is replaced by a strong π-acceptor ligand such as CO or CN^-, an associative mechanism is favoured. This is because the stronger π-accepting CO or CN^- ligand removes the electron density from the metal centre, hence increasing its electrophilicity. This allows delocalization of the electron density-received from the incoming nucleophile-away from the Pt(II) centre in a five-coordinate transition-state stabilisation interaction. Therefore, introduction of σ-donor and/or π-acceptor ligands into the Pt(II) complexes provides an electronic torque through the molecule that is a determinant on the type of reaction mechanism.

2.2.3 The Interchange Mechanism (I)

Between the limiting dissociation (**D**) and the limiting association (**A**) mechanisms there exists a continuum of mechanisms that are characterised by a single activated complex in which bond-making and bond-breaking between the metal centre and the entering-plus-the leaving groups are synchronised. If the bond between the metal and the leaving group is weakened before the incoming group tightly binds to the metal centre, then the probability of the solvent attaching to the reactive metal centre is higher leading to a dissociation mechanism.[7] This permits the solvent, which is normally in a higher molar excess to dominate the substitution process, leading to a dissociative-activated interchange mechanism ($\mathbf{I_D}$). If the reaction rate is more dependent on the nature of the incoming group and the leaving group leaves the metal centre only once the incoming group is fully bound to the reactive centre, the mode of activation changes from $\mathbf{I_D}$ to associatively-activated interchange mechanism ($\mathbf{I_A}$).[5]

2.3 Measurements of Integrated Rate Constants

2.3.1 Reversible Second-order Reactions

Often, ligand substitution reactions in square-planar complexes do not go to completion, but have a tendency to attain a state of equilibrium and can be written as:

$$\mathbf{A} + \mathbf{B} \underset{k_{-2}}{\overset{k_2}{\rightleftharpoons}} \mathbf{C}$$

or

$$\mathbf{ML_3X} + \mathbf{Y} \underset{k_{-2}}{\overset{k_2}{\rightleftharpoons}} \mathbf{ML_3Y} + \mathbf{X} \qquad (2.4)$$

where, A = Metal complex (ML_3X), X is the leaving group
B = incoming nucleophile, Y

The forward reaction step is thus second-order, while the reverse reaction step is first-order, which results in mixed order dependence. Because of the complex nature of the reaction, the reaction can be studied by selecting *pseudo* first-order conditions, in which

the concentration of one of the reactants is at least ten-fold excess, *e.g.* $[B]_0 >> [A]_0$. The equation can be treated as a reversible reaction and the rate of formation of C can be given as:

$$-\frac{d[A]}{dt} = -\frac{d[B]}{dt} = \frac{d[C]}{dt} = k_2[A]_t[B]_t - k_{-2}[C]_t$$
$$= k_2[A]_t[B]_t - k_{-2}[A]_0 - [A]_t$$
$$= k_2[A]_t[B]_t - k_{-2}[A]_t - k_{-2}[A]_0 \quad (2.5)$$

Where k_2 = second-order rate constant

k_{-2} = observed first-order rate constant for the reverse reaction.

By applying a mass balance for a given stoichiometry of 1:1:1, at time, t_0 and t

$$[A]_t = [A]_0 - [C]_t, \text{ and } [B]_t = [B]_0 - [C]_t \quad (2.6)$$

At equilibrium,

$$[A]_{eq} = [A]_0 - [C]_{eq}, \text{ and } [B]_{eq} = [B]_0 - [C]_{eq} = [B]_0 - [A]_0 + [A]_{eq} \quad (2.7)$$

Thus, at equilibrium the rates of the forward and reverse reactions are equal resulting in

$$\frac{-d[A]}{dt} = k_2[A]_{eq}[B]_{eq} + k_{-2}[A]_{eq} - k_{-2}[A]_0 = 0$$
$$k_{-2}[A]_0 = k_2[A]_{eq}[B]_{eq} + k_{-2}[A]_{eq} \quad (2.8)$$

Substitution of $k_{-2}[A]_t$ from *Equation 2.8* into *Equation 2.4* gives

$$\frac{-d[A]}{dt} = k_2[A]_t[B]_t - k_{-2}\{(k_2[A]_{eq}[B]_{eq}) + k_{-2}[A]_{eq}\} - k_{-2}[A]_t \quad (2.9)$$

Substitution of $[B]_t$ and $[B]_{eq}$ in *Equations 2.6* and *2.7* into (*2.9*), and approximating

$k_2[A]_t[A]_o \approx k_2[A]_{eq}[A]_o$ and $k_2[A]^2_t \approx k_2[A]^2_{eq}$ leads to

$$\frac{-d[A]}{dt} = k_2[A]_t[B]_o - k_2[A]_{eq}[B]_o + k_{-2}[A]_t - k_{-2}[A]_{eq}$$

$$= (k_2[B]_o + k_{-2})\,([A]_t - [A]_{eq}) \qquad (2.10)$$

Separation of variables and integration gives:

$$\int_{[A]_0}^{[A]_t} \frac{d[A]}{([A]_t - [A]_{eq})} = -(k_2[B]_0 + k_{-2})\int_0^t dt \qquad (2.11)$$

This results in

$$\ln\left(\frac{[A]_t - [A]_{eq}}{[A]_0 - [A]_{eq}}\right) = -(k_2[B]_0 + k_{-2})t$$
$$= -k_{obs}t$$
$$\text{where, } k_{obs} = k_2[B]_0 + k_{-2} \qquad (2.12)$$

Under pseudo first-order conditions, the experimental first order rate constant, k_{obs}, is given by:

$$\frac{-d[ML_3X]}{dt} = k_{obs}[M]$$

with

$$k_{obs} = k_2[Y] + k_{-2} \qquad (2.13)$$

A plot of k_{obs} versus the initial concentration of the nucleophile, $[B]_0 = [Y]_0$, is linear with a slope equal to the second-order rate constant, k_2, and the y-intercept value equal to the first-order rate constant, k_{-2}. Typical kinetic plots are shown in Figure 2.3. A plot which passes through zero implies that the forward reaction is irreversible and directly goes to completion, whereas a non-zero y-intercept signifies a back reaction in which the nucleophile Y is being substituted from the metal centre by the solvolysis process.

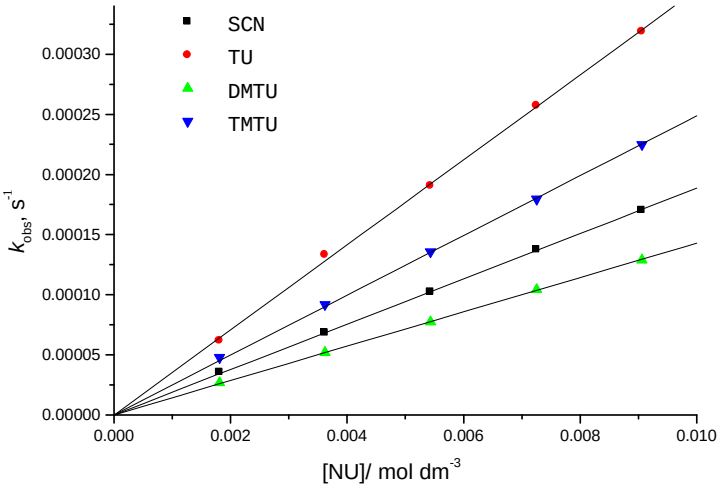

Figure 2.3: Typical plots of the pseudo first-order rate constants, k_{obs} versus. the concentration of the entering nucleophiles for the substitution reaction of a dinuclear Pt(II) complex at 298 K in aqueous solution.

In *Equations 2.12* and *2.13*, the second-order rate constant, k_2, signifies the direct nucleophilic attack on the Pt(II) centre by the incoming nucleophile (Y), while the k_{-2} term represents the existence of a slow back reaction or parallel reaction due to solvolysis. The ratio of k_2/k_{-2} represents the equilibrium constant, K_{eq}, which can be checked thermodynamically.

The two possible mechanistic pathways for associatively-activated substitution reactions at the Pt(II) centre given by the two-term rate law in *Equation 2.13* are summarized in **Scheme 2.2**. The solvolysis pathway follows first-order kinetics and is independent of the concentration of the nucleophile (Y).

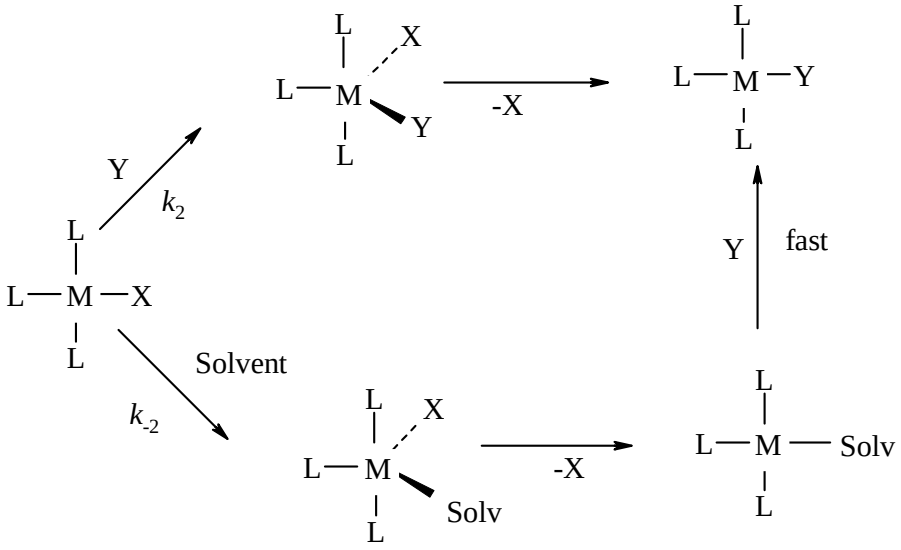

Scheme 2.2: A proposed dual reaction pathway for an associative substitution mechanism at the Pt(II) centre.

Under *pseudo* first-order conditions, the concentration of the incoming nucleophile, Y, is at least 10-fold excess than the metal complex in a 1:1 formation reaction. The k_2 can be determined by measuring the dependence of the observed rate constant, k_{obs}, on the initial concentration of the nucleophile $[B]_0$, using *Equation 2.12*.

2.3.2 Activation Parameters

The reaction rates normally increase with the increase in temperature. The temperature dependency is defined in terms of the rate constant and is useful in determining the activation parameters of a given reaction. This is essential in assigning the mechanism of that reaction. Once the experimental data has been obtained for the various terms that contribute to the rate law, it is analysed using the Arrhenius equation) or by the Transition-State Theory.

2.3.3 The Arrhenius Theory

The rigorous statement of the relationship between temperature and the rate constant, k, was given by Arrhenius in 1889 [26] as *Equations 2.14* and *2.15*:[26]

$$k = Ae^{-Ea/RT} \quad (2.14)$$

$$\ln k = \ln A - \frac{E_a}{R}(1/T) \quad (2.15)$$

where, A = pre-exponential or frequency factor (same units as *k*),

E_a = Arrhenius activation energy (J mol^{-1}),

R = universal gas constant (8.315 J K^{-1} mol^{-1}) and

T = temperature in Kelvin (K).

Over the modest temperature range (10-50 °C) in which the experiment is commonly carried out to determine *k* values, both *A* and *Ea* are independent of temperature. A plot of ln*k* versus $^1/_T$ is linear with a slope of $-Ea/R$. The Arrhenius equation is of great importance for complex systems where measured rate constants are a complex composite of specific rate constants.[26,34]

2.3.4 The Transition-state Theory

H. Eyring, M. Evans and M. Polanyi developed the transition-state theory in 1935.[6,34] The theory works on the assumption that many reactions proceed via a pre-equilibrium mechanism between the reactants and the transition-state species as shown in the following reaction.

$$M—B \overset{K^{\#}}{\rightleftharpoons} [M\text{---}B]^{\#} \xrightarrow{k_2} M + B \quad (2.16)$$

Activated complex or transition-state complex

The equation for the rate of reaction can be written in terms of M as:

$$d[\mathrm{M}]/dt = k_2[\mathrm{M...B}]^{\#} \quad (2.17)$$

but, $$K^{\#} = [\mathrm{M...B}]^{\#}/[\mathrm{M} — \mathrm{B}] \quad (2.18)$$

hence, $$d[\mathrm{M}]/dt = k_2 K^{\#}[\mathrm{M} - \mathrm{B}] \quad (2.19)$$

$$= (k_b \mathrm{T}/h) K^{\#}[\mathrm{M} — \mathrm{B}] \quad (2.20)$$

where, k_b = Boltzmann's constant (1.38×10^{-23} J K^{-1})

h = Plank's constant (6.626×10^{-34} J s^{-1})

$K^{\#}$ = equilibrium constant of the activated complex

Assuming first-order kinetics, the rate expression can be given by

$$d[\mathrm{M}]/dt = k_2[\mathrm{M} — \mathrm{B}] \quad (2.21)$$

Combining equations (2.20) and (2.21), it is found that the experimental rate constant can be equated to

$$k_2 = (k_b \mathrm{T}/h) K^{\#} \quad (2.22)$$

But, the Gibb's free energy of activation, $\Delta G^{\#}$, can be expressed in terms of $K^{\#}$ as

$$\Delta G^{\#} = -\mathrm{RT}\ln K^{\#} = \Delta H^{\#} - \mathrm{T}\Delta S^{\#} \quad (2.23)$$

Substituting equation (2.23) into equation (2.22) gives

$$k_2 = (k_b \mathrm{T}/h) \exp\left(\triangle G^{\#}/\mathrm{RT}\right) \quad (2.24)$$

$$= (k_b \mathrm{T}/h) \exp\left(-\triangle H^{\#}/\mathrm{RT}\right) \exp\left(\triangle S^{\#}/\mathrm{R}\right) \quad (2.25)$$

Subsequent re-arrangement and taking logarithms results in:

$$\ln\left(\frac{k_2}{\mathrm{R}}\right) = \ln\left(\frac{k_b}{h}\right) + \frac{\triangle S^{\#}}{\mathrm{R}} - \frac{\triangle H^{\#}}{\mathrm{RT}} \quad (2.26)$$

$$= \left[23.76 + \frac{\triangle S^{\#}}{R} \right] - \left(\frac{\triangle H^{\#}}{R} \right). 1/T \qquad (2.27)$$

Hence, a plot of $\ln\left(k_2/T\right)$ $\ln\left(k_2/T\right)$ against $1/T$ $1/T$ is linear from which the slope gives the enthalpy of activation, $\Delta H^{\#}$ and the y-intercept provides the value of the activation entropy, $\Delta S^{\#}$. This plot is usually referred to as the *Eyring plot*.[6,16,24]

The important featuring arising out of the thermodynamic activation parameters are:

- The activation parameters are thermodynamic state functions.
- A fast reaction can have a higher enthalpy of activation ($\Delta H^{\#}$), if $\Delta S^{\#}$ is more positive to compensate.
- The activation entropy ($\Delta S^{\#}$) associated with k_2 for a second-order reaction is particularly large and negative, reflecting loss of entropy from the union of two reaction particles into a single transition-state in an associative reaction mechanism dominated by bond formation process; the $\Delta S^{\#}$ is usually large and positive for dissociative activated reactions.
- The values of $\Delta H^{\#}$ determined from the slope is more reliable than that of $\Delta S^{\#}$ that are subjected to large relative errors since the data is calculated from values extracted to infinite temperatures on the y-intercept.
- The uncertainty in $\Delta S^{\#}$ is approximately $1000/T$ $1000/T$ times that of $\Delta H^{\#}$, which amounts to a factor of 3. ($1000/T$, involves conversion from joule for $\Delta S^{\#}$ to kilojoules for $\Delta H^{\#}$).

2.3.5 Effect of Pressure on Rate Constant

A more reliable parameter in diagnosing reaction mechanisms is the activation volume, $\Delta V^{\#}$ since it is particularly less sensitive to temperature. Therefore comparison or contrast between values determined at different temperatures for different reactions can be monitored. The activation volume ($\Delta V^{\#}$) can be determined from a series of experiments in the observed rate constants, k_{obs} measured as a function of applied

pressure on a reaction mixture.[15,25] The rate of reaction becomes sensitive to pressure changes only under extremely vey high pressures 100-200 MPa.

Assuming there is no variation in T, the derivative of the thermodynamic equation for free energy is obtained as:

$$(\partial \Delta G^{\#}/dP)^{o}_{T} = \Delta V^{\#} \qquad (2.29)$$

Differentiating equation (2.29) with respect to pressure and recognizing that $\left\langle k_b \left(T/h\right)\right\rangle$ $(k_b(T/h)$ is independent of pressure gives

$$(\partial \ln K/\partial P)^{o}_{T} = (\partial(\Delta G^{\#}/RT)/\partial P)^{o}_{T} \qquad (2.30)$$

$$= -\Delta V^{\#}/RT \qquad (2.31)$$

Integration of equation (2.31) taking into consideration that the equilibrium constant is $K = k_2/k_{-2}$, results in:

$$\ln k_2 = \ln(k_{-2})_0 - \left(\Delta V^{\#}/RT\right)P \qquad (2.32)$$

where, $\Delta V^{\#}$ is the *volume of activation* for the forward step of the reaction and is the difference in molar volumes of the activated complex and the reactants under the experimental conditions; $(k_{-2})_0$ coefficient of compressibility of the solvent.

A plot of $\ln k_2$ against pressure (P) is linear, and $\Delta V^{\#}$ is calculated from the slope.

$\Delta V^{\#}$ takes values in the range $-20 \le x \ge 10$ ($cm^3\ mol^{-1}$)$-20 \le x \ge 10$, through zero, whereby:

i. $\Delta V^{\#}$ = -20 $cm^3\ mol^{-1}$ signifies electrostriction of the solvent due to the formation of ions in the transition-state.

ii. $\Delta V^{\#} \approx$ -10 $cm^3\ mol^{-1}$ is characteristic of an associative mechanism, in which the activated complex is dominated by the formation of M---Y bond and not by the dissociation of the M---X bond.

iii. $\Delta V^{\#} \approx 10$ cm^3 mol^{-1} features bond breaking in the dissociative mechanism. Since the volume of activation, $\Delta V^{\#}$, is obtained from the slope, it is more reliable than the entropy of activation, $\Delta S^{\#}$, which is an extrapolation of the *Eyring plot* as a y-intercept in determining the substitution reaction mechanism. A positive value indicates a dissociative mechanism, whereas a negative value indicates an associative mechanism.[15]

2.4 Instrumental Techniques Used in Chemical Kinetics

A kinetic study is usually accomplished by monitoring the dependence of time on some variable that is proportional to the concentration of the reactant or product.[26] A large proportion of the chemical reactions are investigated in solution. The appropriate technique used must fulfil the following criteria:[27]

- Bring the reactants together, mix them and initiate the reaction in the shortest time possible in comparison to the time scale of the reaction.
- Measure the physical property of the mixture that is proportional to the concentration of the reactants or product as a function of time after initiation.
- In some reactions, accurately measure and control temperature and the pressure at which the reaction proceeds.

Then the acquired data is processed using an appropriate kinetic model from which the rate constant can be determined. A number of techniques are available for monitoring chemical kinetics. These include infrared (IR), nuclear magnetic resonance (NMR), UV-Visible Spectrophotometry (UV-Vis) and pulse methods. A summary of the different reaction techniques employed in kinetic analysis are given in Figure 2.4.[28] The different chemical and physical processes that can be investigated, in a given time scale, are shown in the upper and the lower regions. In addition the corresponding techniques that can be used to study the kinetic behaviour and the years in which they became in use are provided. From Figure 2.4, the choice of the method depends on the nature and the rate of the reaction under investigation.

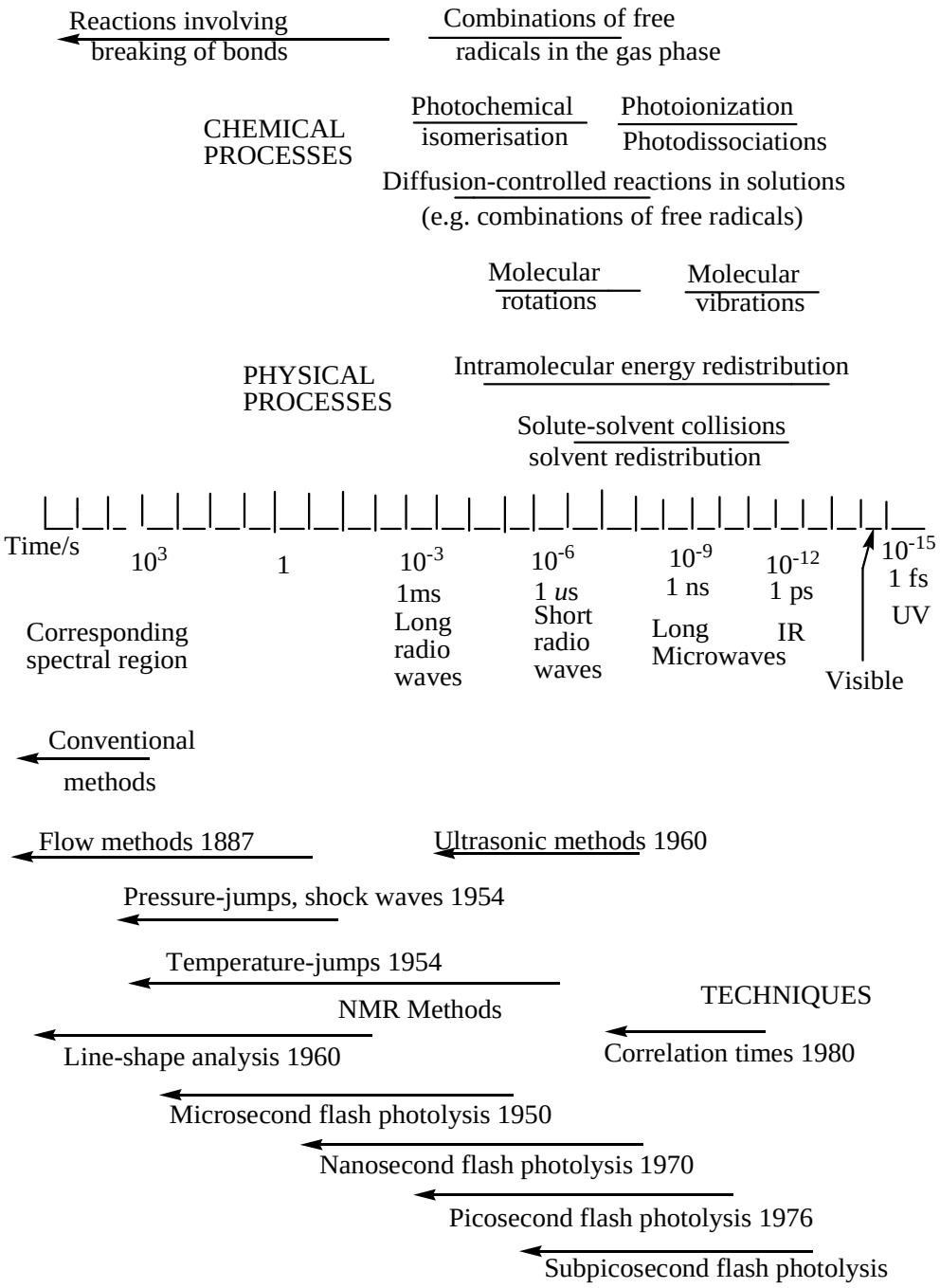

Figure 2.4: Summary of reaction techniques and their associated time scales available for the monitoring chemical kinetics.[28]

In the study of chemical reactions occurring at *conventional* rates, the reagents are first mixed and the decrease in the concentration of the reactant(s) or the increase in the concentration of the product(s) with respect to time is determined. Among the

conventional methods are classical methods such as volumetric and gravimetric techniques that are routinely applied in standardisation of new methods.

The other method is referred to as intermittent sampling where the samples are quenched immediately after they are withdrawn. This can be accomplished by addition of a chemical reagent, changing the pH or temperature of the reaction mixture to stop the reaction.[8] This method is useful for very slow reactions with a half-life in excess of several minutes. Therefore, Conventional techniques are inadequate for very fast reactions which take a very short period of time for the reaction to reach completion. Fast reactions are in the range of 1 minute to 10^{-14} seconds.[25] Such reactions require automated methods such as flow-through and pulse methods.[28,29] Examples of the flow current methods in use are UV-Vis Spectrophotometry and stopped-flow techniques and are further discussed below.

2.4.1 Flow Methods

For fast reactions, the period for mixing varies from 10^{-3} s to 10 seconds in the flow methods. As a result, reactions whose half-lives are about 10^{-2} seconds are normally studied by the flow methods, by the continuous flow or the stopped-flow method.[30]

In the continuous-flow method, first pioneered by Roughton and Hartridge[29], the two solutions (A &B) are forced into the mixing chamber-where the reaction is initiated-by use of pistons (Figure 2.5). The resultant mixture immediately flows out into the observation chamber, where at some distance (d) a steady-state is attained, allowing maximum spectroscopic detection. Since the reaction passes through a steady-state, the observation may be a slow process. The method is also wasteful since large amounts of solutions are required. These problems were solved by application of the stopped-flow technique (Figure 2.6).

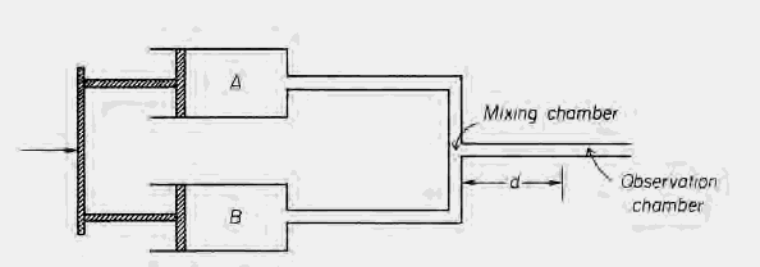

Figure 2.5: A schematic diagram of a continuous flow kinetic system. *d* = distance from the mixer to the point of observation.

In the stopped-flow method the two reagents (A &B) are rapidly mixed under pressure (800 kPa) into the reaction chamber (Mixing jet in Figure 2.6). The mixing takes about 10^{-3} s, then the solution is driven into the cuvette where the solution mixture is allowed to rest at a fixed time interval (rest period), when the stop syringe rests against its seat. During the rest period, the reactive species is monitored and detected spectrophotometrically. The reaction manifold is maintained at a pre-determined constant temperature during the reaction stage and at the injection point. Once the reactants impinge on each other in the observation chamber, the data acquisition system promptly records the absorbance-time resolved kinetic trace at a set wavelength. The kinetic traces are processed and the observed (*pseudo*) first-order rate constants evaluated by an online computer program.[16,28] A typical single exponential kinetic trace acquired on a stopped-flow reaction analyzer is shown in Figure 2.7.

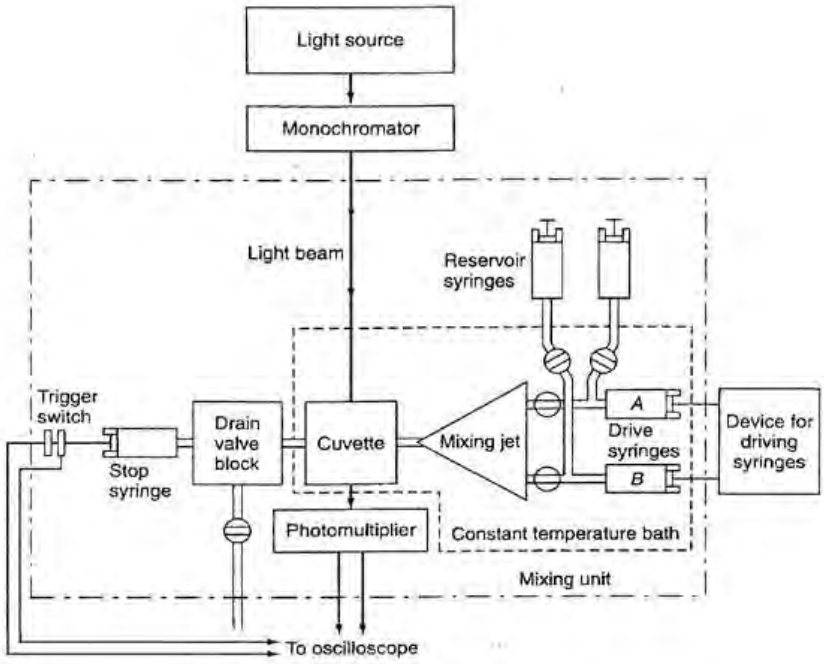

Figure 2.6: Schematic diagram of a stopped flow apparatus.[13]

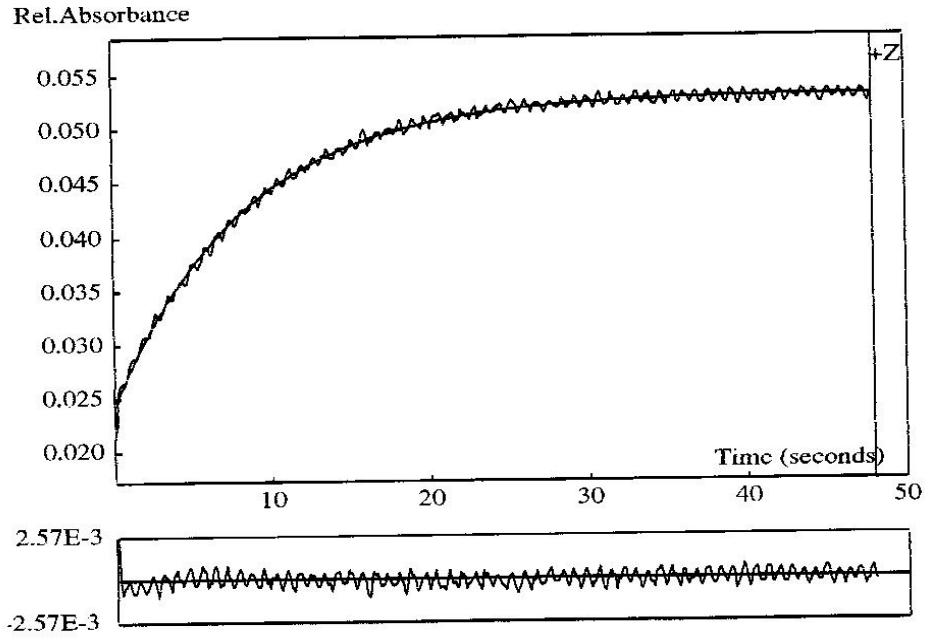

Figure 2.7: Kinetic trace at 448 nm for the substitution reaction between **CH_3PhisoqPtCl** (0.054 mM) and I^- (6.06 mM) at 298 K, I = 0.1 M $Li(SO_3CF_3)$ in methanol.

2.4.2 UV-Visible Spectrophotometry

UV-Visible Spectrophotometry is a sensitive technique which can detect the sample concentrations in the optimum range of 10^{-4} to 10^{-6} M.[31] The method is useful for detecting electronic transitions originating from highest occupied molecular orbital (HOMO) to the lowest unoccupied molecular orbital (LUMO) in compounds which have π-electrons or non-bonding electron pair upon absorption of light in the ultraviolet and visible regions. This results in absorption bands in the spectra by the UV-visible absorption spectrophotometer. A sketch diagram of the UV-Vis spectrophotometer is illustrated in Figure 2.8.

The instrument comprises of two sources of radiation spanning from the Visible (800-400 nm) and ultra-violet range (400-200 nm), reference and sample compartment, wavelength selector (monochromator), the detecting device, the output-readout system, and a temperature control unit. In order to acquire kinetic data, special tandem cuvettes (made of quartz or silica glass) are used for initiating the reaction.

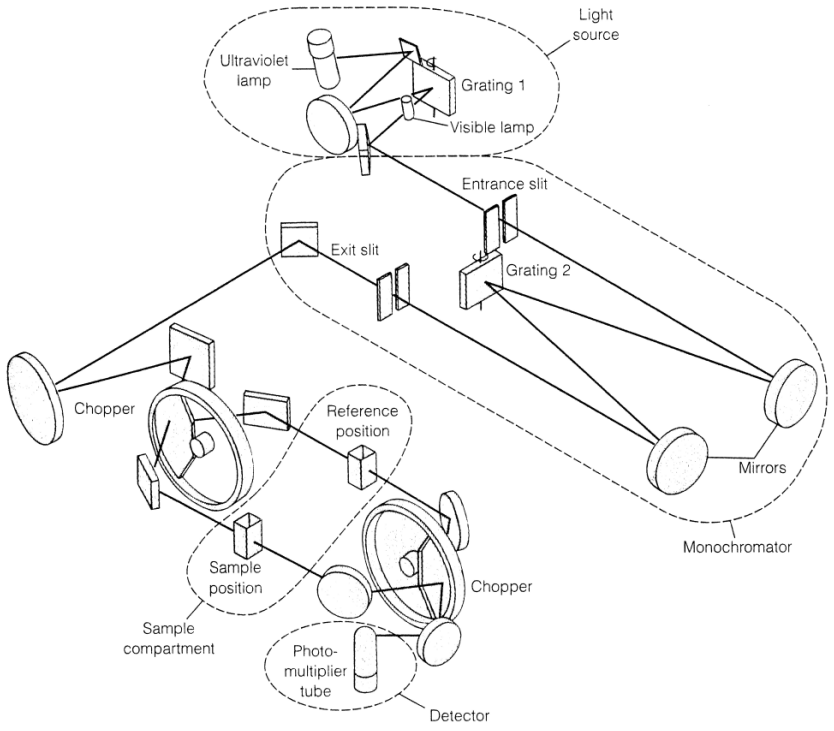

Figure 2.8: A schematic diagram of a UV-Visible Spectrophotometry set-up.[32]

The light transmitted from the sample can be represented as

$$T = \frac{I_0}{I} \tag{2.33}$$

Where I_0 = the intensity of the incident light obtained from the solvent reference cell

I = the intensity of the transmitted light from the power source after passing through the analyte cell

The absorbance can then be written as

$$A = -\log T \tag{2.34}$$

By measuring the absorbance of the reaction mixture at specific time intervals or in a continuous manner, the concentration-time-resolved spectrum of the system can be determined from the Beer's law (*Equation 2.35*).[30]

$$A = \varepsilon c l \tag{2.35}$$

where, A = absorbance

ε = molar absorptivity (L mol^{-1} cm^{-1})

c = Concentration (mol dm^{-3})

l = path length (cm)

UV-Visible absorption spectra usually contain broad absorptions that overlap with other species in the solution, which makes the analysis of the product more difficult. However, kinetic analysis can be done on overlapping absorption spectra.[6]

For a given first-order reaction,

$$X \xrightarrow{k_1} Y \tag{2.36}$$

At any time *t,* the absorption is then given by

$$A_t = \varepsilon_X [X] + \varepsilon_Y [Y] \tag{2.37}$$

where, A_t = the absorbance at any time, t

$\varepsilon_X, \varepsilon_Y$ = molar absorptivity of X and Y respectively

Once the reaction goes to completion, the absorption is given by

$$A_\infty = \varepsilon_X [X]_0 + \varepsilon_Y [Y]_0 \tag{2.38}$$

where A_∞ = absorbance upon completion of reaction

$[X]_0$ *and* $[Y]_0$ = initial concentration of X and Y respectively

For the kinetic analysis of *equation 2.35*, the absorbance can be obtained from *equation 2.39*

$$\ln\frac{[X]_o}{[X]_t} = \ln\left(\frac{A_o - A_\infty}{A_t - A_\infty}\right) = k_1 t \qquad (2.39)$$

Often, the absorbance-time resolved data is used directly to evaluate the observed rate constants using *Equation 2.39*. Apart from its use in monitoring the kinetics of conventionally slow reactions, the UV-visible absorption spectroscopy is also used to perform spectrophotometric titrations, especially in pK_a determinations. The pK_a values of the coordinated aqua ligand are important thermodynamic set of data used as indicator of the electrophilicity of the metal centre.[33]

2.5 Factors Affecting the Rate of Substitution

2.5.1 Effect of the Entering Group

In an associative substitution reaction mechanism, the second order-rate constant, k_2, is strongly dependent on the nucleophilicity of the entering nucleophile. Nucleophilicity is a measure of how readily the nucleophile is able to attack an electron-deficient atom, in this case Pt metal centre, in exclusion of the proton. That is the stronger the nucleophile the greater the rate of substitution reaction of a particular Pt(II) complex. It is derived from the second-order rate constant, k_2, for the substitution process.[5,15] The nucleophilicity of the ligand is usually influenced by several factors:[6,26, 34]

a. Basicity: Basicity of the entering nucleophile is characterised by its pK_a and correlates well with the nucleophilicity of the entering nucleophile towards the metal centre.

b. Polarisability: Polarisability of the nucleophile is an important consideration for the rates rather than for equilibria of chemical reactions.[35] An increase in [1†]polarisability reflects the effectiveness of the ligand as an electron donor.

[1]† The polarisability of a ligand is better explained by Pearson's "Hard Soft Acid Base" theory which states that hard acids, i.e. those metal ions that are small bear a high charge and possess a valence electron shell

c. Oxidizability: Ligands that are readily oxidized, i.e. strong reducing agents are good nucleophiles. The oxidizability of the ligands are characterised by their electrode reduction potentials.

d. Solvation Energy: Those ligands that are strongly solvated are considered weak nucleophiles because energy is required to free the nucleophile from the bonded solvent, before it can coordinate to the metal centre.

e. Metal Centre: Nucleophilicity depends much on the nature of the metal centre. Heavier elements are better polarised in the transition state. The corresponding rates of substitution follow the trend: Ni(II)>> Pd(II) >> Pt(II). This factor limits the application of the nucleophilicity scales in the Inorganic Chemistry as most are dependent on the nature of the metal centre.

Studies which were performed on complexes of Pt(II) established that the nucleophilic reactivity of different nucleophiles is of the order:[36]

R_3P > TU > I^- ~ SCN^- ~ N^{3-} > NO_2^- > Br^- > py > aniline ~ olefin ~NH_3 ~ Cl^- > H_2O > OH^- > F^-

However, it should be noted that the reactivity of the entering nucleophile is more of a function of its polarisability than its base strength. In protic solvents (hydrogen bond donors) the direct relationship between nucleophilicity and its pK_a is the inverse.[37] This results from the ion-dipole interactions between the solvent and the nucleophile. In aprotic solvents nucleophilicity remains directly related to basicity. The most comprehensive study on the relative reactivity and nucleophilicity was performed using *trans*-[$Pt(py)_2Cl_2$] in methanol at 30 ˚C (*Equation 2.40*)

---

that is not easily distorted, prefer hard bases, e.g. Li^+, Mg^{2+} and F^-. Similarly, soft acids, i.e. those metal ions that are large, bear a low charge and have a valence electron shell that is easily distorted or removed, prefer soft bases, e.g. Pt^{2+} and SCN^-.

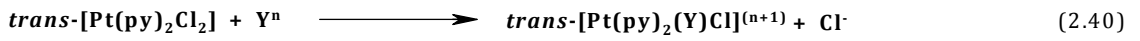

(2.40)

When *trans*-$[Pt(py)_2Cl_2]$ was used as the standard, the nucleophilicity constant of the incoming ligand, n°_{pt}, is defined as:[26,35]

$$\log\left(\frac{k_y}{k^o_s}\right) = n^o_{Pt} \qquad (2.41)$$

where, k_Y = the measured second-order rate constant for the reaction of the entering nucleophile, Y

k^o_S = the second-order rate constant for attack of the solvent (methanol) in an associative mechanism and is equal to $\{k_S/[MeOH]\}$

k_S = the rate constant for attack of the solvent, MeOH, on the complex.

At 30 °C, the concentration of pure methanol is assumed to be 24.3 M and the equation simplifies to:

$$n^o_{pt} = n_{pt} + 1.39 \qquad (2.42)$$

By definition the n^o_{pt} for methanol as the entering group is zero, while that for triphenylphosphine ligand, $\{(Ph)_3P\}$, is a high value of 8.99. The typical n^o_{pt} data obtained for *Equation 2.42* is summarised in Table 2.1 for different entering nucleophiles (Y).

Table 2.1: A selection of n^o_{pt} values listed according to donor atom,[18,38]

Nucleophile	n^o_{pt}	Nucleophile	n^o_{pt}
O-Donor		**S-Donor**	
CH_3O^-	< 2.4	$(CH_3)_3S$	4.87
N-Donor		SCN^-	5.75
NH_3	3.07	SO_3^{2-}	5.79
C_5H_5N	3.19	$(NH_2)_2CS$	7.17
NO^{2-}	3.22	**Selenium-Donor**	
$C_3H_3N_2$	3.44	$(CH_3)_2Se$	5.70
N_3^-	3.58	$SeCN^-$	7.11
NH_2NH_2	3.86	**Antimony-Donor**	
Halogens		Ph_3Sb	6.79
Cl^-	3.04	**C-Donor**	
Br^-	4.18	CN^-	7.14
I^-	5.46	**P-Donor**	
		Ph_3P	8.99

The nucleophilic reactivity constant provides a measure of the reactivity of a nucleophile towards Pt(II) metal centre. For many Pt(II) complexes, plots of $\log k_Y$ for given nucleophiles against n^o_{pt} values are linear as illustrated in Figure 2.9.[18]

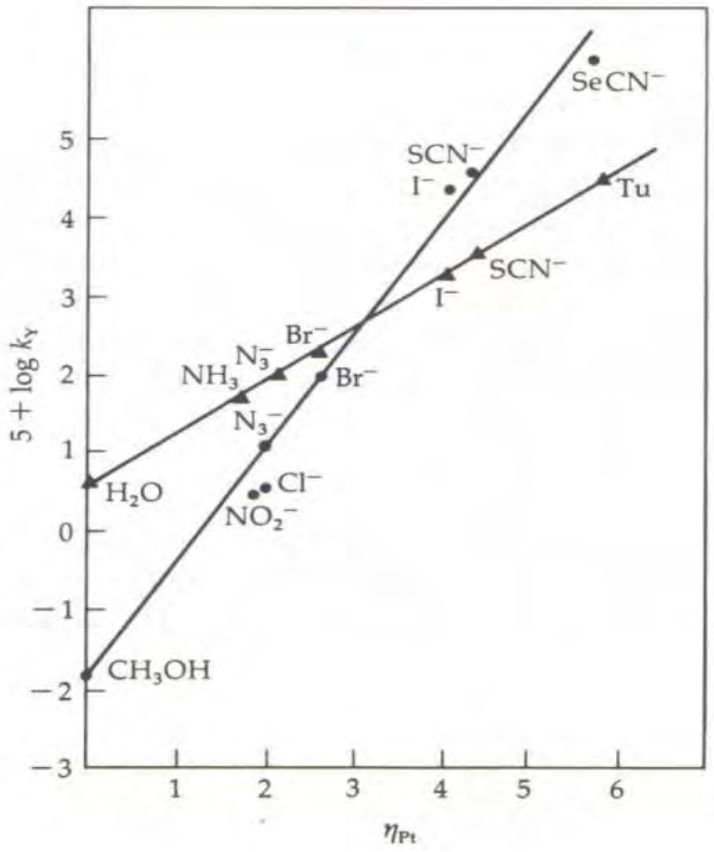

Figure 2.9: Rates of Pt(II) complexes correlated with *trans*-$[Pt(py)_2Cl_2]$ as reference, for different entering nucleophiles: • = trans-$[Pt(PEt_3)_2Cl_2]$ in methanol at 30 °C; ▲ = $[Pt(en)Cl_2]$ in water at 35 °C.[18]

The free energy linear relationship (LFER) obtained is given as:[18]

$$\log k_Y = S.\, n^o_{pt} + C \qquad (2.43)$$

where, *S* is the *nucleophilic discrimination factor* and depends on the complex.

C is the *intrinsic* reactivity.

The value of *S* reflects the electrophilicity and steric properties at the site of substitution felt by the entering nucleophiles. A value of *S* equal to 1 is given to the reference complex, *trans*-$[Pt(py)_2Cl_2]$.[15,26] Values of $S > 1$ show increased reactivity of a particular complex toward the range of nucleophiles used relative to reference complex. The intercept, *C*, estimates the reactivity of the weakest nucleophile at the metal site and its effect can be likened to that of a solvent. Since the complex is more discriminating in a

reaction with different nucleophiles a small intercept corresponds to a large S values.[18,26]

Another important factor that affects the rate of substitution on the square-planar geometry is the polarisability of the incoming nucleophile. In many substitution reactions high nucleophilicity constants are reported for polarisable ligands such as iodide and S-donor nucleophiles.[39] These are attributed to the large size and markedly diffuse valence orbitals of the Pt atom, which enables the metal ion to form stronger bonds with softer (easily polarisable) ligands. Thus, highly polarisable ligands substitute the leaving groups more rapidly at the Pt(II) centre.

It is now clear that the n^{o}_{pt} scale is more applicable to charged nucleophiles. This because charged nucleophiles have been observed to have a greater influence on reactivity as opposed to steric crowding which only has a minor effect.[17,40] In addition nucleophiles such as $SeCN^-$ and NO_2^{2-} deviate from LFER as seen in Figure 2.9. The plausible explanation put forward is that such entering groups with better π-acceptor ability would accelerate reactivity by lowering the energy of the transition state through metal to ligand π-interactions.[38] Hence the complex $[PtCl_4]^{2-}$ would be more reactive to these π-acceptor nucleophiles than $[Pt(dien)Br]^+$ that has a poor π-donating ability relative to the reference *trans*-$[Pt(py)_2Cl_2]$.[41]

2.5.2 Effect of the Leaving Group

The effect of the leaving group is of less importance in reactions following the associative mode of substitution. However, in order for one to investigate the effect of the leaving group the *cis* and the *trans* ligands should be the same.

The reaction below has been extensively studied.[42,43]

$$[Pt(dien)X]^{(2-n)} + py \longrightarrow [Pt(dien)py]^{2+} + X^{n-} \qquad (2.44)$$

The data for this reaction is shown in Table 2.2.

Table 2.2: The effect of the leaving group on the lability of $[Pt(dien)X]^+$

Leaving group (X)	k_{obs} (s^{-1})
NO_3^-	Very fast
H_2O	1900
Cl^-	35
Br^-	23
I^-	10
N_3^-	0.83
SCN^-	0.30
NO_2^{2-}	0.050
CN^-	0.017

This produces a leaving group dependence of the order:

$$NO_3^- > H_2O >> Cl^- > Br^- > I^- >> N_3^- > SCN^- > NO_2^{2-} > CN^-$$

In general it easier to substitute leaving groups which have a low nucleophilicity. For example the replacement of CN^- as the leaving group by Cl^- results in the reduction of the rate by a factor of 2×10^3. But when CN^- is the entering group, it is 10^4 times better than Cl^-.[18] Therefore for an associative mechanism, a substantial amount of metal-ligand bond breaking occurs in the transition state which depends on a specific reaction.[26,35]

2.5.3: Effect of Steric Hindrance

Steric effects are generally space-filling effects[37] and are categorised as, *steric bulky* and *steric hindrance*. Steric bulky is due to mutual repulsion of electron densities brought about by overcrowding of a group of atoms around the metal atom. The magnitude of resulting steric effect is proportional to the spatial size (i.e. a volume effect) of the substituent(s) that causes it. On the other hand, steric hindrance is the shielding of the

reaction site from direct attack by an incoming reagent. The magnitude of this type of steric effect depends on

(i) the spatial size or volume occupied,

(ii) relative spatial orientation or configuration of the substituent with respect to the target metal centre,

(iii) the position of the steric imposing substituents relative to the leaving group.[44]

Generally, the larger the entering groups the slower the reaction.

The transition state of an associated-type of mechanism is accompanied by an increase in the coordination number. This results from the bonding between the metal centre and the incoming ligand. It is expected that steric hindrance is increased in the transition state. This slows down the substitution process because the transition state is destabilized by the increased steric interactions. The retardation effect on the rate of substitution is more prominent if the steric effect imparting substituent is located in a *cis*-position relative to the leaving group rather than in the *trans*-position on a square-planar geometry.[15]

Example is the substitution of pyridine into a series of complexes of the form *cis*-/*trans*-$[Pt(PEt_3)_2(R)X]$ given in *Equation 2.45*. The data is summarised in Table 2.3.[15]

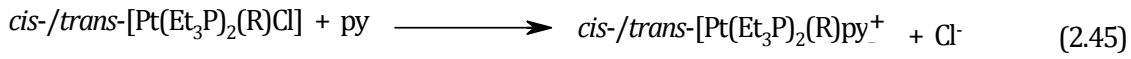

(2.45)

Table 2.3: Rate constants for the substitution of Cl^- in $[Pt(PEt_3)_2LCl]$ by pyridine.[15,44]

	k_{obs} (s^{-1})	
L—Pt	***cis* (0 °C)**	***trans* (25 °C)**
phenyl 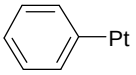	8.0×10^{-2}	1.2×10^{-4}
o-tolyl 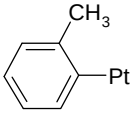	2.0×10^{-4}	1.7×10^{-5}
mesityl 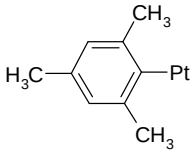	1.0×10^{-6} (25 °C)	3.4×10^{-6}

When the ligand L *cis* to the leaving group increases in bulk from phenyl to mesityl, the rate decreases by a factor of 1/80 000 while for the trans-isomer it drops by 1/35.[15,34,35] In the transition state of the *cis*-isomer the bulky group occupies an axial position as shown in Figure 2.10. This causes greater repulsions between its *ortho*-methyl groups, the leaving group and the incoming ligand. In the case of the trans-isomer the phenyl group lies in the equatorial position at an angle of 120°.[35] As a result, repulsions between the *ortho*-methyl groups, the leaving group and the incoming ligand are reduced. Thus, the corresponding reduction in rate of reaction is less affected.[34] It can then be concluded that steric hindrance from a substituent in the *cis*-position to the leaving group exerts higher effect on the rate of substitution than in the *trans*-position of d^8 square-planar geometry.

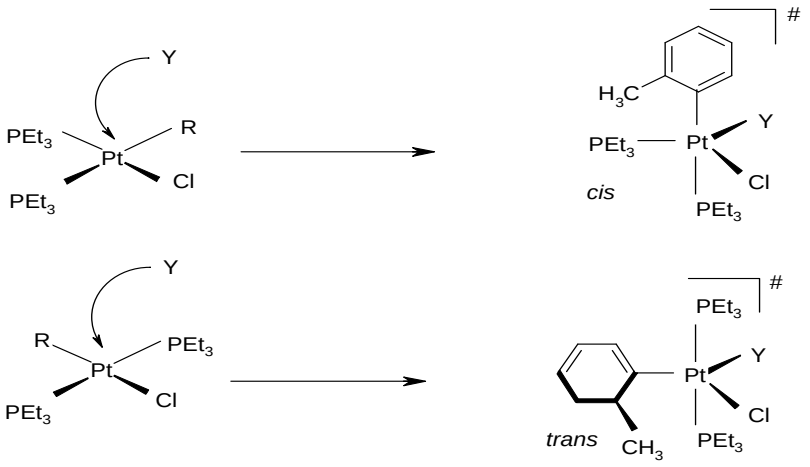

Figure 2.10: The steric effect on the trigonal bipyramidal intermediate of the *cis* isomer in comparison to *trans*-isomer.[34]

Another reason for the retardation of rate of substitution as the size of the ligand increases is the orientation. X-ray crystallography and molecular models show that the orientation of the aromatic ring of the R ligand lies perpendicular to the plane of the molecule. This causes the *o*-methyl substituents on the phenyl ring to lie above and below the plane of molecules effectively blocking the site of attack on the platinum metal centre (Figure 2.11).[6,26,35,]

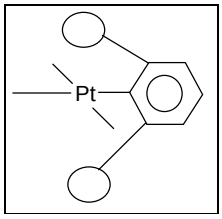

Figure 2.11: Geometry of an aryl square-planar complex showing the *ortho*-substituents block the site of attack.[6,26,35]

Steric effect also may cause mechanistic-changer over to a dissociative mechanism as a result of the favourable change from square-planar to a three-coordinate, T-shaped intermediate,[7] and is only more probable when two bulky groups occupy the cis position relative to leaving group.[34] This is dependent on the ground-state

destabilisation. It is suggested that if the ground-state effects are dominant relative to transition state, then an unusual acceleration in the rate of substitution occurs in order to relief the repulsive forces associated with a crowded metal centre. However, studies have shown that steric hindrance through introduction of methyl and ethyl substituents on the tridentate R_5dien chelate slows down the substitution rate of a series of $[Pd(R_5dien)Cl]^+$ complexes, spanning 5 orders of magnitude in comparison to the unhindered systems, without having any effect on the substitution mechanism (Table 2.4).

Table 2.4: Rate constants and activation parameters for the substitution of coordinated chloride by I^- in $[Pd(R_ndien)Cl]^+$ (n = 0, 3-5) in aqueous solution at 25 °C.[45]

R_5dien	k_1, s^{-1}	$\Delta H^{\neq}$, kJ mol^{-1}	$\Delta S^{\neq}$, J $K^{-1}mol^{-1}$	$\Delta V^{\neq}$, cm^3 mol^{-1}
dien	44	43	-69	-10.0
1,4,7-Et_3dien	10	41	-86	-10.8
1,1,7,7-Et_4dien	2.2×10^{-3}	66	-74	-14.9
1,1,4,7,7-me_5dien	0.28×10^{-4}	50	-88	-10.9
1,1,4,7,7-Et_5dien	7.2×10^{-4}	59	-106	-12.8

It is known that the large negative values of activation entropies and negative volumes of activation are indicative of associative mode of substitution mechanism. However, it is difficult to make a distinction between true steric effects and electronic influence of the alkyl substituents or a change in mechanism through the series. This is because at 80 °C $[Pd(R_5dien)Cl]^+$ complex was found to follow the dissociative mechanism.

2.5.4 Effect of Solvent

The solvent is the reaction medium and through solvation of the ground and the activated states it may influence the energy of activation process. The two-term rate law[15] (*Equation 2.13*) for the substitution reactions of d^8 square-planar complexes includes a term that is independent of the incoming nucleophile. This is ascribed to a parallel solvolysis pathway that involves direct participation of the solvent through

direct displacement of the leaving group (Scheme 2.2). The net effect is increase the rate of substitution with higher coordination ability of the solvent.

A prime example is the chloride exchange reaction with radio-labelled $^{36}Cl^-$:

$$\textit{trans}\text{-}[Pt(py)_2Cl_2] + {}^{36}Cl^- \longrightarrow \textit{trans}\text{-}[Pt(py)_2Cl(^{36}Cl)] + Cl^- \qquad (2.46)$$

The data for the reaction is given in Table 2 5.

Table 2.5: Effect of solvent on the rate of chloride exchange from *trans*-[Pt(*py*)$_2$Cl$_2$][46].

Coordinating solvents	$k_{-2}/(10^{-5}\ s^{-1})$	**Non-/weakly coordinating solvents**	$k_2/\ M^{-1}\ s^{-1}$
DMSO	380	CCl_4	10^4
H_2O	3.5	C_6H_6	10^2
EtOH	1.4	*i*-BuOH	10^{-1}
PrOH	0.4	Me_2CO	10^{-2}
		DMF	10^{-3}

The results show that in the presence of a highly coordinating solvent, the reaction proceeds predominantly through the solvolytic pathway, which is independent of the entering nucleophile. This means that k_{-2} value for the parallel solvolysis pathway is much greater than the second order-rate (k_2) of the product, $k_2[Cl^-]$. The rates also show a direct dependence on the nucleophilicity of the solvent in the order, ROH < H_2O ≈ CH_3NO_2 < DMSO. This is of great significance because it indicates that Pt-solvent bond-making is an important process in the transition state compared to bond-breaking. For instance, if the role of the solvent was to solvate the Cl^-, then H_2O instead of DMSO should be the more efficient solvent. It is known that DMSO is a better nucleophile towards Pt(II) centre than H_2O as Pt(II) forms stable complexes with a Pt–S bond in DMSO.[47] The rate of exchange is therefore faster in dimethylsulphoxide than in H_2O as shown in Table 2.5.

In poor coordinating solvents such as tetrachloromethane, benzene and the sterically hindered alcohols, the reaction occurs only by the attack of the entering nucleophile on

the complex, where $k_{2(Cl)}[^{36}Cl^-] > k_{-2}$. As a result larger rates occur in nonpolar solvents like tetrachloromethane, where the Cl^- would not be solvated compared to polar solvents such as dimethylformamide (DMF).

2.5.5 Effect of Non-participating Groups

2.5.5.1 *cis*-and *trans*-Effects of Platinum(II) Complexes

The effect that a ligand has on another in the *cis* and *trans* positions is referred to as the *cis*- and *trans*-effects, respectively. Chernayev and colleagues[48] introduced these studies while they investigated square-planar platinum (II) complexes. Both the *trans*- and *cis*-carrier ligands affect the rate of substitution at the metal centre, but in different ways.[15] The effect on the reactivity is more pronounced from non-labile ligands that are in *trans*-position to the leaving group than it does on the ligand that is in the *cis*-position.[19,26]

2.5.2.2 The *Trans*-effect

The *trans-effect* is best defined as the effect of a coordinated ligand upon the rate of substitution of ligands opposite to it; or is the ability of a ligand in a square planar complex to direct the replacement of the ligand *trans* to it.[8,35] From extensive investigations performed on the effect of the ligand on substitution reactivity at a Pt(II) centre, using many different nucleophiles, the trans-effect in increasing order of power is :[6,8,49]

$CO \sim C_2H_4 \sim CN^- > R_3P \sim H^- > CH_3^- \, C_6H_5^- > I^- > SR_2 > SC(NH_2)_2 > SO_3^{2-} > NO_2^{2-} \sim N_3^- < SCN^- \sim Br^- > Cl^- > py > RNH_2 \sim NH_3 > OH^- > H_2O.$

This sequence covers the rate effects in the range 10^6 to 10^{11}-fold increase on the lability of the complex when a strong trans-labilizing ligand is present.[50,51] Since the *trans-effect* is a kinetic phenomenon, its origin lies in reactant destabilisation and /or in the transition state stabilisation. In order to have a better insight of the *trans-effect* series and acceleration of the rate of substitution, its effect at the ground state and the transition state levels should be considered. For instance, a stabilisation of the transition state may reduce the activation energy barrier or a destabilisation of the ground state would increase the rate. A ligand high up in the *trans-effect* series may

therefore, weaken the bond of the ligand that is *trans* to it or stabilise the transition state or simply affect both the transition state and the ground state.[7,26]

Closely related to, but characteristically distinct from the *trans-effect* is the *trans-influence*. This is defined as the influence of a coordinated ligand on the strength of the metal-ligand bond *trans* to itself. The *trans-influence* is an equilibrium phenomenon that affects the ground state properties of the metal complexes.[5,15] The *trans*-effect is purely a kinetic factor, which affects the relative stabilities of both the ground and the activated transition states of the reactants during substitution reactions. As illustrated in *Scheme 2.3*, an increase in rate of reaction is due to either a ground state destabilisation (increase in energy) or a transition state stabilisation (decrease in energy).

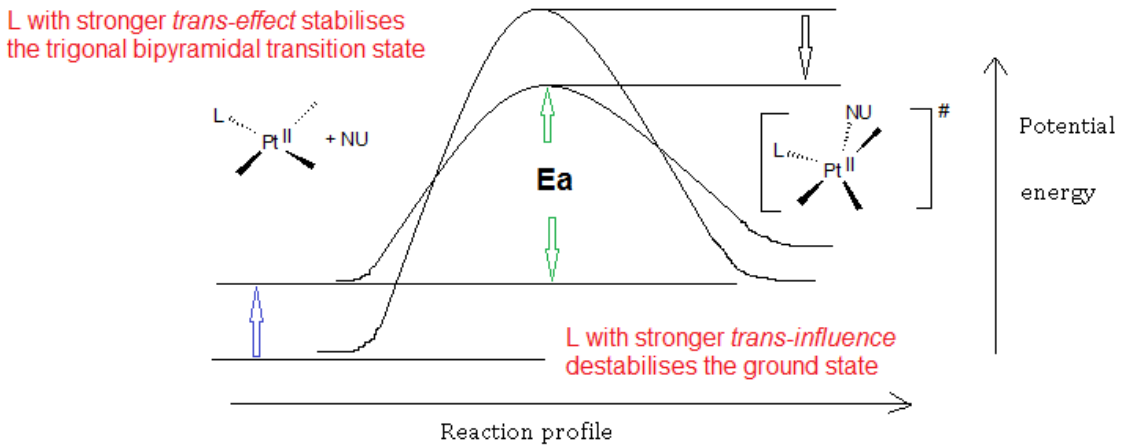

Scheme 2.3: Sketch diagram showing the effect of *trans* ligand on energies of ground state and transition state of a square-planar Pt(II) complex.

The *trans-influence* is measurable in ground state properties such as Pt-*trans* ligand bond elongation (obtained from X-ray structural data) and force constants (obtained from infra red (IR) frequencies) and changes in chemical shifts (observed in nuclear magnetic resonance (NMR) spectra). The frequency of the M–X bond drops as X (the leaving group) becomes more polarisable.[52] Which shows that the negative charge donated from the *trans* ligand to the metal atom through the σ-bond is the dominant contribution to the *trans- influence* (Scheme 2.4). Such a ligand usually has a large σ-

inductive donor capacity and weak π-acceptor ability. Hence, the stronger the *trans-influence*, the weaker is the bond.[53] The weakening of the M–X bond accelerates rates of substitution at the square-planar Pt(II) centre.[54]

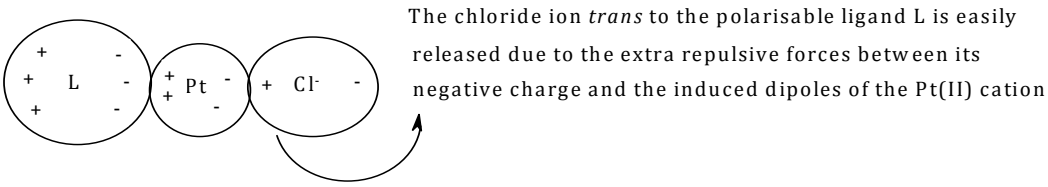

Scheme 2.4: Distribution of charge in induced dipoles in the L–Pt–Cl coordinate of *trans*-[PtA_2LX][35] due to polarisation (where L = non-leaving *trans* ligand, X = leaving group *e.g*. Cl^-).

Therefore, ligands with stronger *trans influence* weaken the bond between Pt and the *trans* ligand to be displaced and increase the energy of ground state accordingly (*polarisation theory* by Griberg).[55]

In the Pt(II) complexes both the σ-donor and π-acceptor capacities are involved in the *trans-effect as* illustrated in *Figure 2.12.* A ligand which exhibits a strong *trans-effect* is either a good σ-donor, e.g. H^-, CH_3^- (Figure 2.12) (a) or a good π-acceptor such as C_2H_4 (Figure 2.12 (b)) or has both σ-donor and π-acceptor properties like CN^- and CO.

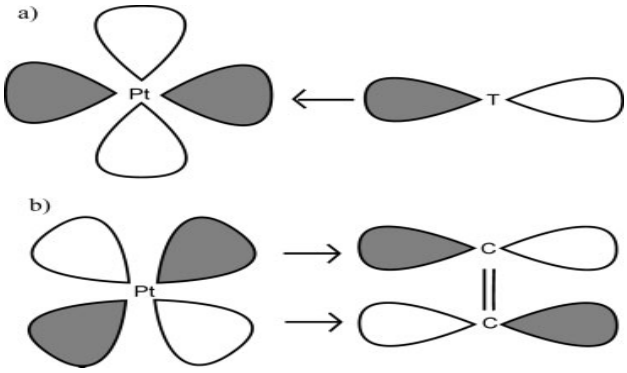

Figure 2.12: (a) σ-donation from the filled ligand p_x orbital to vacant metal $5d_{x^2-y^2}$ orbital. (b) π-back-donation from the filled metal d_{xz} orbital to the antibonding linear combination of carbons' p_x orbitals in C_2H_4.[49]

σ-Donation

According to classical explanation, the *trans*-effect causes electrostatic destabilisation of the ligand in the *trans* position and it is observable in the Pt–*trans* ligand bond length elongation through σ-donation. The *trans* ligand T and the leaving group (X) both share the metal dsp^2 orbital in the ground stat (Scheme 2.5).

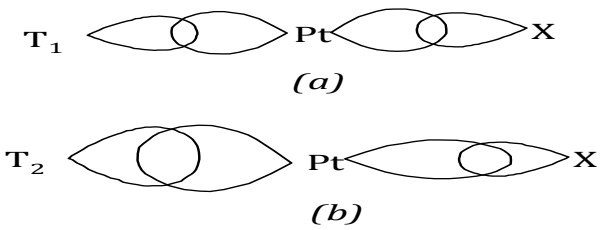

Scheme 2.5: A schematic diagram showing the difference in the Pt–X bond strengths for a (a) weak and (b) strong σ-donor ligand T_1 and T_2, respectively. In (b) the strong *trans* σ-donor weakens the bond to the *trans* ligand (Pt–X).

The stronger of the two contributes more electron density towards the shared orbital. If the *trans* ligand (T) is the stronger σ-donor, the Pt–T bond shortens while that of Pt–X is elongated and weakened as a result of less electron density being availed to this bond. Hence, in the normal *trans*-effect one bond shortens while the other lengthens. Bond cleavage of the weakened bond (Pt–X), *trans* to strong σ-donors occurs very fast during substitution reactions and as a result reduces the significance of nucleophilicity of the incoming ligand.

π-back-donation or the π-Acceptor Effect

Ligands such as CO and C_2H_4 stabilise the complex also by π-back-donation. It is the interaction of filled $5d_{xz}$ or $5d_{xy}$ orbital of the Pt metal (suppose the trans ligand lies on the x or y-axis) with empty $\pi(p_x)$ or $\pi(p_y)$ orbital of the ligand. Hence, π-back-donation increases the positive charge of the Pt(II) atom by a decrease of electron density in the *xz* or *xy* plane. This facilitates nucleophilic attack in the *xz* or *xy* plane and stabilises the corresponding five-coordinate transition state relative to the ground state by withdrawing the π-electron density of the metal into its own empty π*-orbitals as

shown in Figure 2.12 (b).The overall activation energy needed for substitution is reduced while the ground state energy remains unaffected.[56] Thus, the net effect of a strong π-acceptor ligand occupying a *trans*-position is to stabilise the trigonal-bipyramidal transition state by lowering the activation energy. This enhances the addition of the incoming ligand resulting in a rapid substitution reaction. The overall effect is called the *trans-effect.*

Recent studies have reported that systematic variation of the π-acceptor effect of different ligands, substantially enhances reactivity of Pt(II) complexes.[33,57,58] A comparison of NBO charges[49] of *cis*- and *trans*-isomers of $[Pt(NH_3)_2(C_2H_4)_2]^{2+}$ shows that a higher positive charge on the platinum atom is in the *cis*-isomer[33(b)] since two orbitals ($5d_{xz}$ and $5d_{yz}$) are involved in π-backbonding. Only one ($5d_{xz}$) orbital is available for the two π-back-donating ligands in the *trans*-isomer. It is clear changes in σ-donor, π-acceptor and steric properties of the cis ligand have opposite effects on reactivity of a complex. Until very recently,[33,59,60] studies on the effect of the σ-donor and π-acceptor properties of the *cis* ligand had not been separately investigated. In one of the studies, a replacement of the outer pyridyl unit by a phenyl group (a strong σ-donor) in the *cis* position of $[Pt(N\text{-}N\text{-}N)Cl]^+$ complex, where N-N-N is a terpyridine ligand, led to a reduction in reactivity of the complex by a factor of about 16 when thiourea (TU) was the incoming ligand.[60]

Whilst an extensive review of the current research is impossible to present here, efforts are being directed at developing a detailed understanding of the substitution behaviour of mono-, di- and trinuclear platinum-based anticancer drugs. In particular understanding the role of σ-donicity and π-acceptor properties of polydentated mononuclear Pt(II) complexes and the structural complexity of the bridging ligand in controlling reactivity at the Pt(II) metal centres constitutes a major challenge. The details of the objectives are given in Chapter one.

References

1 (a) J. Reedijk, *Chem. Rev*., 1999, **99**, 2499; (b) J. Reedijk, *PNAS*., 2003, **100**, 3611; (c) J. Reedijk, *Eur. J. Inorg. Chem.,* 2009*,* 1303

2 N. De Barrios, G. González, A. Grandas, M. Martinez and V. Moreno, *Inorganic Reaction Mechanisms*, 1999, **1**, 205.

3 G. Wilkinson, *Comprehensive coordination chemistry, Late Transition Elements*, Vol.**5**, Pergamon Press, Oxford, 1987.

4 C. W. Schwietert and J. P. McCue, *Coord. Chem. Rev*., 1990, **184**, 67.

5 C. H. Langford and H. B. Gray, *Ligand Substitution Processes*, Benjamin, New York, 1965.

6 S. Ašperger, *Chemical Kinetics and Inorganic Reaction Mechanisms*, 2nd Ed., Kluwer Academic/Plenum Publisher, New York, 2003, p. 38-39,105- 106, 140-153.

7 R. A. Henderson, *The Mechanisms of Reactions at Transition Metal Sites*, Oxford University Press, Oxford, 1993, p. 1-22.

8 R. G. Wilkins, *Kinetics and Mechanisms of Reactions of Transition Metal Complexes*, 2nd Ed., VCH, Weinheim, 1991, p. 199- 201, 232- 237.

9 M. J. Cleare and J. D. Hoeschele, *Plat. Met.Rev*., 1973, **17**,3.

10 M. J. Cleare and J. D. Hoeschele, *Bioinorg. Chem*., 1973, **2**, 187.

11 X. Wang and Z. Guo, *Dalton Trans.,* 2008, 5121.

12 X. L. Gao, X. Y. Wang, J. Ding, L. P. Lin, Y. Z. Li and Z. J. Guo, *Inorg. Chem. Commun*., 2006, **9**, 722.

13 D. Kovala-Demertzi, P. N. Yadav, M. A. Demertzis and M. Coliccia, *J. Inorg. Biochem*., 2000, **78**, 347.

14 Y. Chen, Z. Guo, S. Parsons and P. J. Sadler, *Chem. Eur. J.* 1998, **4**, 672.

15 M. L. Tobe and J. Burgess, *Inorganic Reaction Mechanisms*, Addison Wesley, Longman, Ltd., Essex, 1999, pp. 30-33; 70-112.

16 K. A. Connors, *Chemical Kinetics*: *The Study of Reaction Rates in Solution*, Wiley-VCH, New York, 1990, pp.1-22, 57-68, 177-180.

17 D. Banerjea, F. Basolo and R. G. pearson, *J. Am. Chem. Soc*., 1957, **79**, 4055.

18 U. Belluco, L. Cattallini, F. Basolo, R. G. Pearson and A. Turrco, *J. Am. Che. Soc*., 1965, **87**, 241.

19 L. Cattallini, *Prog. Inorg. Chem*., 1970, **13**, 263.

20 S. Lanza, D. Minniti, P. Moore, J. Sachinidis, R. Romeo and M. L. Tobe, *Inorg. Chem*., 1984, **23**, 4428.

21 S. Lanza, D. Minniti, P. Moore, J. Sachinidis, R. Romeo and M. L. Tobe, J. Chem. Soc. Chem Commun., 1984, 542.

22 R. Romeo, A. Grassi and L. M. Scolaro, *Inorg. Chem*., 1992, **31**, 4383.

23 M. LR. Plutino, L. M. Scolaro, R. Romeo and A. Grassi, *Inorg. Chem.,* 2000, **39**, 2712.

24 S. R. Logan, *Fundamentals of Chemical Kinetics*, Longman, Essex, 1996, p. 1-27.

25 J. H. Espenson, Chemical Kinetics and Reaction Mechanisms, 2nd Ed., McGraw-Hill, New York, 19977, p. 11-86,252-255.

26 J. D. Atwood, *Inorganic and Organometallic Reaction Mechanisms*, 2nd Ed., Wiley-VCH, New York, 1997, p 749-771.

27 M. J. Pilling, and P. W. Seakins, *Reaction Kinetics*, Oxford Science Publications, Oxford, 1995, pp 25, 38-39.

28 K. J. Laidler, J. H. Meiser and B. C. Sanctuary, *Physical Chemistry*, 4th Ed., Houghton Mifflin Company, New York, 2003, pp 374-379, 390-393.

29 (a) H. Hartridge and F. J. W. Roughton, *Proc. R. Soc*., London, 1923, A**104**, 376; (b) J. W. Moore and R. G. Pearson, *Kinetics and Mechanism*, 3rd *Ed.*, John Wiley & Sons, New York, 1981, 12-36.

30 D. A. Skoog, A. M. West, F. J. Holler and S. R. Crouch, *Fundamentals of Analytical Chemistry*, 8th Ed., Thomson Brooks/Cole, Canada, 2002, p. 374-379, 720, 769-7.

31 D. Reddy, *PhD Thesis, Tuning the Reactivity of Platinum(II) Complexes*, University of Natal, Pietermaritzburg, South Africa, 2009, pp. 88, 90.

32 D. C. Harris, *Quantitative Chemical Analysis*, 4th Ed., W. H. Freeman and Company, New York, 1995, p 480.

33 (a) D. Jaganyi, A. Hofmann and R. van Eldik, *Angew. Chem. Int. Ed.,* 2001, **40**, 1680; (b) A. Hofmann, D. Jaganyi, O. Q. Munro, G. Liehr and R. van Eldik, *Inorg. Chem.*, 2003, **42**, 1688.

34 R. B. Jordan, *Reaction Mechanisms of Inorganic and Organometallic Systems*, Oxford university Press Inc., New York,1991, p 29, 30,53-54, 60.

35 F. Basolo and R. G. Pearson, *Mechanisms of Inorganic Reactions*, 2nd, Ed., WileyNew York,1967, p 1, 351-356, 369-400.

36 (a) R. G. Pearson, *J. Chem. Edu*., 1987, **64**, 561; (b) R. G. Pearson, *Inorg. Chem*., 1988, **27**, 734.

37 P. Y. Bruice, *Organic Chemistry*, 2nd *Ed*., Prentice Hall, 1998, pp. 363-366.

38 R. G. Pearson, H. Sobel, and J. Songstad, *J. Am. Chem. Soc.,* 1968, **90**, 319.

39 K. F. Purcell, I. Kotz, *Inorganic Chemistry*, Holt-Saunders, 1977, pp. 694-755.

40 H. Kruger and R. van Eldik, *J. Chem Soc., Chem. Commun*., 1990, 330.

41 L. Cattallini, A. Orio and M. Nicolini, *J. Am. Chem. Soc.*, 1966, **88**, 5734.

42 F. Basolo, H. B. Gray and R.G. Pearson, J. Am. Chem. Soc., 1960, **82**, 4200.

43 H. G. B. Gray and R. J. Olcott, *Inorg. Chem*., 1662, **1**, 481.

44 (a) F. Basolo, J. Chatt, H. B. Gray, R. G. Pearson and B. L. Shaw, *J. Chem. Soc.*, 1961, 2207; (b) G. Faroare, V. Ricevuto, R. Romeo and M. Trozzi, *J. Chem. Soc. (A)*, 1971, 1877; (c) R. Romeo, M. L. Tobe and M. Trozzi, *Inorg. Chim. Acta.*, 1974, **11**, 231; (d) R. Romeo, D. Minniti and M. Trozzi, *Inorg. Chim. Acta.*, 975, **14**, L15; (e) R. Romeo, D. Minniti and M. Trozzi, *Inorg. Chem.*, 1976, **15**, 1134. (f) R. Romeo, *Inorg. Chem.*, 1978, **17**, 2040; (g) R. van Eldik, D. A. Palmer and H. Kelm, *Inorg. Chem.*, 1978, **18**, 572.

45 (a)M. Kotowski and R. van Eldik, *Inorg. Chem.,* 1984, **23**, 3310; (b) J. B. Goddard and F. Basolo, *Inorg. Chem.*, 1968, **7**, 2456; (c) M. Kotowski and R. van Eldik, *Inorg. Chem.*, 1986, **25**, 3896; (d) J. J. Pienaar, M. Kotowski and R. van Eldik, *Inorg. Chem.*, 1989, **28**, 373; (e) J. Berger, M. Kotowski, R. van Eldik, U. Frey, L. Helm and A. E. Merbach, *Inorg. Chem.*, 1989, **28**, 3759.

46 R. G. Pearson, H. B. Gray and F. Basolo, *J. Am. Chem. Soc.*, 1960, **82**, 787.

47 F. A. Cotton and R. Francis, *J. Am. Chem. Soc*., 1960, **82**, 2986.

48 I. I. Chernayev, *Ann. Inst. Platine USSR,* 1926, **1**, (4), 243; 1927, **1**, (5), 118, cited in therein.

49 Z. Chval, M. Sip and J. V. Burda, *J. Comput. Chem*., 2008, **29**, 2370

50 S. Otto and L. I. Elding, *J. Chem. Soc., Dalton Trans*., 2002, 2354.

51 O. F .Wendt and L. I. Elding, *J. Chem. Soc., Dalton Trans*., 1997, 4725.

52 (a) A. Grinberg, *Acta Physicochim*. *SSSR*, 1935, **3**, 573; (b) A. A. Grinberg, *Ann. Inst. Platine* SSSR, 1927, **5**, 109.

53 (a) A. Pidcock, R. E. Richards and L. M. Venanzi, *J. Chem. Soc. (A)*, 1966, 1707; (b) T. G. Appleton, H. C. Clark and L. E. Manzer, *Coord. Chem. Rev.,* 1973, **10**, 335.

54 D. S. Gill, In *Platinum Coordination Complexes in Cancer Chemotherapy*, M. P. Hacker, E. B. Douple, I. H. Krakoff *Eds*., Martinus Nijhoff Publishing, Boston MA, 1984, 267.

55 (a) A. Grinberg, *Acta Physicochim*. *SSSR*, 1935, **3**, 573; (b) A. A. Grinberg, *Ann. Inst. Platine* SSSR, 1927, **5**, 109.

56 D. R. Armstrong, R. Fortune and P. G. Perkins, *Inorg. Chim. Acta*., 1974, **9**, 9.

57 B. Pitteri, G. Marangoni, L. Cattallini, F. Viseutin, V. Bertelasi and P. Villi, *Polyhedron*, 2001, **20**, 41.

58 B. Petrovic, Ž. D. Bugarčić, A. Dees, I. Ivanović-Burmazović, F. W. Heinemann, R. Puchta, S. N.Steinmann, C. Corminboeuf and R. van Eldi, *Inorg. Chem*., 2012, **51**, 1516.

59 A. Hofmann, L. Dahlenburg and R. van Eldik, *Inorg. Chem*., 2003, **42**, 6528.

60 D. Jaganyi, D. Reddy, J. A. Gertenbach, A. Hofmann and R. van Eldik, *Dalton Trans*., 2004, 299

Table of Contents-3

.

List of figures

List of Tables

Chapter 3

The π-Acceptor Effect in the Substitution Reactions of Tridentate *N*-Donor Ligand Complexes of Platinum(II): A Detailed Kinetic and Mechanistic study

3.0 Abstract

The nucleophilic substitution reactions of the complexes of [Pt{4'-(2'''-CH_3-phenyl)-2,2':6',2''-terpyridine}Cl]CF_3SO_3,**CH_3PhPtCl**,[Pt{4'-(2'''-CH_3-phenyl)-6-(3''-isoquinoyl)-2,2'-bipyridine}Cl]SbF6, CH_3PhisoqPtCl,[Pt{2-(2'-pyridyl)-1,10-phenanthroline}Cl]Cl, **pyPhenPtCl**, and [Pt(terpy)Cl]$^+$, **PtCl** with a series of nucleophiles, *viz.*: thiourea (TU), *N*,*N*-dimethylthiourea (DMTU), *N*,*N*,*N*,*N*-tetramethylthiourea (TMTU), I^-, Br^-, and SCN^- in 0.1 M $LiCF_3SO_3$ in methanol, have been studied. The order of reactivity of the complexes under investigation was found to decrease as follows **pyPhenPtCl** > **PtCl** > **CH_3PhPtCl** > **CH_3PhisoqPtCl**. The lability of the chloride of the starting complexes is dependent on the strength of π-backbonding of the spectator ligands around the platinum centre. This effect is controlled by how the fused ring system around the terpy moiety is structured. The experimental data is strongly supported by the DFT-calculations. The dependence of the second order rate constants on concentration of the nucleophiles and the large and negative values of the activation entropies ($\Delta S^{\neq}$) support an associative mode of activation for the substitution of the chloride ligand.

3.1 Introduction

Since the discovery of anticancer activity of *cis*-$Pt(NH_3)_2Cl_2$ (cisplatin) by Rosenberg *et al*.,[1] many new Pt(II) complexes have been developed with the aim of obtaining better antitumor activity, increased solubility and reduced toxicity.[2] This list includes complexes of Pt(II) with 2,2':6',2''-terpyridine (terpy) or related polypyridine ligands that have widely recognised spectrochemical interaction with DNA and proteins.[3-5] These Pt(II) terpy complexes have been found to be cytotoxic against *Trypanosoma* and

Leishmania parasites in addition to human ovarian carcinoma.[6] However, interactions of Pt species with sulphur-donor ligands have been associated with negative phenomena such as renal toxicity, neurotoxicity and other side effects limiting their widespread clinical use.[7] Therefore, establishing appropriate properties of the Pt(II) complexes that may satisfy the criteria as potential medicinal agents has attracted considerable attention. This search includes the need to understand the kinetics of the interactions of these compounds with biological sulphur-donor nucleophiles.

The monofunctional $[Pt(terpy)Cl]^+$ and related compounds are good models for studying ligand substitution in square-planar d^8 complexes because only the fourth coordinated ligand is labile. The tridentate terpy ligand is stable due to the "chelate effect" and aromatic stability. The role of the π-backbonding in substitution reactions has been shown to enhance the reactivity, for instance, chloride substitution in $[Pt(terpy)Cl]^+$ in methanol is 10^2 to 10^4 times faster than for the cation $[Pt(dien)Cl]^+$ having saturated diethylenetriamine (dien) ligand as the chelating ligand.[8-10] The reactivity difference has been attributed to delocalisation of the π-system in the terpy ligand, which stabilises the five-coordinate transition state relative to the ground state by accepting electron density from platinum 5*d* orbitals into the π* molecular orbitals of the terpy ligand.[11,12] In a related study,[13] addition of electron-donating groups on the ancillary positions of the terpy ligand has been shown to retard the rate of substitution of chloride ligand. The opposite is true for electron-withdrawing groups.[13-15]

Limited information relating to the factors that influence the activity of these compounds such as the role of extended π-conjugation has been reported.[16,17] A systematic investigation involving the variation of the position of pyridine or amine donors in the *cis* and *trans* positions of complexes of the type $[PtL(OH_2)]^{+2}$ where L = tridentate ligand, has been documented.[16,18]The rates of substitution were shown to increase in a stepwise manner by addition of π-acceptor ligands. The results also indicated that the *cis* π-acceptors are superior to the *trans π*-acceptors in enhancing the rate of ligand substitution.

In order to extend our understanding on the role of the π-backbonding beyond the first pyridine ring surrounding the Pt(II) centre, we have investigated substitution reactions of complexes of the type $[Pt(N\text{-}N\text{-}N)Cl]^+$, (N-N-N = terpy; 4'-(2'''-CH_3-phenyl)terpy; 4'-(2'''-CH_3-phenyl)-6-(3''-isoquinoyl)-2,2'-bipyridine and 2-(2'-pyridyl)-1,10-phenanthroline), with three neutral sulphur nucleophiles (TU, DMTU, and TMTU) and three anionic nucleophiles (I^-, Br^-, and SCN^-). The structures of the investigated complexes are shown in *Scheme* 3.1.

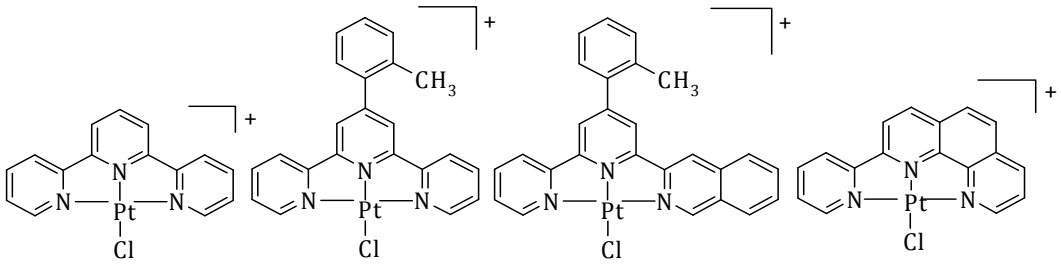

Scheme 3.1: Stuctures of the investigated Pt(II) polypyridyl complexes

3.2 Experimental

3.2.1 Materials and Procedures

Methanol (Saarchem) was purchased from Merck and used after purification and drying over magnesium. Lithium trifluoromethanesulfonate (96%) and the nucleophiles: §thiourea (TU, 99%), *N*,*N*-dimethyl-2-thiourea (DMTU, 99%), *N*,*N*,*N*,*N*-tetramethyl-2-thiourea (TMTU, 98%), sodium bromide (99%) and sodium thiocyanide (98%) were obtained from Aldrich and was used as supplied. Sodium iodide (NaI, 99%, Saarchem) was obtained from Merck and used as supplied. The platinum complexes, [Pt{4'-(2'''-CH_3-phenyl)-2,2':6',2''-terpyridine}Cl]CF_3SO_3 **CH_3PhPtCl** and [Pt{4'-(2'''-CH_3-phenyl)-6-(3''-isoquinoyl)-2,2'-bipyridine}Cl]SbF_6 **CH_3PhisoqPtCl** were synthesised and characterised using literature methods.[18,19] Details of the synthesis and characterisation of CH_3PhPtCl and CH_3PhisoqPtCl have been reported previously by Field[19] and our group.[20] The complex, [Pt{2-(2'-pyridyl)-1,10-phenanthroline}Cl]Cl, **pyPhenPtCl,** was a donation from McMillin and co-workers[21] (University of Purdue, West Lafayette, Indiana, USA). Solutions of the nucleophiles were prepared shortly before use by dissolution in a 0.1 M $LiCF_3SO_3$ solution in methanol whose ionic strength had been

adjusted by addition of 0.01 M LiCl to prevent spontaneous solvolysis. The ionic strength of the solution was maintained using lithium trifluoromethanesulfonate ($LiCF_3SO_3$) because the triflate ion, ($CF_3SO_3^-$), does not coordinate to Pt(II) in solution.[22,23] Similarly, stock solutions of the metal complexes (*ca*. 10^{-5} mol dm^{-3}) were prepared using 0.1 M $LiCF_3SO_3$ solution.

3.2.1.1 Synthesis of the ligands and complexes

The platinum complexes, [Pt{4'-(2"'-CH_3-phenyl)-2,2':6',2''-terpyridine}Cl]CF_3SO_3 **CH_3PhPtCl** and [Pt{4'-(2"'-CH_3-phenyl)-6-(3''-isoquinoyl)-2,2'-bipyridine}Cl]SbF_6 **CH_3PhisoqPtCl** were synthesised and characterised using literature methods.[18,24] Details of the synthesis and characterisation of CH_3PhPtCl and CH_3PhisoqPtCl have been reported previously by Field[19] and our group.[20] The complex, [Pt{2-(2'-pyridyl)-1,10-phenanthroline}Cl]Cl, **pyPhenPtCl,** was a donation from McMillin and co-workers[21] (University of Purdue, West Lafayette, Indiana, USA).

3.2.1.2 Synthesis of [Pt{2–(2'–pyridyl)–1,10–phenanthroline}Cl]Cl

Synthesis of pyphen ligand

The synthesis of the 2-(2'-pyridyl)-1,10-phenanthroline (pyphen) ligand[21] for the preparation of the complex **pyPhenPtCl** is illustrated in Scheme 3.2.

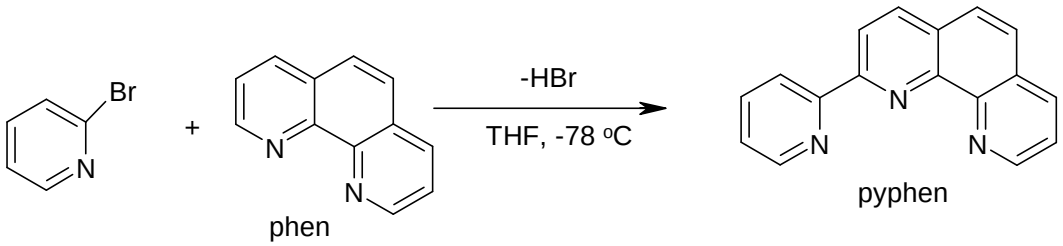

Scheme 3.2: Preparation pathway for pyphen ligand

To a solution of 2-bromopyridine in dry tetrahydrofuran (THF) was added stoichiometric amount of n-butyllithium at -78 °C, under argon atmosphere. A red solution resulted. After stirring for 15 min, 1.2 equiv. of the n-butyllithium reagent (mixture) was transferred, via a cannula, to a solution of 1,10-phenanthroline in dry THF at -78 °C also under Ar to produce a deep red solution. The mixture was stirred for 2 h,

after which water was added to quench the unreacted lithium reagent and the organics extracted into dichloromethane. All the organics were re-aromatized on addition of excess MnO_2 as oxidant and left to stand for 2 h, filtered and the solution dried over Na_2SO_4 and concentrated to yellow oil. The crude product was purified on an alumina column with THF/hexane (5:1). The final white solid product was recrystallized from 1:1 (v/v) dichloromethane/hexanes. 2-(2'-pyridyl)-1,10-phenanthroline **(pyphen**): Anal. Calcd for $C_{17}H_{11}N_3.1/4(CH_2Cl_2)$: C, 74.26; H, 4.04; N, 15.02. Found: C, 74.38; H, 4.16; N, 15.08%. ^{1}H NMR in $CDCl_3$ (in ppm): 9.25 (dd, 1 H), 9.00 (d, 1 H), 8.80 (d, 1 H), 8.75, (m, 1 H), 8.38 (d, 1 H), 8.25 (dd, 1H), 7.92 (td, 1 H), 7.82 (m, 2 H), 7.65 (m, 1 H), 7.38 (m, 1 H).

Preparation of pyPhenPtCl

The synthesising of **pyPhenPtCl** was according to the procedure published by McMillin and co-workers (Scheme 3.3), with $[Pt(COD)Cl_2]$ as the starting material.[21]

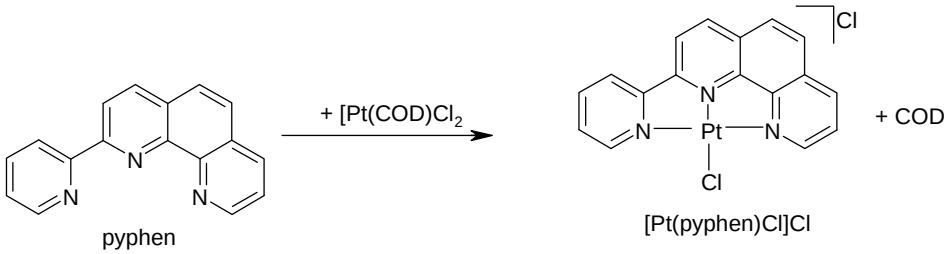

Scheme 3.3: synthesis of [Pt(pyphen)Cl]Cl complex

A solution of the pyphen ligand (100 mg) in a small amount of acetone was added to a suspension of 1 molar equiv. of $[Pt(COD)Cl_2]$ in aqueous 0.05 M 2-(*N*-morpholine)ethanesulfonic acid. The solution turned yellow on heating. After filtration, a saturated aqueous solution of NaCl was added to yield a red precipitate of [Pt(pyphen)Cl]Cl. [Pt(pyphen)Cl]Cl: Anal. Calcd for $C_{17}H_{11}N_3Cl_2Pt$.

3.2.1.3 Synthesis of Dichloro(1,5-cyclooctadiene) Platinum(II)

Literature method yielded [**Pt(CODCl$_2$**]][25] as described in Scheme3.4

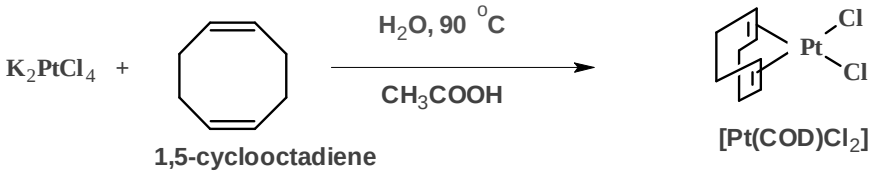

Scheme 3.4: Synthesis of [**Pt(COD)Cl$_2$**]

A solution of 1,5-cyclooctadiene (2.10 ml, 17 mmol) in glacial acetic acid (35 ml) was added to an aqueous solution of K_2PtCl_4 (2.17 g, 5.23 mmol). The mixture was stirred for 30 minutes at 90 ^oC under reflux. After 30 minutes a pale-yellow crystals started to precipitate. The solution was allowed to cool down and the compound formed, [**Pt(COD)Cl$_2$**], was filtered off. The yellow crystals were washed with copious amounts of water, ethanol, and diethyl ether and finally dried in the oven at 100 ^oC for 1 hour. [**Pt(COD)Cl$_2$**]: yield, 87% (1.71g, 4.57mmol).

3.2.1.4 *Synthesis of 4'-(2'''-CH$_3$-phenyl)-6-(3''-isoquinoyl)-2,2'-bipyridine ligand*[20,26]

The synthesis of the ligand followed the Kröhnke method[27] and is illustrated in Scheme 3.5.

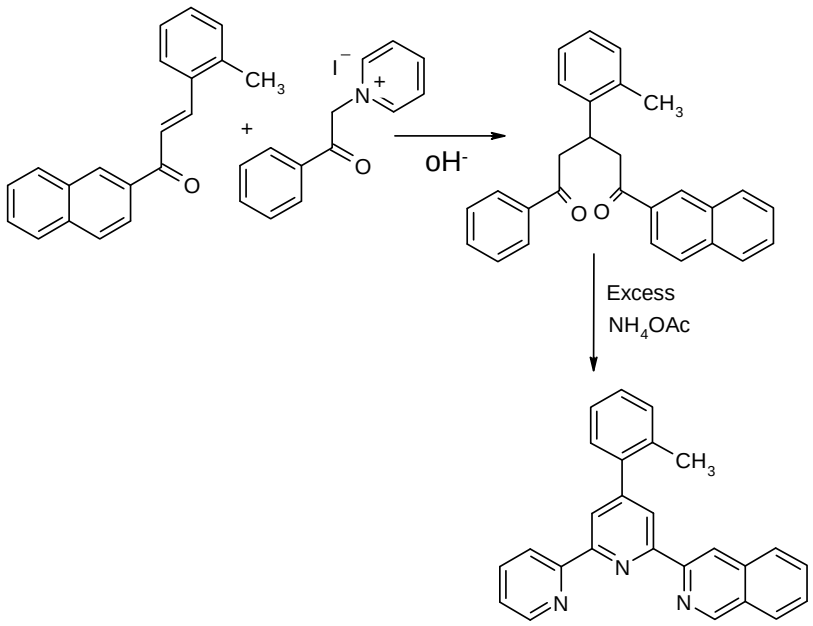

Scheme 3.5: Route used for the synthesis of **4'–(2'''–CH_3–phenyl)–6–(3''–isoquinolyl)–2,2'–bipyridine.**

A solution of a mixture of 1-(3-isoquinoyl)-3-(*o*-tolyl)-prop-2-en-1-one (0.892 g, 3.26 mmol), *N*-{1-(2´-pyridyl)-1-oxo-2-ethyl}pyridinium iodide (1.06 g, 3.26 mmol) and ammonium acetate (16.2 g, excess) in absolute ethanol (10 ml) was stirred for 1 h under reflux. The solution was allowed to cool, the resultant precipitate filtered off and washed with 50% aqueous ethanol. The product was recrystallised from ethanol (95%), after which it was dried under vacuum, to yield analytically pure off-white needle like crystals. **4'–(2'''–CH_3–phenyl)–6–(3˝–isoquinoyl)–2,2´–bipyridine**: Yield: 34% (0.410 g, 1.10 mmol). ^{1}HNMR ($CDCl_3$); 9.37 (s, 1H), 9.07 (s, 1H), 8.77 (d, 1H), 8.74 (dd, 1H), 8.62 (d, 1H), 8.49 (d, 1H), 8.08 (t, 2H), 7.95 (m, 1H) 7.77 (m, 1H), 7.66 (m, 1H), 7.42 (d, 1H), 7.38 (m, 1H), 7.33 (m, 3H), 2.40 (s, 3H, CH_3). LC/MS; [m/z, M + Na] = 396.1476. Anal. Calcd: C, 83.6; H, 5.1; N, 11.3; Found: C, 84.1; H, 5.2; N, 11.4%.

3.2.1.5 Synthesis of [Pt{4'–(2'''–CH_3–phenyl)–6–(3'''–isoquinoyl)–2,2'–bipyridine}Cl]SbF_6

The complex, **[Pt{4'–(2'''–CH_3-phenyl)–6–(3''–isoquinoyl)–2,2'–bipyridine}Cl]SbF_6 (CH_3PhisoqPtCl)** was synthesised using a modification of the method used by Summerton (Scheme 3.6).[28]

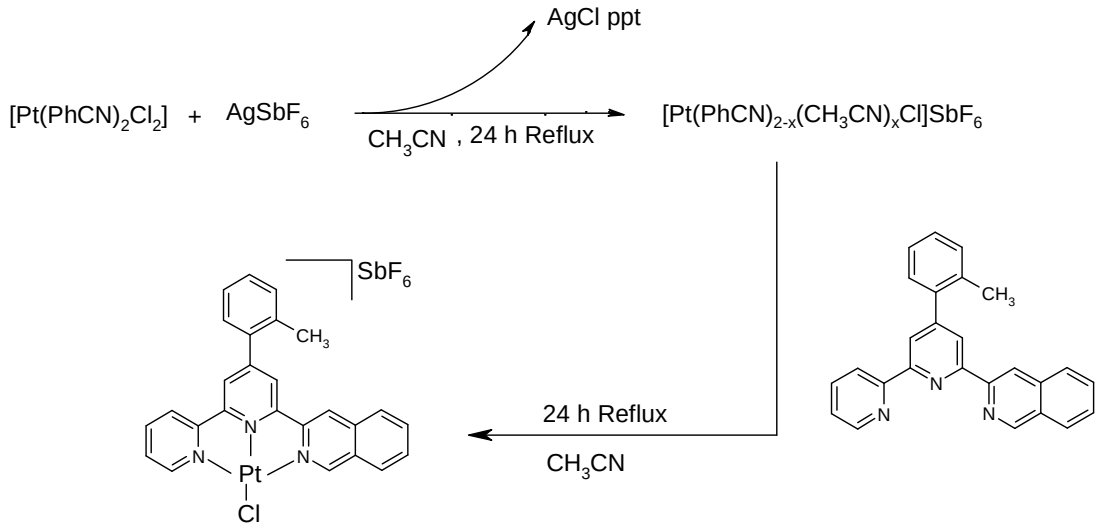

Scheme 3.6: Synthesis of the complex **CH_3PhisoqPtCl**

A solution of $AgSbF_6$ (24.6 mg, 0.0702 mmol) in acetonitrile (5 ml) was added to a suspension of [**$Pt(PhCN)_2Cl_2$**] (34.8 mg, 0.0737 mmol) in acetonitrile (12 ml). The mixture was stirred for 24 h under refluxed under nitrogen atmosphere. The precipitated AgCl was filtered off using 0.45 μm nylon filter membrane on a Millipore filtration unit. To the filtrate an equimolar amount of solid 4'–(2'''–phenyl)–6–(3″–isoquinoyl)–2,2´–bipyridine (24.6 mg, 0.0737 mmol) was added and the mixture was stirred for a further 24 hours under reflux. The solution was filtered while still hot; the precipitate of [**Pt{4'–(*2'''*–CH_3–phenyl)–6–(3''–isoquinoyl)2,2'–bipyridine}Cl]SbF_6** was carefully washed with copious amounts of diethyl ether, cold acetonitrile and dried under vacuum. A scarlet red powder was obtained. Characterisation of [**Pt{4'–(*2'''*–CH_3–phenyl)–6–(3''–isoquinoyl)2,2'–bipyridine}Cl]SbF_6** was by means of elemental analysis for % C, H and N, as well as by infrared, ^1H and ^{13}C NMR spectroscopy. [Pt{4'-(2'''-CH_3-phenyl)-6-(3″-isoquinoyl)-2,2´-bipyridine}Cl]SbF_6 **(CH_3PhisoqPtCl)**: Yield:

84% (34.7 mg, 0.0618 mmol). ^{1}H NMR (DMSO): 9.13 (s, 1H), 9.06 (s, 1H), 8.66/8.64 (dd, 2H), 8.48 (m, 2H), 8.17 (m, 2H), 7.93 (d, 1H), 7.80 (m, 1H), 8.80 (m, 1H), 7.95-7.51 (m, 5H), 2.50 (m, 3H, CH_3). ^{195}Pt NMR (DMSO): -2661.76 ppm. Anal. Calcd: C, 37.2; H, 2.3; N, 5.0; Found: C, 37.4; H, 2.3; N, 5.2%.

3.2.1.6 Synthesis of 2,2´:6´,2˝-terpyridine Platinum(II) (PtCl)[29]

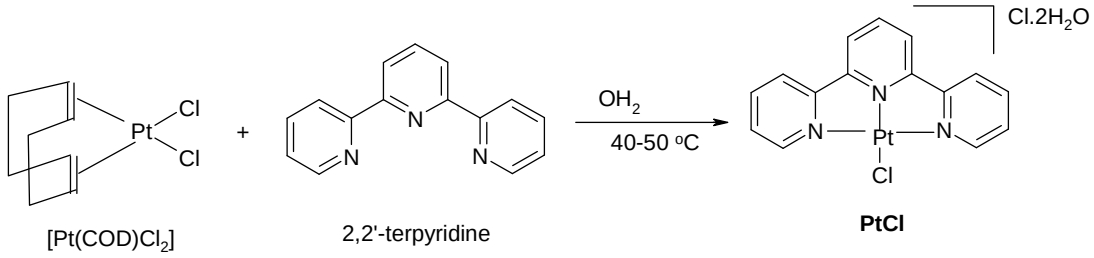

Scheme 3.7: Synthesis of the complex **PtCl**

An aqueous solution of [**Pt(COD)Cl$_2$**] (500 mg, 1.34 mmol) (30 ml) was added to 2,2´:6´,2˝-terpyridine (313 mg, 1.34 mmol) in a small amount of water. The mixture was stirred for 15 minutes at 45-50 °C. The clear orange-red solution obtained was allowed to cool down and any unreacted [Pt(COD)Cl_2] filtered off. The solvent was evaporated under reduced pressure. The orange-red solid, [Pt(terpy)Cl]Cl·2H_2O, (**PtCl**) was washed with diethyl ether, re-crystallized in a hot methanol/water mixture (50: 50), after which the orange needle like crystals were washed with diethyl ether and air dried to give analytically pure material of [Pt(terpy)Cl]Cl·2H_2O (**PtCl):** Yield: 89% (0.64 g, 1.19 mmol). Anal. Calcd: C, 33.7; H, 2.8; N, 7.9; Found: C, 33.9; H, 2.8; N, 7.8%.

3.2.1.7 Synthesis of 4'–(2'''–CH_3–phenyl)–2,2':6',2''–terpyridine ligand

The Synthesis of **4'-(2'''-CH_3-Ph)-2,2':6',2''-terpyridine** ligand **(Scheme 3.8)** as described by Summerton and Field, *et al.*[18,19]

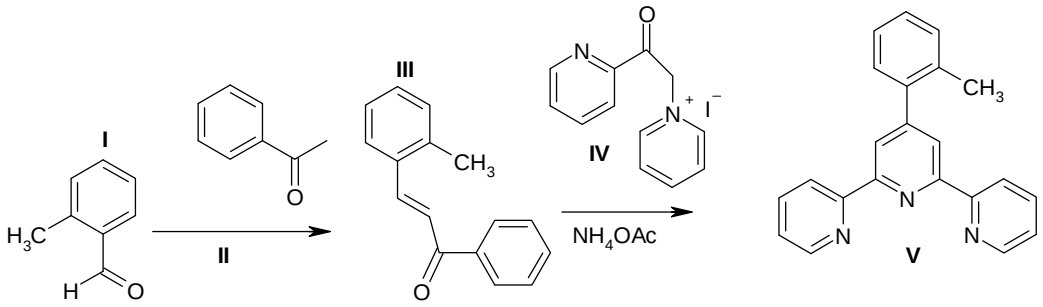

Scheme 3.8: Synthesis of **4'–(2'''–CH_3–Ph)–2,2':6',2''–terpyridine** ligand

One equiv. of 2-acetylpyridine (**II**) was reacted with one equiv. of [2-methylbenzaldehyde (**I**) in acetonitrile to yield the enone intermediate [2-CH_3-1-{3-(2-pyridyl)-3-oxo-prophenyl} benzene] (**III**) as yellow solid in high yield. To the suspension of the enone and ammonium acetate in boiling ethanol was added the enolate acylpyridinium iodide salt, N-{1-(2'-pyridyl)-oxo-2-ethyl}pyridinium iodide (**IV**) and heated under reflux for 2 h. the product was collected by filtration, washed with 50% ethanol and dried *in vacuo*. Colourless crystals of the required ligand, **4'–(2–CH_3–phenyl)–2,2':6',2''–terpyridine** (**V**) were obtained when crystallized from ethanol.

The ligand was characterised by elemental analysis, 1H NMR, 13C NMR, UV-Vis spectrophotometry, and GC-MS. **4'–(2–CH_3–phenyl)–2,2':6',2''–terpyridine** (**V**): Anal. Calcd for $C_{22}H_{17}N_3$: C, 81.7; H, 5.3; N, 13.0. Found: c, 81.6; H, 5.0; N, 13.0%.

3.2.1.8 Synthesis of [Pt{4'–(2'''–CH_3-phenyl)–2,2':6',2''–terpyridine}Cl]CF_3SO_3 (CH_3PhPtCl)

Synthesis of the complex **CH_3PhPtCl** followed literature procedure as described by Summerton[18] (Scheme 3.9).

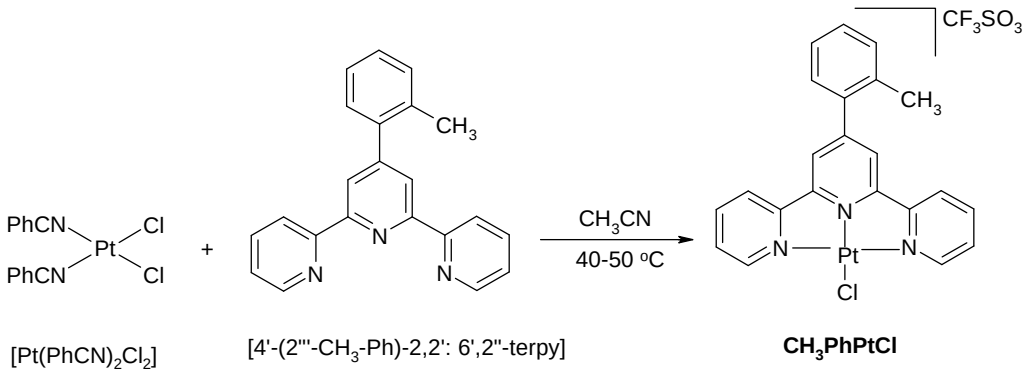

Scheme 3.9: Synthesis of the complex **$CH_3PhPtCl$**

To a solution of 1.0 mol of [**$Pt(PhCN)_2Cl_2$**] in acetonitrile was added slowly and with constant stirring an equimolar amount of $AgCF_3SO_3$. The contents were refluxed for 16 h under nitrogen. The precipitated AgCl was filtered off, and one equiv. of 4'**–(2'''–CH_3–phenyl)–2,2':6',2''–terpyridine** ligand was added to the filtrate and refluxed for a further 24 h. The solution was allowed to cool down, which resulted in the separation of a red solid that was filtered, washed with small amounts of diethyl ether, acetonitrile and dried *in vacuo*. The required product, [**$CH_3PhPtCl$**], was characterised by elemental analysis, IR (KBr disc), 1H and 13C NMR and UV-Vis spectroscopy.[18] [**CH_3PhPtC**l]: Anal. Calcd for $C_{23}H_{17}ClF_3N_3PtS$: C, 39.24; H, 2.58; N, 5.97. Found: C, 38.96; H, 2.94; N, 5.68%.

3.2.2 Physical Measurements and Instrumentation

Kinetic Analyses

All kinetic measurements were performed under *pseudo* first-order conditions using at least a 10-fold excess of the entering nucleophile. The wavelengths chosen for the kinetic investigations were determined from UV/Visible absorption spectra obtained from measurements on a Varian Cary 100 Bio UV/Visible spectrophotometer. The wavelengths at which there was greatest absorbance change were used for the subsequent kinetic analyses. These are summarised in Table SI 3.1 (appendix). An Applied Photophysics SX.18MV (v 4.33) stopped-flow analyzer coupled to an online data acquisition system was used to determine the observed rate constants, k_{obs}. All measurements were carried out in a thermostated environment to within ± 0.1 ^oC using

a coupled temperature control unit. All data were graphically analysed using the Origin 5.0® [30] graphical analysis software package.

3.2.3 Computational Modelling

Ground-state electronic structures calculations of **CH_3PhPtCl**, **CH_3PhisoqPtCl**, **pyPhenPtCl** as well as **PtCl** were optimized, as cations of +1 charge in gas phase, by the density functional theory (DFT) method using Spartan `04 for Windows®. The functional used throughout this study was the B3LYP, [31] a non-local hybrid exchange functional defined by Becke's three parameter equation, utilizing LACVP** (Los Alamos Core Valence Potentials) [32] pseudo-potential basis set.

3.3 Results

3.3.1 Computational Analysis

Computational modelling of the Pt(II) complexes, in gaseous phase, were determined in order to help explain the kinetic trends observed and the influence of the molecular structures as well as the electronic properties of the complexes on the observed reactivity. An extract of the geometry optimized structures of the complexes **CH_3PhPtCl, pyPhenPtCl**, **CH_3PhisoqPtCl** and **PtCl** are shown in Figure 3.1. A summary of corresponding properties of the frontier molecular orbitals: HOMO-LUMO energies, NBO atomic charges, and bond lengths and angles are presented in Table 3.1

Complex Structure	HOMO	LUMO
 PtCl		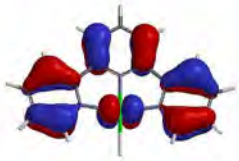
 $CH_3PhPtCl$	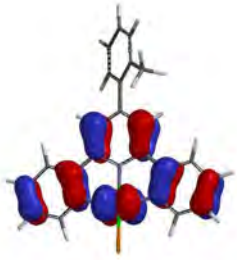	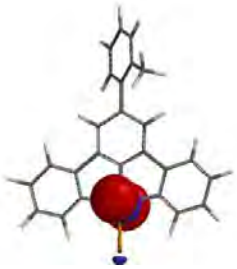
 $CH_3PhisoqPtCl$		
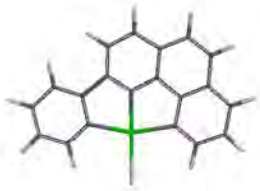 pyPhenPtCl	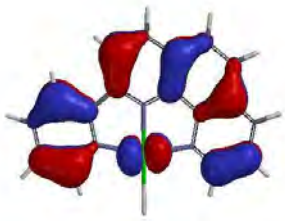	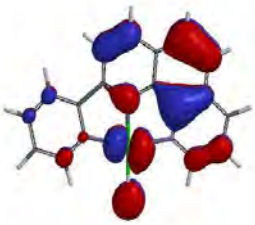

Figure 3.1 DFT-calculated (B3LYP/LACVP+**) HOMOs and LUMOs for polypyridyl complexes.

Table 3.1: Summary of DFT-calculated parameters and numbering system used for the calculation is in the structure shown as an inset.

Parameter	Complex			
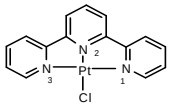	**$CH_3PhPtCl$**	**$CH_3PhisoqPtCl$**	**PtCl**	**pyPhenPtCl**
LUMO /eV	-5.92	-5.62	-6.16	-6.24
HOMO/eV	-9.14	-8.95	-9.45	-9.37
ΔE /eV	3.22	3.33	3.29	3.13
NBO Charges				
Pt	1.222	1.218	1.226	1.225
N_1	-0.60	-0.59	-0.60	-0.61
N_2	-0.57	-0.56	-0.57	-0.58
N_3	-0.60	-0.60	-0.60	-0.60
Cl	-0.645	-0.654	-0.637	-0.638
Bond Length (Å)				
Pt- $N_{1\ cis}$	2.05	2.07	2.05	2.05
Pt- $N_{2\ trans}$	1.97	1.97	1.96	1.97
Pt- N_{3cis}	2.05	2.06	2.05	2.05
Pt-Cl	2.35	2.34	2.35	2.36
Bond Angles (°)				
N_1-Pt-Cl	99.2	98.6	99.4	99.0
N_2-Pt-Cl	179.9	179.9	179.9	180.0
N_3-Pt-Cl	99.3	101.0	99.3	99.5
N_1-Pt-N_2	80.8	81.3	80.6	81.0
N_1-Pt-N_3	161.6	160.3	161.2	161.5

The geometry-optimised structures in Table 3.1 reveal that the molecular structures of all the complexes are similar as far as planarity, bond length and bond angles are concerned. The calculated data for the **PtCl** and **pyPhenPtCl** analogues are in good agreement with those reported in literature for corresponding complex ions $[Pt(terpy)Cl]^+$ and $[Pt(pyphen)Cl]^+$, where pyphen = 2-(2'-pyridyl)-1,10-phenanthroline.[23,33]

The DFT-calculations reveal that in the **pyPhenPtCl** complex, the HOMO molecular orbitals of the complex are delocalised over both metal and ligand centres, whereas the LUMO is localised on the phen ligand, the metal and chlorine atom, with essentially no contribution from the lateral pyridine ring (Figure 3.1). This is consistent with the fact that the phen moiety is a better π-acceptor than pyridine, a fact that is supported by having the lowest value for ΔE (Table 3.1). Compared to **PtCl**, the **pyPhenPtCl** has a more delocalised π-system which is a result of the extra fused ring in the pyphen ligand. This leads to favourable overlap of the *d*π orbitals of the metal and π*-orbitals of ligands in **pyPhenPtCl**. The DFT-calculated HOMO in **CH_3PhisoqPtCl** shows only the Pt (*5d*) character. This picture reveals that the metal centre is more electron-rich when compared to **CH_3PhPtCl**. This effect can only be due to the presence of the isoquinoyl moiety. This is supported by the DFT-calculations, which shows that **CH_3PhisoqPtCl** complex has the highest HOMO-LUMO energy gap and the least positive (NBO) charge at the Pt(II) centre as seen in Table 3.1.

3.3.2 Kinetic Measurements

Substitution of coordinated chloride (Equation 1) from each of the four square planar platinum(II) complexes was investigated using a series of neutral sulphur-donor nucleophiles, *viz*. TU, DMTU and TMTU, as well as ionic nucleophiles, namely I^-, Br^- and SCN^-, under *pseudo* first-order conditions using the stopped-flow technique.

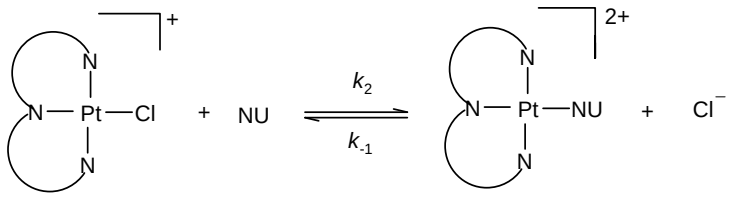

[1]

where NU = TU, DMTU, TMTU, SCN^-, I^-, Br^-

A typical kinetic trace recorded by mixing solutions of **$CH_3PhPtCl$** (2.50 x 10^{-5} M) and DMTU (1.25 x 10^{-3} M) at an ionic strength of 0.1 M ($CF_3SO_3^-$) is shown in Figure 3.2 (also Figure SI 3.1 appendix).

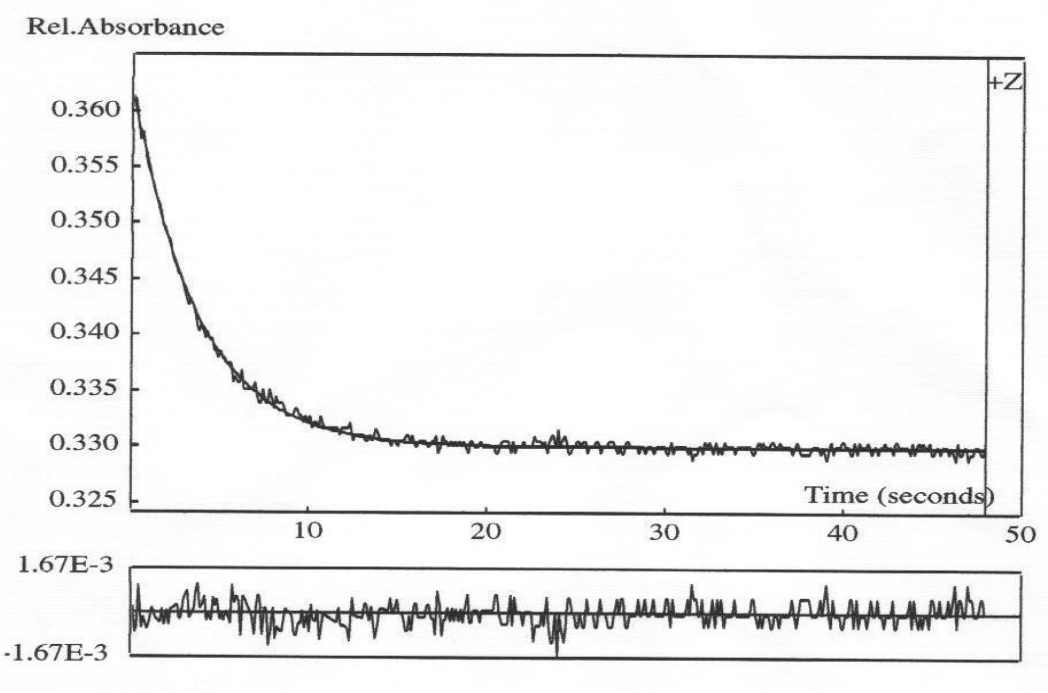

Figure 3.2: Spectrum obtained from the stopped-flow spectrometer with a single exponential fit for the reaction between **$CH_3PhPtCl$** (2.50 x10^{-5} M) and DMTU (1.25 x 10^{-3} M) in methanol followed at 308 nm, I = 0.1 M ($LiCF_3SO_3$), T = 298.15 K.

All the kinetic traces gave excellent fits to first-order exponential decays to generate observed *pseudo* first-order rate constants, k_{obs}, at specific concentrations of the nucleophiles and temperature. The *pseudo* first-order rate constants, k_{obs}, were plotted

against the concentration of the incoming nucleophiles to determine the second-order rate constant, k_2, which were obtained from the slopes of the plots and k_{-2} that were obtained from the y-intercept in some of the complexes. The k_{obs} values used were an average of five to eight runs. All the kinetic data obtained gave straight-line fits with significant non-zero intercepts in some cases for each of nucleophiles as shown in Figures 3.3(a & b) (also Figures SI 3.2(a & b) and Tables SI 3.2(a & b) and 3.3 (a & b) appendix). The mechanistic pathway is irreversible and independent of the solvent when k_{-2} is zero. Therefore, the mechanism of the substitution can be represented by Equation 1 and the corresponding rate law is given by Equation 2.

$$k_{obs} = k_2 [NU] + k_{-2} \quad (2)$$

The representative plots shown in Figures 3.3(a & b) clearly illustrate that the substitution reactions are first-order with respect to the incoming nucleophile. The values of k_2 obtained are summarised in Table 3.2. Also included in Table 3.2 are literature values for **PtCl** for comparison.

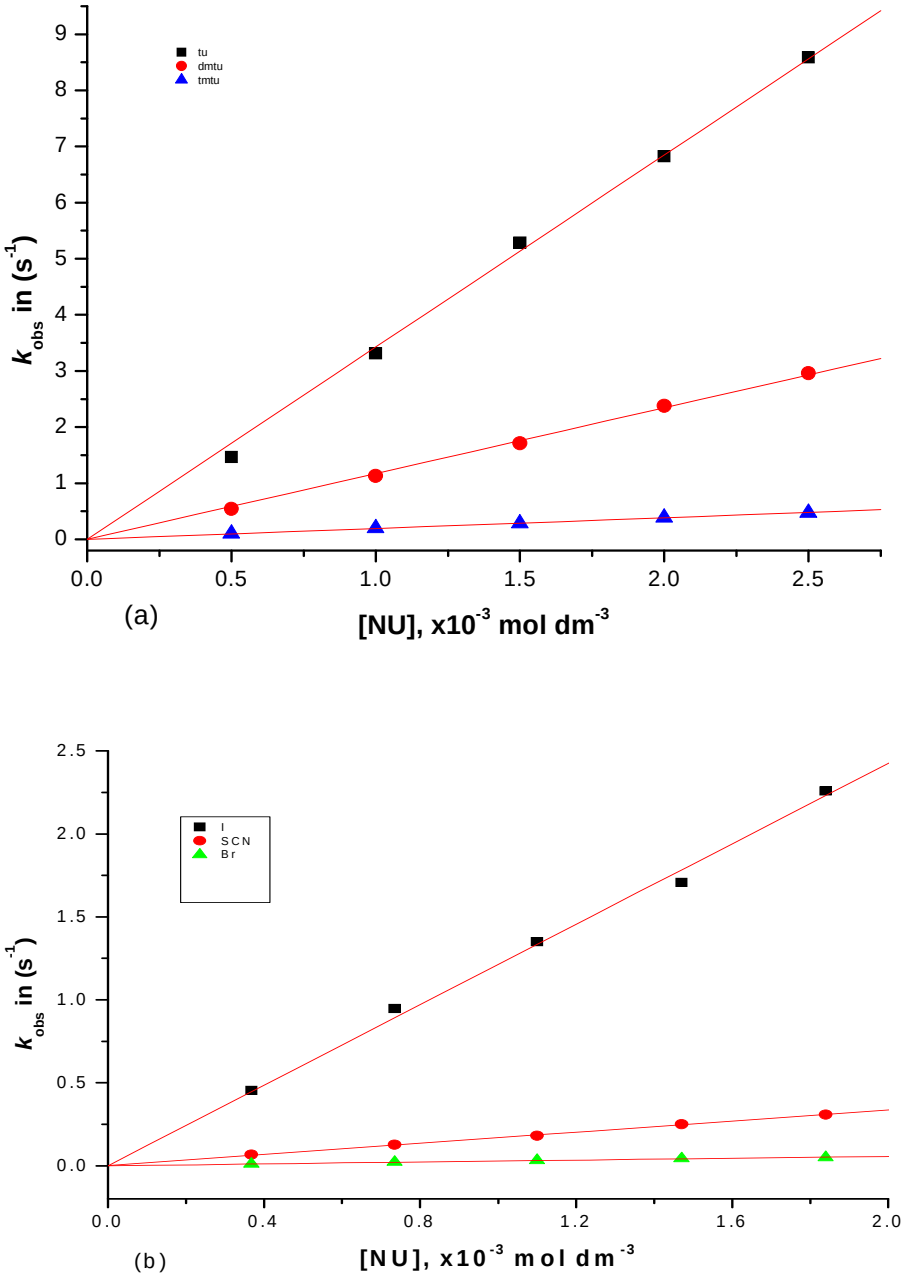

Figure 3.3: Concentration dependence of k_{obs} for the substitution of chloride from **pyPhenPtCl** (5.0 x 10^{-5} M) by (a) thiourea nucleophiles and (b) anionic nucleophiles in methanol, I = 0.1 M ($LiCF_3SO_3$), T = 298.15 K.

Table 3.2: Summary of the second-order rate constants at 25 °C and activation parameters for the substitution of chloride from Pt(II) polypyridyl complexes by TU, DMTU, TMTU, and in methanol, I = 0.1 M ($LiCF_3SO_3$).

Complex	Nu	k_2/ M^{-1} s^{-1}	$\Delta H^{\#}$/kJ mol^{-1}	$\Delta S^{\#}$/J K^{-1} mol^{-1}
	**TU**	1264.2 ± 8.4	39 ± 1	-111 ± 3
	DMTU	426.4 ± 5.2	43 ± 1	-105 ± 5
	TMTU	83.6 ± 0.9	36 ± 1	-141 ± 3
	I^-	213.3 ± 2.0	44 ± 2	-113 ± 7
	Br^-	3.7 ± 0.1	34 ± 1	-172 ± 4
$CH_3PhPtCl$	**SCN^-**	11.3 ± 0.3	50 ± 2	-112 ± 7
	**TU**	375.8 ± 2.7**	40 ± 1	-121 ± 2
	DMTU	127.0 ± 0.7	43 ± 2	-116 ± 6
	TMTU	21.5 ± 0.2	39 ± 1	-141 ± 2
	I^-	80.2 ± 0.7	47 ± 1	-104 ± 4
	Br^-	2.2 ± 0.02	59 ± 1	-89 ± 3
$CH_3PhisoqPtCl$	**SCN^-**	3.2 ± 0.1	62 ± 2	-78 ± 7
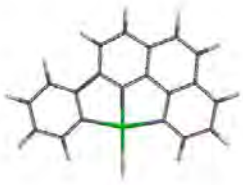	**TU**	3424.7 ± 41.9	41 ± 2	-94 ± 6
	DMTU	851.8 ± 8.9	39 ± 1	-110 ± 4
	TMTU	139.5 ± 1.3	38 ± 1	-129 ± 3
	I^-	454.0 ± 2.9	52 ± 3	-70 ± 9
	Br^-	10.3 ± 0.3	43 ± 1	-67 ± 13
pyPhenPtCl	**SCN^-**	168.5 ± 1.5	64 ± 4	-97 ± 2
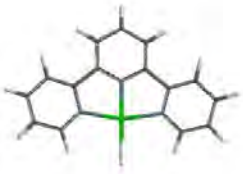	**TU**	1494.0 ± 10.0	29 ± 2	-88 ± 5
	DMTU	448.0 ± 10.0	36 ± 1	-73 ± 4
	TMTU	82.0 ± 0.4	35 ± 2	-91 ± 8
	I^-	243.0 ± 4.0	47 ± 3	-42 ± 11
[a] PtCl	**Br^-**	8.1 ± 0.5	-	-
	SCN^-	17.0 ± 0.2	48 ± 2	-61 ± 1

a = Values extracted from reference 13. ** k_{-2} values of 0.0111± 0.00122 (TU);0.00219 ± 0.00118 (DMTU)

The second order rate constant, k_2, was also determined as a function of temperature, over a temperature range of 15-35° C. Typical Eyring plots obtained for **pyPhenPtCl** for the six nucleophiles are shown in Figure 3.4 (also Figure SI 3.3 and Tables SI 3.4(a &b) and SI 3.5(a & b) appendix). The thermodynamic parameters, activation enthalpies, $\Delta H^{\neq}$, and the activation entropies, $\Delta S^{\neq}$, were calculated and the values are recorded in Table 3.2.

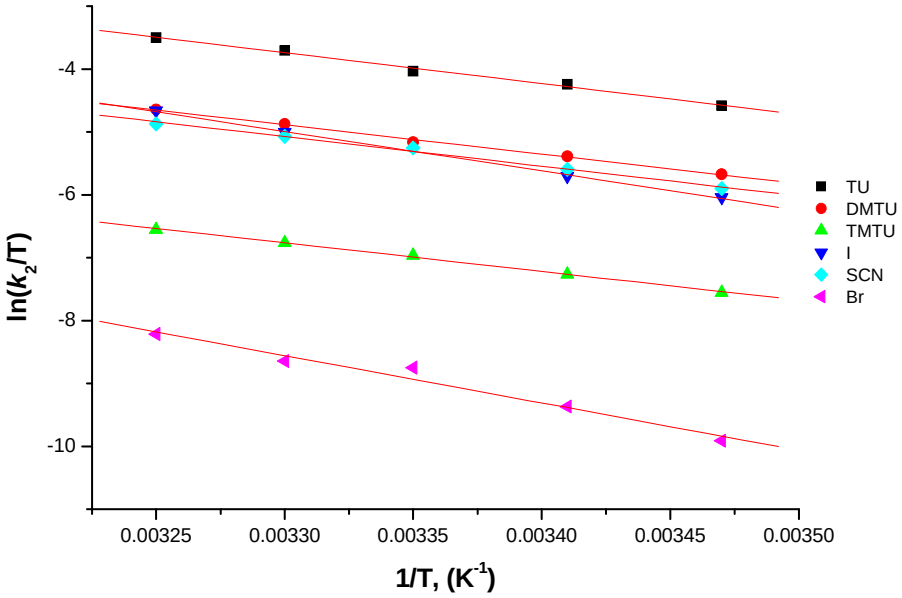

Figure 3.4: Plots of ln (k_2/T) against 1/T for the substitution of chloride from **pyPhenPtCl** by TU, DMTU, TMTU, I-, SCN- and Br- in methanol, I = 0.1 M ($LiCF_3SO_3$), over the temperature range 288-308 K.

3.4 Discussion

Comparing the rates of substitution of the chloride from the complexes, a clear general trend is observed from the reactivity data in Table 3.2. Using the reaction of **PtCl** with TU as the basis of comparison the order of reactivity is **CH_3PhisoqPtCl** < **CH_3PhPtCl** < **PtCl** < **pyPhenPtCl**. A similar order of reactivity trend was observed for all the nucleophiles investigated as given in Table 3.2. When one looks at the structures of **CH_3PhPtCl** and **CH_3PhisoqPtCl,** the only difference is the introduction of isoquinoline moiety in place of the pyridine. Somewhat surprising is that the second-order rate

constants of **CH_3PhisoqPtCl** decrease by a factor of about three or lower depending on the nucleophiles. The expectation would be an increase in the rate of substitution due to the extended π-conjugation, which should enhance π-backbonding effect.[16,17] In the case of **pyPhenPtCl** and **PtCl** the expected trend is observed with **pyPhenPtCl** being more reactive than **PtCl**.

To provide an explanation to this trend it is important that the properties of the coordinated ligand to the platinum metal is understood. Looking at the structures of the Pt(II) complexes which are shown in *Scheme* 3.1, one notes that they are all characterised by the presence of a delocalised π-system that allows for facile electron transfer from the metal to the ligand. This giving rise to metal-to-ligand-charge transfer (MLCT) absorption spectra that are usually found in the wavelength range 350-450 nm,[33-35] and is also seen in Figure 3.5 Since the π-acceptor property of the complex can be viewed as transfer of electron density from the HOMO orbital of the complex into the LUMO, any difference in energies of the *d*-orbital HOMOs of the complex and the π*-LUMOs localised on the ligands, would determine the HOMO-LUMO energy gap and hence the energy of the MLCT absorption, and hence the reactivity.

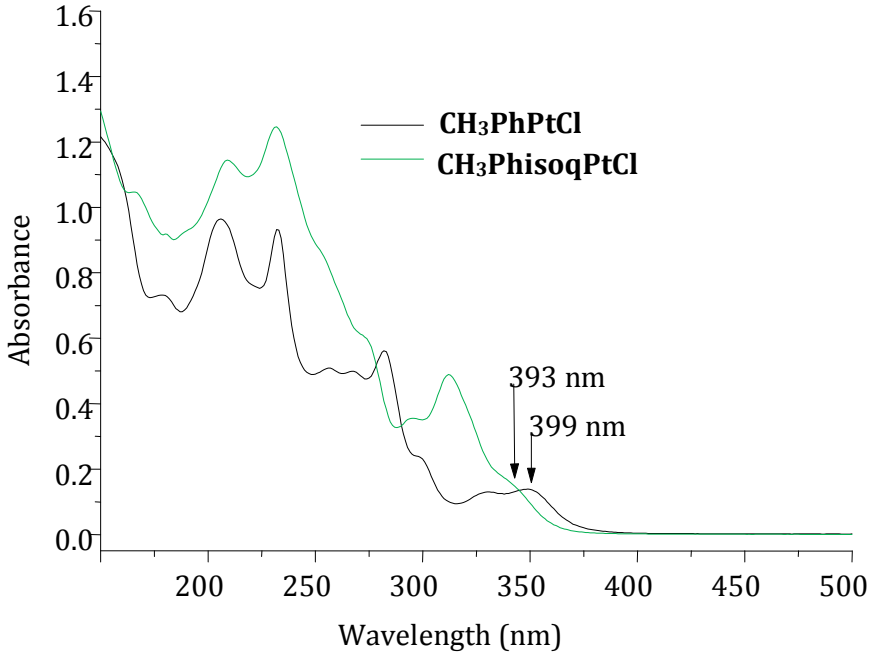

Figure 3.5: Absorption spectra of **CH_3PhPtCl** and **CH_3PhisoqPtCl** in acetonitrile

The electronic absorption spectra of **CH_3PhPtCl**, **CH_3PhisoqPtCl**, **PtCl** and **pyPhenPtCl** have been reported in literature.[20,21] These results reveal that the order of decreasing MLCT absorption energies follow the trend: **CH_3PhisoqPtCl** > **CH_3PhPtCl > PtCl > pyPhenPtCl**. This observation is consistent with the understanding that pyphen ligand is the strongest π-acceptor and **4'–(2'''–CH_3–phenyl)–6–(3''–isoquinoyl)–2,2'–bipyridine** the weakest. The results also represent the electronegativiy of the ligands as well as the extent of π-delocalisation.[36] These results are in agreement with the DFT-calculations which illustrate the π-acceptor properties of the tridentate ligands and quantify the HOMO-LUMO energy gap of the frontier orbitals.

Given the typically associative character of the d^8 square-planar Pt(II) complexes, the transition state is stabilised by the transfer of the electron density to the tridentate N-donor ligands, making the metal centre more positively charged, thus enhancing the substitution reactions. This is in contrast to the increase of electron density around the Pt(II) centre which tends to stabilise the ground state while destabilising the 18-electron five-coordinate transition state with a net effect of slowing substitution reactions.

Therefore, the difference in reactivity of investigated complexes can be accounted for in terms of the strength of the π-backbonding of the coordinating ligand. The higher reactivity of **CH_3PhPtCl** compared to **CH_3PhisoqPtCl** is due to the fact that the three coplanar pyridine rings of terpy ligand are better at delocalising the negative charge from the Pt(II) centre through π-backbonding. The "unusual" decrease in reactivity of **CH_3PhisoqPtCl** is due to the relative poor π-acceptor property of the isoquinoline ligand. This means that the electrophilicity of the metal centre is decreased, resulting in the retardation of the incoming nucleophiles. Similar results have been reported by our group [14] and other workers, [9, 22] but these have been due to the increase in the *cis* σ-effect and not the decrease in the delocalisation of the π-electron density being reported here. The results show that isoquinoline ligand is a net σ-donor.

The difference in reactivity between **PtCl** and **pyPhenPtCl** is because of the fused-ring system in the latter that gives rise to a favourable overlap of the $d\pi$ orbitals of the metal

with π*-orbitals of the ligand. This allows electron density flow from the filled 5*d*π and 6p_z-orbitals of the metal into the empty π*-orbitals of the ligand,[37] making the trigonal bipyramidal transition state in **pyPhenPtCl** more stable and the Pt(II) centre more electrophilic, thereby enhancing the departure of the chloride. This is supported by the DFT-calculations which show that this system has the smallest HOMO-LUMO energy gap. This effect is far reduced in the case of **CH_3PhisoqPtCl**. Thus, the extensive π-conjugation in the fused-ring system of the Phen ligand, accompanied by enhanced electronic communication in the aromatic system around the Pt-metal centre, results in increased reactivity of the **pyPhenPtCl** complex compared to **PtCl**.

The trend of reactivity observed in this study between **CH_3PhPtCl** and **PtCl** has been reported before in the literature. [14, 15] The positive σ-inductive effect associated with the 4′-(2′″-CH_3-phenyl) group decreases the electrophilicity of the metal while increasing the energy gap between the HOMO-LUMO orbitals,[9,13,1517] resulting in decreased reactivity as compared to **PtCl**.

The substitution of chloride by the nucleophiles TU, DMTU and TMTU decreases according to the increasing steric hindrance of the nucleophiles for all the complexes with the most sterically hindered TMTU, reacting significantly slower. The reactivity of the anionic nucleophiles follows the order I^- > SCN^- > Br^-; an order that depicts the nucleophilicity and polarisability of the incoming ligands and correlates well with previous studies.[16, 38] The iodide ion being the most polarisable reacts faster than the other nucleophiles, and is aided by its strong electrostatic attraction forces with the monocationic complexes. It is a well documented fact that soft (polarisable) nucleophiles have a high affinity for softer substrates like Pt(II) ion. [39]

The activation enthalpies ($\Delta H^{\neq}$) as tabulated in Table 3.2 are low and positive, and activation entropies ($\Delta S^{\neq}$) are large and negative. The sensitivity of the second-order rate constants to different nucleophiles and the significantly negative intrinsic entropies of activation ($\Delta S^{\neq}$) values as a result of bond formation in the transition state, support the associative mechanism well known for d^8 square-planar metal complexes.[39-41]

3.5 Conclusion

This study has demonstrated that the lability of the chloride from the complexes **pyPhenPtCl**, **PtCl, CH_3PhPtCl** and **CH_3PhisoqPtCl**, is strongly influenced by the strength of the π-backbonding through the extended π-conjugation of tridentate (N, N, N) ligand around the metal centre. The slower reactivity of **CH_3PhisoqPtCl** is attributed to the net σ-donor of the isoquinoline ligand, which is in the *cis*-position to the leaving group that effectively decreases the electrophilicity of the Pt(II) centre by aiding accumulation of the electron density at the metal centre. The results are clearly supported by the DFT- calculations for NBO charges and HOMO-LUMO energy gap. It can therefore be anticipated that in complex systems where the isoquinoline moiety is on the *trans*-position to the leaving group, an increase in reactivity is likely to occur due to ground state destabilisation of the transition state as a result of *trans-effect*.[22] The negative values for $\Delta S^{\neq}$ and dependence of the second-order rate constants on concentration of the nucleophiles support the associative mechanism that involves a five-coordinate transition state strongly dominated by bond making.

3.6 References

1 D. Rosenberg, L. Van Camp, J. E. Trusko and V. H. Mansour, *Nature*, 1969, **222**, 385.

2 V. X. Jin, S. I. Tan and J. N. Ranford, *Inorg. Chim. Acta*, 2005, **358**, 677.

3 C. S. Peyratout, T. K. Aldridge, D. K. Crites and D.R. McMillin, *Inorg. Chem*., 1995, **34**, 4484.

4 M. Casamento, G. E. Arena, C. Lo Passo,I. Pernice, A. Romeo and L. M. Scolaro, *Inorg. Chim. Acta*, 1998, **276**, 242-249.

5 S. Bonse, J. M. Richards, S. A. Ross, G. Lowe and R. L. Krauth-Siegel, *J. Med. Chem.*, 2000, **43**, 4812.

6 (a) G. Lowe, A. S. Droz, T. Vilaivan, G. W. Weaver, L. Tweedale, J. M. Pratt, P. Rock, V. Yardley and S. L.Croft, *J. Med. Chem*., 1999, **42**, 999; (b) G. Lowe, A. S. Droz, G. W. Weaver, J. J. Park, J. M. Pratt, L. Tweedale and L. R. J. Kelland, *J. Med. Chem*., 1999, **42**, 3167.

7 Z. D.Bugarčić, G. Liehr and R. van Eldik, *J. Chem. Soc., Dalton Trans*., 2002, 2825.

8 B. Pitteri, G. Marangoni, L. Cattalini and T. J. Bobbo, *J. Chem. Soc., Dalton Trans*., 1995, 3853.

9 R. Romeo, M. R. Plutino, L. M. Scolaro, S. Stoccoro and G. Minghetti, *Inorg. Chem*., 2000, **39**, 4749, and references therein.

10 J. Fazlur-Rahman and G. Verkade, *Inorg. Chem*., 1992, **31**, 2064.

11 B. Pitteri, G. Marangoni, L. Cattalini, F. Visentin, V. Bertolasi and P. Gilli, *Polyhedron*, 2001, **20**, 869.

12 R. J. Mureinik, M Bidani, *Inorg. Chim. Acta*, 1978, **29**, 37.

13 D. Reddy and D. Jaganyi, *Dalton Trans*., 2008, 6724.

14 D. Jaganyi, D. Reddy, J-A. Gertenbach, A. Hofmann and R. van Eldik, *Dalton Trans.,* 2004, 299.

15 D. Jaganyi, K-L, De Boer, J-A. Gertenbach and J. Perils, *Int. J. Chem. Kinet.,* 2008, 807.

16 A. Hofmann, D. Jaganyi, O, Q. Munro, G. Liehr and R. van Eldik, *Inorg. Chem*., 2003, **42**, 1688.

17 D. Jaganyi, A. Hofmann and R. van Eldik, *Angew. Chem. Int. Ed. Engl*. 2001, **40**, 1680.

18 G. C. Summerton, Ph. D. Thesis, University of Natal, Pietermaritzburg, Republic of South Africa, 1997, pp. 51, 53, 71-77, 94, 107.

19 J. S. Field, R. J. Haines, D. R. McMillin, G. C. Summerton, *J. Chem. Soc., Dalton Trans*., 2002, 1369.

20 J. S. Field, J-A, Gertenbach, D. Jaganyi, D. R. McMillin, D. J. Stewart and A. Shaira, *Z. Naturforsch*., 2010, **65b**, 1318.

21 J. J. Moore, J. J. Nash, P. E. Fanwick and D. R. McMillin, *Inorg. Chem*., 2002, **41**, 6387.

22 A. Hofmann, L. Dahlenburg, and R. van Eldik, *Inorg. Chem*., 2003, **42**, 6528-6538.

23 T. G. Appleton, J. R. Hall, S. F. Ralph and C. S M. Thompson, *Inorg. Chem*., 1984, **41**, 3521.

24 J. S. Field, R. J. Haines, D. R. McMillin, G. C. Summerton, *J. Chem. Soc., Dalton Trans*., 2002, 1369.

25 J. X. McDermott, J. F. White and G. M. Whitesides, *J. Am. Chem. Soc.,* **1976**, *98*, 6521.

26 A. Shaira, MSC Thesis, *A Kinetic and Mechanistic study into the Substitution Behaviour of Platinum(II) Polypyridyl Complexes with a Series of Azole Ligands*, University of KwaZulu-Natal, Pietermaritzburg, 2010.

27 E. Kröhnke, *Synthesis,* 1976, 1.

28 G. C. Summerton, PhD Thesis*, Solid State Structures and Photophysical Properties of Polypyridyl Complexes of platinum(II)*, University of Natal, Pietermaritzburg, South Africa, **1997**, pp. 23-25,32-33,70-75,153-154.

29 G. Annibale, M. Brandolisio and B. Pitteri, *Polyhedron,* **1995**, *14*, 451.

30 Microcal ™ Origin ™ Version 5.0, Microcal Software, Inc.,One Roundhouse Plaza, Northampton, MA, 01060, USA, 1991-1997.

31 A. D. Becke, *J. Chem Phys.*, 1993, **98**, 5648.

32 V. A. Rassolov, J. A. Pople, M .A. Ratuer and J. L. Windus, *J. Chem Phys.*, 1998, **109**, 1223.

33 H. K. Yip, L. K. Cheng, K. K. Cheung and C. M. Che, *J. Chem. Soc., Dalton Trans*., 1993, 2933.

34 R. Buchner, Field, J. S., R. J. Haines, G. C. Summerton and D. R. McMillin, *Inorg. Chem*., 1997, 36, 3952.

35 D. R. McMillin and J. J.Moore, *Coord. Chem. Rev*., 2002, **229**, 113.

36 R. Zong, G. Zhang, S. V. Eliseeva, J-C. G. Bünzli and R. P. Thummel, *Inorg. Chem*., 2010, 49, 4647.

37 M. Schülling, D. M. Grove, G. Van Koten, R. van Eldik, N. Veldman and A. L. Spek, *Organometallics*, 1996, **15**, 1384.

38 D. Jaganyi, F. Tiba, O. Q. Munro, B. Petrović and Z. D. Bugarčić, *Dalton Trans*., 2006, 2943.

39 M. L. Tobe and J. Burgess, *Inorganic Reaction Mechanisms*; Addison-Wesley Longman: Essex, England, 1999, pp.30-33; 70-112.

40 J. D. Atwood, *Inorganic and Organometallic Reaction Mechanisms*, 2nd Ed; Wiley-VCH: New York, 1997, pp. 13, 14; 43-61.

41 R. Van Eldik, T. Asano and W. Le Noble, *Chem. Rev*., 1989, **89**, 549.

Appendix 3

A summary of wavelengths for kinetic measurements for **CH_3PhisoqPtCl** and **pyPhenPtCl**; kinetic traces, concentration and temperature dependent studies of selected complexes; tables summarising all values of k_{obs} determined for reactions at different concentrations and temperatures for selected complexes; electrostatic potential surfaces of the calculated DFT structures accompany the work reported in this paper as supporting information.

The π-Acceptor Effect in the Substitution Reactions of Tridentate *N*-Donor Ligand Complexes of Platinum(II): A Detailed Kinetic and Mechanistic study

Table S3.1: Summary of the wavelengths (nm) used for monitoring the reactions between a series of Pt(II) complexes with tridentate ligands and neutral S-donor and ionic nucleophiles.

Complex	Nucleophiles	Wavelength, λ (nm)
CH_3PhisoqPtCl	TU	363
	DMTU	363
	TMTU	386
	I^-	448
	SCN^-	412
	Br^-	412
pyPhenPtCl	TU	308
	DMTU	313
	TMTU	339
	I^-	309
	SCN^-	415
	Br^-	302

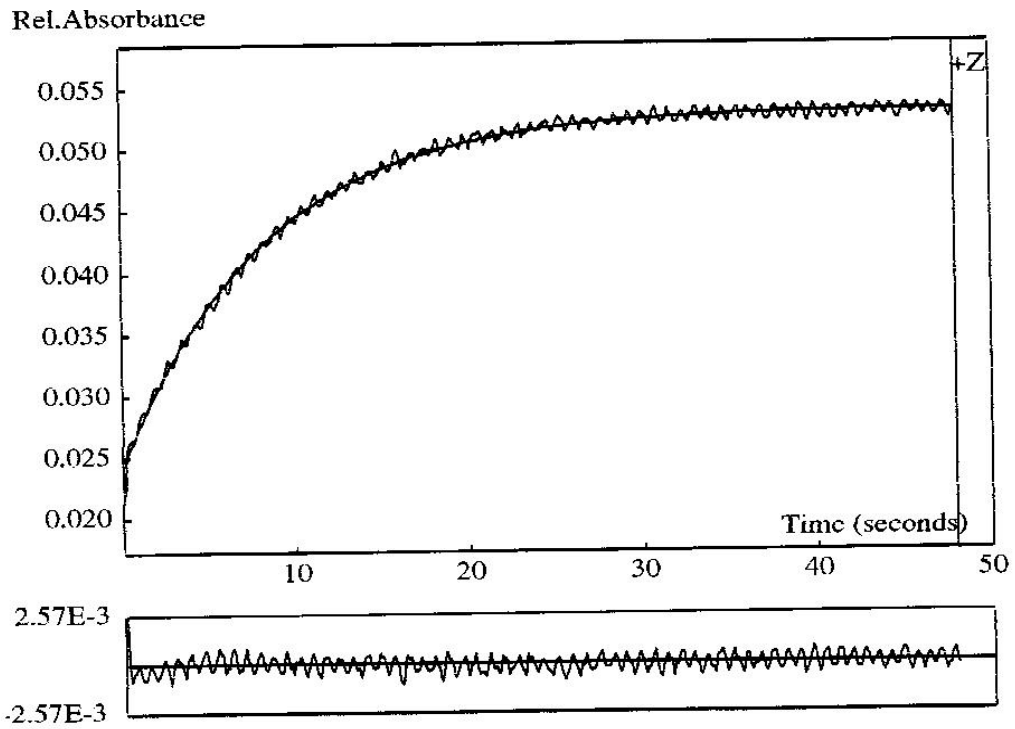

Figure S3.1: Kinetic trace at 448 nm for the substitution reaction between **CH_3PhisoqPtCl** (0.054 mM) and I^- (6.06 mM) at 298 K, I = 0.1 M Li(SO_3CF_3) in methanol.

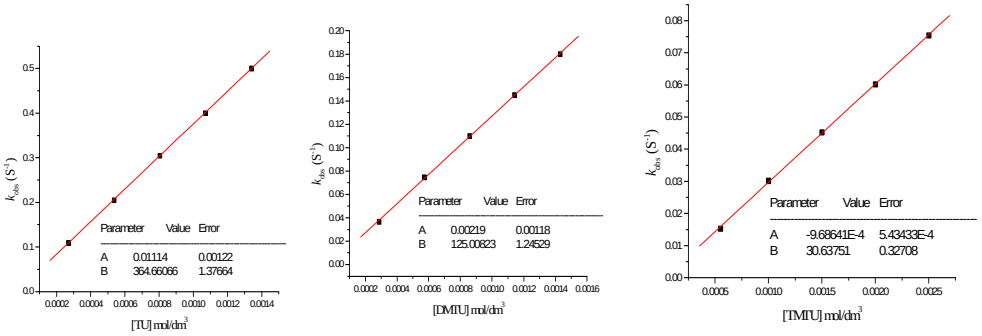

Figure S3.2 (a): Concentration dependence of $k_{obs/}$ s^{-1}, for the substitution of the chloride ligand in **CH_3PhisoqPtCl** by a series of nucleophiles, T = 298 K, I = 0.1 M ($LiSO_3CF_3$) in methanol.

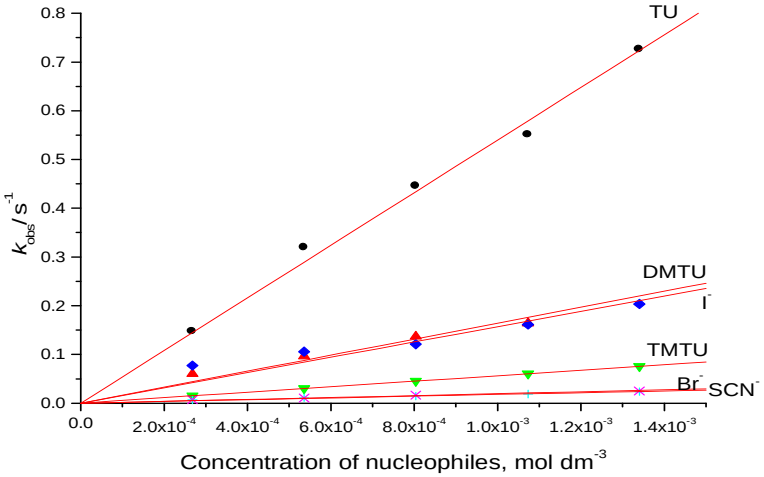

Figure S3.2 (b): Concentration dependence of $k_{obs/}$ s^{-1}, for the substitution of the chloride ligand in **CH_3PhisoqPtCl** by a series of nucleophiles, T = 298 K, I = 0.1 M ($LiSO_3CF_3$) in methanol.

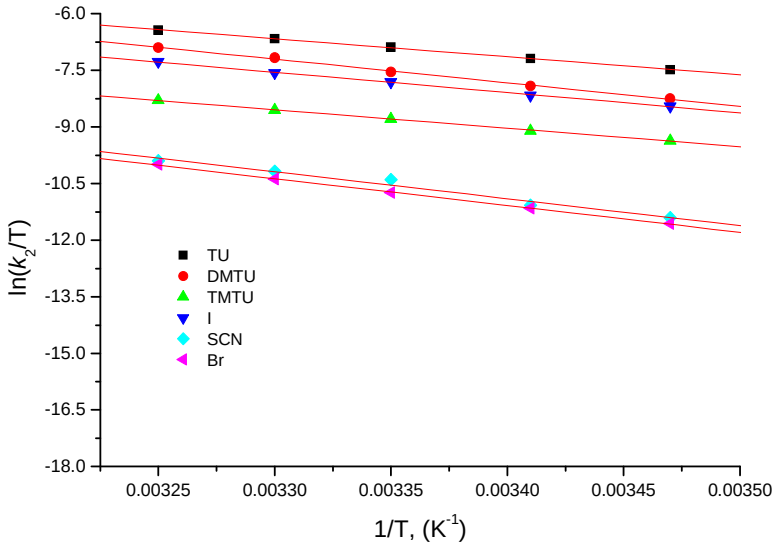

Figures S3.3: Temperature dependence of k_2, $M^{-1}s^{-1}$, for the substitution of the chloride from **CH_3PhisoqPtCl**, by thiourea nucleophiles I = 0.1 M ($LiSO_3CF_3$) in methanol.

Table S3.2a: Average observed rate constants, k_{obs}, s^{-1}, for substitution of chloride from **pyPhenPtCl** by thiourea nucleophiles, T = 298 K, I = 0.1 M ($LiSO_3CF_3$)

TU (λ = 308 nm)		**DMTU** (λ =370 nm)		**TMTU** (λ = 339 nm)	
Conc., M	k_{obs}, s^{-1}	Conc., M	k_{obs}, s^{-1}	Conc., M	k_{obs}, s^{-1}
0.0005	1.4628	6.88×10^{-4}	0.5415	6.88×10^{-4}	0.1032
0.001	3.3150	0.00138	1.1255	0.00138	0.1995
0.0015	5.2825	0.00206	1.7128	0.00206	0.2821
0.002	6.8256	0.00275	2.3766	0.00275	0.3885
0.0025	8.5872	0.00344	2.9588	0.00344	0.475

Table S3.2b: Average observed rate constants, k_{obs}, s^{-1}, for substitution of chloride from **pyPhenPtCl** by ionic nucleophiles, T = 298 K, I = 0.1 M ($LiSO_3CF_3$).

I^- (λ = 308 nm)		**SCN^-** (λ =415 nm)		**Br^-** (λ = 339 nm)	
Conc., M	k_{obs}, s^{-1}	Conc., M	k_{obs}, s^{-1}	Conc., M	k_{obs}, s^{-1}
3.675×10^{-4}	0.454	3.675×10^{-4}	0.06798	3.675×10^{-4}	0.0108
7.350×10^{-4}	0.946	7.350×10^{-4}	0.12574	7.350×10^{-4}	0.0216
0.00110	1.350	0.00110	0.18135	0.00110	0.0326
0.00147	1.708	0.00147	0.25052	0.00147	0.0432
0.00184	2.260	0.00184	0.30788	0.00184	0.0493

Table S3.3a: Average observed rate constants, k_{obs}, s^{-1}, for substitution of chloride from **CH_3PhisoqPtCl** by thiourea nucleophiles, T = 298 K, I = 0.1 M ($LiSO_3CF_3$).

TU (λ = 363 nm)		**DMTU**(λ = 363 nm)		**TMTU** (λ = 386 nm)	
Conc., M	k_{obs}, s^{-1}	Conc., M	k_{obs}, s^{-1}	Conc., M	k_{obs}, s^{-1}
2.679×10^{-4}	0.1094	2.859×10^{-4}	0.03674	5.5×10^{-4}	0. 01532
5.358×10^{-4}	0.2054	5.718×10^{-4}	0.07474	1.0×10^{-3}	0.03022
8.037×10^{-4}	0.3053	8.577×10^{-4}	0.01100	1.5×10^{-3}	0.04530
1.070×10^{-3}	0.4003	1.140×10^{-3}	0.14510	2.0×10^{-3}	0.06022
1.340×10^{-3}	0.5003	1.430×10^{-3}	0.18010	2.5×10^{-3}	0.07541

Table S3.3b: Average observed rate constants, k_{obs}, s^{-1}, for substitution of chloride from **CH_3PhisoqPtCl** by ionic nucleophiles, T = 298 K, I = 0.1 M ($LiSO_3CF_3$).

I^- (λ = 448 nm)		**SCN^-**(λ = 412 nm)		**Br^-** (λ = 412 nm)	
Conc., M	k_{obs}, s^{-1}	Conc., M	k_{obs}, s^{-1}	Conc., M	k_{obs}, s^{-1}
0.00101	0.07716	0.00101	0.00680	0.00200	0. 00740
0.00127	0.10554	0.00127	0.01085	0.00250	0.01069
0.00152	0.12108	0.00152	0.01463	0.00300	0.01638
0.00202	0.16142	0.00202	0.01872	0.00375	-
0.00253	0.20340	0.00253	0.02330	0.00500	0.02508

Table S3.4a: Temperature dependence of k_2, M^{-1} s^{-1}, for substitution of chloride from **pyPhenPtCl** by thiourea nucleophiles at 30-fold excess of [metal complex], T = 298 K, I = 0.1 M ($LiSO_3CF_3$).

TU (λ = 308 nm)		**DMTU** (λ = 313 nm)		**TMTU** (λ = 386 nm)	
(1/T), K^{-1}	ln(k_2/T)	(1/T), K^{-1}	ln(k_2/T)	(1/T), K^{-1}	ln(k_2/T)
0.00347	-4.5802	0.00347	-5.6746	0.00347	-7.5524
0.00341	-4.2442	0.00341	-5.3850	0.00341	-7.2611
0.00335	-4.0327	0.00335	-5.1589	0.00335	-6.9626
0.00330	-3.7067	0.00330	-4.8711	0.00330	-6.7590
0.00325	-3.4966	0.00325	-4.6417	0.00325	-6.5508

Table S3.4b: Temperature dependence of k_2, M^{-1} s^{-1}, for substitution of chloride from **pyPhenPtCl** by ionic nucleophiles at 30-fold excess of [metal complex], T = 298 K, I = 0.1 M ($LiSO_3CF_3$).

I^- (λ = 309 nm)		**SCN^-**(λ = 415 nm)		**Br^-** (λ = 302 nm)	
(1/T), K^{-1}	ln(k_2/T)	(1/T), K^{-1}	ln(k_2/T)	(1/T), K^{-1}	ln(k_2/T)
0.00347	-6.0403	0.00347	-5.8971	0.00347	-9.9127
0.00341	-	0.00341	-5.5947	0.00341	-9.3691
0.00335	-5.7060	0.00335	-5.2524	0.00335	-8.7501
0.00330	-5.0057	0.00330	-5.0685	0.00330	-8.6466
0.00325	-4.6598	0.00325	-4.8690	0.00325	-8.2166

Table S3.5a: Temperature dependence of k_2, M^{-1} s^{-1}, for substitution of chloride from **CH_3PhisoqPtCl** by thiourea nucleophiles at 30-fold excess of [metal complex], T = 298 K, I = 0.1 M ($LiSO_3CF_3$).

TU (λ = 363 nm)		**DMTU**(λ = 363 nm)		**TMTU** (λ = 386 nm)	
(1/T), K^{-1}	ln(k_2/T)	(1/T), K^{-1}	ln(k_2/T)	(1/T), K^{-1}	ln(k_2/T)
0.00347	-7.4827	0.00347	-8.2511	0.00347	-9.3656
0.00341	-7.1918	0.00341	-7.9115	0.00341	-9.1025
0.00335	-6.8836	0.00335	-7.5483	0.00335	-8.7915
0.00330	-6.6624	0.00330	-7.1682	0.00330	-8.5540
0.00325	-6.4338	0.00325	-6.8974	0.00325	-8.2937

Table S3.5b: Temperature dependence of k_2, M^{-1} s^{-1}, for substitution of chloride from **CH_3PhisoqPtCl** by ionic nucleophiles at 30-fold excess of [metal complex], T = 298 K, I = 0.1 M ($LiSO_3CF_3$).

I^- (λ = 448 nm)		**SCN^-** (λ = 423 nm)		**Br^-** (λ = 412 nm)	
(1/T), K^{-1}	ln(k_2/T)	(1/T), K^{-1}	ln(k_2/T)	(1/T), K^{-1}	ln(k_2/T)
0.00347	-8.4525	0.00347	-11.4029	0.00347	-11.567
0.00341	-8.1633	0.00341	-11.0728	0.00341	-11.157
0.00335	-7.8082	0.00335	-10.3975	0.00335	-10.745
0.00330	-7.5678	0.00330	-10.1735	0.00330	-10.385
0.00325	-7.2753	0.00325	-9.8964	0.00325	-9.997

Table S3.6: Average observed rate constants, k_{obs} [a], at varied temperatures for the reactions of **CH_3PhisoqPtCl** (0.054 mM) with a series of different nucleophiles whilst maintaining nucleophile concentrations at ≈ 30x [metal complex].

	Observed rate constant/ k_{obs} s^{-1}					
T (K)	TU	DMTU	TMTU	I^-	SCN^-	Br^-
288.15	0.3196	0.07512	0.0261	0.0615	0.00404	0.00273
293.15	0.4200	0.1074	0.0323	0.0835	0.00455	0.00400
298.15	0.5578	0.1447	0.0450	0.1211	0.00909	0.00649
303.15	0.7950	0.2343	0.0566	0.1566	0.01157	0.0133
308.15	1.1067	0.3084	0.0771	0.2133	0.01551	-

[a] Taken as an average of at least five kinetic runs with a SD between 0.1 and 2%.

Table S3.7: Average observed rate constants, k_{obs} [a], at varied temperatures for the reactions of **pyPhenPtCl** (0.054 mM) with a series of different nucleophiles whilst maintaining nucleophile concentrations at ≈ 30x [metal complex].

			Observed rate constant/ k_{obs} s^{-1}			
T (K)	TU	T (K)	TU	T (K)	TU	T (K)
288.15	2.863	0.9886	0.1534	0.7140	0.7890	0.0143
293.15	4.350	1.3429	0.2095	1.0408	1.0862	0.0250
298.15	5.278	1.6759	0.2748	1.3496	1.4857	0.0324
303.15	8.916	2.3807	0.3459	2.0383	1.9349	0.0533
308.15	12.723	3.1928	0.4346	2.9314	2.4492	0.8470

[a] Taken as an average of at least five kinetic runs with a SD between 0.1 and 2%.

Table S3.8: DFT calculated electrostatic potential surfaces (EPS) of the chloro Pt(II) complexes with tridentate ligands. The blue region indicates the most electropositive areas and the red area indicates the most electronegative areas.

Complex	**CH_3PhPtCl**	**CH_3PhisoqPtCl**	**PtCl**	**pyPhenPtCl**
EPS	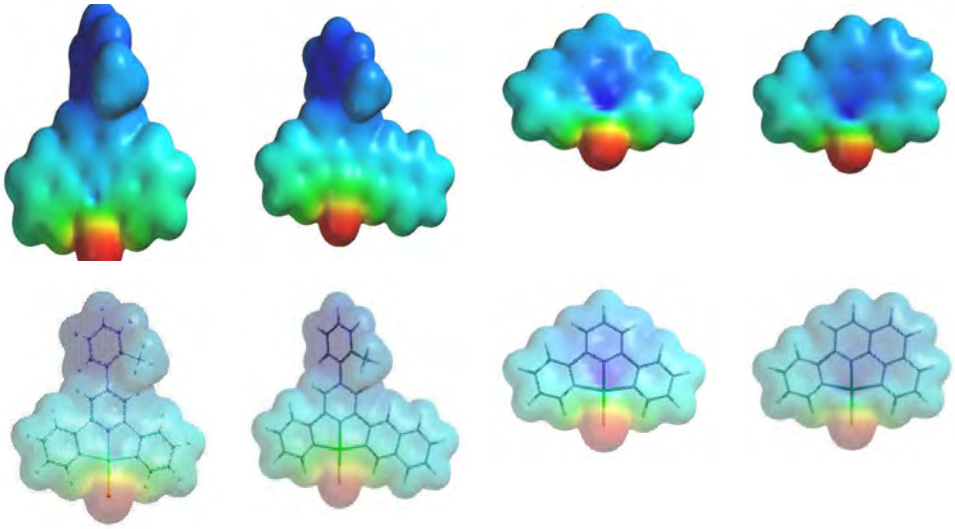			

Table of Contents-4

List of Figures

List of Tables

CHAPTER 4

Substitution of Aqua Ligands in Pyrazine-Bridged Pt(II) Dinuclear Complexes: Influence of the Ancillary Substituents.

4.0 Abstract

The rate of substitution of coordinated water molecules by three nucleophiles of different steric demand, *viz*. TU, DMTU and TMTU for the complexes: [*cis*-{$PtOH_2(NH_3)_2$}$_2$-μ-pzn]$(ClO_4)_2$ (**pzn**), [*cis*-{$PtOH_2(NH_3)_2$}$_2$-μ-2,3pzn]$(ClO_4)_2$ (**2,3pzn**), [*cis*-{$PtOH_2(NH_3)_2$}$_2$-μ-2,5pzn]$(ClO_4)_2$ (**2,5pzn**) and [*cis*-{$PtOH_2(NH_3)_2$}$_2$-μ-2,6pzn]$(ClO_4)_2$ (**2,6pzn**) was investigated under *pseudo* first-order conditions as a function of concentration and temperature by stopped-flow and UV-Visible spectrophotometry . The reaction proceeded in three consecutive steps; each step follows first order kinetics with respect to each complex and nucleophile. The *pseudo* first-order rate constants, $k_{obs1/2/3}$ for sequential substitution of the aqua ligands and subsequent displacement of the linker obeyed the rate law: $k_{obs1/2/3} = k_{1/2/3}$[nucleophile].

The order reactivity of the complexes is **2,3pzn** ≈ **2,5pzn** < **2,6pzn** < **pzn**. The difference in reactivity is due to electronic and steric effects at the Pt(II) centre. An increase in steric crowding at the Pt(II) centre imposed by the methyl groups decelerates the lability of the aqua ligands in the dinuclear complexes by increasing the negative charge and obstructs the entry of the incoming nucleophile from above or below the reaction metal centre. The ^{1}H and ^{195}Pt NMR spectroscopic results confirmed the observed dissociation of the bridging ligand from the metal centre of the *cis*-dinuclear complexes, caused by thiourea and its derivatives in the third step.

The order of reactivity of the nucleophiles is based on the order of steric hindrance, which is TU > DMTU > TMTU. The low enthalpy of activation $\Delta H^{\neq}$ and large negative entropy of activation $\Delta S^{\neq}$ values support an associative mode of activation for both the aqua ligand substitution reactions and the displacement of the linker.

4.1 Introduction

Platinum compounds play an important role in the treatment of many cancers[1-4], as well as nucleic acid probes[5, 6] and DNA molecular light switches.[7] It is estimated that 50-70 % of cancer patients are treated with a platinum drug.[8] The complex ***cis*-[$PtCl_2(NH_3)_2$]**, cisplatin, remains the most widely used anticancer drug against ovarian, testicular and non-small cell lung cancers.[1-4] Driven by the impressive success of cisplatin and despite its limited spectrum of activity due to the development of high toxicity and cross-resistance in many cell lines,[8,9] thousands of new platinum containing compounds have been developed and screened for anti-cancer activity. Only a small fraction has shown sufficient promise during pre-clinical evaluation.[10]

Recently, many multinuclear Pt(II) complexes that incorporate flexible diamine chains or rigid aromatic bridging ligands such as azoles and diazine molecules[10,11] have been synthesized and tested with the aim of obtaining better anti-tumour activity through increased solubility and lower toxic effects. These di-and tri-nuclear Pt(II) complexes are well suited for the anti-tumour activity compared to their mononuclear analogues because they are ionic, more soluble and exhibit a high degree of cellular uptake. Secondly, they possess Pt---Pt distances that are flexible enough to offer minimal distortion of the DNA molecule. In addition their 1,3- and 1,4-GG interstrand cross-links persist longer than the intrastrand cross-links and are less susceptible to repair.[12]

A number of ligand substitution reactions involving dinuclear Pt(II) complexes have been reported in literature.[12-17] Studies have shown that the reactivity of the complexes is dependent on the Pt---Pt distance separating the centres.[18] The electronic and steric properties of the complexes as well as the symmetry of the complexes have been put forward to explain reactivity at the metal centres. Kinetic studies have also shown that some dinuclear complexes undergo ring opening of their chelate during the substitution reactions involving strong *trans*-influencing donor ligands such as TU, PPh_3 and I^-.[15,16,18,19] Despite this, there is evidence that complexes such as [{*cis*-$PtCl(NH_3)_2$-μ-y]$^{n+}$ (where y = $NH_2(CH_2)_6NH_2$),[20] which has a *cis*-geometry at the Pt(II) centre does not undergo degradation by strong sulphur donor nucleophiles. However, some studies have demonstrated the release of the bridge in complexes of similar geometry following

coordination of sulphur nucleophiles.[21] Vasak *et al*.[22] have also shown that whereas all ligands in *cis*-Pt(II)-based compounds were replaced by cysteine and thiolates, *trans*-Pt(II)-compounds retained their N-donor ligands; thereby remaining in a potentially active form. Factors that mediate these reaction processes remain least understood. It would, therefore, be interesting and useful to study the kinetics of the pyrazine-bridged dinuclear Pt(II) complexes with a common *cis* geometry, to understand the mode of *in vivo* activities of these complexes with sulphur-donor ligands.

To gain further insight into the influence of the rigid bridging ligand on the reactivity of the platinum(II) centres in dinuclear complexes, a series of bridged dinuclear platinum(II) complexes of the type, [*cis*-{$Pt(H_2O)(NH_3)_2$}$_2$-μ-pzn]$^{4+}$ (where pzn = pyrazine), was investigated structures of the complexes are given in Figure 4.1).

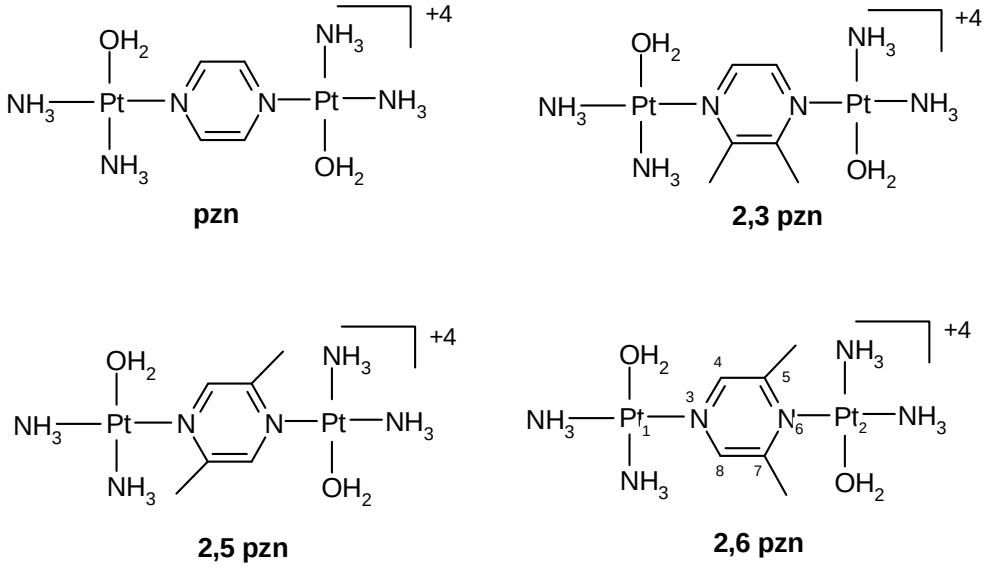

Figure 4.1: Structures of the investigated dinuclear Pt(II) complexes. The numbering scheme employed for pK_{a1} and pK_{a2}, the NBO charges, bond length and bond angles for the complexes is shown on the structure of **2,6pzn**.

Isomeric dimethylpyrazine bridging ligands were used in this study because by varying the position of the methyl groups on the pyrazine ring, the basic strength and σ-donor properties of the tertiary amine (sp^2) N-atom coordinated to the Pt(II) centre is expected to change. This would affect the basicity of the whole complex, especially in the

cis geometry, leading to dramatic changes in the substitution of the aqua ligands. At the same time, the bulky methyl substituents would introduce steric hindrance on the *cis*-Pt(II) centre. Therefore, the variation of the substituents on the pyrazine-bridge enabled a systematic study of the thermodynamic (pK_a, where coordinated water was deprotonated) and kinetic properties of the Pt(II) centres.

4.2 Experimental

4.2.1 Chemicals and Reagents

Pyrazine (99%), 2,3-dimethylpyrazine (99%), 2,5-dimethylpyrazine (99%), 2,6-dimethylpyrazine (99%), †$NaClO_4.H_2O$ (98%), and $HClO_4$ (70%) were obtained from Aldrich and were used without further purification. $AgClO_4$ (99.98%, Aldrich) was stored under nitrogen and used as supplied. *Cis-(*$PtCl_2(NH_3)_2$ (99%) was purchased from Strem chemicals. The nucleophiles §thiourea (TU, 99%), *N*,*N*-dimethyl-2-thiourea (DMTU, 99%), *N*,*N*,*N*,*N*-tetramethyl-2-thiourea (TMTU, 98%) used in the kinetic measurements were obtained from Aldrich.

Stock solutions of the nucleophiles were prepared, shortly before use, by dissolving known amounts of the nucleophiles in 0.1M $NaClO_4/HClO_4$ aqueous solution of constant ionic strength. Since it is well-known that the perchlorate ion, (ClO_4^-), does not coordinate to Pt(II),[23] its presence in aqueous solution would not interfere with the kinetic measurements. Ultrapure water (Modulab Systems) was used in all experiments. All other reagents were of analytical grade quality and were used without further purification.

Caution! †Perchloric acid and salts are potentially explosive, particularly at high temperatures and must be handled with caution and in small amounts.

§Thiourea and its substituted derivatives are suspected carcinogens and the necessary safety measures must be adhered to when handling these reagents.

4.2.2 Synthesis of compounds

A total of four dinuclear Pt(II) complexes, namely [*cis*-{PtCl(NH_3)$_2$}$_2$-μ-pzn](ClO_4)$_2$ (**pzn**) (pzn = pyrazine), [*cis*-{PtCl(NH_3)$_2$}$_2$-μ-2,3 pzn](ClO_4)$_2$ (**2,3pzn**) (2,3pzn = 2,3-dimethylpyrazine), [*cis*-{PtCl(NH_3)$_2$}$_2$-μ-2,5pzn](ClO_4)$_2$ (**2,5pzn**) (2,5pzn = 2,5-dimethylpyrazine), and [*cis*-{PtCl(NH_3)$_2$}$_2$-μ-2,6pzn]Cl_2 (**2,6pzn**) (2,6pzn = 2,6-dimethylpyrazine) were synthesized starting from the precursor compound [*cis*-{PtCl(NH_3)$_2$(DMF)}]ClO_4 using $AgClO_4$ following the procedure reported in literature.[24, 25]

4.2.3 Preparation of platinum complexes

cis-[{PtCl(NH_3)$_2$}$_2$–μ–pzn](ClO_4)$_2$(pzn)

The *cis*-[{PtCl(NH_3)$_2$}$_2$-μ-pzn](ClO_4)$_2$ (**pzn**) was prepared following a modified procedure to that used previously for similar compounds as illustrated in Scheme 4.1.[26]

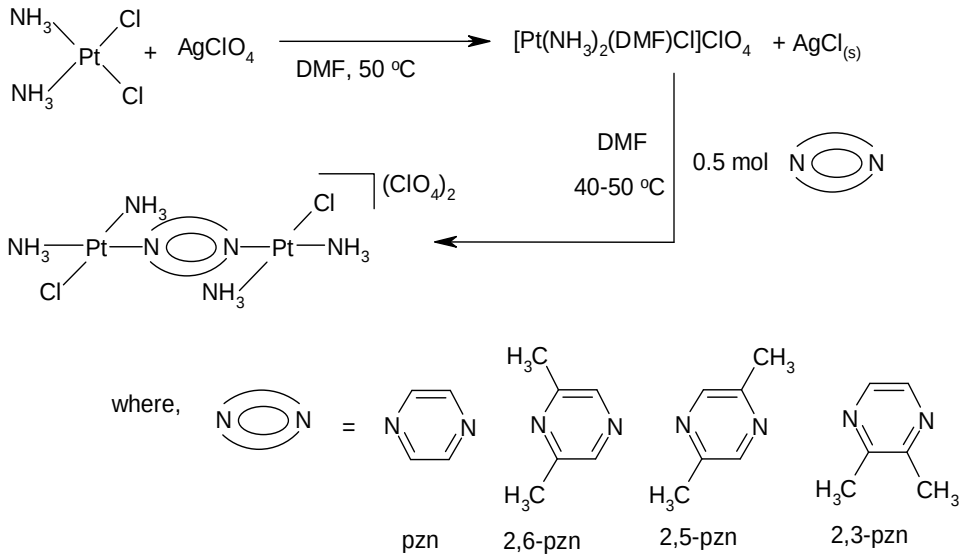

Scheme 4.1 Synthetic route for the complexes **pzn**, **2,3pzn**, **2,5pzn** and **2,6pzn**

To 50 ml of stirred solution of (1.039 mmol) [{cis-PtCl (NH_3)$_2$(DMF)]ClO_4 was added in the dark (78.2 mg, 0.976 mmol) of pyrazine ligand (pzn) at room temperature. The

ligand was added to the [{*cis*-PtCl(NH_3)$_2$(DMF)]ClO_4 solution slowly, in order to have constantly excess of [{cis-PtCl(NH_3)$_2$(DMF)]ClO_4 in the solution and stirred for 12 h and after cooling at 5-10 °C for 1h, was filtered to remove any undissolved material. The solvent was evaporated under vacuum. The residue was washed with diethyl ether, re-dissolved in warm water (40-50 °C) and the water evaporated under vacuum to dryness. The light yellow solid was washed with a minimal amount of ethanol followed by concomitant amounts of diethyl ether and dried over potassium hydroxide (KOH) in a desiccator. This process was repeated for **2,3pzn** and **2,5pzn**, using stoichiometric amounts (0.279 mmol, 30.21 mg 2,3pzn; and 0.289 mmol, 31.22 mg 2,5pzn, respectively) of the appropriate nitrogen ligand.

***cis*- [{PtCl(NH_3)$_2$}$_2$–μ–2, 6 pzn]Cl_2 (2,6pzn)**

Literature procedure was used for the synthesis of the platinum complex, **[{cis–PtCl(NH_3)$_2$}$_2$–μ–2,6pzn]Cl_2 (2,6pzn)**.[25] A solution (5 mL) of 2,6pzn ligand (18.3 mg, 0.170 mmol) in water was added to a solution (10 mL) of **cis–[Pt(NH_3)$_2$$Cl_2$]** (101.5 mg, 0.338 mmol) in water. The mixture was stirred for 3 days at 40 °C in the dark, filtered to remove any unreacted material and concentrated to 1-2 mL under vacuum. The compound formed, **[{*cis*–Pt(NH_3)$_2$Cl}$_2$–μ–2,6–pzn]Cl_2**, was filtered off, washed with a small amount of ethanol, diethyl ether and dried under vacuum.

Their purity was confirmed by micro-elemental analysis, infrared (IR), ^{1}H and ^{195}Pt NMR. The IR spectra of all the complexes exhibited common characteristic peaks in the range 326-400 cm^{-1} (weak) for Pt–Cl and 1090-1100 cm^{-1} (broad, strong) for Cl–O (perchlorate counter ion) vibration stretches, respectively. The results obtained from the analysis of the complexes are given below.

(**pzn**) Yield: 382.8 mg (45.5%). ^{1}H NMR (500 MHz, D_2O), δ /ppm: 8.99, s (4H). ^{195}Pt NMR (107 MHz, D_2O) δ/ppm: -2302.2. IR (KBr, 4000-300 cm^{-1}): 3305, 3224, 3107 (N–H stretch); 1090-1100 (perchlorate counter ion); 340 (Pt–Cl stretch). Anal. Calc. for $C_4H_{16}N_6Cl_4O_8Pt_2$: H, 2.00; C, 5.94; N, 10.40; Found H, 2.23; C, 5.50; N, 9.90 %.

(**2,3pzn**) Yield: 137.2 mg (58.8 %). ^{1}H NMR (500 MHz, D_2O), δ /ppm: 8.80 (d, 2H); 3.2 (s. 6H). ^{195}Pt NMR (107 MHz, D_2O) δ /ppm: -2312.2. IR (KBr, 4000-300 cm^{-1}): 3303, 3227, 3057 (N–H stretch); 1090-1100 (Perchlorate counter ion); 338 (Pt–Cl stretch). TOF MS/ES^+. (m/z, M^{2+}): 318 ($C_3H_{10}N_3PtCl$ species). Anal. Calc. for $C_6H_{20}N_6Cl_4O_8Pt_2$: H, 2.39; C, 8.61; N, 10.05; Found H, 2.17; C, 8.23; N, 10.28%.

(**2,5pzn**) Yield: 179.9 mg (74.4%). ^{1}H NMR (500 MHz, D_2O) δ / ppm: 9.05 (s, 2H); 3.04 (s, 6H). ^{195}Pt NMR (107 MHz, D_2O) δ / ppm: -2344.34. IR (KBr, 4000-300 cm^{-1}): 3300, 3228, 3057 (N–H stretch); 1090-1100 (perchlorate counter ion); 338 (Pt–Cl stretch). TOF MS/ES^+. (m/z, M^{2+}): 318 ($C_3H_{10}N_3PtCl$ species). Anal. Calc. for $C_6H_{20}N_6Cl_4O_8Pt_2$: H, 2.39; C, 8.61; N, 10.05; Found H, 2.21; C, 8.11; N, 9.87%.

(**2,6pzn**) Yield: 103.0mg (44.8%). ^{1}H NMR (500 MHz, D_2O) δ /ppm: 8.95 (s, 2H); 3.05 (s, 6H). ^{195}Pt NMR (107 MHz, D_2O) δ /ppm: -2320.36, -2461.82. IR (KBr, 4000-300 cm^{-1}): 3285, 3207, 3075 (N–H stretch); 1090-1100 cm^{-1} (perchlorate counter ion); 326 (Pt–Cl stretch). TOF MS/ES^+. (m/z, M^{2+}): 318 ($C_3H_{10}N_3PtCl$ species). Anal. Calc. for $C_6H_{20}N_6Cl_4Pt_2$: H, 2.82; C, 10.17; N, 11.80; Found H, 2.78; C, 9.99; N, 11.27%.

4.2.4 Preparation of the dinuclear Pt(II) diaqua aqueous complexes

The solutions of the diaqua complexes **pzn**, **2,3pzn**, **2,5pzn** and **2,6pzn** were prepared as described in the literature,[26] by addition of appropriate amount of $AgClO_4$ to each of corresponding chloro complexes. The chloro Pt(II) complex and $AgClO_4$ (1: 1.98 molar ratio) were dissolved in 0.1M $HClO_4$ and the mixture stirred vigorously at 50 °C for 24 h in the dark. The precipitated AgCl was removed by filtration through a 0.45 μm nylon membrane using Millipore filtration unit. The filtrate was diluted with 0.1 M $HClO_4$ solution to give the required complex concentrations which were 3.52 x 10^{-4}, 1.0 x 10^{-3}, 1.06 x 10^{-3}, and 1.0 x 10^{-3} M for **2,6pzn**, **2,3pzn**, **2,5pzn** and **pzn**, respectively.

4.2.5 Instrumentation and Physical measurements

Elemental analyses of the complexes were performed on a Carlo Erba Elemental Analyzer 1106. The infrared spectra in the range 4000-300 cm^{-1} were recorded in the solid state (KBr pellets) using Perkin Elmer Spectrum One FT-IR spectrometer. The NMR

spectra were measured in and referenced to the solvent (D_2O) signal at 30 °C, on a Bruker Avance DPX 500 spectrometer (^{1}H, 500 MHz) and (^{195}Pt, 107.5 MHz), respectively, to confirm the purity and identity of the complexes as well as to follow the reaction kinetics of the dinuclear complex **pzn** containing two Pt–Cl bonds with TU. The ^{195}Pt chemical shifts were referenced externally to $K_2[PtCl_6]$. Both ^{1}H and ^{195}Pt NMR are effective methods for the determination of the coordination details at the metal centre because their chemical shifts are usually influenced by the solvent, temperature and the coordinated donor atoms.[27] UV-Visible absorption spectra for the determination of pK_a values and kinetic measurements of slow reactions were recorded on a Varian Cary 100 Bio UV-Visible spectrophotometer equipped with a thermostated cell holder. The pH of the aqueous solutions of the complexes were measured using a Jenway 4330 Conductivity/pH meter equipped with a Micro 4.5 diameter glass electrode. The electrode was calibrated at 25 °C using standard buffer solutions of pH 4.0, 7.0 and 10.0 (Merck). The pH electrode was filled with 3.0 M NaCl instead of KCl to prevent precipitation of $KClO_4$ during use. An Applied Photophysics SX 18 MV (v4.33) stopped-flow reaction analyzer coupled to an online data acquisition system was used for fast reactions. The temperature of the instruments was controlled to within ± 0.1°C for all the measurements. Mass spectra were obtained on Hewlett Packard LC-MS using electron impact (EI) ionization. Analyses of the pH and time-dependent kinetic spectral data were graphically performed using Origin 5.0® [28]software package.

4.2.6 Computational details

DFT calculations were performed on all the complexes so as to provide an insight into their observed kinetic results. Ground-state electronic structures were optimized using density functional theory (DFT) method on Spartan `04 for Windows® quantum chemical package. The functional used throughout this study was the B3LYP,[29] a non-local hybrid exchange functional defined by Becke`s three parameter equation, utilizing LACVP†** (Los Alamos Core Valence Potentials) [30] *pseudo* potential basis set. The ground-state geometries of the complexes were modelled as cations of total charge of +4 in the gas phase.

4.2.7 Determination of pK_a values of the diaqua complexes

Spectrophotometric pH titrations were performed using NaOH as the base, in pH range 2-10. A large volume (200.0 mL) of each of the complex solutions was used during the titration to avoid absorbance corrections due to dilution. Solid NaOH pellets was added stepwise in the pH range 2-3, while micropipette dropwise additions of saturated, 1.0 M and 0.1 M NaOH or conc. $HClO_4$ (for reversibility of the pH) were added to the solution until the desired pH was attained prior to withdrawal of 2.0 mL aliquots from the solution for pH measurement. The 2.0 mL aliquots were discarded after each measurement to avoid *in situ* contamination of the complex solution by the chloride released from the pH electrode. The concentrations of the Pt(II) complexes used during these titrations ranged from 3.52×10^{-5} to 1.06×10^{-4} M.

4.2.8 Kinetic measurements

All the kinetic measurements were performed under *pseudo* first-order conditions in order to force the reactions to go to completion. The desired concentration of the nucleophile was achieved by using at least a 20-fold (1:2 complex formation) excess of the nucleophile over the dinuclear metal complex. This afforded at least a 10-fold excess of the nucleophile at each centre. The kinetic reactions were studied at pH *ca*. 2.0 to guarantee the presence of only the diaqua form of the complexes. The suitable wavelengths at which the kinetic measurements could be followed were established spectrophotometrically by monitoring the change in absorbance of the mixture of the metal complex and the nucleophile as a function of time and are summarised in Table **S4.1**, (appendix). The temperature dependence was studied at five different temperatures ranging from 15 to 35 °C at intervals of 5 °C.

4.3 Results

The role of the pyrazine as a bridging ligand and the influence of steric and electronic effects of the methyl substituents attached to it, on the kinetics and thermodynamic properties of each of the Pt(II) centres of the dinuclear platinum(II) complexes were investigated using the four complexes shown in Figure 4.1.

4.3.1 DFT calculated Optimized Structures

The representative geometry- optimized structures for the complexes and the extract of the calculated data are shown in Figure 4.2 and Table 4.1, respectively. The data in Table 4.1 shows that the calculated geometries around each of the Pt(II) centres exhibit a slightly distorted square planar arrangement. The metrics agrees well with those from previously described crystallographic data published in literature [24,25] for the complexes *cis*-[{$Pt(NH_3)_2Cl$}$_2$-μ-pzn]$(ClO_4)_2$/or $(NO_3)_2$. As the pyrazine ligand is characterised by π-acceptor ability. The calculations, on the other hand, show that the pyrazine ligand and its methyl-substituted analogues all lie perpendicular to the Pt(II) centre, which means that "electronic communication" between the Pt(II) centres through π-backbonding is absent.

Complex	Structure	HOMO	LUMO
pzn D_{2h}	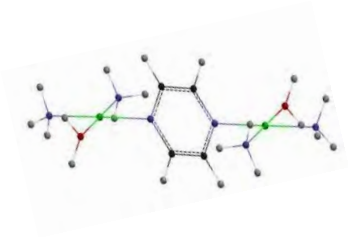	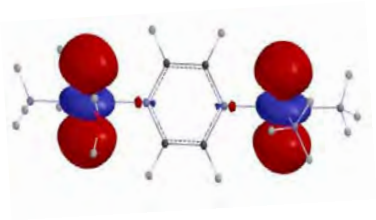	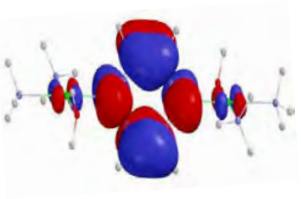
2,6pzn C_{2h}	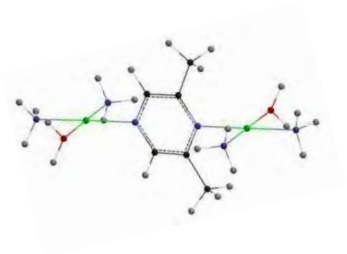		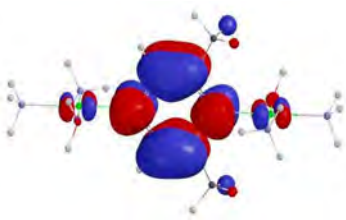
2,3pzn C_{2v}	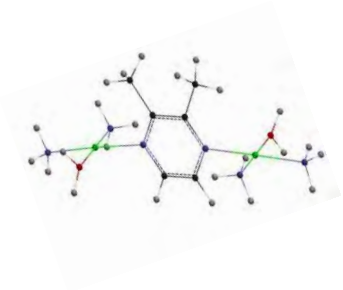	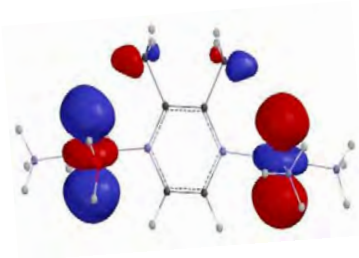	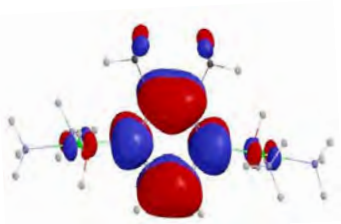
2,5pzn C_{2v}	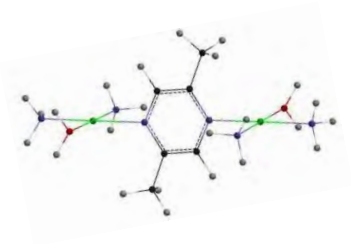	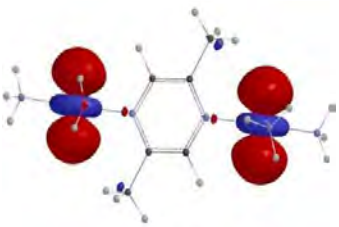	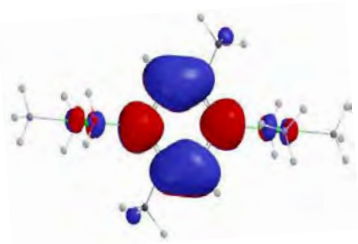

Figure 4.2: Density functional theoretical (DFT) minimum structures, HOMO and LUMO frontier molecular orbitals for dinuclear Pt(II) complexes.

Table 4.1: A summary of the DFT calculated data for the investigated **[{*cis*–$Pt(OH_2)(NH_3)_2$}$_2$–μ–pzn]$^{4+}$** complexes at B3LYP/LACVP ** level of theory

NBO charges *	**pzn**	**2,3pzn**	**2,5pzn**	**2,6pzn**
Pt 1	1.2192	1.2173	1.2150	1.2167
Pt 2	1.2192	1.2171	1.2149	1.2155
Pt_1-O (H_2O)	-1.0050	-1.0015	-1.0011	-1.0023
Pt_2-O (H_2O)	-1.0050	-1.0018	-1.0001	-0.9994
Bond length (Å)				
Pt_1-$N3_{(pyrazine)}$	2.131	2.138	2.131	2.129
Pt_2-$N6_{(pyrazine)}$	2.131	2.138	2.129	2.148
Pt_1-OH_2	2.129	2.130	2.130	2.123
Pt_2-OH_2	2.129	2.131	2.135	2.134
Pt_1-NH_3(*trans* to H_2O)	2.072	2.071	2.070	2.068
Pt_2-NH_3(*trans* to H_2O)	2.072	2.071	2.069	2.071
Bond angles (°)				
$N3_{(pyrazine)}$-Pt_1-OH_2	86.61	86.84	86.83	87.21
$N6_{(pyrazine)}$-Pt_2- OH_2	86.61	86.84	86.86	93.47
NH_3-Pt_1-OH_2	90.80	90.88	91.05	90.48
NH_3-Pt_2-OH_2	90.81	90.84	90.75	84.10
OH_2-Pt_1-NH_3(*trans* to H_2O)	179.96	179.78	179.02	179.22
OH_2-Pt_2-NH_3(*trans* to H_2O)	179.98	179.29	179.46	174.33
NH_3-Pt ½-$N2/6_{(pyrazine)}$	177.41	176.98	177.63	177.65
MOs Energies/ (eV)				
HOMO	-19.97	-19.66	-19.68	-19.65
LUMO	-15.75	-15.05	-15.20	-15.20
ΔE/(eV)	4.22	4.61	4.48	4.45

In addition, in all the complexes the HOMO is concentrated above and below the metal centres, primarily in the d_z^2 orbital whilst the LUMO is centred on the bridging ligand (Figure 4.2). The HOMO-LUMO energy gap does show an increase with the introduction

of the σ-electron donating methyl groups[31] that could be associated with a decrease in the electrophilicity of the platinum atom, but is little influenced by the position to which they are attached to the pyrazine ligand.

4.3.2 Acid-base equilibria of the diaqua complexes

The representative spectral changes recorded during the pH titration with NaOH are shown in Figure 4.3 for the diaqua **2,5pzn** complex (also Figures **S4.2 – S4.4** for the corresponding data for the **pzn**, **2,3pzn** and **2,6pzn**, appendix). The pK_a of the coordinated water molecules were determined by plotting absorbance at a specific wavelength as a function of pH. A typical example is presented as an inset in Figure 4.3.

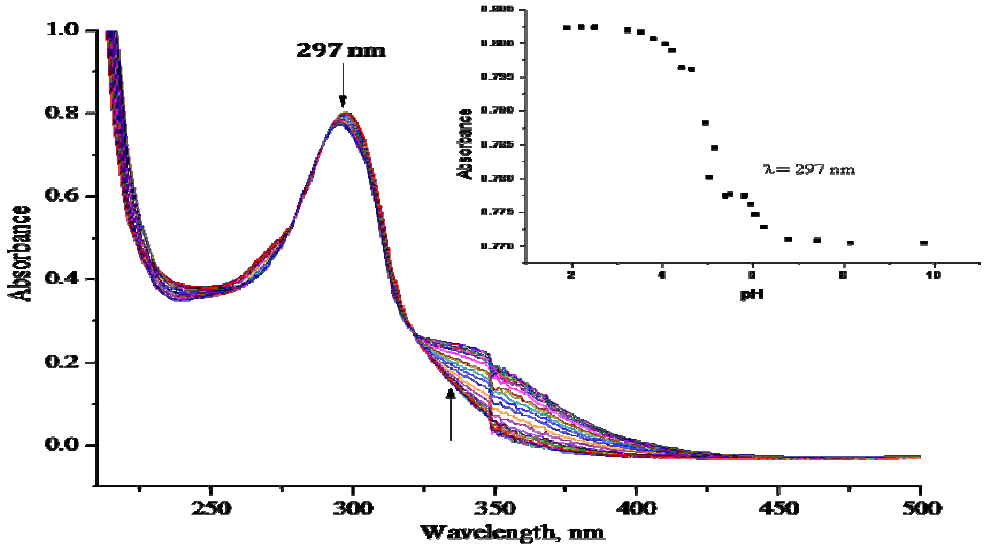

Figure 4.3: UV-Visible spectra for the titration of 0.1 mM 2,5pzn with NaOH as a function of pH in the range 1 to 10 at I = 0.1 M ($NaClO_4$) and T = 298.15 K. Inset: Plot of absorbance versus pH at 297 nm for **2,5pzn**.

All the diaqua complexes exhibited two inflection points an indication of two pH dependent deprotonation steps with equilibrium constants K_{a1} and K_{a2} as shown in reaction *Scheme* 4.1.

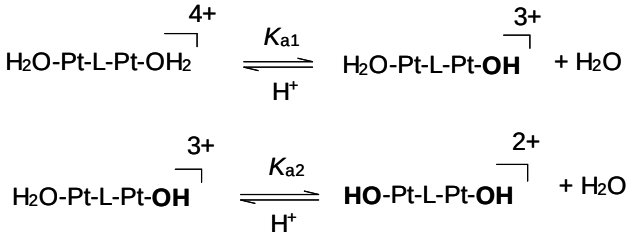

***Scheme* 4.1:** Proposed stepwise deprotonation for the pH dependence of the dinuclear Pt(II) complexes.

The resulting pK_a values for the coordinated water molecules were obtained by fitting the data, for all the dinuclear complexes, to a standard Boltzmann equation describing two pK_a values using Origin 5.0® [28] software. The data obtained are summarised in Table 4.2 and included for comparison are the pK_a values for related *trans*-complexes.[32]

Table 4.2: Summary of pK_a values for the deprotonation of platinum-bound water in the [**{*cis*–Pt$OH_2$$(NH_3)_2$}$_2$–μ–pzn**]$^{4+}$ complexes, I = 0.1 M $HClO_4$, T = 298.15 K.

	pzn	**2,3pzn**	**2,5pzn**	**2,6pzn**
pK_{a1}	3.32 ± 0.06	3.98 ± 0.02	3.96 ± 0.12	3.48 ± 0.51
	(3.59 ± 0.33)[a]	(3.66 ± 0.11)[a]	(3.68 ± 0.26)[a]	
pK_{a2}	5.64 ± 0.09	6.01 ± 0.18	6.13 ± 0.05	6.88 ± 0.04
	(4.36 ± 0.30)[a]	(4.61 ± 0.22)[a]	(4.62 ± 0.21)[a]	
ΔpK_a	2.32	2.03	2.17	3.40

[a]pK_a values for [**{*trans*–Pt$(NH_3)_2(OH_2)$}$_2$–μ–pzn**]$^{4+}$ complexes extracted from reference.[31]

Inspection of the data in Table 4.2 shows that the pK_{a1} values of the deprotonation of the first coordinated aqua molecule increase in the order **pzn** (pK_a 3.29) < **2,6pzn** (pK_a 3.48) < **2,3pzn** (pK_a 3.98) ≈ **2,5pzn** (pK_a 3.96). Also noted is that the second deprotonation of the aqua molecule from the aqua/hydroxo species to form the hydroxo/hydroxo species occurs at higher pH values than the first.

Since pK_a values have been associated with the electrophilicity of the metal centre, [33-36] it can be concluded that introduction of the methyl groups to the pyrazine moiety decreases the electrophilicity of the metal centre through σ-electron donation via the pyrazine nitrogen bound to the Pt(II) centre. The position of the methyl groups also influences the electron density on the pyrazine ligand. In cases of **2,3pzn** and **2,5pzn,** the charges are symmetrically distributed resulting in pK_a values that are approximately equal, since the methyl groups are symmetrically distributed at the *ortho* position of the pyrazine linker. However, in **2,6pzn**, the N6 being more negative than the **N3** results in Pt1 centre being slightly more positively charged compared to **Pt2**. This is seen in the ΔpK_a values (Table 4.2) for which **2,6pzn** has the biggest difference compared to the other complexes, signifying the difference in terms of electrophilicity between the two platinum centres. This is supported by the ^{195}Pt NMR which shows chemical shift signals at δ (^{195}**Pt**) = -2320.36 for **Pt1** and -2461.82 ppm for **Pt2**. These differences exist for the other complexes, but the gap is relatively constant across the other complexes. In general, the DFT calculated NBO charges in Table 4.1 are in agreement with the observed experimental data.

When the current pK_a results are compared to that of *trans*-analogues (shown in Table 4.2), the pK_a values due to the first deprotonation of the coordinated aqua ligands are similar in magnitude within the limits of experimental errors. The second pK_a values for the *cis*-complexes are less acidic, a factor that can be linked to their geometric differences. First, introduction of the methyl groups on the pyrazine moiety in the *trans*-complexes results in elongation of the Pt-OH_2 bond due to the *trans-effect,* [32] and as a consequent enhances the lability and acidity of coordinated aqua ligands of these complexes. On the other hand, the influence of the *cis* ligand is mainly to bring about change of electron density at the Pt(II) centre. This causes a decrease in the

electrophilicity and acidity of the Pt(II) centre, from which as expected would result in higher pK_a values for the *cis*-complexes. Secondly, lack of intramolecular hydrogen bonding contacts between the H_2O/OH ligands and the N-heterocyclic linker results in a slightly lower pKa_1 values in the *trans*-complexes[37] compared to some of their *cis*-counterparts. The higher pK_{a2} values observed in the second deprotonation step of the aqua ligand to form hydroxo/hydroxo species have been reported before in related studies involving dinuclear complexes,[18,21] and is a result of general reduction in the overall charge on the platinum atom on formation of the hydroxo species. Lack of intramolecular hydrogen bonding contacts between the H_2O/OH ligands and the N-heterocyclic linker results in a slightly lower pKa_1 values in the *trans*-complexes[38] compared to their *cis*-counterparts. Overall, the higher pK_a values for **2,3pzn**, **2,5pzn** and **2,6pzn** compared to **pzn** are indicative of the positive inductive effect of the methyl substituents on the pyrazine moiety that increases the electron density at the Pt(II) centre.

4.3.3 Kinetic studies on substitution reactions of the diaqua complexes

The substitution reactions of all the dinuclear complexes **pzn**, **2,3pzn, 2,5pzn** and **2,6pzn** with thiourea and its derivatives occurred in three consecutive steps as shown in Scheme 4.2. The aqua ligands in *cis*-$[H_2O\text{-Pt-L-Pt-}HO_2]^{4+}$ moiety can be synthesised with the cation being centrosymmetric, with the H_2O ligands pointing in opposite directions (*trans*-) as shown in Scheme 4.2, or *cis*-to each other. The DFT calculated HOMO-LUMO energy gaps are very similar in the two configurations. The X-rays structures of closely related compounds *cis*-$[\{(NH_3)_2PtCl\}_2\text{-}\mu\text{-pzn}](NO_3)_2/(ClO_4)_2$, in which the Cl ligand is pointing *trans*- or *cis*- to each other have been reported before.[24,25] The crystallographic data are in good agreement with the DFT calculations.

The substitutions of the aqua ligands proceed via three steps characterised by rate constants k_1, k_2 and k_3 shown in Scheme 4.2. The three substitution steps differ by a factor of at least 10 between k_1 and k_2, and at least 100 from k_2 to k_3.

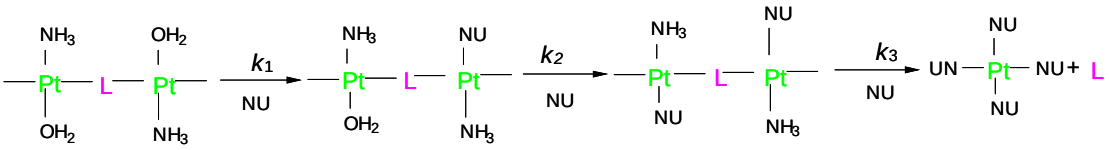

where, L = bridge = pzn, 2, 3pzn, 2, 5pzn, and 2, 6pzn
nu = nucleophile = TU, DMTU, TMTU
Charges are omitted for clarity

***Scheme* 4.2** Proposed reaction pathways for the reactions between the Pt(II) complexes and the thiourea nucleophiles at a pH of 2.0.

The first two steps represent the nucleophilic substitutions of one of the coordinated aqua ligands in each step. The reduced reactivity at the second Pt(II) centre in the second step is attributed to steric hindrance around the Pt(II) centre arising from the first substituted thiourea nucleophile and the methyl substituents on the pyrazine-bridging linker. The final step is the slowest and is ascribed to the release of the linker and ammines following the coordination of a further thiourea ligands to the Pt(II) centre in all the complexes. This was confirmed by monitoring the release of free pyrazine using the ^{1}H NMR. [39,40] The spectral arrays can be seen in Figure 4.8.

The substitution of the first aqua ligands by TU and its derivatives for all the complexes was too fast to be monitored on the UV-Visible or NMR time-scale and was followed by the stopped-flow technique. The second and third substitution steps were monitored from the UV-Visible kinetic traces. Representative plots of the time-resolved stopped-flow and UV-Visible kinetic traces for the reaction of **2,5pzn** and TU are shown in Figure 4.4. The UV-Visible kinetic traces were fitted using a double exponential function to give k_{obs} for the second and the third substitution, respectively.

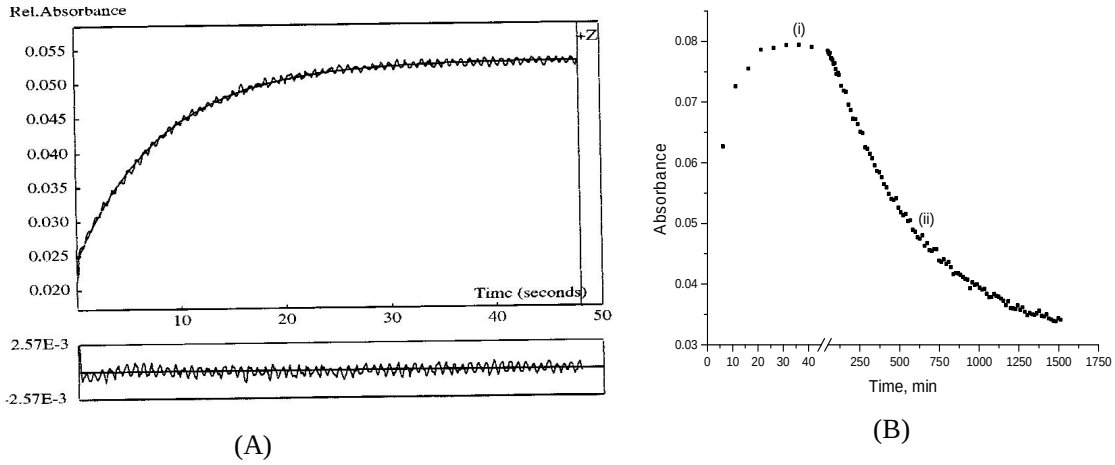

Figure 4.4: Typical three well-separated kinetic traces for the three steps reaction between **pzn** (2.14×10^{-5} M) and TU (1.00×10^{-3} M) monitored at 395 nm, T= 298.15 K, pH = 2.0, I = 0.1 M $NaClO_4$, adjusted with 0.01 M $HClO_4$. Step (A): the substitution of the first aqua ligand by stopped-flow technique. Step (B): (i) the substitution of the second aqua ligand and (II) the dissociation of the diazine linker and substitution of ancillary ligands in the third step studied by UV-Vis Spectrophotometric technique.

The observed *pseudo* first-order rate constant values ($k_{obs\ 1/2/3}$) of each step were found to vary linearly with the concentration of the nucleophiles. The plots of k_{obs} versus nucleophile concentrations were found to be linear, passing through the origin with positive slopes as shown in Figures 4.5, 4.6 and 4.7, for the **2,5pzn** complex (also Figures.**S4.5**-**S4.7**, **S4.11–S4.13** and **S4.17–S4.19** for the corresponding complexes **pzn**, **2,6pzn** and **2,3pzn**, appendix).

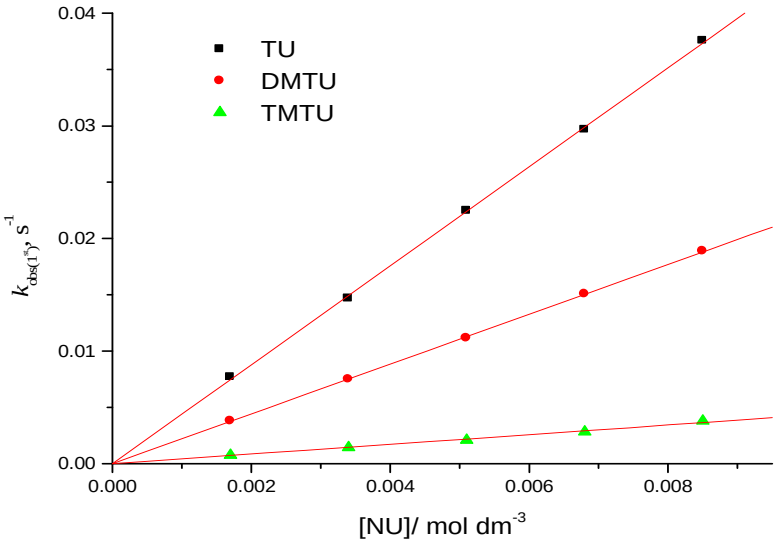

Figure 4.5: Concentration dependence of $k_{obs(1^{st})}$ for the substitution of first aqua ligand in **2,5pzn** by thiourea nucleophiles, pH = 2.0, T = 298.15 K, I = 0.10 M (0.01 M $HClO_4$, adjusted with $NaClO_4$).

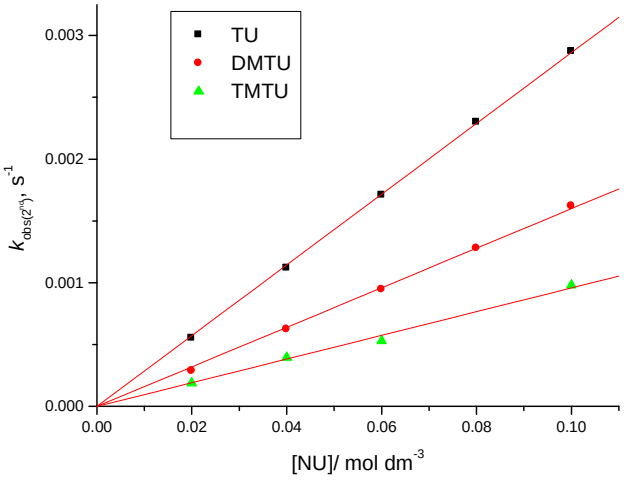

Figure 4.6: Concentration dependence of $k_{obs(2^{nd})}$ for the substitution of second aqua ligand in **2,5pzn** by thiourea nucleophiles, pH = 2.0, T = 298.15 K, I = 0.10 M (0.01 M $HClO_4$, adjusted with $NaClO_4$).

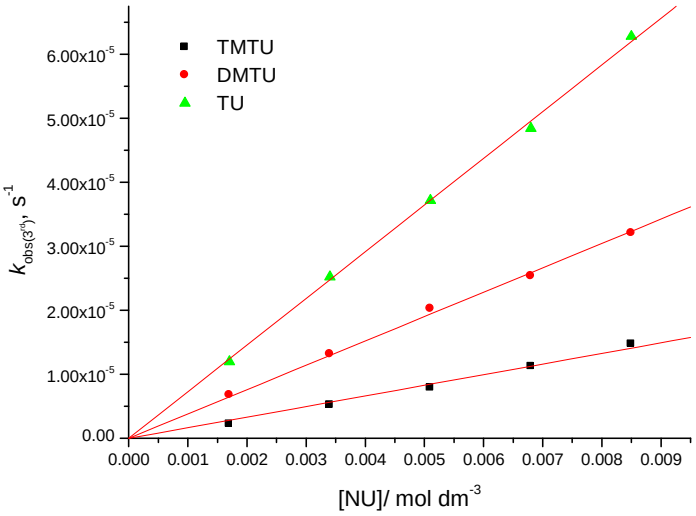

Figure 4.7: Concentration dependence of $k_{obs(3^{rd})}$ for the release of bridging ligand in **2,5pzn** by thiourea nucleophiles, pH = 2.0, T = 298.15 K, I = 0.10 M (0.01 M $HClO_4$, adjusted with $NaClO_4$).

The graphs indicate that in each step the reaction is first order with respect to nucleophile concentration. The slopes of the plot gave the second order rate constants ($k_{1/2/3}$) in each step and the values are summarized in Table 4.3.

Table 4.3: Summary of second order rate constants for the substitution of coordinated aqua ligands and dissociation of the linker by thiourea nucleophiles in the **[{*cis*-Pt(OH$_2$)(NH$_3$)$_2$–μ–pzn]$^{+4}$**complexes, I = 0.1 M (0.01 M $HClO_4$, adjusted by $NaClO_4$), T = 298.15 K

Complex	NU	k_1/M^{-1} s^{-1}	k_2/M^{-1} s^{-1}	k_3/10^{-3} M^{-1} s^{-1}
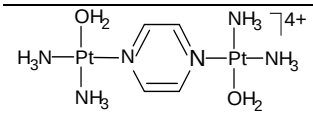 **pzn**	**TU**	42.04 ± 0.56	0.30 ± 0.01	2.86 ± 0.07
	DMTU	22.46 ± 0.23	0.15 ± 0.01	3.65 ± 0.15
	TMTU	4.02 ± 0.06	0.09 ± 0.0.003	1.54 ± 0.10
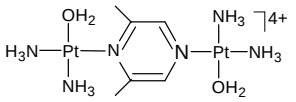 **2,6pzn**	**TU**	8.13 ± 0.03	0.06 ± 0.003	7.89 ± 0.53
	DMTU	10.50 ± 0.24	0.04 ± 0.003	6.08 ± 0.10
	TMTU	3.53 ± 0.07	0.01 ± 0.002	2.73 ± 0.10
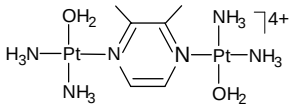 **2,3pzn**	**TU**	5.36 ± 0.10	0.19 ± 0.0	5.13 ± 0.01
	DMTU	2.14 ± 0.04	0.17 ± 0.04	1.81 ± 0.03
	TMTU	0.44 ± 0.001	0.02 ± 0.01	0.19 ± 0.003
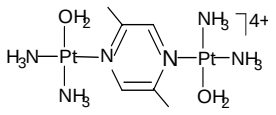 **2,5pzn**	**TU**	4.39 ± 0.19	0.19 ± 0.01	7.29 ± 0.01
	DMTU	2.21 ± 0.06	0.16 ± 0.01	3.81 ± 0.04
	TMTU	0.41 ± 0.001	0.015 ± 0.003	0.20 ± 0.02

The linear regression plots had non-zero intercept for all the complexes, suggesting that little or no reverse reaction due to solvolysis or parallel reaction had occurred and the corresponding rate law can be given by Equation 4.1.

$$k_{obs} = k_{1/2/3}\,[\mathrm{NU}] \qquad (4.1)$$

4.3.4 Kinetics with NMR

The substitution reaction of **pzn** as a chloride, *i.e.* [*cis*-{$PtCl(NH_3)_2$}$_2$-μ-pzn}]$^{+2}$ with excess TU (6 equiv.), was studied by ^{1}H and ^{195}Pt NMR spectroscopy. The ^{1}H and ^{195}Pt NMR spectra of the substitution reaction of the [{***cis*–PtCl(NH$_3$)$_2$}$_2$–μ–pzn**](**ClO$_4$**)$_2$ with TU are presented in Figures 4.8 and 4.9, respectively. The NMR spectral arrays were also used to determine the rate of dechelation of the pyrazine ligand as shown in figure 4.10.

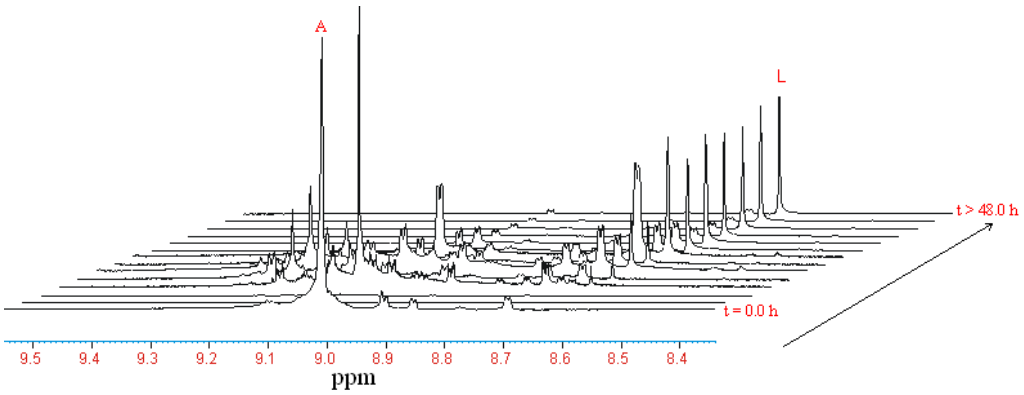

Figure 4.8: ^{1}H NMR spectra in D_2O of the aromatic region of 0.022mM [{**cis-PtCl (NH$_3$)$_2$}$_2$-μ-pzn**]$^{+2}$ reaction with TU at 30°C showing the production of the major degradation product free pyrazine (L) at δ 8.68 ppm and the starting complex (A) at δ = 9.04 ppm. These spectra are indicative of the formation of other minor transient intermediate products.

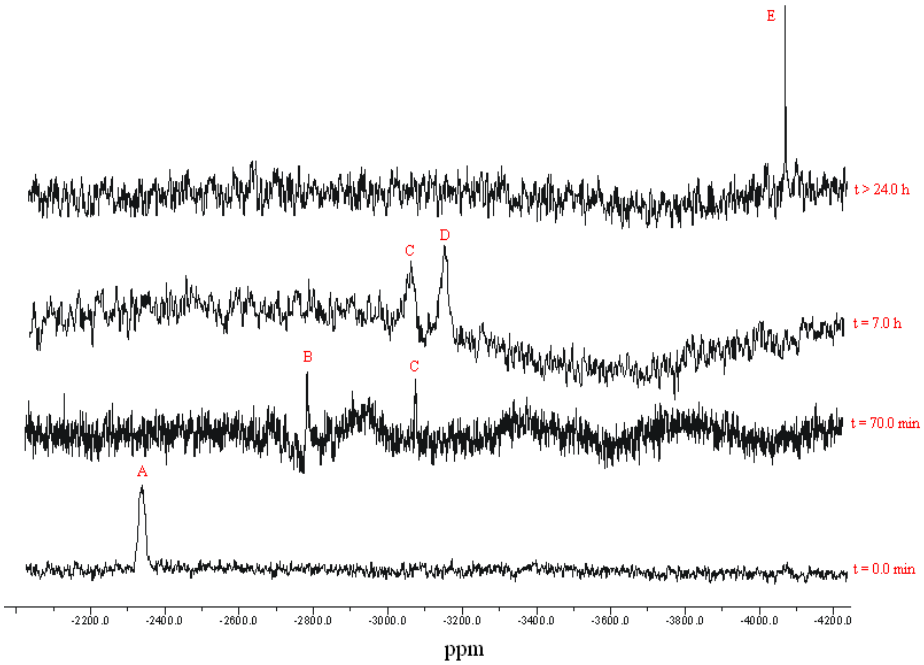

Figure 4.9: ^{195}Pt NMR spectra of the reaction mixture of **pzn–Cl** with six mole equivalents TU, showing pure dinuclear Pt(II) complex **pzn–Cl** (A, δ = -2302.2 ppm)before the reaction and the final degradation product (E, δ = -4045.0 ppm) corresponding to **$[Pt(TU)_4]^{+4}$,** 24.0 h after the reaction. Proposed minor transient products (B, C and D, at δ = -2962.0, -3125.0, and -3276.0 ppm, correspond to $[Cl(NH_3)_2Pt\text{-}pzn\text{-}Pt(NH_3)_2(TU)]^{+3}$ (where, $Cl(NH_3)_2Pt$ = B fragment; $Pt(NH_3)_2(TU)$ = C fragment) and $[(TU)(NH_3)_2Pt\text{-}pzn\text{-}Pt(NH_3)_2(TU)]^{+4}$ corresponds to species D.

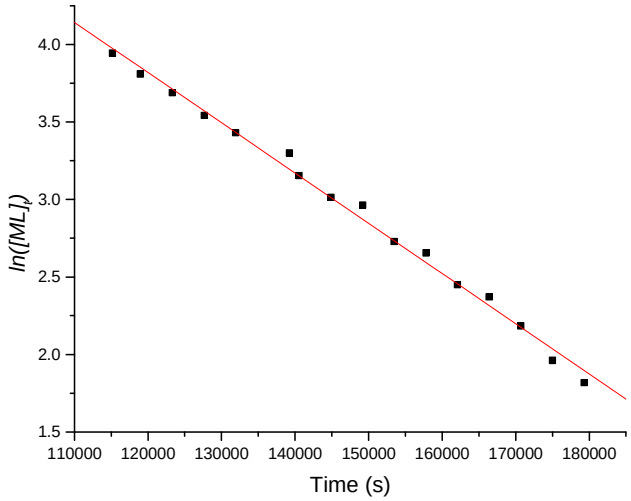

Figure 4.10: First order plot for the reaction of cis-[{PtCl(NH_3)$_2$}$_2$-μ-pzn]$^{+2}$ (0.221 mM) with excess TU (1.323 mM) (in the molar ratio complex: ligand = 1:6) in D2O at 30° C, using ^{1}H NMR spectroscopy. The equation used in calculation is: $\ln[ML]_t = -k_{obs1} + \ln[ML]_0$, where $[ML]_0$ = [free pyrazine ligand] = $[L]_{infinite\ time}$, and $[ML]_t = [L]_{infinite} - [L]_t$ using the area of the signals for released pyrazine ligand.

Looking at Figure 8 & 9, at t = 0, a signal due to the starting complex [{***cis*–PtCl(NH_3)$_2$}$_2$–μ–pzn](ClO$_4$)$_2$** (δ ^{195}Pt = -2302.2ppm or δ^1_H = 9.04 ppm) is observed. The ^{1}H NMR spectra shows that after 48 h only two main products had been formed. These are identified as uncoordinated pyrazine ligand (L), which is expected to appear as a singlet at δ ^{1}H = 8.64 ppm,[39,40] and a singlet at δ ^{195}Pt = -4146.6 ppm [17] corresponding to Pt(TU)$_4$, which is supported by the ^{195}Pt NMR spectra. The ^{1}H and ^{195}Pt NMR spectra reveal the formation of intermediate species, [PtCl–L–Pt(TU)]$^{+3}$, that exhibits two chemical shifts of Pt(N_3Cl) as B at δ^{195}_{Pt} = -2962.0 ppm and Pt(N_3TU) as C at δ^{195}_{Pt} = -3125.0 ppm (Figure 4.9). Pyrazine (L) protons appear as pairs of doublets at δ ^{1}H = 8.96 as residual coordinated ligand and 8.68 ppm as free ligand seen in Figure 4.8.[39,40] Thus, the coordinated aqua molecules are sequentially substituted from Pt(II) centres in the first two steps. The ^{195}Pt NMR signals at -3125.0 ppm (marked as **C**) and -3276.0 ppm (marked as **D**) in Figure 4.9, are both typical of PtN_3S coordinating sphere [41] and -4146.6

ppm shown as **E** corresponds to $[Pt(TU)4]^{+2}$, the end-product when the linker is replaced by thiourea in the third step. The disappearance of the signal at δ = 9.04 ppm for the coordinated pyrazine in dinuclear complex, and the appearance of the corresponding signal for the free pyrazine at δ = 8.68 ppm in the ^{1}H NMR spectra together with ^{195}Pt NMR results all support the proposed reaction given in Scheme 4.2.

Based on the NMR study it is reasonable to conclude that the presence of strong labilising thiourea nucleophiles at the Pt(II) centre enhances stepwise cleavage of the linker and the ammine groups attached to the metal centre. This conclusion contrasts previous studies by Farrell and his group [20] who reported that the integrity of the flexible diamine linker remains intact for the reactions of *cis*-1,1/c,c compound and related novel dinuclear platinum (II) complexes using S-donor nucleophiles. The results however, are consistent with the induced ring opening of bis-(2-pyridylmethethyl)amine chelate by strong labilising thiourea nucleophiles as reported in recent studies by van Eldik and co-workers.[17, 18]

4.4.5 Thermodynamic Parameters

The temperature dependence study of the second order rate constants, $k_{1/2/3}$ was investigated over the temperature range of 15 to 35 °C at intervals of 5 °C. The thermodynamic activation parameters, enthalpy of activation ($\Delta H^{\neq}$) and entropy of activation ($\Delta S^{\neq}$), were calculated from the Eyring plots which are shown in Figures4.10, 4.11 and 4.12 for the **2,5pzn** complex (see Figures. **S4.8**-**S4.10**, **S4.14-S4.16** and **S4.20-S4.22** for the corresponding complexes **pzn**, **2,6pzn** and **2,3pzn**, appendix), and the data is recorded in Table 4.4 as $\Delta H_i^{\neq}$ and $\Delta S_i^{\neq}$ for the individual substitutions.

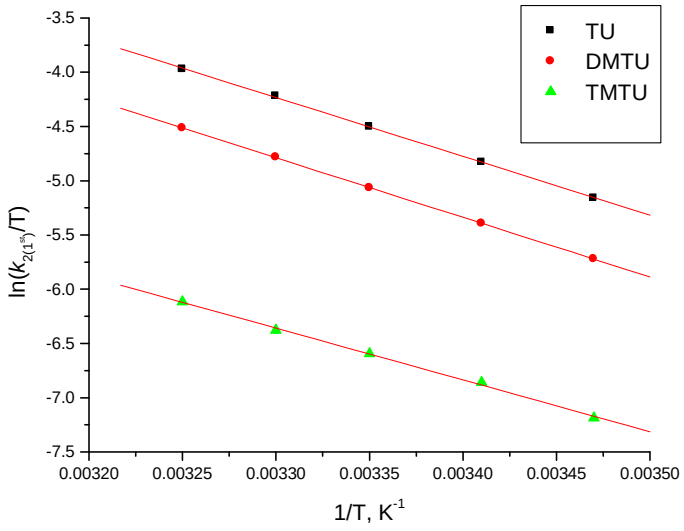

Figure 4.11: Plots of ln(k_2/ T) versus 1/T for the first reaction step of **2,5pzn** with a series nucleophiles in the temperature range 15-35 °C.

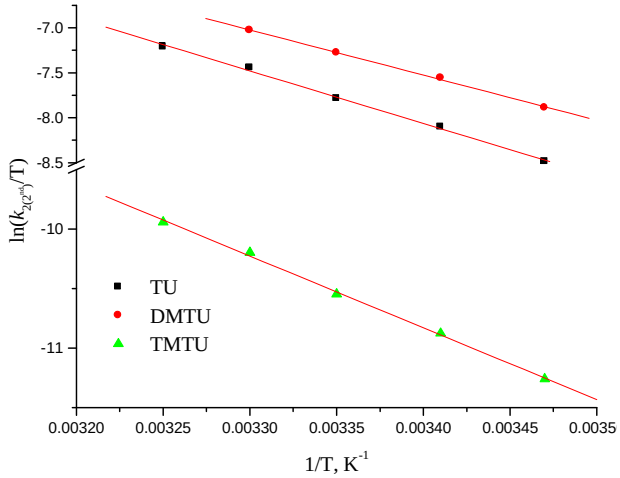

Figure 4.12: Plots of ln(k_2 /T) versus 1/T for the substitution reaction of second step of **2,5pzn** with thiourea nucleophiles in the temperature range 15-35 °C.

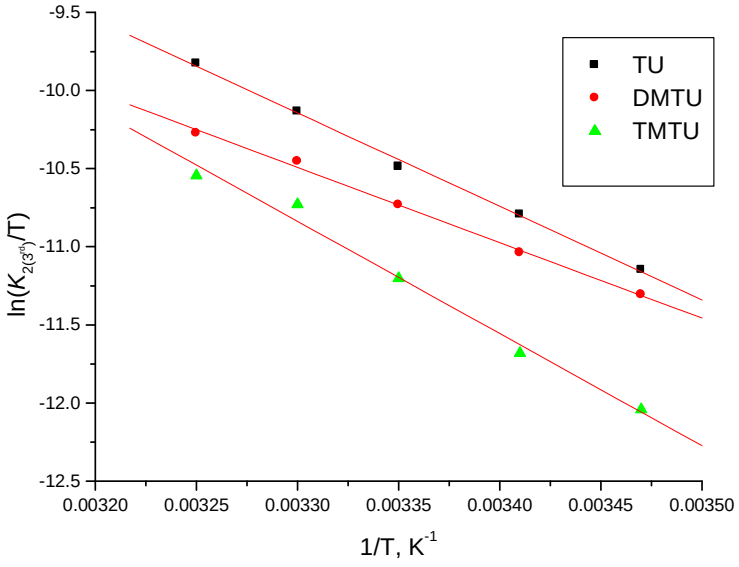

Figure 4.13: Plots of ln(k_2 / T) versus 1/T for the substitution reaction of third step of **2,5pzn** with thiourea nucleophiles in the temperature range 15-35 °C.

Table 4.4: Summary of Activation parameters for the substitution of coordinated water ligands and the displacement of the linker by thiourea nucleophiles in *cis*-[{$PtOH_2(NH_3)_2$–μ–pzn]$^{+4}$ complexes, I = 0.1 M (0.01 M $HClO_4$, adjusted by $NaClO_4$).

Complex	NU	$\Delta H^{\#}_1$ /kJ mol^{-1}	$\Delta H^{\#}_2$ /kJ mol^{-1}	$\Delta H^{\#}_3$ / kJ mol^{-1}	$\Delta S^{\#}_1$ / J mol^{-1}K^{-1}	$\Delta S^{\#}_2$ / J mol^{-1} K^{-1}	$\Delta S^{\#}_3$ / J mol^{-1} K^{-1}
pzn	**TU**	44.7 ± 0.3	55.4 ± 4.2	88.4 ± 1.8	-86.9 ± 1.0	-89.7 ± 14.0	-40.8 ± 6.2
	DMTU	47.6 ± 0.6	67.9 ± 0.4	70.3 ± 6.7	-84.6 ± 1.9	-51.5 ± 1.4	-98.5 ± 22.4
	TMTU	44.6 ± 1.3	60.1 ± 1.2	72.0 ± 3.7	-103.4 ± 4.2	-118.8 ± 4.1	-80.8 ± 12.1
2,6pzn	**TU**	45.3 ± 0.9	50.8 ± 2.9	58.1 ± 1.3	-76.1 ± 2.9	-141.6 ± 9.8	-89.7 ± 4.3
	DMTU	51.4 ± 2.1	56.2 ± 0.4	64.4 ± 4.7	-56.7 ± 7.2	-133.4 ± 1.3	-74.6 ± 15.7
	TMTU	32.3 ± 2.7	48.0 ± 0.8	43.6 ± 2.7	-142.9 ± 9.0	-162.6 ± 1.1	-154.0 ± 9.0
2,3pzn	**TU**	49.7 ± 2.0	55.1 ± 2.5	47.8 ± 1.1	-67.4 ± 6.6	-91.1 ± 0.7	-127.4 ± 3.8
	DMTU	44.3 ± 0.2	63.3 ± 1.0	55.5 ± 1.1	-92.5 ± 0.7	-48.2 ± 1.6	-102.7 ± 3.6
	TMTU	39.5 ± 2.3	59.1 ± 1.7	56.6 ± 2.1	-128.5 ± 8.1	-81.0 ± 5.8	-105.2 ± 6.3
2,5pzn	**TU**	45.1 ± 0.5	48.6 ± 1.4	49.8 ± 1.4	-84.3 ± 1.6	-99.8 ± 4.7	-118.0 ± 4.8
	DMTU	45.6 ± 0.1	41.7 ± 1.0	38.6 ± 2.1	-87.1 ± 0.5	-118.5 ± 3.4	-157.6 ± 7.2
	TMTU	39.7 ± 1.0	50.1 ± 1.2	59.7 ± 3.8	-119.7 ± 3.4	-117.4 ± 3.9	-90.9 ± 12.9

4.5 Discussion

By introducing the methyl groups at the 2,3-, 2,5-,and 2,6-positions of the pyrazine bridge, it was possible to investigate their role as electron-donating groups in controlling the extent of σ-electron density at the metal centre and also the influence of steric hindrance on reactivity at the Pt(II) centres. As the number of methyl groups is increased on the pyrazine moiety, the σ-electron donating ability of the linker improves.[31, 32] Pyrazine is the smallest and most rigid linear aromatic linker, which due to the short distance between the two Pt(II) centres and the resonance effect of pyrazine induces "metal-metal electronic communication" by electrostatic charge transfer from the metal centre into the lowest unoccupied molecular orbitals (LUMO) of the bridging ligand,[42] and as expected will result in a more electron-deficient Pt(II) centre.

Comparing the reactivity of the aqua complexes in Table 4.3, the ratio of the substitution of the first aqua ligand by TU is: 1: 1: 2: 10, respectively for **2,5pzn**, **2,3pzn**, **2,6pzn** and **pzn**. This means that the rate of substitution of the aqua ligand by the S-donor nucleophiles increases in the order of **2,5pzn ≈ 2,3pzn < 2,6pzn < pzn** for the first step.

The high reactivity of **pzn** is attributed to a more positively charged metal centres that also experiences less steric hindrance. This is in line with the determined lower pK_a values (Table 4.2), higher values of DFT calculated positive NBO charges on the Pt(II) ions and narrow HOMO-LUMO energy gap (Table 4.1). These findings support higher electrophilicity and hence, enhanced reactivity at the Pt(II) centre.[18-35,43] On the contrary, due to lack of appropriate overlapping of orbitals between the metal centred HOMO mapped on the dz^2 orbitals and the linker lying perpendicular to the plane of the Pt(II) centre (Figure 2), π-back bonding between the metal and the pyrazine ligand [42,43] is missing.

To understand further the role of the linker σ-donor effect on the rate of substitution of the *cis*-aqua ligand for the first step, the reactivity of **pzn** and **2,6pzn** are compared. The difference between them is on the second **Pt2(II)** centre of **2,6pzn** that is surrounded by methyl groups. From the kinetic data in Table 4.3, the lability of the aqua ligand in **2,6pzn** (k_1 = 8.13 M^{-1} s^{-1}) is reduced by a factor of 5 compared to **pzn** (k_1 = 42.02 M^{-1} s^{-1}).

The decrease in reactivity of **2,6pzn** for the first substitution is due to the positive inductive effect of the 2,6-dimethylpyrazine ring that leads to accumulation of electron density at metal centre. This makes the Pt1(II) centre less electrophilic, resulting in lower reactivity towards the nucleophiles. This is well supported by the large HOMO-LUMO energy gap coupled with reduced positive NBO charges (Table 4.1) for **2,6pzn**. Smaller values of k_1 were observed for the first substitution step of the aqua ligand in the complexes **2,3pzn** and **2,5pzn** by a factor of 10 than **pzn** and also smaller than that of **2,6pzn**. Previous studies have shown that methyl groups and other electron-donating groups collectively lead to a reduction in the rate of ligand substitution, by reducing the positive charge density on the platinum atom, thereby lowering the electrophilicity of the metal centre.[3,31,32,36,44,45] As a result, the incoming nucleophile is repelled by the increased amount of electron density around the metal centre**,** leading to a less stable five-coordinate transition state and decreased rate of substitution.

The difference between the **2,6pzn** and the **2,3pzn** and **2,5pzn** indicates that the distribution of the methyl groups around the pyrazine linker plays a role in controlling the reactivity. This is because the position of the methyl group influences the electronic as well as the steric effects around the Pt(II) centres. The reactivity of **2,3pzn** and **2,5pzn** are similar because of having symmetrically equal effects in terms of electronic and steric hindrance.

The reactions for the second step are significantly slower, by a factor of 10, than for the first in all cases. This is probably because of the electronic communication between the two platinum atoms and also steric hindrance from the first substitution at the Pt(II) centre. The DFT calculations show a change in NBO charges if TU is substituted to one platinum centre as can be seen in Table 5, suggesting that electronic information is somehow conveyed through the bridging ligand. The order of reactivity for the second step is **pzn** > **2,3pzn** ≈ **2,5pzn** > **2,6pzn**. In case of **2,6pzn** there is additional steric effect which blocks entry of the incoming nucleophile on both sides of the Pt2 centre (Figure 4.14),[3, 39,46-52] accounting for the slowest rate of reactivity.

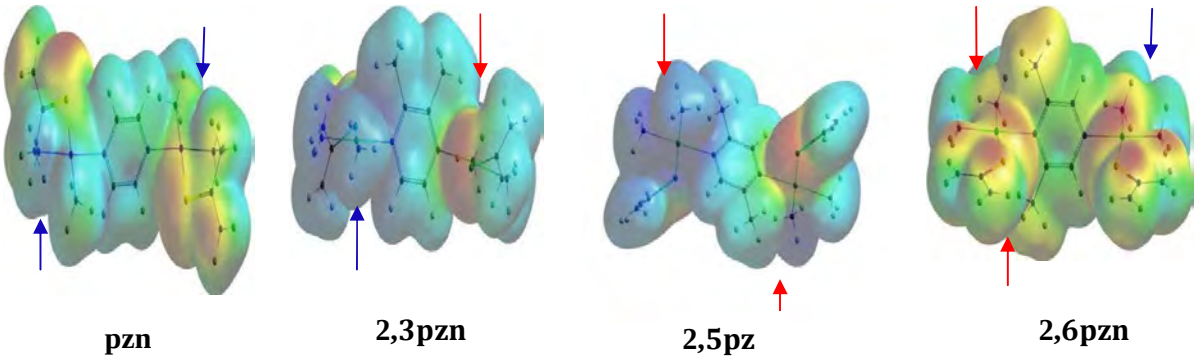

Figure 4.14: DFT-calculated electron density distribution plots for the investigated complexes illustrating steric hindrance by the bridging pyrazine ligand and the coordinated thiourea nucleophiles. The blue (arrows indicate the least sterically hindered pathway for the incoming thiourea nucleophiles, while the red arrows indicate pathways that are subject to increased axial steric hindrance by the methyl groups present on the linker and the already attached thiourea ligand.

Table 4.5: DFT calculated (NBO) charges for Pt atoms of optimised structures of monoaquaTU-substituted complexes.

Complex	Structure	Pt1	Pt2
pzn-TU	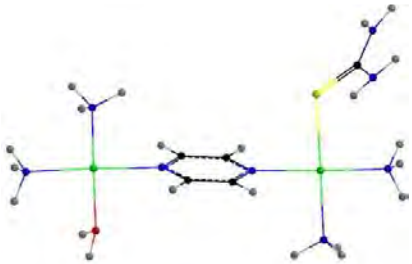	1.0568	1.2184
2,6pzn-TU	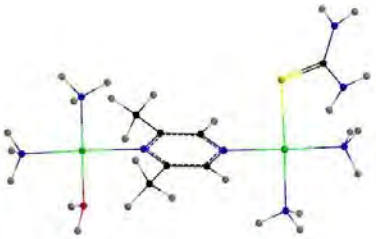	1.0557	1.2158
2,3pzn-TU		1.0527	1.2192
2,5pzn-TU	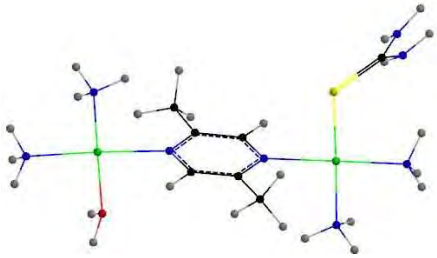	1.0534	1.2158

The third step which is the replacement of the linker is initiated by the coordination of thiourea nucleophiles *trans* to the NH_3 ligands. Because of the strong *trans-effect* of sulphur atom, the NH_3 *trans* to the sulphur atom are slowly substituted.[50] This increases

the number of sulphur bound molecules per Pt(II) atom in the products, thereby weakening the amine N–Pt bond, which becomes susceptible to further substitution reactions, leading to the simultaneous displacement of the linker and formation of $[Pt(TU)_4]^{2+}$. Based on the NMR studies one can conclude that the third step observed in all these dinuclear complexes is due to degradation of the dinuclear Pt(II) complex to release the bridging ligand and form $[Pt(TU)_4]^{+2}$. The results show that the rate constants of the third step are not dependent on the nature of the pyrazine linker, but are sensitive to the steric nature of the nucleophile.

The value of the rate constant of the third step from the ^{1}H NMR spectral data was calculated from the observed first-order rate constant, k_{obs}, obtained from Figure 4.10 and converted to second-order rate constant ($k_2 = k_{obs}/$ [TU]) based on *equation* 1 and found to be ($k_{3,3}^{rd} = 2.44 \times 10^{-3}$ M^{-1} s^{-1}), which is in close agreement with the value ($k_3 = 2.86 \times 10^{-3}$ M^{-1} s^{-1}) obtained from the concentration dependence study at 25 °C for **pzn,** as the thiourea in each case attacks a thiourea substituted Pt(II) centre.

When the TU results of the *cis*-complexes **pzn**, **2,3pzn** and **2,5pzn** are compared with those of the recently published *trans*-complexes[32], the second-order rate constants *(k_1)* of the *cis*-complexes for the first step are slightly bigger. This indicates that *cis*-analogue undergoes substitution reactions slightly faster than its *trans*-counterpart. This small difference is possibly due to a very weak hydrogen bond between NH---OH_2 in case of **pzn** or CH---OH for the other complexes, which stabilizes the five-coordinate trigonal bipyramidal transition state as illustrated in Scheme **S4.1** and Figure **S4.1**. This phenomenon was reported by Klein and co-workers,[53] while investigating intramolecular C-H bond activation by the Pt(II) centre and its ability to form hydrogen bonding amongst the dimethylpyrazine ligands;[54] and has also been reported by Munro and his group in crystallographic studies.[55]

The results as tabulated in Table 4.4 show that the activation entropies ($\Delta S^{\#}_{1/2/3}$) are large and negative whereas the activation enthalpies ($\Delta H^{\#}_{1/2/3}$) are small and positive. It is also noted that steric effects decelerate the reactivity between the *cis*-complexes **2,3pzn**, **2,5pzn** and **2,6pzn** and the S-donor nucleophiles, which helps confirm that the

reaction proceeds via bimolecular path with no hydrolysis step. All these are in support of associative mode of substitution mechanism known for d^8 square-planar complexes.[47,48,56]

In terms of steric effects, substitution of coordinated aqua ligands shows a clear dependence on the steric hindrance of the incoming nucleophiles. Thus, the order of reactivity exhibited by the S-donor nucleophiles at the Pt(II) centres increased in the order: TU > DMTU > TMTU and is line with the steric retardation in the case of TMTU.

4.6 Conclusion

From the results of this study, we have shown that all the dimethylpyrazine substituted Pt(II) complexes: **2,3pzn**, **2,5pzn** and **2,6pzn** reacted more slowly with thiourea ligands compared to unsubstituted **pzn**. The order of reactivity of the complexes is **2,5pzn** ≈ **2,3pzn** < **2,6pzn** < **pzn**. Substitution in the pyrazine backbone influences the rate of the substitution at the Pt(II) centre by controlling mainly the steric effects. A highly symmetrical bridging ligand like the unsubstituted pyrazine ring with electronegative N-atoms, will pull electron-density away from the positively charged metal centre, making the Pt(II) centre more electrophilic and susceptible to attack by the S-donor nucleophiles. On the other hand, the bridging ligands possessing the methyl moiety, which is an electron-donating moiety, reduces the positive charge at the Pt(II) centre. This makes the platinum centre less electrophilic, and hence, less susceptible to nucleophilic attack resulting into a slowed down substitution reactions. In addition, the bulky methyl substituent on the pyrazine linker introduces steric crowding on the reaction centre retarding the reactivity of **2,3pzn**, **2,5pzn** and **2,6pzn.** The electronic communication between the two metal centres results in two distinct pK_a values and substitution reactions.

The ^{1}H and ^{195}Pt NMR results collectively support the experimentally observed dissociation of the linker by thiourea nucleophiles as the third step in all the cases. The study confirmed the release of free pyrazine (singlet, at $\delta\ ^{1}_{H} = 8.64$ ppm) and $[Pt(TU)_4]^{2+}$ ($\delta\ _{195Pt}$ = -4146.6 ppm), for the reaction of **pzn** with excess TU. Given the high nucleophilicity of the sulphur bearing thiourea nucleophiles at the Pt(II) centres coupled

with the weaker σ-donor ability of pyrazine ligand, degradation of the *cis*-dinuclear integrity occurred in a slow reaction process.

The large and negative values of $\Delta S^{\neq}$ coupled with small positive values of the $\Delta H^{\neq}$ and the fact that the substitution reaction was dependent on the steric nature of the nucleophiles, plus the second order rate constants ($k_{1/2/3}$) varying linearly with nucleophile concentration for all the complexes, support an associative mode of reaction mechanism.

References

1 T. Storr, K. H.Thomson and C. Orvig, 2006, *Chem. Soc. Rev*., **35**, 534.

2 J. Reedijk, 2003, PNAS, **100**, 3611-3616.

D. Jaganyi, E. Pantoja, A. Gallipoli, S. van Zutphen, S. komeda, D. Reddy, M. Lutz, D. M. Tooke, A. L. Spek, C. Navarro-Ranninger and J. Reedijk, 2006, *J. Inorg. Biochem.***, 100,** 1955-1964.

4 E. Wong and C. M. Giandomenico, 1999, *Chem. Rev*., **99**, 2451-2466.

5 E. R. Jameison and S. J .Lippard, 1999, *Chem. Rev*., **99**, 2467.

6 V. Balzani, A. Juris, M. Venture, S. Campagna and S. Serroni, 1996, *Chem. Rev*., **96**, 759.

7 N. Farrell, Y. Qu and J. D. Roberts, 1999, *Top. Biol. Inorg. Chem*., **1**, 99.

8 P. J. Dyson, G. Sava, 2006, *Dalton Trans*. 1929-1933.

9 Y. Qu, J.A. Fitzgerald, H. Rauter and N. Farrell, 2001, *Inorg. Chem*., **40**, 6324-6327.

10 S. Komeda, M. Lutz, A. L Spek, Y. Yamanaka, T. Sato, M.Chikuma and J. Reedijk, 2002, *J. Am. Chem. Soc*., **124,** 4738.

11 S. Komeda, G. V. Kalayda, M. Lutz, A. L. Spek, Y. Yamanaka, T. Sato, M. Chikuma and J. Reedijk, 2003, *J. Med. Chem*., **46**, 1210.

12 M. S. Davies, J. W. Cox, S. J. Berners-Price, W. Barklage, Y. Qu and N. Farrell, 2000, *Inorg. Chem*., **39**, 1710-1715.

13 M. S. Davies, D. S. Thomas, A. Hegmans, S. J. Berners-Price and N. Farrell, 2002, *Inorg. Chem*., **41**, 1101-1109.

14 D. Jaganyi, V. M. Munisamy and D. Reddy, 2006, *Int. J. Chem.Kinet*., **38**, 202.

15 S. J. Hoseini, S. M. Nabavizadeh, S. Jamali, and M Rashidi, 2007, *J.Organomet. Chem*., **692**, 1990-1996.

16 N. Summa, J. Maigut, R. Puchta and R. van Eldik, 2007, *Inorg. Chem*., **46**, 2094-2104.

17 H. Ertuerk, J. Maigut, R. Puchta and R. van Eldik, 2008, *Dalton Trans*., **20**, 2759-2766.

18 D.Jaganyi, A. Mambanda, S. Hochreuther and R. van Eldik, 2010. *Dalton Trans*., **39**, 3595-3608.

19 (a) V. X. Jin, S. I. Tan and J. D. Ranford, 2005, *Inorg. Chim. Acta*, **358**, 677- 686, (b) M.E. Oehlsen, Y. Qu, N. Farrell, 2003, *Inorg. Chem*. **42**, 5498-5506.

20 (a) J. W. Williams, Y. Qu, G. H. Bulluss, E. Alvorado and N.P. Farrell, 2007, *Inorg. Chem*., **46**, 5820-5822; (b) M. E. Oehlsen, A. Hegmans, Y. Qu and N. Farrell. 2005, *J. Biol. Inorg. Chem*. **10**, 433-442.

21 H.Ertuerk, R. Puchta and R. van Eldik, 2009. *Eur. J. Inorg. Chem*., 1331-1338 and references cited therein.

22 M. Vasak, M. Knipp, A.V. Karortki, S. Chesnov, G. Natile, P.J. Sadler and V. Brabec. 2007. *J. Med. Chem*., 50, 4075 – 4086.

23 T. G. Appleton, J. R. Hall, S. F. Ralph and C. S. M. Thompson, 1984, *Inorg. Chem*., **23**, 3521.

24 G.V. Kalayda, S. Komeda, K. Ikeda, T. Sato, M. Chikuma and J. Reedijk, 2003, *Eur. J. Inorg. Chem*., 4347-4355.

25 M. Willermann, C. Mulcahy, R. K. O. Sigel, M. M. Cerdà, E. Freisinger, P. J. Sanz Migul, M. Roitzsch, B. Lippert, 2006, *Inorg. Chem*., **45**, 2093-2099.

26 Z. D. Bugarčič, B. V. Petrović, R. Jelić, 2001, *Trans. Met. Chem*., **26**, 668.

27 A. K. Connors, *Chemical Kinetics the of Reaction rates in Solution*, Wiley-VCH, New York, 1990, pp 334 – 337.

28 Microcal™ Origin™ Version 5.0, Microcal software, Inc., One Roundhouse Plaza, Northampton, MA, 01060, USA, 1991-1997.

29 A. D. Becke, 1993, *J. Chem. Phys*., **98,** 5648-5652.

30 P. J. Hay and W.R Wadt, 1985, *J. Chem. Phys*., **82**, 299.

31 D. Reddy and D. Jaganyi, 2008, *Dalton Trans*. 6724-6731.

32 D. Reddy and D. Jaganyi, 2011, *Int. J. Chem.Kinet*., **43**, 161-174.

33 H. Erturk, A. Hofmann, R. Puchta and R. van Eldik, 2007, *Dalton Trans*. 2295-2301A

34 Hofmann, A, D. Jaganyi, O. Q. Munro, G. Leihr and R. van Eldik, 2003, *Inorg. Chem*. **42**, 1688-1700.

35 D. Jaganyi, A. Hofmann, R. van Eldik, 2001, *Angew Chem. Int., Ed*., **40**, 1680-1683.

36 D. Jaganyi, D. Reddy, J.A. Gertenbach, A. Hofmann and R. van Eldik, 2004, *Dalton Trans*. 299-304.

37 P. M. Lax, M. G. Anorbe, B. Muller, E. Y. Bivian-Castro and B. Lippert, 2007, *Inorg. Chem., **46**, 4036-4043.*

[38]. P. M. Lax, M. G. Anorbe, B. Muller, E. Y. Bivian-Castro and B. Lippert, *Inorg. Chem.*, 2007, **46**, 4036.

39 M. A. Nazif, J-A, Bangert, I. Ott, R. Gust, R. Stoll and W. S. sheldrick, 2009, *J. Inorg. Biochem*. **103**, 1405-1414.

40 F. D. Rochon and M. Fakhfakh, 2009, *Inorg. Chim.Acta*, **362**, 458-470.

41 T. G. Appleton, J. R. Hall and S. F. Ralph, 1985, *Inorg. Chem*., **24**, 4685.

42 (a) J. S. Field, J.A. Gertenbach, R. J. Haines, O. Q. Munro and D. R. McMillin, 2007, *Z. Naturforsch*, **62b**, 447-452; (b) T Soldatović, S. Jovanović, Ž. B. Bugarčić and R. van Eldik, 2012, *Dalton Trans*. **41**, 876.

43 D. Reddy, K. J. Akerman, M. P. Akerman and D. Jaganyi, 2011, *Transition Met. Chem*., **36**, 593.

44 A. Hofmann, L. Dahlernburg and R. van Eldik, 2003, *Inorg. Chem*., **42**, 6528-6538.

45 A. Pasini, L. Rigamonti, A. Forni, M, Manassero, C. Manassero, 2010, *Inorg. Chem*., **49**, 125-135.

46 (a) S. Asperger, *Chemical Kinetics and Inorganic Reaction Mechanisms*, 2nd Edn. Kluwer Academic/ Plenum Publishers, New York, 2003, pp.152-3; (b) C. Jones and J. R. Thornback, *Medicinal Applications of Coordination Chemistry*, RSC, Cambridge CB4 0WF, UK, 2007, pp. 219-257.

47 M .l. Tobe and J. Burgess, *Inorganic Reaction Mechanisms*, Addison Wesley Longman Inc: 1990, pp. 70-112.

48 J. D. Atwood, 1997, *Inorganic and Organometallic Reaction Mechanisms*, 2nd Ed., Wiley-VCH Inc., NY, p.43-61.

49 (a)R.Romeo, L. m. Scolaro, M. R. Plutino, F. F. de Biani, G. Bottari, A. Romeo, 2003, *Inorg. Chim. Acta*, **350**, 143-151; (b) R. Romeo, L. M. Scolaro, N. Natasi, G. Arena, 1996, *Inorg. Chem*., **35**, 5087.

50 M. E. Oehlsen, A. Hegmans, Y. Qu, N. Farrell, 2005, *J. Biol. Inorg. Chem*., **10**, 433-442.

51 O. F. Wendt, L. I. Elding, 1997. *J. Chem. Soc., Dalton Trans*., **24**, 4725-4731.

52 Y. Chen, Z. Guo, S. Parsons, P. J. sadler, 1998. Chem.-Eur. J., **4**, 672-676.

53 A. Klein, T. Schurr, A. Knodler, D. Gudat, K. W. K. Klinkhammer, V. Jain, S. Zalis, W. Kaim. 2005, *Organometallics*, **17**, 4125.

54 V. R. Thalladi, A. Gehrke, R. Boese, 2000. *New J. Chem*., **24**. 463-470.

55 A. Mambanda, D. Jaganyi, and O. Q Munro, *Acta Cryst*., 2007, **C63**, o676–o680.

56 F. Basolo and R. G. Pearson, *Mechanisms in Inorganic Reactions*, 2nd Ed., Wiley, New York, 1967.

Appendix 4

THE INFLUENCE OF THE PYRAZINE BRIDGE ON SUBSTITUTION REACTIONS OF DINUCLEAR Pt(II) COMPLEXES-*cis* σ-EFFECT VERSUS STERIC HINDRANCE

Figures **S4.2**-**S4.4** show UV-Visible spectra for **pzn**, **2,3pzn** and **2,6pzn** at different of pH values. Figures **S4.5-S4.22** illustrates different concentration and temperature dependent studies for all nucleophiles and complexes. Table S1 shows a summary of the used wavelengths and Tables **S4.2-S4.24** summarise all values of k_{obs} determined for all reactions at different concentrations and temperatures for all nucleophiles. Included is Figures **S4.23-S4.27** for ^{1}H and ^{195}Pt NMR spectra of the complexes.

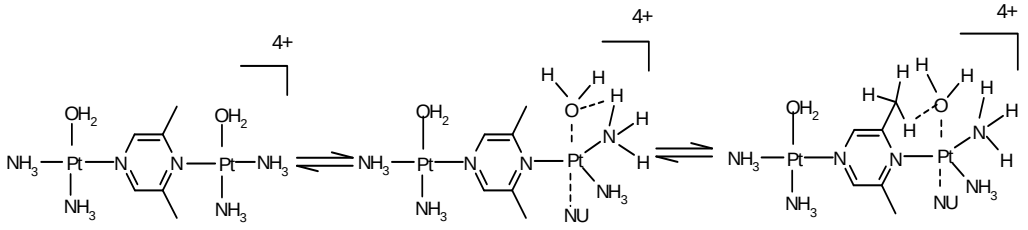

Scheme S4.1: stabilization of the transition-state by hydrogen bonding

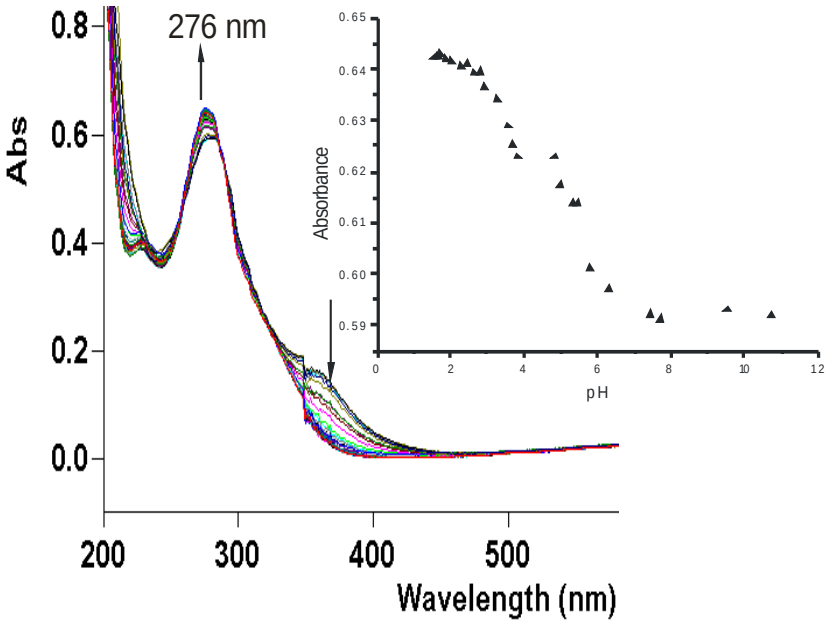

Figure S4.2: UV/Visible spectra for the titration of 0.1 mM **pzn** with NaOH in the pH range 2-11, T = 25 °C. Inset is the titration curve at 276 nm.

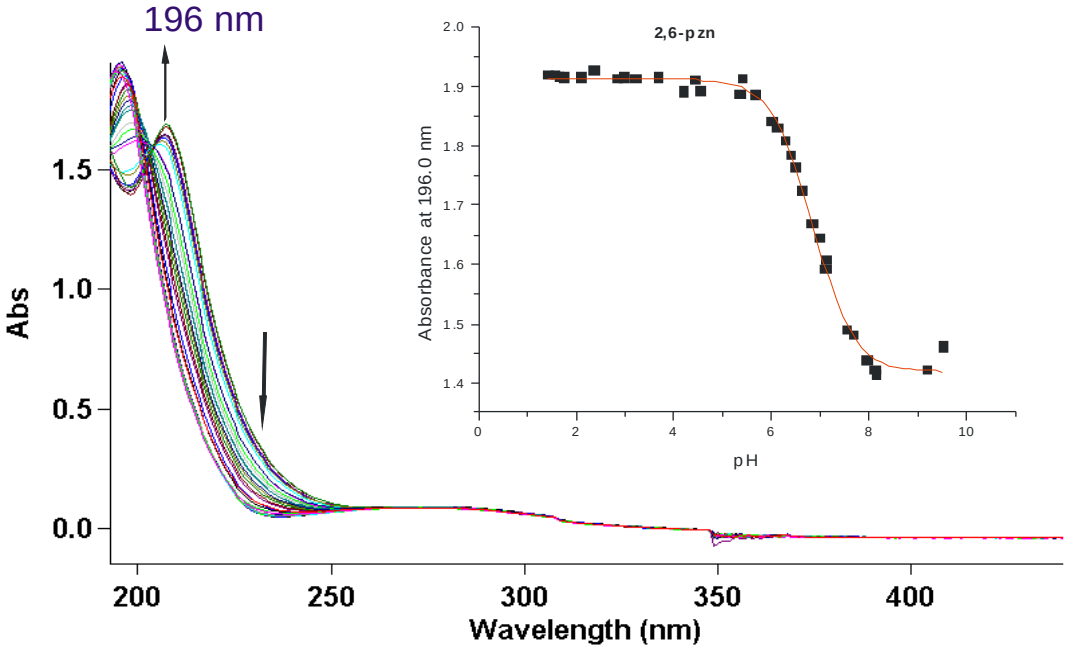

Figure S4.3: UV/Visible spectra for the titration of 0.1 mM **2,6pzn** with NaOH in the pH range 2-10, T = 25 °C. Inset is the titration curve at 196 nm.

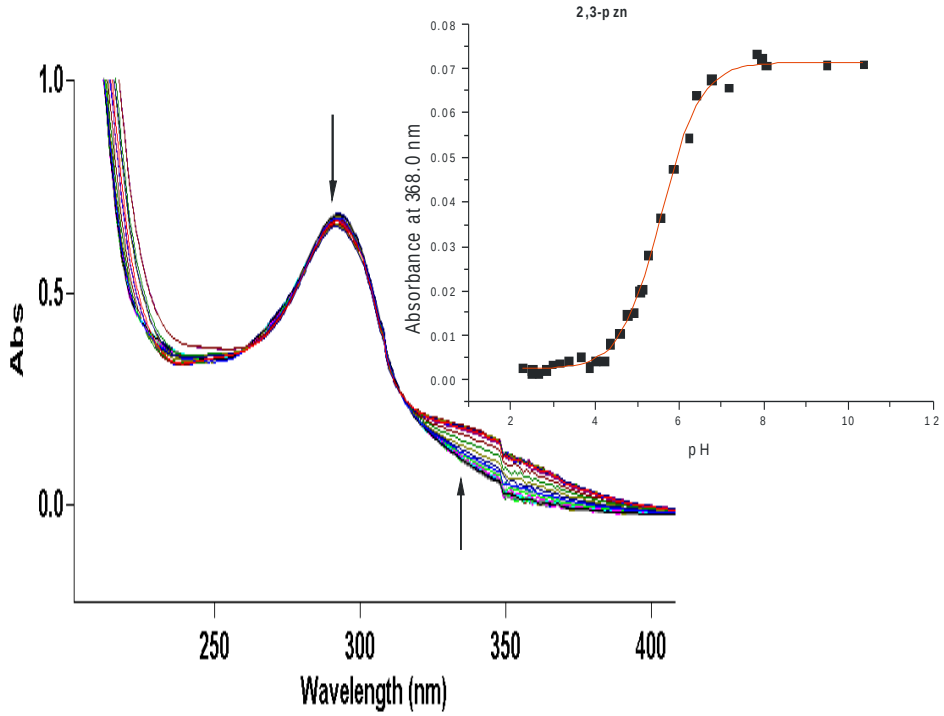

Figure S4.4: UV/Visible spectra for the titration of 0.1 mM **2,3pzn** with NaOH in the pH range 2-10, T = 25 °C. Inset is the titration curve at 368 nm.

Table S4.1: Summary of the wavelengths (nm) used for monitoring the reactions between a series of dinuclear Pt(II) complexes with thiourea nucleophiles.

Complex	Nucleophile	Wavelength (λ) nm
pzn	TU	395
	DMTU	411
	TMTU	411
2,6pzn	TU	342
	DMTU	342
	TMTU	342
2,3pzn	TU	390
	DMTU	390
	TMTU	390
2,5pzn	TU	390
	DMTU	390
	TMTU	390

Table S4.2: Average observed rate constants, $k_{obs(1^{st})}$, at 298.15 K, for the reactions of **pzn** with a series of nucleophiles at different concentrations.

[NU]/ M	$\boldsymbol{k_{obs(1)}}$, $\mathbf{s^{-1}}$		
	TU	**DMTU**	**TMTU**
0.02	0.0689	0,0444	0.0081
0.04	0.1681	0.0863	0.0164
0.06	0.2571	0.1337	0.0241
0.08	0.3434	0.1784	0.0321
0.1	0.4232	0.2217	0.0398

Table S4.3: Average observed rate constants, $k_{obs}(2^{nd})$, at 298.15 K, for the reactions of **pzn** with a series of nucleophiles at different concentrations.

[NU]/M	$k_{obs(2)}$, **s^{-1}**		
	TU	**DMTU**	**TMTU**
0.02	5.543 x 10^{-4}	2.873 x 10^{-4}	1.889 x 10^{-4}
0.04	1.120 x 10^{-3}	6.239 x 10^{-4}	3.959 x 10^{-4}
0.06	1,710 x 10^{-3}	9.470 x 10^{-4}	5.294 x 10^{-4}
0.08	2.300 x 10^{-3}	1.280 x 10^{-3}	
0.1	2.870 x 10^{-3}	1.620 x 10^{-3}	9.805 x 10^{-4}

Table S4.4: Average observed rate constants, $k_{obs(3^{rd})}$, at 298.15 K, for the reactions of **pzn** with a series of nucleophiles at different concentrations.

[NU]/ M	$k_{obs(3^{rd})}$, **(x10^{-5} s^{-1})**		
	TU	**DMTU**	**TMTU**
0.02	0.4065	-	0.3378
0.04	1.1172	1.2512	0.7180
0.06	1.6147	2.0745	1.1125
0.08	2.3859	2.9302	1.5227
0.1	2.8822	3.7350	1.8200

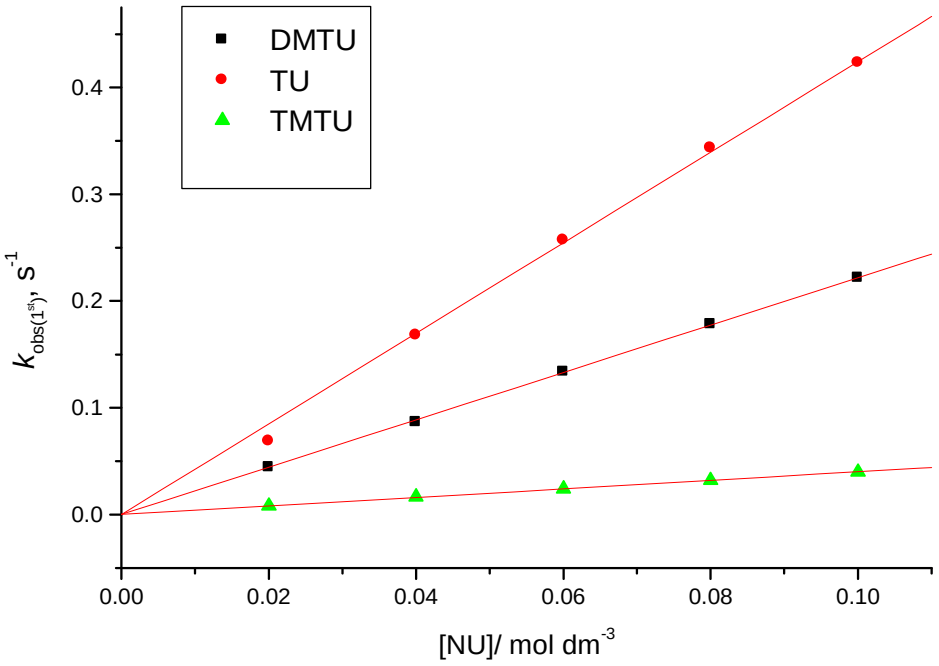

Figure S4.5: Concentration dependence of $k_{obs(1^{st})}$ for the displacement of first aqua ligand in **pzn** by thiourea nucleophiles, pH = 2.0, T = 298.15 K, I = 0.10 M (0.01 M $HClO_4$, adjusted with $NaClO_4$).

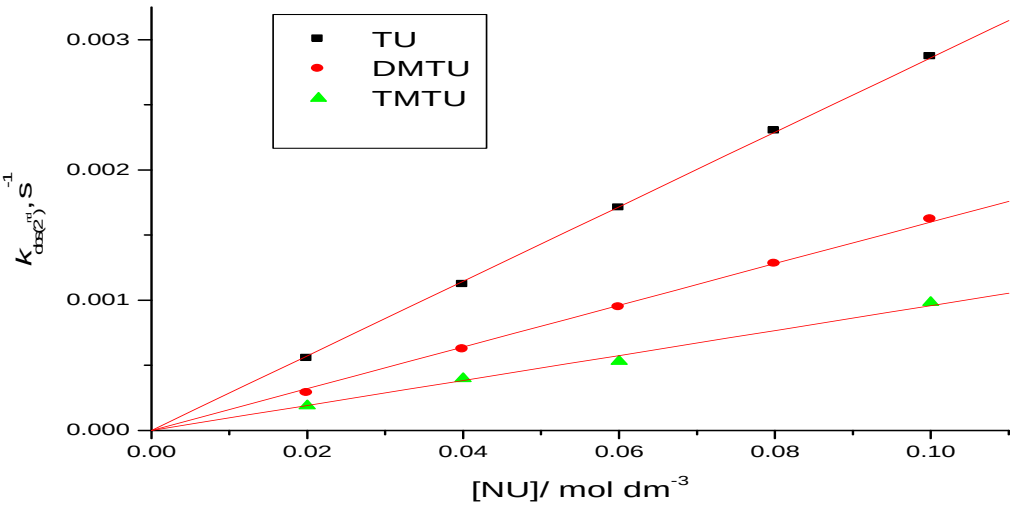

Figure S4.6: Concentration dependence of $k_{obs(2^{nd})}$ for the displacement of second water ligand in **pzn** by thiourea nucleophiles, pH = 2.0, T = 298.15 K, I = 0.10 M (0.01 M $HClO_4$, adjusted with $NaClO_4$).

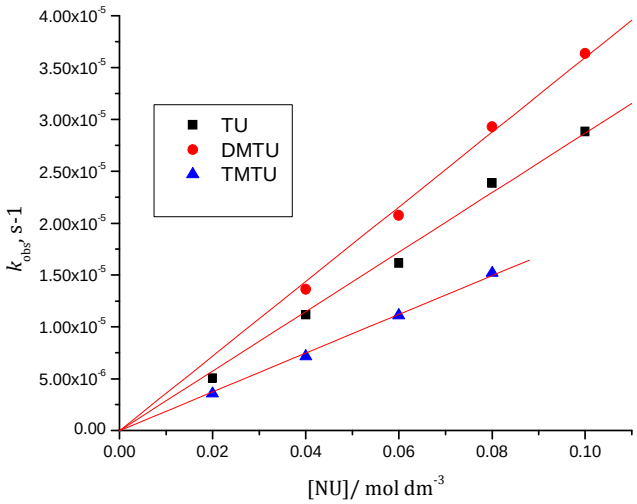

Figure S4.7: Concentration dependence of $k_{obs(3^{rd})}$ for the displacement of second water ligand in **pzn** by thiourea nucleophiles, pH = 2.0, T = 298.15 K, I = 0.10 M (0.01 M $HClO_4$, adjusted with $NaClO_4$).

Table S4.5: Average observed rate constants, $k_{obs(1^{st})}$, for the reactions of **pzn** at varied temperatures in the range 15 to 35 °C while maintaining nucleophile concentration at ≈ 60x [**pzn**].

1/T, K^{-1}	**TU**		**DMTU**		**TMTU**	
	$k_{obs(1^{st})}$, s^{-1}	**ln(k_2/T)**	**$k_{obs(1^{st})}$, s^{-1}**	**ln(k_2/T)**	**$k_{obs(1^{st})}$, s^{-1}**	**ln(k_2/T)**
0.00347	0.08503	-5.3143	0.0332	-6.2548	0.0118	-7.2892
0.00341	0.1201	-4.9862	0.0468	-5.9286	0.0172	-6.9296
0.00335	0.1666	-4.6758	0.0671	-5.5853	0.0235	-6.6344
0.00330	0.2224	-4.4036	0.0911	-5.2961	0.0324	-6.3299
0.00325	0.2985	-4.1257	0.1253	-4.9737	0.0409	-6.1133

Table S4.6: Average observed rate constants, $k_{obs(2^{nd})}$, for the second step reactions of **pzn** at varied temperatures in the range 15 to 35 °C while maintaining nucleophile concentration at ≈ 60x [**pzn**].

1/T, K^{-1}	**TU**		**DMTU**		**TMTU**	
	$k_{obs(2^{nd})}$, s^{-1}	**ln(k_2/T)**	**$k_{obs(2^{nd})}$, s^{-1}**	**ln(k_2/T)**	**$k_{obs(2^{nd})}$, s^{-1}**	**ln(k_2/T)**
0.00347	7.626 x 10^{-4}	-10.028	3.707 x 10^{-4}	-10.750	5.376 x 10^{-5}	-12.681
0.00341	1.079 x 10^{-3}	-9.698	6.237 x 10^{-4}	-10.247	6.521 x 10^{-5}	-12.505
0.00335	1.692 x 10^{-3}	-9.266	1.022 x 10^{-3}	-9.770	7.691 x 10^{-5}	-12.357
0.00330	2.133 x 10^{-3}	-9.051	1.585 x 10^{-3}	-9.347	9.343 x 10^{-5}	-12.179
0.00325	3.697 x 10^{-3}	-8.519	2.391 x 10^{-3}	-8.953	1.105 x 10^{-4}	-12.027

Table S4.7: Average observed rate constants, $k_{obs(3^{rd})}$, for the third step reactions of **pzn** at varied temperatures in the range 15 to 35 °C while maintaining nucleophile concentration at ≈ 60x [**pzn**].

1/T, K^{-1}	**TU**		**DMTU**		**TMTU**	
	$k_{obs(3^{rd})}$, s^{-1}	**ln(k_2/T)**	**$k_{obs(3^{rd})}$, s^{-1}**	**ln(k_2/T)**	**$k_{obs(3^{rd})}$, s^{-1}**	**ln(k_2/T)**
0.00347	4.280 x 10^{-6}	-18.0244	1.466 x 10^{-5}	-16.810	2.070 x 10^{-5}	-16.449
0.00341	8.348 x 10^{-6}	-17.3735	1.665 x 10-^{5}	-16.666	5.406 x 10^{-5}	-15.488
0.00335	1.655 x 10^{-5}	-16.7085	2.073 x 10^{-5}	-16.480	1.025 x 10^{-4}	-14.882
0.00330	2.714 x 10^{-5}	-16.2282	3.572 x 10^{-5}	-15.954	1.565 x 10^{-4}	-14.476
0.00325	8.304 x 10^{-5}	-15.1263	5.811 x 10^{-5}	-15.483	2.320 x 10^{-4}	-14.099

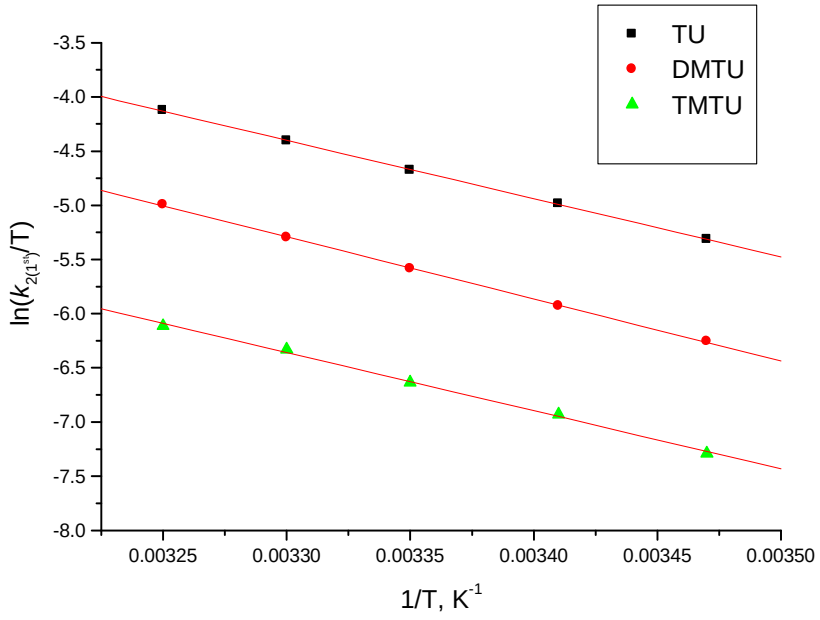

Figure S4.8: Plots of ln(k_1/ T) versus (1/T) for the first step reaction of **pzn** with a series of different nucleophiles at varying temperatures.

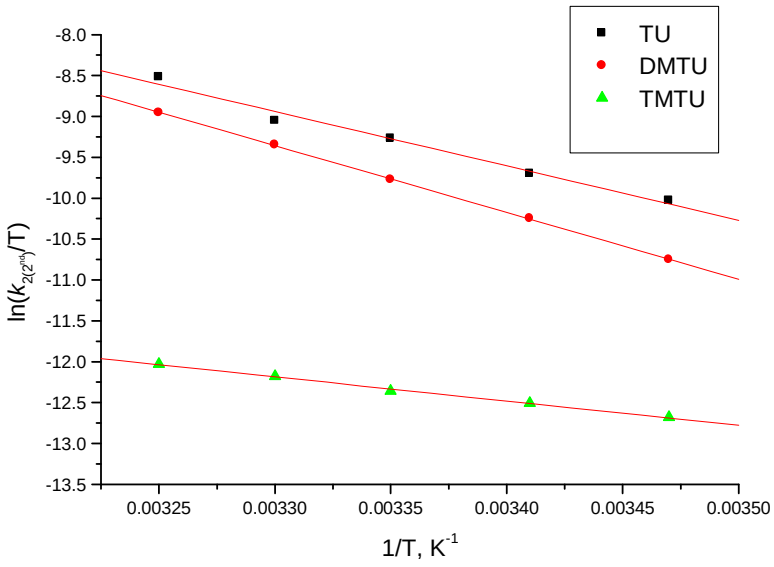

Figure S4.9: Plots of ln(k_2/ T) versus (1/T) for the second step reaction of **pzn** with a series of different nucleophiles at varying temperatures.

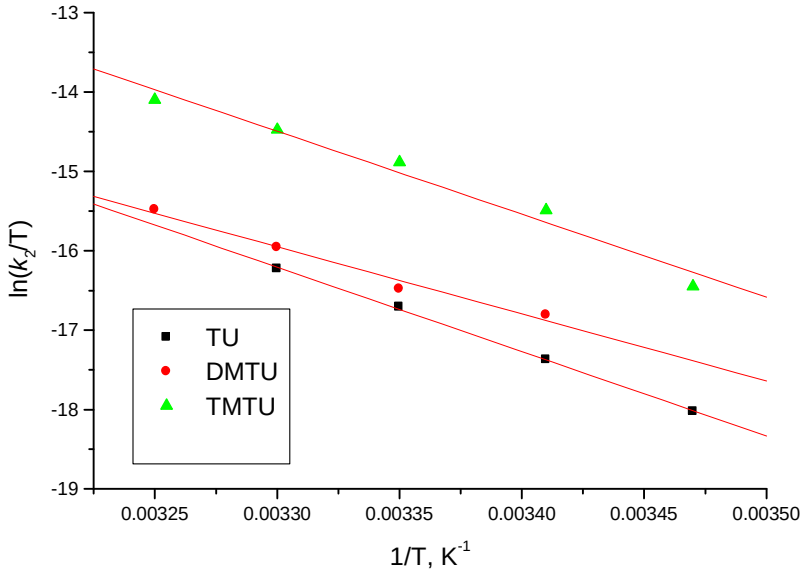

Figure S4.10: Plots of ln(k_3/ T) versus (1/T) for the third step reaction of **pzn** with a series of different nucleophiles at varying temperatures.

Table S4.8: Average observed rate constants, $k_{obs(1^{st})}$, at 298.15 K, for the first step reactions of **2, 6-pzn** with a series of nucleophiles at different concentrations.

[NU]/M	$k_{obs(1^{st})}$, **s^{-1}**		
	TU	**DMTU**	**TMTU**
0.00209	0.01710	0.02483	0.00759
0.00418	0.03424	0.04634	0.01372
0.00627	0.05140	0.06305	0.02285
0.00836	0.06827	0.08788	0.02944
0.01045	0.08428	-	-

Table S4.9: Average observed rate constants, $k_{obs(2^{nd})}$, at 298.15 K, for the second step reactions of **2, 6pzn** with a series of nucleophiles at different concentrations.

[NU]/ M	$k_{obs(2^{nd})}$, **s^{-1}**		
	TU	**DMTU**	**TMTU**
0.004	4.279×10^{-5}	3.670×10^{-5}	4.804×10^{-6}
0.008	8.743×10^{-5}	7.345×10^{-5}	9.711×10^{-6}
0.012	1.294×10^{-4}	1.075×10^{-4}	1.486×10^{-5}
0.016	1.739×10^{-4}	1.463×10^{-4}	2.008×10^{-5}
0.02	2.190×10^{-4}	1.798×10^{-4}	2.497×10^{-5}

Table S4.10: Average observed rate constants, $k_{obs(3^{rd})}$, at 298.15 K, for the second step reactions of **2, 6pzn** with a series of nucleophiles at different concentrations.

[NU]/ M	$k_{obs(3^{rd}),}$ s^{-1}		
	TU	DMTU	TMTU
0.004	3.287×10^{-5}	2.455×10^{-5}	1.087×10^{-5}
0.008	6.287×10^{-5}	4.899×10^{-5}	2.201×10^{-5}
0.012	9.643×10^{-5}	7.412×10^{-5}	3.318×10^{-5}
0.016	1.287×10^{-4}	9.811×10^{-5}	4.375×10^{-5}
0.02	1.567×10^{-4}	1.234×10^{-4}	5.434×10^{-5}

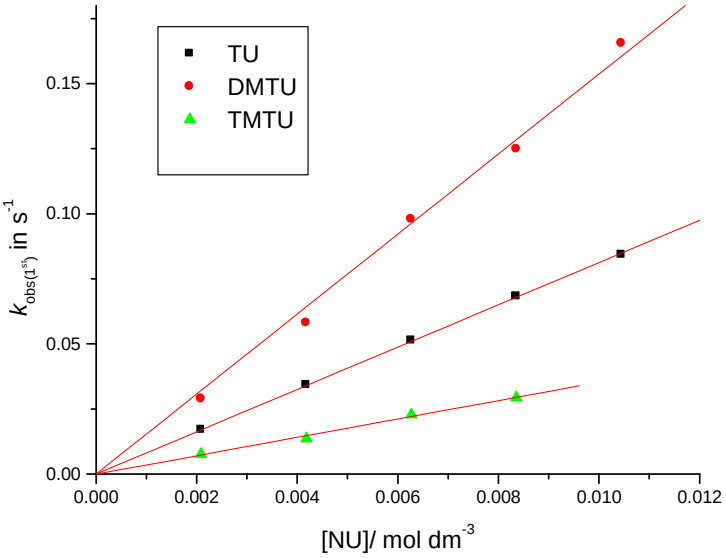

Figure S4.11: Concentration dependence of $k_{obs(1^{st})}$ for the displacement of first aqua ligand in **2,6pzn** by thiourea nucleophiles, pH = 2.0, T = 298.15 K, I = 0.10 M (0.01 M $HClO_4$, adjusted with $NaClO_4$).

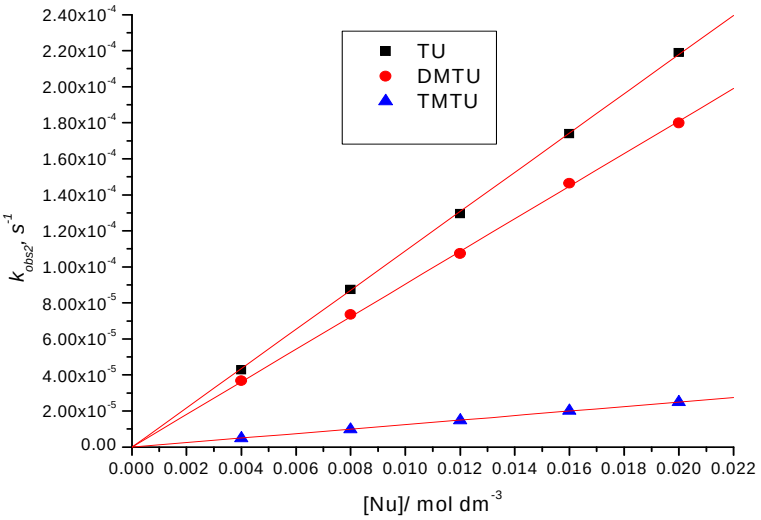

Figure S4.12: Concentration dependence of $k_{obs(2^{nd})}$ for the displacement of first aqua ligand in **2,6pzn** by thiourea nucleophiles, pH = 2.0, T = 298.15 K, I = 0.10 M (0.01 M $HClO_4$, adjusted with $NaClO_4$).

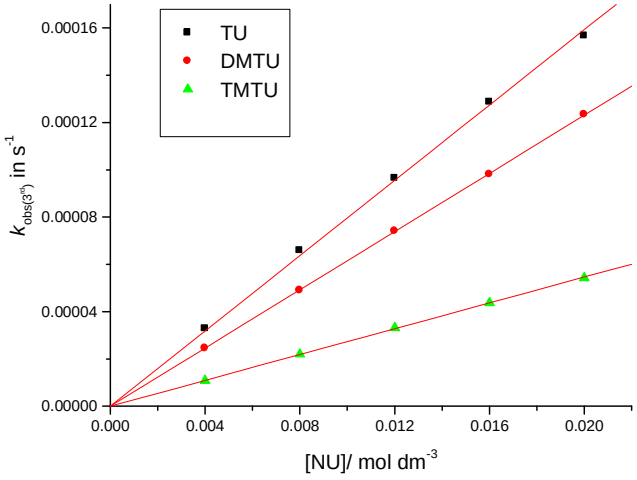

Figure S4.13: Concentration dependence of $k_{obs(3^{rd})}$ for the displacement of linker in **2,6pzn** by thiourea nucleophiles, pH = 2.0, T = 298.15 K, I = 0.10 M (0.01 M $HClO_4$, adjusted with $NaClO_4$).

Table S4.11: Average observed rate constants, $k_{obs(1^{st})}$, for the reactions of **2,6pzn** at varied temperatures in the range 15 to 35 °C while maintaining nucleophile concentration at ≈ 60x [**2,6pzn**].

1/T, K^{-1}	**TU**		**DMTU**		**TMTU**	
	$k_{obs(1^{st})}$, s^{-1}	**ln(k_2/T)**	**$k_{obs(1^{st})}$, s^{-1}**	**ln(k_2/T)**	**$k_{obs(1^{st})}$, s^{-1}**	**ln(k_2/T)**
0.00347	0.02538	-4.2648	0.02038	-4.4842	1.759 x 10^{-3}	-6.9340
0.00341	0.03571	-3.9405	0.03240	-4.0378	2.564 x 10^{-3}	-6.5744
0.00335	0.05140	-3.5932	0.04336	-3.7633	3.116 x 10^{-3}	-6.3963
0.00330	0.06903	-3.3150	0.06447	-3.3833	3.837 x 10^{-3}	-6.2048
0.00325	0.08866	-3.0811	0.08594	-3.1122	4.532 x 10^{-3}	-6.0547

Table S4.12: Average observed rate constants, $k_{obs(2^{nd})}$, for the reactions of **2,6pzn** at varied temperatures in the range 15 to 35 °C while maintaining nucleophile concentration at ≈ 60x [**2,6pzn**].

1/T, K^{-1}	**TU**		**DMTU**		**TMTU**	
	$k_{obs(2^{nd})}$, s^{-1}	**ln(k_2/T)**	**$k_{obs(2^{nd})}$, s^{-1}**	**ln(k_2/T)**	**$k_{obs(2^{nd})}$, s^{-1}**	**ln(k_2/T)**
0.00347	1.501 x 10^{-4}	-10.0431	-	-	1.759 x10^{-3}	-7.583
0.00341	2.286 x 10^{-4}	-9.641	1.360 x 10^{-4}	-10.160	2.564 x 10^{-3}	-7.224
0.00335	3.670 x 10^{-4}	-9.184	2.079 x 10^{-4}	-9.723	2.837 x 10^{-3}	-7.139
0.00330	4.503 x 10^{-4}	-8.997	3.021 x 10^{-4}	-9.396	3.116 x 10^{-3}	-7.062
0.00325	6.193 x 10^{-4}	-8.694	3.945 x 10^{-4}	-9.145	4.532 x 10^{-3}	-6.704

Table S4.13: Average observed rate constants, $k_{obs(3^{rd})}$, for the reactions of **2,6pzn** at varied temperatures in the range 15 to 35 °C while maintaining nucleophile concentration at ≈ 60x [**2,6pzn**].

1/T, K^{-1}	**TU**		**DMTU**		**TMTU**	
	$k_{obs(3^{rd})}$, s^{-1}	**ln(k_2/T)**	**$k_{obs(3^{rd})}$, s^{-1}**	**ln(k_2/T)**	**$k_{obs(3^{rd})}$, s^{-1}**	**ln(k_2/T)**
0.00347	4.429 x 10^{-5}	-11.265	-	-	-	-
0.00341	6.957 x 10^{-5}	-10.831	3.237 x10^{-5}	-11.596	1.214 x 10^{-5}	-12.576
0.00335	1.093 x 10^{-4}	-10.396	4.842 x 10^{-5}	-11.210	1.591 x 10^{-5}	-12.323
0.00330	1.484 x 10^{-4}	-10.106	8.249 x 10^{-5}	-10.694	2.133 x 10^{-5}	-12.046
0.00325	2.254 x 10^{-4}	-9.705	1.129 x 10^{-4}	-10.396	2.952 x 10^{-5}	-11.738

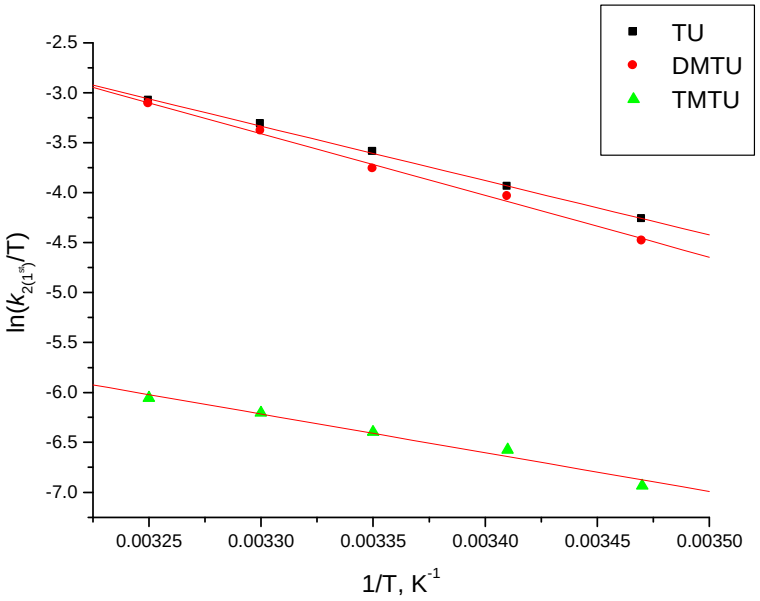

Figure S4.14: Graph of ln(k_2/ T) versus (1/T) for first step of the reaction of **2,6pzn** with a series of different nucleophiles at varying temperatures.

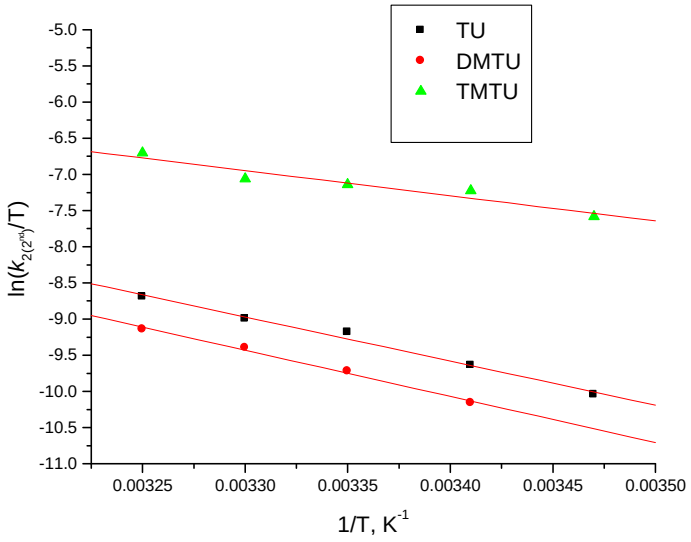

Figure S4.15: Graph of ln (k_2/ T) versus (1/T) for second step of the reaction of **2,6pzn** with a series of different nucleophiles at varying temperatures.

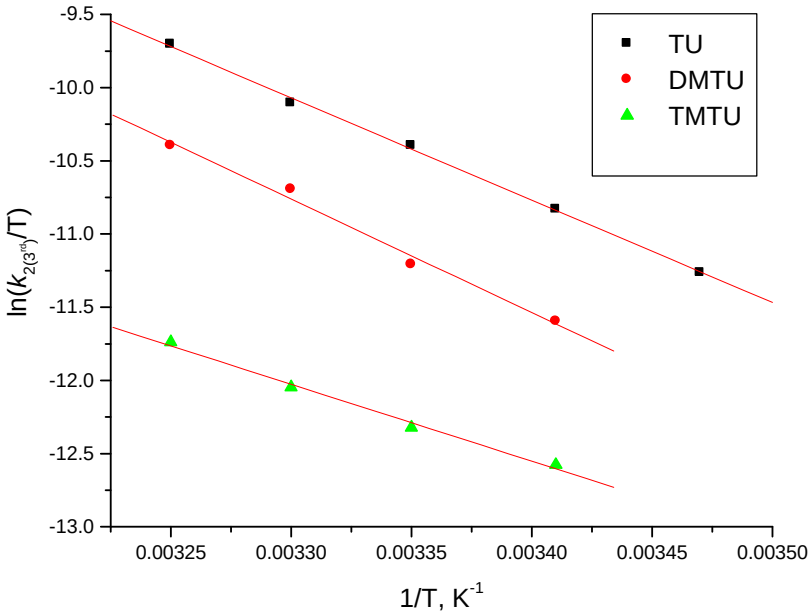

Figure S4.16: Graph of ln (k_2/ T) versus (1/T) for third step of the reaction of **2,6pzn** with a series of different nucleophiles at varying temperatures.

Table S4.14: Average observed rate constants, $k_{obs(1^{st})}$, at 298.15 K, for the first step reactions of **2, 5-pzn** with a series of nucleophiles at different concentrations.

[NU]/ M	$k_{obs(1^{st})}$, **s^{-1}**		
	TU	**DMTU**	**TMTU**
0.0017	0.007685	0.00379	0.000747
0.0034	0.014670	0.00749	0.001430
0.0051	0.022450	0.01115	0.002080
0.0068	0.029650	0.01505	0.002820
0.0085	0.037570	0.01887	0.003800

Table S4.15: Average observed rate constants, $k_{obs(3^{rd})}$, at 298.15 K, for the third step reactions of **2, 5pzn** with a series of nucleophiles at different concentrations.

[NU]/ M	$k_{obs(3^{rd})}$, **s^{-1}**		
	TU	**DMTU**	**TMTU**
0.0017	1.198×10^{-5}	6.790×10^{-6}	2.225×10^{-6}
0.0034	2.523×10^{-5}	1.318×10^{-5}	5.199×10^{-6}
0.0051	3.720×10^{-5}	2.027×10^{-5}	7.883×10^{-6}
0.0068	4.842×10^{-5}	2.538×10^{-5}	1.123×10^{-5}
0.0085	6.280×10^{-5}	3.208×10^{-5}	1.475×10^{-5}

Table S4.16: Average observed rate constants, $k_{obs(1^{st})}$, for the reactions of **2,5pzn** at varied temperatures in the range 15 to 35 °C while maintaining nucleophile concentration at ≈ 60x [**2,5pzn**].

1/T, K^{-1}	**TU**		**DMTU**		**TMTU**	
	$k_{obs(1^{st})}$, s^{-1}	**ln(k_2/T)**	**$k_{obs(1^{st})}$, s^{-1}**	**ln(k_2/T)**	**$k_{obs(1^{st})}$, s^{-1}**	**ln(k_2/T)**
0.00347	8.44 x 10^{-3}	-5.1592	4.813 x10^{-3}	-5.7209	1.110 x 10^{-3}	-7.1870
0.00341	0.01197	-4.8272	6.796 x 10^{-3}	-5.3931	1.571 x 10^{-3}	-6.8578
0.00335	0.01684	-4.5026	9.592 x 10^{-3}	-5.0654	2.083 x 10^{-3}	-6.5924
0.00330	0.02270	-4.2206	0.01292	-4.7842	2.626 x 10^{-3}	-6.3775
0.00325	0.02958	-3.9722	0.01718	-4.5156	3.472 x 10^{-3}	-6.1146

Table S4.17: Average observed rate constants, $k_{obs(2^{nd})}$, for the reactions of **2**,**5pzn** at varied temperatures in the range 15 to 35 °C while maintaining nucleophile concentration at ≈ 60x [**2**,**5pzn**].

1/T, K^{-1}	**TU**		**DMTU**		**TMTU**	
	$k_{obs(2^{nd})}$, s^{-1}	**ln(k_2/T)**	**$k_{obs(2^{nd})}$, s^{-1}**	**ln(k_2/T)**	**$k_{obs(2^{nd})}$, s^{-1}**	**ln(k_2/T)**
0.00347	3.030 x 10^{-4}	-8.4862	5.510 x 10^{-4}	-7.8882	1.982 x 10^{-5}	-11.2600
0.00341	4.520 x 10^{-4}	-8.1035	7.800 x 10^{-4}	-7.5579	2.854 x 10^{-5}	-10.8765
0.00335	6.318 x 10^{-4}	-7.7855	1.050 x 10^{-3}	-7.2775	3.995 x 10^{-5}	-10.5465
0.00330	9.040 x 10^{-4}	-7.4438	1.372 x 10^{-3}	-7.0282	5.763 x 10^{-5}	-10.1967
0.00325	1.160 x 10^{-3}	-7.2109	-	-	7.560 x 10^{-5}	-9.941

Table S4.18: Average observed rate constants, $k_{obs(3^{rd})}$, for the reactions of **2,5pzn** at varied temperatures in the range 15 to 35 °C while maintaining nucleophile concentration at ≈ 60x [**2,5pzn**].

1/T, K^{-1}	**TU**		**DMTU**		**TMTU**	
	$k_{obs(3^{rd})}$, s^{-1}	**ln(k_2/T)**	**$k_{obs(3^{rd})}$, s^{-1}**	**ln(k_2/T)**	**$k_{obs(3^{rd})}$, s^{-1}**	**ln(k_2/T)**
0.00347	2.117 x 10^{-5}	-11.1475	1.802 x 10^{-5}	-11.3084	8.652 x 10^{-6}	-12.0422
0.00341	3.070 x 10^{-5}	-10.7931	2.654 x 10^{-5}	-10.9384	1.264 x 10^{-5}	-11.6805
0.00335	4.234 x 10^{-5}	-10.4885	3.315 x 10^{-5}	-10.7330	2.075 x 10^{-5}	-11.2015
0.00330	6.139 x 10^{-5}	-10.1335	4.453 x 10^{-5}	-10.4545	2.528 x 10^{-5}	-11.0207
0.00325	8.467 x 10^{-5}	-9.8283	5.417 x 10^{-5}	-10.2749	4.154 x 10^{-5}	-10.5445

Table S4.19: Average observed rate constants, $k_{obs(1^{st})}$, at 298.15 K, for the first step reactions of **2, 3pzn** with a series of nucleophiles at different concentrations.

[NU]/ M	**$k_{obs(1^{st})}$, s^{-1}**		
	TU	**DMTU**	**TMTU**
0.02	0.0096	0.00477	8.936 x 10^{-4}
0.04	0.0204	0.00841	0.00174
0.06	0.0316	0.01241	0.00260
0.08	0.0428	0.01772	0.00348
0.1	0.0552	0.02129	0.00436

Table S4.20: Average observed rate constants, $k_{obs(2^{nd})}$, at 298.15 K, for the second step reactions of **2,3pzn** with a series of nucleophiles at different concentrations.

[NU]/ M	$k_{obs(1)}$, **s^{-1}**		
	TU	**DMTU**	**TMTU**
0.0017	5.543 x 10^{-4}	2.873 x 10^{-4}	1.889 x 10^{-4}
0.0034	0.00112	6.239 x 10^{-4}	3.959 x 10^{-4}
0.0051	0.00171	9.470 x 10^{-4}	5.294 x 10^{-4}
0.0068	0.00230	0.00128	-
0.0085	0.00287	0.00162	9.805 x 10^{-4}

Table S4.21: Average observed rate constants, $k_{obs(3^{rd})}$, at 298.15 K, for the second step reactions of **2,3pzn** with a series of nucleophiles at different concentrations.

[NU]/ M	$k_{obs(3^{rd})}$, **s^{-1}**		
	TU	**DMTU**	**TMTU**
0.004	2.152 x 10^{-5}	7.850 x 10^{-6}	5.685 x 10^{-6}
0.008	4.141 x 10^{-5}	1.596 x 10^{-5}	1.042 x 10^{-5}
0.012	6.259 x 10^{-5}	2.320 x 10^{-5}	1.652 x 10^{-5}
0.016	8.098 x 10^{-5}	3.125 x 10^{-5}	2.287 x 10^{-5}
0.02	9.997 x 10^{-5}	3.921 x 10^{-5}	2.953 x 10^{-5}

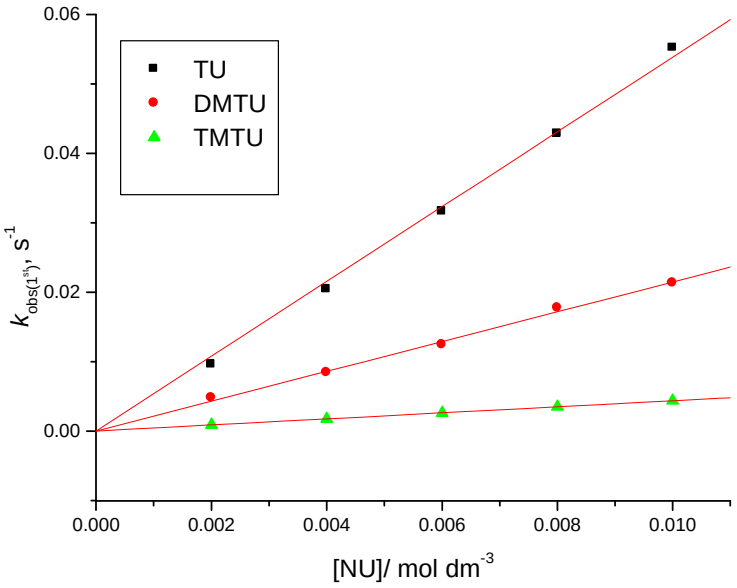

Figure S4.17: Concentration dependence of $k_{obs(1^{st})}$ for the displacement of first aqua ligand in **2,3pzn** by thiourea nucleophiles, pH = 2.0, T = 298.15 K, I = 0.10 M (0.01 M $HClO_4$, adjusted with $NaClO_4$).

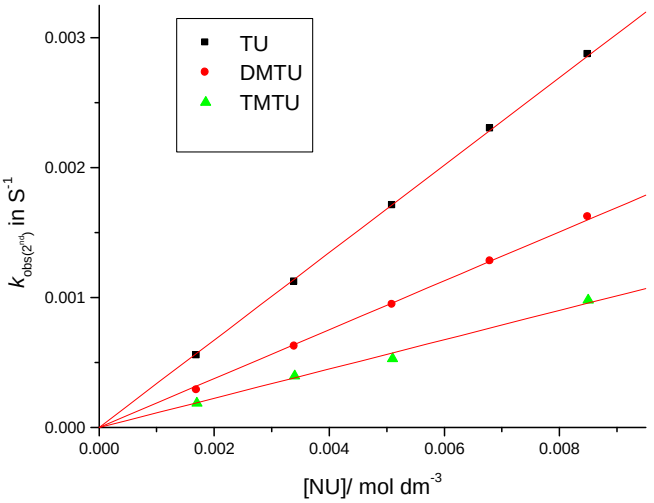

Figure S4.18: Concentration dependence of $k_{obs(1^{st})}$ for the displacement of first aqua ligand in **2,3pzn** by thiourea nucleophiles, pH = 2.0, T = 298.15 K, I = 0.10 M (0.01 M $HClO_4$, adjusted with $NaClO_4$).

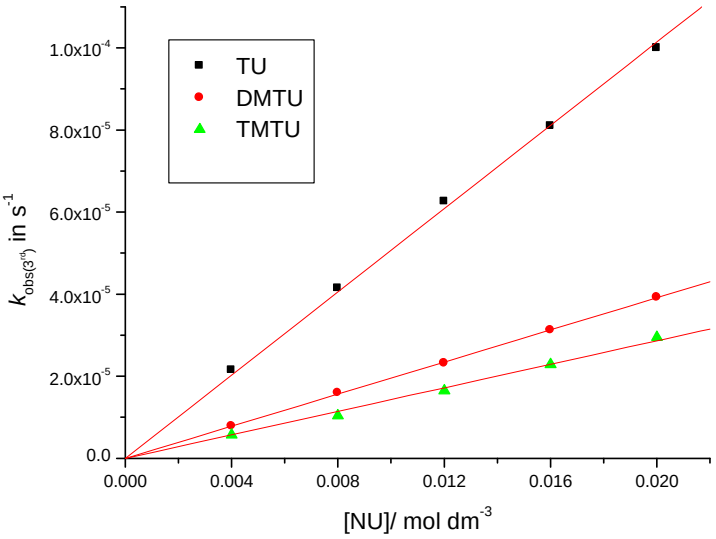

Figure S4.19: Concentration dependence of $k_{obs(3^{rd})}$ for the displacement of linker in **2,3pzn** by thiourea nucleophiles, pH = 2.0, T = 298.15 K, I = 0.10 M (0.01 M $HClO_4$, adjusted with $NaClO_4$).

Table S4.22: Average observed rate constants, $k_{obs(1^{st})}$, for the first step reactions of **2,3pzn** at varied temperatures in the range 15 to 35 °C while maintaining nucleophile concentration at ≈ 60x [**2,3pzn**].

1/T, K^{-1}	**TU**		**DMTU**		**TMTU**	
	$k_{obs(1^{st})}$, s^{-1}	**ln(k_2/T)**	**$k_{obs(1^{st})}$, s^{-1}**	**ln(k_2/T)**	**$k_{obs(1^{st})}$, s^{-1}**	**ln(k_2/T)**
0.00347	0.01113	-5.0451	5.104 x 10^{-3}	-5.8247	1.4165 x 10^{-3}	-7.1065
0.00341	0.01570	-4.7183	7.192 x 10^{-3}	-5.4990	1.9177 x 10^{-3}	-6.7413
0.00335	0.02167	-4.4129	0.01011	-5.1753	2.6020 x 10^{-3}	-6.5488
0.00330	0.03145	-4.0571	0.01332	-4.9162	3.1454 x 10^{-3}	-6.3595
0.00325	0.04456	-3.7250	0.01766	-4.6506	4.2479 x 10^{-3}	-6.0754

Table S4.23: Average observed rate constants, $k_{obs(2^{nd})}$, for the second step reactions of **2,3pzn** at varied temperatures in the range 15 to 35 °C while maintaining nucleophile concentration at ≈ 60x [**2,3pzn**].

1/T, K^{-1}	**TU**		**DMTU**		**TMTU**	
	$k_{obs(2^{nd})}$, s^{-1}	**ln(k_2/T)**	**$k_{obs(2^{nd})}$, s^{-1}**	**ln(k_2/T)**	**$k_{obs(2^{nd})}$, s^{-1}**	**ln(k_2/T)**
0.00347	6.932 x 10^{-5}	-10.1238	3.947 x 10^{-4}	-8.3844	4.218 x 10^{-5}	-10.6210
0.00341	1.041 x 10^{-4}	-9.7340	6,237 x 10^{-4}	-7.9440	6.521 x 10^{-5}	-10.2021
0.00335	1.578 x 10^{-4}	-9.3351	9.737 x 10^{-4}	-7.5155	1.084 x 10^{-4}	-9.7108
0.00330	2.070 x 10^{-4}	-9.0807	1.493 x 10^{-3}	-7.1050	1.526 x 10^{-4}	-9.3851
0.00325	3.313 x 10^{-4}	-8.6265	2.256 x 10^{-3}	-6.6500	2.109 x 10^{-4}	-9.0783

Table S4.24: Average observed rate constants, $k_{obs(3^{rd})}$, for the reactions of **2**,**3pzn** at varied temperatures in the range 15 to 35 °C while maintaining nucleophile concentration at ≈ 60x [**2**,**3pzn**].

1/T, K^{-1}	**TU**		**DMTU**		**TMTU**	
	$k_{obs(3^{rd})}$, s^{-1}	**ln(k_2/T)**	**$k_{obs(3^{rd})}$, s^{-1}**	**ln(k_2/T)**	**$k_{obs(3^{rd})}$, s^{-1}**	**ln(k_2/T)**
0.00347	1.823 x 10^{-5}	-11.4603	1.357 x 10^{-5}	-11.7546	6.486 x 10^{-6}	-12.4928
0.00341	2.509 x 10^{-5}	-11.1574	2.161 x 10^{-5}	-11.3065	1.065 x 10^{-5}	-12.0140
0.00335	3.643 x 10^{-5}	-10.8013	3.154 x 10^{-5}	-10.9454	1.547 x 10^{-5}	-11.6578
0.00330	4.984 x 10^{-5}	-10.5207	4.573 x 10^{-5}	-10.5906	2.139 x 10^{-5}	-11.3545
0.00325	7.257 x 10^{-5}	-10.1950	6.363 x 10^{-5}	-10.2765	3.243 x 10^{-5}	-10.9505

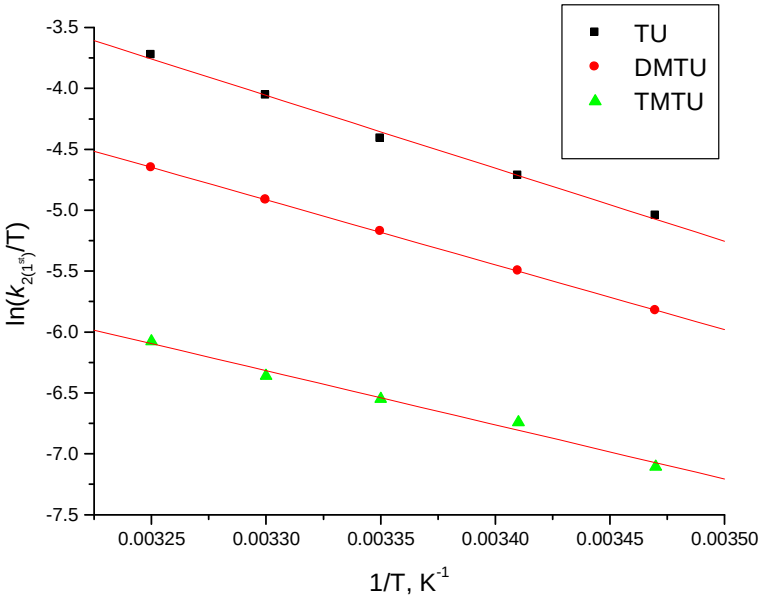

Figure S4.20: Graph of ln (k_2/ T) versus (1/T) for first step of the reaction of **2,3pzn** with a series of different nucleophiles at varying temperatures.

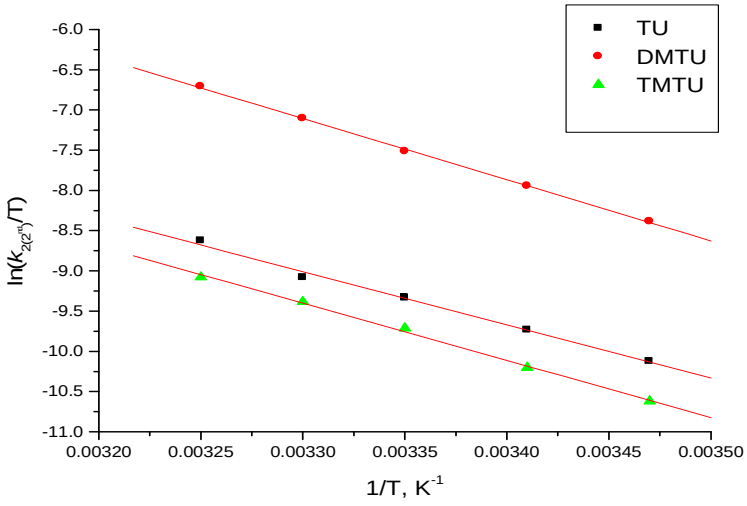

Figure S4.21: Graph of ln (k_2/ T) versus (1/T) for second step of the reaction of **2,3pzn** with a series of different nucleophiles at varying temperatures.

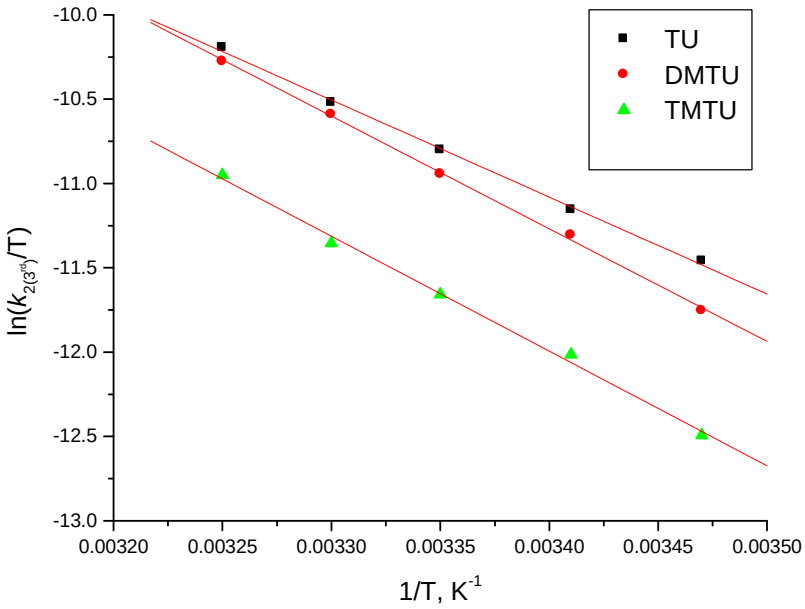

Figure S4.22: Graph of ln (k_2/ T) versus (1/T) for third step of the reaction of **2,3pzn** with a series of different nucleophiles at varying temperatures.

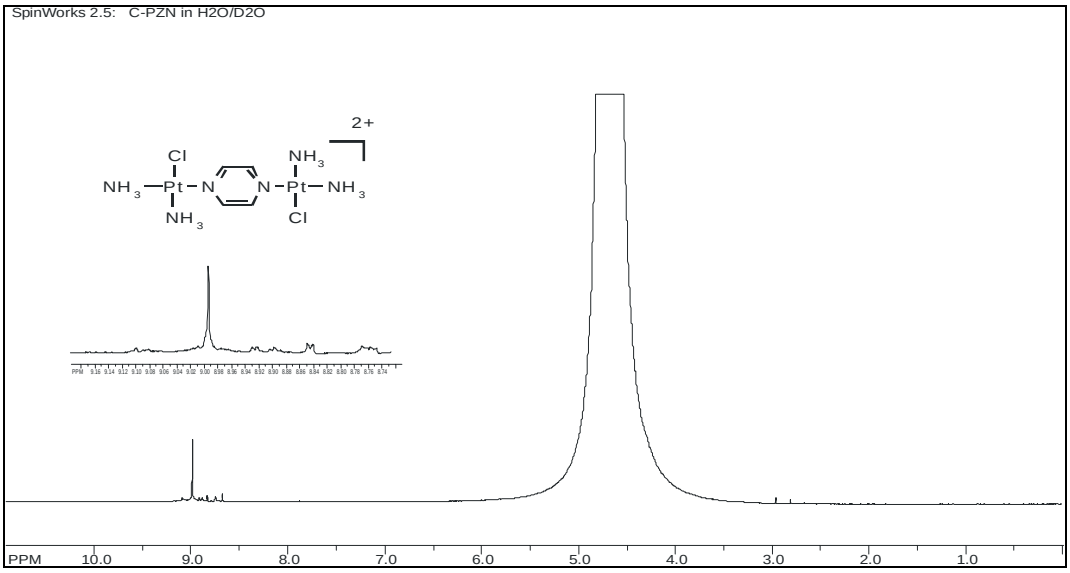

Figure S4.23: 500MHz ^{1}H NMR spectrum of a D_2O solution of **[*cis*–{PtCl(NH$_3$)$_2$}$_2$–μ–pzn]**$(ClO_4)_2$ showing pyrazine ring proton assignment.

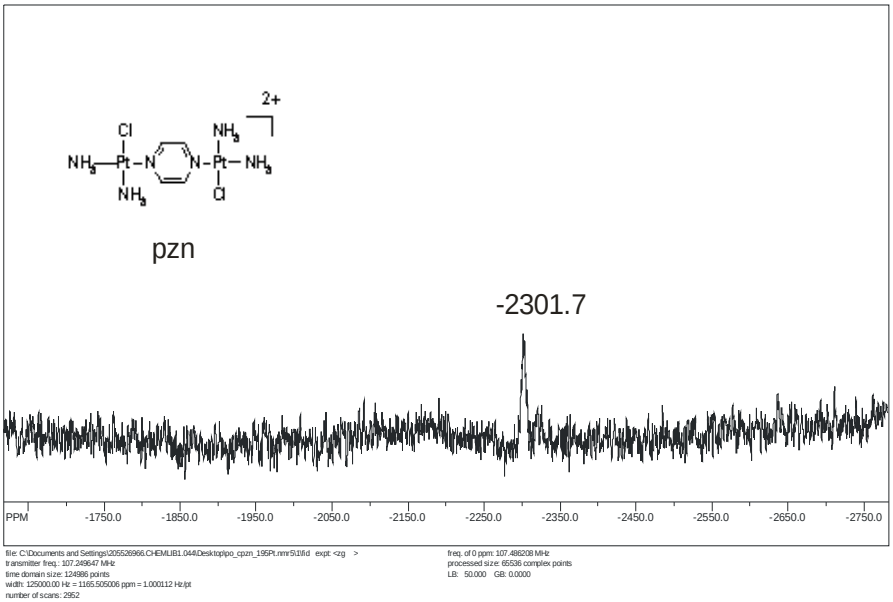

Figure S4.24: The 107 MHz ^{195}Pt NMR spectrum of [***cis*–{PtCl(NH$_3$)$_2$}$_2$–μ–pzn](ClO$_4$)$_2$** showing PtN_3Cl coordination.

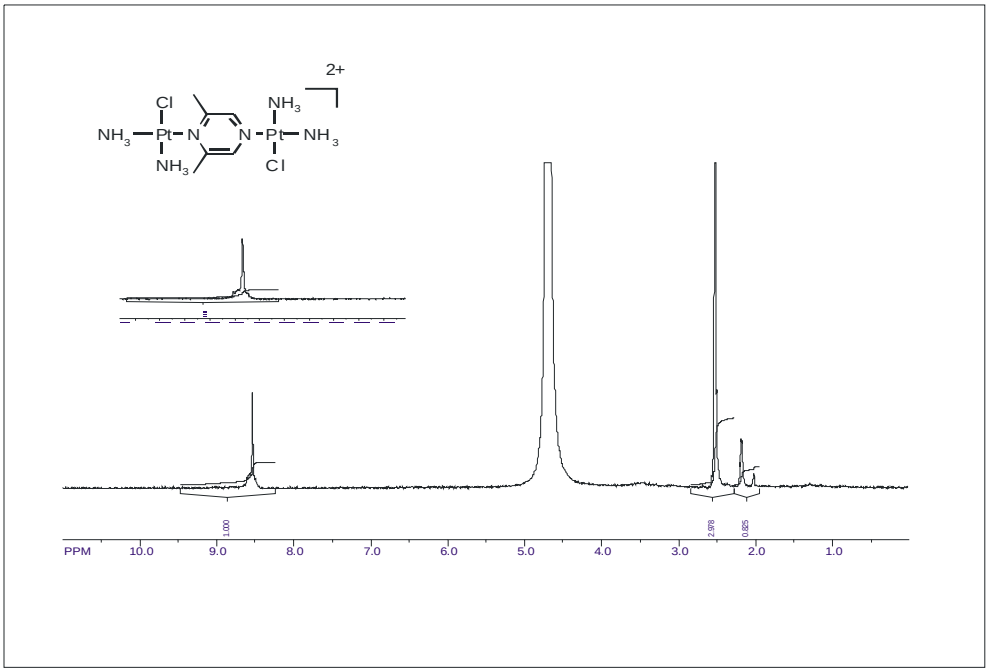

Figure S4.25: 500MHz ^{1}H NMR spectrum of a D_2O solution of **[*cis*–{PtCl(NH$_3$)$_2$}$_2$–μ–2,6pzn](ClO$_4$)$_2$** showing pyrazine ring and methyl proton assignments.

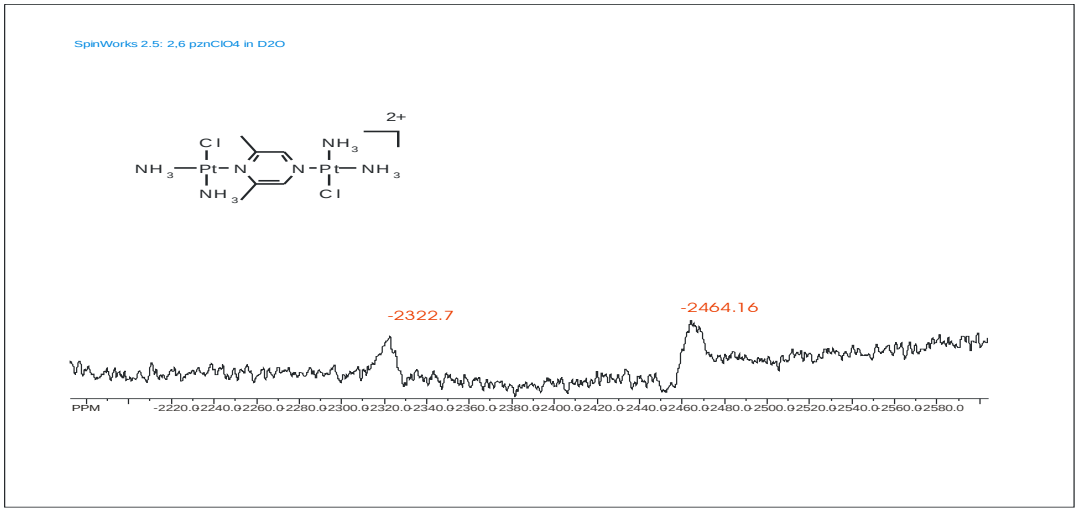

Figure S4.26: The 107 MHz ^{195}Pt NMR spectrum of **[*cis*–{PtCl(NH$_3$)$_2$}$_2$–μ–2,6pzn](ClO$_4$)$_2$** showing Pt1N$_3$Cl and Pt2N$_3$Cl coordination Pt labels are as defined in Scheme 4.1.

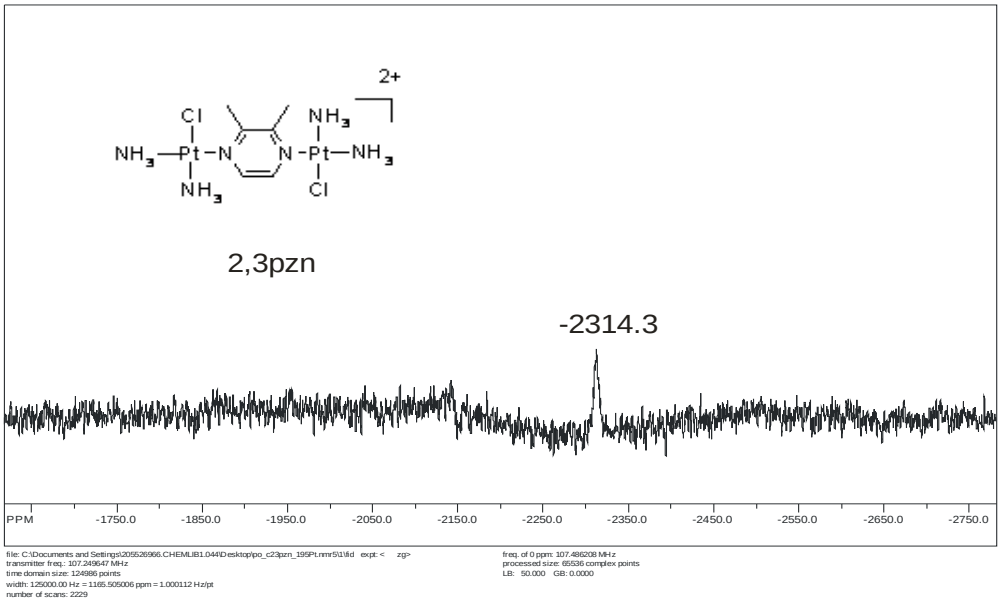

Figure S4.27: The 107 MHz ^{195}Pt NMR spectrum of **[*cis*–{PtCl(NH$_3$)$_2$}$_2$–μ–2,3pzn](ClO$_4$)$_2$**.

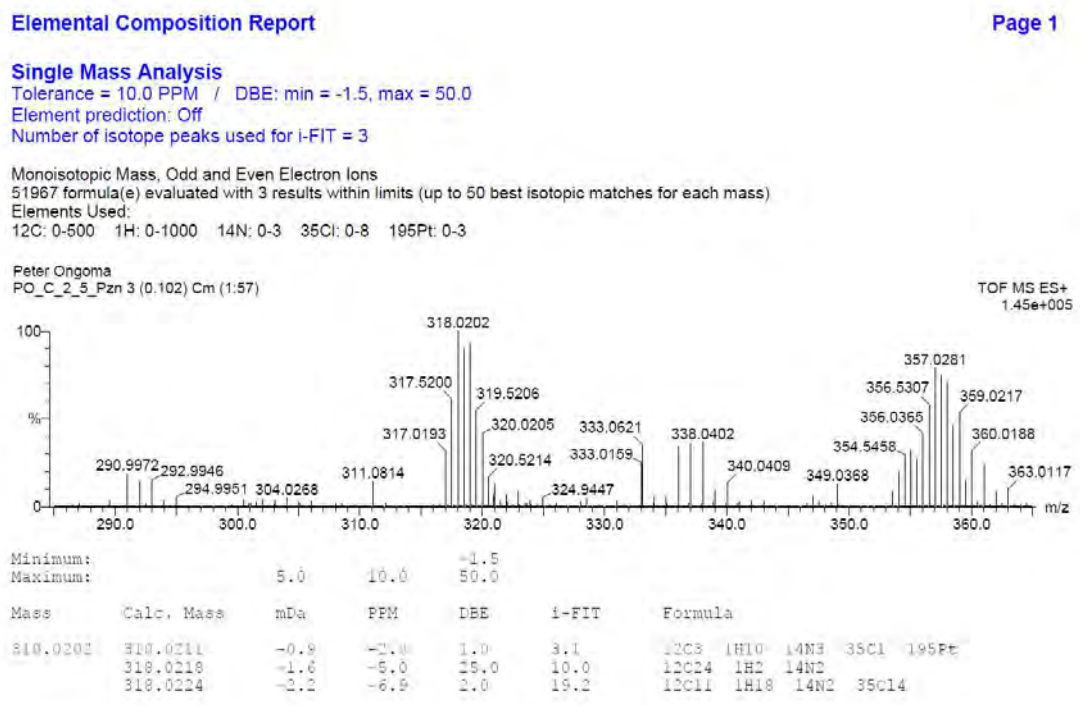

Figure S29: Mass spectrum for complex **2,5pzn (**m/e, M^{2+})

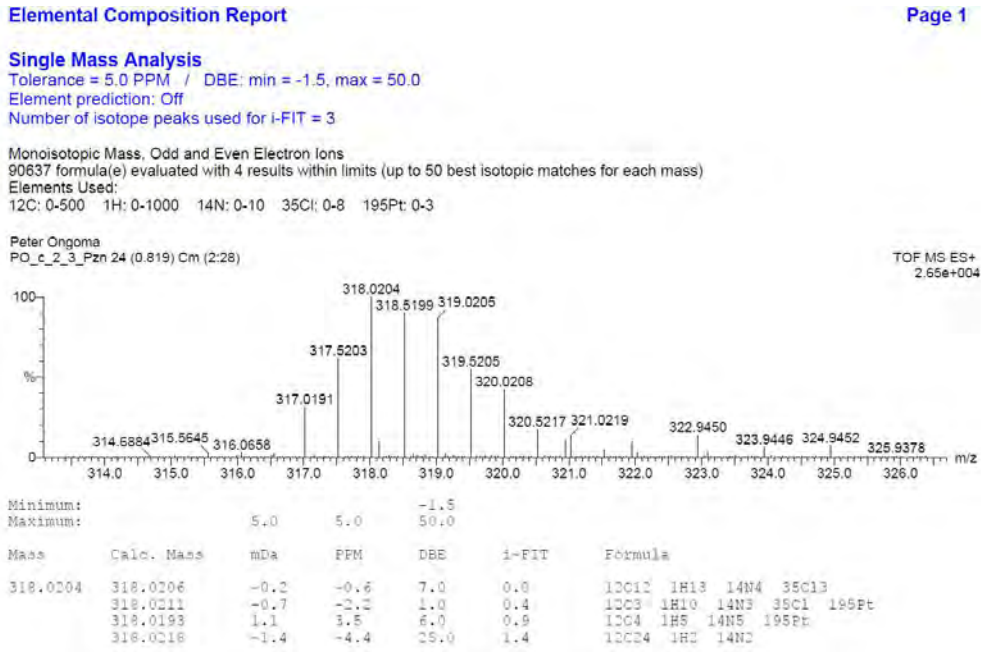

Figure S30 Mass spectrum for complex **2,3pzn (**m/e, M^{2+})

Table of Contents-5

List of Figures

List of Tables

Chapter 5

Substitution Reactions in Dinuclear Platinum(II) Complexes: *an Evaluation of the Influence of the Diazine-bridge on Reactivity*

5.0 Abstract

The kinetics of substitution reactions of aqua dinuclear Pt(II) complexes, **[{cis–Pt(OH$_2$)(NH$_3$)$_2$}$_2$–μ–pmn](ClO$_4$)$_2$** (**pmn**), **[{cis–Pt(OH$_2$)(NH$_3$)$_2$}$_2$–μ–pdn](ClO$_4$)$_2$** (**pdn**), **[{cis–Pt(OH$_2$)(NH$_3$)$_2$}$_2$–μ–qzn](ClO$_4$)$_2$** (**qzn**), **[{cis–Pt(OH$_2$)(NH$_3$)$_2$}$_2$–μ–pht](ClO$_4$)$_2$** (**pht**), and **[{cis–Pt(OH$_2$)(NH$_3$)$_2$}$_2$–μ–pzn](ClO$_4$)$_2$** (**pzn**) (pmn = pyrimidine, pdn = pyridazine, qzn = quinazoline, pht = phthalazine, pzn = pyrazine) and sulphur-donor nucleophiles, *viz*. thiourea (TU), *N,N*–dimethylthiourea (DMTU) and *N,N,N,N*–tetramethylthiourea (TMTU) were investigated. The reactions were followed under *pseudo* first-order conditions as a function of nucleophile concentration and temperature using stopped-flow and UV-Vis Spectrophotometric methods. The reactivity of the nucleophiles follows the order TU > DMTU > TMTU. The results of the rate constants for the consecutive substitution of the aqua ligand showed that **pzn** is more reactive than the rest of dinuclear complexes. The reactivity of the aqua complexes follows the order **pzn** > **qzn** > **pmn** > **pdn** > **pht** which was confirmed by the quantum chemical (DFT) NBO charges and the pK_a calculations. The results indicate that changing the position or distance of the N atoms of the bridging ligand controls the electrophilicity of the metal centre and hence its reactivity. The results further indicate that the metal centre is activated differently in the cases of **qzn** and **pht,** even though both are part of a π–conjugated system. The negative values reported for the activation entropy confirm the associative nature of substitution process. ^{1}H NMR was used to follow the substitution of the aqua ligand by excess thiourea and confirmed the displacement of the bridging ligand in the third step in all cases. The results clearly demonstrate a strong connection between the reactivity of the dinuclear Pt(II) complexes with sulphur nucleophiles and their structural and electronic characteristics.

5.1 Introduction

Multinuclear platinum(II) complexes containing heterocyclic amine carrier ligands represent a novel class of anticancer drugs[1–7] that can overcome both acquired and intrinsic resistance to cisplatin, *cis*-$PtCl_2(NH_3)_2$. In addition, they also form different binding modes to DNA.[6,8] One of the advantages of these dinuclear platinum(II) complexes compared to cisplatin, is their strong binding affinity for intracellular polyanionic DNA due to their relatively large positive charge (+4/+2).[9] Studies in this area of multinuclear complexes are motivated by the tenet that bridging ligands play important roles in regulating reactivity of the metal ions by controlling the geometric symmetry, distance separating the coordinated metal ions, steric and electronic features at the metal centre.[3,10–12] However, systematic investigation of the kinetic and thermodynamic properties of the dinuclear platinum (II) complexes in which the aromatic diazine ligands act as linkers is relatively unexplored with only one paper reported in literature.[13]

Most of the studies that are available in the public domain involve α,ω-alkanediamine[10] and bis-(2-pyridylmethyl) amine-bridged dinuclear platinum(II) complexes.[12–18] The results from these investigations show that as the aliphatic-chain separating the two platinum centres increases the extent of reactivity reaches a maximum.[17,18] Such behaviour is consistent with the decrease in charge additions as well as the steric influences, which decrease proportionally as the chain length increases in dinuclear complexes.[18] However, it is unclear whether such metal-to-metal interactions would be mediated by direct binding between the platinum atoms or by the bridging ligands when the distance is shortened using rigid aromatic bridging ligands like azoles and diazines. In most cases, long distance metal-to metal interactions are transmitted through conjugated π-systems.[19–21] In fact, the rate of substitution decreases by a factor of 60, if communication between aromatic rings is destroyed.[22]

Recent studies in our research group involving dimethypyrazine and pyridyl-bridging ligands have shown degradation of the linker; which is contrary to the commonly accepted knowledge that the *cis* geometry, in the species such **as [{*cis*–$PtCl(NH_3)_2$}$_2$–μ–$H_2N(CH_2)_6NH_2$]$^{+2}$**, is less susceptible to metabolic decomposition by the sulphur

nucleophiles.[23] What's more is that *trans*-$Pt(NH_3)_2(H_2N(CH_2)_6NH_2)_2$ (**BBR3464**) molecule and related structures are susceptible to decomposition,[4,24,25] since the *trans*-influence of S donors has the propensity to liberate the alkanediamine linker, especially where the Pt–Cl bond is *trans* to the linking diamine.[26]

Heterocyclic diazines such as pyrazine, pyrimidine, pyridazine and related N-containing heterocyclic derivatives are excellent bridging ligands when coordinated to transition metals.[27,28] These heterocyclic ligands are π-electron deficient (i.e., have low-lying empty π*-orbitals),[29] and hence, are capable of withdrawing electron density from soft metal centres like Pt(II) leading to increased electrophilicity at the metal centre.[30] In addition, their complexes have high stability with respect to metal ion dissociation owing to the synergistic combination of σ-donating N atoms and π-accepting heterocycles coupled with the ability to form chelates.[29] Dinuclear metal complexes bridged by pyridazine and phthalazine are of particular interest because the bridge provides a shorter metal-metal separation distance of 3.2-4.5 Å, which makes them unstable compared to typical diamine ligands such as phenanthroline and bipyridine due to steric and electronic properties.[29]

Therefore in the present study, the kinetics and mechanism of substitution of coordinated water ligands from rigid diazine-bridged dinuclear platinum(II) complexes of the type **$[\{cis\text{–}Pt(NH_3)_2(H_2O)\}_2\text{–}\mu\text{–}z]^{+2}$**, (z = diazine heterocyclic ring like pyrazine, pyrimidine, pyridazine and related benzodiazines presented in Scheme 1 using sulphur-donor nucleophiles is reported. These dinuclear complexes differ in the relative disposition of the two Pt(II) centres (e.g. 180° with pyrazine; 120° with pyrimidine, pyridazine and their benzodiazine derivatives, quinazoline and phthalazine); metal-metal (Pt---Pt) distances, steric and electronic properties of the linker. Thus, by incorporating higher steric crowding around the platinum(II) centre using different diazine ligands of varying structural geometry will open an avenue for exploring the mechanistic aspect of the nucleophilic interaction with the metal centre under different structural environment. Herein, thiourea and its derivatives are chosen as nucleophiles because of their varying nucleophilicity and steric effects. Thiourea ligands may act as strong σ-donors with a metal ion and at the same time stabilized by $d\pi$–$p\pi$ back

bonding. For this reason, pK_a titrations and nucleophilic substitution reactions of the complexes shown in Scheme 5.1 were performed. The experimental work is supported by computational (DFT) calculations.

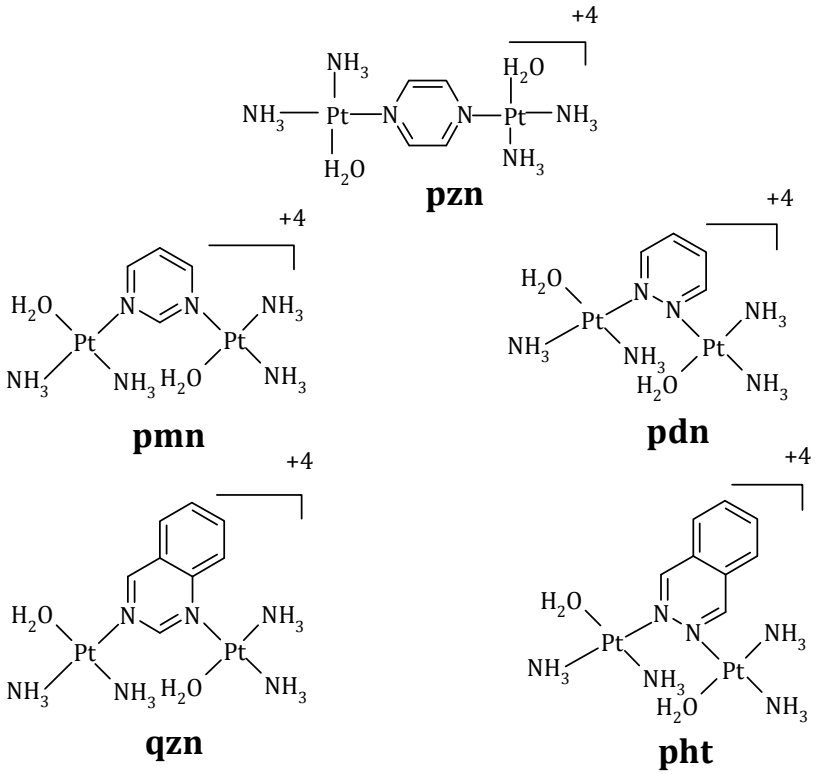

Scheme 5.1: Representative structures and abbreviations of the azine-bridged dinuclear complexes.

5.2 Experimental

5.2.1 Chemical and Solutions

Cisplatin *(cis*-($PtCl_2(NH_3)_2$, 99%) was purchased from Strem Chemicals. The nucleophiles thiourea (TU, 99%), 1,3-dimethyl-2-thiourea (DMTU, 99%), 1,1,3,3-tetramethyl-2-thiourea (TMTU, 98%)and diazine ligands: pyrazine (pzn, 99%), pyrimidine (pmn, 99%), pyridazine (pdn, 99%), quinazoline (qzn, 99%), phthalazine

(pht, 99%), including sodium perchlorate monohydrate †($NaClO_4.H_2O$, 98%)and perchloric acid ($HClO_4$, 70%) were purchased from Aldrich and used without further purification. Silver perchlorate ($AgClO_4$, 99.9%) from Aldrich was stored under nitrogen and used as supplied. Methanol (Saarchem) was distilled and dried over magnesium before use.[31] For all preparations of aqueous solutions, ultrapure water (Modulab Systems) was used.

5.2.2 Synthesis of the Dinuclear Pt(II) chloro-complexes (pzn to pht)

The dinuclear platinum(II) complexes **[{*cis*–PtCl(NH_3)$_2$}$_2$–μ–pzn](ClO$_4$)$_2$** (**pzn**), **[{*cis*–PtCl(NH_3)$_2$}$_2$–μ–pmn](ClO$_4$)$_2$** (**pmn**), **[{*cis*–PtCl(NH_3)$_2$}$_2$–μ–pdn](ClO$_4$)$_2$** (**pdn**), [{***cis*–PtCl(NH_3)$_2$}$_2$–μ–qzn]Cl$_2$** (**qzn**), and **[{*cis*–PtCl(NH_3)$_2$}$_2$–μ–pht](ClO$_4$)$_2$** (**pht**), were synthesized from the precursor molecule, **[{*cis*–PtCl(NH_3)$_2$(DMF)]ClO$_4$**, according to a literature method[32] using $AgClO_4$. The synthetic method is the same as described in chapter 4 (section 4.2.3).

Their purity was confirmed by micro-elemental analysis, infrared (IR), ^{1}H and ^{195}Pt NMR. The IR spectra of all the complexes exhibited common characteristic peaks in the range 326-400 cm^{-1} (weak) for Pt–Cl and 1090-1100 cm^{-1} (broad, strong) for Cl–O (perchlorate counter ion) vibration stretches, respectively.

pzn: Yield: 382.8 mg (0. 474 mmol, 45.5%). ^{1}H NMR (500.5 MHz, D_2O) δ /ppm: ^{1}H: 8.99, s (4H). ^{195}Pt NMR (107.5 MHz, D_2O): δ/ ppm: -2302.20. IR (KBr, 4000-300 cm^{-1}): 3305, 3224, 3107 (N–H stretch); 1658 (C=N, pyrazine group stretch); 1090-1100 (perchlorate counter ion); 450-490 (Pt–N stretch); 340 (Pt–Cl stretch). *Anal. Calcd for* $C_4H_{16}N_6Cl_4O_8Pt_2$: H, 2.00; C, 5.94; N, 10.40. *Found*: H, 2.23; C, 5.45; N, 9.90%.

pmn: Yield: 220.9 mg (0. 273 mmol, 44.3%). ^{1}H NMR (500.5 MHz, D_2O) δ/ppm:10.01 (s, 1H); 9.26 (d, 2H); 7.85, (t, 1H). ^{195}Pt NMR (107.5 MHz, D_2O) δ/ ppm: -2320.55. IR (KBr,

---

Caution! †Metal perchlorate complexes and perchloric acid are potentially explosive. They should be handled with care, and the complexes should be prepared in small quantities.

400-300 cm^{-1}): 3308, 3117, 3071 (N–H stretch); 1670 (C=N, pyrimidine group stretch); 1090-1100 (perchlorate counter ion); 450-490 (Pt–N stretch); 315 (Pt–Cl stretch). TOF MS/ES^+. (m/z, M^{2+}): 304 ($C_2H_8N_3PtCl$ species). *Anal. Calcd for* $C_4H_{16}N_6Cl_4O_8Pt_2$: H, 2.00; C, 5.94; N, 10.40. *Found*: H, 2.08; C, 6.18; N, 10.14%.

pdn: Yield: 235.5 mg (0. 291mmol, 35.4%). ^1H NMR (500.5 MHz, D_2O), δ /ppm: 9.60, (d, 2H); 8.11, (dd, 2H). ^{195}Pt NMR (107.5 MHz, D_2O) δ/ ppm: -2244.82. IR (KBr, 4000-300 cm^{-1}): 3303, 3230, 3105 (N–H stretch); 1678 (C=N, pyridazine group stretch); 1090-1100 (perchlorate counter ion) 333 (Pt–Cl stretch). *Anal. Calcd for* $C_4H_{16}N_6Cl_4O_8Pt_2$: H, 2.00; C, 5.94; N, 10.05. *Found*: H, 2.00; C, 5.56; N, 9.98%.

qzn: Yield: 182.0 mg (0. 212 mmol, 36.0 %). ^1H NMR (500.5 MHz, D_2O), δ / ppm: 10.16, (s,1H); 10.05, (s, 1H); 9.53, (d, 1H); 8.50, (d, 1H); 8.38, (t, 1H); 8.11, (t,1H). ^{195}Pt NMR (107.5 MHz, D_2O) δ/ ppm: -2321.65, -2345.01. IR (KBr, 4000-300 cm^{-1}): 3285, 3207, 3075 (N–H stretch); 1678 (C=N, quinazoline group stretch); 1090-1100 (perchlorate counter ion); 450-490 (Pt–N stretch); 326 (Pt–Cl stretch). TOF MS/ES^+. (m/z, M^{2+}): 329 ($C_4H_9N_3PtCl$ species). *Anal. Calcd for* $C_8H_{18}N_6Cl_4O_8Pt_2$: H, 2.11; C, 11.19; N, 9.79. *Found*: H, 2.47; C, 11.69; N, 9.56%.

pht: Yield: 139.7 mg (0.163 mmol, 36.3%). ^1H NMR (500.5 MHZ, D_2O), δ/ppm:10.04, (s, 2H); 8.40, (m, 2H); 8.34, (m, 2H). ^{195}Pt NMR (107.5 MHz, D_2O) δ/ ppm: -2241.03. IR (KBr, 4000-300 cm^{-1}): 3299 (N–H stretch); 1678 (C=N, phthalazine group stretch), 1090-1100 (perchlorate counter ion); 450-490 (Pt–N stretch); 338 (Pt–Cl stretch). TOF MS/ES^+. (m/z, M^{2+}): 329 ($C_4H_9N_3PtCl$ species). *Anal. Calcd for* $C_8H_{18}N_6Cl_4O_8Pt_2$: H, 2.11; C, 11.09; N, 9.79. *Found*: H, 2.25; C, 10.67; N, 9.39%.

5.2.3 Instrumentation and Physical Measurements

Microanalysis of C, H, and N was done on a Carlo Erba Elemental Analyzer 1106. The infrared spectra were recorded in the 4000-300 cm^{-1} range on a Perkin Elmer Spectrum One-FTIR spectrophotometer using KBr pellets. The NMR spectra were measured on a Bruker Avance 500 spectrometer (^1H, 500 MHz) and (^{195}Pt, 107.5 MHz), respectively, at

ambient temperature of 30°C. Values of ^{1}H are given in δ (ppm) relative to tetramethylsilane (δ = 0.00) and ^{195}Pt chemical shifts were externally referenced to $K_2[PtCl_6]$ in D_2O. Mass spectrometric analyses were collected on Hewlett Packard LC-MS using electron impact ionization (ESI-TOF).

5.2.4 Computational Details

In an effort to gain further insight into the role of the diazine bridging ligand in such dinuclear Pt(II) complexes, the corresponding diaqua cationic complexes of total charges of 4+ were optimized at the B3LYP/[33]LACVP** (Los Alamos Core Valence pseudo-potentials set)[34] hybrid level, utilizing density functional computation method (DFT), in gaseous phase. B3LYP relates to the hybrid functional Becke's three parameter formulation[33] which has been proven to be superior to traditional functionals. The Spartan `04 for Windows® quantum chemical software package was used.

5.2.5 Preparation of the Aqueous Complex Solutions

The chloro complexes were converted into aqua analogues in solution by addition of 1.98 equiv. $AgClO_4$ using literature procedure.[35] Since perchlorate ions do not coordinate to Pt(II) the kinetic investigations were studied at pH *ca*.2.0 to prevent deprotonation of the aqua ligand,[36] and the ionic strength was adjusted to I = 0.10 M ($NaClO_4$ adjusted with perchloric acid). The resultant aqueous solutions were brought to a final complex concentration of 1.34 x 10^{-4}, 1.0 x 10^{-3}, 9.20 x 10^{-4}, 1.79 x 10^{-3} and 1.0 x 10^{-3} M, respectively, for **[{*cis*–$PtOH_2(NH_3)_2$}$_2$--μ–pmn]$(ClO_4)_2$** (**pmn**), **[{*cis*–$PtOH_2(NH_3)_2$}$_2$–μ–pdn]$(ClO_4)_2$ (pdn), [{*cis*–$PtOH_2(NH_3)_2$}$_2$–μ–qzn]$(ClO_4)_2$** (**qzn**), **[{*cis*–$PtOH_2(NH_3)_2$}$_2$–μ–pht]$(ClO_4)_2$** (**pht**), and **[{*cis*–$PtOH_2(NH_3)_2$}$_2$–μ–pzn]$(ClO_4)_2$** (**pzn**). A series of nucleophile concentrations in the order: 20, 40, 60, 80 and 100-fold excess of appropriate metal complex concentration, were prepared using the 0.10 M $NaClO_4/HClO_4$, at pH *ca.*2.0.

5.2.6 Spectrophotometric pK_a Titrations

The UV-Vis spectra were recorded on a Varian Cary 100 Bio spectrophotometer equipped with a thermostated cell holder. The pH of the aqueous solutions was measured at 25°C, using a Jenway 4330 Conductivity/pH meter equipped with a Micro 4.5 diameter glass electrode. The electrode was calibrated using standard buffer solutions at pH 4.0, 7.0 and 10.0, purchased from Saarchem chemicals. The pH electrode was filled with 3 M NaCl electrolyte to prevent precipitation of $KClO_4$. Spectrophotometric pH titrations were carried out using NaOH as the base. In order to avoid absorbance corrections due to dilution, a large volume (200ml) of each of the complex solution was used during the titration. Subsequent pH changes were obtained by stepwise additions of crushed solid NaOH pellets in the pH range 2-3, micropipette dropwise addition of saturated, 1.0 and 0.1 M NaOH or conc. $HClO_4$ (for reversibility of the pH) to the complex solution, prior to withdrawal of 2 ml aliquots of the solution for pH determination. After each of the measurements, the aliquots were discarded to avoid contamination by chloride ions coming from the pH electrode.

5.2.7 Kinetic Measurements

Spectral changes resulting from mixing separately each of the complexes **pzn**, **pmn**, **pdn**, **qzn** and **pht** with ligand solutions were recorded over the wavelength range 200-600 nm to establish a suitable wavelength at which the kinetic measurement would be performed on a Varian Cary 100 Bio spectrophotometer. The kinetics of the lability of coordinated water was followed spectrophotometrically by monitoring the change in absorbance at suitable wavelengths. An Applied Photophysics SX 18MV (v4.33) stopped-flow system coupled to an online data acquisition system was used for fast substitution reactions. The UV-Vis spectrophotometer was used for subsequent slow reaction steps. The reactions were studied under *pseudo* first-order conditions with at least 10-fold excess of nucleophile concentration per Pt-atom. The temperature of both instruments was controlled to within ± 0.1° C. Analyses of the pH- and time-dependent spectra were graphically performed using Origin 7.5®[37] software package.

5.2.8 Properties of the Ligands

Before discussing the results, it is worth looking at the properties of the ligand so as to understand the forces at hand. The introduction of heteroatoms into a benzene ring results in an irregular distribution of the electron density which strongly influences the physical properties and reactivity of the ligand as well as the corresponding metal complex.[38] In the case of diazines in these systems, two contradictory factors are in place: the strong electron-acceptor influence of the nitrogen and the weak electron-donor influence due to re-organisation of the π-cloud by inductive effect. The sequence of the π-acceptor effect of these diazines decreases from pyrazine > pyridazine > pyrimidine.[38] This is supported by the DFT –calculations on NBO charges and Pt-OH_2 bond lengths (Table 5.1).

5.3 Results

5.3.1 Computation Calculations

Representative geometry-optimized structures for the complexes are shown in Figure 1. Selected bond lengths and angles, natural atomic bond orbital (NBO) charges as well as HOMO-LUMO energy gap are given in Table 5.1. From Table 5.1, it is observed that the coordination around each of the Pt(II) atoms corresponds to a square-planar geometry with slight distortions from ideal values according to the observed N–Pt–N and N–Pt–OH_2 angles. The optimized geometries are in agreement with the available crystallographic structures of [{*cis*-$PtCl(NH_3)_2$}$_2$-μ-pzn]$(ClO_4)_2$/$(NO_3)_2$.[39,40] The Pt–$N_{1/2}$ bond distance in all the complexes is found to be shorter than the Pt–N_{py} (2.159 Å) distance in the mononuclear analogue $Pt(pipNCN)_2(py)^+$ [41] (py = pyridine), which is an indication that the diazine ligands have better π-acceptor properties compared to pyridine. (Figure 5.1), π-back-bonding is of less or no significance in the complexes **pzn**, **pmn** and **pdn**.

Table 5.1: A summary of DFT-calculated parameters for the aqua complexes pzn to pht. The table is ordered according to increasing values of Natural Atomic charges (NBO) of Pt(II) centres.

Complexes	**pht** 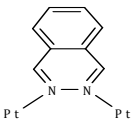	**pdn** 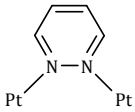	**qzn** 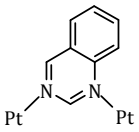	**pmn** 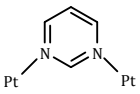	**pzn** 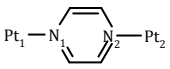
NBO charges					
Pt1/Pt2	1.204	1.208	1.209/1.210	1.213	1.219
N1/N2	-0.402	-0.406	-0.624	-0.639	-0.574
$Pt_{(TU)\text{-substituted}}$	1.052	1.052	1.043	1.043	1.057
$Pt_{(OH2)\text{-substituted}}$	1.202	1.214	1.211	1.213	1.218
MO energies /eV					
E_{HOMO}	-18.65	-20.68	-18.67	-20.18	-19.97
E_{LUMO}	-15.08	-15.86	-14.64	-15.28	-15.75
ΔE	3.57	4.82	4.03	4.90	4.22
Bond lengths / Å					
Pt---Pt	3.905	4.022	6.040	6.174	7.063
N_1---N_2	1.352	1.360	2.387	2.378	2.804
$Pt_{1/2}$---$N_{1/2}$	2.114	2.147	2.123/2.128	2.146	2.131
Pt---OH_2	2.148	2.143	2.131/2.129	2.130	2.127
Bond angles (°)					
α	5.73	7.16	12.44	17.05	179.89
OH_2-Pt-*trans* NH_3	91.13	91.05	91.35	91.14	90.82
$N_{1/2}$-Pt-*cis* NH_3	87.85	87.71	87.19	86.81	86.66
OH_2-Pt-*trans* NH_3	176.94	177.94	179.17	179.06	179.65
Dipole moment/D	2.13	1.28	3.83	3.21	0.27
Symmetry group	C_{2v}	C_{2v}	C_1	C_{2v}	D_{2h}

Structure	HOMO	LUMO
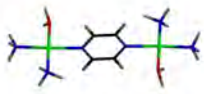 **pzn** (D_{2h})	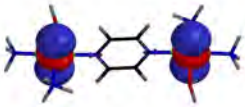	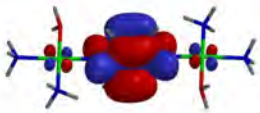
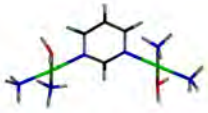 **pmn** (C_{2v})		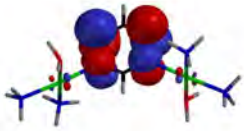
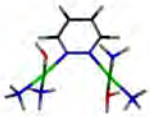 **pdn** (C_{2v})		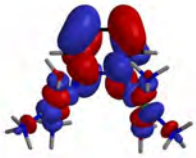
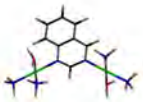 **qzn** (C_1)	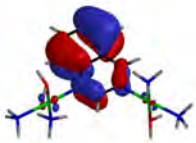	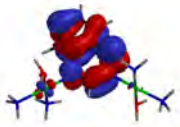
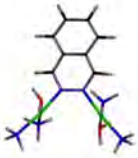 **pht** (C_{2v})	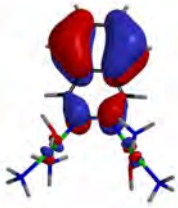	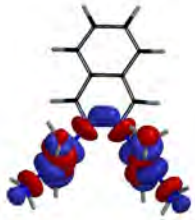

Figure 5.1: Frontier molecular orbitals HOMO–LUMO of the complexes

However, because the highest occupied molecular orbitals (HOMO) on the metal atom are centred on the d_z^2 orbitals whilst the lowest unoccupied molecular orbitals (LUMO) are located on the N-heterocyclic ligand that is lying perpendicular to the plane of the Pt(II) centre. Moreover, in the complexes **qzn** and **pht,** the HOMO orbitals are concentrated on the N-heterocyclic ligands and display a significantly higher energy HOMO level, which suggests that the extra aromatic ring on the benzodiazine ligand enables **qzn** and **pht** to possess better π-acceptor ability due to the extended π-system. This is supported by the smaller HOMO-LUMO (ΔE) energy gap (Table 5.1). Compared to that of **pzn**, the electron-acceptor properties of **qzn** and **pht** are only moderate since their LUMO is not as low in energy.

It can also be seen from the DFT-calculations (Table 5.1) that the positive (NBO) charges at the Pt(II) centres are symmetrically distributed. Their values steadily increase as the (N_1–N_2) and Pt---Pt distances increase further along the series **pht** through **pdn**, to **pzn**, respectively. In addition, the corresponding Pt–$N_{1/2}$ bond distances are also dependent on the structure of the diazine ligand, which also determines the average negative charge carried on the $N_{1/2}$ atoms of the bridging ligands due to electronic charge transfer from the metal centre to the diazine ligand through the electronegative N atoms. This results in differential transfer of electron density from the metal centre to the diazine ligand, leading to variations in the positive charge on the metal centres and hence, in the electrophilicity of the Pt(II) centres. This simultaneously decreases or increases the lability of the aqua complexes as will be discussed further.

5.3.2 Acid Dissociation Constants (pK_a) of the Diaqua Complexes

Titrations of the diazine-bridged dinuclear Pt(II) complexes with NaOH show that deprotonation of the two aqua ligands occurred in two successive steps. Thus, the stepwise deprotonation steps for the pH dependence of the dinuclear system can be presented by Scheme 5.2.

$$[H_2O\text{-}Pt\text{-}(NN)\text{-}Pt\text{-}OH_2]^{4+} + OH^- \overset{K_{a1}}{\rightleftharpoons} [H_2O\text{-}Pt\text{-}(NN)\text{-}\mathbf{OH}]^{3+} + H_2O$$

$$[H_2O\text{-}Pt\text{-}(NN)\text{-}\mathbf{OH}]^{3+} + OH^- \overset{K_{a2}}{\rightleftharpoons} [\mathbf{HO}\text{-}Pt\text{-}(NN)\text{-}\mathbf{OH}]^{2+} + H_2O$$

where, *NN* = pzn, pmn, pdn, qzn, pht bridging ligand

Scheme 5.2: Proposed stepwise deprotonation for the pH dependence of the dinuclear Pt(II) complexes.

A typical plot of the UV-Visible spectra obtained during the pH titrations for **qzn** is given in Figure 5.2 (see also under Supplementary information Figure S5.2, for **pmn**). The pK_a values of the aqua Pt(II) complexes were calculated from the pH profiles, an example is shown as an inset in Figure 5.2.

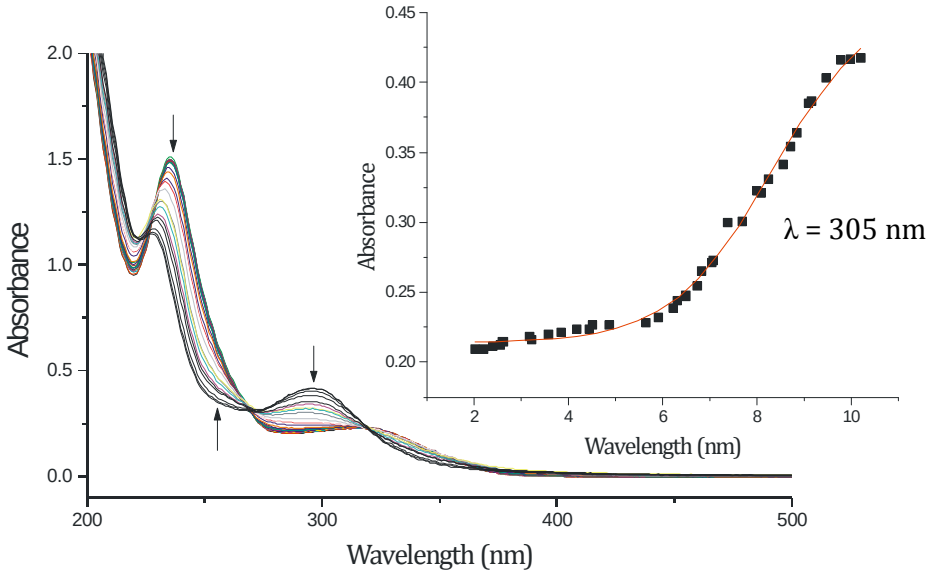

Figure 5.2: Variation of absorbance with pH for **qzn** complex in the pH range 2-10, I = 0.1 M $HClO_4$, T = 25 °C. Inset: Titration curve at 305 nm for **qzn** complex.

All the diaqua complexes exhibited two inflection points and a fit of the absorbance data to the standard Boltzmann equation, taken one at a time using the Origin 7.5®[37] software, resulted in two pK_a values which are presented in Table 5.2.

Table 5.2: Acid dissociation constants of platinum(II) complexes determined spectrophotometrically at 25 °C (Ionic strength, I = 0.1 M NaClO4/ HClO4).

	pzn	**pmn**	**pdn**	**qzn**	**pht**
pK_{a1}	3.29 ± 0.06	3.27 ± 0.20	4.87 ± 0.07	3.27 ± 0.05	3.59 ± 0.12
pK_{a2}	5.55 ± 0.09	5.92 ± 0.23	5.96 ± 0.08	8.62 ± 0.12	9.61 ± 0.06
ΔpK_a	2.32	2.65	1.09	5.35	6.02

The results shown in Table 5.2 indicate a correlation between pK_a values and the properties of the linkers, and the DFT calculations of the complexes. The pK_{a1} values for the first deprotonation of the aqua ligand coordinated to Pt(II) centre fall in the range **qzn** (pK_{a1} = 3.27) to **pdn** (pK_{a1} = 4.87) and increases in the order: **qzn** ≈ **pmn** < **pzn** < **pht** < **pdn**. This is attributed to the π-acceptor properties of the linker and the difference in the distance separating the two Pt(II) centres, which has an influence on the overall charge observed on the Pt(II) atoms (Table 5.1). Previous studies have established that a short distance between the Pt atoms results in the addition of single charges to the Pt(II) centres, [16–18,42] which enables each metal centre to become more electrophilic and more acidic, leading to lower pK_a values. As a consequence of the short distance coupled with extended π-conjugation in the benzodiazine ligands, good electronic communication between the ligand and the Pt centres is present.[30,43] This results in additional charge increments on the Pt(II) centres and is the reason for the significantly lower pK_{a1} values of **qzn** and **pht** in comparison to **pmn** and **pdn**, respectively. This trend is in line with the π-acceptor properties of the ligand and DFT calculations. The results also show that when the number of aromatic rings is increased the complex becomes more acidic, showing that the electron density on the Pt(II) centre and on the hydroxo ligand are stabilised better by extended π-conjugation of the

benzodiazine ring. This is supported by the lower energy gap (ΔE) values for **qzn** and **pht** complexes.

It is also noted that the pK_{a2} values for deprotonation of the second water molecule from the aqua/hydroxo complex species to form hydroxo/hydroxo species occurred at higher pH. Following deprotonation of the first aqua ligand the overall charge of the complexes decreases to +3 on forming the hydroxo species on the first Pt(II) centre.[14,18] Because of this, the electrophilicity of the second Pt(II) centre is decreased, resulting in higher pK_{a2} values in all cases.

However, in the case of **pht** and **qzn**, the pK_{a2} values are exceptionally high. After deprotonation of the first aqua ligand, the second nitrogen atom bound to Pt(II) centre bearing the aqua ligand causes a destabilising effect on the metal centre, due to the excess negative charges carried by adjacent N atoms. This results in elongation of the Pt–OH_2 bond as observed from the DFT calculations (Table 5.3). Also, the π-donor character is significantly increased in the benzodiazines which have higher energy HOMOs compared with their monocyclic analogues (Table 5.3). Thus, phthalazine ligand is the strongest heterocyclic π-donor in the series, quite consistent with its electron-rich structure that is supported by the bigger value of the HOMO-LUMO energy gap and lowest NBO charges for the aqua/Hydroxo derivative of the **pht** complex. These factors collectively are responsible for the remarkable high pK_{a2} values in **qzn** and **pht,** respectively.

Table 5.3: A summary of DFT calculated Parameters for aqua/hydroxo complex systems of benzodiazines and their monocyclic analogues.

Complex	**pzn**	**pmn**	**qzn**	**pdn**	**pht**
	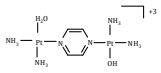	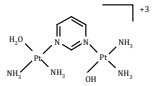	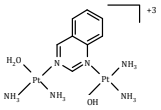	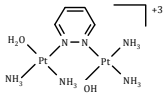	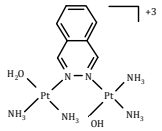
NBO charges					
Pt_{OH}	1.222	1.201	1.191	1.193	1.183
Pt_{H2O}	1.214	1.216	1.208	1.201	1.194
Pt–OH_2 **(Å)**	2.214	2.129	2.136	2.158	2.159
MO energies/eV					
HOMO	-15.02	-16.04	-15.57	-16.63	-15.85
LUMO	-12.48	-12.18	-11.74	-12.67	-11.56
ΔE/eV	2.54	3.86	3.83	3.96	4.29

5.3.3 NMR Study

To add further insight into the kinetics and mechanism of the substitution reactions of the diazine complexes, substitution reaction of **pzn** as chloride, and diaqua **pdn** complex with a large excess (6 equiv. TU for **pzn–Cl** and 20-fold excess TU for aqua **pdn**) of the nucleophile, were studied by ^{1}H NMR and ^{195}Pt NMR spectroscopy (in D_2O). The ^{1}H and ^{195}Pt NMR spectra of the complex, *cis*-[{$PtCl(NH_3)_2$}$_2$-μ-pzn]$^{+2}$ (**pzn–Cl**) with thiourea (TU) has been described in details in Chapter 4 (section 4.3.4). This information is now used as a reference for these dinuclear complexes. In general, it can be concluded that the substitution reactions proceeded in three successive steps, *viz*. stepwise substitution of the aqua ligands and dissociation of the linker.

The proton resonances for the coordinated aqua of **pdn** complex appeared within 45 min**,** while the reaction of chlorido**–pzn** took over 48 h to reach completion. The substitution reactivity of the Pt–Cl bond in **pzn** was slower as expected compared with the corresponding Pt–OH_2 bond of the **pdn** complex because aqua ligand is more labile and a better leaving group than the chloride ligand.[44] Only a section of the ^{1}H NMR spectra showing the first resonance for the unreacted complex and last resonance due to the displaced pyrazine bridging ligand are presented in Figure 5.3, *i.e*. resonance at δ = 9.04 ppm due to the symmetrically coordinated pyrazine ligand at the beginning of the reaction, while a second singlet resonance at δ = 8.64 ppm, was observed after 48 h and is assigned to free pyrazine ligand that resulted after release of the linker.[39,45] Similarly, the ^{195}Pt NMR spectra of the reaction of *cis*-[{PtCl $(NH_3)_2$}$_2$-μ-pzn]$^{+2}$ with TU also revealed the presence of two main resonances: one peak at -2302 ppm consistent with the N_3Cl coordination sphere of unreacted **pzn** and at -4140 ppm for the degradation product $[Pt(TU)_4]^{+2}$[15] as shown in Chapter 4 (Section4.3.4, Figure 4.9).

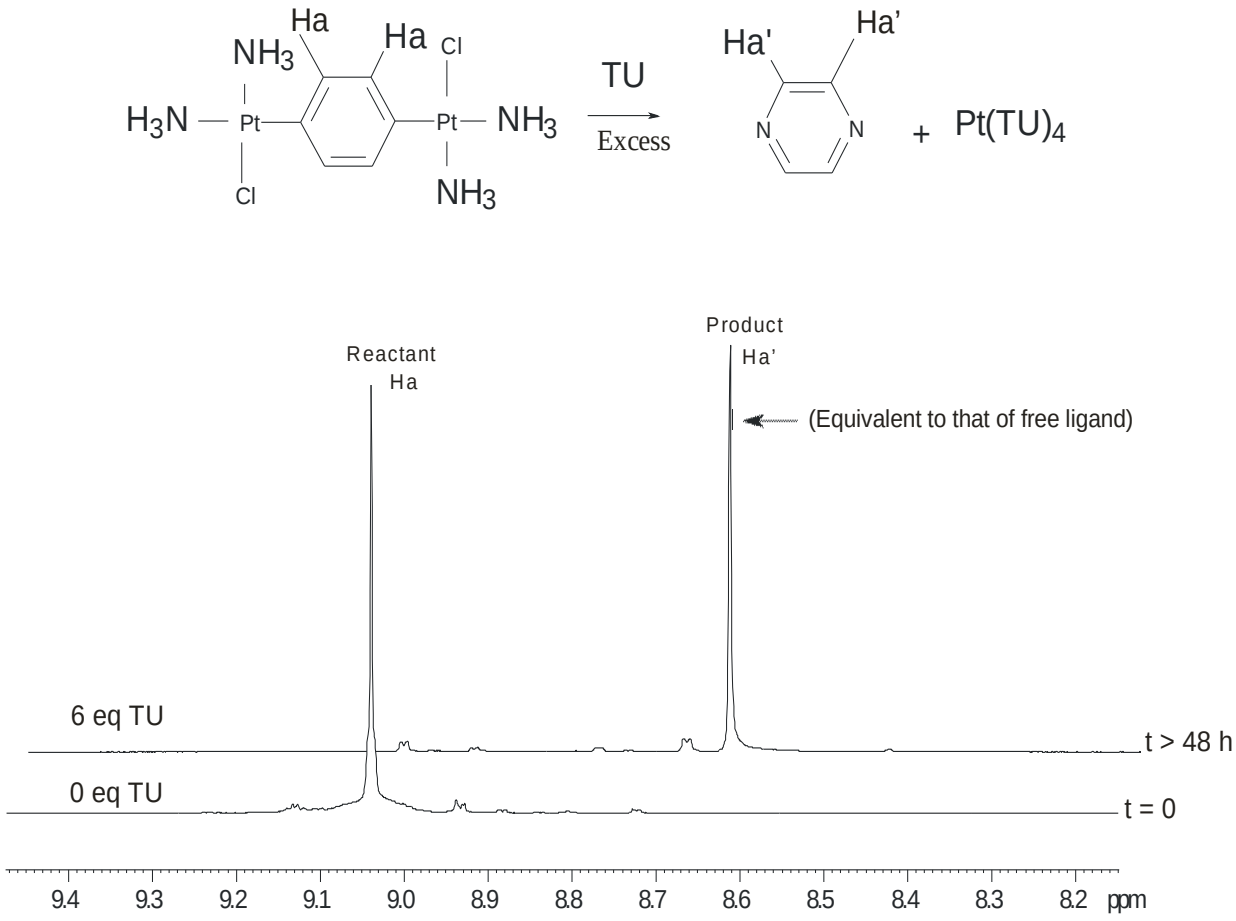

Figure 5.3: ^{1}H NMR spectra of the reaction of cis-[{PtCl(NH_3)$_2$}$_2$-μ-pzn]$^{+2}$ and excess thiourea (TU). Charges omitted for clarity.

The ^{1}H NMR spectra of **pdn** showed two resonances H_a and H_b, at the beginning of the reaction. After 45 minutes a second set of non-symmetrical pyridazine resonances were clearly resolved (Figure 5.4) at δ = 9.19 ppm (*pseudo* triplet for equivalent $H`_a$ protons) and 7.83 ppm (*pseudo* triplet for equivalent $H`_b$ protons)[46] that are assigned to the degradation product, *i.e*. free pyridazine ligand. The proton labels are shown on the structures of the **pdn** complex and the free ligand presented below in Scheme 5.3.

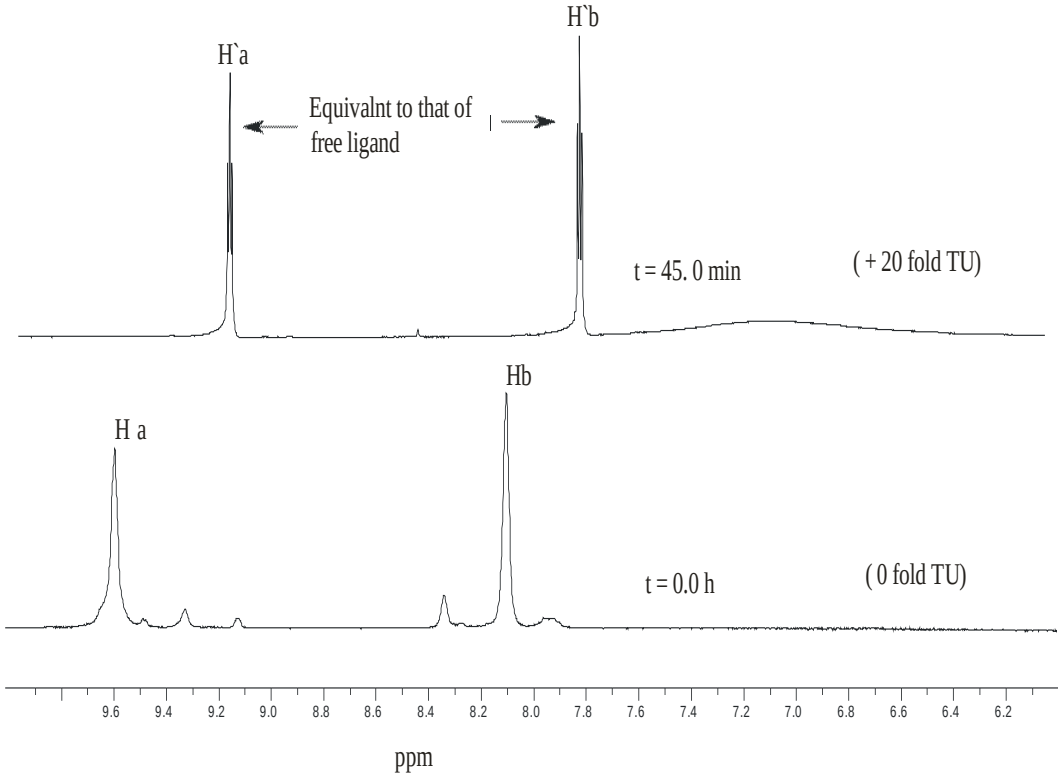

Figure 5.4: ^{1}H NMR spectra of the reaction of *cis*-$[\{Pt(OH_2)(NH_3)_2\}_2$-μ-pdn$]^{+2}$ and 20 fold excess thiourea (TU).

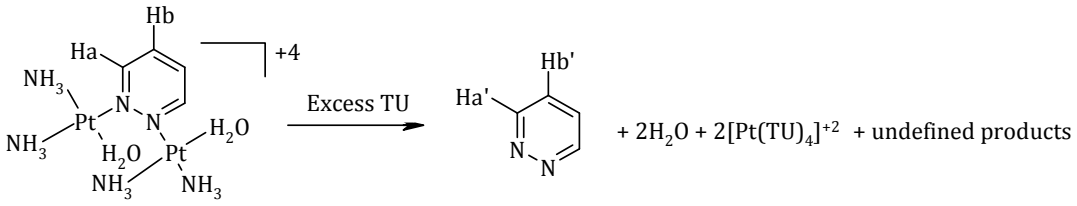

Scheme 5.3: Structure and proton labels H_a, H_b, H_a' and H_b' for coordinated and un-coordinated pyridazine ligand after dissociation of the bridging ligand.

Examination of the reaction products of the metal complexes **pzn** and **pdn** with thiourea, using ^{1}H and ^{195}Pt NMR, reveals the formation of free linker ligand-pyrazine and pyridazine, and a $[Pt(TU)_4]^{2+}$ unit yielding a ^{195}Pt resonance at around -4145 ppm, which is consistent with value of -3999 ppm reported by van Eldik, *et.al*.[15] This is attributed to release of the linker and the ammine ligands from the Pt(II) centre in the

third step due to the *trans*-effect of the S-donor ligands. All the complexes exhibited this step.

5.3.4 Kinetic Measurements with Thiourea Nucleophiles

The substitution reactions of coordinated aqua ligands from **pzn**, **pmn, pdn**, **qzn** and **pht** (Scheme 5.4) by S-bonding nucleophile, TU, DMTU and TMTU were studied spectrophotometrically by following the change in absorbance at suitable wavelengths (supporting information Table **S1**) as a function of time. A typical kinetic trace recorded for the reaction between **qzn** (0.17 mM) and TU (16.9 mM) at an ionic strength of 0.10 M ($NaClO_4$) by the stopped-flow is shown in Figure 5.5a. The data obtained were fitted to a single exponential model and gave values $k_{obs\ (1^{st})}$ for the first steps. The observed rate constant values of the successive second $k_{obs(2^{nd})}$ and the third $k_{obs(3^{rd})}$ steps were obtained by UV-Vis spectrophotometric technique. Typical kinetic traces of the second and third step recorded for **qzn** are shown in Figure 5.5b. By fitting the data successively to a single exponential model, we obtained the values for *pseudo* first-order rate constants for the second and third steps, respectively.

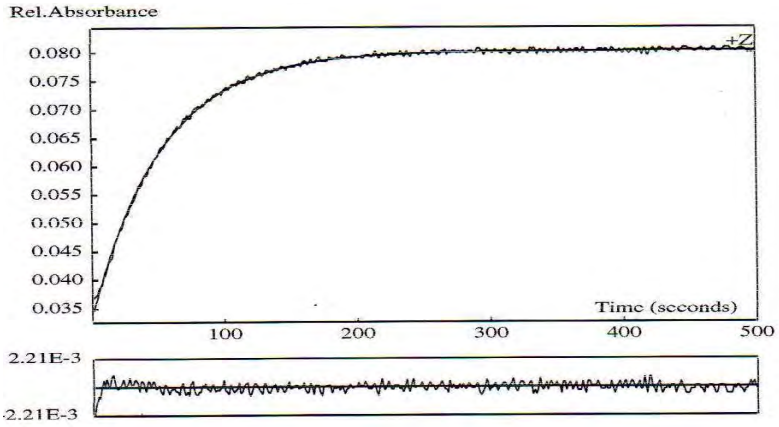

(a)

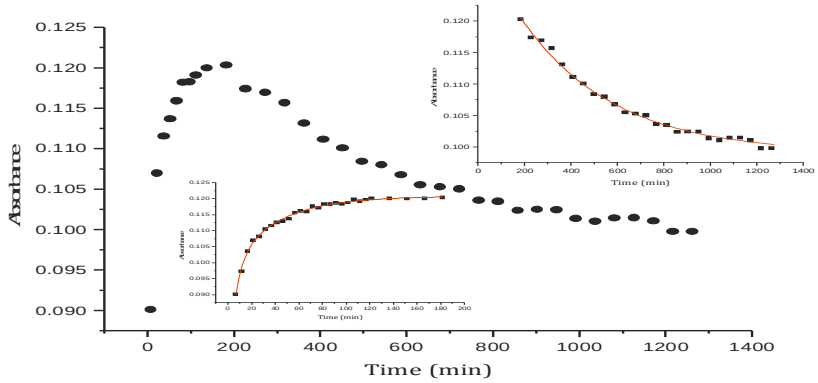

(b)

Figure 5.5: (a) Stopped-flow and (b) UV-Vis Spectrophotometric kinetic traces for the reaction between **qzn** and TU recorded at 305 nm, T = 25 °C, *I* = 0.10 M (0.01 M $HClO_4$, adjusted with $NaClO_4$), pH = 2.0. The inserts in (b) represent the substitution of the second and third steps.

The substitution reactions of the studied complexes with S-nucleophiles can be summarised as outlined in Scheme 5.4, showing the three sequential steps.

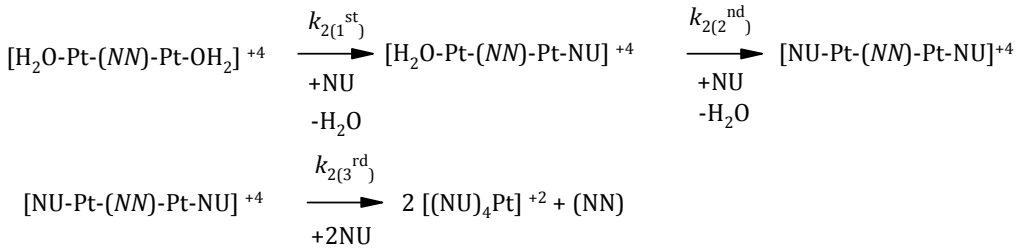

where, (*NN*) = pzn, pmn, pdn, qzn, pht bridging ligand

NU = nucleophile

Scheme 5.4: Suggested Substitution Mechanism for the Dinuclear Pt(II) complex system with Thiourea and its substituted derivatives.

The observed *pseudo* first order rate constants, k_{obs}, as a function of total concentration of nucleophile are shown in Figures 5.6, 5.7 and 5.8 for **pmn** complex (0.17 mM) with the TU, DMTU and TMTU, and can be described by equation 1.

$$k_{obs}(1^{st}/2^{nd}/3^{rd}) = k_2(1^{st}/2^{nd}/3^{rd})\,[NU] \qquad (1)$$

The plots show that all the k_{obs} linearly depend on concentration of the entering nucleophile with zero intercepts, an indication that there was little or no reverse reaction. The values of the observed rate constants, k_{obs}, used in determining $k_{2(1^{st})}$ were an average of five to seven independent runs obtained from the stopped-flow; while an average of multiple readings obtained from the UV-Vis spectrophotometer were used for the second and third steps. The second-order rate constants, $k_{2(i)}$, for the first, second and third steps for all the reactions were obtained from the slope of plots of k_{obs} vs. [NU], using Origin 7.5®[37] program. The values of the second order rate constants are summarized in Table 5.4.

Table 5.4: Summary of second order rate constants of diazine-bridged dinuclear Pt(II) complexes; I = 0.1 M ($NaClO_4$, adjusted with $HClO_4$), T = 298.15 K.

Complex	NU	$k_{2(1^{st})}$ /M^{-1} s^{-1}	$k_{2(2^{nd})}$ /M^{-1} s^{-1}	$k_{2(3^{rd})}$ /10^{-3} M^{-1} s^{-1}
pzn	TU	42.04 ± 0.56	0.30 ± 0.01	2.86 ± 0.07
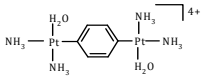	DMTU	22.46 ± 0.23	0.15 ± 0.001	3.65 ± 0.15
	TMTU	4.02 ± 0.06	0.09 ± 0.003	1.54 ± 0.10
pmn	TU	8.50 ± 0.07	0.12 ± 0.002	27.81± 1.53
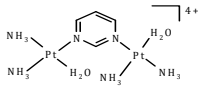	DMTU	13.15 ± 0.76	0.073 ± 0.001	23.16 ± 1.64
	TMTU	0.83 ± 0.003	0.04 ± 0.001	3.45 ± 0.01
pdn	TU	2.04 ± 0.03	0.12 ± 0.003	4.64 ± 0.10
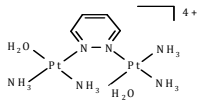	DMTU	2.78 ± 0.07	0.17 ± 0.001	9.56 ± 0.46
	TMTU	0.70 ± 0.01	0.07 ± 0.001	1.59 ± 0.03
qzn	TU	19.80 ± 0.26	0.11 ± 0.002	12.15 ± 0.06
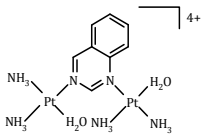	DMTU	15.63 ± 0.27	0.09 ± 0.001	5.92 ± 0.004
	TMTU	2.99 ± 0.02	0.03 ± 0.001	3.73 ± 0.03
pht	TU	0.94 ± 0.01	0.054 ± 0.0001	17.40 ± 0.14
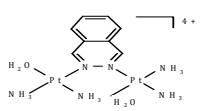	DMTU	0.25 ± 0.01	0.045 ± 0.0001	5.49 ± 0.02
	TMTU	0.11 ± 0.02	0.002 ± 0.00003	1.03 ± 0.06

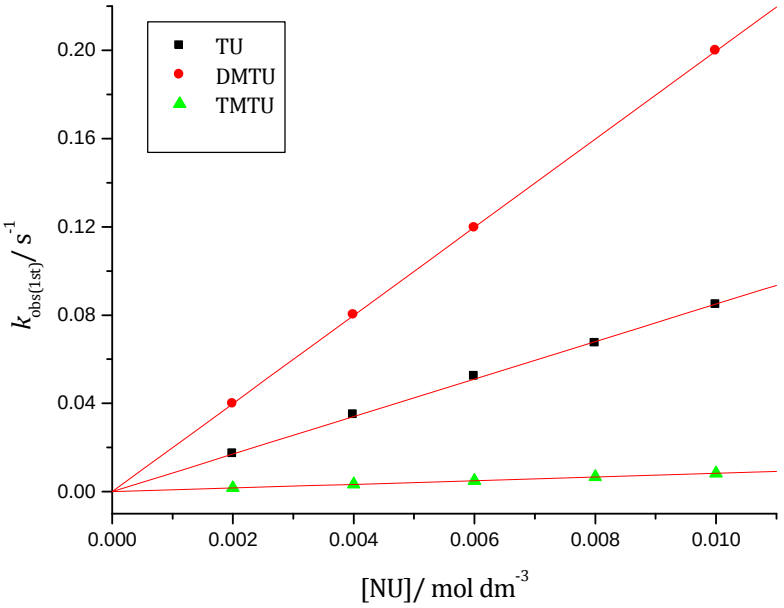

Figure 5.6: Concentration dependence of $k_{obs}(1^{st})$ for the displacement of first aqua ligand in **pmn** by thiourea and its substituted derivatives, pH = 2.0, T = 298.15 K, I = 0.10 M (0.01 M $HClO_4$, adjusted with $NaClO_4$).

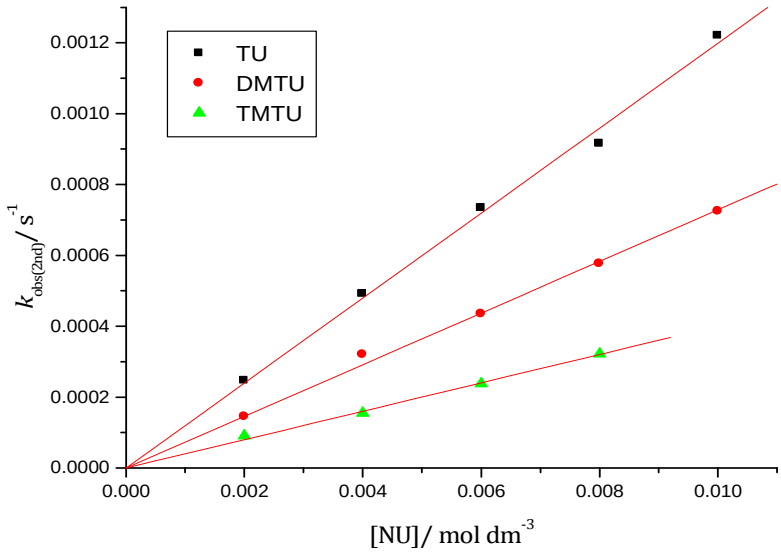

Figure 5.7: Concentration dependence of $k_{obs(2nd)}$ for the displacement of second aqua ligand in **pmn** by thiourea and its substituted derivatives, pH = 2.0, T = 298.15 K, I = 0.10 M (0.01 M $HClO_4$, adjusted with $NaClO_4$).

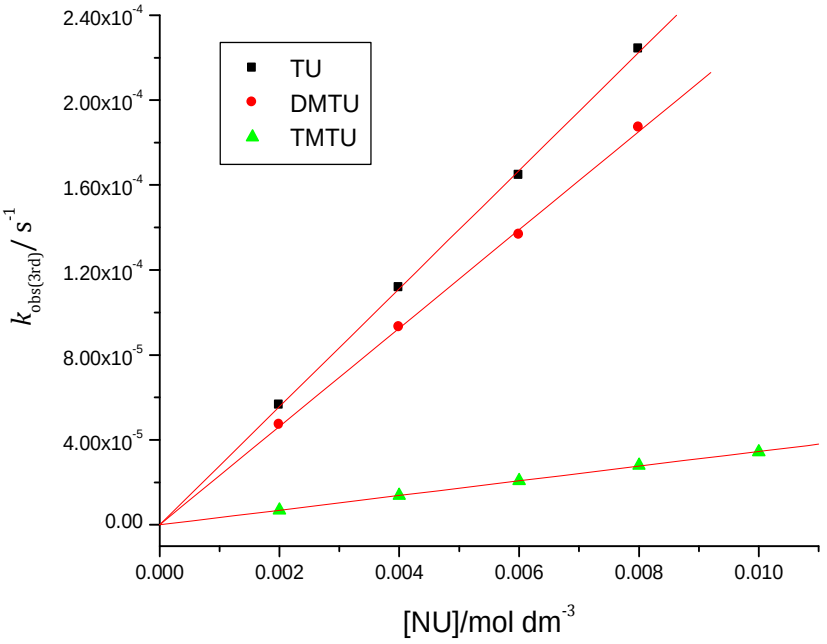

Figure 5.8: Concentration dependence of $k_{obs(3rd)}$ for the displacement of the bridging ligand in **pmn** by thiourea and its substituted derivatives, pH = 2.0, T = 298.15 K, I = 0.10 M (0.01 M $HClO_4$, adjusted with $NaClO_4$).

The first and second substitution steps, $k_{2(1^{st})}$ and $k_{2(2^{nd})}$ respectively, represents the consecutive substitution of the water ligand on the coordination sphere of each of the Pt(II) centres of the dinuclear diaqua Pt(II) complexes. The second substitution step is up to 2-orders of magnitude slower compared to the first one. This is ascribed to a communication between the two metal centres after the first substitution which results into a change in the environmental conditions around the second metal centre.[47] The DFT calculations show a change in NBO charges if TU is substituted to one platinum centre, *i.e.* from Pt(OH_2) to Pt(TU), as can be seen in Table 5.1, suggesting that electronic charge is conveyed through the bridging ligand. The third step involves the dissociation of the bridging ligand from the Pt(II) centre. The degradation process occurs as a result of the ability of the S-donor ligands to displace simultaneously both the linker and the am(m)ine ligands through the *trans*-effect, a process that is accelerated by protonation of the released nitrogen atom at pH 2.0[16,18] preventing any possibility of reverse reaction and therefore, forces the reaction forward as shown in Scheme 5.4. The excess

thiourea nucleophile is large enough to displace the bridging ligand to produce $[Pt(TU)_4]^{2+}$ and any other undefined products. This degradation process is 10 to 1000 times slower when compared to the first and the second substitution process respectively. Similar results have been observed by Reedijk, *et al*., [32] where degradation of the Pt-$N_{(pht/pdn)}$ bond occurred after initial substitution of the aqua ligands by 9EtG in **pdn** and **pht** complexes. In all the cases, the rates of the successive substitution of the aqua ligands and displacement of linker are influenced by the structure of the bridging ligand.

5.3.5 Thermodynamic Parameters

To confirm that these complexes follow an associative mode of substitution, characteristic of square-planar complexes, the enthalpy of activation ($\Delta H^{\#}$) and entropy of activation ($\Delta S^{\#}$) were determined in the temperature range 15-35 °C. The activation enthalpies and entropies were calculated from the slope and y-intercept, respectively, from the Eyring plots (Figure 5.9, 5.10 and 5.11) and these are summarised in Table 5.5.

Table 5.5: Summary of Activation parameters for the displacement of coordinated water by a series of nucleophiles in complexes of the Type [cis-{$PtOH_2(NH_3)_2$-μ-pzn]$^{4+}$, I = 0.1 M $NaClO_4$.

Complex	**NU**	$\Delta H^{\#}_1$ /kJ mol^{-1}	$\Delta H^{\#}_2$ /kJ mol^{-1}	$\Delta H^{\#}_3$ / kJ mol^{-1}	$\Delta S^{\#}_1$ / J mol$^{-1}K^{-1}$	$\Delta S^{\#}_2$ / J mol$^{-1}K^{-1}$	$\Delta S^{\#}_3$ / J mol$^{-1}K^{-1}$
pzn	TU	45 ± 0.3	55 ± 4.2	88 ± 1.8	-63 ± 1.0	-113 ± 14.0	-41 ± 6.2
	DMTU	48 ± 0.6	49 ± 3.3	70 ± 6.7	-108 ± 1.9	-140 ± 11.0	-99 ± 22.4
	TMTU	45 ± 1.3	60 ± 1.2	72 ± 3.7	-127 ± 4.4	-119 ± 4.1	-81 ± 12.1
pmn	TU	43 ± 0.1	43 ± 0.1	43 ± 0.6	-107 ± 0.3	-218 ± 0.2	-156 ± 2.0
	DMTU	47 ± 0.2	46 ± 0.2	52 ± 0.6	-82 ± 0.8	-159 ± 0.7	-132 ± 2.0
	TMTU	51 ± 0.8	49 ± 0.4	50 ± 0.6	-95 ± 2.5	-150 ± 1.3	-142 ± 1.8
pdn	TU	46 ± 1.2	61 ± 1.7	61 ± 1.7	-105 ± 4.0	-81 ± 5.6	-107 ± 5.6
	DMTU	63 ± 3.5	61 ± 1.3	53 ± 1.1	-45 ± 11.8	-75 ± 4.2	-145 ± 3.8
	TMTU	53 ± 1.5	57 ± 1.9	70 ± 1.3	-92 ± 5.0	-98 ± 6.5	-92 ± 4.4
qzn	TU	46 ± 0.3	56 ± 1.5	51 ± 2.2	-68 ± 0.9	-77 ± 5.1	-112 ± 7.3
	DMTU	41 ± 0.8	68 ± 2.8	50 ± 1.4	-87 ± 2.6	-36 ± 2.8	-112 ± 4.7
	TMTU	53 ± 1.4	54 ± 0.9	63 ± 1.1	-70 ± 4.8	-86 ± 2.9	-69 ± 3.6
pht	TU	48 ± 1.3	60 ± 0.3	64 ± 1.1	-110 ± 4.5	-88 ± 1.1	-74± 3.6
	DMTU	67 ± 1.0	55 ± 0.5	55 ± 1.1	-38 ± 3.5	-103 ± 1.7	-122 ± 3.7
	TMTU	45 ± 0.4	49 ± 0.4	60 ± 2.8	-87 ± 1.2	-104 ± 1.3	-109 ± 9.3

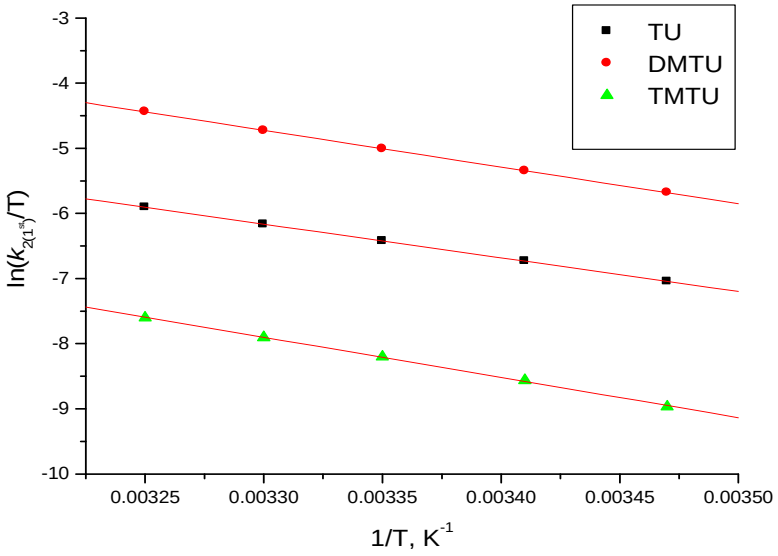

Figure 5.9 : Plots of ln(k_2/ T) versus 1/T for the first reaction step of pmn with a series nucleophiles in the temperature range 15-35 °C, I = 0.10 M (0.01 M $HClO_4$, adjusted with $NaClO_4$).

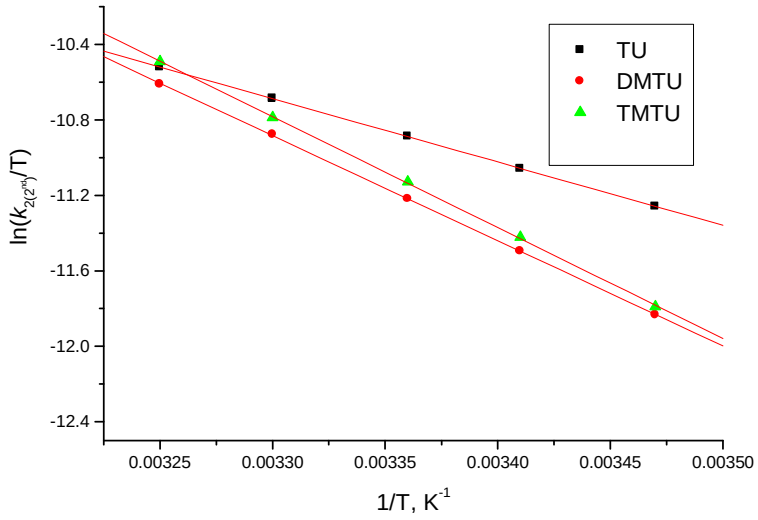

Figure 5.10: Plots of ln(k_2/ T) versus 1/T for the second reaction step of **pmn** with a series nucleophiles in the temperature range 15-35 °C, I = 0.10 M (0.01 M $HClO_4$, adjusted with $NaClO_4$).

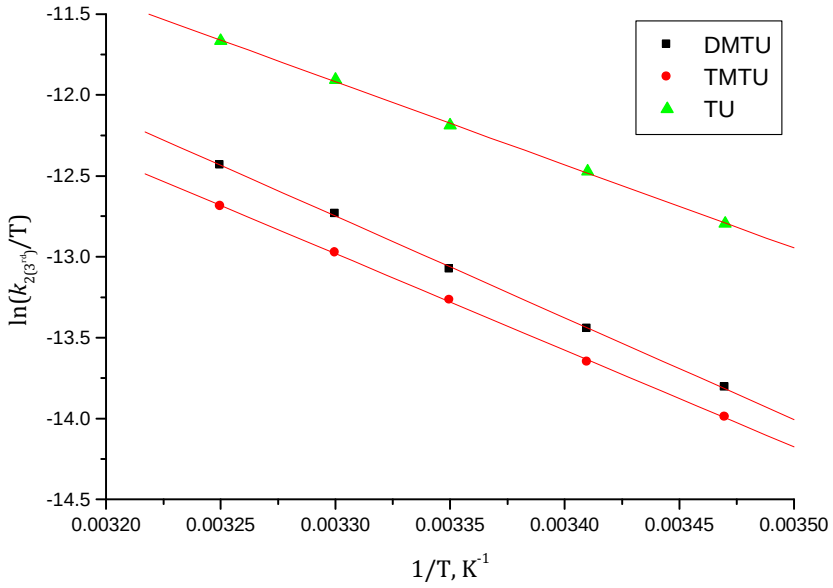

Figure 5.11: Plots of ln(k_2/ T) versus 1/T for the third reaction step of **pmn** with a series nucleophiles in the temperature range 15-35 °C, I = 0.10 M (0.01 M $HClO_4$, adjusted with $NaClO_4$).

5.4 Discussion

In the current study, the investigated complexes are characterized by the two Pt(II) centres that are linked by rigid aromatic ligands of varying Pt---Pt distances due to different positions of the N atoms in the heterocyclic ring. The dinuclear Pt(II) complexes can be classified into two groups as monocyclic diazines: **pzn**, **pmn**, and **pdn**; and benzodiazines- **qzn** and **pht**. From the DFT calculations, the distance separating the two Pt(II) centres varies in the decreasing order: **pzn** (7.063) > **pmn** (6.174) > **qzn** (6.040) > **pdn** (4.022) > **pht** (3.905 Å), respectively. In addition, the complex is symmetry *i.e.* C_{2v} point group symmetry for **pmn**, **pdn**, and **pht**, and D_{2h} for **pzn,** while **qzn** has a C_1 symmetry (Figure 5.1).

The kinetic data in Table 5.3 shows that the lability of the aqua ligands is dependent on the nature, structural geometric, as well as the distance between the N atoms of the coordinated diazine-bridging ligand. A comparison of the k_2-values in Table 5.3 reveals the order of reactivity of the complexes to be **pzn** > **qzn** > **pmn** > **pdn** > **pht**. This order

is the same as the electron-withdrawal ability of the bridge ligand and its ability to stabilize the five-coordinate transition state which increases in the order: pyrazine (pzn) > quinazoline (qzn) > pyrimidine (pmn) > pyridazine (pdn) > phthalazine (pht).[48] Therefore, the difference in reactivity can be ascribed to electronic and steric effects operating around the Pt(II) centre.

To understand fully the influence of the diazine-bridge on the reactivity of the Pt(II) metal centres, the complexes need to be grouped into two clusters. First, is the influence of increasing the distance between the metal atoms, *i.e*. from being *ortho* to each other (**pdn**) to *para* disposition (**pzn**) in the monocyclic diazines. Secondly, is by looking at the influence of increasing the *π-effect* by comparing the monocyclic diazines to the respective benzodiazines, *i.e*. **pmn** versus **qzn** and **pdn** against **pht**.

Using the $k_{2(1^{st})}$ values for TU as a reference one clearly sees that as the position of the metal changes from *ortho* to each other to *para*, the reactivity increases by a factor of 15. One can infer from this that steric hindrance is playing a role in influencing the reactivity of the complexes. This is because as the position changes from *ortho* to *para* the dihedral angle (Pt–N1–N2–Pt), i.e. α in Table 5.1 increases reducing any possible interference from each metal centre. This order of reactivity has been observed for closely related substitution of chloride by guanosine-5'-monophosphate (GMP) studies reported by Reedijk and co-workers.[32]

There is also clear evidence that electronic effect is also playing a role in these reactions. The DFT calculation of the NBO positive charges on the Pt-atoms, shows that the Pt(II) centre in **pzn** is more electrophilic followed by that of **pmn** and then **pdn**, accounting for the order of the reactivity. DFT calculations are supported further by the ^{195}Pt NMR chemical shifts which shows the pyrazine-bridged complex (**pzn**) to have a lower field (б = -2302.2 ppm) while that for the pyrimidine-bridged complex **pmn** appears at (б = -2320.6 ppm) and for pyridazine bridged complex (**pdn**) at (б = -2244.8 ppm). This trend has also been reported by other authors based on photo-physical data and electrochemical properties.[29,49]

Comparing the reactivity of **qzn** against **pmn** and **pht** versus **pdn** provides an understanding of the role of adding π-moiety onto the phenyl part of the chelate. The results show that in case of **qzn**, the π-backbonding into the aromatic ring is dominant. The net result is that the Pt-metal of **qzn** is more electropositive and as such is more reactive than **pmn**. In case of **pht**, the opposite is true, the N=N bond in both pyridazine (pdn) and phthalazine (pht) is a strong electron-withdrawer than the π-backbonding due to the introduced aromatic ring, which makes it more of an electron donor than electron-withdrawer. Because of this the metal centre for **pht** is more electronegative or less electrophilic than the rest of the complexes; as such it is the least reactive. The optimised structures of the LUMO clearly show the difference between the two complexes with respect to electron density around the metal atom.

On the whole, the rate of substitution of the second aqua ligand from the starting complex is slower than in the first substitution step (Table 5.3). The order of substitution with TU decreases by a factor of 140: 247: 71: 19: 9 for **pzn**: **qzn**: **pmn**: **pdn**: **pht**, respectively. The obtained rate constants show the same order of nucleophile reactivity as was observed in the first step. Again, a combination of steric and electronic properties control reactivity at the Pt(II) centre. Finally, a slower third step was observed for all the metal complexes that involves the release of the linker and formation of PtS_4 units, due to the influence of the *trans*-effect of the S-donor ligands. Also the electron density on the metal centre is increased when the number of coordinated S-donor atoms per Pt(II) centre is increased further. This weakens the bond between the metal and the leaving group, but simultaneously obstructs the formation of a bond between the Pt(II) centre and the entering group in the transition state, thus slowing down the reaction.

On the basis of the results summarised in Table 5.3, it can be concluded that the reactivity order of the nucleophiles is the same for all the cases and follows the trend TU > DMTU >TMTU, which is in relation to their order of nucleophilicity and steric properties of the respective nucleophile.[50] The reported activation entropies ($\Delta S^{\neq}_{(1^{st}/2^{nd}/3^{rd})}$) for all systems studied are significantly negative, which is in line with an

associative mode of substitution mechanism, well known for d^8 square planar metal complexes.[50,51–53]

5.5 Conclusion

This work has demonstrated the connection between the structure and position of the N atoms of the bridging diazine ligand and reactivity of the aqua Pt(II) complexes. The substitution kinetics resulted in three k_2 rate constants, the first and second rate constants being due to stepwise substitution of the aqua ligands, while the third is due to the release of the bridging ligand. The results of the observed second-order rate constants for the stepwise substitution of the aqua ligand with thiourea nucleophiles in monocyclic diazine bridged complexes increases in the order **pzn** > **pmn** > **pdn**. This correlates with the mutual disposition of the nitrogen atoms and π-deficiency of the diazine ligands. The higher π-acceptor action due to the added phenyl ring in the **qzn** containing the pyrimidine moiety, accounts for the accelerated nucleophilic substitution compared to the **pht** where the nitrogen atoms are in the *ortho*-position, despite both complexes having an extended π-conjugation. The results are clearly supported by the experimental pK_a values and DFT computations especially for NBO charges and HOMO-LUMO energy gap. While, ^{1}H NMR measurement for the reactions of **pzn–Cl** and **pdn–OH_2** with TU confirmed dissociation of the linker following the coordination of further thiourea to the congested Pt(II) centre in the transition state. It can therefore, be speculated that the biological importance of these complexes as potential anticancer Pt drugs is likely to be limited by their instability.

References

1 N. J. Wheate and J. G. Collins, 2003, *Coord. Chem. Rev*. **241**, 133-145.

2 J. Reedijk, 2003, *Proc. Natl. Acad. Sci. USA*, **100**, 3611-3616.

3 K. Van der Schilden, F. Garcia, H. Kooijman, A. L. Spek, J. G. Haasnoot and J. Reedijk, 2004, *Angew. Chem. Int. Ed*. **43**, 5668.

4 M. E. Oehlsen, Y. Qu, N. Farrell, 2003, *Inorg. Chem.*, **42**, 5498.

5 N. Farrell, in *Platinum-based Drugs in cancer Therapy*, 2000, L. R. Kelland, N. Farrell, (*Ed.*), Human Press, Totowa 321.

6 T. D. McGregor, Z. Balcarova, Y. Qu, M. C.Tran, R. Zaludova, V. Brabec and N. Farrell, 1999, *J. Biol. Inorg. Chem.,* **77**, 43.

7 D. Fan, X. Yang, X. Wang, S. Zhang, J. Mao, J. Ding, L. Lin and Z. Guo, 2007, *J. Biol. Inorg. Chem*., **12**, 655 and references therein.

8 J. Kasparkova, O. Vrana, N. Farrell and V. Brabec, 2004, *J. Inorg.Biochem*., **98**, 1560.

9 Q. Liu, Y. Qu, R.van Antwerpen and N. Farrell, 2006, *Biochemistry*, **45**, 4248.

10 D. Jaganyi, V. M. Munisamy and D. Reddy, 2006, *Int. J. Chem. Kinet.* , **38**, 202.

11 Y. M. Zhao, W. J. He, p. F. Shi, J. H. Zhu, L. Qiu, L. P. Lin and Z. J. Guo, 2006, *Dalton Trans*., 2617.

12 S. Komeda, M. Lutz, A. L. Spek, M. Chikuma and J. Reedijk, 2000, *Inorg. Chem.,* **39**, 4230; (b) S. Komeda, M. Lutz, A. L. Spek, Y. Yamanaka, T. Sato, M. Chikuma and J. Reedijk, 2002, *J. Am. Chem. Soc.*, **124**, 4738.

13 D. Reddy and D. Jaganyi, 2011, *Int. J. Chem. Kinet*., **43**, 161.

14 A. Hofmann and R. van Eldik, 2003, *Dalton Trans.,* 2979.

15 H. Ertürk, A. Hofmann, R. Puchta and R. van Eldik, 2007, *Dalton Trans.,* 2295.

16 H. Ertürk, J. Maigut, R. Puchta and R. van Eldik, 2008, *Dalton Trans.,* 2759.

17 H. Ertürk, R. Puchta and R. van Eldik, 2009, *Eur. J. Inorg. Chem*., 1334.

18 A. Mambanda, D. Jaganyi, S. Hochreuther and R. van Eldik, 2010, *Dalton Trans*., **39**, 3595.

19 S. Bonnet, M. A. Siegler, J. H, van Lenthe, M. Lutz, A. L. Spek, G. van Koten and R. J. M. Klein Gebbink, 2010, *Eur. J. Inorg. Chem*. 4667-4674 and references therein.

20 J. E. Sutton and H. Taube, 1981, *Inorg. Chem*., **20**, 3126.

21 R. Dembinski, T. Bartik, B. Bartik, M. Jaeger and J. Gladysz, 2000. *J. Am. Chem. Soc*., **122**, 810.

22 R. Romeo, M. R. Plutino, M. L. Scolaro, S. Stoccoro and G. Minghetti, 2000, *Inorg. Chem*., **39**, 4749.

23 J. W. Williams, Y. Qu, G. H. Bulluss, E. Alvorado and N. Farrell, 2007, *Inorg. Chem*., **46**, 5821.

24 N. Summa, J. Maigut, R. Puchta and R. van Eldik, 2007. *Inorg. Chem.*, **46**, 2094.

25 V. Vacchina, L. Torte, C. Allievi and R. Lobeinski, 2003, *J. Anal. Atomic Spectrom.*, **18**, 884.

26 S. J. Hoseini, S. M. Nabavizadeh, S. Jamali, and M Rashidi, 2007, *J.Organomet. Chem*., **692**, 1990.

27 S. Budagumpi, G. S. Kurdekar, N. V. Kulkarni and V. K. Revankar, 2010, *J. Incl. Phenom. Macrocyl*. Chem., **67**, 271, and references cited therein.

28 N. Nédélec and F. D. Rochon, 2001, *Inorg. Chem*., **40**, 5236.

29 (a) J. S. Gardner and D. P. Strommen, 2003, *J. Phys. Chem*., **107**, 351; (b) F. D. Rochon and M. Fakhfakh, 2009, *Inorg. Chim. Acta*, **362**. 1455.

30 D. Donghi, G. D`Alfonso, M. Mauro, M. Panigati, P. Mercandelli, A. Sironi, P. Mussini and L. D`Alfonso, 2008, *Inorg. Chem*., **47**, 4243.

31 D. D. Perrin, W. L. F. Armarego, D. R. Perrin, 1980, *Purification of Laboratory Chemicals*, 2nd Ed., Pergamon, Oxford.

32 G. V. Kalayda, S. Komeda,K. Ikeda, T. Sato, M. Chikuma and J. Reedijk, 2003, *Eur. J. Inorg. Chem*., 4347.

33 A. D. Becke, 1993*, J. Chem. Phys.,* **98,** 5648.

34 P. J. Hay and W.R Wadt, 1985, *J. Chem. Phys.,* **82***,* 299.

35 (a) Z. D. Bugarčić, G. Liehr and R. van Eldik, *J. Chem. Soc., Dalton Trans.,* 2002, 951; (b) Z. D. Bugarčič, B. V. Petrović and R. Jelić, 2001*, Transition Met. Chem.,* **26**, 668.

36 T. G. Appleton, J. R. Hall, S. F. Ralph and C. S. M. Thompson, 1984, *Inorg. Chem.,* **23**, 3521.

37 MicrocalTM OriginTM Version 7.5, Microcal Software, Inc., One Roundhouse Plaza, Northampton, MA, 01060, USA, 1991-2003.

38 A. R. Katrityzky, C. A. Ramsden, J. A. Joule and V. V. Zhdankin, 2010, *Handbook of Heterocyclic Chemistry*, 3rd Ed., Elsevier Publishers, UK, pp. 17-20.

39 S. Komeda, G. V. Kalayda, M. Lutz, A. L. Spek, Y. Yamanaka, T. Sato, M. Chikuma and J. Reedijk, 2003, *J. Med. Chem*., **46**, 1210.

40 M. Willermann, C. ulcahy, R. K. O. Sigel, M. M. Cerdià, E. Freisinger, P. J. Sanz Miguel, M. Roitzsch and B. Lippert, 2006, *Inorg. Chem*., **46**, 2093.

41 S. Chatterjee, J. A. Krause, A. G. Oliver and W. B. Connick, 2010, *Inorg. Chem*., **49**, 9798.

42 A. Hofmann, L. Dahlernburg and R. van Eldik, 2003, *Inorg. Chem.,* **42**, 6528.

43 (a) D. Jaganyi, A. Hofmann and R. van Eldik, 2001, *Angew. Chem. Int. Ed*., **40**, 1680; (b) A. Hofmann, D. jaganyi, O. Q. Munro, G. Liehr, and R. van Eldik, 2003, *Inorg. Chem*., **42**, 1688.

44 G. McGowan, S. Parsons and P.J. Sadler, 2005, *Inorg. Chem*., **44**, 7459, and references cited therein.

45 M. A. Nazif, J-A. Bangert, I. Ott, R. Gust, R. Stoll and W. S. Sheldrick, 2009, *J. Inorg. Biochem.*, **103**, 1405.

46 Y. Chen and R. E. Shepherd, 1998, *Inorg. Chim. Acta*, **279**, 85.

47 N. Summa,W. Schiess, R. Puchta, N. van Eikema Hommes and R. van Eldik, 2006. *Inorg. Chem*., **45**, 2948.

48 N. Sato, Pyrazines and their benzo derivatives, in: A. J. Boulton (Ed.), *Comprehensive Heterocyclic Chemistry II,* **Vol. 6(Ch. 6.03)**, Pergamon, Oxford, 1996.

49 G. Ge, J. He, H. Guo, H. Wang, D. Zou, 2009, *J. Organomet. Chem*., **694**, 3050.

50 M. L. Tobe and J. Burgess, 1999, *Inorganic Reaction Mechanisms*, Addison Wesley Longman Ltd., NY, pp. 30-43, 70-112.

51 J. D. Atwood, 1997, *Inorganic and Organometallic reaction mechanisms*, 2nd Ed., Wiley-VCH, NY, pp.43-61.

52 R. G. Wilkins, 1991, *Kinetics and Mechanism of reactions of Transition Metal complexes*, 2nd Ed., VCH, Wienheim, pp. 199-201.

53 F. Basolo and R. G. Pearson, 1967, *Mechanism of Inorganic reactions*, 2nd Ed., Wiley, New York, pp. 80-115.

Appendix 5

Comparative Rates of Ligand Substitution in Diazine-bridged Dinuclear Platinum(II) Complexes in Aqueous Solution

Table S5.1: Summary of the wavelengths (nm) used for monitoring the reactions between a series of aqua Pt(II) complexes with neutral S-donor nucleophiles.

Complex	Nucleophile	Wavelength (λ, nm)
pzn	TU	395
	DMTU	411
	TMTU	411
pmn	TU	325
	DMTU	325
	TMTU	325
pdn	TU	342
	DMTU	290
	TMTU	339
qzn	TU	392
	DMTU	392
	TMTU	343
pht	TU	335
	DMTU	298
	TMTU	307

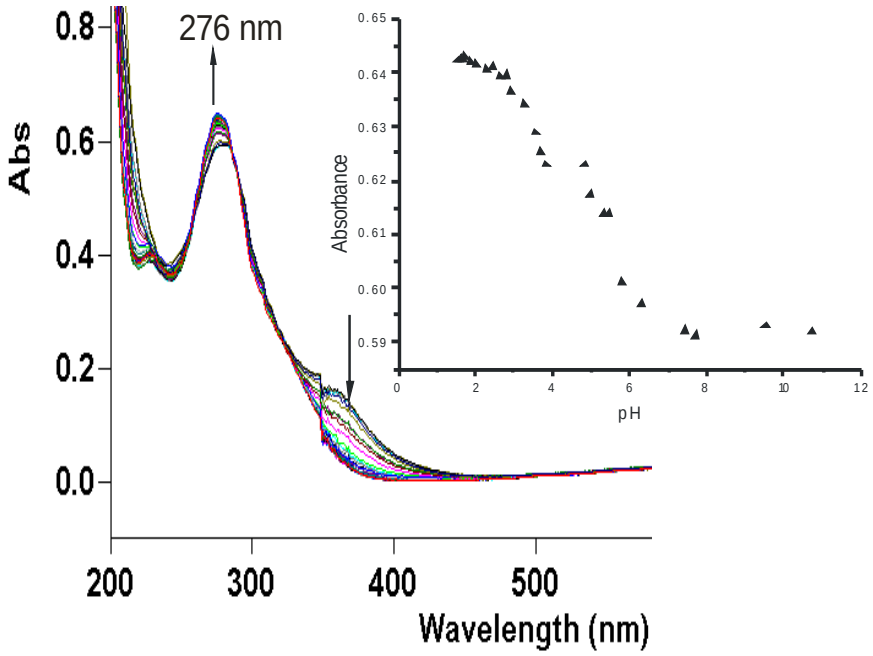

Figure S5.1: UV/Visible spectra for the titration of 0.1 mM **pzn** with NaOH in the pH range 2-11, T = 25° C. Inset is the titration curve at 276 nm.

Table S5.2: Average observed rate constants, $k_{obs(1^{st})}$, at 298.15 K, for the reactions of **pzn** with a series of nucleophiles at different concentrations.

[NU]/ M	$k_{obs(1)}$, s^{-1}		
	TU	**DMTU**	**TMTU**
0.02	0.0689	0,0444	0.0081
0.04	0.1681	0.0863	0.0164
0.06	0.2571	0.1337	0.0241
0.08	0.3434	0.1784	0.0321
0.1	0.4232	0.2217	0.0398

Table S5.3: Average observed rate constants, $k_{obs}(2^{nd})$, at 298.15 K, for the reactions of **pzn** with a series of nucleophiles at different concentrations.

[NU]/M	$k_{obs(2)}$, s^{-1}		
	TU	**DMTU**	**TMTU**
0.02	5.543×10^{-4}	2.873×10^{-4}	1.889×10^{-4}
0.04	1.120×10^{-3}	6.239×10^{-4}	3.959×10^{-4}
0.06	$1,710 \times 10^{-3}$	9.470×10^{-4}	5.294×10^{-4}
0.08	2.300×10^{-3}	1.280×10^{-3}	
0.1	2.870×10^{-3}	1.620×10^{-3}	9.805×10^{-4}

Table S5.4: Average observed rate constants, $k_{obs(3^{rd})}$, at 298.15 K, for the reactions of **pzn** with a series of nucleophiles at different concentrations

[NU]/ M	$k_{obs(3^{rd})}$, ($\times 10^{-5}$ s^{-1})		
	TU	**DMTU**	**TMTU**
0.02	0.4065	-	0.3578
0.04	1.1172	1.2512	0.7180
0.06	1.6147	2.0745	1.1125
0.08	2.3859	2.9302	1.5227
0.1	2.8822	3.7350	1.8200

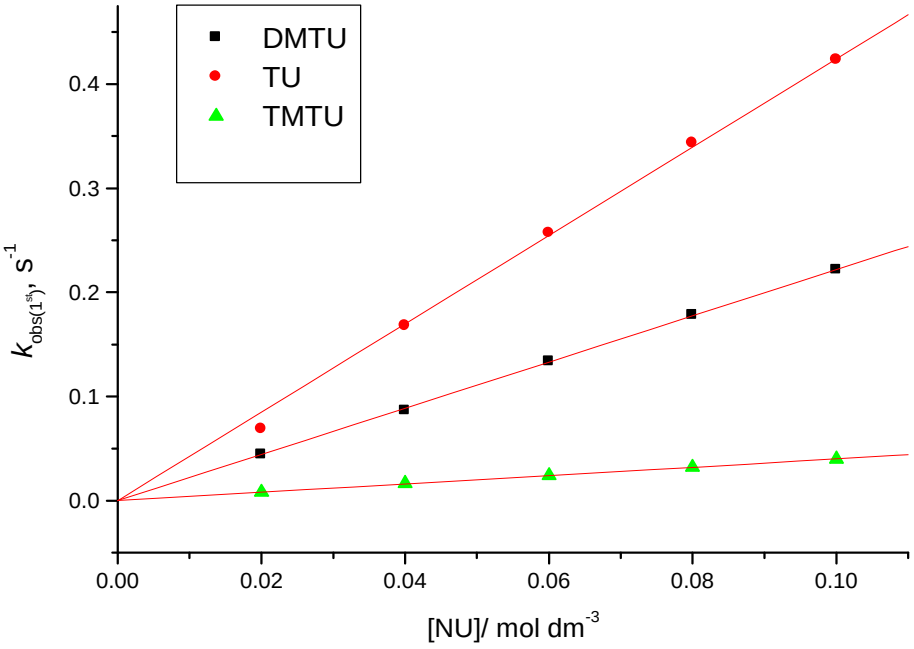

Figure S5.2: Concentration dependence of $k_{obs(1^{st})}$ for the displacement of first aqua ligand in **pzn** by thiourea nucleophiles, pH = 2.0, T = 298.15 K, I = 0.10 M (0.01 M $HClO_4$, adjusted with $NaClO_4$).

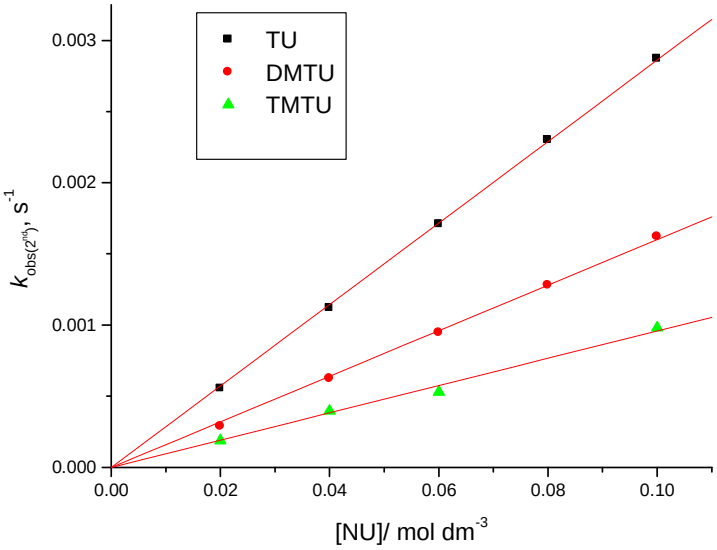

Figure S5.3: Concentration dependence of $k_{obs(2^{nd})}$ for the displacement of second water ligand in **pzn** by thiourea nucleophiles, pH = 2.0, T = 298.15 K, I = 0.10 M (0.01 M $HClO_4$, adjusted with $NaClO_4$).

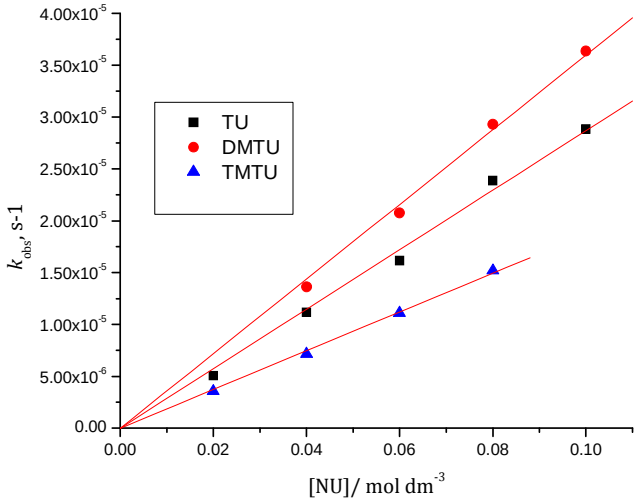

Figure S5.4: Concentration dependence of $k_{obs(3^{rd})}$ for the displacement of bridging ligand in **pzn** by thiourea nucleophiles, pH = 2.0, T = 298.15 K, I = 0.10 M (0.01 M $HClO_4$, adjusted with $NaClO_4$).

Table S5.5: Average observed rate constants, $k_{obs(1^{st})}$, for the reactions of **pzn** at varied temperatures in the range 15 to 35 °C while maintaining nucleophile concentration at ≈ 60x [**pzn**].

1/T, K^{-1}	**TU**		**DMTU**		**TMTU**	
	$k_{obs(1^{st})}$, s^{-1}	**ln(k_2/T)**	**$k_{obs(1^{st})}$, s^{-1}**	**ln(k_2/T)**	**$k_{obs(1^{st})}$, s^{-1}**	**ln(k_2/T)**
0.00347	0.08503	-5.3143	0.0332	-6.2548	0.0118	-7.2892
0.00341	0.1201	-4.9862	0.0468	-5.9286	0.0172	-6.9296
0.00335	0.1666	-4.6758	0.0671	-5.5853	0.0235	-6.6344
0.00330	0.2224	-4.4036	0.0911	-5.2961	0.0324	-6.3299
0.00325	0.2985	-4.1257	0.1253	-4.9737	0.0409	-6.1133

Table S5.6: Average observed rate constants, $k_{obs(2^{nd})}$, for the second step reactions of **pzn** at varied temperatures in the range 15 to 35 °C while maintaining nucleophile concentration at ≈ 60x [**pzn**].

1/T, K^{-1}	**TU**		**DMTU**		**TMTU**	
	$k_{obs(2^{nd})}$, s^{-1}	**ln(k_2/T)**	**$k_{obs(2^{nd})}$, s^{-1}**	**ln(k_2/T)**	**$k_{obs(2^{nd})}$, s^{-1}**	**ln(k_2/T)**
0.00347	7.63 x 10^{-4}	-10.028	3.71 x 10^{-4}	-10.750	5.38 x 10^{-5}	-12.681
0.00341	1.08 x 10^{-3}	-9.698	6.24 x 10^{-4}	-10.247	6.52 x 10^{-5}	-12.505
0.00335	1.69 x 10^{-3}	-9.266	1.02 x 10^{-3}	-9.770	7.69 x 10^{-5}	-12.357
0.00330	2.13 x 10^{-3}	-9.051	1.59 x 10^{-3}	-9.347	9.34 x 10^{-5}	-12.179
0.00325	3.70 x 10^{-3}	-8.519	2.39 x 10^{-3}	-8.953	1.11 x 10^{-4}	-12.027

Table S5.7: Average observed rate constants, $k_{obs(3^{rd})}$, for the third step reactions of **pzn** at varied temperatures in the range 15 to 35 °C while maintaining nucleophile concentration at ≈ 60x [**pzn**].

1/T, K^{-1}	**TU**		**DMTU**		**TMTU**	
	$k_{obs(3^{rd})}$, s^{-1}	**ln(k_2/T)**	**$k_{obs(3^{rd})}$, s^{-1}**	**ln(k_2/T)**	**$k_{obs(3^{rd})}$, s^{-1}**	**ln(k_2/T)**
0.00347	4.28 x 10^{-6}	-18.0244	1.47 x 10^{-5}	-16.810	2.07 x 10^{-5}	-16.449
0.00341	8.35 x 10^{-6}	-17.3735	1.67 x 10-^{5}	-16.666	5.41 x 10^{-5}	-15.488
0.00335	1.66 x 10^{-5}	-16.7085	2.07 x 10^{-5}	-16.480	1.03 x 10^{-4}	-14.882
0.00330	2.71 x 10^{-5}	-16.2282	3.57 x 10^{-5}	-15.954	1.57 x 10^{-4}	-14.476
0.00325	8.30 x 10^{-5}	-15.1263	5.81 x 10^{-5}	-15.483	2.32 x 10^{-4}	-14.099

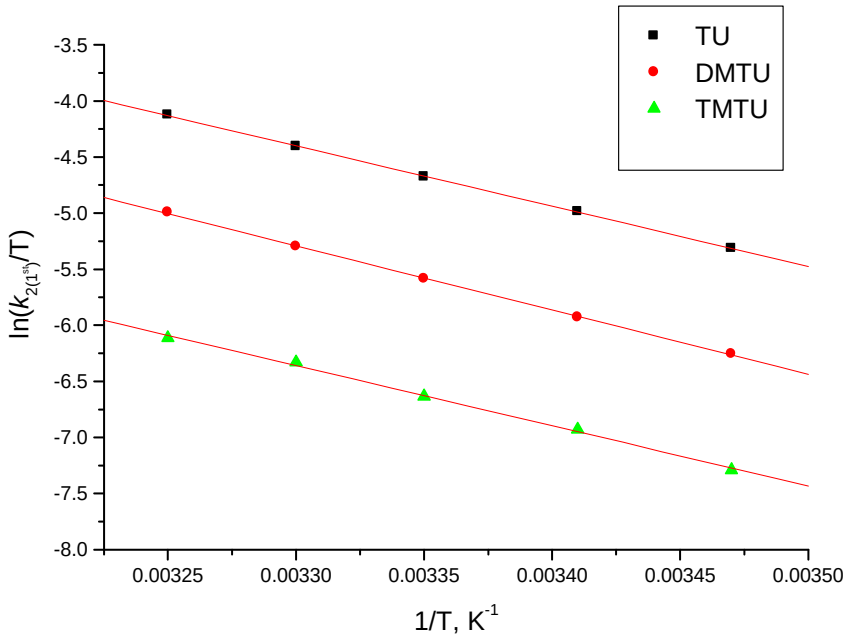

Figure S5.5: Plots of ln(k_1/T) versus (1/T) for the first step reaction of **pzn** with a series of different nucleophiles at varying temperatures.

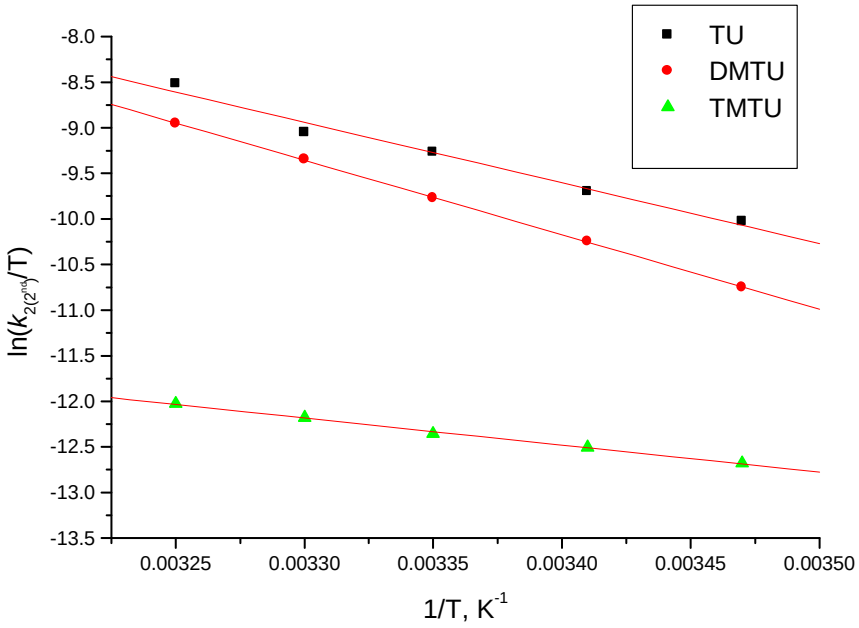

Figure S5.6: Plots of ln(k_2/T) versus (1/T) for the second step reaction of **pzn** with a series of different nucleophiles at varying temperatures.

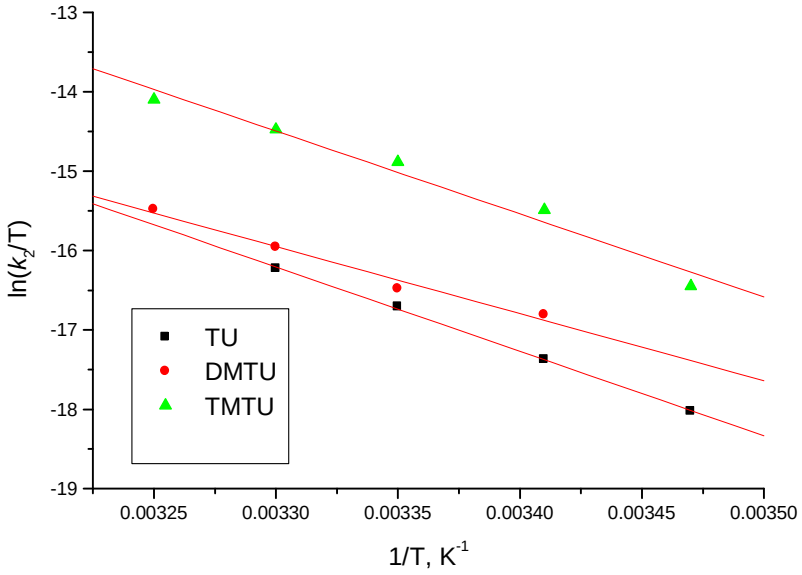

Figure S5.7: Plots of ln(k_3/T) versus (1/T) for the third step reaction of **pzn** with a series of different nucleophiles at varying temperatures.

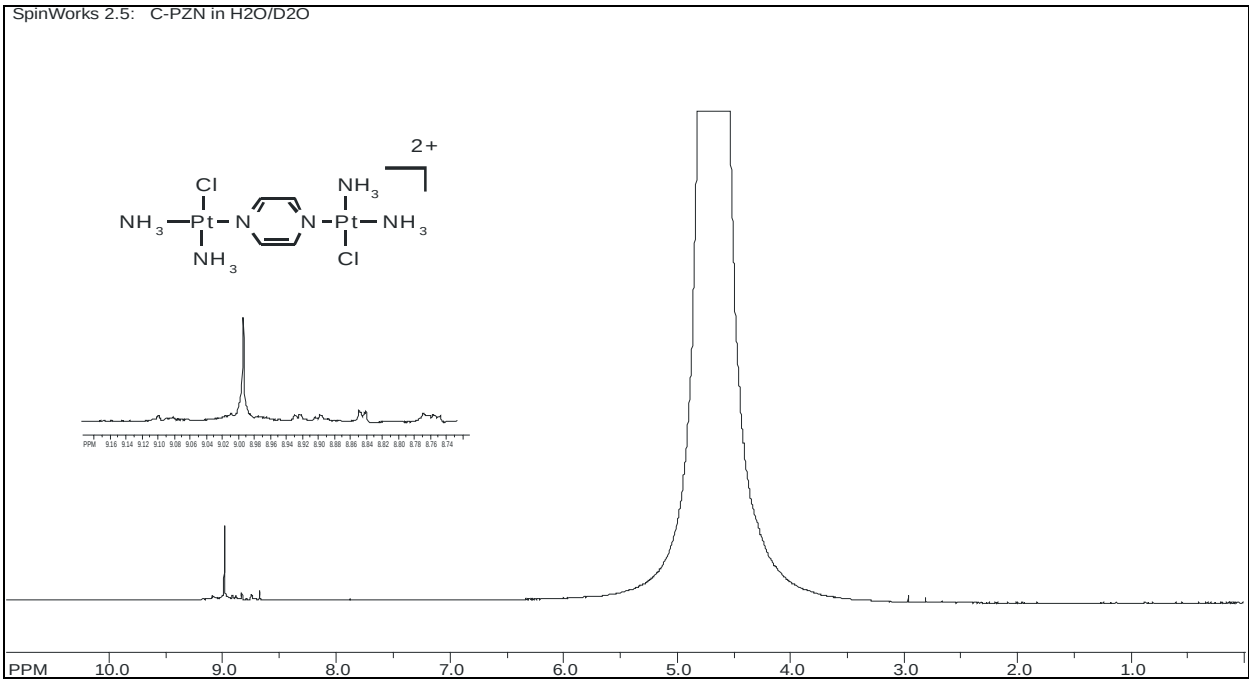

Figure S5.8: ^{1}H NMR (500MHz) spectrum of solution of [*cis*-{$PtCl(NH_3)_2$}$_2$-μ-pzn]$(ClO_4)_2$ in D_2O at 30 °C showing pyrazine ring proton assignment

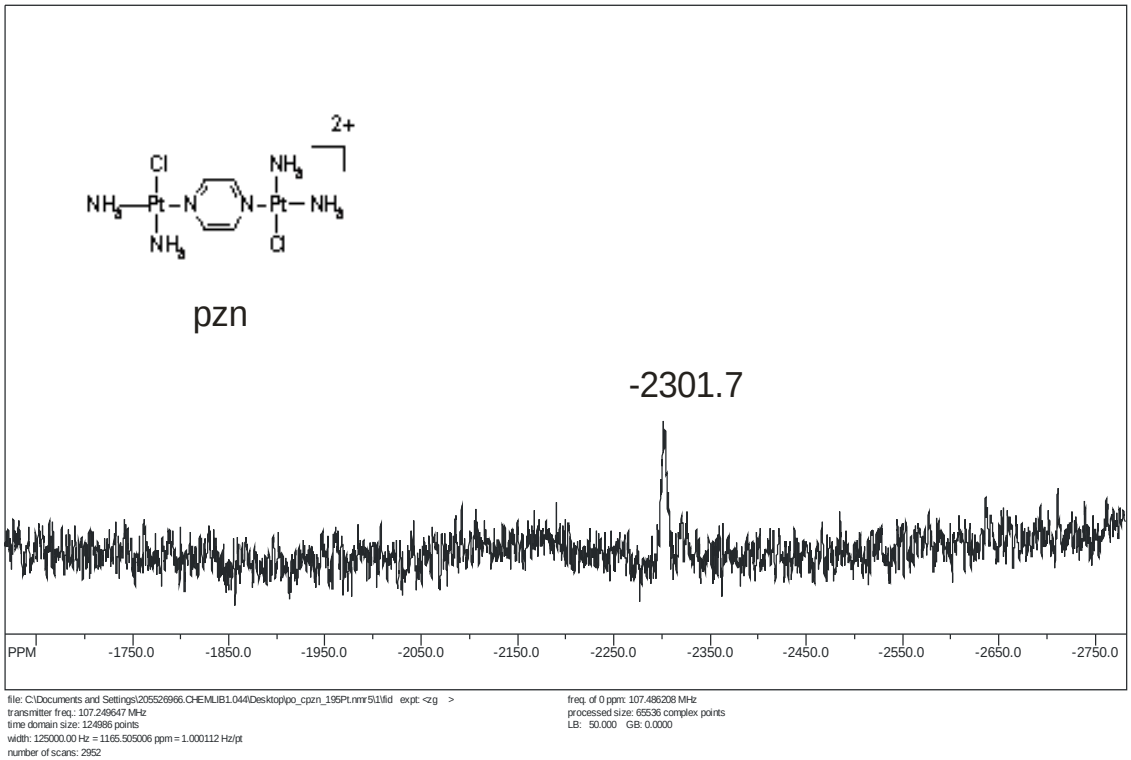

Figure S5.9: ^{195}Pt NMR (107 MHz) spectrum of [*cis*-{PtCl(NH_3)$_2$}$_2$-μ-pzn](ClO_4)$_2$ in D_2O at 30 °C.

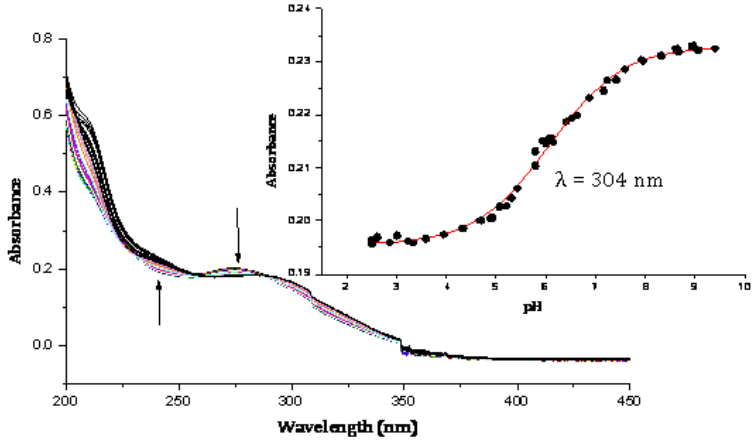

Figure S5.10: UV/Visible spectra for the titration of 0.1 mM **pmn** with NaOH in the pH range 2-10, T = 25° C. Inset is the titration curve at 304 nm.

Table S5.8: Average observed rate constants, $k_{obs(1^{st})}$, at 298.15 K, for the displacement of the first aqua ligand of **pmn** with a series of nucleophiles at different concentrations.

[NU]/ M	$k_{obs(1^{st})}$, s^{-1}		
	TU	**DMTU**	**TMTU**
00.02	0.01705	0.03975	0.00165
0.004	0.03476	0.08004	0.00333
0.006	0.5224	—	0.00492
0.008	0.06716	0.11950	0.00670
0.01	0.08462	0.19978	0.00829

Table S5.9: Average observed rate constants, $k_{obs}(_{2^{nd}})$, at 298.15 K, for the reactions of **pmn** with a series of nucleophiles at different concentrations.

[NU]/ M	$\boldsymbol{k_{obs(2^{nd})}}$**, s^{-1}**		
	TU	**DMTU**	**TMTU**
0.002	2.462×10^{-4}	1.449×10^{-4}	9.097×10^{-5}
0.004	4.909×10^{-4}	3.197×10^{-4}	1.550×10^{-4}
0.006	7.333×10^{-4}	4.3479×10^{-4}	2.380×10^{-4}
0.008	9.149×10^{-4}	5.764×10^{-4}	3.220×10^{-4}
0.01	0.00122	7.244×10^{-4}	—

Table S5.10: Average observed rate constants, $k_{obs(3^{rd})}$, at 298.15 K, for the displacement of the bridging ligand of **pmn** with a series of nucleophiles at different concentrations.

[NU]/ M	$\boldsymbol{k_{obs(3^{rd})}}$**, s^{-1}**		
	TU	**DMTU**	**TMTU**
0.002	5.634×10^{-5}	4.697×10^{-5}	6.858×10^{-6}
0.004	1.115×10^{-4}	9.291×10^{-5}	1.3745×10^{-5}
0.006	1.645×10^{-4}	1.364×10^{-4}	2.065×10^{-5}
0.008	2.240×10^{-4}	1.869×10^{-4}	2.796×10^{-5}
0.010	—	—	3.429×10^{-5}

Table S5.11: Average observed rate constants, $k_{obs(1^{st})}$, for the third step reactions of **pmn** at varied temperatures in the range 15 to 35 °C while maintaining nucleophile concentration at ≈ 60x [**pmn**].

1/T, K^{-1}	**TU**		**DMTU**		**TMTU**	
	$k_{obs(1^{st})}$, s^{-1}	**ln(k_2/T)**	**$k_{obs(1^{st})}$, s^{-1}**	**ln(k_2/T)**	**$k_{obs(1^{st})}$, s^{-1}**	**ln(k_2/T)**
0.00347	0.01509	-7.0433	0.05909	-5.6782	2.207 x 10^{-3}	-8.9658
0.00341	0.02091	-6.7343	0.08372	-5.3470	3.360 x 10^{-3}	-8.5626
0.00335	0.02903	-6.4231	0.01195	-5.0083	4.915 x 10^{-3}	-8.1991
0.00330	0.38118	-6.1674	0.16088	-4.7274	6.713 x 10^{-3}	-7.9041
0.00325	0.50385	-5.9048	0.21880	-4.4363	9.226 x 10^{-3}	-7.6024

Table S5.12: Average observed rate constants, $k_{obs(2^{nd})}$, for the third step reactions of **pmn** at varied temperatures in the range 15 to 35 °C while maintaining nucleophile concentration at ≈ 60x [**pmn**].

1/T, K^{-1}	**TU**		**DMTU**		**TMTU**	
	$k_{obs(2^{nd})}$, s^{-1}	**ln(k_2/T)**	**$k_{obs(2^{nd})}$, s^{-1}**	**ln(k_2/T)**	**$k_{obs(2^{nd})}$, s^{-1}**	**ln(k_2/T)**
0.00347	2.23 x 10^{-4}	-11.2586	1.25 x 10^{-4}	-11.8336	1.31 x 10^{-4}	-11.7896
0.00341	2.77 x 10^{-4}	-11.0576	1.79 x 10^{-4}	-11.4956	1.92 x 10^{-4}	-11.4226
0.00335	3.34 x 10^{-4}	-10.8876	2.34 x 10^{-4}	-11.2186	2.63 x 10^{-4}	-11.1286
0.00330	4.15 x10^{-4}	-10.6866	3.43 x 10^{-4}	-10.8766	3.75 x 10^{-4}	-10.7886
0.00325	4.99 x 10^{-4}	-10.5206	4.56 x 10^{-4}	-10.6106	5.14 x 10^{-4}	-10.4896

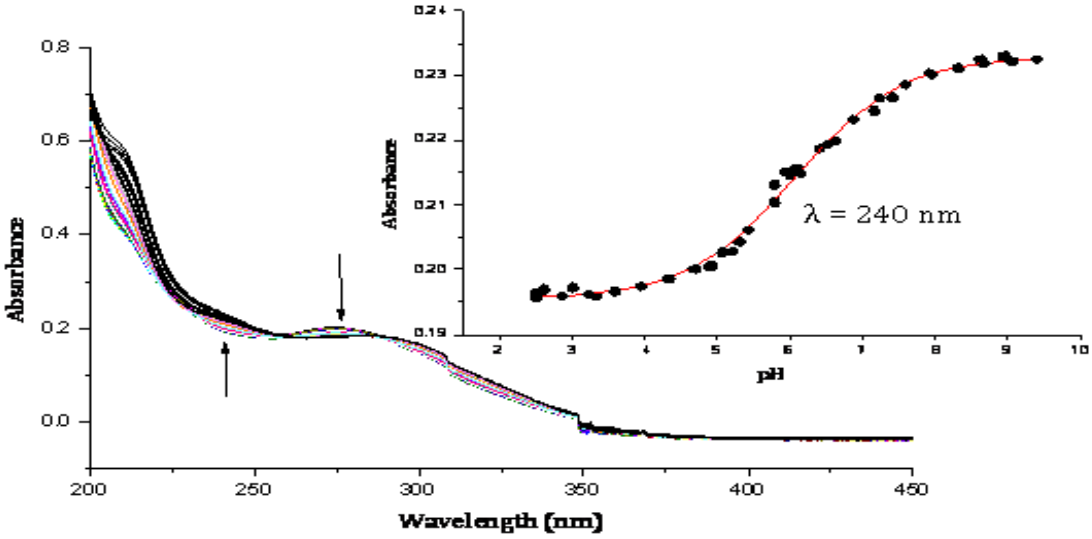

Figure S5.13: UV/Visible spectra for the titration of 0.1 mM **pdn** with NaOH in the pH range 2-10, T = 25° C. Inset is the titration curve at 240 nm.

Table S5.14: Average observed rate constants, $k_{obs(1^{st})}$, at 298.15 K, for the displacement of the first aqua ligand of **pdn** with a series of nucleophiles at different concentrations.

[NU]/ M	$k_{obs(1^{st})}$, s^{-1}		
	TU	**DMTU**	**TMTU**
0.02	0.00372	0.00502	0.00166
0.04	0.00848	0.01096	0.00280
0.06	0.01182	0.01590	0.00398
0.08	0.01672	0.02187	0.00511
0.1	0.02019	0.02879	0.00660

Table S5.15: Average observed rate constants, $k_{obs(2^{nd})}$, at 298.15 K, for the displacement of the second aqua ligand of **pdn** with a series of nucleophiles at different concentrations.

[NU]/ M	$k_{obs(2^{nd})}$, s^{-1}		
	TU	**DMTU**	**TMTU**
0.02	2.029×10^{-4}	3.480×10^{-4}	—
0.04	3.932×10^{-4}	6.850×10^{-4}	2.7357×10^{-4}
0.06	6.084×10^{-4}	0.00103	4.3068×10^{-4}
0.08	8.625×10^{-4}	0.00139	5.1627×10^{-4}
0.1	1.089×10^{-3}	—	6.7520×10^{-4}

Table S5.16: Average observed rate constants, $k_{obs(3^{rd})}$, at 298.15 K, for the displacement of the bridging ligand of **pdn** with a series of nucleophiles at different concentrations.

[NU]/ M	$k_{obs(3^{rd})}$, s^{-1}		
	TU	**DMTU**	**TMTU**
0.002	-	1.8915×10^{-5}	3.1750×10^{-6}
0.004	1.8865×10^{-5}	3.7780×10^{-5}	6.0497×10^{-6}
0.006	2.5761×10^{-5}	6.0950×10^{-5}	9.0890×10^{-6}
0.008	3.8720×10^{-5}	7.5260×10^{-5}	1.3319×10^{-5}
0.01	4.6230×10^{-5}	9.4750×10^{-5}	1.5773×10^{-5}

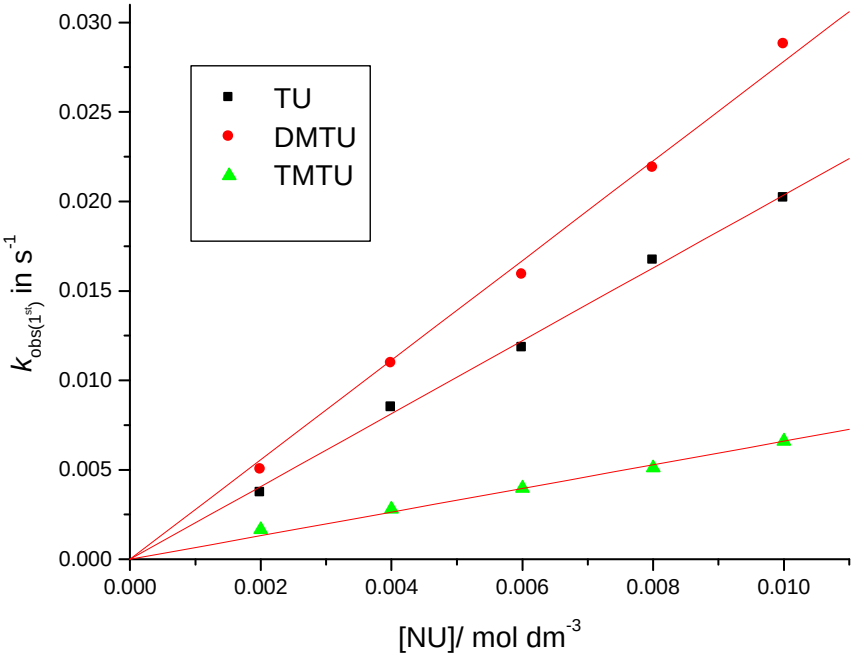

Figure S5.14: Concentration dependence of $k_{obs(1^{st})}$ for the displacement of first aqua ligand in **pdn** by thiourea nucleophiles, pH = 2.0, T = 298.15 K, I = 0.10 M (0.01 M $HClO_4$, adjusted with $NaClO_4$).

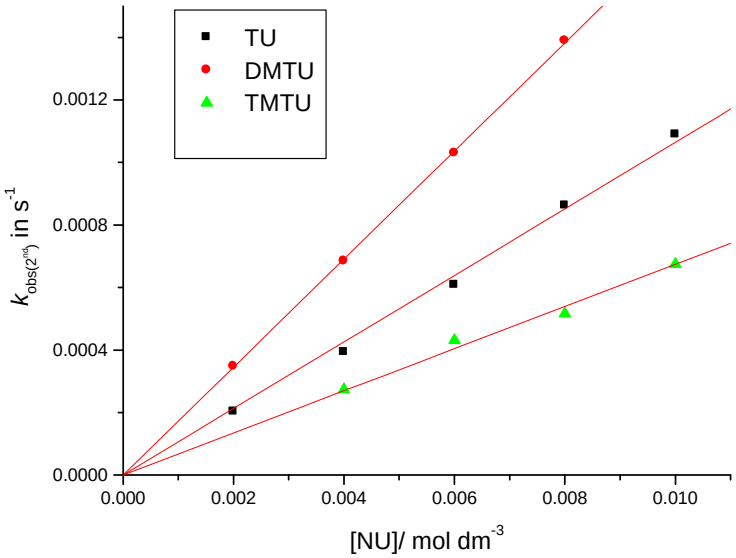

Figure S5.15: Concentration dependence of $k_{obs(2^{nd})}$ for the displacement of second aqua ligand in **pdn** by thiourea nucleophiles, pH = 2.0, T = 298.15 K, I = 0.10 M (0.01 M $HClO_4$, adjusted with $NaClO_4$).

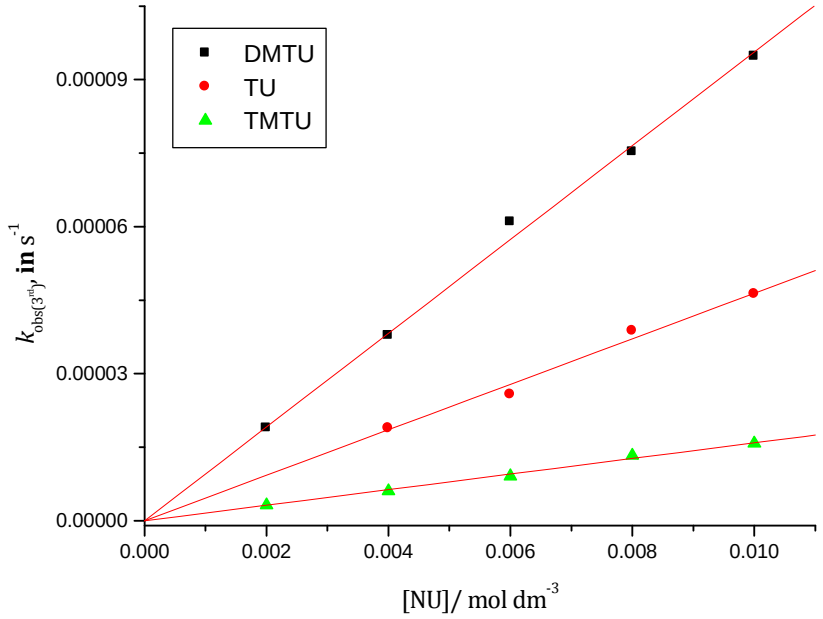

Figure S5.16: Concentration dependence of $k_{obs(3^{rd})}$ for the displacement of first aqua ligand in **pdn** by thiourea nucleophiles, pH = 2.0, T = 298.15 K, I = 0.10 M (0.01 M $HClO_4$, adjusted with $NaClO_4$)

Table S5.17: Average observed rate constants, $k_{obs(1^{st})}$, for the third step reactions of **pdn** at varied temperatures in the range 15 to 35 °C while maintaining nucleophile concentration at ≈ 60x [**pdn**].

1/T, K^{-1}	**TU**		**DMTU**		**TMTU**	
	$k_{obs(1^{st})}$, s^{-1}	**ln(k_2/T)**	**$k_{obs(1^{st})}$, s^{-1}**	**ln(k_2/T)**	**$k_{obs(1^{st})}$, s^{-1}**	**ln(k_2/T)**
0.00347	5.92 x 10^{-3}	-7.9790	5.81 x 10^{-3}	-7.9974	1.76 x 10^{-3}	-9.1903
0.00341	7.93 x 10^{-3}	-7.7039	9.67 x 10^{-3}	-7.5059	2.65 x 10^{-3}	-8.8018
0.00335	0.01151	-7.3485	0.01328	-7.2052	3.98 x 10^{-3}	-8.4112
0.00330	0.01544	-7.0711	0.02280	-6.6813	5.21 x 10^{-3}	-8.1579
0.00325	0.02108	-6.7762	0.03372	-6.3064	7.77 x 10^{-3}	-7.7744

Table S5.18: Average observed rate constants, $k_{obs(2^{nd})}$, for the third step reactions of **pdn** at varied temperatures in the range 15 to 35 °C while maintaining nucleophile concentration at ≈ 60x [**pdn**].

1/T, K^{-1}	**TU**		**DMTU**		**TMTU**	
	$k_{obs(2^{nd})}$, s^{-1}	**ln(k_2/T)**	**$k_{obs(2^{nd})}$, s^{-1}**	**ln(k_2/T)**	**$k_{obs(2^{nd})}$, s^{-1}**	**ln(k_2/T)**
0.00347	1.96 x 10^{-4}	-11.3875	1.91 x 10^{-5}	-13.7182	1.55 x 10^{-4}	-11.6197
0.00341	2.89 x 10^{-4}	-11.0147	3.32 x 10^{-5}	-13.1813	2.25 x 10^{-4}	-11.2668
0.00335	4.58 x 10^{-4}	-10.5723	5.52 x 10^{-5}	-12.6892	3.37 x 10^{-4}	-10.8783
0.00330	6.96 x 10^{-4}	-10.1706	8.35 x 10^{-5}	-12.2913	5.23 x 10^{-4}	-10.4559
0.00325	1.04 x 10^{-3}	-9.7881	1.24 x 10^{-4}	-11.9139	7.22 x 10^{-4}	-10.1499

Table S5.19: Average observed rate constants, $k_{obs(3^{rd})}$, for the third step reactions of **pdn** at varied temperatures in the range 15 to 35 °C while maintaining nucleophile concentration at ≈ 60x [**pdn**].

1/T, K^{-1}	**TU**		**DMTU**		**TMTU**	
	$k_{obs(3^{rd})}$, s^{-1}	**ln(k_2/T)**	**$k_{obs(3^{rd})}$, s^{-1}**	**ln(k_2/T)**	**$k_{obs(3^{rd})}$, s^{-1}**	**ln(k_2/T)**
0.00347	9.69 x10^{-6}	-14.3943	2.58 x 10^{-6}	-15.7169	1.14 x 10^{-6}	-16.5315
0.00341	1.42 x 10^{-5}	-14.0295	3.75 x 10^{-6}	-15.3596	1.85 x 10^{-6}	-16. 0648
0.00335	2.40 x 10^{-5}	-13.5199	5.55 x 10^{-6}	-14.9857	3.34 x 10^{-6}	-15.4926
0.00330	3.41 x 10^{-5}	-13.1867	7.72 x 10^{-6}	-14.6725	5.00 x 10^{-6}	-15.1072
0.00325	5.07 x 10^{-5}	-12.8060	1.13 x 10^{-5}	-14.3085	7.72 x 10^{-6}	-14.6885

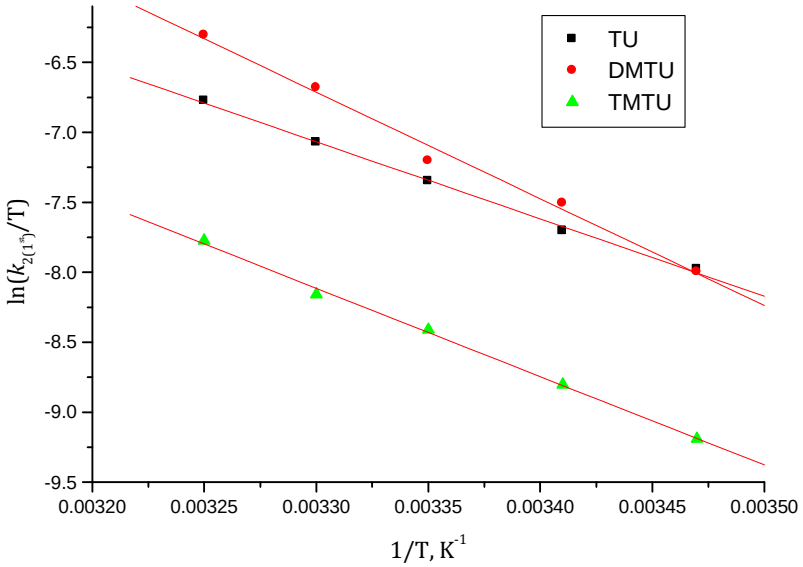

Figure S5.17: Plots of ln(k_1/ T) versus (1/T) for the first step reaction of **pdn** with a series of different nucleophiles at varying temperatures.

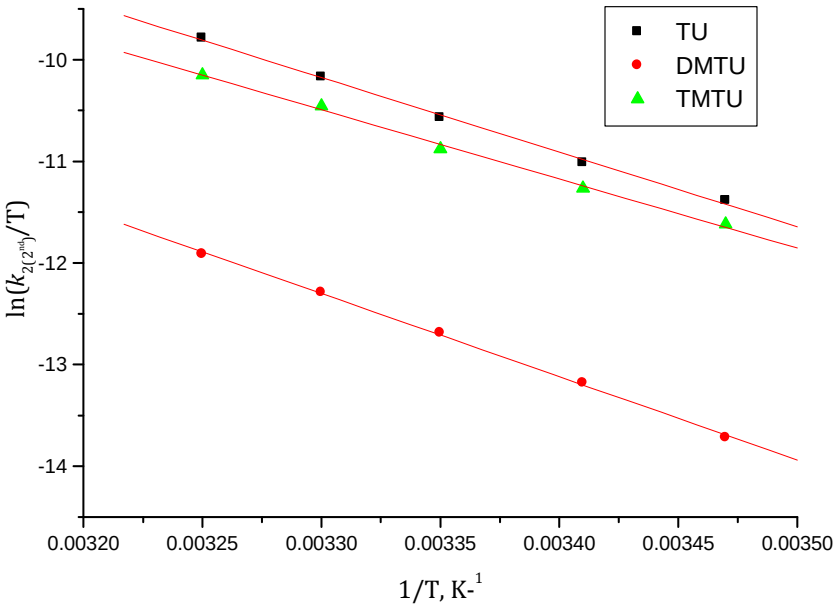

Figure S5.18: Plots of ln(k_2/T) versus (1/T) for the second step reaction of **pdn** with a series of different nucleophiles at varying temperatures.

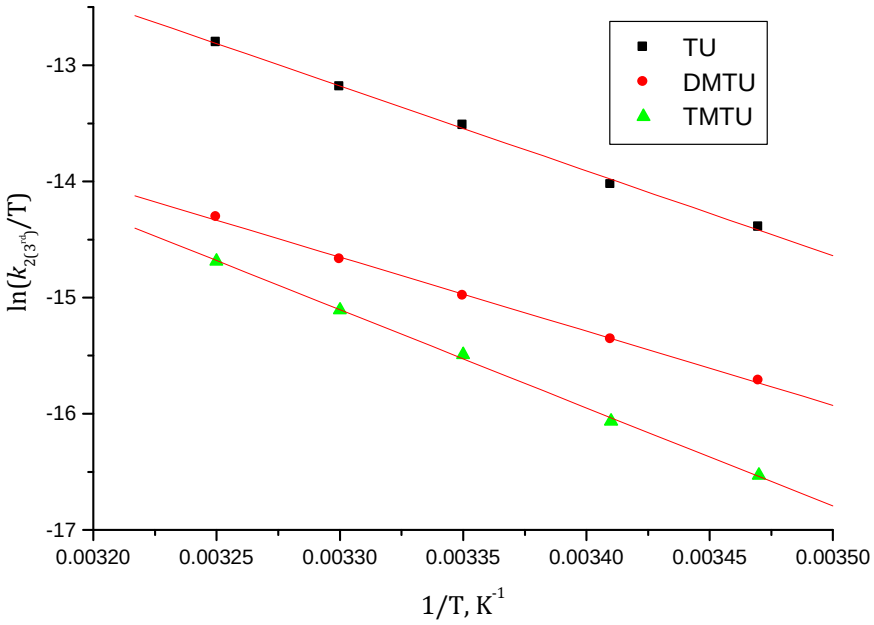

Figure S5.19: Plots of ln(k_3/T) versus (1/T) for the third step reaction of **pdn** with a series of different nucleophiles at varying temperatures.

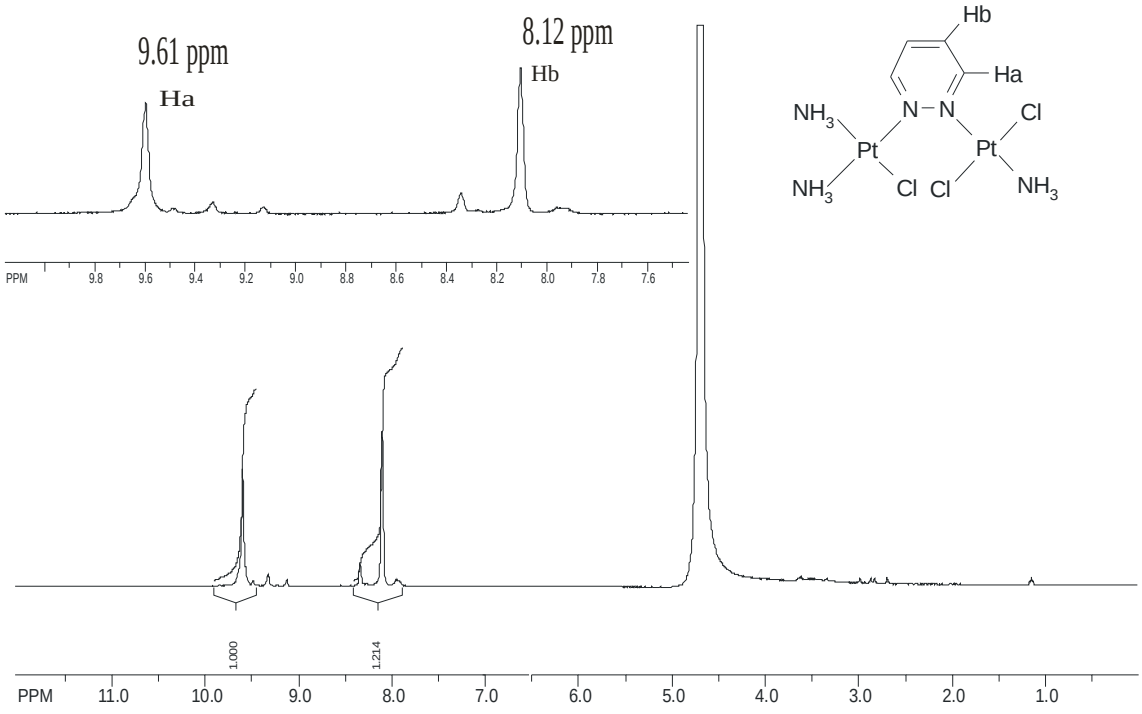

Figure S5.20: ^{1}H NMR (500MHz) spectrum of solution of [*cis*-{$PtCl(NH_3)_2$}$_2$-μ-pdn]$(ClO_4)_2$ in D_2O at 30 °C showing pyrazine ring proton assignment

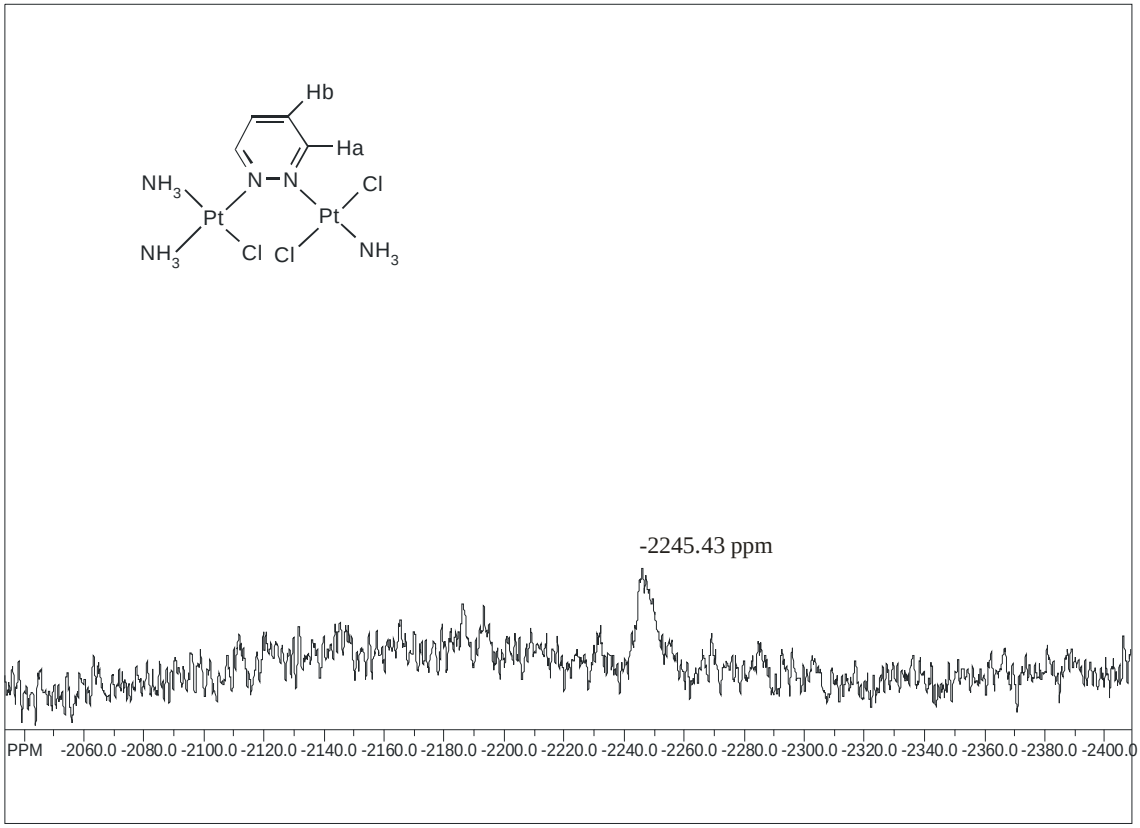

Figure S5.21: ^{195}Pt NMR (107 MHz) spectrum of [*cis*-{PtCl(NH_3)$_2$}$_2$-μ-pdn](ClO_4)$_2$ in D_2O at 30 °C.

Table S5.22: Average observed rate constants, $k_{obs(3^{rd})}$, at 298.15 K, for the displacement of the second aqua ligand of **qzn** with a series of nucleophiles at different concentrations.

[NU]/ M	$k_{obs(3^{rd})}$, s^{-1}		
	TU	**DMTU**	**TMTU**
0.00138		8.1534×10^{-6}	5.0754×10^{-6}
0.00276	3.3360×10^{-5}	1.6310×10^{-5}	1.0567×10^{-5}
0.00414	5.0010×10^{-5}	2.4459×10^{-5}	1.5510×10^{-5}
0.00552	6.7920×10^{-5}	3.2691×10^{-5}	2.0943×10^{-5}
0.00690	8.3342×10^{-5}	—	2.5366×10^{-5}

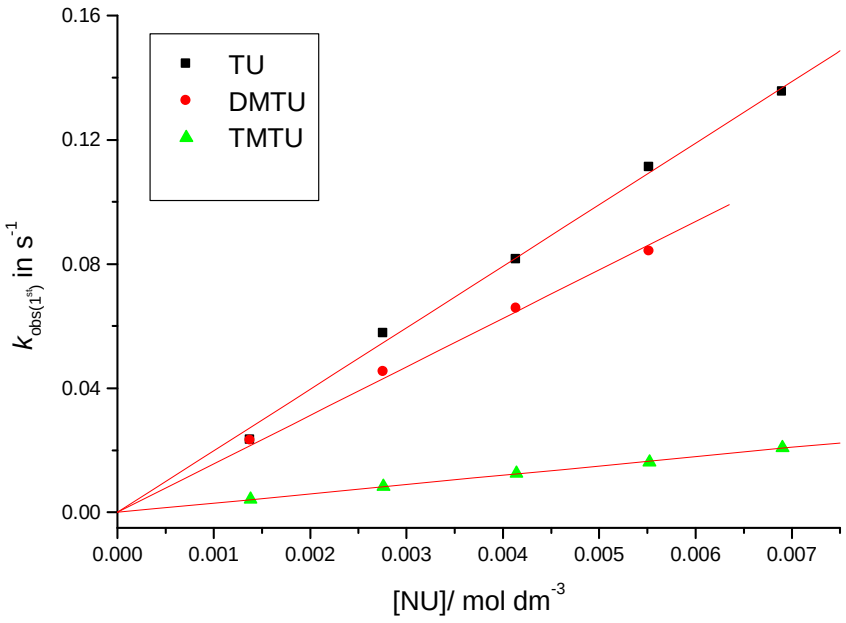

Figure S5.22: Concentration dependence of $k_{obs(1^{st})}$ for the displacement of first aqua ligand in **qzn** by thiourea nucleophiles, pH = 2.0, T = 298.15 K, I = 0.10 M (0.01 M $HClO_4$, adjusted with $NaClO_4$).

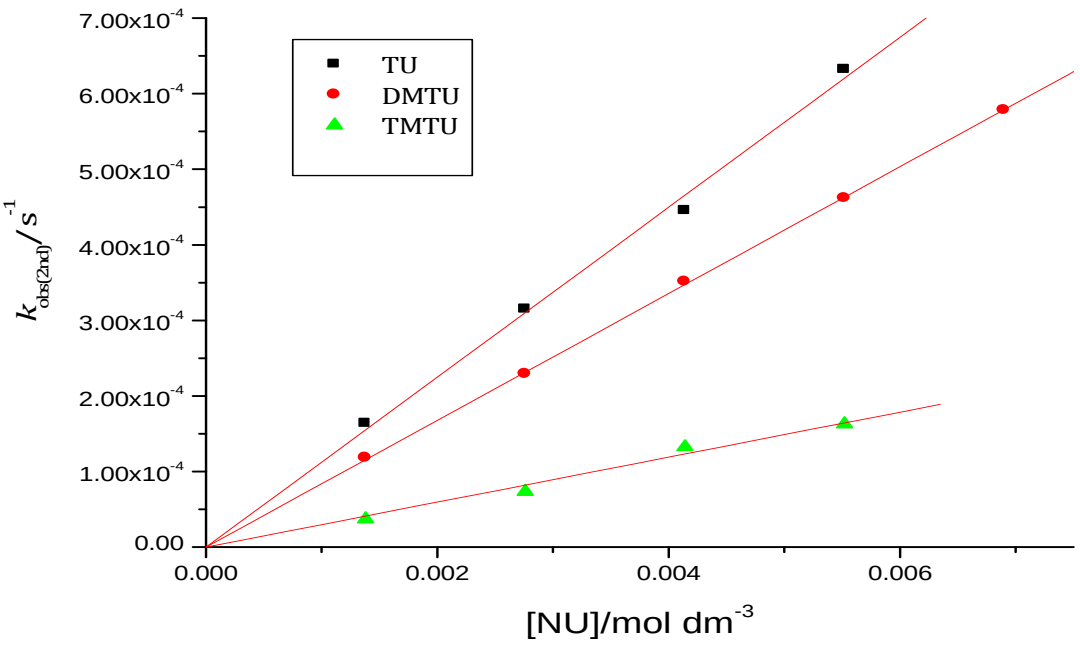

Figure S5.23: Concentration dependence of $k_{obs(2^{nd})}$ for the displacement of first aqua ligand in **qzn** by thiourea nucleophiles, pH = 2.0, T = 298.15 K, I = 0.10 M (0.01 M $HClO_4$, adjusted with $NaClO_4$).

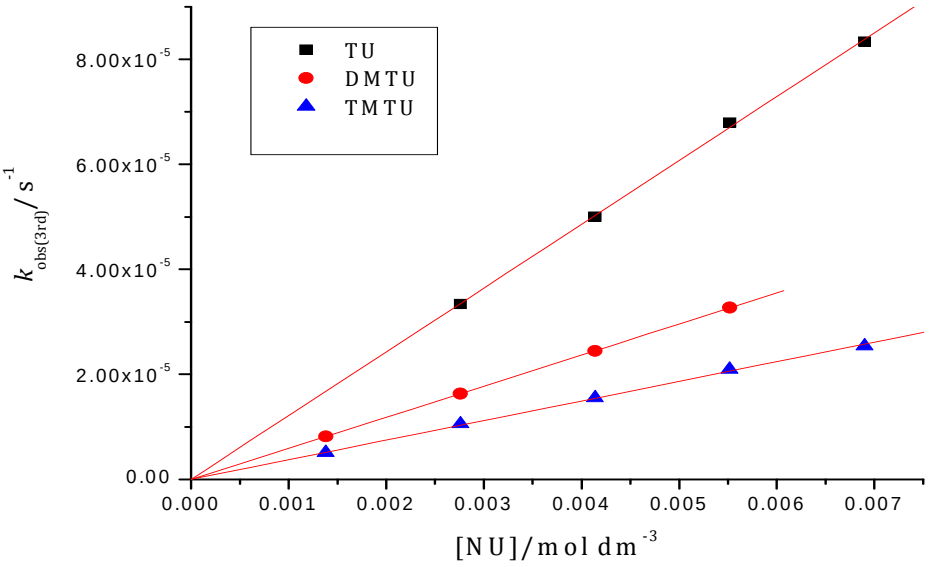

Figure S5.24: Concentration dependence of $k_{obs(3^{rd})}$ for the displacement of first aqua ligand in **qzn** by thiourea nucleophiles, pH = 2.0, T = 298.15 K, I = 0.10 M (0.01 M $HClO_4$, adjusted with $NaClO_4$).

Table S5.23: Average observed rate constants, $k_{obs(1^{st})}$, for the first step reactions of **qzn** at varied temperatures in the range 15 to 35 °C while maintaining nucleophile concentration at ≈ 60x [**qzn**].

1/T, K^{-1}	**TU**		**DMTU**		**TMTU**	
	$k_{obs(1^{st})}$, s^{-1}	**ln(k_2/T)**	**$k_{obs(1^{st})}$, s^{-1}**	**ln(k_2/T)**	**$k_{obs(1^{st})}$, s^{-1}**	**ln(k_2/T)**
0.00347	0.04140	-3.3604	0.03308	-3.5848	0.001683	-6.5633
0.00341	0.05872	-3.0281	0.04548	-3.2836	0.002480	-6.1928
0.00335	0.08197	-2.7114	0.06078	-3.0105	0.003660	-5.8202
0.00330	0.11050	-2.4294	0.08055	-2.7455	0.004959	-5.5332
0.00325	0.14810	-2.1529	—	—	0.007321	-5.2601

Table S5.24: Average observed rate constants, $k_{obs(2^{nd})}$, for the second step reactions of **qzn** at varied temperatures in the range 15 to 35 °C while maintaining nucleophile concentration at ≈ 60x [**qzn**].

1/T, K^{-1}	**TU**		**DMTU**		**TMTU**	
	$k_{obs(2^{nd})}$, s^{-1}	**ln(k_2/T)**	**$k_{obs(2^{nd})}$, s^{-1}**	**ln(k_2/T)**	**$k_{obs(2^{nd})}$, s^{-1}**	**ln(k_2/T)**
0.00347	1.66 x 10^{-4}	-8.8783	1.99 x 10^{-4}	-8.698o	—	—
0.00341	2.57 x 10^{-4}	-8.4495	3.09 x 10^{-4}	-8.2737	3.00 x 10^{-4}	-8.5063
0.00335	4.13 x 10^{-4}	-8.0011	5.01 x 10^{-4}	-7.8092	3.62 x 10^{-4}	-8.0764
0.00330	5.57 x 10^{-4}	-7.7206	7.63 x 10^{-4}	-7.4053	5.23 x 10^{-4}	-7.7822
0.00325	7.86 x 10^{-4}	-7.3917	1.27 x 10^{-3}	-6.8921	7.22 x 10^{-4}	-7.4763

Table S5.25: Average observed rate constants, $k_{obs(3^{nd})}$, for the third step reactions of **qzn** at varied temperatures in the range 15 to 35 °C while maintaining nucleophile concentration at ≈ 60x [**qzn**].

1/T, K^{-1}	**TU**		**DMTU**		**TMTU**	
	$k_{obs(3^{rd})}$, s^{-1}	**ln(k_2/T)**	**$k_{obs(3^{rd})}$, s^{-1}**	**ln(k_2/T)**	**$k_{obs(3^{rd})}$, s^{-1}**	**ln(k_2/T)**
0.00347	2.090 x 10^{-5}	-10.9519	3.798 x 10^{-5}	-10.3563	2.363 x 10^{-5}	-10.8288
0.00341	2.881 x 10^{-5}	-10.6479	5.468 x10^{-5}	-10.0072	3.696 x 10^{-5}	-10.3988
0.00335	4.179 x 10^{-5}	-10.2929	7.582 x 10^{-5}	-9.6972	5.948 x 10^{-5}	-9.9399
0.00330	6.322 x 10^{-5}	-9.8956	1.094 x 10^{-4}	-9.3476	9.029 x 10^{-5}	-9.5392
0.00325	8.358 x 10^{-5}	-9.6328	1.516 x 10^{-4}	-9.0371	—	—

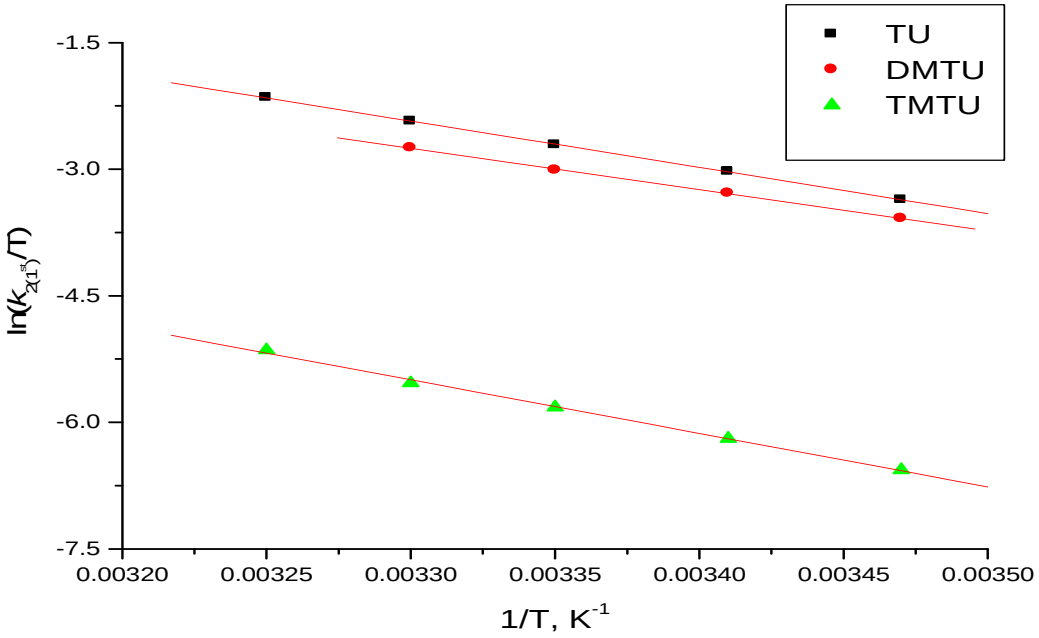

Figure S5.25: Plots of ln(k_2/ T) versus (1/T) for the first step reaction of **qzn** with a series of different nucleophiles at varying temperatures.

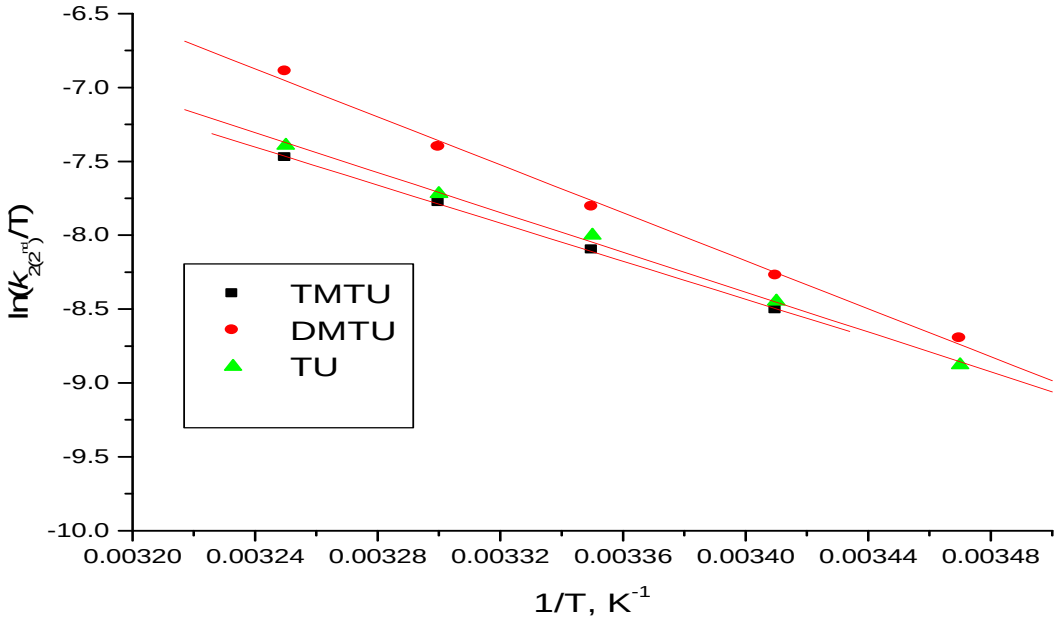

Figure S5.26: Plots of ln(k_2/T) versus (1/T) for the second step reaction of **qzn** with a series of different nucleophiles at varying temperatures.

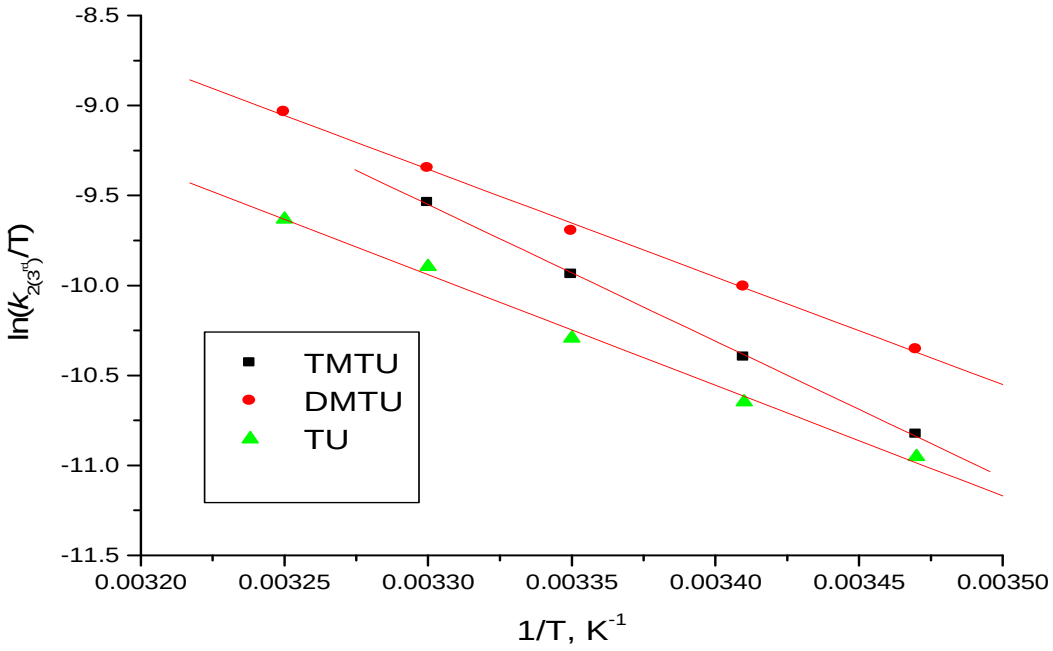

Figure S5.27: Plots of ln(k_2/T) versus (1/T) for the third step reaction of **qzn** with a series of different nucleophiles at varying temperatures.

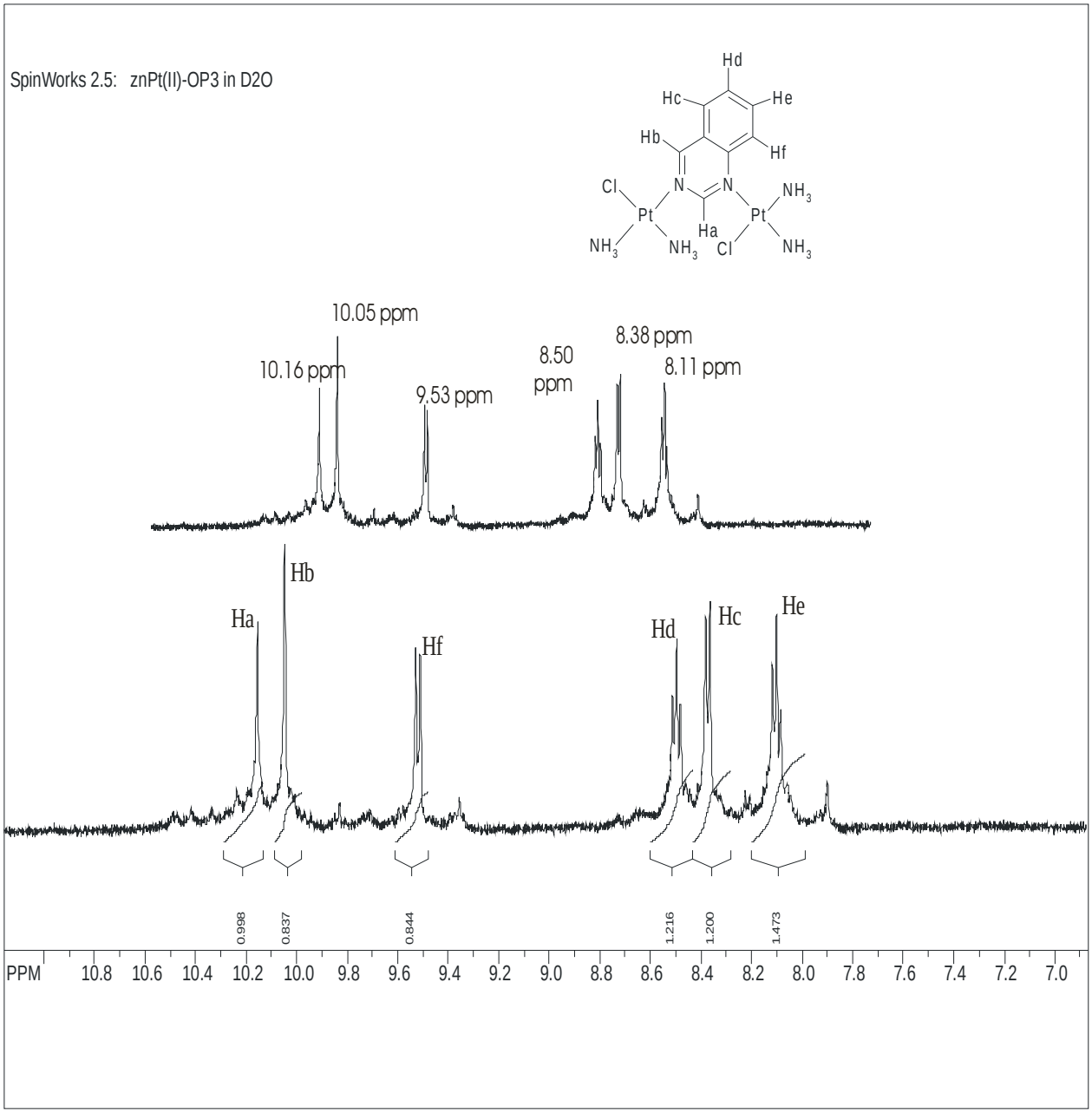

Figure S5.28: ^{1}H NMR (500MHz) spectrum of solution of [*cis*-{$PtCl(NH_3)_2$}$_2$-μ-qzn]$(ClO_4)_2$ in D_2O at 30 °C showing quinazoline ring proton assignment.

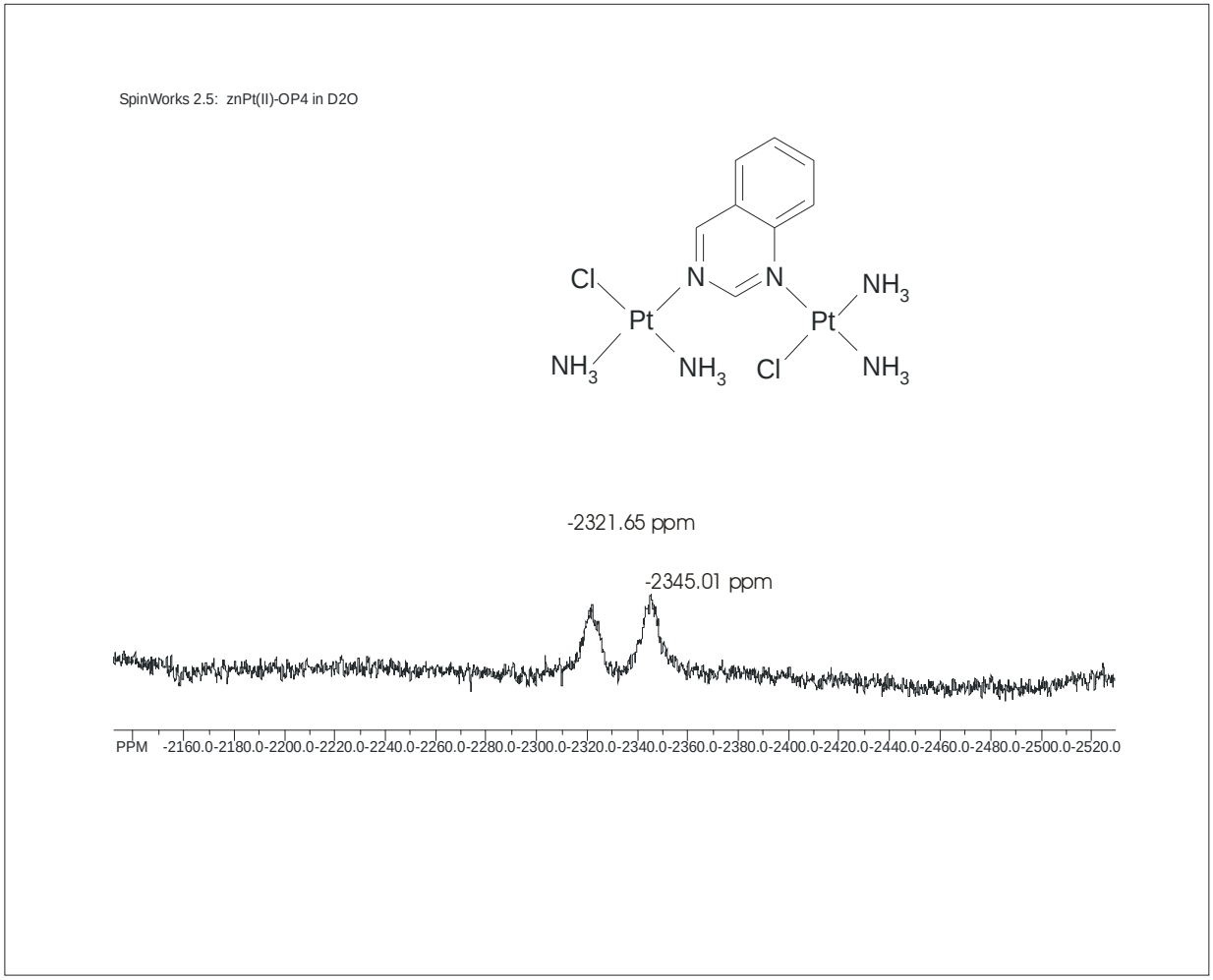

Figure S5.29: ^{195}Pt NMR (107 MHz) spectrum of [*cis*-{PtCl(NH_3)$_2$}$_2$-μ-qzn](ClO_4)$_2$ in D_2O at 30 °C.

Elemental Composition Report **Page 1**

Single Mass Analysis
Tolerance = 5.0 PPM / DBE: min = -1.5, max = 50.0
Element prediction: Off
Number of isotope peaks used for i-FIT = 3

Monoisotopic Mass, Even Electron Ions
1222613 formula(e) evaluated with 19 results within limits (up to 50 best isotopic matches for each mass)
Elements Used:
12C: 0-500 1H: 0-1000 14N: 0-10 35Cl: 0-8 195Pt: 0-3

Peter Ongoma
PO_qzn 16 (0.544) Cm (2:28)

TOF MS ES+
1.01e+004

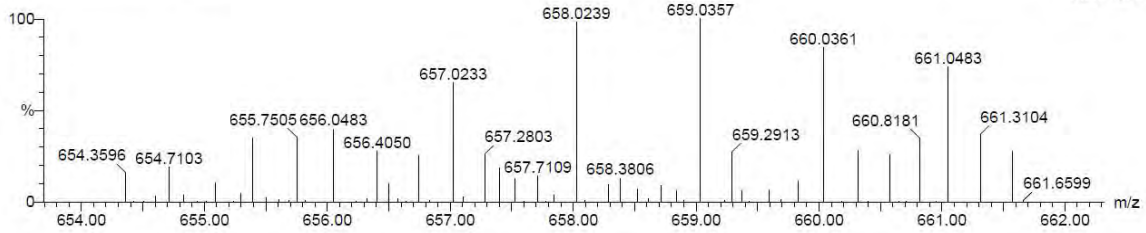

Minimum:				-1.5		
Maximum:		5.0	5.0	50.0		
Mass	Calc. Mass	mDa	PPM	DBE	i-FIT	Formula
659.0357	659.0357	0.0	0.0	4.5	0.0	12C16 1H27 14N5 35Cl5 195Pt
	659.0352	0.5	0.8	10.5	0.0	12C25 1H30 14N6 35Cl7
	659.0362	-0.5	-0.8	-1.5	0.0	12C7 1H24 14N4 35Cl3 195Pt2
	659.0351	0.6	0.9	27.5	0.0	12C29 1H11 14N5 35Cl 195Pt
	659.0364	-0.7	-1.1	28.5	0.0	12C37 1H19 14N4 35Cl4
	659.0369	-1.2	-1.8	22.5	0.1	12C28 1H16 14N3 35Cl2 195Pt
	659.0346	1.1	1.7	33.5	0.1	12C38 1H14 14N6 35Cl3
	659.0344	1.3	2.0	3.5	0.1	12C8 1H19 14N6 35Cl2 195Pt2
	659.0370	-1.3	-2.0	5.5	0.1	12C24 1H35 14N4 35Cl8
	659.0374	-1.7	-2.6	16.5	0.2	12C19 1H13 14N2 195Pt2
	659.0375	-1.8	-2.7	-0.5	0.2	12C15 1H32 14N3 35Cl6 195Pt
	659.0339	1.8	2.7	9.5	0.2	12C17 1H22 14N7 35Cl4 195Pt
	659.0376	-1.9	-2.9	46.5	0.2	12C49 1H8 14N2 35Cl
	659.0333	2.4	3.6	15.5	0.4	12C26 1H25 14N8 35Cl6
	659.0333	2.4	3.6	32.5	0.4	12C30 1H6 14N7 195Pt
	659.0382	-2.5	-3.8	23.5	0.4	12C36 1H24 14N2 35Cl5
	659.0327	3.0	4.6	38.5	0.6	12C39 1H9 14N8 35Cl2
	659.0387	-3.0	-4.6	17.5	0.6	12C27 1H21 14N 35Cl3 195Pt
	659.0326	3.1	4.7	8.5	0.6	12C9 1H14 14N8 35Cl 195Pt2

Figure S5.30: Mass spectrum for [*cis*-{PtCl(NH_3)$_2$}$_2$-μ-qzn]$^{2+}$ complex.

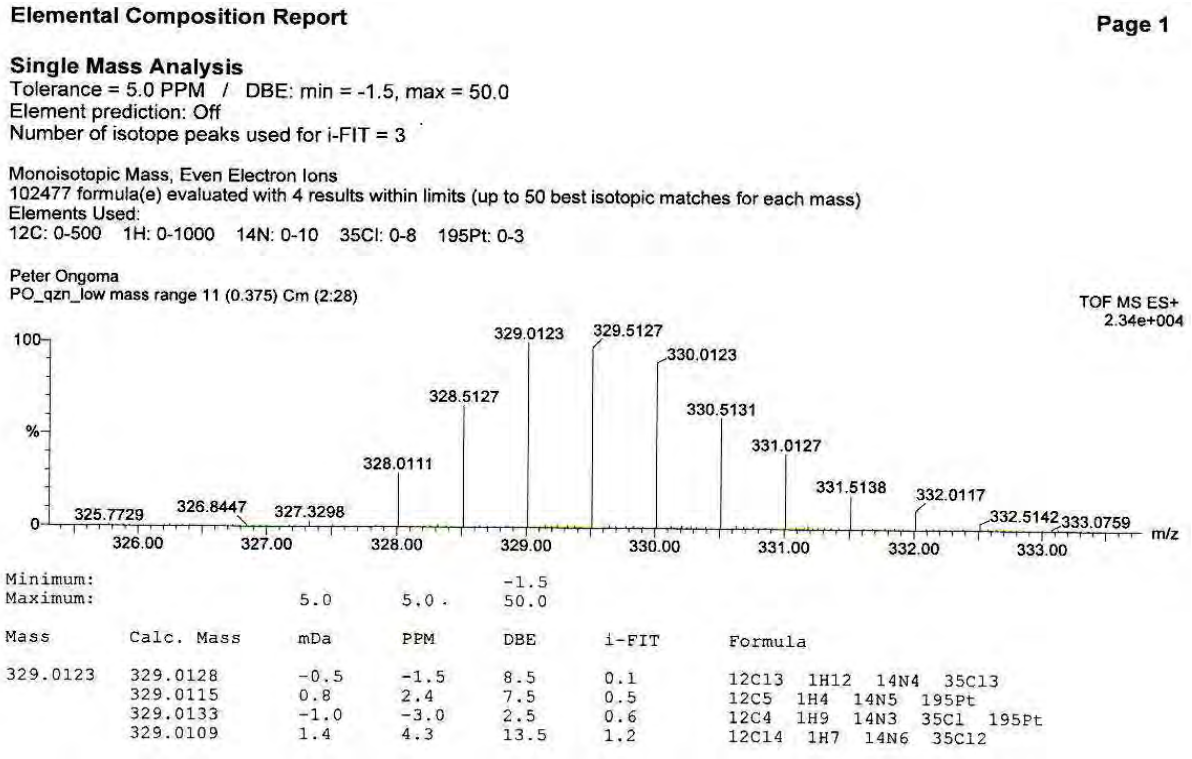

Figure S5.31: Mass spectrum for complex **qzn-Cl (**m /e, M^{2+}).

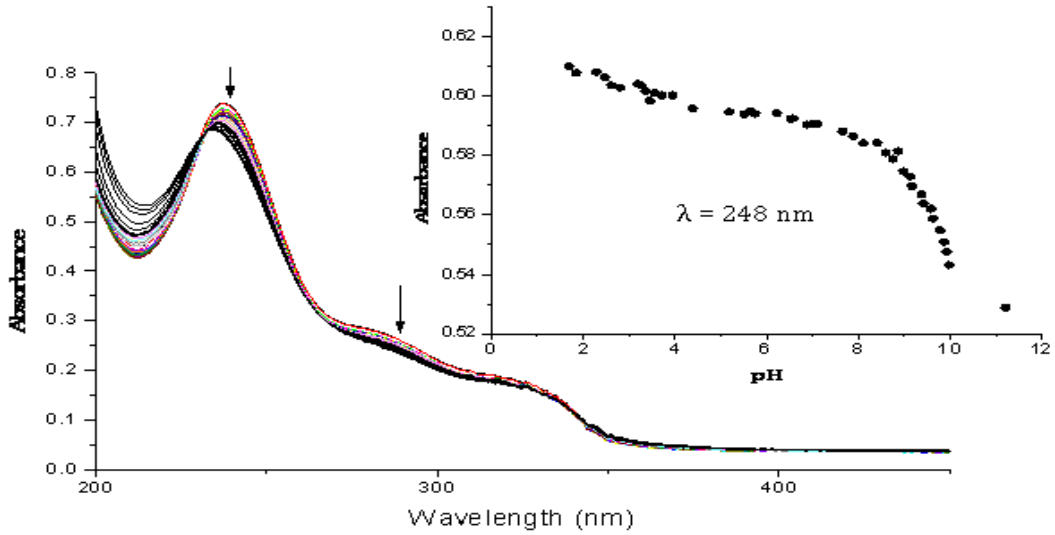

Figure S5.32: UV/Visible spectra for the titration of 0.1 mM **pht** with NaOH in the pH range 2-10, T = 25° C. Inset is the titration curve at 248 nm.

Table S5.26: Average observed rate constants, $k_{obs(1^{st})}$, at 298.15 K, for the displacement of the first aqua ligand of **pht** with a series of nucleophiles at different concentrations.

[NU]/ M	$k_{obs(1^{st})}$, **s^{-1}**		
	TU	**DMTU**	**TMTU**
0.00138	1. 3024 x 10^{-3}	3.480 x 10^{-4}	1.480 x 10^{-4}
0.00276	2.4908 x 10^{-3}	6.850 x 10^{-4}	2.955 x 10^{-4}
0.00414	3.8949 x 10^{-3}	1.030 x 10^{-3}	4.440 x 10^{-4}
0.00552	5.1913 x 10^{-3}	1.390 x 10^{-3}	6.080 x 10^{-4}
0.0069	6.5099 x 10^{-3}	—	7.892 x 10^{-4}

Table S5.27: Average observed rate constants, $k_{obs(2^{nd})}$, at 298.15 K, for the displacement of the second aqua ligand of **pht** with a series of nucleophiles at different concentrations.

[NU]/ M	$k_{obs(2^{nd})}$, **s^{-1}**		
	TU	**DMTU**	**TMTU**
0.00138	7.454 x 10^{-5}	6.299 x 10^{-5}	2.574 x 10^{-6}
0.00276	1.496 x 10^{-4}	1.249 x 10^{-4}	5.618 x 10^{-6}
0.00414	2.235 x 10^{-4}	1.870 x 10^{-4}	7.987 x 10^{-6}
0.00552	3.003 x 10^{-4}	2.524 x10^{-4}	1.109 x 10^{-5}
0.0069	3.732 x 10^{-4}	3.123 x 10^{-4}	1.424 x 10^{-5}

Table S5.28: Average observed rate constants, $k_{obs(3^{rd})}$, at 298.15 K, for the displacement of the second aqua ligand of **pht** with a series of nucleophiles at different concentrations.

[NU]/ M	$k_{obs(3^{rd})}$, s^{-1}		
	DMTU	**TMTU**	**TU**
0.00138	1.4045×10^{-5}	9.885×10^{-7}	2.520×10^{-5}
0.00276	2.8165×10^{-5}	2.059×10^{-6}	4.869×10^{-5}
0.00414	4.2236×10^{-5}	3.769×10^{-6}	6.998×10^{-5}
0.00552	5.6060×10^{-5}	6.047×10^{-6}	9.727×10^{-5}
0.0069	7.0226×10^{-5}	7.482×10^{-6}	1.198×10^{-4}

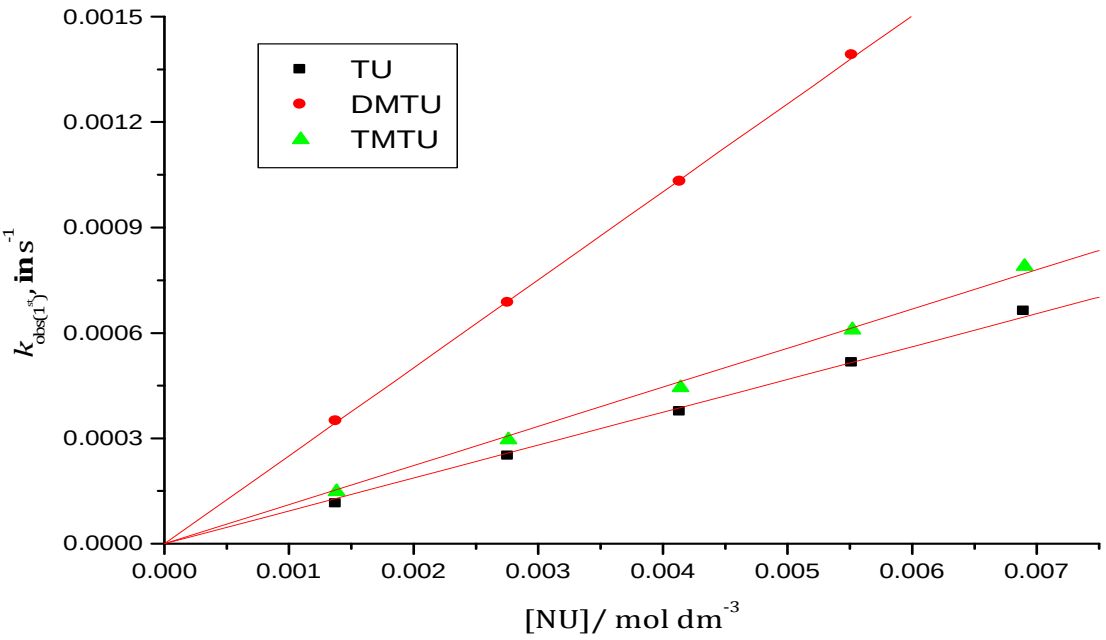

Figure S5.33: Concentration dependence of $k_{obs(1^{st})}$ for the displacement of first aqua ligand in **pht** by thiourea nucleophiles, pH = 2.0, T = 298.15 K, I = 0.10 M (0.01 M $HClO_4$, adjusted with $NaClO_4$).

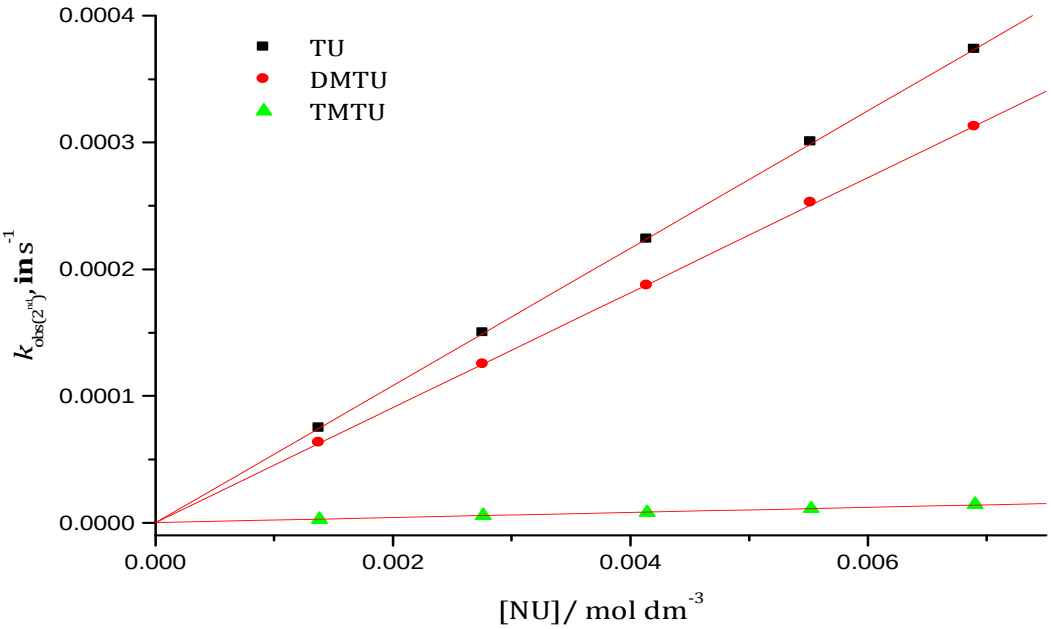

Figure S5.34: Concentration dependence of $k_{obs(2^{nd})}$ for the displacement of first aqua ligand in **pht** by thiourea nucleophiles, pH = 2.0, T = 298.15 K, I = 0.10 M (0.01 M $HClO_4$, adjusted with $NaClO_4$).

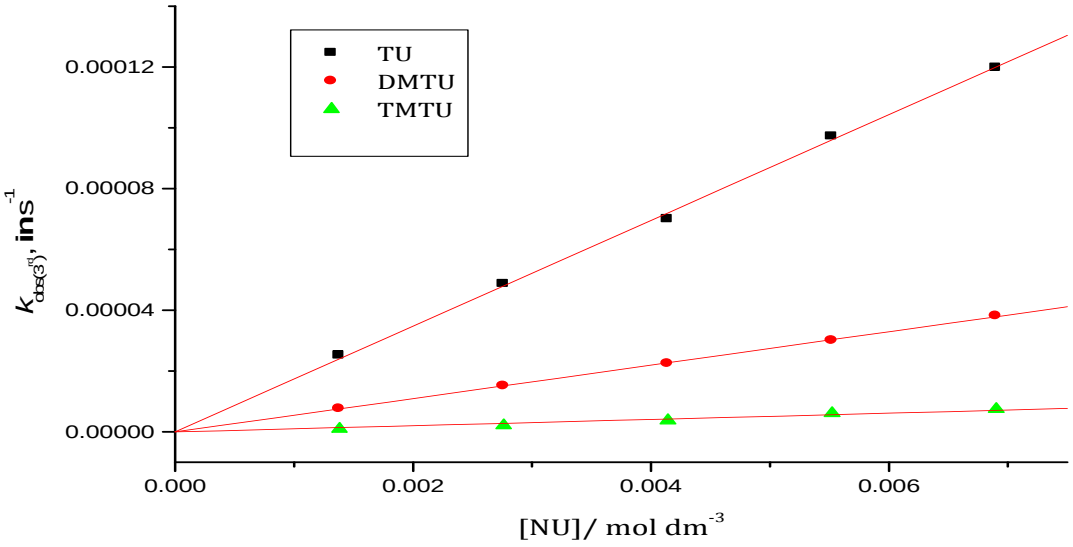

Figure S5.35: Concentration dependence of $k_{obs(3^{rd})}$ for the displacement of first aqua ligand in **pht** by thiourea nucleophiles, pH = 2.0, T = 298.15 K, I = 0.10 M (0.01 M $HClO_4$, adjusted with $NaClO_4$).

Table S5.29: Average observed rate constants, $k_{obs(1^{st})}$, for the first step reactions of **pht** at varied temperatures in the range 15 to 35 °C while maintaining nucleophile concentration at ≈ 60x [**Pht**].

1/T, K^{-1}	**TU**		**DMTU**		**TMTU**	
	$k_{obs(1^{st})}$, s^{-1}	**ln(k_2/T)**	**$k_{obs(1^{st})}$, s^{-1}**	**ln(k_2/T)**	**$k_{obs(1^{st})}$, s^{-1}**	**ln(k_2/T)**
0.00347	1.203 x 10^{-4}	-9.2412	1.754 x 10^{-4}	-8.8246	6.346 x 10^{-3}	-5.2358
0.00341	1.640 x 10^{-4}	-8.9086	3.021 x 10^{-4}	-8.2979	8.933 x 10^{-3}	-4.9111
0.00335	2.282 x 10^{-4}	-8.5953	4.790 x 10^{-4}	-7.8539	0.01263	-4.5814
0.00330	3.104 x 10^{-4}	-8.3044	7.494 x 10^{-4}	-7.4229	0.011679	-4.3138
0.00325	4.425 x 10^{-4}	-7.9661	1.114 x 10^{-3}	-7.0429	0.021998	-4.0598

Table S5.30: Average observed rate constants, $k_{obs(2^{nd})}$, for the second step reactions of **pht** at varied temperatures in the range 15 to 35 °C while maintaining nucleophile concentration at ≈ 60x [**Pht**].

1/T, K^{-1}	**TU**		**DMTU**		**TMTU**	
	$k_{obs(2^{nd})}$, s^{-1}	**ln(k_2/T)**	**$k_{obs(2^{nd})}$, s^{-1}**	**ln(k_2/T)**	**$k_{obs(2^{nd})}$, s^{-1}**	**ln(k_2/T)**
0.00347	1.04 x 10^{-5}	-11.6491	1.35 x 10^{-5}	-11.3876	1.31 x 10^{-4}	-9.1159
0.00341	1.65 x 10^{-5}	-11.2044	2.00 x 10^{-5}	-11.0145	1.92 x 10^{-4}	-8.7489
0.00335	2.56 x 10^{-5}	-10.7831	3.05 x 10^{-5}	-10.6083	2.73 x 10^{-4}	-8.4149
0.00330	3.71 x 10^{-5}	-10.4288	3.94 x 10^{-5}	-10.2687	3.75 x 10^{-4}	-8.1149
0.00325	5.44 x 10^{-5}	-10.0626	5.49 x 10^{-5}	-9.9535	5.14 x 10^{-4}	-7.8159

Table S5.31: Average observed rate constants, $k_{obs(3^{nd})}$, for the third step reactions of **pht** at varied temperatures in the range 15 to 35 °C while maintaining nucleophile concentration at ≈ 60x [**Pht**].

1/T, K^{-1}	**TU**		**DMTU**		**TMTU**	
	$k_{obs(3^{rd})}$, s^{-1}	**ln(k_2/T)**	**$k_{obs(3^{rd})}$, s^{-1}**	**ln(k_2/T)**	**$k_{obs(3^{rd})}$, s^{-1}**	**ln(k_2/T)**
0.00347	1.249 x 10^{-5}	-11.5666	2.116 x 10^{-5}	-13.6129	9.840 x 10^{-6}	-14.3786
0.00341	1.881 x 10^{-5}	-11.0902	3.031 x 10^{-5}	-13.2710	1.651 x 10^{-5}	-13.8781
0.00335	4.214 x 10^{-4}	-10.6760	4.682 x 10^{-5}	-12.8528	2.560 x 10^{-5}	-13.457
0.00330	6.214 x 10^{-4}	-10.2838	6.736 x 10^{-5}	-12.5057	3.356 x 10^{-5}	-13.2025
0.00325	6.600 x 10^{-4}	-9.8689	9.365 x 10^{-5}	-12.1927	5.438 x 10^{-5}	-12.7363

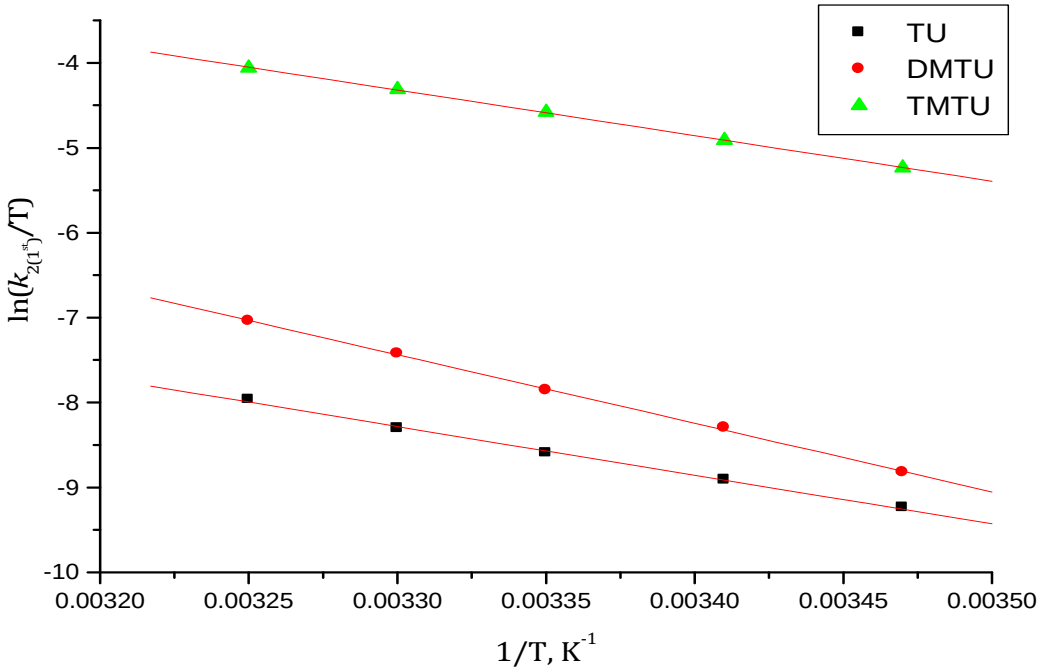

Figure S5.36: Plots of ln(k_2/T) versus (1/T) for the first step reaction of **pht** with a series of different nucleophiles at varying temperatures.

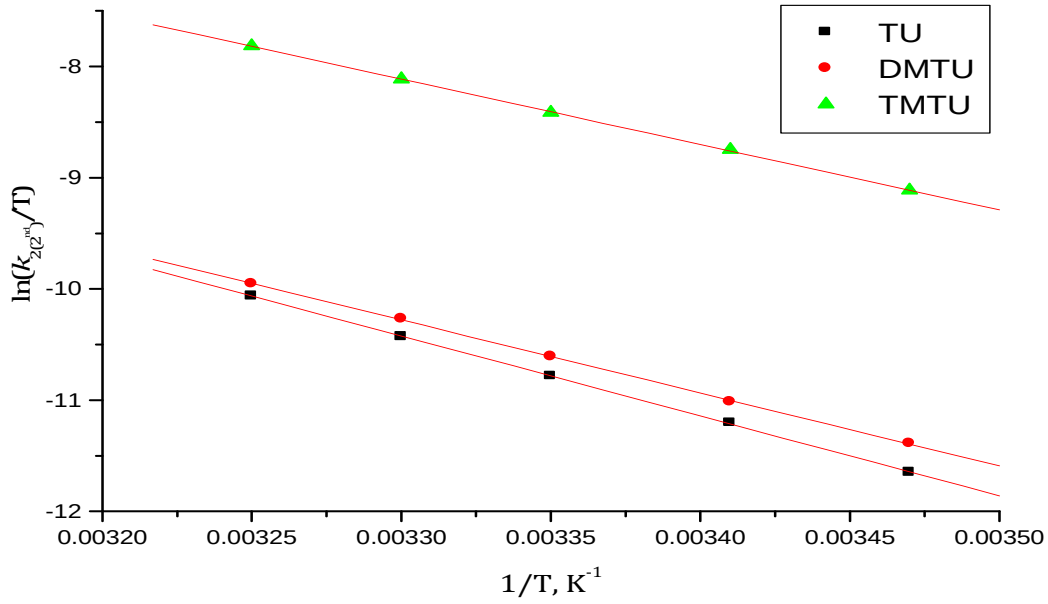

Figure S5.37: Plots of ln(k_2/T) versus (1/T) for the second step reaction of **pht** with a series of different nucleophiles at varying temperatures.

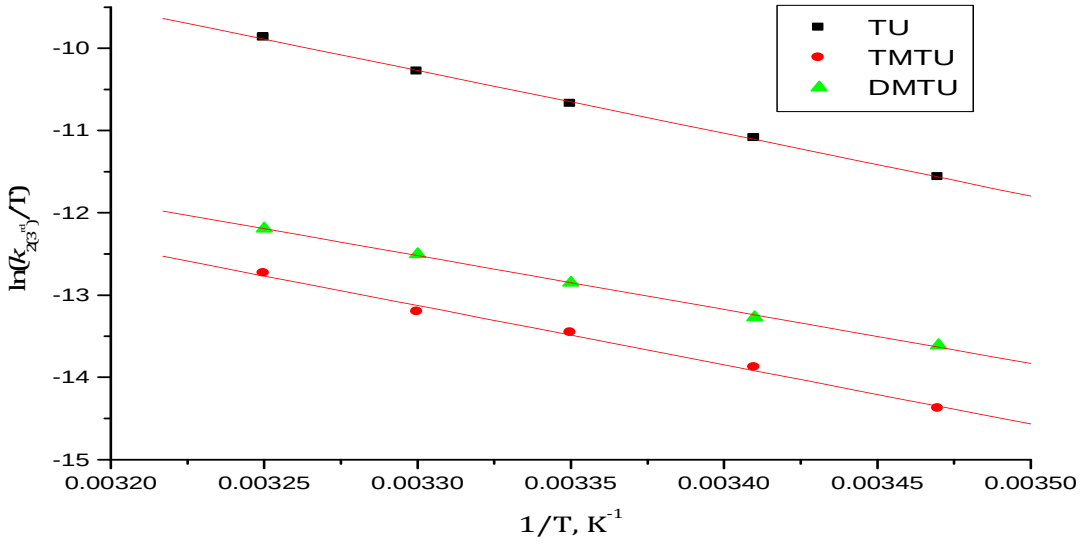

Figure S5.38: Plots of ln(k_2/ T) versus (1/T) for the third step reaction of **pht** with a series of different nucleophiles at varying temperatures.

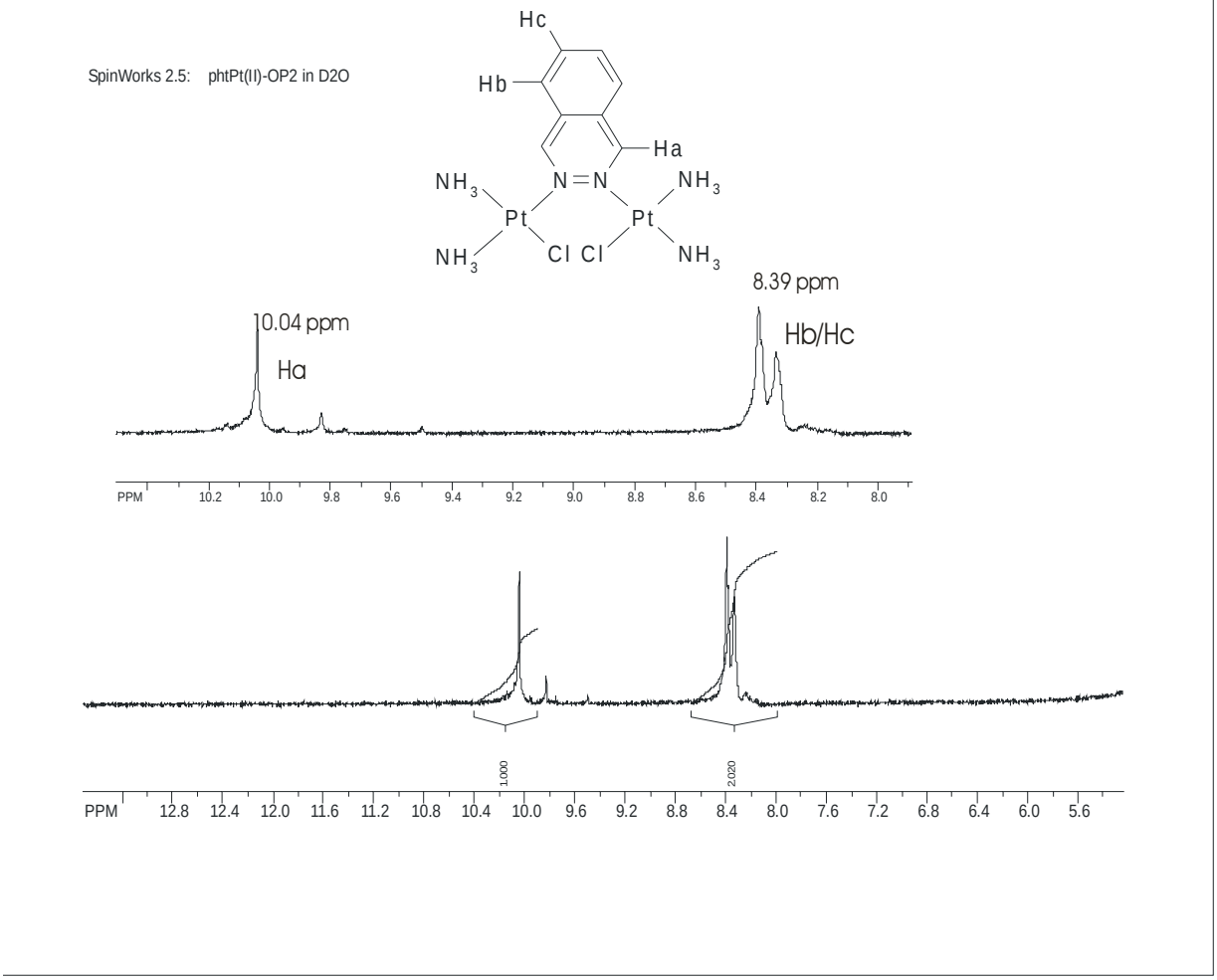

Figure S5.39: ^{1}H NMR (500MHz) spectrum of solution of [*cis*-{$PtCl(NH_3)_2$}$_2$-μ-pht]$(ClO_4)_2$ in D_2O at 30 °C showing phthalazine ring proton assignment.

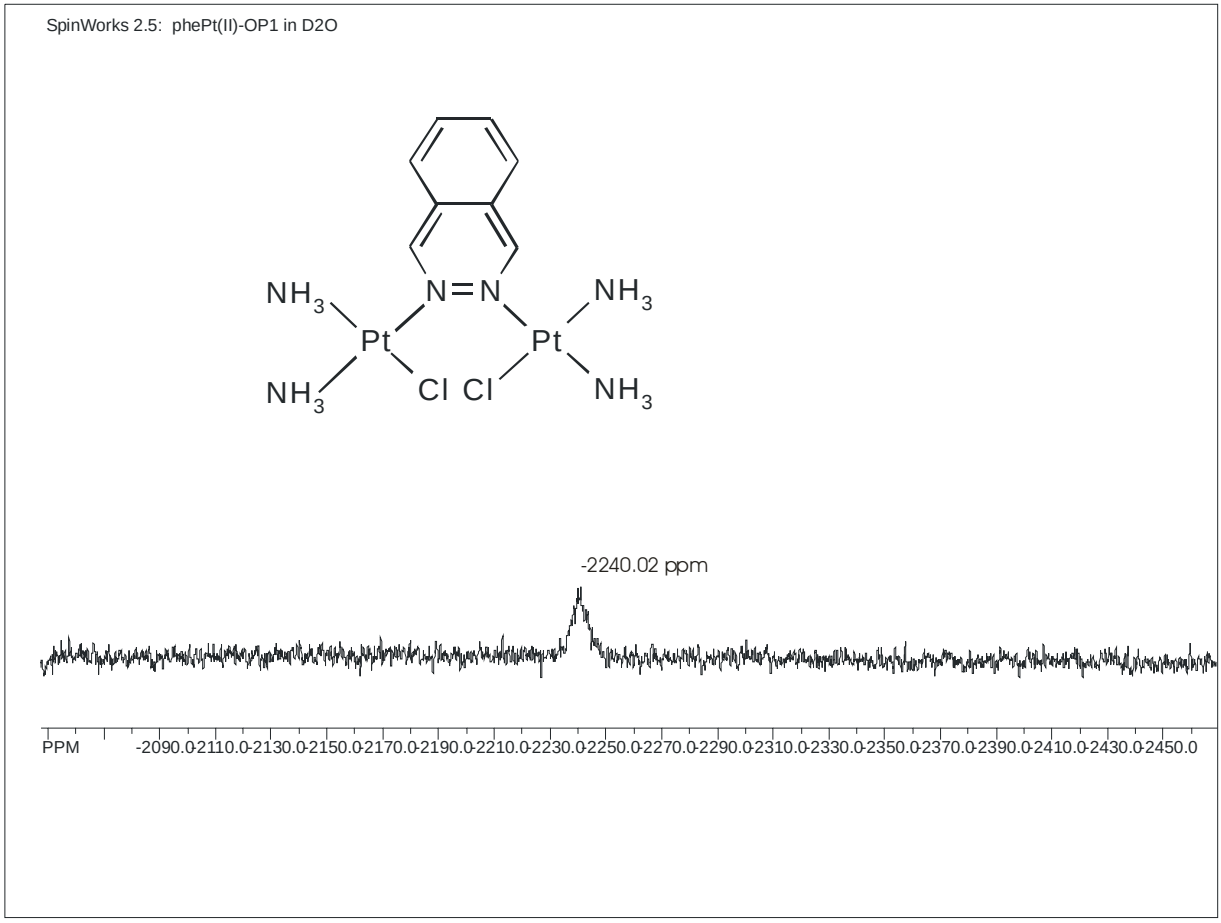

Figure S5.40: ^{195}Pt NMR (107 MHz) spectrum of [*cis*-{PtCl(NH_3)$_2$}$_2$-μ-pht](ClO_4)$_2$ in D_2O at 30 °C.

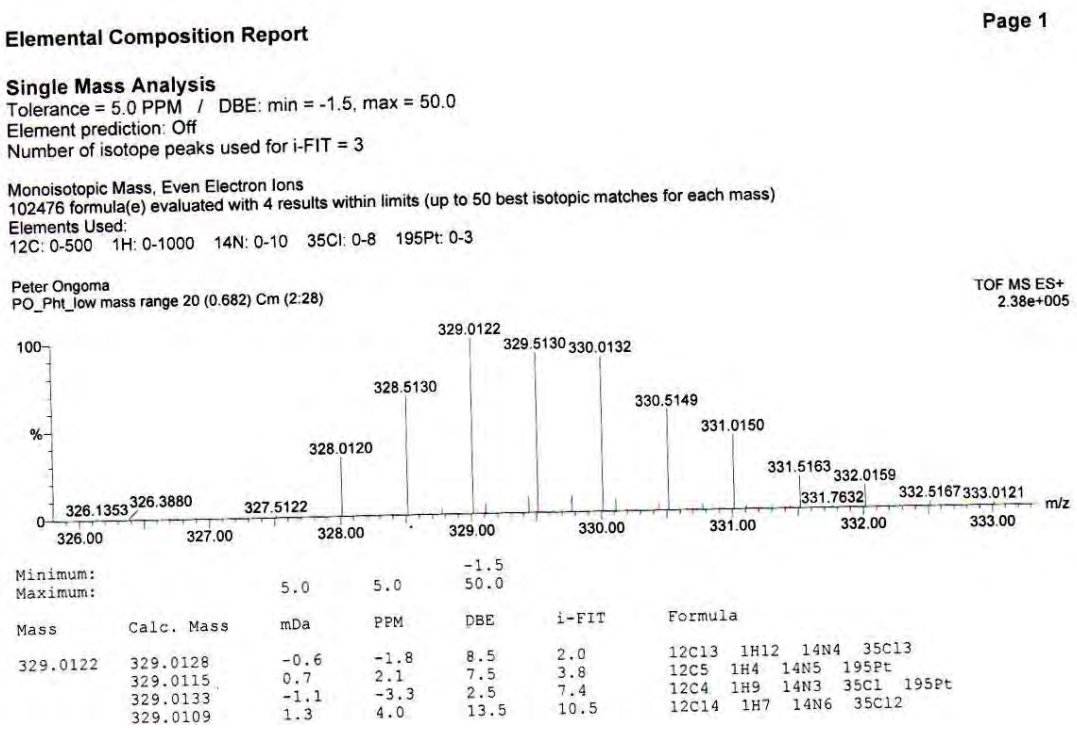

Figure S5.41: Mass spectrum for complex **pht-Cl (**m/e, M^{2+})

Table of Contents-6

List of Figures

List of Tables

Chapter 6

Tuning Reactivity of Platinum(II) Complexes with Parametalated Pyridine Spacer Groups: *A kinetic and Mechanistic Study*

6.0 Abstract

The substitution reactions of dinuclear Pt(II) complexes containing two platinum centres connected by a pyridine bridging ligand of variable length, *viz*. **[{*cis*–Pt(OH$_2$)(NH$_3$)$_2$}$_2$–μ–L]$^{+4}$**, L = 4,4'-bis(pyridine)sulphide (**Pt1**), 4,4'-bis(pyridine)disulphide (**Pt2**) and 1,2-bis(4-pyridyl)ethane (**Pt3**), were investigated with S-donor nucleophiles (TU, DMTU and TMTU) and anionic nucleophiles (SCN^-, I^- and Br^-) under *pseudo* first-order conditions as a function of nucleophile concentration and temperature, using stopped-flow and UV-Vis spectrophotometric methods. In addition, spectrophotometric acid-base titrations were performed to determine the pK_a values of the platinum bound aqua ligands. The pK_a values of the aqua ligands, namely; **Pt1** (pK_{a1}: 4.86; pK_{a2}: 5.53), **Pt2** (pK_{a1}: 5.19; pK_{a2}: 6.42), **Pt3** (pK_{a1}: 5.04; pK_{a2}: 5.45) show a direct correlation between the Pt---Pt distance and acidity of the coordinated water molecules.

The substitution reactions of the dinuclear Pt(II) complexes with a series of nucleophiles occurred in two sequential steps. The second-order rate constants for the simultaneous displacement of aqua ligands in the first step, decreased in the order **Pt2** > **Pt3** > **Pt1.** The DFT calculations for the corresponding **Pt1** complex clearly demonstrated that the structure of the complex is distorted due to non–planarity of the ligand, where repulsions from the two lone pairs on S atom and the pyridine rings prevents **Pt1** to exhibit a perfect C_{2v} symmetry. This distortion is the reason for the lower reactivity of **Pt1** as the aerial attack of a nucleophile on the Pt(II) centre is sterically hindered. The complexes **Pt2** and **Pt3**, both adopt C_{2h} molecular point group symmetry. The lability of **Pt3** is 2 times slower than that of **Pt2**. This could be explained by the higher value of the dipole moment of **Pt2**, which exhibits greater electrophilicity at the metal centre and can account for acceleration of nucleophilic substitution process as compared to **Pt3**. These reactions show that a small change on the structure of the bridging ligand influences the

structure as well as the nucleophilic substitution process of the diaqua Pt(II) complexes. The dissociation of the bridging ligand in the second step was confirmed by the ^{1}H NMR of **Pt1–Cl** with thiourea in DMF-d_7. The temperature dependence of the second–order rate constants for both the processes results in large negative values of activation entropies ($\Delta S^{\#}$) supporting an associative mode of substitution mechanism.

6.1 Introduction

Metal complexes are the main resources for the generation of chemical diversity, which includes novel Pt(II) anti-cancer therapeutic agents.[1] A number of Pt(II) anticancer agents, enjoying widespread use in the clinic owe their anticancer activity to their ability to bind covalently or through intercalation of the aromatic ligands to cellular DNA. This alters the tertiary structure of DNA, resulting in the death of the cancer cell through apoptosis.[2–6] Although, *cis*-diamminedichloridoplatinum(II) (*cis*platin) is one of the most active and clinically effective agents used in 50-70% of all cancer patients, especially against testicular, ovarian, and head and neck carcinomas;[7–9] the impetus to find new drugs stems from difficulties related to its use, because of drug resistance and severe side effects.[10] However, systematic kinetic and mechanistic study of these complexes with relevant biological nucleophiles has not been fully explored to provide detailed insight into the kinetics and thermodynamic properties that control the lability (reactivity) of these complexes.

Over the last few years, many kinetic studies have aimed at tuning reactivity of the dinuclear Pt(II) complexes by altering their structures using a variety of different ligands,[11, 12] e.g. flexible α,ω-alkanediamines[13] or rigid azoles[14] and diazines,[15,16] so as to modulate their reactivity towards nucleic acids and other biological nucleophiles in comparison with their mononuclear analogues. Two approaches have commonly been used to tailor the substitution process at the metal centres, without changing the parent structure of the complex: control of their electronic properties by introducing a σ-donor and/or π-acceptor group or extending the π-conjugation,[17–19] and by introducing steric hindrance around the Pt(II) centre. Steric hindrance is observed for heterocycles containing one or two *ortho* groups and these effects may be additive.[20]

Against this background, several reports have indicated that bulky planar ligands such as pyridine and substituted pyridines attached next to the metal centre in Pt(II) complexes, *e.g.* *cis*-[PtCl(NH_3)$_2$(2-methylpyridine)]$^+$ and *cis*-[Pt(NH_3)$_2$Cl(4-methylpyridine]$^+$,[21] could reduce the rate of reaction between the metal complexes and bio-molecules containing –SH groups due to steric hindrance around the Pt(II) ion,[6,22]. In recent reports, Jaganyi and his group[23] have studied the importance of introducing electron-donating methyl groups at 2,3-, 2,6- and 2,5-positions of the pyrazine bridging moiety (and in Chapter 4 of this study) and noted that increased steric hindrance and σ-inductive effect decreased the positive charge on the metal centre, slowing down reactivity of the Pt(II) complexes. In addition, recent studies[24–26] have established that there is a strong interaction between the two Pt(II) centres of dinuclear complexes, which proportionately weakens as the chain-length and flexibility of the linker is increased. The other factors which influence reactivity of multinuclear Pt(II) complexes include hydrogen-bonding capacity, charge at the metal centre and the linker, and the geometry of the leaving group relative to the linker.[27–29]

It was systematically demonstrated in this work (Chapters 4 & 5) that the *cis*-dinuclear Pt(II) complexes bridged by the diazine ligands are degraded by thiourea, resulting in the loss of the integrity of the dinuclear structure and eventually releases the linker, in contrast to what was reported by Farrell and co-workers.[30] This is because of the strong *trans* influence of the sulphur atom that weakens the am(m)ine nitrogen–platinum bond, making it susceptible to further substitution reactions.[31]

Pyridine has extensively been used as a ligand for the synthesis of new platinum coordination compounds because of its ability to connect metal centres by forming metal-to-ligand bonds. To try and shed some light with respect to the degradation of the bridging ligand that has been observed in a number of studies,[21,32–34] sp^3 hybridized sulphur spacer groups at the 4-position of the pyridine unit were investigated.

In this study we report the kinetic and thermodynamic data for the substitution of the aqua ligand of the dinuclear Pt(II) complexes of the type [{*cis*-Pt(NH_3)$_2$$H_2O$}$_2$L]$^{+4}$ (L = 4,4'-bis(pyridine)sulphides or 1,2-bis(4-pyridyl)ethane) (Scheme 6.1), by thioureas (TU, DMTU and TMTU) and ionic (Br^-, I^- and SCN^-) nucleophiles. The pK_a values have also

been determined for the two aqua ligands and together with the DFT calculations interpreted in terms of the ability to stabilize the transition state of the reaction.

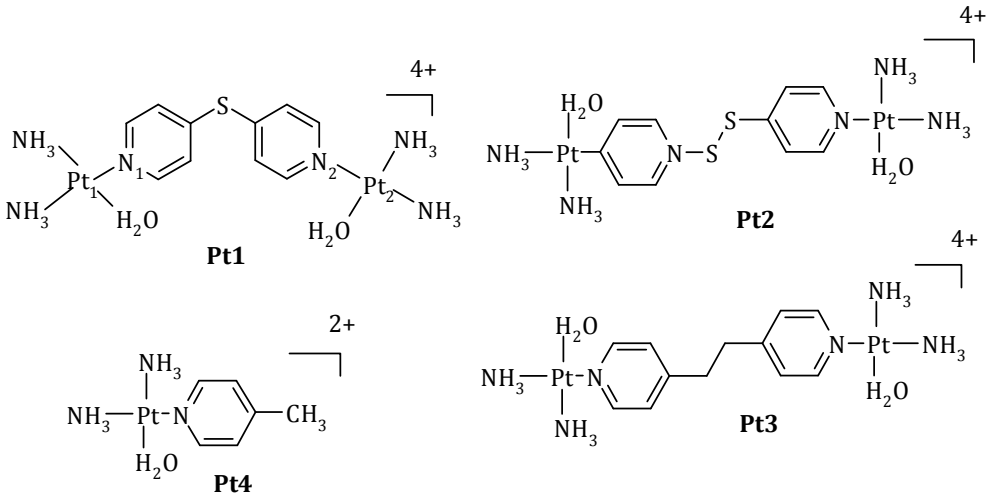

Scheme 6.1: Structures of the investigated dinuclear Pt(II) complexes. Included for comparison of pK_a and computation data purposes is the mononuclear complex **Pt4**. The numbering system adopted for the Pt centres is indicated on the structure of **Pt1**

6.2 Experimental

6.2.1 Materials

*Cis*platin *(cis*-($PtCl_2(NH_3)_2$, 99%) was purchased from Strem Chemicals. Methanol (Saarchem) was distilled over magnesium before use.[35] The nucleophiles thiourea (TU, 99%), 1,3-dimethyl-2-thiourea (DMTU, 99%), 1,1,3,3-tetramethyl-2-thiourea (TMTU, 98%), sodium bromide (NaBr, 99%), sodium iodide (NaI, 99%), sodium thiocyanide (NaSCN, 99%) and the ligands: 4-mercaptopyridine (95%), 4,4'-dipyridyldisulphide (dpss, 98%), 1,2-bis(4-pyridyl)ethane (bpe, 99%), dipyridinium hydrochloride (98%), 4-bromopyridine hydrochloride (99%), sodium perchlorate monohydrate ($NaClO_4.H_2O$, 98%) and perchloric acid ($HClO_4$, 70%) were obtained from Aldrich and used without further purification. Silver perchlorate ($AgClO_4$, 99.9%) from Aldrich was stored under nitrogen and used as supplied. Ultrapure water (Modulab Systems) was used in all experiments.

6.2.2 Instruments

Microanalyses were carried out on a Carlo Erba CHNS Elemental Analyzer 1106. Infrared spectra (KBr pellet, range 4000-300 cm^{-1}) were recorded on a Perkin Elmer Spectrum One-FTIR spectrophotometer. NMR spectra were acquired from a Bruker Avance DPX 500 instrument (^{1}H, 500 MHz) and (^{195}Pt, 107.5 MHz), respectively, at ambient temperature of 30°C. Values of ^{1}H are given in δ (ppm) relative to tetramethylsilane (δ = 0.00) and ^{195}Pt the chemical shifts were externally referenced to $K_2[PtCl_4]$ in D_2O. Mass spectrometric analyses were collected on Hewlett Packard LC-MS using electron impact (EI) ionization. All pK_a titrations, kinetic and spectroscopic measurements for slower reactions were recorded on a Varian Cary 100 Bio spectrophotometer equipped with a thermostated cell holder. Kinetic measurements on fast substitution reactions were monitored using an Applied Photophysics SX 18 MV (v4.33) stopped-flow reaction analyzer coupled to an online data acquisition system. The temperature of instrument was controlled to within ± 0.1 °C. pK_a values, rate constants and standard deviations were calculated using Microcal-origin version Origin-7.5® [36] software package.

6.2.3 Preparation of 4,4'–dipyridylmonosulphide Ligand (dps)

The ligand 4,4'-dipyridylmonosulphide (dps) was prepared using a slightly modified method previously described in literature as presented in Scheme **S6.1** (**Appendix 6**).[37] A mixture of 4-mercaptopyridine (1.8 g, 16.2 mmol), 4-bromopridine (3.0 g, 15.4 mmol) and potassium carbonate (2.0 g) in dimethylformamide (15.0 mL) was kept under reflux at 120 °C, for 48 h. After the reaction was complete, the mixture was cooled and the crude product was treated with water and then extracted with dichloromethane (5 x 20 mL).The organic layer was dried over anhydrous sodium sulphate. The solvent was evaporated under reduced pressure and the residue purified by column chromatography on silica gel (eluent: hexane/ethylacetate 7:1) to afford a yellow solid of 4,4'-dipyridylmonosulphide. The purity of the isolated product was confirmed by: the IR, mass spectroscopy, ^{1}H and ^{13}C NMR spectra, and were in satisfactory agreement with values found in literature.[37,38]

Ligand 4,4'-dipyridylmonosulphide (dps)

Yield: 1805.4 mg (9.60 mmol, 64.0%). ^{1}H NMR (500.5 MHz, D_2O) δ /ppm: ^{1}H: 8.53 (d, 4H; H1, H5); 7.22 (d, 4H; H2, H4)). ^{13}C NMR (75.5 MHz, D_2O): δ/ppm: 149.12 (C1, C5), 145.44 (C3), 125.45 (C2, C4). IR (KBr, 4000-300 cm^{-1}): 3054 (m, N–H stretch); 1567, 1225 (C=N/C=C, pyridine ring stretch); 1107, 991 (C–H, aromatic stretch). TOF MS/ES^+. (m/z, MH^+): 189.05 ($C_{10}H_9N_2S$, species).

6.2.4 Synthesis of Pt(II) Complexes

The dinuclear platinum(II) complexes (Pt1 to Pt3): **[{*cis*–PtCl(NH$_3$)$_2$}$_2$–μ–dps](ClO$_4$)$_2$** (**Pt1**), **[{*cis*–PtCl(NH$_3$)$_2$}$_2$–μ–dpss](ClO$_4$)$_2$** (**Pt2**) and **[{*cis*–PtCl(NH$_3$)$_2$}$_2$–μ–bpe](ClO$_4$)$_2$** (**Pt3**), were prepared by a reported procedure,[38,39] starting from the precursor **[{*cis*–PtCl(NH$_3$)$_2$(DMF)]ClO$_4$**, using $AgClO_4$. Micro-analytical data of the complexes are as follows.

Metal Complex Pt1

Yield: 62.8 mg (0. 069 mmol, 57.8 %). ^{1}H NMR (500.5 MHz, D_2O) δ /ppm: ^{1}H: 8.78 (d, (4H); 7.60 (d, 4H). ^{195}Pt NMR (107.5 MHz, D_2O): δ/ ppm: -2303.88. IR (KBr, 4000-300 cm^{-1}): 3179 (m, N–H stretch); 1598, 1480 (C=N/C=C, pyridine ring stretch); 1090-1100 (perchlorate counter ion); 505 (Pt–N stretch); 302 (Pt–Cl stretch). TOF MS/ES^+. (m/z, M^{2+}): 358.005 ($C_{10}H_{18}N_6SPt_2Cl_2$ species). *Anal. Calcd for* $C_{10}H_{20}N_6SCl_4O_8Pt_2$: H, 2.20; C, 13.1; N, 9.17; S, 3.49. *Found*: H, 2.23; C, 13.45; N, 9.50; S, 3.35%.

Metal Complex Pt2

Yield: 91.6 mg (0. 097 mmol, 79.2%). ^{1}H NMR (500.5 MHz, D_2O), δ /ppm: 8.53 (d, 4H in dpss); 7.60 (d, 4H in dpss). ^{195}Pt NMR (107.5 MHz, D_2O) δ/ ppm: -2304.16. IR (KBr, 4000-300 cm^{-1}): 3179 (N–H stretch); 1598, 1480 (C=N/C=C, pyridine ring stretch), 1421 (s, dpss), 1213 (w, dpss), 818 (m, dpss), 731 (m, dpss); 1090-1100 (perchlorate counter ion); 507 (Pt–N stretch); 385 (Pt–Cl stretch). *Anal. Calcd for* $C_{10}H_{20}N_6Cl_4S_2O_8Pt_2$: H, 2.13; C, 12.65; N, 8.86; S, 6.76. *Found*: H, 2.19; C, 13.15; N, 8.82; S, 6.77%.

Metal Complex Pt3

Yield: 52.5 mg (0. 058 mmol, 65.0 %). ^{1}H NMR (500.5 MHz, D_2O) δ/ppm: 8.96 (d, 4H of py in bpe); 7.78 (d, 4H of py in bpe); 3.66 (s, 4H for $2CH_2$ of bpe). ^{195}Pt NMR (107.5 MHz, D_2O) δ/ ppm: -2284.66. IR (KBr, 400-300 cm^{-1}): 3285 (N–H stretch); 1621 (C=N/C=C, pyridine ring stretch), 1436 (m, bpe), 1340 (vw, bpe), 1212 (w, bpe); 1090-1100 (perchlorate counter ion); 556 (Pt–N stretch). TOF MS/ES^{+}. (m/z, M^{2+}): 356.535 ($C_{12}H_{22}N_6Pt_2Cl_2$, species). *Anal. Calcd for* $C_{12}H_{24}N_6Cl_4O_8Pt_2$: H, 2.65; C, 27.64; N, 9.21. *Found*: H, 2.59; C, 27.69; N, 9.71%.

6.2.5 Preparation of the Dinuclear Pt(II) Diaqua Complexes

The chloro complexes (**Pt1** to **Pt3**) were converted into aqua analogues using literature procedure.[40] The resultant aqua solutions were brought to a final complex concentration of 4.41 x 10^{-4}, 4.43 x 10^{-4} and 1.13 x 10^{-4} M for **[{*cis*–PtOH$_2$(NH$_3$)$_2$}$_2$–μ–dps](ClO$_4$)$_2$** (**Pt1**), **[{*cis*–Pt(OH$_2$)(NH$_3$)$_2$}$_2$–μ–dpds](ClO$_4$)$_2$** (**Pt2**), **[{*cis*–Pt(OH$_2$)(NH$_3$)$_2$}$_2$–μ–bpe](ClO$_4$)$_2$** (**Pt3**), respectively. The solution was acidified with $HClO_4$ to pH 1.0 (for determination of pK_a values) and pH 2.0 (for kinetic measurements). The ionic strength was adjusted to 0.10 M with $NaClO_4$.

6.2.6 Preparation of Kinetic Solutions

The kinetic measurements were studied in 0.10 M $NaClO_4$, at pH *ca*. 2.0, since the perchlorate ions do not coordinate to Pt(II) in aqueous solution, and in order to prevent deprotonation of the aqua ligand.[20(b)] Nucleophile solutions of different concentrations, *viz*. 20, 40, 60, 80 and 100-fold excess of appropriate metal complex concentration were prepared shortly before use by quantitative dilution of the corresponding stock solution using the 0.10 M ($NaClO_4$, adjusted with $HClO_4$ to pH 2.0).[41] This was to maintain the reaction under *pseudo* first-order conditions and drive the reaction to completion.

6.2.7 Spectrophotometric pK_a Titrations

The pH of the aqueous solutions was measured using a Jenway 4330 Conductivity/pH meter equipped with a Micro 4.5 diameter glass electrode after calibration with standard buffers pH 4.0, 7.0 and 10.0 at 25 °C. The pH electrode was filled with 3M NaCl electrolyte to prevent precipitation of $KClO_4$ during use. In order to avoid absorbance

corrections due to dilution, a large volume (200ml) of each of the complex solutions was used during the titrations. Spectrophotometric pH titrations were carried out using NaOH as the base. Subsequent pH changes were obtained by stepwise additions of crushed solid NaOH pellets in the pH range 2-3, micropipette dropwise addition of saturated, 1.0 and 0.1 M NaOH or conc. $HClO_4$ (for reversibility of the pH) to the bulk of the complex solution, prior to withdrawal of 2 ml aliquots of the solution. After each of the measurements, the aliquots were not returned to the sample solutions to avoid *in situ* contamination by chloride ions from the pH electrode.

6.2.8 Computational Details

The geometries of all the complexes in aqua-form with total charges of +4 were optimized, in *vacuo*, using Density functional Theory (DFT) utilizing the B3LYP,[42] a three parameter hybrid functional method, and the LACVP** (Los Alamos Core Valence Potentials)[43] pseudo-potentials basis set as implemented in Spartan `04 for Windows® program. B3LYP relates to Becke's three parameter hybrid functional[42] that has been proven to be superior to traditional functionals. The mononuclear complex**,** *cis*-$[Pt(H_2O)(NH_3)_2(4\text{-methylpyridine})]^{+2}$, **Pt4**, is included for comparative purposes with respect to the pK_a and DFT results of **Pt3**

6.2.9 Kinetic Measurements

Spectral changes resulting from mixing separately each of the complexes **Pt1**, **Pt2**, and **Pt3** with ligand solutions were recorded over the wavelength range 200-600 nm to establish a suitable wavelength at which the kinetic measurement would be performed on a Varian Cary 100 Bio spectrophotometer. The kinetics of the lability of coordinated water was followed spectrophotometrically by monitoring the change in absorbance at suitable wavelengths. The wavelength values are given as supplementary information in Table **S6.1** (Appendix 6).

6.3 Results

6.3.1 Synthesis and Characterization of Compounds Pt1, Pt2 and Pt3

In this study, each of the three dinuclear Pt(II) complexes was prepared "*in situ"* from the cation *cis*-$[Pt(NH_3)_2(DMF)Cl]^+$. The DMF was selectively displaced by the ligands giving the desired dimer. The details of the spectroscopic data for the ligand dps and the complexes are listed in the experimental section (section 6.2.4). The characteristic IR bands at *ca.* 1570 cm^{-1} for the highest–energy pyridine ring vibration of the ligands are shifted by *ca.* 25-29 to higher frequencies upon complexation, suggesting that the nitrogen atoms of pyridine are coordinated to platinum metal.[44] The presence of bands in the IR spectra of the perchlorate complexes at 1090-1100 cm^{-1} (O–Cl vibration stretch) indicates that ionic perchlorate is present.[41(b)] In the ^1H NMR spectra of the three complexes, there are only two signals in the aromatic region, indicating that the structures of these complexes are symmetric due to coordination of the pyridyl rings at the Pt(II) centres. The ^{195}Pt signals for the three complexes appear within the range of -2284 and -2305 ppm which is typical of (PtN_3) coordination environment.[44]

6.3.2 Acidity of the Coordinated Aqua Ligands

In order to investigate the impact of the different diamine spacer groups on the reactivity of the diaqua Pt(II) complexes, the pK_a values of the coordinated water ligands were initially determined. A typical example of the UV-Vis spectral changes observed during the pH titration with NaOH is shown in Figure 6.1 for **Pt3** complex.

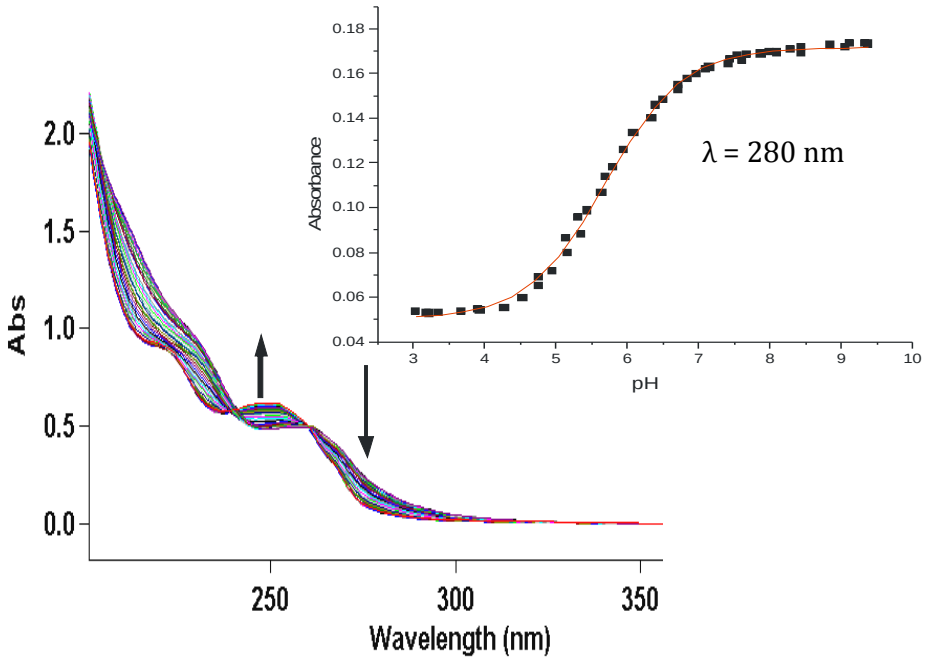

Figure 6.1: UV-Vis spectrophotometric titration curve of **Pt3** with NaOH in the pH range 2-9, I = 1.0 M ($NaClO_4$), T = 25 °C. Inset: plot of Absorbance vs pH at 280 nm.

When the UV-Vis data was fitted using a non-linear least squares procedure, as represented by the inset in Figure 6.1, and Figures S6.17 and S6.21 for the corresponding data for the **Pt1** and **Pt2** complexes (Appendix 6), the pK_a values for the deprotonation of the coordinated aqua molecules were obtained from the standard Boltzmann equation. The data gave an excellent fit for a system with two dissociation steps with equilibrium constants K_{a1} and K_{a2}, for which the overall process can be presented by the reaction given in Scheme 6.2.

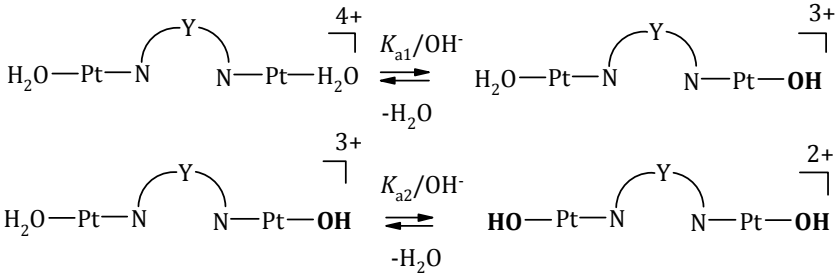

Scheme 6.2: Summary of the stepwise deprotonation of the dinuclear Pt(II) complexes as function of pH

The pK_a values obtained are summarized in Table 6.1. Included for comparison purpose in Table 6.1 is the pK_a value of the mononuclear analogue, *cis*-[Pt$(NH_3)_2H_2O$(4-methylpyridine)]$^{+2}$, **Pt4**.[21(a)]

Table 6.1: Summary of the pK_a values obtained for the deprotonation of platinum-bound water of the different complexes.

Complex	**Pt1**	**Pt2**	**Pt3**	***Pt4**
pK_{a1}	4.86 ± 0.05	5.19 ± 0.02	5.04 ± 0.15	5.63 ± 0.01
pK_{a2}	5.53 ± 0.03	6.42 ± 0.04	5.45 ± 0.17	N/A

* The pK_a value was extracted from reference 21(a).

6.3.4 Computation Calculations

Representative geometry-optimized structures for the complexes are shown in Figure 6.2 while key geometrical data including HOMO-LUMO energy gap are summarized in Table 6.2.

Figure 6.2 shows the minimum energy structures of the studied diaqua complexes calculated at DFT (B3LYP/LACVP**) level of theory. The geometry about the Pt atoms is slightly distorted square-planar as the bond angles show in Table 6.2. It is also noted that the angle labelled *c* is smaller than all the other angles around the Pt(II) centre an indication of a possible hydrogen bonding interaction (average separation distance = 2.484 Å) between the H_2O/NH_3 moieties.

The DFT calculated data from Table 6.2 shows that the NBO charges on the platinum atoms, to a large extent, remain almost constant across the series of the investigated complexes. This is not unexpected. X-rays structures of other Pt(II) complexes with such aromatic bridging ligands (*e.g*. 4,4'-bis(pyridine)ethane, 4,4'-bis(pyridine)sulphide, 4,4'-bis(pyridine)disulphide) indicate that the aromatic ring lies almost perpendicular to the plane of the Pt(II) centre.[23,45] Therefore, the interaction between the metal centre and the π-electrons of the pyridine ring is expected to be extremely small, if it exists.

The DFT calculations also reveal that the major influence of the *para*-substituent (Y), *i.e. pyridyl 4-position*, is on the HOMO energy level-"ground-state effect" and not the LUMO (Figure 6.2). The electron density of the HOMO orbitals are localized between the pyridyl π-acceptor bridging ligand and the spacer S atom(s) in **Pt1** and **Pt2**, whereas in **Pt3** the HOMO orbitals lie entirely on the Pt(II) centres and very sparsely on the bridging moiety. In case of the LUMO orbitals, these comprise of contributions from the metal centres and the donor atoms of the am(m)ine ligands in all the three complexes. The effect of increasing the number of S-atoms results in decreasing the HOMO–LUMO energy gap while replacing the S-atoms with $–CH_2–CH_2–$ group raises the energy level as the data in Table 6.2 shows.

Table 6.2: DFT-calculated parameters for platinum(II) complexes

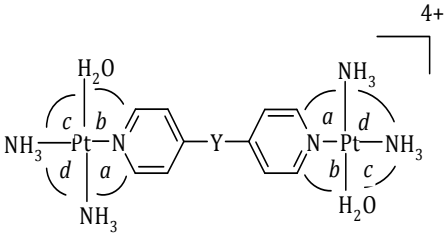

	Pt1	**Pt2**	**Pt3**	**Pt4**
HOMO-LUMO energy (ΔE) /eV	4.14	3.72	5.33	4.52
NBO charges				
Pt1/ Pt2	1.207	1.206	1.205	1.199
Pt–**OH**/Pt–HO_2	1.177/1.201	1.173/1.201	1.169/1.201	
N_{py}	-0.650	-0.657	-0.648	-0.658
Bond length/ Å				
Pt–N_{py}	2.089	2.082	2.082	2.055
Pt–H_2O	2.128	2.129	2.128	2.126
Pt---Pt	12.07	13.74	13.54	
H_2O–Pt–NH_3*cis* to O	2.484	2.493	2.475	
Ortho–H_{py}---Pt	3.006	3.013	3.027	
Bond angle (°)				
N_{py}–Pt–NH_3*trans* to py	177.9	177.1	176.9	177.3
H_2O–Pt–NH_3*trans* to O	175.6	176.1	176.1	178.9
b	94.4	93.4	93.4	93.3
a	90.0	90.3	90.5	87.9
c	83.7	83.7	83.5	84.1
d	92.4	92.5	92.6	94.8
Dipole moment/ Debye (D)	1.93	4.01	0.16	2.18

Structure	HOMO	LUMO
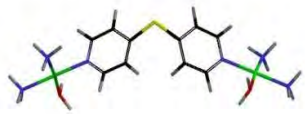 **Pt1** (C_{2v})	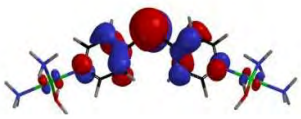	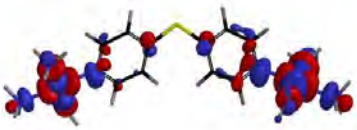
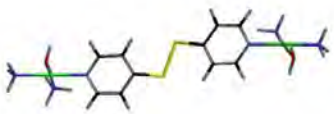 **Pt2** (C_{2h})	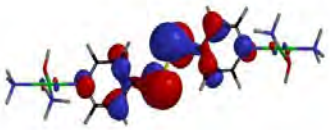	
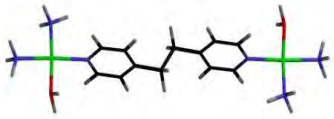 **Pt3** (C_{2h})	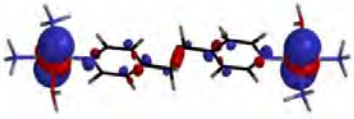	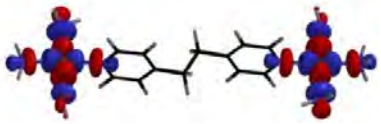
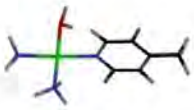 **Pt4** (C_s)	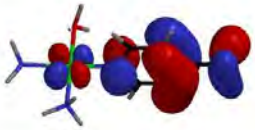	

Figure 6.2: DFT optimised structures of the dinuclear platinum(II) complexes.

From this study the most important structural features revealed by the optimized structures shown in Figure 6.2 and the data in Table 6.2, is that the structural geometry of each complex depends on the angular conformation of the spacer group. For instance, when the sp^3 hybridized S atom is incorporated between the two pyridine rings in the **Pt1** complex, it assumes a V-shaped structure, which results in a C_{2v} point group symmetry. In the case of **Pt2** and **Pt3**, the pyridyl units run nearly parallel, which adopts a slip-up structure that belongs to C_{2h} point group symmetry. Such a structure resembles

that of dinuclear Pt(II) complexes bridged by the flexible α,ω-alkyldiamine, with $(CH_2)_n$ groups that have even numbers of carbon atoms.[24,25(b)]

The conformational differences significantly influenced the DFT calculated values of the Pt---Pt separation distances (through-space), *i.e*. **Pt1** (12.07), **Pt2** (13.74) and **Pt3** (13.54 Å); and the dipole moments exhibited by **Pt1** (1.93), **Pt2** (4.01) and **Pt3** (0.16 D) recorded in Table 6.2. These structural metrics are brought about by the smaller C–C (Å) bond length relative to that of S–S (Å) due to the larger size of S atom and also are influenced by the symmetry of the complex. These structural features together with the steric influences on the square-planar planes at the Pt(II) centres, as will be discussed later, are expected to control reactivity with the incoming nucleophiles.

6.3.5 Kinetic Measurements

The substitution reactions of the complexes with thioureas (TU, DMTU, TMTU) and ionic nucleophiles (Br^-, I^-, SCN^-) were carried out at pH 2.0. The purpose of keeping the solutions acidic was to make sure that the complex remains in aqueous form and at the same time protonate the released N-donor pyridyl bridging ligand so as to prevent it from re-coordination to the metal centre as shown in Scheme 6.4. Besides, protonation of thiourea (TU, pK_a = -1.3) can be ruled out as reported recently.[46] As already mentioned, all the kinetic measurements were done under *pseudo* first-order conditions with respect to the nucleophile, in order to drive the reactions to completion.

The results of the substitution reaction with bromide for all the studied complexes gave only one substitution process (Table 6.3) because of being a weak nucleophile. However, the substitution reactions of the aqua complexes with nucleophiles of stronger nucleophilicity like the thioureas (TU, DMTU, TMTU) and the other anionic nucleophiles (I^-, SCN^-) showed two reaction steps. The first step is attributed to simultaneous substitution of both aqua ligands by the nucleophiles. The second step is much slower by 1 to 3 orders of magnitude compared to the first step, and is assigned to the release of the linker following coordination of further nucleophiles to the Pt(II) centre. This conclusion is arrived at after monitoring the reaction between **Pt1–Cl** and TU (6 equiv.) by ^{1}H NMR spectroscopy in DMF-d_7. An array of the proton NMR spectra, showing the aromatic region only, is recorded in Figure 6.3. The adopted numbering system for the

pyridyl protons Ha/Hb used to monitor the progress of the reaction is shown on the structure of the **Pt1–Cl** complex as an inset in Figure 6.3. The signals of the coordinated ligand appear at Ha = 8.78 and Hb = 7.60 ppm as doublet resonances, which decreased during the reaction. After 1.5 h of the reaction, a broad singlet signal was observed at Ha* = 8.53 ppm, representing the released (free) pyridyl bridging ligand, because the excess thiourea displaces the last N-donor atom in the bridging system to produce $[Pt(TU)_4]^{+2}$ and/or any other undefined products. However, the Hb*-signal at 7.22 ppm for the second aromatic proton of the freed ligand was obscured by the broad peak due to thiourea, TU, at 7.20 ppm and is not shown on Figure 6.3.

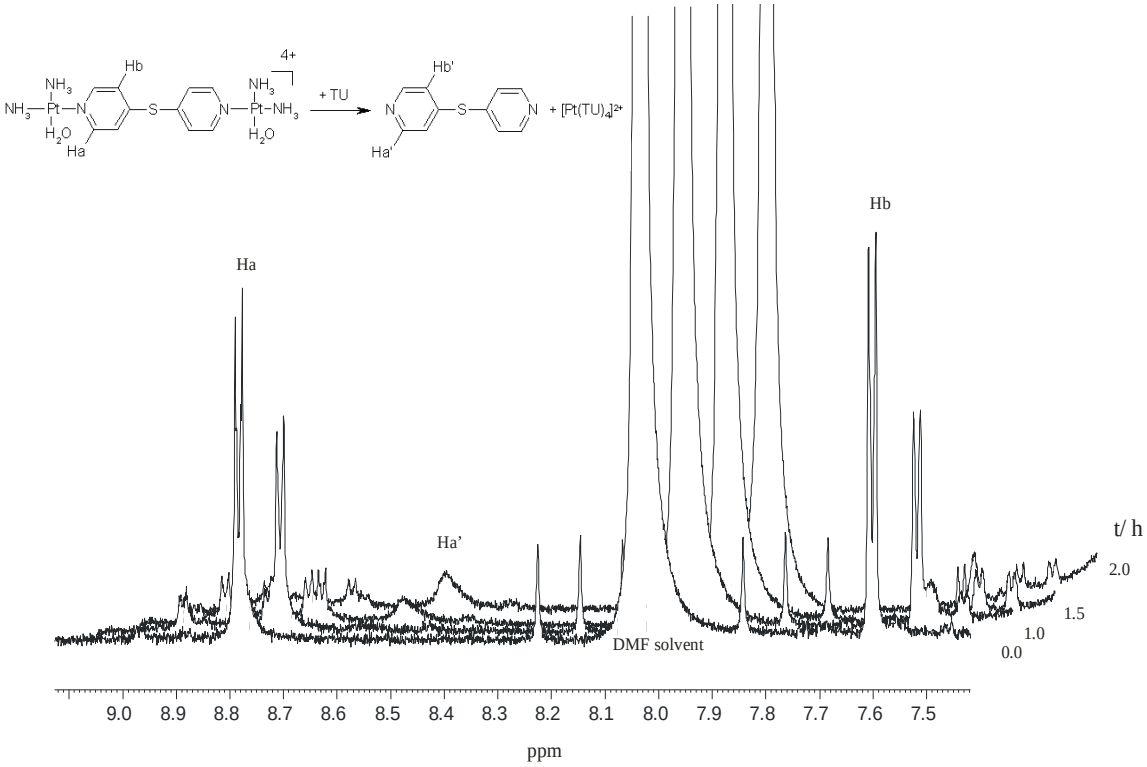

Figure 6.3: The ^{1}H NMR spectra of the reaction of **Pt1** with thiourea (2.0 mM) in DMF-d_7, at 30 °C showing the release of the dps bridging ligand.

Because of the low concentration of the **Pt1–Cl** complex, the aromatic resonances corresponding to the unreacted complex appears as downfield–shifted peaks as the reaction progressed. This is consistent with what has been reported before for bidentate coordinated Pt(II)-based DNA intercalators.[47]

It can be concluded that substitution of the aqua ligands at each of Pt(II) centres occurs simultaneously in all the complexes investigated irrespective of the nature of the spacer group. This is consistent with the symmetrical nature of the complexes. But, the second and slower subsequent step is due to the strong labilising thiourea and other nucleophiles inducing dissociation of the linker. The second step also is sensitive to variations in the nature and size of spacer group of the pyridyl moiety. Thus, the overall substitution process can be represented by the reaction shown in Scheme 6.3.

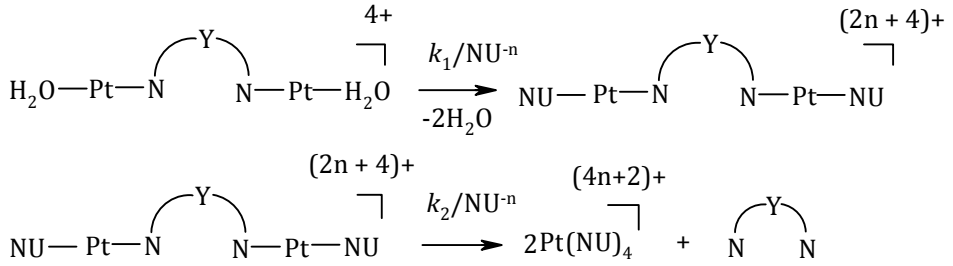

Scheme 6.3: Substitution Mechanism for the reaction between the S, S–S and C–C dinuclear Pt(II) complexes with selected nucleophiles.

In all cases, the first step was fast and was therefore studied on the stopped-flow reaction analyzer whereas the subsequent slower step was studied by the UV-Vis spectroscopic method. The general course of the substitution reactions for 1.0 mM **Pt2** with 3.0 mM TU are recorded in Scheme 6.4.

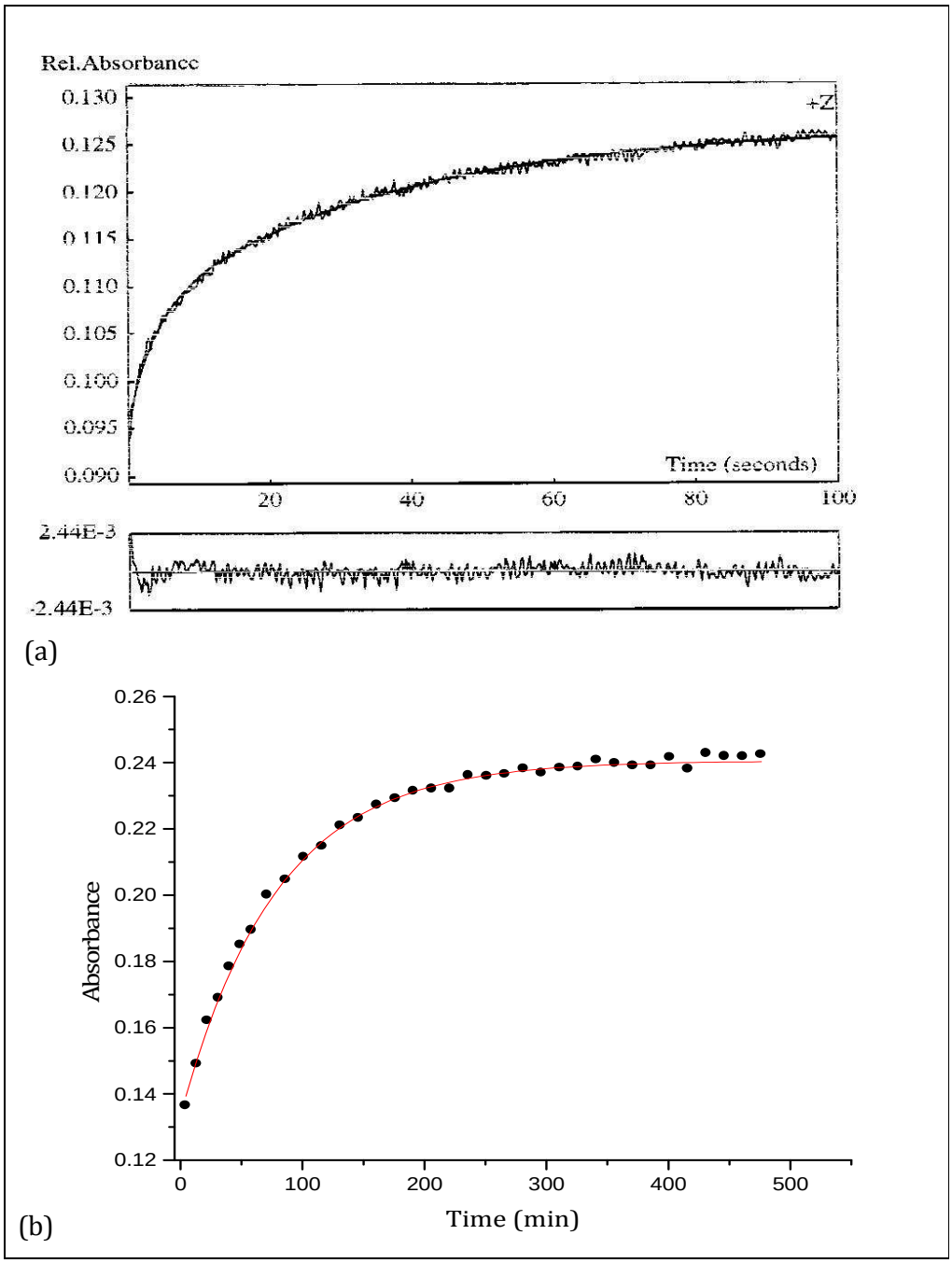

Figure 6.4: (a) Stopped-flow and (b) UV-Vis spectrophotometric curves for **Pt2** with TU at 305 nm, T = 298 K, I = 0.10 M (0.01 M $HClO_4$, adjusted with $NaClO_4$), pH = 2.0.

Both the first and second substitution steps fitted well to a single-exponential model to give the observed rate constants $k_{obs(1st)}$ and $k_{obs(2^{nd})}$. The determined *pseudo* first-order

rate constants, $k_{obs(1^{st}/2^{nd})}$, were plotted against nucleophile concentration. A linear dependency of the observed rate constants on the concentration of the nucleophiles was obtained as shown for **Pt1** complex in Figures 6.5 and 6.6 (also Figures **S6.1-S6.2** and **S6.9-S6.10**, **Appendix 6**). The second-order rate constants, $k_{2(1^{st}/2^{nd})}$, were derived from the slopes of the plots and are summarized for all the complexes investigated in this study in Tables 3 and 4.

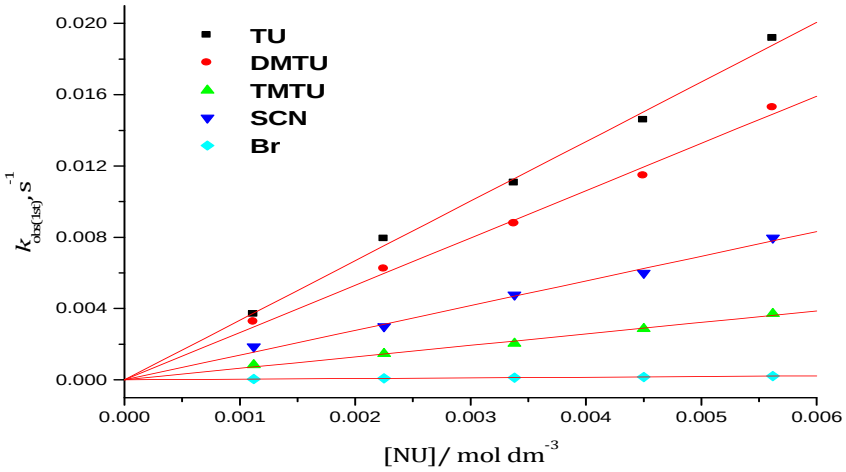

Figure 6.5: Concentration dependence of $k_{obs(1^{st})}$ for the simultaneous substitution of aqua ligands in **Pt1** by thiourea nucleophiles and ionic nucleophiles at pH = 2.0, T = 298.15 K, I = 0.10 M (0.01 M $HClO_4$, adjusted with $NaClO_4$).

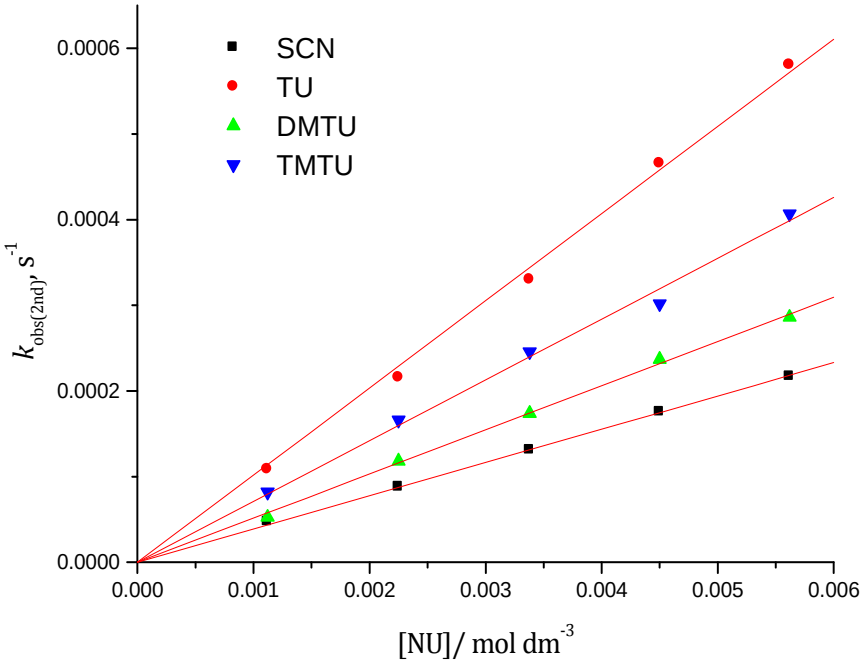

Figure 6.6: Concentration dependence of $k_{obs(2^{nd})}$ for the dissociation of bridging ligand in **Pt1** by thiourea nucleophiles and ionic nucleophiles at pH = 2.0, T = 298.15 K, I = 0.10 M (0.01 M $HClO_4$, adjusted with $NaClO_4$).

Table 6.3: Summary of rate constants and activation parameters with the corresponding standard deviations for the substitution of aqua ligands by neutral (TU, DMTU, and TMTU) and ionic (I^-, Br^- and SCN^-) nucleophiles, I = 0.10 M ($NaClO_4$).

Complex	NU	$k_{2,1}^{st}$ / M^{-1} s^{-1}	$\Delta^{\neq}H_1^{st}$ /kJmol^{-1}	$\Delta^{\neq}S_1^{st}$ /J mol^{-1} K^{-1}
Pt1 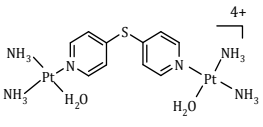	TU	33.5 ± 0.5	63 ± 1.4	-41 ± 4.6
	DMTU	25.9 ± 1.1	56± 1.5	-64 ± 5.0
	TMTU	6.4 ± 0.1	58 ± 2.5	-57 ± 8.3
	SCN^-	14.0 ± 0.6	60 ± 4.9	-52 ± 16.3
	Br^-	0.4 ± 0.01	73 ± 2.3	-26 ± 7.5
Pt2 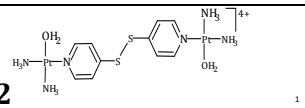	TU	244.6 ± 2.9	53 ± 0.4	-52 ± 1.4
	DMTU	179.0 ± 2.8	48 ± 2.8	-111 ± 9.3
	TMTU	86.2 ± 1.8	48 ± 1.6	-91 ± 5.4
	SCN^-	542.0 ± 14.1	69 ± 1.0	-26 ± 3.4
	Br^-	13.0 ± 0.2	74 ± 2.3	-25 ± 7.7
Pt3 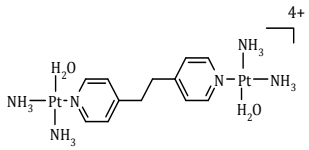	TU	129.5 ± 1.6	53 ± 0.4	-53 ± 1.3
	DMTU	65.6 ± 0.6	44 ± 1.6	-85 ± 5.5
	TMTU	13.4 ± 0.2	41 ± 0.5	-112 ± 1.8
	SCN^-	258.2 ± 2.5	54 ± 3.0	-39 ± 10.0
	I^-	129.5 ± 1.6	42 ± 1.7	-83 ± 5.6
	Br^-	11.8 ± 0.2	50 ± 2.0	-104 ± 6.6

At pH 2.0, the S–S bond scission occurred reversibly in a redox reaction with iodide: py–S–S-py + $2I^-$ ↔ 2py–S^-+ I_2. This limited further kinetic studies for **Pt1** and **Pt2** complexes.

Table 6.4: Summary of rate constants and activation parameters with the corresponding standard deviations for the release of bridging ligand by neutral (TU, DMTU, and TMTU) and ionic (I^-, Br^- and SCN^-) nucleophiles, I = 0.10 M ($NaClO_4$).

Complex	NU	$k_{2,2}^{nd}$ / 10^{-3} M^{-1} s^{-1}	$\Delta H^{\neq}{}_2^{nd}$ /kJ mol^{-1}	$\Delta S^{\neq}{}_2^{nd}$ /J mol^{-1} K^{-1}
Pt1	TU	102.1 ± 0.20	49 ± 3.2	-107 ± 10.7
	DMTU	51.5 ± 0.64	53 ± 0.6	-99 ± 1.9
	TMTU	70.6 ± 1.52	48 ± 1.9	-117 ± 6.4
	SCN^-	39.0 ± 0.28	65 ± 1.7	-61 ± 5.8
Pt2	TU	35.4 ± 0.23	53 ± 1.3	-95 ± 4.5
	DMTU	14.3 ± 0.05	62 ± 1.1	-73 ± 3.6
	TMTU	24.9 ± 0.12	49 ± 0.9	-116 ± 2.9
	SCN^-	18.8 ± 0.41	49 ± 1.0	-83 ± 3.5
Pt3	TU	23.8 ± 0.18	59 ± 1.2	-80 ± 4.1
	DMTU	7.6 ± 0.36	49 ± 1.2	-122 ± 4.1
	TMTU	1.4 ± 0.22	50 ± 1.1	-133 ± 3.6
	SCN^-	14.7 ± 0.14	49 ± 1.1	-78 ± 3.5
	I^-	1.2 ± 0.14	50 ± 1.2	-133 ± 3.9

Br^- = No reaction was observed in the second step in all cases.

None of the plots exhibited an intercept in all the reactions of the complexes with the nucleophiles, indicating that both steps are irreversible in nature, and k_{-1} and k_{-2} are zero since the reverse reaction is too slow, if it exists. Thus, the rate equations for the two substitution reaction steps can be expressed by *Equation 1*.

$$k_{obs(1^{st}/2^{nd})} = k_{2(1^{st}/2^{nd})}[NU] \quad (1)$$

6.3.6 Activation Parameters

The activation parameters were determined through systematic variation of temperature within the range 15-35 °C, at 5 °C interval. The Eyring plots depicted in Figure 6.7 and 6.8 (also Figures **S6.3-S6.4** and **S6.11-S6.12**, **Appendix 6**) resulted in the activation parameters: activation enthalpy, $\Delta H^{\neq}_{(1^{st}/2^{nd})}$ from the slopes, and activation entropy, $\Delta S^{\neq}_{(1^{st}/2^{nd})}$ from the intercept. The values obtained are tabulated in Tables 6.3 and 6.4.

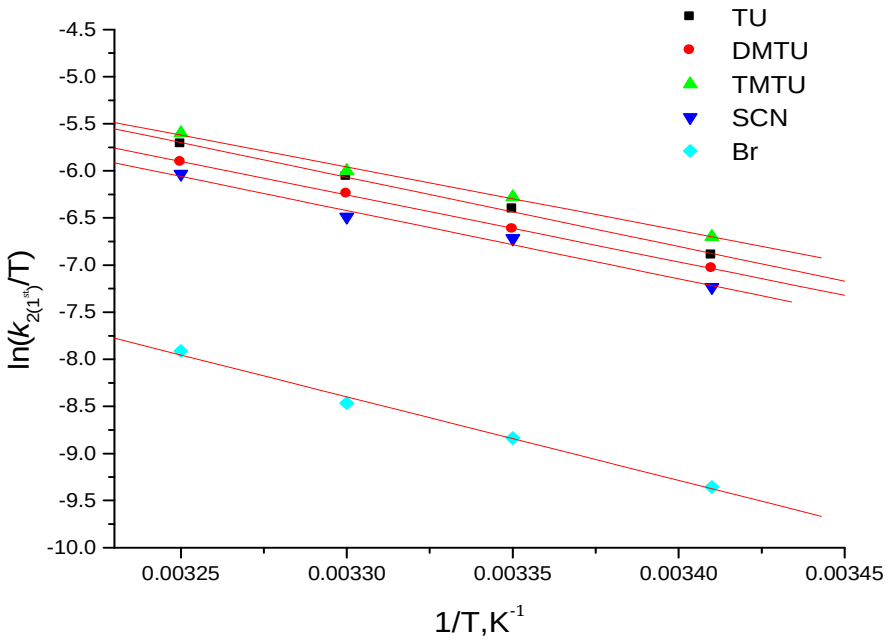

Figure 6.7: Plots of $\ln(k_{2(1^{st})}/T)$ versus (1/T) for the first step reaction of **Pt1** with a series of different nucleophiles at varying temperatures.

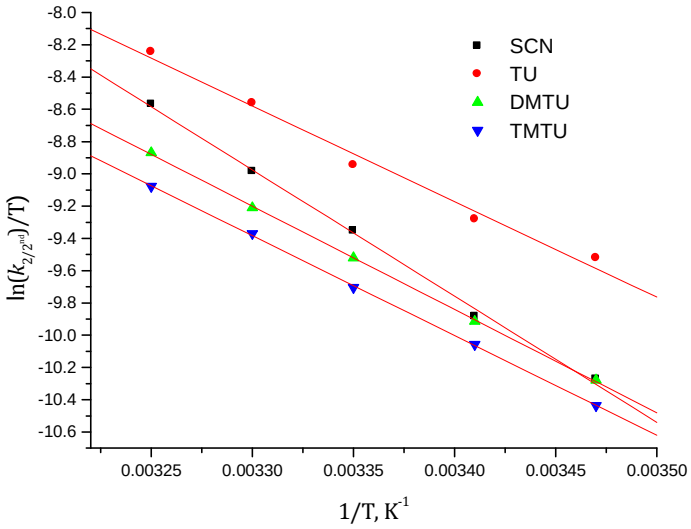

Figure 6.8: Plots of $\ln(k_{2(2^{nd})}/T)$ versus (1/T) for the second step reaction of **Pt1** with a series of different nucleophiles at varying temperatures.

6.4 Discussion

6.4.1 pK_a Determination for the Diaqua Complexes

The thermodynamic data in Table 6.1 demonstrates that the pK_a values of the coordinated aqua moieties are dependent on the nature of the linker. The pK_{a1} values of the studied dinuclear complexes **Pt1**, **Pt2** and **Pt3** (ranging from 4.86 ± 0.05 to 5.19 ± 0.02) are lower than that of the mononuclear analogue **Pt4** (pK_a = 5.63 ± 0.01) and those of the Pt(II) amphiphiles recently published:[48] [Pt(H_2O)(N,N-bis(2-pyridylmethyl)-$NCH_2)_n$-CH_3; NH]$^{+2}$ n = 1, 2, 3, 4, 5, 9 (pK_a = 5.45 ± 0.05 to 5.52 ± 0.02); signifying an increase in acidities of the coordinated water molecules in these dinuclear complexes. This is in agreement with what has been reported in other studies which have shown that Pt atoms in dinuclear complexes are more acidic than the Pt atoms of the mononuclear complexes.[24,25,48] A higher overall positive charge of +4 on the Pt atoms coupled with higher electrophilicity is the reason for the lower pK_a value observed in the dinuclear complexes than that found for +2 charged Pt(II) centres of the mononuclear complexes. Furthermore, a short distance between the Pt(II) centre of the dinuclear complexes, results in single charge additions (controlled by in-space electrostatic forces and/or H-bond) on the platinum atoms that increases the effective positive charge at the metal centre.[25(b & c)] This explains why with decreasing Pt---Pt separation distance the

pK_{a1} values become smaller. In addition, the difference in the observed pK_a values is also due to the σ-donor properties of the spacers.

This is supported by the differences in the ^{195}Pt NMR chemical shifts of **Pt1** (-2303.9), **Pt2** (-2304.2), **Pt3** (-2284.7) and **Pt4** (-2299 ppm), respectively. Since the position of the ^{195}Pt resonance is influenced by the donor strength of the ligands attached to the platinum,[49] the results indicate that the σ-inductive effect of *para*-substituent on the pyridyl linker towards the Pt(II) centre differ in strength and as a result controls the bacisity of the aqua complexes. However, the difference of only 0.3 pK_{a1} units between pK_{a1} values of the complexes of shortest and longest spacer length shows the result is more of a charge effect than σ–donor effect by the bridging ligand. The pK_{a1} value of the diaqua **Pt3** complex is in agreement with the recently published value for its *trans*-isomer.[34(c)]

Further observation shows that deprotonation of the second coordinated water molecule to the hydroxo/hydroxo species occurs at higher pH values than in the first step in all the three complexes. This results from a reduction of the overall charge to +3 after deprotonation of one coordinated water molecule. Hence, the Pt(II) centre of the aqua/hydroxo species is less electrophilicity compared to that of the diaqua complex,[25,31] leading to higher pK_{a2} values. As already mentioned for the first deprotonation step, the pK_{a2} values also depend on the nature and length of the spacer group.

These σ–inductive effects on the ground-state properties of the Pt(II) complexes are supported by the computational data, which shows that the DFT calculated NBO charges at the Pt(II) centres decreased after deprotonation of the first water molecule as follows: Pt–**OH** (1.177): Pt–H_2O (1.201) for **Pt1**, Pt–**OH** (1.173): Pt–H_2O (1.201) for **Pt2**, and Pt–**OH** (1.169): Pt–H_2O (1.201), respectively compared with values of the diaqua complexes in Table 6.2. The trend is also in the order of the magnitude of the dipole moments of the complexes, which is a measure of the electronegativiy of the complexes.

6.4.2 Ligand Substitution

Based on the DFT calculated Pt---Pt distances between the complexes, one can conclude that the distances are long enough to prevent strong intramolecular "electronic communication" between the two Pt(II) centres. This makes the two Pt(II) centres kinetically indistinguishable from each other, and therefore, react independently. Analysis of the rate constants (Table 6.3) shows that the two metal centres could not be discriminated by the incoming nucleophiles, resulting in the simultaneous substitution of both aqua ligands as the first reaction step.

From the values of the second-order rate constants (Table 6.3), the order of reactivity of the diaqua Pt(II) complexes for the direct attack pathway, k_1, is **Pt2** > **Pt3** > **Pt1**. The difference in reactivity can be attributed to steric and electronic effects attributed to different structural or geometrical arrangement of the spacer atom(s) of the pyridyl linker.

It is widely accepted that the pK_a value of the coordinated water molecule is an indicator of the electron density around the metal centre and hence, of the electrophilicity of the Pt(II) centre.[19,45] Since the pK_{a1} value of the **Pt1** complex is smaller than that of either **Pt2** or **Pt3**, one would expect higher reactivity for **Pt1**. The data in Table 6.3 shows the contrary. In addition, enhanced reactivity due to the "entrapment effect" expected of complexes with C_{2v} point group symmetry,[24] was also not observed in the first substitution step of **Pt1**. As seen from the optimised structure of the complex (Figure 6.8), the central cavity is blocked by the pyridine ring that protrudes into the cavity preventing the entrapment effect to the incoming nucleophiles. The DFT calculated C-S-C angles of 94.5 and 112.8° for the 4,4'-bis(pyridine)sulphide ligand and the **Pt1** complex, respectively, show that the ligand has a perfect V-shaped planar structure (C_{2v}), whereas **Pt1** is highly distorted (Figure 6.8). The lone pairs on sp^3 hybridized S atom in **Pt1** occupy less geometrical angles about the atom and cause greater repulsions, which forces the Pt coordination planes to sit in a twisted anti-conformation relative to each other as seen in Figure 6.8. The pyridine ring is inclined at an angle which is almost perpendicular to the Pt(II) centre, such that the *ortho*-Hydrogen atom on the aromatic ring (H_{py}) poses steric influence to aerial approach of the nucleophile on each Pt(II) centre, leading to a slower nucleophilic attack. It can be presumed that an equal amount

of steric influence is felt by the Pt atoms of the investigated dinuclear complexes. However, the DFT calculated inclination distance between the *ortho*-Hydrogen atom and the Pt(II) centre (H_{py}---Pt) increases in the order 3.006, 3.013 and 3.027 Å (Table 6.2) for **Pt1**, **Pt2** and **Pt3**, respectively, showing that the greatest steric hindrance is present in **Pt1**. The observed distortion of the bridging ligand in **Pt1** is absent in **Pt2**.

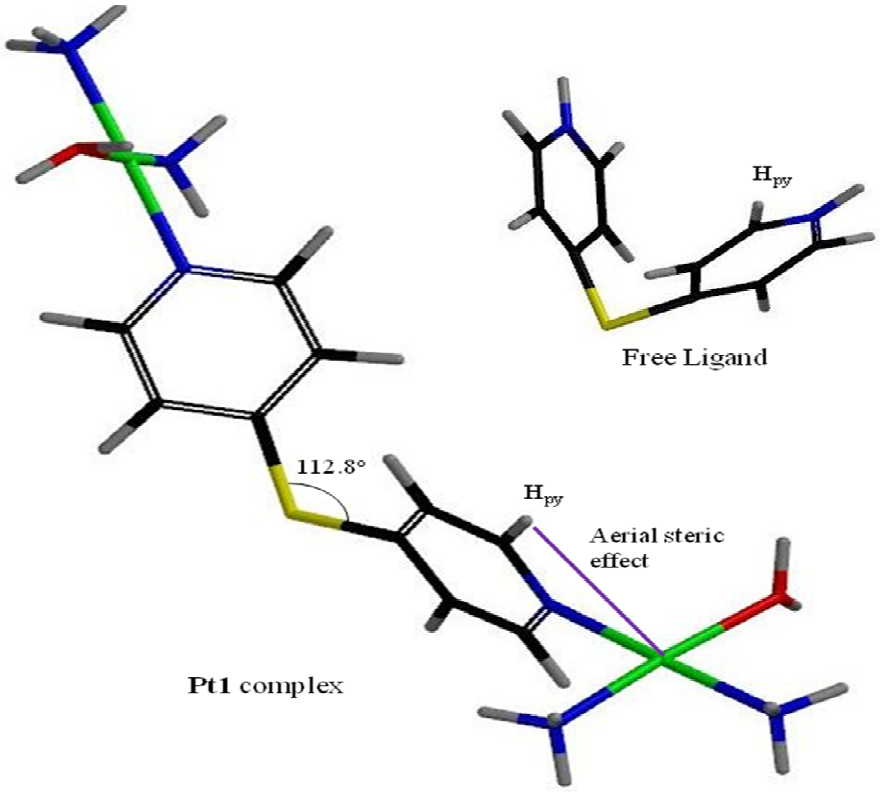

Figure 6.9: Schematic structures of **Pt1** and free ligand illustrating the twisted conformation of **Pt1** and steric factor

To understand further the role of the linker on the rate of substitution, the reactivity of **Pt2** and **Pt3** are compared. **Pt2** and **Pt3** complexes both adopt C_{2h} molecular point symmetry, but differ by what link the two pyridines attach to Pt atoms. This difference makes the **Pt2** complex to have the highest dipole moment (Table 6.2), an indication that its Pt(II) centre is more electrophilic, as such it could be more reactive in comparison to the other complexes as observed. This is supported by the NBO charge on **Pt3** which is slightly less positive compared to that of **Pt2**. In addition, the HOMO-LUMO energy gap (Table 1) is wider for **Pt3** than for **Pt2**, suggesting an increase in the energy barrier and therefore a slower substitution reaction.

A further observation is that the second step is remarkably slower than the simultaneous substitution of the aqua ligands in the first step in all cases. It is assigned to the release of the bridging pyridyl ligand following the coordination of further nucleophiles to the already sterically crowded Pt(II) centre. Because of these factors, the congested Pt(II) centre in the transition state weakens the bonds, forcing the dissociation of pyridyl linker. The order of reactivity of the complexes is **Pt1** > **Pt2** > **Pt3**, mostly controlled by the structural differences. The entrapment of the incoming nucleophiles coupled with the release of strain imposed on the structure by lone pair repulsions in the twisted conformation in **Pt1** accounts for its much higher reactivity compared to **Pt2** and **Pt3**.

The order of reactivity of the thiourea nucleophiles at the Pt(II) centres during the simultaneous substitution of the aqua ligands increases in order TU > DMTU > TMTU, which reflects the steric characteristics of a mechanism involving bond making in the 5-coordinate transition state. The most sterically hindered nucleophile TMTU reacts significantly slower than the less hindered TU in all cases.

The order of reactivity for the anionic nucleophiles is SCN^- > I^- > Br^-, which is in line with the polarisability of the ions *i.e*. 3.05 x 10^{-24}, 4.70 x 10^{-24} and 6.1 x 10^{-24} cm^3 for Br^-, I^- and SCN^-, respectively,[50,51] as well as the electrostatic attraction forces between the anions and the doubly charged terminal Pt(II) centres. [52]

Activation parameters obtained for the simultaneous substitution of the aqua ligands in the first step (Table 6.3) and the release of the linker in the second step (Table 6.4) are characterized by large negative activation entropies ($\Delta S^{\neq}_{(1^{st}/2^{nd})}$) and low activation enthalpies ($\Delta H_{(1^{st}/2^{nd})}$), all supporting an associative substitution mechanism dominated by bond making in the transition state.[53,54]

6.5 Conclusion

The present study has demonstrated that small modifications of the bridging moiety has a strong influence on the properties and reactivity of diaqua Pt(II) complexes.
Spectrophotometric acid-base titrations of these complexes gave two pK_a values. The ^{1}H NMR measurement for the reaction of **Pt1–Cl** with TU confirmed the replacement of the bridging pyridyl ligand following coordination of further thiourea to the already congested Pt(II) centre in the transition state. The substitution process of the studied systems remains associative mechanism. This is supported by the large negative activation entropies.

The pK_{a1} values for deprotonation of the first water molecule increases with increasing Pt---Pt distance in the order **Pt1** < **Pt3** < **Pt2**, showing there is direct correlation between the Pt---Pt distance and the acidity of the coordinated aqua ligand. This has been explained to be due to the charge additions and to the decreasing communication/interactions between the two Pt atoms. The substitution kinetics resulted into two k_2 rate constants, simultaneous substitution of the coordinated H_2O molecules and the release of the linker ligand. The order of the reactivity is mostly dependent on the structure of the complexes where steric hindrance plays a major role. The second factor is the electronic effect where the charge addition has some influence. Computation studies support the experimental trend of pK_a values and substitution reactivity of the diaqua Pt(II) complexes. It can be concluded that the dissociation of the linker is a possible indication that if these compounds are used for treatment of cancer, they are likely to be unstable.

References

1 R. E., J. Cummings, A. A. Ritchie, M. Muir, R. E. Morris and H. Chen, 2002, *British J. Cancer*, **86**, 1652.

2 S. J. Lippard, D. Wang, 2005. *Nat. Rev. Drug*., **4**, 307.

3 S. E. Miller and D. A. House, 1990, *Inorg. Chim. Acta*, **173**, 53.

4 G. Momekov, A. Bakalova and M. Karaivanova, 2005, *Curr. Med. Chem*., **12**, 2177.

5 (a) C. X. Zhang and S. J. Lippard, 2003, *Curr. Opin. Chem. Biol*., **7**, 481; (b) Y. Jung and S. J. Lippard, 2007. *Chem. Rev*., **107**, 1387.

6 E. Pantoja, A. Gallipoli, S. Van Zutphen, S. Komeda, D. Reddy, D. Jaganyi, M. Lutz, M. D. Tooke, A. L. Spek, C. Ravarro-Ranninger and J. Reedijk, 2006, *J. Inorg. Biochem*., **100**, 1955 (and references cited therein).

7 (a) G. Natile and M. Coluccia, 2001. *Coord. Chem. Rev*., **216**, 383; (b) P.J.Dyson and G. Sava, 2006, *Dalton Trans*., 1929.

8 T. W. Hambley, 1997, *Coord. Chem. Rev*., **166**, 181.

9 N. J. Wheate, S. Walker, G. E. Craig and R. Oun, 2010, *Dalton Trans*., **39**, 8113.

10 (a) A. G. Sykes, 1988, *Platinum Met. Rev*., **32**, 170; (b) A. Pasini and F. Zunino, 1987, *Angew. Chem. Int. Ed*., **26**, 615; c) N. Farrell, Y. Qu and M. P. Hacker, 1990, *J. Med. Chem*., **33**, 2179.

11 J. Reedjik, 2008, *Platinum Met. Rev*., **52**, 2.

12 S. Rubino, P. Portanova, F. Giammalva, M. A. Girasolo, S. Orecchio, G. Calvaruso and G. C. Stocco, 2011, *Inorg. Chim. Acta*, **370**, 207 (and reference cited therein).

13 (a) U. Kalinowska-Lis, J. Ochocki and K. Matlawska-Wasowska, 2008, *Coord. Chem. Rev*., **252**, 1328; (b) N. J. Wheate and J. G. Collins. 2003, *Coord. Chem. Rev*., **241**, 133; c) B. A. J. Jansen, J. Van Der Zwan, , H. den Dulk, J. Brouwer and J. Reedijk, 2001, *J. Med. Chem*., **44**, 245.

14 S. Komeda, M. Lutz, A. L. Spek, M. Chikuma and J. Reedijk, 2000, *Inorg. Chem*., **39**, 4230.

15 S. Komeda, G. V. Kalayda, M. Lutz, A. L. Spek, Y. Yamanaka, T. Sato, M. Chikuma and J. Reedijk, 2003, *J. Med. Chem*., **46**, 1210.

16 G. V. Kalayda, S. Komeda, K. Ikeda, T. Sato, M. Chikuma and J. Reedijk, 2003, *Eur. J. Inorg. Chem*., 4347.

17 O. F. Wendt and L. I. Elding, 1997, *J. Chem. soc., Dalton Trans*., 4725.

18 D. Reddy and D. Jaganyi, 2008, *Dalton Trans*., 6724.

19 A. Hofmann, D. Jaganyi, O. Q. Munro, G. Liehr and R. van Eldik, 2003, *Inorg. Chem*., **42**, 1688.

20 H. Krüger and R. van Eldik, 1990, *J. Chem. Soc., Chem. Commun*., 330; b) B. Pitteri and M. Bortoluzzi, 2008, *Polyhedron*, **27**, 2259.

21 (a) V. X. Jin, S. I. Tan and J. D. Ranford, 2005, *Inorg. Chim. Acta*, **358**, 677; (b) E. Wong and C. M. Giandomenico, 1999, *Chem. Rev*., **99**, 2451.

22 P. Sarmah and R. C. Deka, 2010, *J. Mol. Str.: THEOCHEM*, **955**, 53.

23 D. Reddy and D. Jaganyi, 2011, *Int. J. Chem. Kinet*. **43**,161.

24 A. Mambanda, D. Jaganyi, S. Hochreuther and R. van Eldik, 2010, *Dalton Trans*., **39**, 3595.

25 (a) A. Hofmann and R. van Eldik, 2003, *Dalton Trans*., 2979; (b) H. Ertürk, A. Hofmann, R. Puchta and R. van Eldik, 2007, *Dalton Trans*., 2295; (c) H. Ertürk, J. Maigut, R. Puchta, R. van Eldik, 2008, *Dalton Trans*., 2759.

26 D. Jaganyi, V. M. Munisamy and D. Reddy, 2006, *Int. J. of Chem. Kinet.*, ***38***, 202.

27 A. Hegmans, S. J. Berners-Price, M. S. Davies, D. S. Thomas, A. S. Humphreys and N. Farrell, 2004, *J. Am. Chem. Soc*., **126**, 2166.

28 E. I. Montero, B. T. Benendetti, J. B. Mangrum, M. J. Oehlsen, Y. Qu and N. P. Farrell, 2007, *Dalton Trans*., 4938.

29 R. A. Ruhayel, I. Zgani, S. J. Berners-Price and N. P. Farrell, 2011, *Dalton Trans*., **40**, 4154 (and references cited therein).

30 (a) J. W. Williams, Y. Qu, G. H. Bulluss, E. Alvorado and N. P. Farrell, 2007, *Inorg. Chem*. **46**, 5820; (b) D. Fan, X. Yang, X. Wang, S. Zhang, J. Ding, *et al*. 2007, *J. Biol. Inorg. Chem*., **12**, 655.

31 H. Ertürk, R. Puchta and R. van Eldik, 2009, *Eur. J. Inorg. Chem*., 1331.

32 (a) M. E. Oehlsen, Y. Qu and N. Farrell, 2003, *Inorg. Chem*., **42**, 5498; (b) V. Vacchina, L. Torti, C. Allievi and R. Lobinski, 2003, J. *Anal. At. Spectros*., **18**, 884.

33 (a) N. Farrell, in *Platinum-based Drugs in Cancer Therapy*, 2000, L. R. Kelland and N. Farrell, (Ed.), Humana Press, Totowa, 321; (b) T. D. McGregor, Z. Balcarova, Y. Qu, M. C. Tran, R. Zaludova, V. Brabec and N. Farrell, 1999, *J. Biol. Inorg. Chem*., **77**,

43; (c) E. I. Montero, J. Zhang, J. I. Moniodis, S. J. Berners-Price and N. P. Farrell, 2010, *Chem. Eur. J*., **30**, 9175.

34 (a) N. Summa, J. Maigut, R. Puchta and R. van Eldik, 2007, *Inorg. Chem*., **46**, 2094; (b) S. Hochreuther, R. Puchta and R. van Eldik, 2011, *Inorg. Chem*., **50**, 12747; (c) T. Soldatović, S. Jovanović, Ž. D. Bugarčić and R. van Eldik, 2012, *Dalton. Trans*., **41**, 876.

35 D. D. Perrin, W. L. F. Armarego, D. R. Perrin, *Purification of Laboratory, Chemicals*, Pergamon, Oxford, 2nd edn, 1980.

36 MicrocalTM OriginTM Version 7.5, Microcal Software, Inc., Northampton, MA, 1991-2003.

37 (a) D. M. De Faria, M. I. Yoshida, et al. 2007, *Polyhedron*, **26**, 4525; (b) M. V. Marinho, M. I. Yoshida, K. Krambbrock, L. Fernando, C. De Oliveira, R. Diniz and F. C. Machado, 2009, *J. Mol. Str*., **923**, 60.

38 G. Zhao, H. Lin, S. Zhu, H. Sun, Y. Chen, 1998. *J. Inorg. Biochem*., **70**, 219.

39 L. S. Hollis, A. R. Amundsen, E. W. Stern, 1989, *J. Med. Chem*., **32**, 128.

40 Z. D. Bugarčić, G. Liehr and R. van Eldik, 2002, *J. Chem. Soc., Dalton Trans*., 951.

41 (a) A. D. Appleton, J. R. Hall, S. F. Ralph and C. S. M. Thompson, 1984, *Inorg. Chem*., **23**, 3521; (b) R. Romeo and M. Cusumano, 1981, *Inorg. Chim. Acta*, **49**, 167.

42 A. D. Becke, 1993, *J. Chem. Phys*., **98**, 5648.

43 P. J. Hay and W. R. Wadt, 1985, *J. Chem. Phys*., **82**, 299.

44 G. Zhao and X. Hu, 2004, *Trans. Metal Chem*., **29**, 607 (and references therein).

45 N. Summa, W. Schiessl, R. Puchta, N. Van Eikema Hommes and R. van Eldik, 2006, *Inorg. Chem*., **45**, 2948.

46 W. C Schiessl, N. Summa, C. F. Weber, S. Gubo, C. Ducker-Benfer, R. Puchta, N. J. R. van Eikema Hommes and R. van Eldik, 2005, *Z. Anorg. Allg. Chem*., **631**, 2812.

47 S. Kemp, N. J. Wheate, S. Wang, J. G. Collins, S. F. Ralph, A. I. Day, V. J. Higgins and J. R. Aldrich-Wright, 2007, *J. Biol. Inorg. Chem*., **12**, 969.

48 A. Mambanda and D. Jaganyi, 2011, *Dalton, Trans*., **40**, 79.

49 (a)P. S Pregonsin, 1982, *Coord. Chem. Rev*., **33**, 512; (b) T. G. Appleton, J. R. Hall and S. F. Ralph, 1985, *Inorg. Chem*., **24**, 4685.

50 D. Jaganyi, F. Tiba, O. Q. Munro, B. Perović and Ž. D. Bugarčić, 2006, *Dalton Trans*., 2943.

51 Y. Iwadata, K. Kawamura, K. Igarashi and J. Mochinaga, 1982, J. Phys. Chem., 86, 5206.

52 R. G. Pearson, 1963, *J. Am. Chem. Soc*., **85**, 3533.

53 (a) S. Aŝperger, *Chemical Kinetics and Inorganic Reaction Mechanisms*, Kluwer/ Plenum Publishers, New York, 2nd Ed., 2003; (b) M. L. Tobe and J. Burges, *Inorganic Reaction Mechanisms*, Addison Wesley, Longman Ltd, London, 1999.

54 J. D. Atwood, *Inorganic and Organometallic Reaction Mechanisms*, 2nd Ed., Wiley-VCH Inc., New York, 1997, pp. 43-61.

Appendix 6

Table S6.1: Summary of the wavelengths (nm) used for monitoring the reactions between a series of aqua Pt(II) complexes with neutral S-donor and ionic nucleophiles.

Complex	Nucleophile	Wavelength, λ (nm)
Pt1	TU	330
	DMTU	333
	TMTU	346
	SCN^-	315
	Br^-	232
Pt2	TU	321
	DMTU	305
	TMTU	340
	SCN^-	298
	Br^-	236
Pt3	TU	311
	DMTU	299
	TMTU	241
	SCN^-	248
	I^-	290
	Br^-	276

Table S6.2: Average observed rate constants, $k_{obs(1^{st})}$, at 298.15 K, for the reactions of **Pt3** with a series of nucleophiles at different concentrations.

[NU]/ M	$k_{obs(1^{st})}, s^{-1}$					
	TU	**DMTU**	**TMTU**	**SCN^-**	**I^-**	**Br^-**
0.00207	0.0256	0.00794	0.00158	0.0530	0.02558	0.00224
0.00414	0.0528	0.01443	0.00293	0.1024	0.05286	0.00505
0.00621	0.0840	0.02175	0.00441	0.1580	0.08398	0.00789
0.00828	0.1042	0.02916	0.00623	0.2110	0.10416	0.00956
0.01034	0.1347	0.03740	0.00743	0.2724	0.13465	0.01194

Table S6.3: Average observed rate constants, $k_{obs(2^{nd})}$, at 298.15 K, for the reactions of **Pt3** with a series of nucleophiles at different concentrations.

[NU]/ M	$k_{obs(2^{nd}),s^{-1}}$				
	TU	**DMTU**	**TMTU**	**SCN^-**	**I^-**
0.00125	2.253×10^{-5}	9.510×10^{-6}	1.782×10^{-6}	1.820×10^{-5}	1.577×10^{-6}
0.00225	4.595×10^{-5}	1.632×10^{-5}	3.164×10^{-6}	3.330×10^{-5}	2.825×10^{-6}
0.00338	6.983×10^{-5}	2.628×10^{-5}	4.911×10^{-6}	5.170×10^{-5}	4.025×10^{-6}
0.0045	9.253×10^{-5}	3.384×10^{-5}	6.401×10^{-6}	6.580×10^{-5}	5.200×10^{-6}
0.00653	1.326×10^{-4}	4.899×10^{-5}	9.513×10^{-6}	9.460×10^{-5}	7.873×10^{-6}

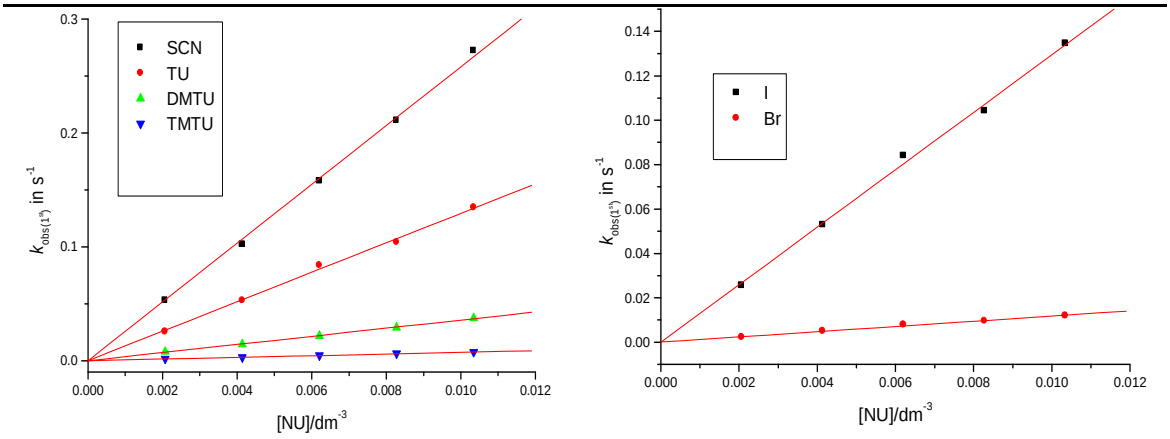

(a) **(b)**

Figure S6.1: Concentration dependence of $k_{obs(1^{st})}$ for the simultaneous substitution of aqua ligands in **Pt3** by (a) thiourea nucleophiles and (b) ionic nucleophiles at pH = 2.0, T = 298.15 K, I = 0.10 M (0.01 M $HClO_4$, adjusted with $NaClO_4$).

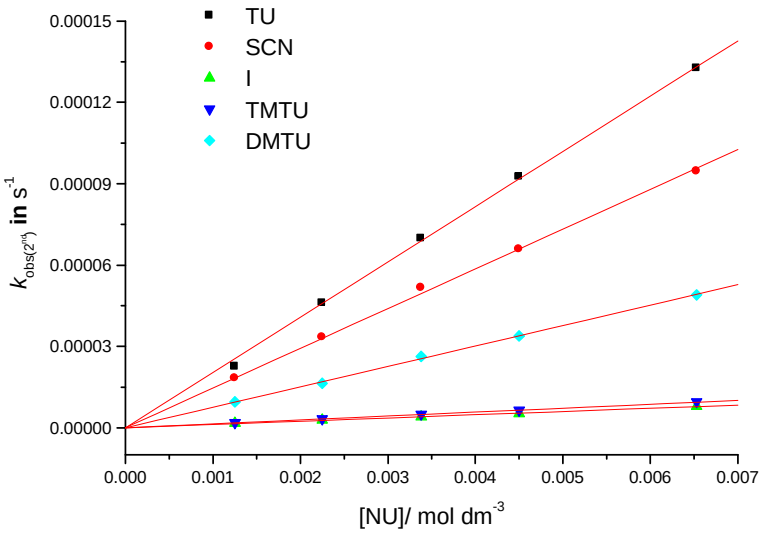

Figure S6.2: Concentration dependence of $k_{obs(2^{nd})}$ for the dissociation of the bridging ligand in **Pt3** by thioureas and ionic nucleophiles at pH = 2.0, T = 298.15 K, I = 0.10 M (0.01 M $HClO_4$, adjusted with $NaClO_4$).

Table S6.4(a): Average observed rate constants, $k_{obs(1^{st})}$, for the reactions of **Pt3** at varied temperatures in the range 15 to 35 °C while maintaining nucleophile concentration at ≈ 60x [**Pt3**].

1/T, K^{-1}	**TU**		**DMTU**		**TMTU**	
	$k_{obs(1^{st})}$, s^{-1}	**ln(k_2/T)**	**$k_{obs(1^{st})}$, s^{-1}**	**ln(k_2/T)**	**$k_{obs(1^{st})}$, s^{-1}**	**ln(k_2/T)**
0.00347	0.0148	-4.7945	0.0145	-4.8179	2.396×10^{-3}	-6.6153
0.00341	0.0225	-4.3937	0.0213	-4.4467	3.230×10^{-3}	-6.3338
0.00335	0.0332	-4.0217	0.0278	-4.1993	4.408×10^{-3}	-6.0399
0.00330	0.0467	-3.6959	0.0390	-3.8759	5.664×10^{-3}	-5.8057
0.00325	0.647	-3.3868	0.0497	-3.6494	7.527×10^{-3}	-5.5377

Table S6.4(b): Average observed rate constants, $k_{obs(1^{st})}$, for the reactions of **Pt3** at varied temperatures in the range 15 to 35 °C while maintaining nucleophile concentration at ≈ 60x [**Pt3**].

1/T, K^{-1}	**SCN$^-$**		**I$^-$**		**Br$^-$**	
	$k_{obs(1^{st})}$, s^{-1}	**ln(k_2/T)**	**$k_{obs(1^{st})}$, s^{-1}**	**ln(k_2/T)**	**$k_{obs(1^{st})}$, s^{-1}**	**ln(k_2/T)**
0.00347	0.0631	-3.3446	0.0455	-3.6714	1.159 x 10^{-4}	-9.6443
0.00341	0.1079	-2.8248	0.0663	-3.3116	1.586 x 10^{-4}	-9.3477
0.00335	0.1580	-2.4607	0.0840	-3.0927	2.314 x 10^{-4}	-8.9853
0.00330	0.2095	-2.1952	0.1144	-2.8004	3.175 x 10^{-4}	-8.6881
0.00325	0.2901	-1.8861	0.1501	-2.5447	4.678 x 10^{-4}	-8.3159

Table S6.5(a): Average observed rate constants, $k_{obs(2^{nd})}$, for the reactions of **(Pt3)** at varied temperatures in the range 15 to 35 °C while maintaining nucleophile concentration at ≈ 60x [**Pt3**].

1/T, K^{-1}	**TU**		**DMTU**		**TMTU**	
	$k_{obs(2^{nd})}$, s^{-1}	**ln(k_2/T)**	**$k_{obs(2^{nd})}$, s^{-1}**	**ln(k_2/T)**	**$k_{obs(2^{nd})}$, s^{-1}**	**ln(k_2/T)**
0.00347	3.023 x 10^{-5}	-10.3797	1.314 x 10^{-5}	-11.2129	2.462 x 10^{-6}	-12.8876
0.00341	4.706 x 10^{-5}	-9.9544	1.834 x 10^{-5}	-10.8967	3.408 x 10^{-6}	-12.5797
0.0033	6.983 x 10^{-5}	-9.5766	2.628 x 10^{-5}	-10.5539	4.911 x 10^{-6}	-12.2312
0.00335	1.060 x 10^{-4}	-9.1755	3.421 x 10^{-5}	-10.2978	6.963 x 10^{-6}	-11.8987
0.00325	1.546 x 10^{-4}	-8.8148	5.128 x 10^{-5}	-9.9184	9.692 x 10^{-6}	-11.5844

Table S6.5(b): Average observed rate constants, $k_{obs(2^{nd})}$, for the reactions of **Pt3** at varied temperatures in the range 15 to 35 °C while maintaining nucleophile concentration at ≈ 60x [**Pt3**].

1/T, K^{-1}	**SCN$^-$**		**I$^-$**	
	$k_{obs(2^{nd})}$, s^{-1}	**ln(k_2/T)**	**$k_{obs(2^{nd})}$, s^{-1}**	**ln(k_2/T)**
0.00347	2.524 x 10^{-3}	-5.9550	1.993 x 10^{-6}	-13.0992
0.00341	3.648 x 10^{-3}	-5.6038	2.757 x 10^{-6}	-12.7915
0.0033	5.175 x 10^{-3}	-5.2711	4.148 x 10^{-6}	-12.4001
0.00335	6.952 x 10^{-3}	-4.9926	5.674 x 10^{-6}	-12.1035
0.00325	9.947 x 10^{-3}	-4.6507	7.962 x 10^{-6}	-11.7811

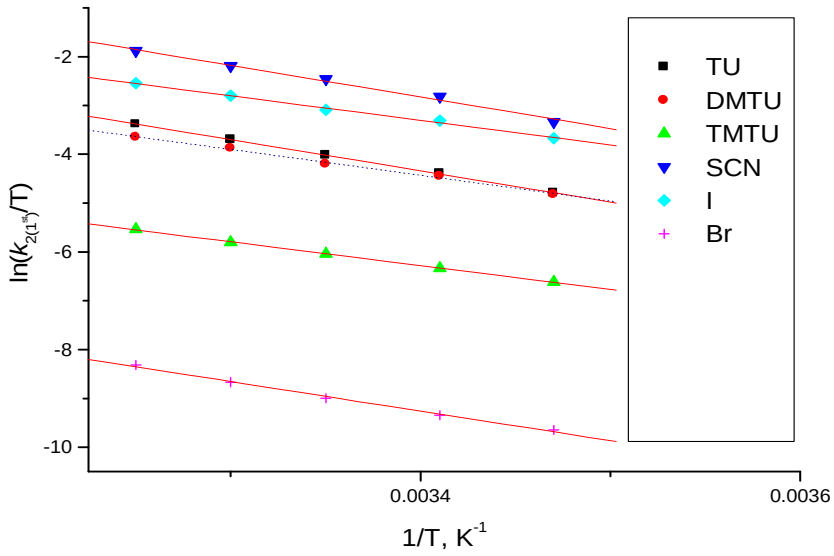

Figure S6.3: Plots of ln($k_{2(1^{st})}$/T) versus (1/T) for the first step reaction of **Pt3** with a series of different nucleophiles at varying temperatures.

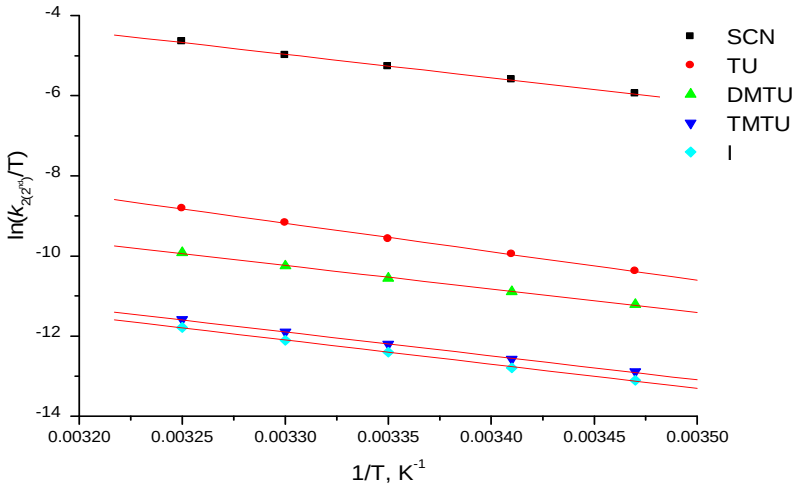

Figure S6.4: Plots of ln($k_{2(2^{nd})}$/T) versus (1/T) for the second step reaction of **Pt3** with a series of different nucleophiles at varying temperatures.

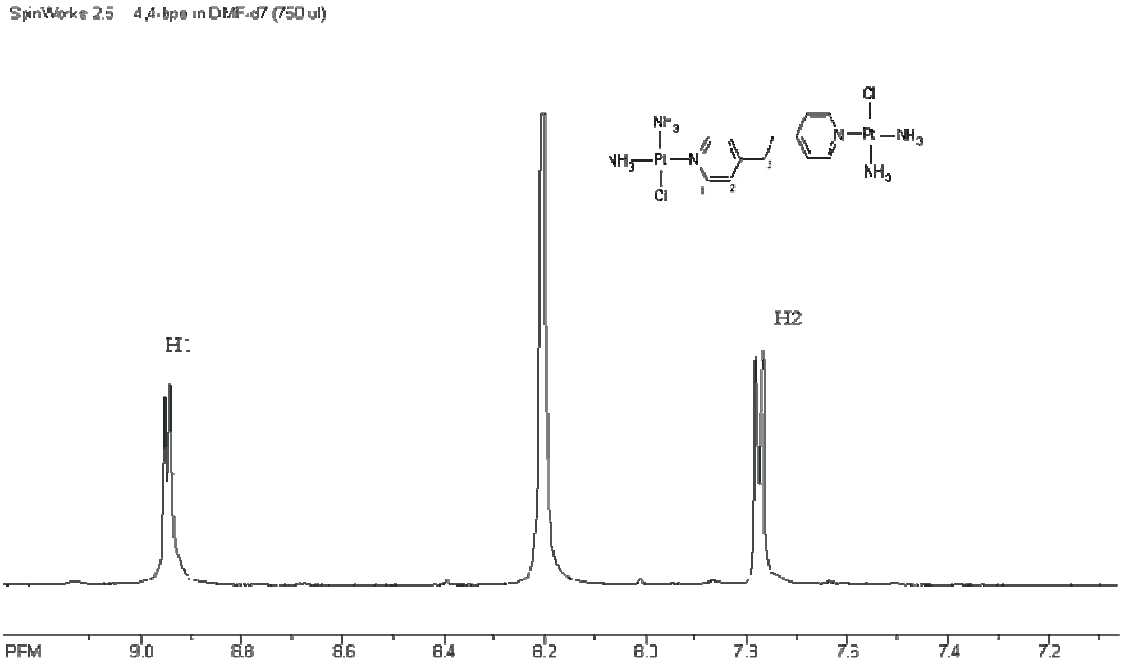

Figure S6.5: ^{1}H NMR spectrum of **Pt3–Cl** in DMF-d_7 at 30 °C

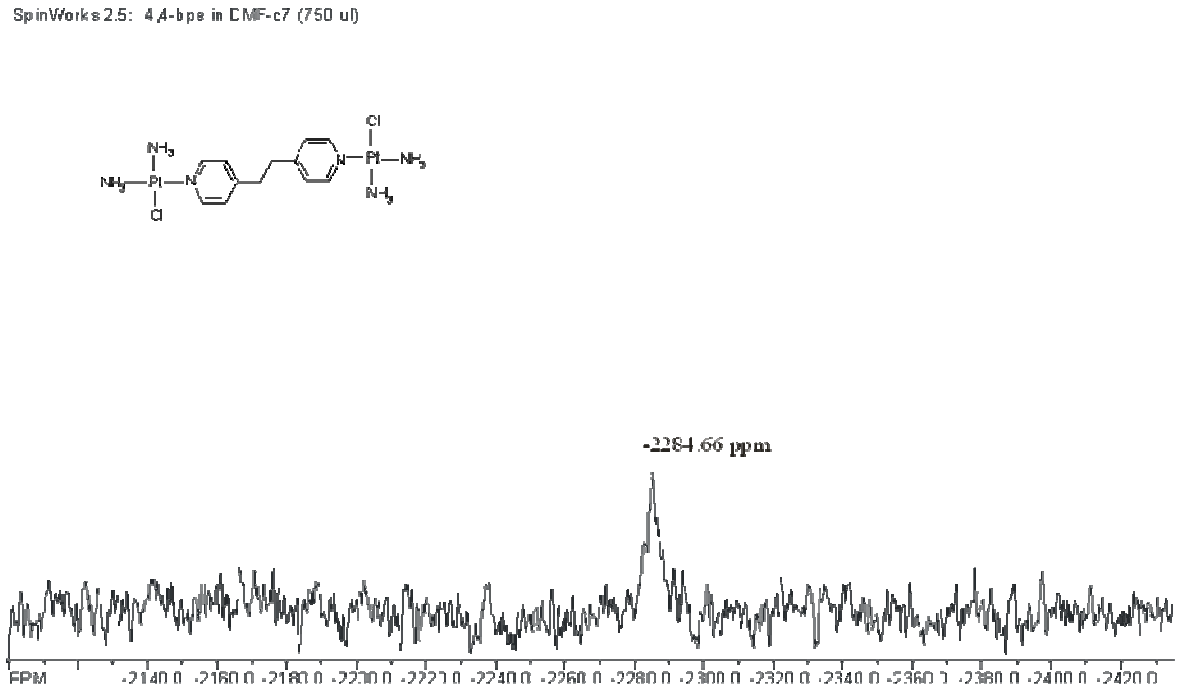

Figure S6.6:^{195}Pt NMR spectrum of **Pt3–Cl** in DMF-d_7 at 30 °C

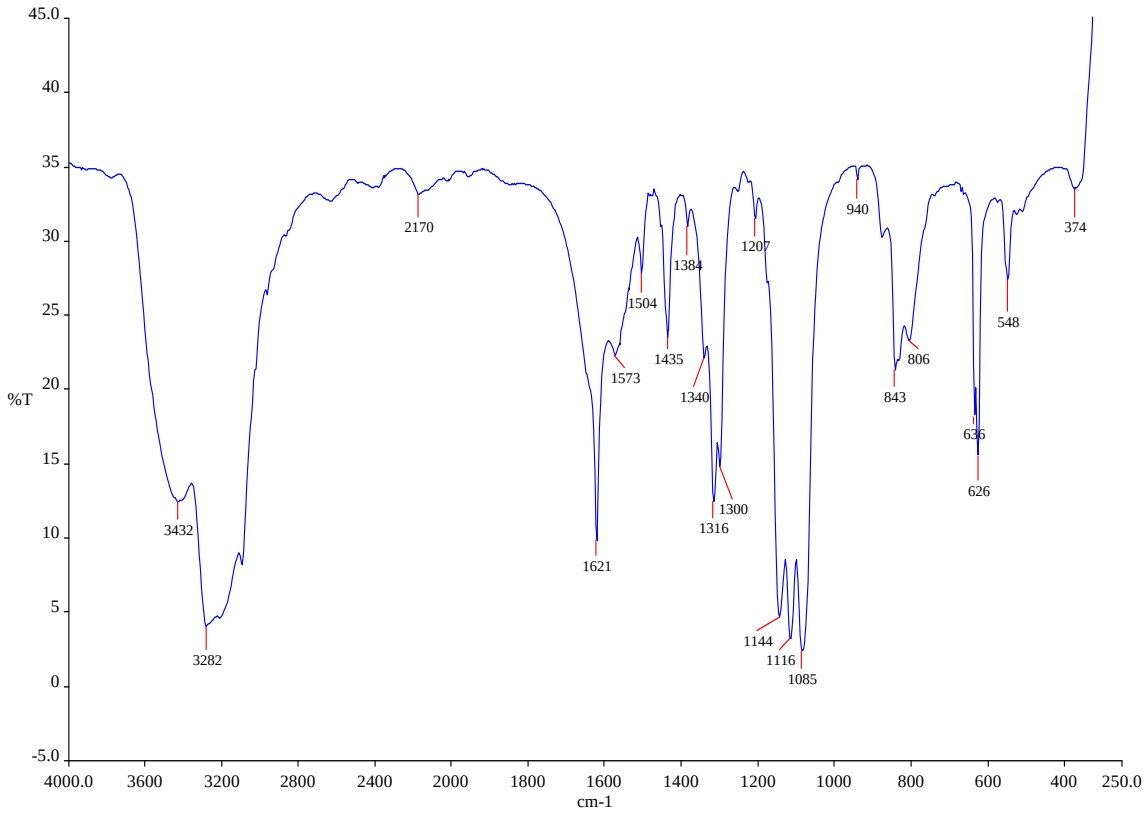

Figure S6.7: Infra red (IR, KBr disc) spectrum of **Pt3–Cl**

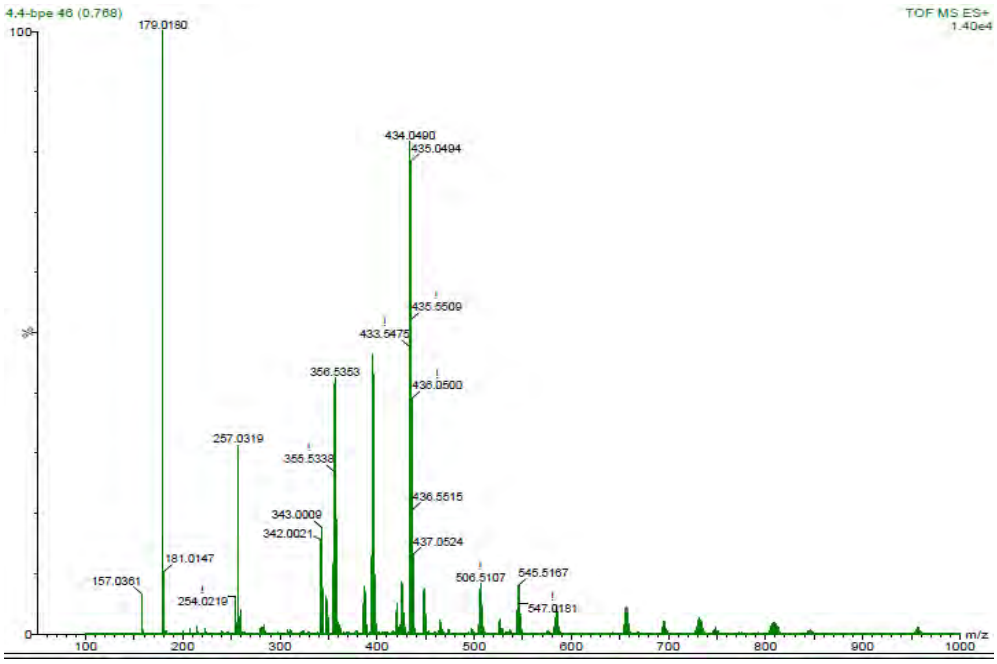

Figure S6.8: Mass spectra (TOF/ES$^+$) of complex **Pt3–Cl**.

Table S6.6: Average observed rate constants, $k_{obs(1^{st})}$, at 298.15 K, for the reactions of **Pt2** with a series of nucleophiles at different concentrations.

[NU]/ M	$\boldsymbol{k_{obs(1^{st}),s^{-1}}}$				
	TU	**DMTU**	**TMTU**	**SCN^-**	**Br^-**
0.00181	0.02952	0.02092	0.01008	0.04650	0.00226
0.00362	0.05761	0.04061	0.01882	0.12325	0.00427
0.00543	0.08435	0.06447	0.02797	0.17537	0.00679
0.00725	0.11156	0.08001	0.03737	0.24724	0.00961
0.00906	0.13447	0.09893	0.05074	0.31090	0.01201

Table S6.7: Average observed rate constants, $k_{obs(2^{nd})}$, at 298.15 K, for the reactions of **Pt2** with a series of nucleophiles at different concentrations.

[NU]/ M	$k_{obs(2^{nd}),}\ s^{-1}$			
	TU	**DMTU**	**TMTU**	**SCN^-**
0.00181	6.1692×10^{-5}	2.6921×10^{-5}	4.7605×10^{-5}	3.554×10^{-5}
0.00362	1.3311×10^{-4}	5.1852×10^{-5}	9.1658×10^{-5}	6.845×10^{-5}
0.00543	1.9063×10^{-4}	7.7446×10^{-5}	1.3553×10^{-4}	1.022×10^{-4}
0.00725	2.5717×10^{-4}	1.0416×10^{-4}	1.7934×10^{-4}	1.375×10^{-4}
0.00906	3.1888×10^{-4}	1.2887×10^{-4}	2.2486×10^{-4}	1.701×10^{-4}

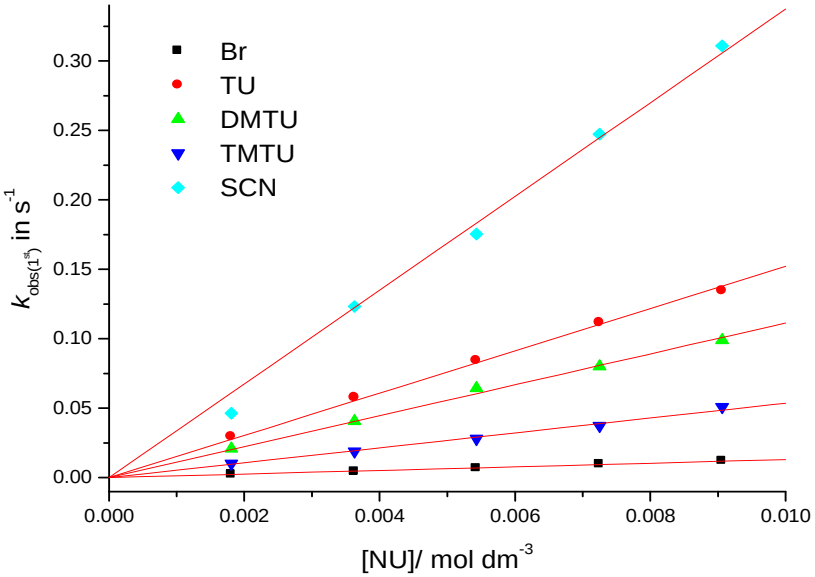

Figure S6.9: Concentration dependence of $k_{obs(1^{st})}$ for the simultaneous substitution of aqua ligands in **Pt2** by thiourea nucleophiles and ionic nucleophiles at pH = 2.0, T = 298.15 K, I = 0.10 M (0.01 M $HClO_4$, adjusted with $NaClO_4$).

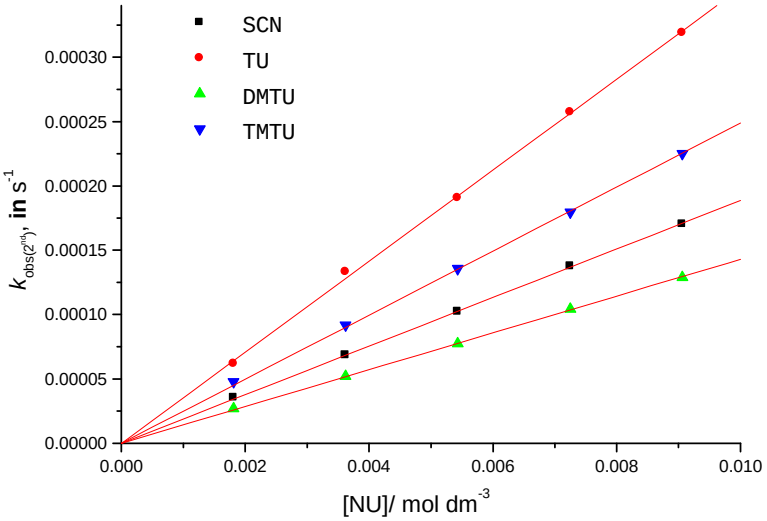

Figure S6.10: Concentration dependence of $k_{obs(2^{nd})}$ for the dissociation of bridging ligand in **Pt2** by thiourea nucleophiles and ionic nucleophiles at pH = 2.0, T = 298.15 K, I = 0.10 M (0.01 M $HClO_4$, adjusted with $NaClO_4$).

Table S6.8(a): Average observed rate constants, $k_{obs(1^{st})}$, for the reactions of **Pt2** at varied temperatures in the range 15 to 35 °C while maintaining nucleophile concentration at ≈ 60x [**Pt2**].

1/T, K^{-1}	**TU**		**DMTU**		**TMTU**	
	$k_{obs(1^{st})}$, s^{-1}	**ln(k_2/T)**	**$k_{obs(1^{st})}$, s^{-1}**	**ln(k_2/T)**	**$k_{obs(1^{st})}$, s^{-1}**	**ln(k_2/T)**
0.00347	0.01480	-4.6603	1.206 x 10^{-4}	-9.4701	1.182 x 10^{-3}	-7.1879
0.00341	0.02248	-4.2595	—	—	1.579 x 10^{-3}	-6.9155
0.00335	0.03317	-3.8895	2.292 x 10^{-4}	-8.8621	2.391 x 10^{-3}	-6.5174
0.00330	0.04672	-3.5615	3.336 x 10^{-4}	-8.4712	3.183 x 10^{-3}	-6.2479
0.00325	0.06468	-3.2526	4.477 x 10^{-4}	-8.2257	4.461 x 10^{-3}	-5.9267

Table S6.8(b): Average observed rate constants, $k_{obs(1^{st})}$, for the reactions of **Pt2** at varied temperatures in the range 15 to 35 °C while maintaining nucleophile concentration at ≈ 60x [**Pt2**].

1/T, K^{-1}	**SCN$^-$**		**Br$^-$**	
	$k_{obs(1^{st})}$, s^{-1}	**ln(k_2/T)**	**$k_{obs(1^{st})}$, s^{-1}**	**ln(k_2/T)**
0.00341	7.130 x 10^{-4}	-7.7104	1.141 x 10^{-4}	-9.5428
0.00335	1.217 x 10^{-3}	-7.1929	1.872 x 10^{-4}	-9.0646
0.00330	1.880 x 10^{-3}	-6.7743	3.148 x 10^{-4}	-8.5613
0.00325	2.833 x 10^{-3}	-6.3805	4.908 x 10^{-4}	-8.1338

Table S6.9: Average observed rate constants, $k_{obs(2^{nd})}$, for the reactions of **Pt2** at varied temperatures in the range 15 to 35 °C while maintaining nucleophile concentration at ≈ 60x [**Pt2**].

1/T, K^{-1}	**TU**		**DMTU**		**TMTU**		**SCN$^-$**	
	$k_{obs(2^{nd})}$, 10^{-4} s^{-1}	**ln(k_2/T)**	**$k_{obs(2^{nd})}$, 10^{-4} s^{-1}**	**ln(k_2/T)**	**$k_{obs(2^{nd})}$, 10^{-4} s^{-1}**	**ln(k_2/T)**	**$k_{obs(2^{nd})}$, 10^{-3} s^{-1}**	**ln(k_2/T)**
0.00347	1.0005	-9.6570	0.2768	-10.942	0.3521	-10.701	2.5339	-6.4291
0.00341	1.4024	-9.3365	0.4490	-10.476	0.4993	-10.369	3.6482	-6.0779
0.00335	2.1253	-8.9376	0.6802	-10.077	0.7280	-10.009	5.1750	-5.7452
0.00330	3.0225	-8.6022	1.0499	-9.6596	1.0283	-9.6804	6.9517	-5.4667
0.00325	4.2855	-8.2694	1.5539	-9.2912	1.3610	-9.4164	9.9468	-5.1248

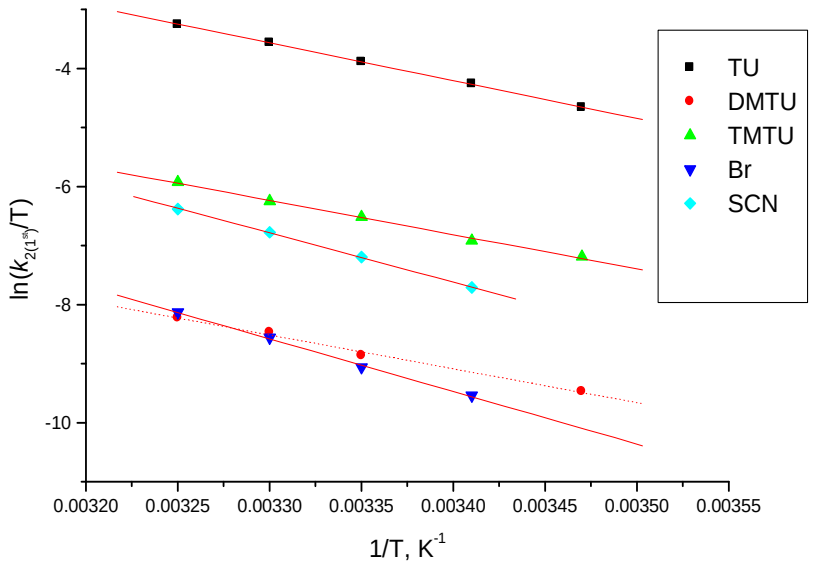

Figure S6.11: Plots of ln($k_{2(1^{st})}$/T) versus (1/T) for the first step reaction of **Pt2** with a series of different nucleophiles at varying temperatures.

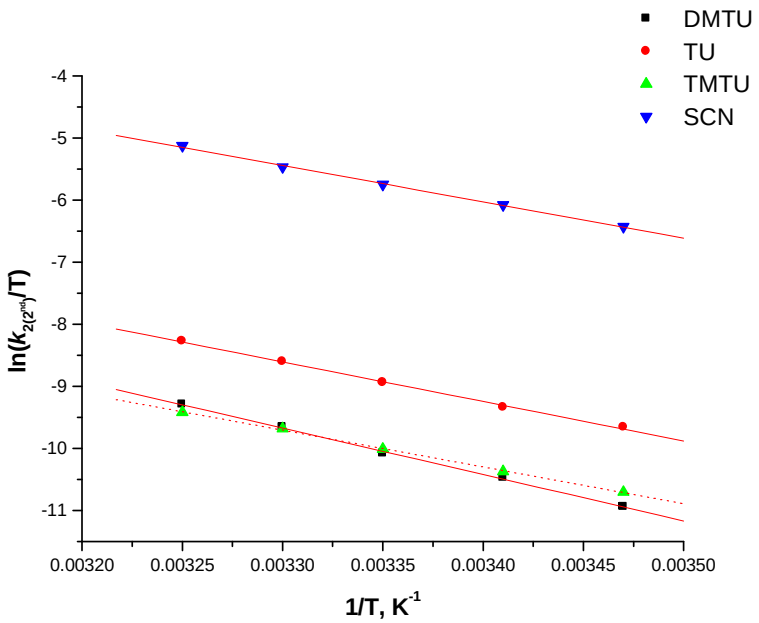

Figure S6.12: Plots of $\ln(k_{2(2^{nd})}/T)$ versus $(1/T)$ for the second step reaction of **Pt2** with a series of different nucleophiles at varying temperatures.

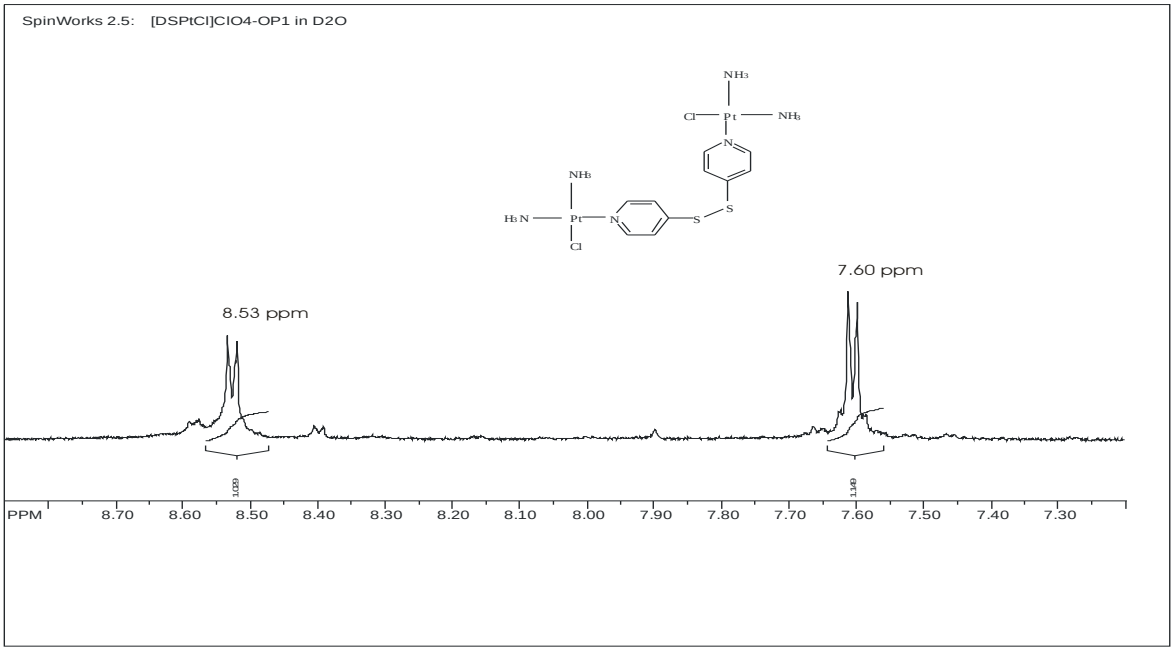

Figure S6.13: ^{1}H NMR spectrum of **Pt2–Cl** in DMF-d_7 at 30 °C

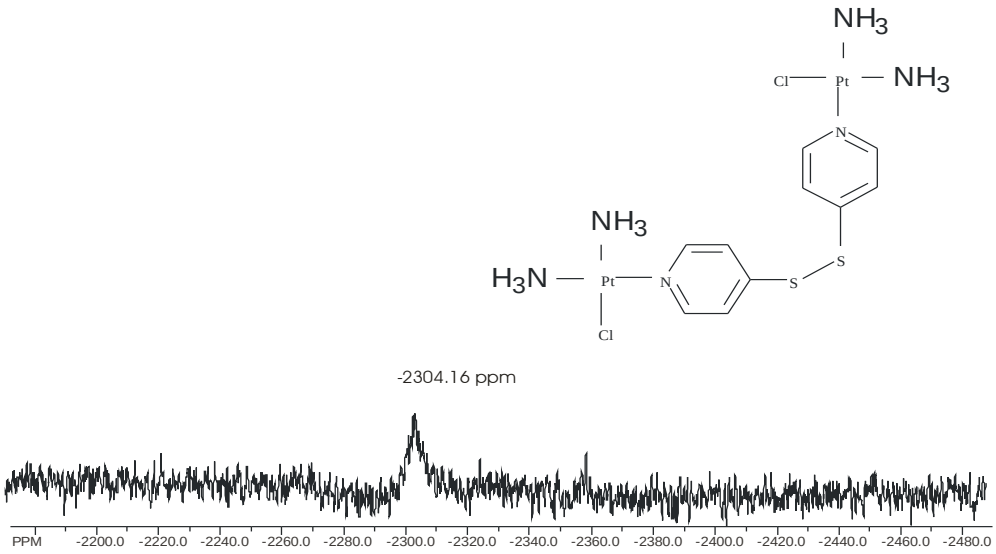

Figure S6.14: ^{195}Pt NMR spectrum of **Pt2–Cl** in DMF-d_7 at 30 °C

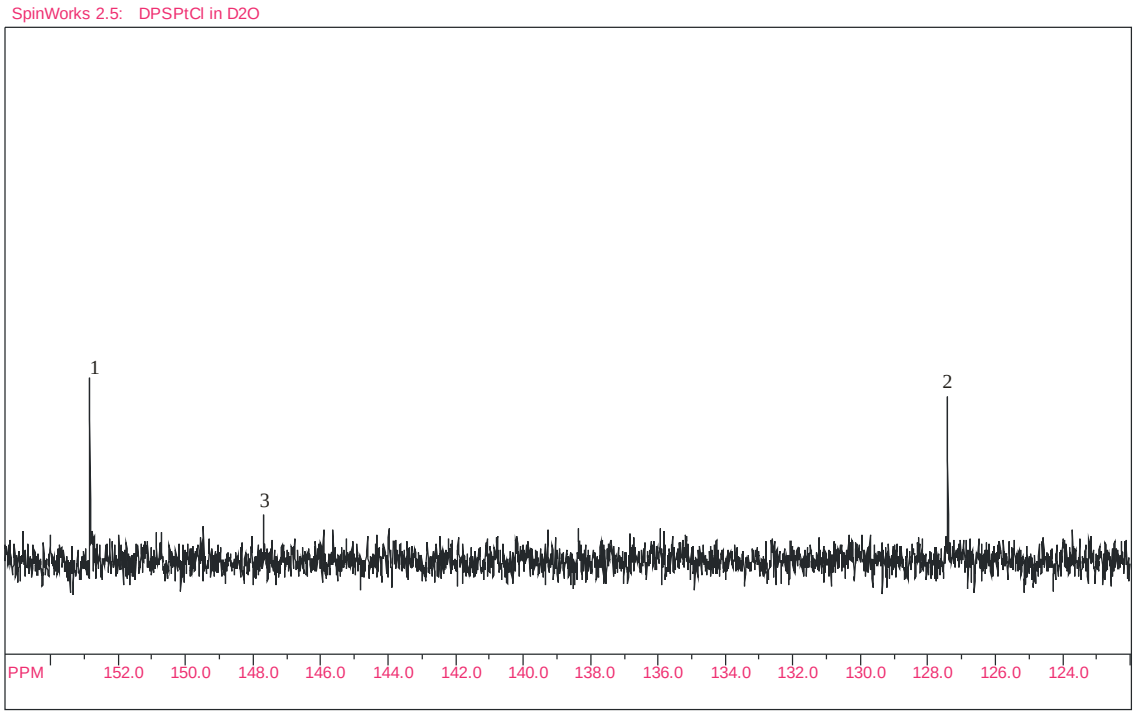

Figure S6.15: ^{13}C NMR spectrum of **Pt2–Cl** in D_2O at 30 °C

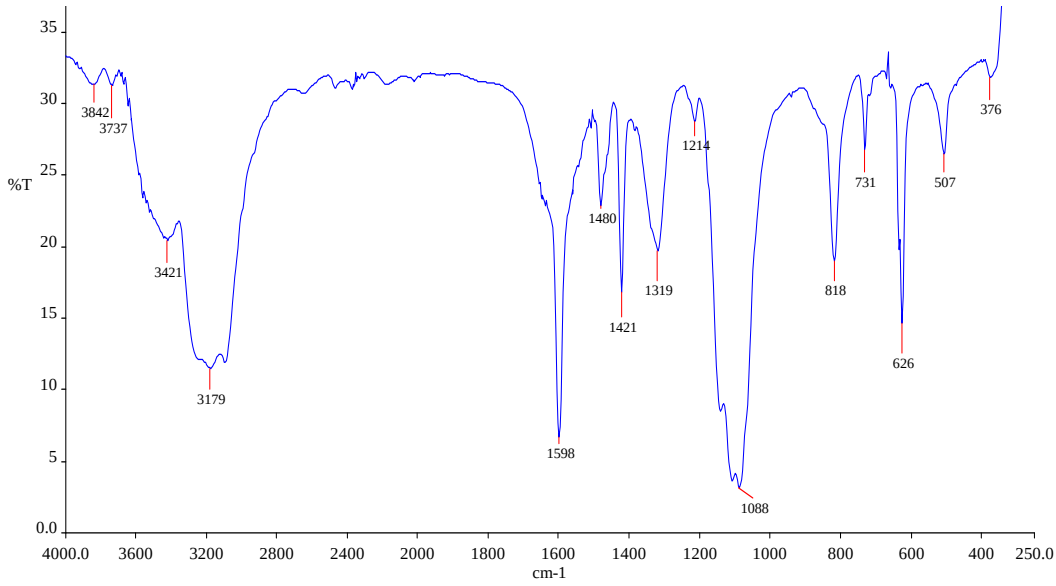

Figure S6.16: Infra red (IR) spectrum of **Pt2–Cl** in KBr disc

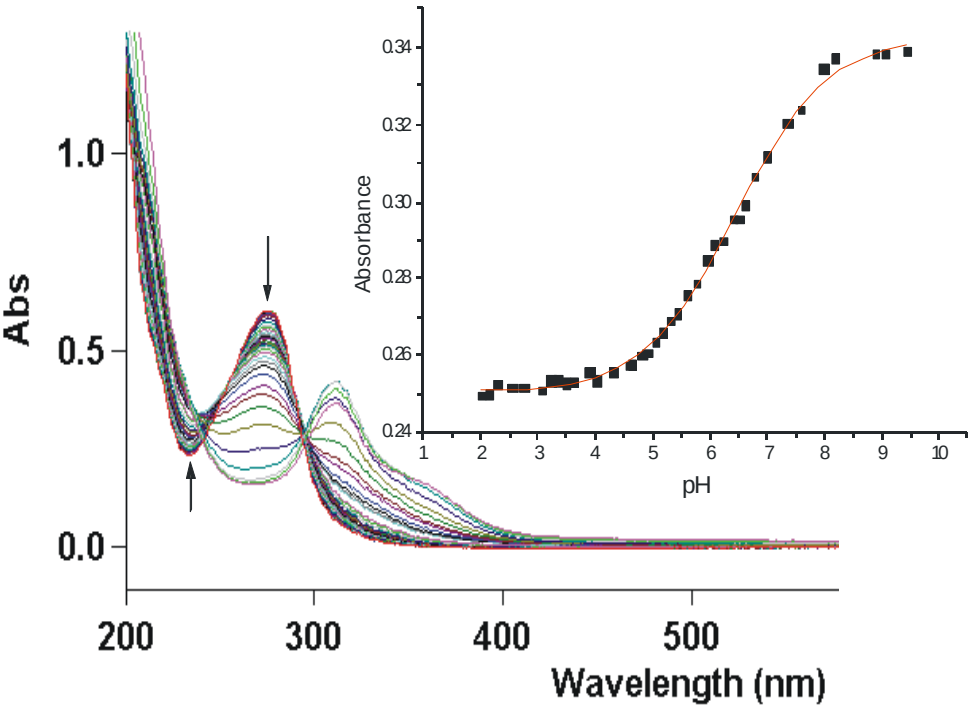

Figure S6.17: Uv-Vis spectrophotometric titration curve of **Pt2** with NaOH in the pH range 2-10, I = 1.0 M ($NaClO_4$), T = 25 °C. Inset: plot of Absorbance vs pH at 238 nm.

Table S6.10: Average observed rate constants, $k_{obs(1^{st})}$, at 298.15 K, for the reactions of **Pt1** with a series of nucleophiles at different concentrations.

[NU]/ M	$k_{obs(1^{st}),s^{-1}}$				
	TU	**DMTU**	**TMTU**	**SCN^-**	**Br^-**
0.00112	0.00367	0.00325	8.232×10^{-4}	0.00186	4.135×10^{-5}
0.00225	0.00791	0.00622	0.00145	0.00299	8.386×10^{-5}
0.00338	0.01105	0.00876	0.00204	0.00476	1.197×10^{-4}
0.00450	0.01457	0.01145	0.00286	0.00598	1.597×10^{-4}
0.00562	0.01917	0.01528	0.00371	0.00796	2.077×10^{-4}

Table S6.11: Average observed rate constants, $k_{obs(2^{nd})}$, at 298.15 K, for the reactions of **Pt1** with a series of nucleophiles at different concentrations

[NU]/ M	$k_{obs(1^{st}),s^{-1}}$			
	TU	**DMTU**	**TMTU**	**SCN^-**
0.0112	1.0848×10^{-4}	5.2685×10^{-5}	8.1784×10^{-5}	4.7272×10^{-5}
0.0025	2.1573×10^{-4}	1.1820×10^{-4}	1.6592×10^{-4}	8.7770×10^{-5}
0.00338	3.2998×10^{-4}	1.7383×10^{-4}	2.4546×10^{-4}	1.3093×10^{-4}
0.0045	4.6576×10^{-4}	2.3680×10^{-4}	3.0170×10^{-4}	1.7552×10^{-4}
0.00562	5.8060×10^{-4}	2.8611×10^{-4}	4.0660×10^{-4}	2.1694×10^{-4}

Table S6.12(a): Average observed rate constants, $k_{obs(1^{st})}$, for the reactions of **Pt1** at varied temperatures in the range 15 to 35 °C while maintaining nucleophile concentration at ≈ 60x [**Pt1**].

1/T, K^{-1}	**TU**		**DMTU**		**TMTU**	
	$k_{obs(1^{st})}$, s^{-1}	**ln(k_2/T)**	**$k_{obs(1^{st})}$, s^{-1}**	**ln(k_2/T)**	**$k_{obs(1^{st})}$, s^{-1}**	**ln(k_2/T)**
0.00341	1.0020 x 10^{-3}	-6.8961	7.1300 x 10^{-4}	-7.0363	1.2210 x 10^{-3}	-6.6984
0.00335	1.6610 x 10^{-3}	-6.4075	1.2167 x 10^{-3}	-6.6188	1.8849 x 10^{-3}	-6.2788
0.00330	2.3843 x 10^{-3}	-6.0627	2.4334 x 10^{-3}	-6.2428	2.5404 x 10^{-3}	-5.9993
0.00325	3.4351 x 10^{-3}	-5.7139	2.8330 x 10^{-3}	-5.9065	3.8539 x 10^{-3}	-5.5989

Table S6.12(b): Average observed rate constants, $k_{obs(1^{st})}$, for the reactions of **Pt1** at varied temperatures in the range 15 to 35 °C while maintaining nucleophile concentration at ≈ 60x [**Pt1**].

1/T, K^{-1}	**SCN$^-$**		**Br$^-$**	
	$k_{obs(1^{st})}$, s^{-1}	**ln(k_2/T)**	**$k_{obs(1^{st})}$, s^{-1}**	**ln(k_2/T)**
0.00341	7.1302 x 10^{-4}	-7.2363	8.5550 x 10^{-5}	-9.3567
0.00335	1.2167x 10^{-3}	-6.7188	1.4624 x 10^{-4}	-8.8375
0.00330	1.5558 x 10^{-3}	-6.4896	2.1610 x 10^{-4}	-8.4636
0.00325	2.4920 x 10^{-3}	-6.0349	3.8147 x 10^{-4}	-7.9117

Table S6.13: Average observed rate constants, $k_{obs(2^{nd})}$, for the reactions of **Pt1** at varied temperatures in the range 15 to 35 °C while maintaining nucleophile concentration at ≈ 60x [**Pt1**].

1/T, K^{-1}	**TU**		**DMTU**		**TMTU**		**SCN$^-$**	
	$k_{obs(2^{nd})}$, 10^{-4} s^{-1}	**ln(k_2/T)**	**$k_{obs(2^{nd})}$, 10^{-4} s^{-1}**	**ln(k_2/T)**	**$k_{obs(2^{nd})}$, 10^{-4} s^{-1}**	**ln(k_2/T)**	**$k_{obs(2^{nd})}$, 10^{-4} s^{-1}**	**ln(k_2/T)**
0.00347	0.7128	-9.5220	0.3344	-10.279	0.2856	-10.4365	0.3363	-10.2731
0.00341	0.9226	-9.2812	0.4899	-9.9142	0.4248	-10.0568	0.5048	-9.8843
0.00335	1.312	-8.9457	0.6688	-9.6198	0.6143	-9.7049	0.8724	-9.3541
0.00330	1.958	-8.5623	1.0243	-9.2102	0.8726	-9.3705	1.2835	-8.9846
0.00325	2.736	-8.2439	1.4646	-8.869	1.1887	-9.0777	1.9770	-8.5690
0.00319	—	—	—	—	1.5081	-8.8558	—	—

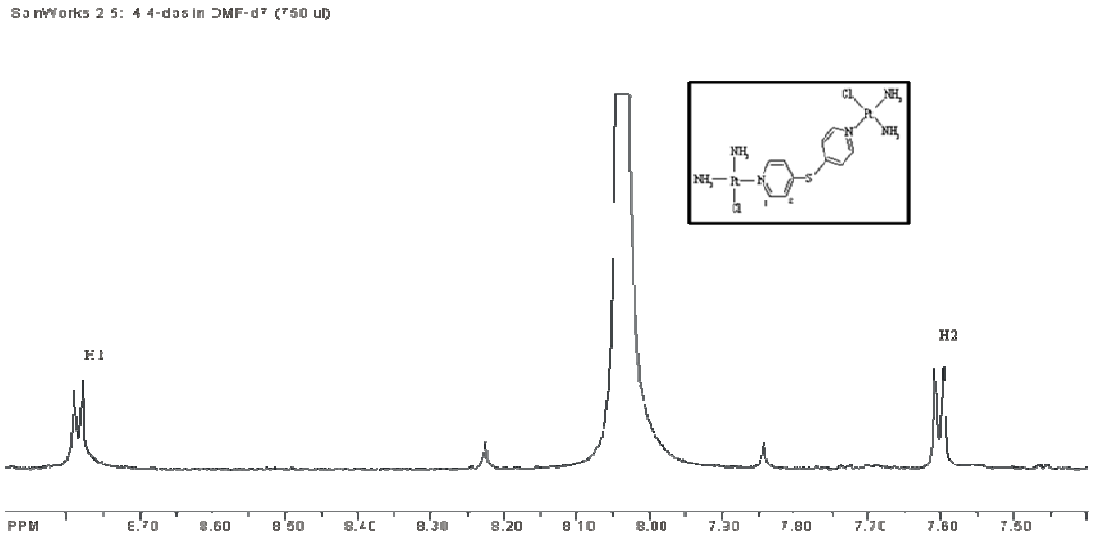

Figure S6.18: ^{1}H NMR spectrum of **Pt1–Cl** in DMF-d_7 at 30 °C

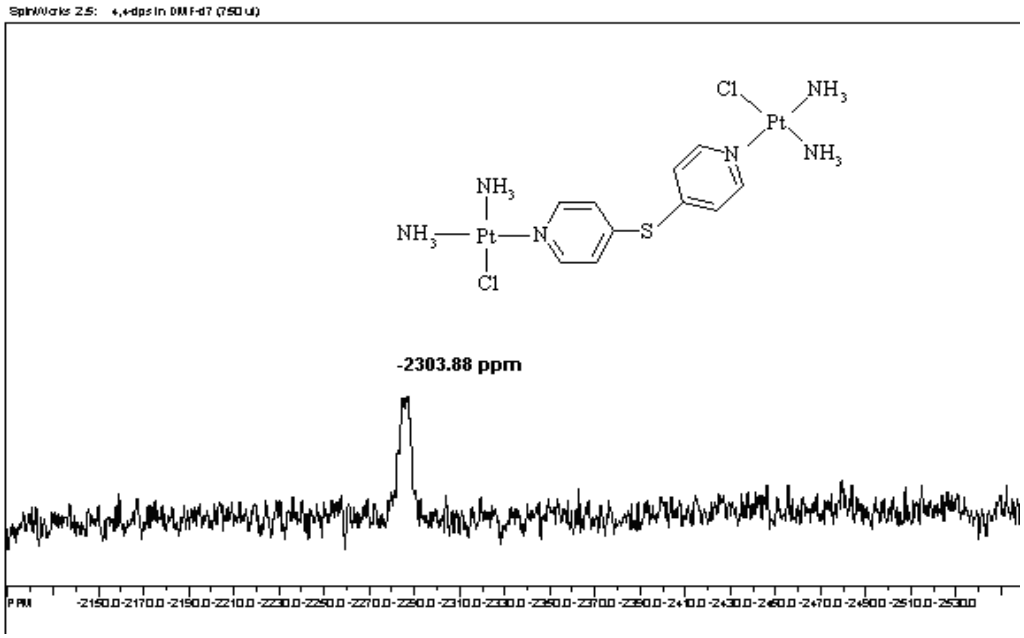

Figure S6.19: ^{195}Pt NMR spectrum of **Pt2–Cl** in DMF-d_7 at 30 °C

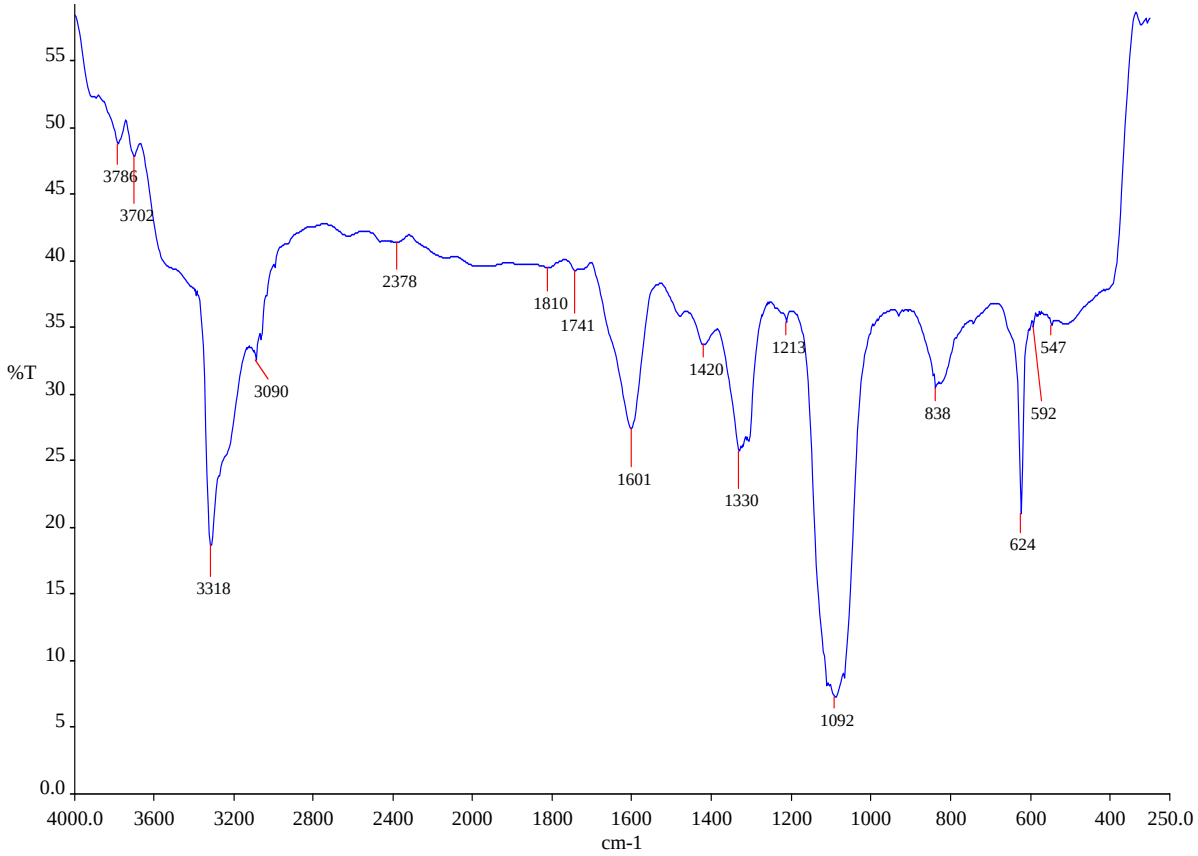

Figure S6.20: Infra red (IR, KBr disc) spectrum of **Pt2–Cl**.

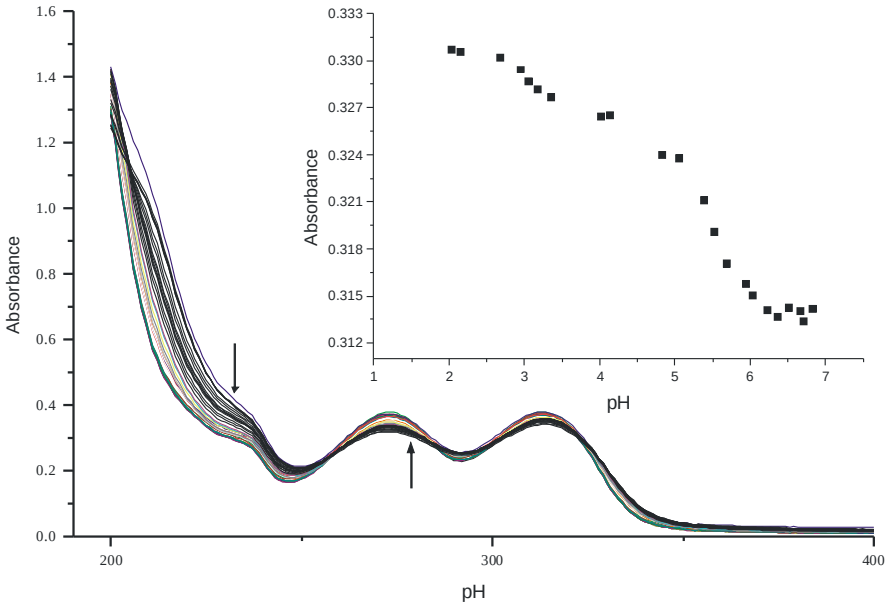

Figure S6.21: UV-Vis spectrophotometric titration curve of **Pt1** with NaOH in the pH range 2-9, I = 1.0 M ($NaClO_4$), T = 25 °C. Inset: plot of Absorbance vs pH at 280 nm.

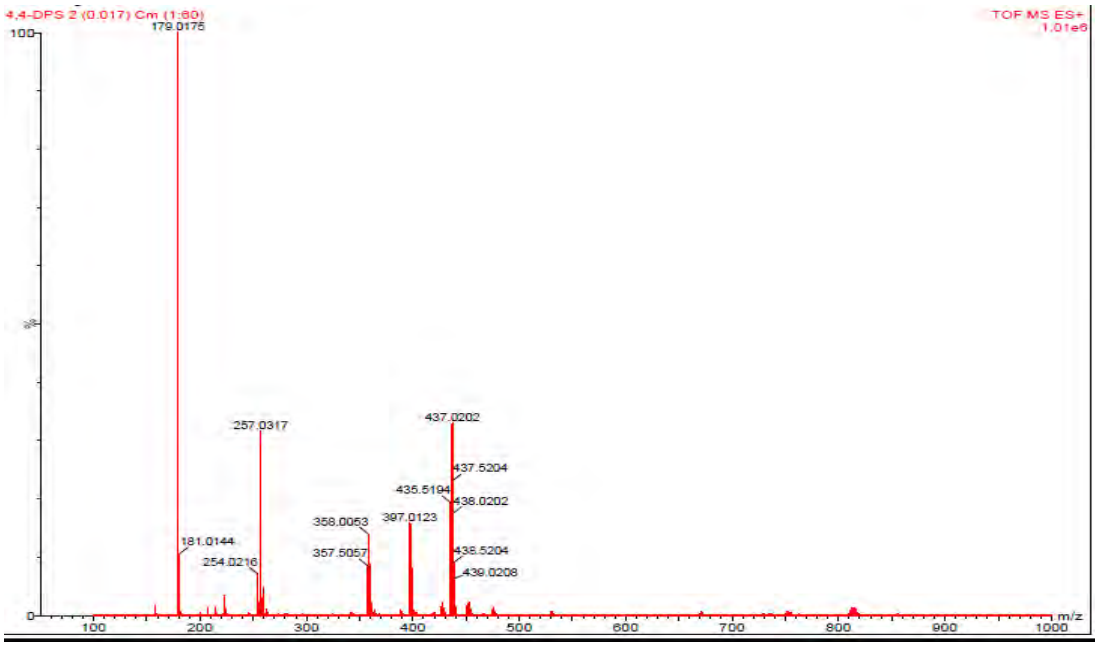

Figure S6.22: Mass spectrum for complex **Pt1–Cl**

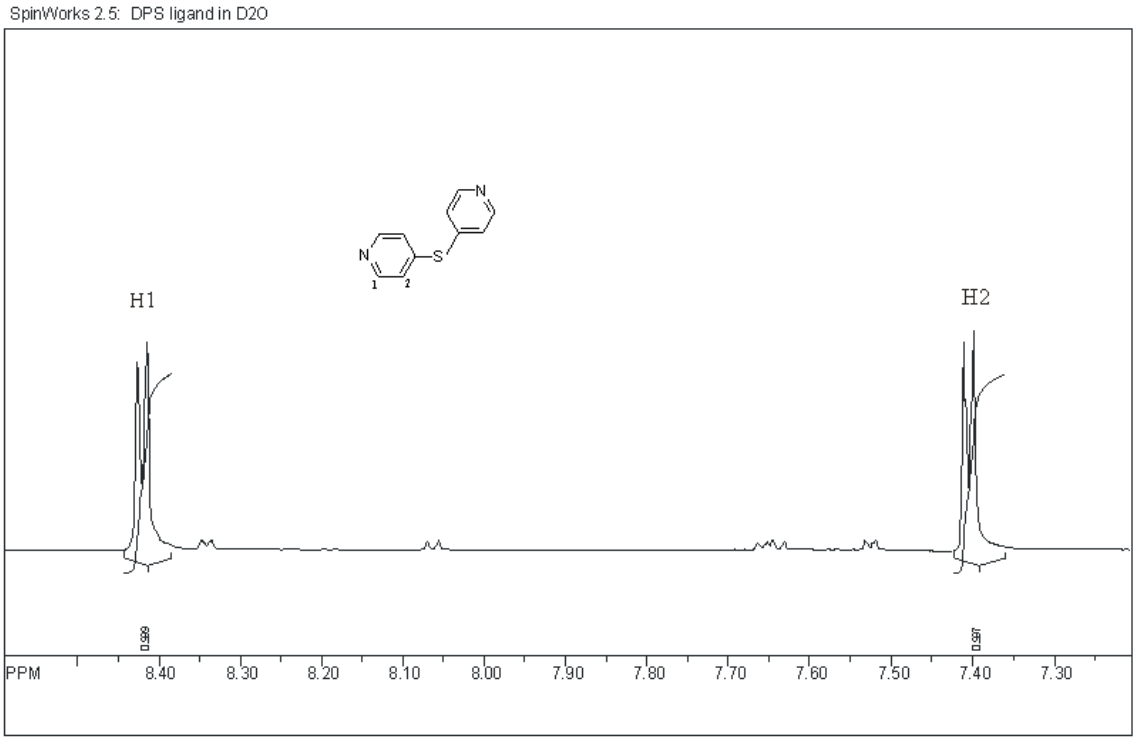

Figure S6.23: ^{1}H NMR spectrum of 4,4'-dipyridine ligand in D_2O at 30 °C

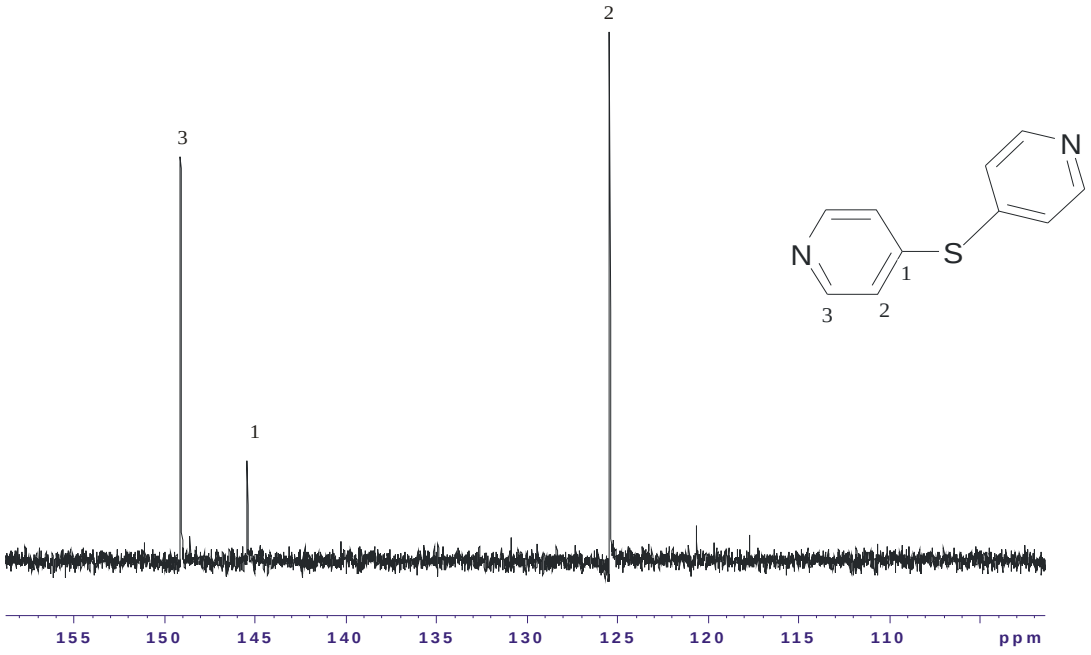

Figure S6.24: ^{13}C NMR spectrum of 4,4'-dipyridine ligand in D_2O at 30 °C

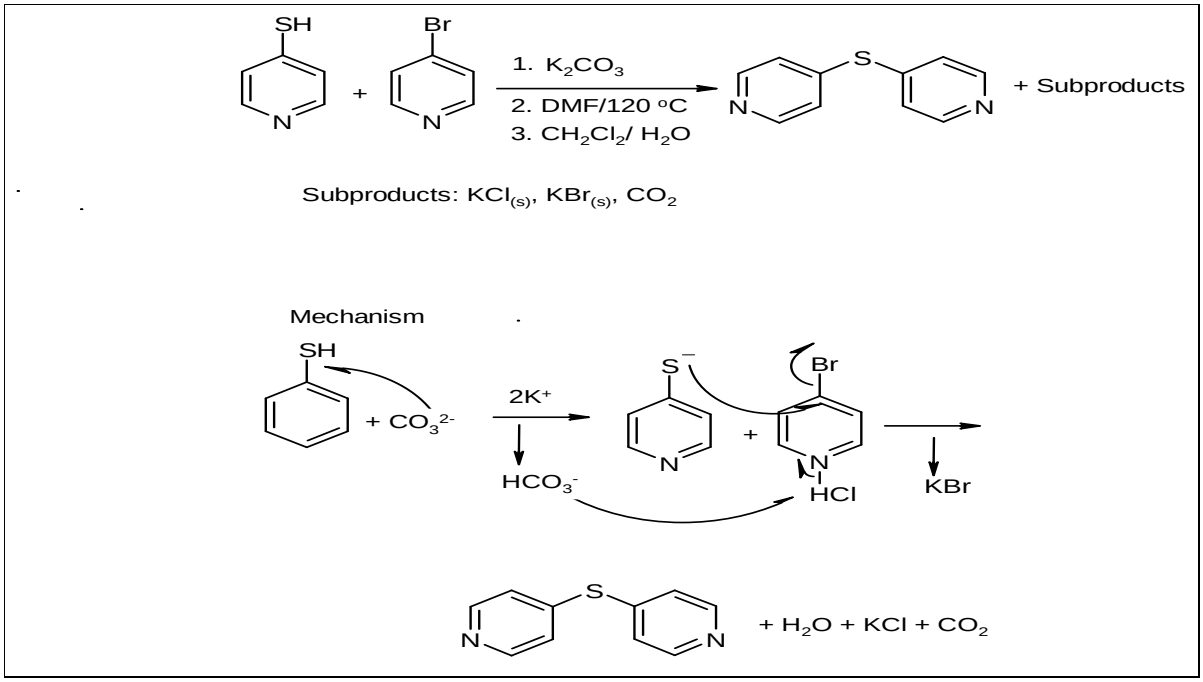

Scheme S6.1: Sythetic path and mechanism for 4,4'-Dipyridinesulphide ligand.

Table of Contents-7

List of Figures

List of Tables

Chapter 7

The Influence of α,ω-Diamine Linker on Ligand Substitution of Dinuclear Pt(II) Complexes: *A Thermodynamic and Kinetic Study*

7.0 Abstract

Substitution of the coordinated water molecules from the **[{*cis*–Pt(NH$_3$)$_2$H$_2$O}$_2$–μ–NH$_2$(CH$_2$)$_n$NH$_2$]$^{+4}$** (n = 2, 3, 4, 6, 8, 10) complexes: **EnPt**, **PropPt**, **ButPt**, **HexPt**, **OctPt** and **DecPt** with S-donor nucleophiles of different steric demand, thiourea (TU), *N*,*N*-dimethyl-2-thiourea (DMTU) and *N*,*N*,*N*,*N*-tetramethylthiourea (TMTU) was studied under *pseudo* first-order conditions as a function of concentration and temperature, using stopped-flow and UV–Vis Spectrophotometric techniques. The substitution reaction proceeded in two steps: simultaneous substitution of the aqua ligands and subsequently, release of the ammine ligand in the *trans*-position by the strong *trans*–*effect* of the coordinated thiourea, with each of the steps being sensitive to steric and σ-electronic properties of the alkanediamine linker. A comparison of the second-order rate constants, $k_{2,1^{st}}$ and $k_{2,2^{nd}}$, shows that the rate constants of the first step are 1-2 orders of magnitude larger than those of the second step in all cases.

The pK_a of the coordinated water molecules in the complexes were determined by spectrophotometric acid-base titrations. The obtained pK_a values clearly demonstrated their dependency on the σ-donor capacity of the bridging ligand which increases with increasing aliphatic chain length. This effect reflects a less electrophilic and less acidic Pt(II) centre as the aliphatic chain is increased further. This relationship shows also that the calculated second-order rate constants decreases as the alkanediamine chain length is increased from **EnPt** to **DecPt**. The experimental data is supported by the Density Functional theory (DFT) calculated data, where reduction in the NBO charges on the Pt atom and increased HOMO-LUMO energy gap in the ground state of the Pt(II) complexes clearly demonstrates an increase in the σ-inductive effect of the alkanediamine bridging ligand, thereby leading to a less reactive metal centre. The large negative values of activation entropy, $\Delta S^{\neq}$, confirmed an associative mode of substitution mechanism for both steps. Proton (^{1}H) and ^{195}Pt NMR spectroscopy established that α,ω-alkanediamine

linker remained coordinated to the metal centres possibly due to their *cis* geometry to the incoming thiourea nucleophiles.

7.1 Introduction

The anticancer properties of *cis* diamine platinum(II) compounds is now well known since *cis*-diamminedichloridoplatinum(II), *cis*-$Pt(NH_3)_2Cl_2$, (cisplatin) and its analogues oxaliplatin and carboplatin[1] are effective anti-tumour agents. They have been used either singularly or in combination in the treatment of many tumours such as testicular, ovarian, cervical, head/neck and colorectal cancer.[2-7] However, their clinical use has been compromised by severe side effects *e.g.* nausea, ear damage, loss of sensation in hands, vomiting, kidney toxicity,[8-11] and the emergence of platinum resistance, especially those caused by the reduction of intracellular accumulation. These limitations have stimulated great interest in the development of new platinum compounds; approximately 30,000 new platinum complexes have been synthesised and screened with the intention of overcoming cisplatin resistance or enlarging the spectrum of activity.[10-13] Part of the search includes understanding the kinetics and thermodynamic properties of the platinum complexes for a better understanding of the mechanistic pathway of these reactions in biological systems.

Multinuclear Pt(II) complexes represent a novel class of compounds that have shown great potential in cancer chemotherapy.[14] This family includes dinuclear complexes consisting of two or more platinum(II) centres that are bridged by long and flexible aliphatic diamine chains,[15,16] rigid aromatic diamines such as azoles,[17] diazines[18] or, a semi-rigid linker like 4,4′-dipyrazolylmethane[19] and 4,4′-methylenedianiline[14] structural groups, and the trinuclear $[\{trans\text{-}Pt(NH_3)_2\}_2(\mu\text{-}trans\text{-}Pt(NH_3)_2\{NH_2(CH_2)_nNH_2\}_2]^{+4}$ (1,0,1/*t,t,t*, n = 6, or **BBR3464**), which has entered phase II clinical evaluation.[20,21] Collectively, multinuclear platinum(II) complexes exhibit a significantly different binding mechanism to DNA that involves electrostatic and hydrogen bonding interactions with polyanionic DNA,[22] and therefore, display attractive biological properties over classical drugs cisplatin and its analogues. For instance, the overall high charge coupled to flexibility and lipophilicity of the linker chains, confers improved water solubility and enhanced cellular drug uptake. Furthermore, because of the markedly longer distances between the leaving groups, these complexes are capable of forming long-range (Pt, Pt)

interstrand and *intrastrand* DNA adducts that are more difficult to repair by the cellular proteins, and could lead to enhanced cytotoxicity.[23-25]

Nonetheless, the actual contribution of the bridge, *i.e*. its steric and electronic properties, to the mechanism of the substitution of the leaving group remains unclear, especially in dinuclear Pt(II) complexes in which the carbon chain length of α,ω-alkanediamine linker is varied. Results from recent studies by Jaganyi *et al*.,[26] Hoffmann *et al.* [27] and Farrell *et al*.,[28] have shown that the reactivity of dinuclear Pt(II) complexes bridged by flexible α,ω-alkanediamines is dependent on the average distance separating the Pt(II) centres, and decreases as the length of the aliphatic chain is increased. More importantly, the molecular geometry and symmetry adopted by these type of complexes is another critical factor controlling the reactivity of the Pt(II) centres.[27,29,30] In particular, studies indicate that **BBR3464** and its analogues, which have monodentate amine ligands around the platinum(II) centres and leaving groups in *trans* geometry to the alkanediamine linker, are degraded *in vitro* through liberation of the alkanediamine bridge under the strong *trans*-influence of coordinated sulphur and nitrito nucleophiles,[2,31] leading to substitution of the Pt–Cl bond.[32] In contrast, the *cis* geometry as in 1,1/*c,c* dinuclear structure [*cis*-{$Pt(NH_3)_2Cl$}$_2$-μ-Y]$^{+n}$, exhibits enhanced stability to metabolic deactivation; the reactions are slower than their *trans*-counterparts, but eventually the NH_3 group *trans*- to the sulphur atom is lost because of the strong labilising Pt–S bond.[33] However, 1,1/c,c compounds based on 1,2-diaminecyclohexane (dach) as the carrier ligand show enhanced robustness attributable to the chelate effect of the dach ring.[34,35]

A great attention has been so far paid mostly to multinuclear *trans* Pt(II) complexes whose clinical application is limited due to their lowered stability to metabolic deactivation. In an effort to gain more insight into the role of the flexible α,ω-diaminealkane linker on reactivity of each of the two platinum(II) centres of the dinuclear *cis*-Pt(II) complexes, this study was undertaken using the complexes presented in *Scheme* 7.1, by measurement of the pK_a values of the coordinated water ligands in their aquated derivatives, and also substitution reactions using sulphur nucleophiles thiourea (TU), *N*,*N*-dimethylthiourea (DMTU), and *N*,*N*,*N*,*N*-tetramethylthiourea (TMTU). Deprotonation of the aquated complexes to give hydroxo complexes is of interest because the latter complexes are less reactive than the aqua

complexes, have a lower charge and will associate differently with the DNA. In addition, Density Functional Theory (DFT) calculations were performed on the geometry–optimised structures of the studied complexes.

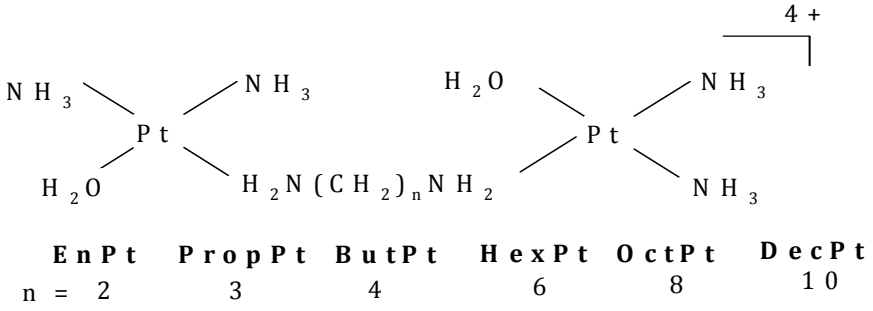

Scheme 7.1: Structures and abbreviations of the investigated dinuclear Pt(II) complexes

7.2 Experimental Section

Chemicals: *Cis*platin (*cis*-$PtCl_2(NH_3)_2$, 99%) was purchased from Strem Chemicals. The nucleophiles, *viz*. thiourea (TU, 99%), *N*,*N*-dimethyl-2-thiourea (DMTU, 99%), *N*,*N*,*N*,*N*-tetramethyl-2-thiourea (TMTU, 98%) and the ligands: 1,2-diaminoethane (99%), 1,3-diaminopropane (99%), 1,4-diaminobutane (99%), 1,6-diaminohexane (98%), 1,8-diaminooctane (98%) and 1,10-diaminodecane (97%), including †$NaClO_4.H_2O$ (98%) and $HClO_4$ (70%) were obtained from Aldrich and used without further purification. $AgClO_4$ (99.99%, Aldrich) was stored under nitrogen and used as supplied. Methanol (Saarchem) was distilled and dried over magnesium before use.[36] Ultrapure water (Modulab Systems) was used in all experiments. All other reagents used were of analytical grade quality.

Caution: † Metal perchlorate complexes and perchloric acid are potentially explosive. They should be handled with care, and the complexes should be prepared in small quantities.

7.2.1 Synthesis of Pt(II) Compounds (EnPt up to DecPt)

The general synthetic pathway for the dinuclear Pt(II) complexes (**EnPt** to **DecPt**) involved preparing *in situ* the precursor cation [{*cis*-$PtCl(NH_3)_2(DMF)]^+$,[18,37] using $AgClO_4$ instead of $AgNO_3$ as shown in *Scheme* 7.2. The DMF is selectively displaced by involving slow dropwise addition of diaminoalkane to [{*cis*-$PtCl(NH_3)_2(DMF)]^+$ (1: 1.98 equiv), while stirring at room temperature (30-40 °C) for 24 h in the absence of light. After removal of the AgCl precipitate, the filtrate was cooled and filtered again to remove any undesirable impurities and rotary evaporated under low pressure to a volume of approximately 2 mL and methanol (50 mL) was added. The resulting off-white precipitate was filtered off and repeatedly recrystallized in minimum H_2O/ethanol to remove a brown sticky mass. The off-white solid of good purity was dried over KOH in a desiccator, giving the desired dinuclear Pt(II) complexes: [{*cis*–$PtCl(NH_3)_2$}$_2$–μ–en]$(ClO_4)_2$ (**EnPt**) (en = 1,2-diaminoethane), [{*cis*–$PtCl(NH_3)_2$}$_2$–μ–prop]$(ClO_4)_2$ (**PropPt**) (prop =1,3-diaminopropane), [{*cis*–$PtCl(NH_3)_2$}$_2$–μ–but]$(ClO_4)_2$ (**ButPt**) (but = 1,4-diaminobutane), [{*cis*–$PtCl(NH_3)_2$}$_2$–μ–hex]Cl_2 (**HexPt**) (hex = 1,6-diaminohexane), [{*cis*–$PtCl(NH_3)_2$}$_2$–μ–oct]Cl_2 (**OctPt**) (oct = 1,8-diaminooctane), and [{*cis*–$PtCl(NH_3)_2$}$_2$–μ–dec]Cl_2 (**DecPt**) (dec = 1,10-diaminodecane).

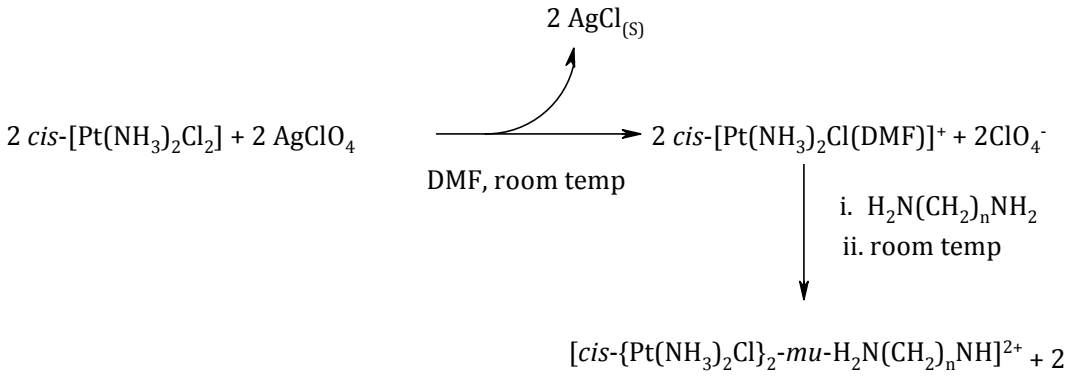

Scheme 7.2: Synthesis of [*cis*-{$PtCl(NH_3)_2$}$_2$-μ-$NH_2(CH_2)_nNH_2$]$(ClO_4)_2$ (**EnPt** to **DecPt**), where μ = *mu.*

Their purity was confirmed by micro-elemental analysis, infrared (IR), ^1H and ^{195}Pt NMR. The IR spectra of all the complexes exhibited common characteristic peaks in the

range 326-400 cm^{-1} (weak) for Pt–Cl and 1090-1100 cm^{-1} (broad, strong) for Cl–O (perchlorate counter ion) vibration stretches, respectively. The typical spectra are as shown in Figures S7.5, S7.15-S7.16, S7.21-S7.25 and S7.31-S7.35 (**Appendix 7**).

The analysis data for the different complexes is as follows.(**EnPt**) Yield: 86.2 mg (36.0%). ^{1}H NMR (550 MHz, D2O), δ /ppm: 2.87 (dd, 4H). ^{195}Pt NMR (107 MHz, D_2 O) δ/ppm: -2415.6. IR (KBr, 4000-300 cm^{-1}) (cm^{-1}): 3290, 3257, (N–H stretch); 1090-1100 (perchlorate counter ion); 326.47 (Pt–Cl stretch); 517.5 (Pt–N stretch). Anal. Calcd for $C_2H_{20}N_6Cl_4O_8Pt_2$.0.25 methanol: H, 2.56; C, 3.05; N, 10.66.; Found H, 2.89; C, 3.39; N, 11.03%.

(**PropPt**) Yield: 20.7 mg (8.5%). ^{1}H NMR (500 MHz, D_2O), δ /ppm: 3.32 (quintet, 4H); 1.28 (s/br, 2H). ^{195}Pt NMR (107 MHz, D_2 O) δ /ppm:-2421.7 IR (KBr, 4000-300 cm^{-1}): 3073 (N-H stretch); 1090-1100 (Perchlorate counter ion); 341.8 (Pt–Cl stretch); 561.7 (Pt–N stretch); 2966, 2925 (C-H stretch). TOF MS/ES^+. (m/z, M^{2+}): 318 ($C_3H_{10}N_3PtCl$ species). Anal. Calcd for $C_3H_{22}N_6Cl_4O_8Pt_2$: H, 2.76; C, 4.49; N, 10.48.; Found H, 2.56; C, 4.23; N, 9.98%.

(**ButPt**) Yield: 60.0 mg (26.6%). ^{1}H NMR (500 MHz, D_2O) δ / ppm: 3.32 (quintet, 4H); 1.28 (s, 4H). ^{195}Pt NMR (107 MHz, D_2 O) δ / ppm: -2344.3. IR (KBr, 4000-300 cm^{-1}): 3158, 3078 (N–H stretch); 1090-1100 (perchlorate counter ion); 333.7 (Pt–Cl stretch); 516.8 (Pt-N stretch); 2951, 2931, 2862.7 (C-H stretch). TOF MS/ES^+. (m/z, M^{2+}): 308 ($C_2H_{12}N_3PtCl$ species). Anal. Calcd for $C_4H_{24}N_6Cl_4O_8Pt_2$: H, 2.96; C, 5.83; N, 10.30.; Found H, 2.95; C, 5.78; N, 9.96%.

(**HexPt**) Yield: 98.4 mg (36.9%). ^{1}H NMR (500 MHz, D_2O) δ /ppm: 2.67 (t/br, 4H), 1.67 (s/br, 4H), 1.37 (s/br, 4H). ^{195}Pt NMR δ /ppm: -2420.2. IR (KBr, 4000-300 cm^{-1}): 3283 (N-H stretch); 1090-1100 cm^{-1} (perchlorate counter ion); 324 (Pt-Cl stretch); 515.9 (Pt-N stretch); 2926.9, 2854.7 (C-H stretch). TOF MS/ES^+. (m/z, M^{2+}): 322 ($C_3H_{14}N_3PtCl$ species). Anal. Calcd for $C_6H_{26}N_6Cl_4Pt_2$: H, 3.34; C, 8.53; N, 9.96.; Found: H, 3.38; C, 9.00; N, 9.58%.

(**OctPt**) Yield: 65.0 mg (29.6%). ^{1}H NMR (500 MHz, D_2O) δ /ppm: 2.65 (quintet, 4H); 1.55 (t, 4H), 1.28 (t, 4H). ^{195}Pt NMR δ /ppm: -2320.4, -2461.82. IR (KBr, 4000-300 cm^{-1}): 3268 (N–H stretch); 1090-1100 cm^{-1} (perchlorate counter ion); 333.7 (Pt–Cl stretch); 507 (Pt–N stretch); 2928, 2856 (C–H stretch). TOF MS/ES$^+$. (m/z, M^{2+}): 336 ($C_4H_{16}N_3PtCl$ species). Anal. Calcd for $C_8H_{30}N_6Cl_4Pt_2$: H, 3.70; C, 11.01; N, 9.64.; Found: H, 3.78; C, 11.44; N, 9.36%.

(**DecPt**) Yield: 159.7 mg (59.8%). ^{1}H NMR (500 MHz, D_2O) δ /ppm: 2.64 (quintet, 4H); 1.66 (quintet, 4H); 1.28 (s/broad, 12H). ^{195}Pt NMR δ /ppm: -2413.2. IR (KBr, 4000-300 $cm^{-1)}$: 3285.6, 3237.8 (N–H stretch); 1090-1100 cm^{-1} (perchlorate counter ion); 333.8 (Pt–Cl stretch); 516 (Pt–N stretch); 2925, 2853 (C-H stretch). TOF MS/ES$^+$. (m/z, M^{2+}): 350 ($C_5H_{18}N_3PtCl$ species). Anal. Calcd for $C_{10}H_{32}N_6Cl_4Pt_2$: H, 4.03; C, 13.34; N, 9.34.; Found: H, 3.94; C, 12.93; N, 9.07%.

7.2.2 Physical Measurements

C, H, and N analyses were performed with a Carlo Erba Elemental Analyzer 1106. The infrared spectra (4000-300 cm^{-1}, KBr disc) were recorded on a Perkin Elmer Spectrum One-FTIR spectrophotometer. All NMR spectra were measured at ambient temperature of 30°C with a Bruker Avance 500 spectrometer equipped with a variable-temperature control unit. Chemical shift values are given in δ (ppm): ^{1}H relative to tetramethylsilane (δ = 0.00) and ^{195}Pt were externally referenced to $K_2[PtCl_6]$ in D_2O. Mass spectrometric analyses were collected on Hewlett Packard LC-MS using electron impact (EI) ionization. Kinetic measurements of fast reactions were performed on an Applied Photophysics SX 18MV stopped-flow instrument coupled to an online data acquisition system. A Varian Cary 100 Bio spectrophotometer equipped with a thermostated cell holder was used to record UV–Vis spectra for the determination of the pK_a values of the aqua complexes and for the study of the slow reactions. The temperature of both instruments was controlled to an accuracy of ± 0.1 °C. The pH and time-dependent kinetic spectra were graphically analysed using Origin 7.5® [38] software package.

7.2.3 Computational Details

To gain insight to the experimental data obtained, computational calculation was carried out. The geometries and energies of molecular orbitals of aqua complexes **EnPt**, **PropPt**,

ButPt, **HexPt**, **OctPt** and **DecPt**, were optimised using the B3LYP [39] hybrid density functional and the LACVP** (Los Alamos Core Valence Potentials)[40] basis set, using the Spartan`04 for windows computational software package. All structures were characterised as cationic species of formal charges of 4+.

7.2.4 Preparation of Aqueous Complex Solutions

The desired solutions of the diaqua complexes were prepared by removal of Cl^- with Ag^+, (1: 1.98 molar ratio of the chloro complexes (**EnPt** to **DecPt**) to silver perchlorate) in 0.1M $HClO_4$, as described in the literature for Pt(II) aqua complexes.[41] The mixture was vigorously stirred at 50°C for 24h in the dark. After cooling on ice cold water, the precipitated AgCl was filtered off. The resulting aqueous solution was brought to a final complex concentration of respectively, 1.09×10^{-4}, 5.33×10^{-4}, 2.29×10^{-4}, 1.17×10^{-3}, 1.34×10^{-3} and 1.00×10^{-4} M for **EnPt**, **PropPt**, **ButPt**, **HexPt**, **OctPt** and **DecPt**, using 0.1M $HClO_4$ and stored in a fridge until use. For all the kinetic investigations, the pH of the solutions was maintained at *ca*. 2.0, in order to guarantee the presence of only the diaqua form of the complexes. Since perchlorate ion, (ClO_4^-), does not coordinate to Pt(II),[42] the ionic strength was adjusted to 0.1M using 0.1M $NaClO_4/HClO_4$ solution. A series of nucleophile concentrations in the order: 20, 40, 60, 80 and 100-fold excess to the metal complex concentration were obtained using the 0.1M $NaClO_4/HClO_4$ solution.

7.2.8 pK_a Titrations of the Diaqua Complexes

For the pK_a determination, the pH of each aqueous solution was measured using a Jenway 4330 Conductivity/pH meter equipped with a Micro 4.5 diameter glass electrode. This electrode was filled with 3M NaCl as the electrolyte to prevent precipitation of $KClO_4$, and was standardised at 25 °C using buffer solutions at pH 4.0, 7.0 and 10.0, purchased from Merck. In order to avoid absorbance corrections due to dilution, a large volume (200ml) of the metal complex solution was used during the titration. Adjustments in pH were made by stepwise additions of crushed solid NaOH pellets in the pH range 2-3, micropipette dropwise addition of saturated, 1.0 and 0.1M NaOH or conc. $HClO_4$ (for reversibility of the pH) to the sample solution. After each addition of base, aliquots of 2 mL of the solution were placed in small vials and the pH monitored by UV–Vis spectroscopy. Afterwards, the aliquot samples were discarded to avoid contamination by chloride ions leaching from the pH electrode.

7.2.6 Kinetic Measurements

All kinetic reactions of the complexes **EnPt**, **PropPt**, **ButPt**, **HexPt**, **OctPt** and **DecPt** were monitored under *pseudo* first-order conditions with at least a twenty-fold excess of the nucleophile. The reactions were started by the mixing of equal volumes of a solution of the Pt (II) complex with a solution of the nucleophile directly in the stopped-flow instrument or UV-Vis spectrophotometer at suitable wavelengths (Table S7.1). Observed rate constants were calculated by a single exponential function or double exponential fit to the kinetic traces. The reported *pseudo* first-order rate constants, k_{obs}, are mean values of at least five independent kinetic runs on the stopped-flow or duplicate measurements on the UV-Vis spectrophotometer. Second-order rate constants, k_2, were obtained by a fit of a straight line to the plot of *pseudo* first-order rate constants k_{obs} versus concentration of nucleophile [NU], using a standard least-squares minimizing routine by Origin 7.5®[38] software package. Enthalpies and entropies of activation, $\Delta H^{\neq}$ and $\Delta S^{\neq}$, were obtained by a fit of the natural logarithm of the second-order rate constant, $\ln(k_2/T)$ versus $1/T$ to the Eyring equation.

7.3 Results

7.3.1 DFT Calculations

The optimised structures are given in Figure 7.1 and a complete list of the calculated results, including the Natural atomic Bond Order (NBO) charges, bond lengths and angles is recorded in Table 7.1. The data shows that the d^8 Pt(II) centre adopts a distorted square planar coordination geometry with an average bite angle, *trans* OH_2–Pt–NH_3, of 178 °C and *cis* H_2O–Pt–$NH_{2diamine}$ of 84.2 °C. In addition, the "even" complexes **EnPt**, **ButPt**, **HexPt**, **OctP**t and **DecPt** adopt C_{2h} symmetry, while a C_{2v} symmetry is adopted for **PropPt**.

It is seen from the data in Table 7.1 and Figure 7.3 that the energies of HOMO and LUMO frontier orbitals increase proportionately with the length of the aliphatic chain, whereas ΔE values follow the order **EnPt** < **PropPt** < **ButPt** < **HexPt** > **OctPt** > **DecPt**. This trend is a result of the differential σ-donation of electron density towards the Pt(II) centre created by the introduction of the alkanediamine bridge. The σ-donation of electron density increases with increasing HOMO and LUMO orbital energy levels, while its σ-inductive effect towards the Pt(II) atoms lessens on increasing the chain length of the aliphatic bridge further. The overall effect of increasing the alkanediamine chain is that the HOMO–LUMO energy gap increases to a maximum at **HexPt** before it starts to decrease with respect to **OctPt** and **DecPt**. A similar trend is observed when looking at rate of reduction of the NBO charges. The results indicate that after the $(CH_2)_n$ group (n = 6), the interaction between the two Pt(II) centres decreases significantly which, in turn, is accompanied by a decrease in electrophilicity of the metal centre.

Table 7.1: Summary of selected DFT-calculated NBO charges, HOMO-LUMO energy gaps, bond lengths and angles of the studied Pt(II) complexes.

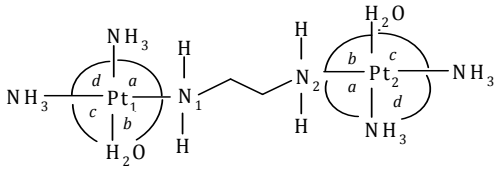

	EnPt	PropPt	ButPt	HexPt	OctPt	DecPt
MO energy/ eV						
HOMO	-19.50	-18.98	-18.55	-17.89	-16.98	-15.81
LUMO	-14.47	-13.86	-13.38	-12.68	-12.21	-11.88
ΔE/eV	5.03	5.12	5.17	5.21	4.77	3.93
Bond length (Å)						
Pt---Pt	7.797	9.040	10.302	12.824	15.349	17.890
Pt–N_{amine}	2.168	2.143	2.132	2.115	2.107	2.104
Pt–OH_2	2.134	2.132	2.130	2.129	2.129	2.129
Bond angles (°)						
N_{amine}–Pt–NH_3	176.3	175.3	175.8	176.2	176.5	176.6
H_2O–Pt–NH_3	177.8	178.1	178.0	177.7	177.3	176.3
a	94.1	95.3	94.5	93.9	93.3	91.5
b	85.4	83.5	84.0	84.1	84.2	91.1
c	91.7	92.1	92.1	92.3	92.4	84.6
d	88.8	88.9	89.3	89.8	90.1	91.8
NBO charges						
Pt1/Pt2	1.1925	1.1924	1.1909	1.1888	1.1860	1.1850
Symmetry	C_{2h}	C_{2v}	C_{2h}	C_{2h}	C_{2h}	C_{2h}

Structure	HOMO	LUMO
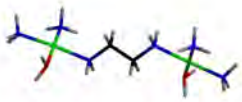 **EnPt** (C_{2h})	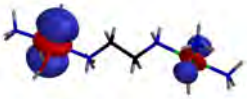	
 **PropPt** (C_{2v})		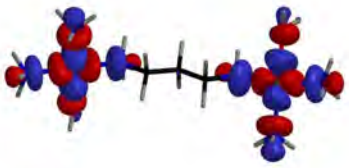
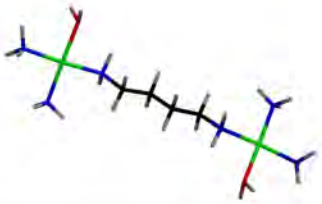 **ButPt** (C_{2h})	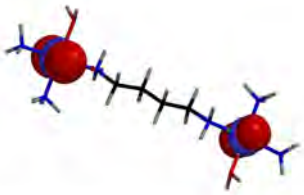	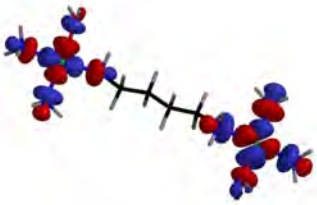
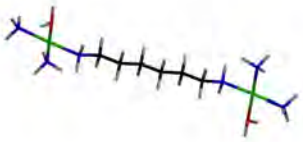 **HexPt** (C_{2h})	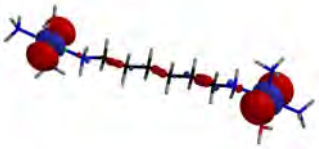	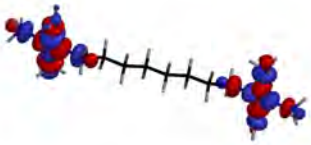
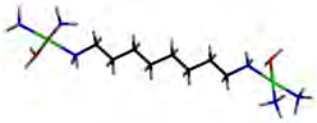 **OctPt** (C_{2h})	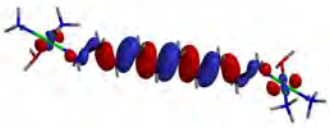	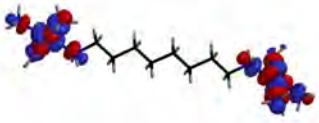
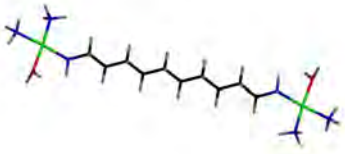 **DecPt** (C_{2h})	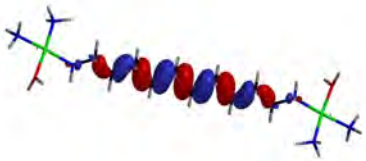	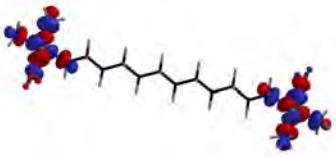

Figure 7.1: Density Functional theoretical (DFT) minimum energy structures, HOMO and LUMO frontier molecular orbitals for investigated diaqua Pt(II) complexes.

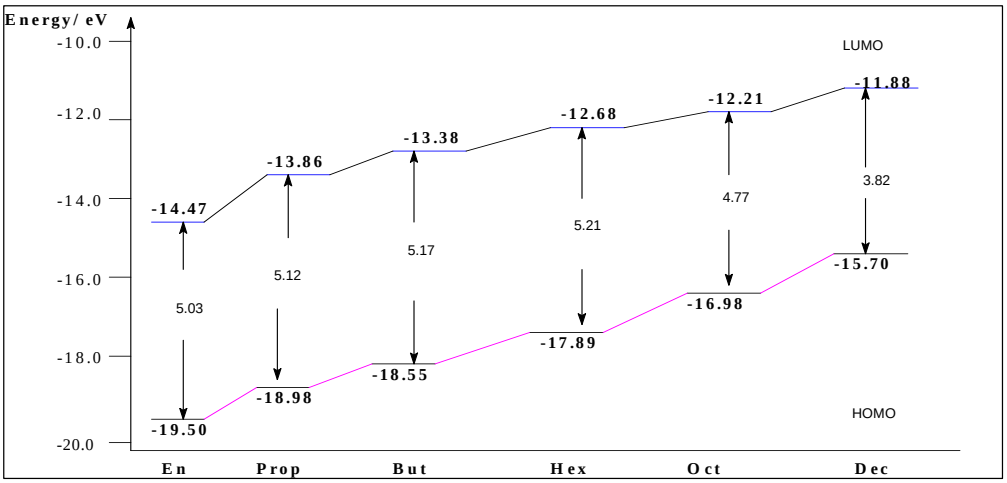

Figure 7.2: HOMO-LUMO Energy gap as a function of number of carbons for the diaqua complexes.

7.3.2 Acidity of the Diaqua Complexes

A typical plot of the UV/Vis spectra in the pH range 2-9 obtained during the course of the titration of the complex **OctPt** with NaOH is shown in Figure 7.3 (also Figures **S7.10**, **S7.15** and **S7.30** for the corresponding data for the pK_a of the complexes **PropPt**, **ButPt** and **DecPt**, **Appendix 7**). The pK_a values of the aqua complexes were calculated from the pH profiles, an example is shown as an inset in Figure 7.3, recorded as a plot of absorbance versus pH at 241 nm. When the data were fitted to the standard Boltzmann equation, the pK_a values for the deprotonation of the platinum bound water molecules were obtained and are summarised in Table 7.2.

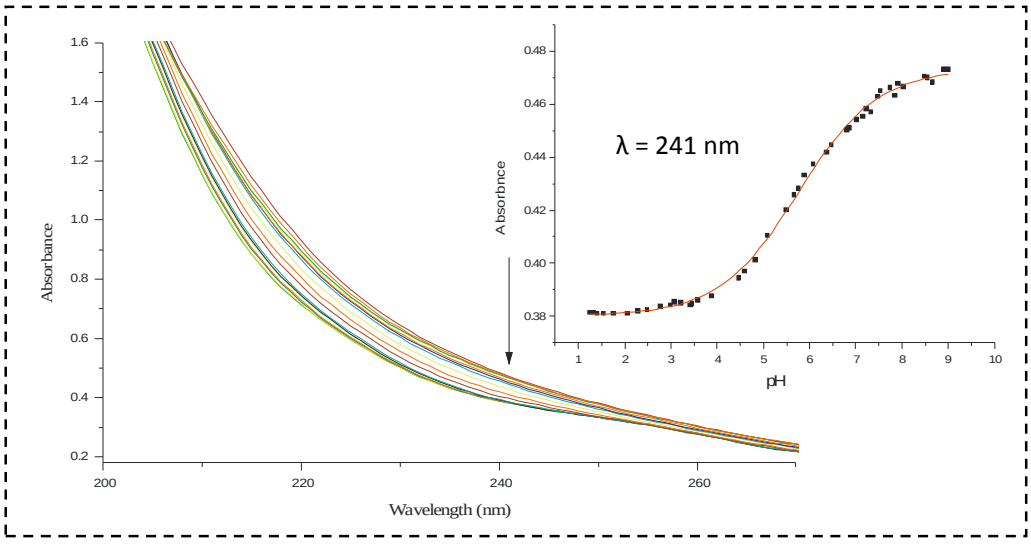

Figure 7.3: UV-Vis spectra of the diaqua **OctPt** complex recorded as a function of pH in the range of 2- 10; *I* = 0.10 M (NaClO4), T = 25 ºC. Inset: Plot of absorbance vs. pH at 241 nm.

Table 7.2: Summary of pK_a values for the deprotonattion steps of aqua platinum(II) complexes at 25 °C. pK_a values of *trans*-isomers are included for comparison purposes.

	EnPt	**PropPt**	**ButPt**	**HexPt**	**OctPt**	**DecPt**
p*K*a (*cis*)	-	5.34 ± 0.18	5.51 ± 0.05	6.01 ± 0.03[a]	5.76 ± 0.03	6.22 ± 0.12
[b]pK_a (*trans)*	4.98 ± 0.09	5.30 ± 0.12	5.50 ± 0.02	5.62 ± 0.03	-	-

[a] Extracted data from reference 43 and [b] from reference 26.

Despite the possibility of hydrogen bonding between the aqua/hydroxo groups that would result after the first deprotonation step due to the *cis*-orientation and flexibility of $(CH_2)_n$ chain of the linker, only one inflection point was detected in the titration curves of the complexes, indicating that $K_{a1} \approx K_{a2}$.[43] Moreover, both the {PtN_3O} sites carry a positive charge (+2) and also the same charge difference (+1) occurs during the deprotonation steps of the two coordinated water molecules.[43] When these facts are coupled with the σ-donor ability of the primary amine function on the linker, any

differences in the pK_a values due to electrostatic forces can be assumed to be insignificant. Consequently, a single pK_a value is obtained for the two water molecules in all cases. This corroborates the reports by Jaganyi *et al*.[26] and Davies *et al*.[44] Hence; the overall process can be presented by *Scheme 7.*3.

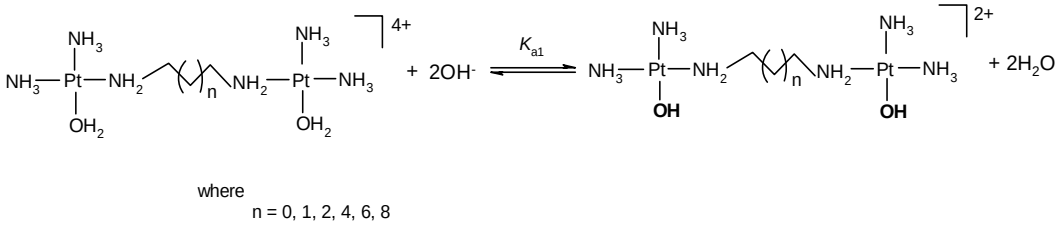

***Scheme* 7.3**: Proposed mechanism for simultaneous deprotonation of the aqua ligands for the pH dependence of the dinuclear Pt(II) complexes

The data in Table 7.2 indicates that the pK_a values increase from 5.34 to 6.01 as the number of the $(CH_2)_n$ groups of the alkanediamine bridge increases from **PropPt** to **HexPt**, whereas the pK_a values for the latter complexes **HexPt**, **OctPt** and **DecPt** with longer bridges remain statistically constant. Also included for comparison purposes in Table 7.2 are the pK_a values of the related *trans*-isomers,[26] which shows that no difference exists between the *cis* and the *trans* complexes with respect to deprotonation of the coordinated aqua ligand.

7.3.3 Kinetics

Substitution of the coordinated aqua ligands from each of the six Pt(II) complexes (*Scheme 7.*1) by three different thiourea nucleophiles *i.e.* thiourea (TU), *N*,*N*-dimethyl-2-thiourea (DMTU), and *N*,*N*,*N*,*N*-tetramethyl-2-thiourea (TMTU), was investigated under *pseudo* first-order conditions using conventional stopped-flow and UV–Vis spectrophotometric techniques. Two separate reaction steps were observed. The first step involves simultaneously substitution of the two water ligands since the coordinated water ligands are equivalent in nature.[45]

The second slower step is ascribed to substitution of the labilised ammine (NH_3) ligand at the *trans* position to TU, as a result of the strong *trans effect* of sulphur atom from TU, and also due to the stronger *trans*-labilisation of the S-donor nucleophiles following its

coordination to the soft Pt(II) centre. At pH 2.0, protonation of the released ammine ligand serves as the driving force which prevents the reverse reaction. This step is slower because of the steric hindrance of the coordinated thiourea and its σ-electron donation toward the Pt(II) centre makes the metal centre less electrophilic, leading to repulsion of the incoming nucleophile in the five-coordinate transition state. The release of ammine has been detected in the reaction of cisplatin with methionine in blood[46] and has also been reported in previous studies using S-donor nucleophiles TU and glutathione for mononuclear analogues *trans*-$[PtCl(NH_3)_3]^+$ and *trans*-$[PtCl(NH_3)_2CH_3NH_2]^+$ [47] and 1,1/c,c dinuclear complexes.[14,31(a),32]

To confirm the stepwise mechanism proposed in *Scheme* 7.4, the reaction between **HexPt** as a chloride and TU (at 2, 4, 6 equiv.) in D_2O was monitored by ^1H and ^{195}Pt NMR and the NMR spectra are recorded in Figures 7.4 & 7.5. An array of the $(CH_2)_n$ protons of the linker showing: δ /ppm H_a = 2.69 (CH_2, 1/6), H_b = 1.72 (CH_2, 2/5) and H_c = 1.40 (CH_2, 3/4) in the absence of TU is recorded as a reference point provided as Figure 7.4 as spectra "a". During the course of substitution (refer to spectral array Figure 7.4), both H_b and H_c resonances are shifted upfield, due to coordination of sulphur to the metal centre consistent with the substitution of either chloro or ammine ligand by thiourea. The broad multiplet resonance H_a underwent a downfield shift. The distinct broadened multiplet resonance for H_a protons results from coordination of S to form PtN_3S intermediate species upon subsequent addition of larger amounts of TU to the complex solution, which demonstrates further the sensitivity of the protons on the linker to electronic changes at the Pt(II) centre upon coordination of the second TU moiety. Kasherman *et al*.[47] have demonstrated that the formation of *trans*-$[Pt(NH_3)_3TU]^{+2}$ from the mononuclear complex *trans*-$[PtCl(NH_3)_2L]^+$ (where L = CH_3NH_2 or NH_3) occurred in the first 100 minutes, explaining why in the current study cleavage of the linker was not observed. This is supported by the absence of the diagnostic triplet peak at 3.0 ppm assigned to the free hexanediamine.[31(a)]

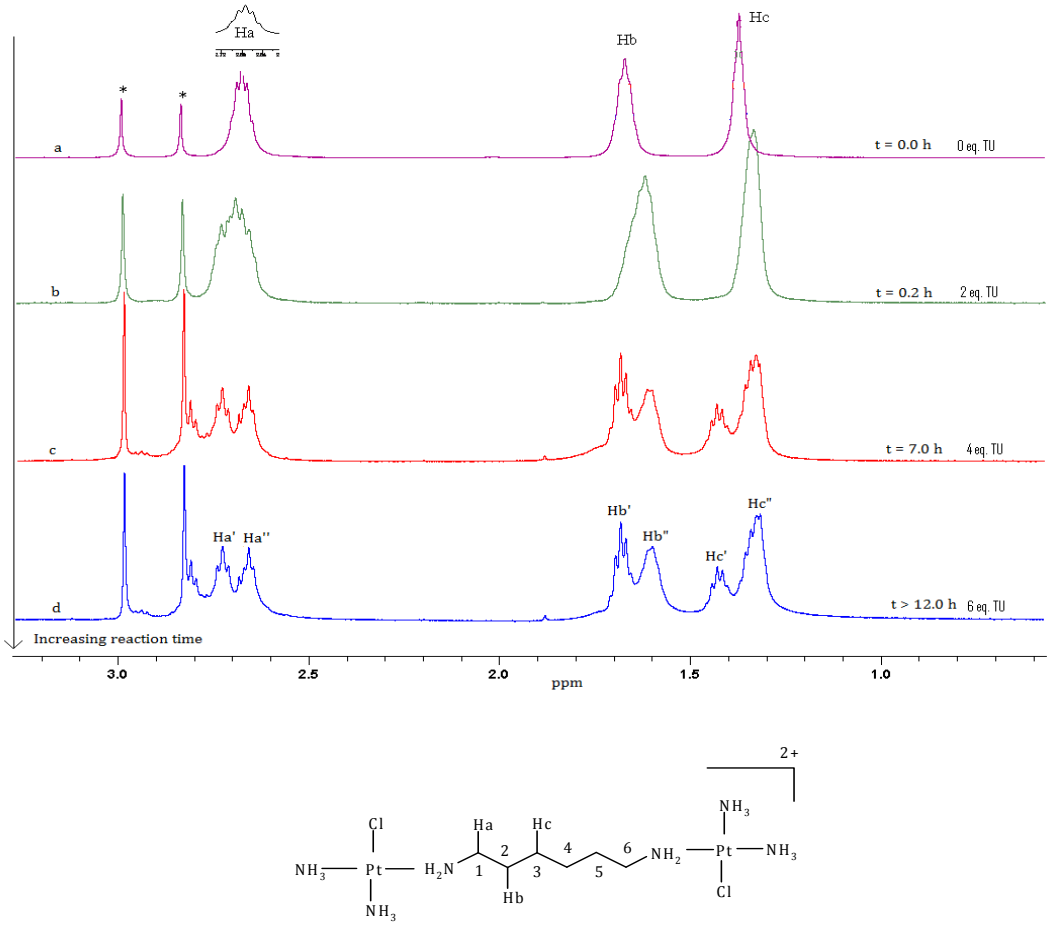

Figure 7.4: An array of ^{1}H NMR spectra of **HexPt–Cl** (showing methylene (CH_2) protons only) acquired during the reaction with 6 equiv. TU in D_2O, at 30 °C, with spectrum "a" at zero time and "d" after 12.0 h reaction time, respectively. Where Ha = (CH_2, 1/6), Hb = (CH_2, 2/5) and Hc = (CH_2, 3/4) represent the methylene protons as shown in the structure for starting complex above, showing the formation of substituted thiourea products described in Scheme 7.4. The protons Ha'/Ha" are (CH_2, 1/6), Hb'/Hb" are (CH_2, 2/5) and Hc'/Hc" are (CH_2, 3/4) protons for *cis*–[{Pt(TU)$(NH_3)_2$}$_2$–μ–$NH_2(CH_2)_6NH_2$]$^{+4}$ and *cis*–[{Pt(TU)$_2$$(NH_3)$}$_2$–μ–$NH_2(CH_2)_6NH_2$]$^{+4}$ species, respectively. * are peaks due to unknown impurities in solution or solvent.

The ^{195}Pt NMR is an effective method to determine the coordination details of the complexes, since the chemical shift of the ^{195}Pt resonance is influenced by the number of coordinated donor atoms surrounding the Pt(II) centre. The peak (**A**) at -2420 ppm in Figure 7.5 corresponds to the unreacted starting complex **HexPt–Cl**. This peak disappeared within the first 30 minutes and was replaced by two new peaks (**B** and **C**)

observed at -2962.4 and -3024.1 ppm, respectively, suggesting that two new species had been formed in the solution. In the presence of a large excess TU (≥ 4 equiv.), two persistence peaks were observed at -3024.1 ppm (C, small) and a doublet (D) at -3275.6/-3282.5 ppm (12.0 h). It is well known from literature that the ^{195}Pt NMR chemical shift of Pt(II) compounds with [PtN_3S] coordination sphere appears in the range -2800 to -3000 ppm, whereas complexes with [PtN_2S_2] coordination sphere resonate around -3150 to -3250 ppm.[30,31(a),47] Therefore, the observed peaks at -2962.4 and -3024.1 ppm are mainly due to *cis*-[{$PtCl(NH_3)_2$}-μ-NH_2-$(CH_2)_6$-NH_2-{$PtTU(NH_3)_2$}]$^{+3}$ and *cis*-[{$Pt(TU)(NH_3)_2$}$_2$-μ-$NH_2(CH_2)_6NH_2$]$^{+4}$ species, respectively. The persistence conformer at -3024.1 ppm is more likely to be the intermediate species *cis*-[{$PtTU(NH_3)_2$}-μ-linker-$Pt(NH_3)_2TU$]$^{+4}$; whereas the latter doublet peak at -3279 ppm is indicative of a PtN_2S_2 coordination environment and corresponds to *cis*-[{$Pt(TU)_2NH_3$}$_2$-μ-$NH_2(CH_2)_6NH_2$]$^{+4}$ species. The assignment of the peaks in ^{195}Pt NMR spectra to [PtN_3S] and [PtN_2S_2] coordination spheres are in agreement with that reported by Oehlsen *et al*.[48] and Kasherman *et al*.[47] In case of higher concentration of TU (6 equiv), the reactions are fast such that the only intermediate that is observed is **C**. In addition, no evidence for other decomposition products were observed at higher fields beyond -3400 ppm, an indication that the alkanediamine bridging system in the dinuclear Pt(II) complexes did remain interact, even for a strong nucleophile such as thiourea. This does not rule out that a longer reaction time may be required for the linker cleavage from the Pt metal. These results suggest that increase in steric hindrance and reduced electrophilicity around the Pt(II) centre retards any further substitution and dissociation of the linker.

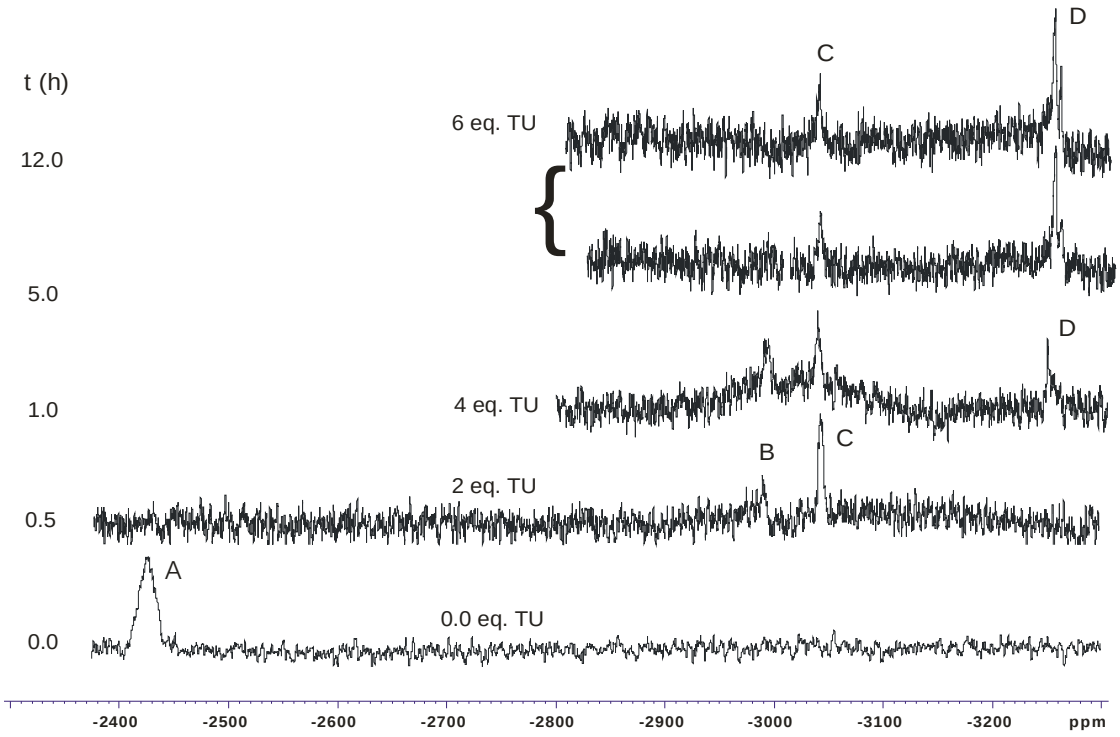

Figure 7.5: ^{195}Pt NMR spectra of mixtures **HexPt-Cl** and TU (1:2; 1:4 and 1:6 equiv.) in D_2O, at 30 °C; where **A** is the peak due to starting complex *cis*–$[\{PtCl(NH_3)_2\}_2–\mu–NH_2(CH_2)_6NH2]^{2+}$, **B** and **C** are intermediates, *cis*–$[\{PtCl(NH_3)_2\}–\mu–NH_2–(CH_2)_6–NH_2–\{PtTU(NH_3)_2\}]^{3+}$ and *cis*–$[\{Pt(TU)(NH_3)_2\}_2–\mu–NH_2(CH_2)_6NH_2]^{4+}$, respectively, while **D** is the final product *cis*–$[\{Pt(TU)_2NH_3\}_2–\mu–NH_2(CH_2)_6NH_2]^{4+}$.

It can therefore be concluded that in this study the final product is a dinuclear Pt(II) complex with two thiourea coordinated to each of the Pt(II) centres, and that the substitution mechanism is a stepwise process as represented by *Scheme* 7.4.

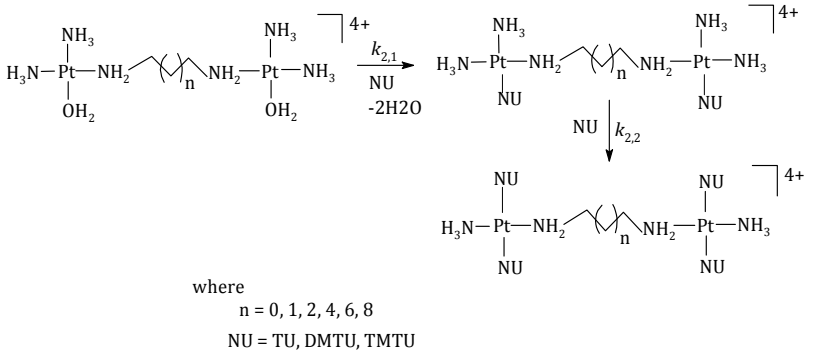

***Scheme* 7.4**: Proposed mechanism of aqua substitution from the investigated complexes by a series of thiourea nucleophiles (NU)

Typical kinetic traces recorded by mixing solutions of **OctPt** (5.285×10^{-5} M) and TU (1.664×10^{-3} M) in the stopped-flow instrument or UV/Vis spectrophotometer, at an ionic strength of 0.1 M ($NaClO_4$), are shown in Figure 7.6. All the kinetic traces were described by single exponential functions. The obtained *pseudo* first-order rate constants, k_{obs}, were found to be directly proportional to the concentration of the S-donor nucleophile. Typical plots for the reactions of **OctPt** with the S-donor nucleophiles at different concentrations are shown in Figures 7.7 & 7.8 (also Figures **S7.1**-**S7.2**, **S7.6-S7.7**, **S7.11-S7.12**, **S7.17-S7.18** and **S7.26-S7.27** for the corresponding complexes **EnPt**, **PropPt**, **ButPt**, **HexPt** and **DecPt**, **Appendix 7**). The second-order rate constant, k_2, for the forward reaction of each complex with a particular nucleophile was calculated from the slope of a plot of the observed rate constant, k_{obs}, versus the nucleophile concentration using Origin 7.5®.[38] The plots obtained can be described by *Equation (1)*. The absence of an intercept indicates a direct ligand-exchange of aqua or ammine ligand for thiourea nucleophile and shows that the nucleophilicity of these sulphur donors is strong enough to suppress the kinetic influence from the solvent path.

$$k_{obs1^{st}/2^{nd}} = k_{2,1^{st}/2,2^{nd}}[NU] \qquad (1)$$

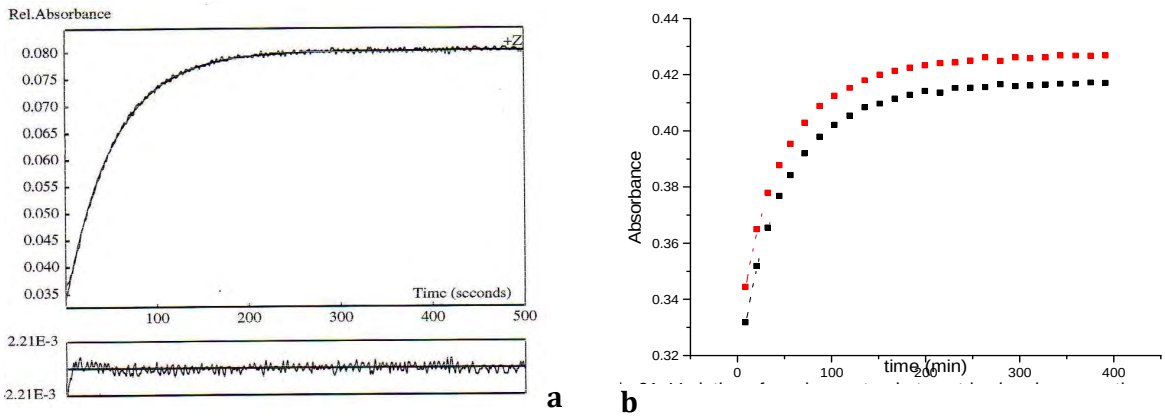

Figure 7.6: Typical kinetic traces for two step reaction between **OctPt** (0.1 mM) and TU (3 mM) recorded at 363 nm, T =298 K, pH = 2.0, I =0.1 M ($NaClO_4/HClO_4$). (a) A typical kinetic trace from the stopped-flow for the simultaneous substitution of the aqua ligand (b) A typical kinetic trace (in duplicate) for the release of ammine acquired by UV-Vis spectroscopy.

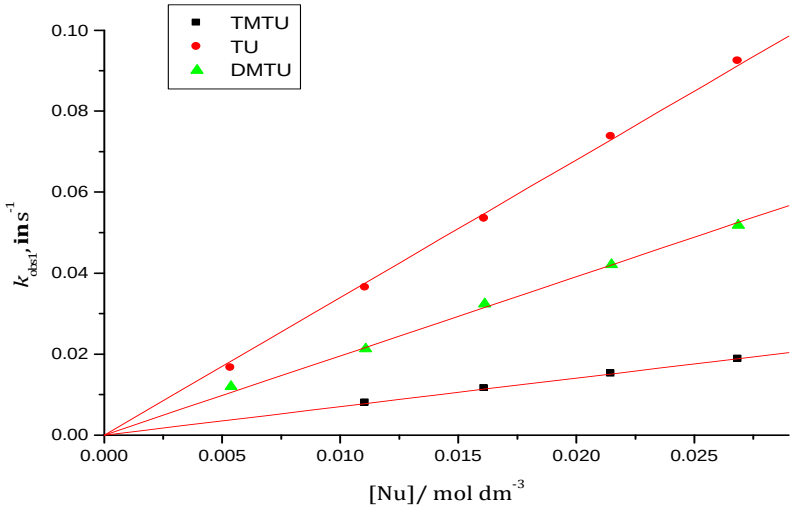

Figure 7.7: Concentration dependence of $k_{obs(1^{st})}$, s^{-1}, for the simultaneous substitution of the aqua ligands in **OctPt** by thiourea nucleophiles at pH =2.0, T =298 K, I = 0.1 M ($NaClO_4$, adjusted with 0.01 M $HClO_4$).

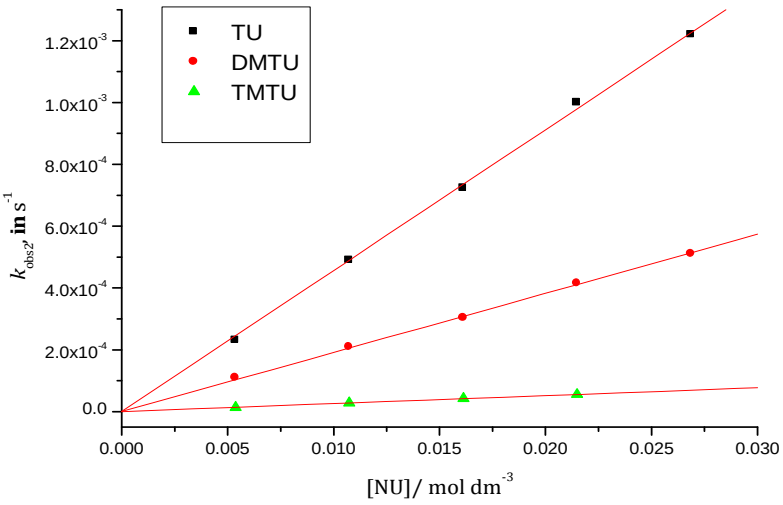

Figure 7.8: Concentration dependence of $k_{obs(2^{nd})}$, s-1, for the release of the ammine ligand in **OctPt** by thiourea nucleophiles at pH =2.0, T =298 K, I = 0.1 M ($NaClO_4$, adjusted with 0.01 M $HClO_4$).

A summary of the values of second-order rate constants, $k_{2,1^{st}/2,2^{nd}}$, calculated from the slopes of such plots at 25°C, for the first and second substitution steps, respectively is tabulated in Table 7.3.

Table 7.3: Summary of second order rate constants and activation parameters for flexible α, ω-alkanediamine-bridged platinum(II) complexes.

Complex	**NU**	$k_{2,\,1^{st}}$ **/M^{-1} s^{-1}**	$\Delta H^{\neq}_{2,\,1^{st}}$ **/kJ mol^{-1}**	$\Delta S^{\neq}_{2,\,1^{st}}$ **/JK^{-1} mol^{-1}**	$k_{2,\,2^{nd}}$ **/10^{-3}. M^{-1} s^{-1}**	$\Delta H^{\neq}_{2,\,2^{nd}}$ **/kJ mol^{-1}**	$\Delta S^{\neq}_{2,\,2^{nd}}$ **/JK^{-1} mol^{-1}**
EnPt	TU	47 ± 0.7	56 ± 1	-45 ± 3	241.0 ± 2.0	52 ± 2	-102 ± 6
	DMTU	26 ± 1	48 ± 1	-76 ± 4	110.0 ± 1.0	54 ± 2	-102 ± 5
	TMTU	6 ± 0.1	66 ± 2	-29 ± 5	8.7 ± 0.01	49 ± 1	-120 ± 4
PropPt	TU	50 ± 1	45 ± 1	-78 ± 3	44.0 ± 0.3	60 ± 2	-70 ± 5
	DMTU	27 ± 1	46 ± 0.1	-75 ± 0.4	19.8 ± 0.03	56 ± 1	-94 ± 5
	TMTU	11 ± 0.3	47 ± 0.2	-92 ± 1	5.7 ± 0.1	48 ± 2	-123 ± 5
ButPt	TU	46 ± 1	61 ± 3	-71 ± 11	41.4 ± 0.3	56 ± 1	-129 ± 4
	DMTU	26 ± 1	65 ± 2	-61 ± 8	15.0 ± 0.1	52 ± 2	-144 ± 6
	TMTU	7 ± 0.03	44 ± 3	-144 ± 10	8.3 ± 0.03	69 ± 2	-98 ± 6
HexPt	TU	40 ± 0.1	37 ± 0.2	-109 ± 1	40.2 ± 0.1	64 ± 1	-56 ± 4
	DMTU	21 ± 0.4	57 ± 1	-46 ± 3	10.6 ± 0.1	51 ± 2	-113 ± 7
	TMTU	8 ± 0.1	54 ± 1	-67 ± 2	2.3 ± 0.02	66 ± 1	-70 ± 3
OctPt	TU	34 ± 0.3	52 ± 1	-61 ± 3	45.7 ± 0.4	61 ± 1	-67 ± 4
	DMTU	20 ± 0.2	47 ± 2	-81 ± 5	19.1 ± 0.1	54 ± 1	-99 ± 4
	TMTU	7 ± 0.1	52 ± 1	-72 ± 4	2.6 ± 0.03	56 ± 4	-133 ± 13
DecPt	TU	27 ± 0.2	50 ± 1	-74 ± 1	42.1 ± 0.3	53 ± 0.3	-98 ± 1
	DMTU	19 ± 0.1	62 ± 1	-39 ± 7	7.0 ± 0.3	69 ± 1	-52 ± 3
	TMTU	4 ± 0.3	53± 1	-73 ± 2	4.0 ± 0.04	73 ± 1	-40 ± 4

7.3.4 Activation Parameters

The temperature dependence of the rate constant, k_2, was studied over the range 15-35°C in increments of 5 °C. Figures 7.9 & 7.10 (also Figures **S7.3-S7.4**, **S7.8-S7.9**, **S7.13-S7.14**, **S7.19-S7.20**, and **S7.28-S7.29**, for the corresponding complexes **EnPt**, **PropPt**, **ButPt**, **HexPt** and **DecPt**, **Appendix 7**) show the representative Eyring plots, for the reaction of **OctPt** with the different nucleophiles. The corresponding activation parameters $\Delta H^{\neq}$ and $\Delta S^{\neq}$ in Table 7.3, were calculated using the Eyring equation.

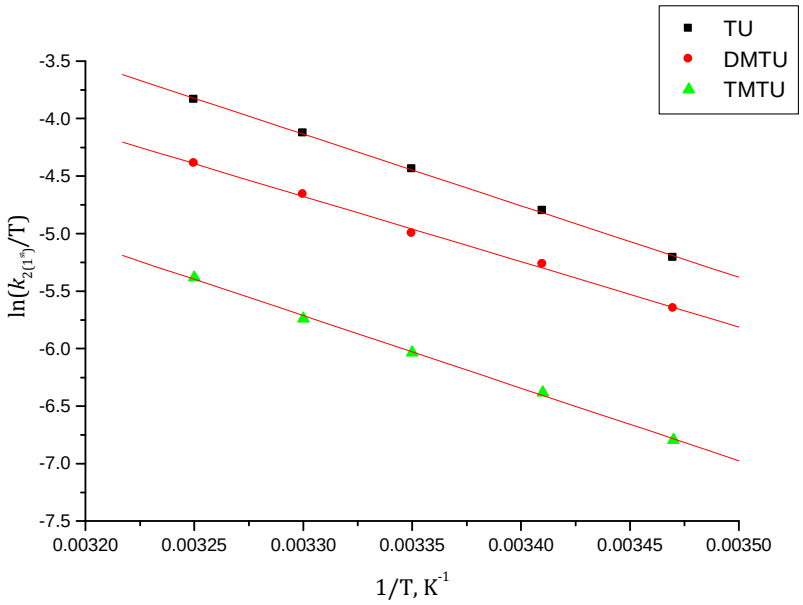

Figure 7.9: Eyring plots forthe determination of the activation enthalpies and entropies for $k_{2,1st}$ of all nucleophiles studied with **OctPt** complex.

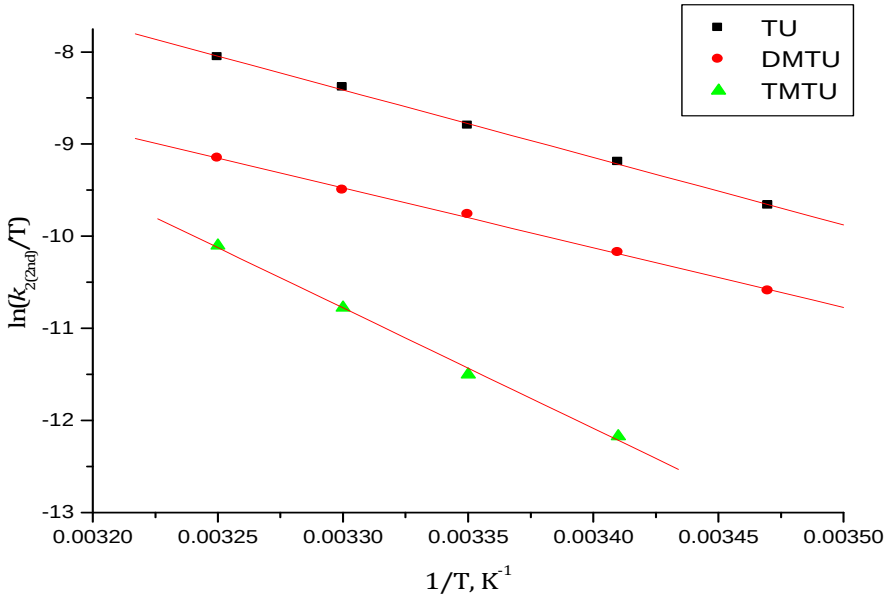

Figure 7.10: Eyring plots forthe determination of the activation enthalpies and entropies for $k_{2,2^{nd}}$ of all nucleophiles studied with **OctPt** complex .

7.4 Discussion

7.4.1 pK_a of the Diaqua Complexes

From previous studies, it has been reported that pK_a values obtained for coordinated aqua ligand at the Pt(II) centre is a good indicator of the electrophilicity of the metal centre,[49] and therefore, of the reactivity of the aqua complex. The results in Table 7.2 indicate that the pK_a values of the studied complexes increase as the number of $(CH_2)_n$ groups of the alkanediamine bridge increases from n = 3 to 10. The slight increase in pK_a values follows the order **PropPt** < **ButPt** < **HexPt** ≤ **OctPt** < **DecPt**. This order is due to the lengthening of the alkanediamine chain, which causes a decrease in localised charge on the Pt(II) centre, reducing electronic communication between the two Pt(II) centres as the separation distance is increased (see Table 7.1). A short distance between the Pt(II) centres in dinuclear Pt(II) complexes results in additional charge increases, which add to an overall of +4 at each Pt centre.[45] As a consequence of this higher charge, each Pt(II) centre becomes more electrophilic and more acidic, leading to lower pK_a values for the coordinated water ligands. The effect of charge additions is more important when the distance between the Pt(II) centres is relatively shorter.[29,30,50] Secondly, the electron-releasing inductive effect of the alkanediamine linker means more electron

density is located on the metal centre, which makes the Pt(II) centre less electrophilic and less acidic. This is supported by the shortening of the Pt–$N_{diamine}$ bond lengths and the reduction in the NBO charges on the Pt(II) centres as the chain length of the linker increases across the series (Table 7.1).

Compared to the mononuclear analogues: *cis*-$[Pt(NH_3)_3H_2O]^{2+}$ (pK_a = 6.37) [51] the pK_a values (5.31-6.22) for most of the investigated dinuclear complexes are slightly lower. As already explained, the inductive effect of the linker and a higher overall charge of +4 on the Pt atom are the reasons for the lower pK_a values of the dinuclear complexes compared with the +2 charged mononuclear analogues. By increasing the chain length of the system, the individual metal centre environment approaches that of the mononuclear analogue. These findings are in agreement with reports by Farrell and co-workers[43] and van Eldik and his group.[30] Changing the position of the water ligand from *trans*- to *cis*- has little or no effect, if at all, on the value of the pK_a of Pt-metal complex, shown in Table 7.2 where the values of *cis* and *trans*- counterparts[26] are compared.

7.4.2 Substitution Process

Comparing the general reactivity, using the TU nucleophile as a reference, the second-order rate constants for the first step lie in the range $5.0 \pm 0.1 \geq k_{2,1}^{st} \geq 2.6 \pm 0.02$ M^{-1} s^{-1}, progressively decreasing marginally from **EnPt** to **DecPt**. The difference in reactivity can be attributed to the decrease in the overall effect of charge additions experienced by the metal centre and σ–donicity of the coordinated alkanediamine linker in these complexes. [26, 29,52]

The retardation of the rate of substitution in the first step, on increasing the alkanediamine chain length from **EnPt** up to **DecPt**, is attributed to the strong σ-donor ability of the $(CH_2)_n$ moiety, which causes accumulation of the electron density at the metal centre.[52,53] This decelerates the substitution process by making the Pt(II) centre more electronegative or less electrophilic. The σ-inductive effect does not only prevent the approach of the nucleophile, but also through the accumulation of electron density at the metal centre suppresses the stabilization of the transition state, which slows down the substitution reaction. Consistent with this view is that the pK_a and HOMO-LUMO energy gap values of the ground state of the dinuclear Pt(II) complexes increase on

introduction of a greater number of $(CH_2)_n$ from n = 2 up to 10. A further factor is the decrease in-space electrostatic charge additions at the metal centre due to the increase in the linker chain.[13,29,30] This leads to a decrease in electrophilicity at the Pt(II) centre thereby making the metal centre less reactive.

It has been demonstrated that the 1,1/c,c geometry results in slower substitution reactions because of the steric hindrance of the bridge around the Pt(II) centre.[14] The steric factor is mainly due to the flexibility of the $(CH_2)_n$ units of the alkanediamine ligand.[26] In this study the overall steric effect was found to have been non-existent or had no significant influence on the first substitution step of the aqua ligands. It can therefore be concluded that electronic effect is the main factor that controls the first substitution step.

A general look at the results in Table 7.3 shows that the rate constants, $k_{2,2^{nd}}$, for the second substitution step are about 1-2 orders of magnitude smaller than those obtained for the simultaneous substitution of the aqua ligands in the first step in all the six complexes. The second substitution reaction is slower than the first step due to a number of reasons. Firstly, a facilitated attack (due to the strong *trans*-effect of the first coordinated TU) by a second thiourea molecule on the *trans*-positioned ammine nitrogen is slowed down as a result of steric constraints around the Pt(II) centre from the first substitution. Secondly, is the increase in electron donation to the Pt metal due to the coordinated TU from the first substitution reactions. The third reason is the fact that the leaving group in the first substitution is different to that in the second substitution. The Pt–OH_2 bond is stronger than that of Pt–NH_3.[54] Finally, the *trans*-effect of the two substitution process is also different, as such influencing the overall reactivity

In this study, the proton (^{1}H) and ^{195}Pt NMR data have demonstrated that for 1,1/c,c dinuclear Pt(II) complexes, a second step which involved release of ammine ligand following the coordination of a further thiourea to the Pt(II) centre is observed. In contrast, the first data reported in literature on di-platinum metal complexes for the *trans* analogues (1,1/t,t)[26] gave only a single reaction step, which is most likely a combination of the two steps. The results of the *trans* analogues (1,1/t.t) also contradicts NMR studies by Farrell *et al*.[31(a)] for the reaction of 1,1/t,t (n =6) with N-

acetylmethionine, which reported that the release of the aliphatic chain occurred within 5.0 h of the reaction. Since the nucleophilicity of thiourea is higher than that of methionine, the release of bridge in 1,1/t,t dinuclear complexes should have occurred within the *ca*. 1500 min, time window used in the study.

Substitution reactions with the sterically hindered nucleophiles DMTU and TMTU show a clear dependence on the steric bulkiness of the nucleophiles. The most sterically hindered nucleophile TMTU reacts significantly slower than the less hindered TU, which means the associative bond formation process in the trigonal-bipyramidal transition state is less favoured.

The mode of activation remains associative in nature throughout the studied systems, since the activation enthalpy change, $\Delta H^{\neq}$, is positive and large, while activation entropy change, $\Delta S^{\neq}$, is large and negative for all cases.[55-57]

7.5 Conclusion

In this study, the effect of increasing the alkanediamine chain length in the **[{*cis*–$Pt(NH_3)_2OH_2$}$_2$–μ–$NH_2(CH_2)_nNH_2$]$^{+4}$** complexes was investigated. It was found that the reactivity of the dinuclear Pt(II) complexes with S-donor nucleophiles decreased with elongation of the length of $(CH_2)_n$ moiety between the Pt(II) centres. This is ascribed to the decrease in the in-space electrostatic interactions between the two Pt(II) centres, which becomes weaker as the chain–length is increased further. In addition, an increase in the σ-inductive effect through the introduction of the alkanediamine bridge results in accumulation of the electronic density at Pt(II) centre, which makes the metal centre less electrophilic. This results in higher pK_a values of the coordinated aqua ligands and also slows down the substitution reaction on going from **EnPt** to **DecP**t by repelling the incoming thiourea nucleophiles.

The results from the ^{1}H and ^{195}Pt NMR studies support the kinetic data clearly showing the two substitution processes, which involves an initial simultaneous displacement of the aqua ligands by thiourea followed by the release of the ammine *trans* to the bound sulphur to form the final product **[{*cis*–$Pt(TU)_2NH_3$}$_2$–μ–$NH_2(CH_2)_nNH_2$]$^{+4}$**. In addition, the results reveal that the alkanediamine linker remained interact during the reaction

with S-donor nucleophiles. This finding concurs with the results reported by Farrell and his group.[31(a), 33, 48]

Compared to the dinuclear complexes containing the rigid aromatic linkers, *viz*. diazines[17, 18] and dipyridyl ligands[14], whose results have been reported elsewhere in the earlier works by our group (Chapters 4, 5 & 6 of this study), it is demonstrated that the dinuclear complexes comprising of rigid aromatic linkers are relatively unstable and readily disintegrate to liberate the diamine bridge by sulphur donor nucleophiles. Taken together, the current results suggest that the *cis*-dinuclear complexes with α,ω-alkanediamine show high stability to strong S-donor nucleophiles that are present in human cells and play an important role in biological reactions. It can therefore be concluded that these compounds are likely to be more stable as anti-tumour drugs. The substitution process remains associative in nature, which is supported by the large negative $\Delta S^{\neq}$ values calculated from the temperature-dependent studies of the reactions.

References

1 (a) B. Rosenberg, L. Van Camp, J. E. Trosko and V. H. Mansour, 1969, *Nature*, **222**, 385; (b) M. A. Fuertes, C. Alonso and J. M. Perez, 2003, *Chem. Rev*., **103**, 645; (c) D. Wang and S. J. Lippard, 2005, *Nat. Rev. Drug Discovery*, **4**, 307; (d) S. Van Zutphen and J. Reedijk, 2005, *Coord. Chem. Rev*., **24**, 2845.

2 E. Wong and C. M. Giandomenico, 1999, *Chem. Rev*., **99**, 2451.

3 R. T. D. Oliver, 2001, *Curr. Opin. Oncol*., **13**, 191.

4 E. R. Jamieson and S. J. Lippard, 1999, *Chem. Rev*., **99**, 2467.

5 J. Reedijk, 1999, *Chem. Rev*., 99, 2499.

6 P. J. Dyson and G. Sava, 2006, *Dalton Trans*., 1929.

7 A. S. Abu-Surrah and M. Kettunen, 2006, *Curr. Med. Chem*., **13**, 1337.

8 L. R. Kelland, 2007, *Nat. Rev. Cancer*, **7**, 573.

9 J. Reedijk, 2009, *Eur. J. Inorg. Chem*., 1303.

10 T. Soldatović, Ž. D. Bugarčić and R. van Eldik, 2009, *Dalton. Trans*., 4526.

11 M. D. Hall and T. W. Hambley, 2002, Coord. *Chem. Rev*., **232**, 49.

12 C. X. Zhang and S. J. Lippard, 2003, *Curr. Opin. Chem. Biol*., **7**, 481.

13 H. Ertürk, R.Puchta, R. van Eldik, 2009. *Eur. J. Inorg. Chem*., 1331.

14 D. Fan, X. Yang, X. Wang, S. Zhang, J. Mao, J. Ding, L. Lin and Z. Guo, 2007, *J. Biol. Inorg. Chem*., **12**, 655, and references therein.

15 N. Farrell, 1995, *Comm. Inorg*. *Chem*., **16**(**6**), 373.

16 N. J. Wheate and J. G. Collins, 2003, *Coord. Chem. Rev.*, 133.

17 G. V. Kalayada, S. Komeda, K. Ekeda, T. Sato, M. Chikuma and J. Reedijk, 2003, *Inorg. Chem*., 4347.

18 S. Komeda, G. V. Kalayda, M. Lutz, A. L. Spek, T, Sato, M. Chikuma and J. Reedijk, 2003, *J. Med. Chem*., **46**, 1210.

19 N. J. Wheate, C. Cullinane, L. K. Webster and J. G. Collins, 2001, *Anti-Cancer Drug Des*., **16**, 91.

20 G. Colella, M. Pennati, A. Bearzatto, R. Leone, D. Colangelo and C. Manzotti, 2001, *Br. J. Cancer*, **84**, 1387.

21 D. I. Jodrell, T. R. J. Evans, W. Steward, D. Cameron, J. Prendiville and C. Aschele, 2004, *Eur. J. Cancer*, **40**, 1872.

22 A. L. Harris, X. Yang, A. Hegmans, L.Povirk, J. J. Ryan, L. Kelland and N. P.Farrell, 2005, *Inorg. Chem*., **44**, 9598.

23 J. Kasparkova, N. Farrell and V. Brabec, 2000, *J. Biol. Chem*., **275**, 15789.

24 M. S. Ali, K. H. Whitmire, T. Toyomasi, Z. H. Siddik and A. R. Khokhar, 1999. *J. Inorg*. *Biochem*., **77**, 231.

25 J. W Cox, S. J. Berners-Price, M. S. Davies, W. Barlage, Y. Qu and N. Farrell, 2000, *Inorg*. *Chem*., **39**, 1710.

26 D. Jaganyi, V. M. Munisamy and D. Reddy, 2006, *Int. J. of Chem. Kinet.*, ***38***, 202.

27 A. Hofmann and R. van Eldik, 2003, *J. Chem. Soc*., *Dalton Trans*., 2979.

28 M. S. Davies, J. W. Cox, S. Berners-Price, W. Barklage, Y. Qu, N. Farrell, 2000, *Inorg. Chem*., **39**, 1710.

29 A. Mambanda, D. Jaganyi, S. Hochreuther and R. van Eldik, *Dalton Trans.*, 2010, **39**, 3595.

30 H. Ertürk, A. Hofmann, R. Puchta and R. van Eldik, 2007, *J. Chem. Soc*., *Dalton Trans*., 2295.

31 (a) M. E. Oehlsen, Y. Qu and N. Farrell, 2003, *Inorg. Chem*., **42**, 5498; (b) E. I. Montero, J. Zhang, J. J. Moniodis, S. J. Berners-Price and N. P. Farrell, 2010, *Chem. Eur. J*., **16**, 1975.

32 N. Summa, J. Maigut, R. Puchta and R. Van Eldik, 2007, *Inorg. Chem*., **46**, 2094.

33 M. Oehlsen, A.Hegmans, Y. Qu and N. Farrell, 2005, *J. Biol. Inorg. Chem*., **10**, 433.

34 J. W. Williams, Y. Qu, G. H. Bullus, E. Alvorado and N. P. Farrell, 2007, *Inorg. Chem*., **46**, 5820.

35 L. Zerzankova, T. Suchankova, O. Vrana, N. P. Farrell, V. Brabec and J. Kasparkova, 2010. *Biochem. Pharmacol.*, **79**, 112.

36 D. D. Perrin, W. L. F. Armarego, D. R. Perrin, *Purification of Laboratory Chemicals*, 2nd Ed., Pergamon, Oxford, 1980.

37 (a) L. S. Hollis, A. R. Amundsen, and E. W. Stern, 1989, *J. Med. Chem*., **32**, 128; b) Y. Qu and N. Farrell, 1992, *Inorg. Chem*., **31**, 930.

38 MicrocalTM OriginTM Version 7.5, Microcal Software, Inc., One Roundhouse Plaza, Northampton, MA, 1060, USA, 1991-2003.

39 A. D. Becke, 1993, *J. Chem. Phys.,* **98**, 5648.

40 P. J. Hay and W. R. Wadt, 1985, *J. Chem. Phys*., **82**, 299.

41 Z. D. Bugarčić, B. V. Petrović and R. Jelić, 2001, *Transition Met. Chem.,* **26**, 66.

42 T. G. Appleton, J. R. Hall, S. F. Ralph and C. M. S. Thompson, 1984, *Inorg. Chem.,* **23**, 3521.

43 J. Zhang, D. S. Thomas, M. S. Davies, S. J. Berners-Price and N. Farrell, 2005. *J. Biol. Inorg. Chem.*, **10**, 652.

44 M. S. Davies, J. W. Cox, S. J. Berners-Price, W. Barklage, Y. Qu and N. Farrell, 2000, *Inorg. Chem*., **39**, 1710.

45 S. Hochreuther, R. Puchta and R. van Eldik, 2011, *Inorg. Chem*., **50**, 8984.

46 R. E Norman, J. Ranford and P. J Sadler, 1992, *Inorg. Chem*., **31**, 880; and reference cited therein.

47 (a) Y. Kasherman, S. Sturup and D. Gibson, 2009, *J. Biol. Inorg. Chem*., **14**, 387; (b) G. Ma, Y. Min, F. Huang, T. Jiang and Y. Liu, 2010, Chem. Commun., 46,

48 M. E. Oehlsen, A. Hegmans, Y. Qu and N. Farrell, 2005, *Inorg. Chem*., **44**, 3004.

49 A. Hofmann, D. Jaganyi, O. Q. Munro, G. Liehr and R. van Eldik, 2003, *Inorg. Chem*., **42**, 1688.

50 A. Mambanda and D. Jaganyi, 2011, *Dalton Trans*., **40**, 79.

51 T. G. Appleton, J. R. Hall, S. F. Ralph and C. S. M. Thompson, 1989, *Inorg. Chem*., **28**, 1989.

52 D. Reddy and D. Jaganyi, 2011, *Int. J. Chem. Kinet*. **43**, 161.

53 A. Hofmann, L. Dahlengburg and R. van Eldik, 2003, *Inorg Chem*., **42**, 6528.

54 J-T, Chen, *"Platinum: Organometallic Chemistry" in Encyclopaedia of Inorganic Chemistry*, John Wiley & Sons, New York, 2006.

55 M. L. Tobe, J. Burgess, *Inorganic Reaction Mechanisms*, Addison Wisey, Longman, Ltd., Essex, 1999, pp. 30-33; 70-112.

56 F. Basolo, R. G. Pearson, *Mechanisms of Inorganic Reactions*, 2nd, Ed., Wiley, New York, 1967, pp. 80-115.

57 J. D. Atwood, *Inorganic and Organometallic Reaction Mechanisms*, 2nd, Ed., Wiley-VCH, NY, 1997, pp. 43-61.

Appendix 7

Table S7.1: Summary of selected wavelengths (nm) used in kinetic studies

Nucleophile	Wavelength (nm)					
	EnPt	**PropPt**	**ButPt**	**HexPt**	**OctPt**	**DecPt**
TU	312	306	305	343	343	308
DMTU	312	306	305	343	337	306
TMTU	340	340	370	370	363	343

Table S7.2: Summary of $k_{obs(1st)}$, values for simultaneous displacement of aqua ligands for **EnPt** complex with thiourea nucleophiles, pH = 2.0, T = 298 K, I = 0.1 M ($NaClO_4$, adjusted with 0.01 M $HClO_4$).

Nucleophile	$k_{obs(1^{st})}$, in s^{-1}		
	TU	**DMTU**	**TMTU**
0.00218	0.00901	0.00432	0.00144
0.00436	0.02068	0.01072	0.00277
0.00654	0.0279	0.01588	0.00404
0.00872	0.03822	0.02223	0.00540
0.0109	0.0493	0.02868	0.00704

Table S7.3: Summary of $k_{obs(2^{nd})}$, values for displacement of ammine (NH_3) ligand for **EnPt** complex with thiourea nucleophiles, pH = 2.0, T = 298 K, I = 0.1 M ($NaClO_4$, adjusted with 0.01 M $HClO_4$).

Nucleophile	$k_{obs(2^{nd})}$, in s^{-1}		
	TU	**DMTU**	**TMTU**
0.00218	4.8990×10^{-5}	2.5630×10^{-5}	1.8956×10^{-5}
0.00436	1.0452×10^{-4}	4.8656×10^{-5}	3.7707×10^{-5}
0.00654	1.5810×10^{-4}	7.1840×10^{-5}	5.6952×10^{-5}
0.00872	2.1030×10^{-4}	9.5300×10^{-5}	7.5834×10^{-5}
0.01090		1.1789×10^{-4}	9.4686×10^{-5}

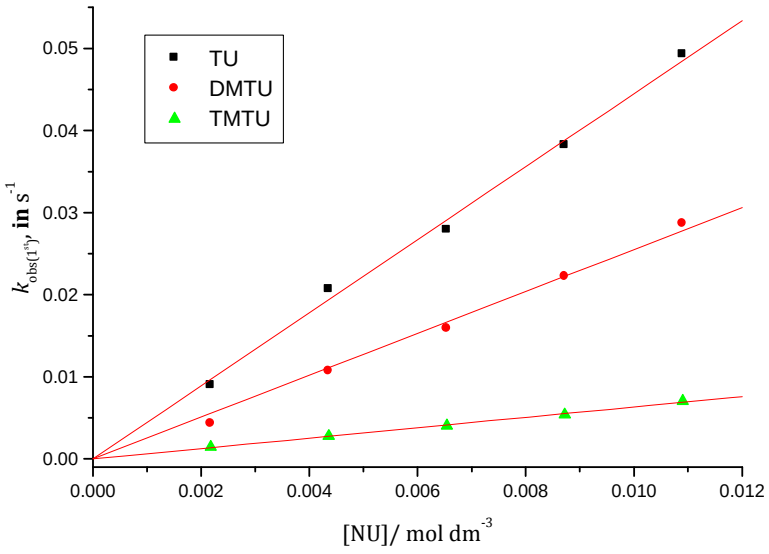

Figure S7.1: Concentration dependence of $k_{obs(1^{st})}$, s^{-1}, for the simultaneous displacement of the coordinated water molecules in **EnPt** by thiourea nucleophiles, pH =2.0, T =298 K, I = 0.1 M ($NaClO_4$, adjusted with 0.01 M $HClO_4$).

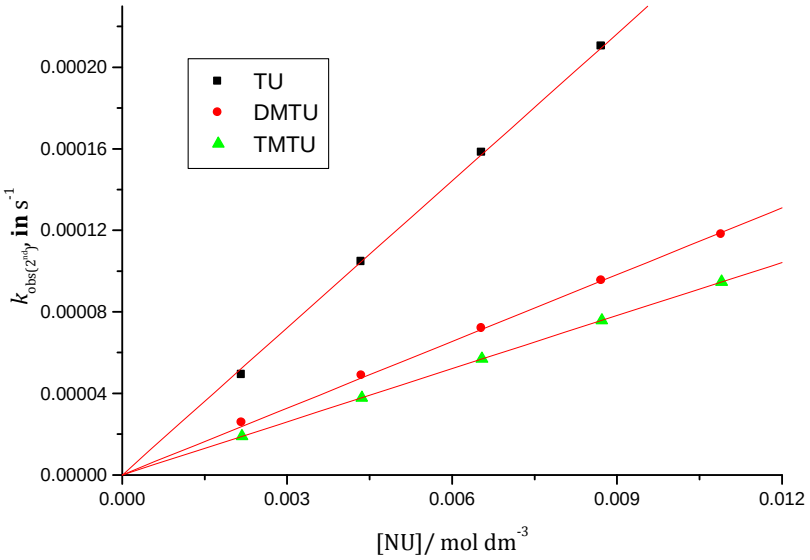

Figure S7.2: Concentration dependence of $k_{obs(2^{nd})}$, s^{-1}, for the displacement of the ammine (NH_3) ligand in **EnPt** by thiourea nucleophiles, pH =2.0, T = 298 K, I = 0.1 M ($NaClO_4$, adjusted with 0.01 M $HClO_4$).

Table S7.4: Average observed rate constants, $k_{obs(1^{st})}$, for the simultaneous displacement of aqua ligands in **EnPt** at varied temperatures in the range 15 to 35 °C while maintaining nucleophile concentration at ≈ 60x [**EnPt**].

1/T, K^{-1}	**TU**		**DMTU**		**TMTU**	
	$k_{obs(1^{st})}$, s^{-1}	**ln(k_2/T)**	**$k_{obs(1^{st})}$, s^{-1}**	**ln(k_2/T)**	**$k_{obs(1^{st})}$, s^{-1}**	**ln(k_2/T)**
0.00347	0.01154	-5.0948	0.007525	-5.5227	0.001363	-7.2310
0.00341	001793	-4.6715	0.01146	-5.1193	0.002223	-6.7595
0.00335	0.02799	-4.2432	0.01588	-4.8101	0.003870	-6.2218
0.00330	0.03799	-3.9543	0.02192	-4.5041	0.005560	-5.8761
0.00325	0.05523	-3.5966	0.02929	-4.2309	0.008305	-5.4912

Table S7.5: Average observed rate constants, $k_{obs(2^{nd})}$, for the displacement of ammine ligand in **EnPt** at varied temperatures in the range 15 to 35 °C while maintaining nucleophile concentration at ≈ 60x [**EnPt**].

1/T, K^{-1}	**TU**		**DMTU**		**TMTU**	
	$k_{obs(2^{nd})}$, s^{-1}	**ln(k_2/T)**	**$k_{obs(2^{nd})}$, s^{-1}**	**ln(k_2/T)**	**$k_{obs(2^{nd})}$, s^{-1}**	**ln(k_2/T)**
0.00347	7.732 x 10^{-5}	-10.1007	3.436 x 10^{-5}	-10.9119	2.784 x 10^{-5}	-11.1220
0.00341	1.083 x 10^{-4}	-9.7813	4.867 x 10^{-5}	-10.5809	3.963 x 10^{-5}	-10.7863
0.00335	1.581 x 10^{-4}	-9.4195	7.184 x 10^{-5}	-10.2084	5.688 x 10^{-5}	-10.4418
0.00330	2.248 x 10^{-4}	-9.0844	1.046 x 10^{-4}	-9.8492	8.158 x 10^{-5}	-10.0979
0.00325	3.251 x 10^{-4}	-8.7316	1.508 x 10^{-4}	-9.4999	1.094 x 10^{-4}	-9.8221

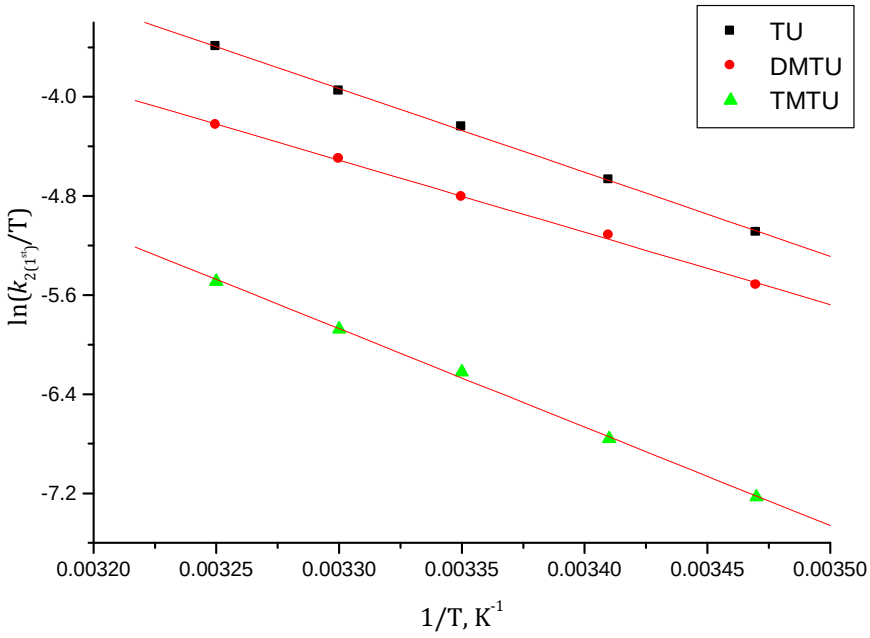

Figure S7.3: Eyring plots forthe determination of the activation enthalpies and entropies for $k_{2,1^{st}}$ of all nucleophiles studied with **EnPt** complex.

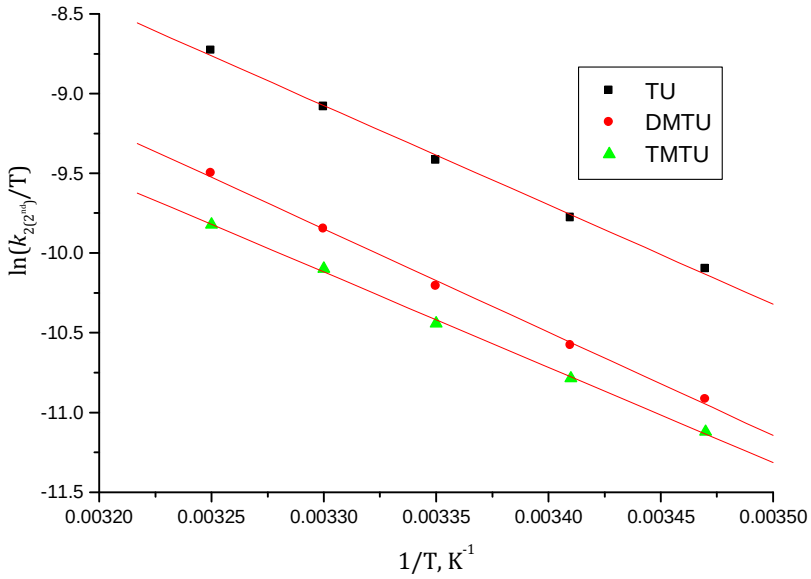

FigureS7.4: Eyring plots forthe determination of the activation enthalpies and entropies for $k_{2,2}^{nd}$ of all nucleophiles studied with **EnPt** complex.

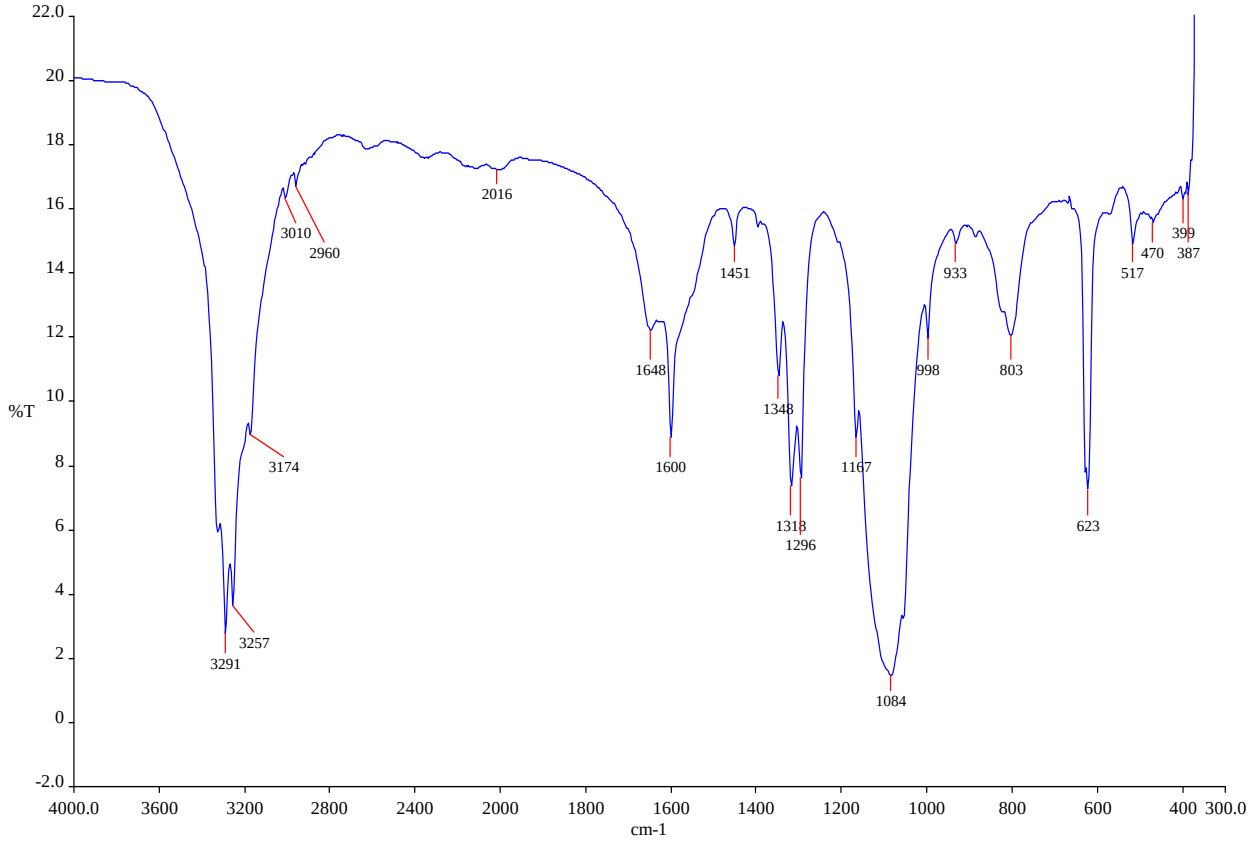

Figure S7.5: Infrared (KBr disc) spectrum for **EnPt** complex.

Table S7.6: Summary of $k_{obs(1^{st})}$, values for simultaneous displacement of aqua ligands for **PropPt** complex with thiourea nucleophiles, pH = 2.0, T = 298 K, *I* = 0.1 M ($NaClO_4$, adjusted with 0.01 M $HClO_4$).

Nucleophile		$k_{obs(1^{st})}$, **in** s^{-1}	
	TU	**DMTU**	**TMTU**
0.00267	0.01035	0.00567	0.00264
0.00533	0.2294	0.01359	0.00602
0.00800	0.03450	0.02227	0.00867
0.01066	0.04436	0.02826	0.01046
0.01333	0.05866		0.01446

Table S7.7: Summary of $k_{obs(2^{nd})}$, values for displacement of ammine (NH_3) ligand for **PropPt** complex with thiourea nucleophiles, pH = 2.0, T = 298 K, *I* = 0.1 M ($NaClO_4$, adjusted with 0.01 M $HClO_4$).

Nucleophile		$k_{obs(2^{nd})}$, in s^{-1}	
	TU	**DMTU**	**TMTU**
0.00267	1.214×10^{-4}	5.615×10^{-5}	1.784×10^{-5}
0.00533	2.360×10^{-4}	9.508×10^{-5}	3.008×10^{-5}
0.00800	3.576×10^{-4}	1.597×10^{-4}	4.230×10^{-5}
0.01066	4.573×10^{-4}	2.157×10^{-4}	5.991×10^{-5}
0.01333	5.802×10^{-4}	2.632×10^{-4}	7.964×10^{-5}

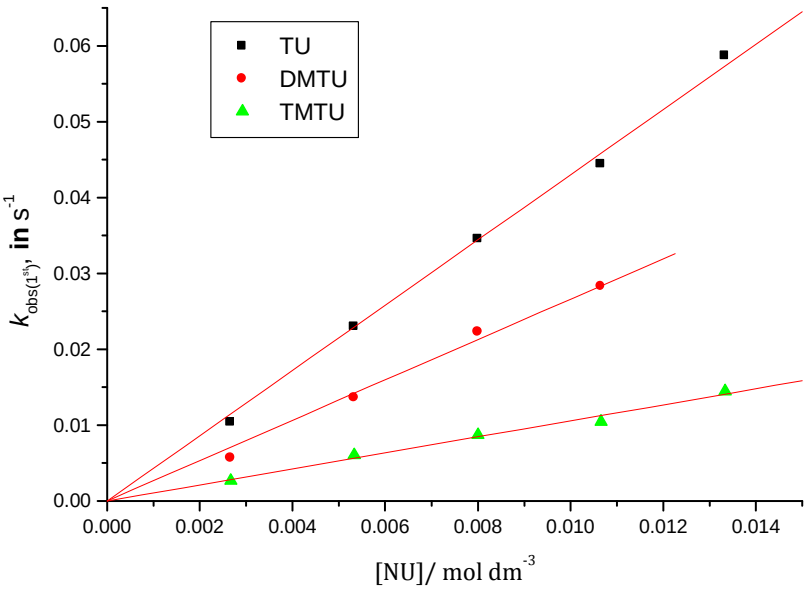

Figure S7.6: Concentration dependence of $k_{obs(1^{st})}$, s^{-1}, for the simultaneous displacement of the coordinated water molecules in **PropPt** by thiourea nucleophiles, pH =2.0, T =298 K, I = 0.1 M ($NaClO_4$, adjusted with 0.01 M $HClO_4$).

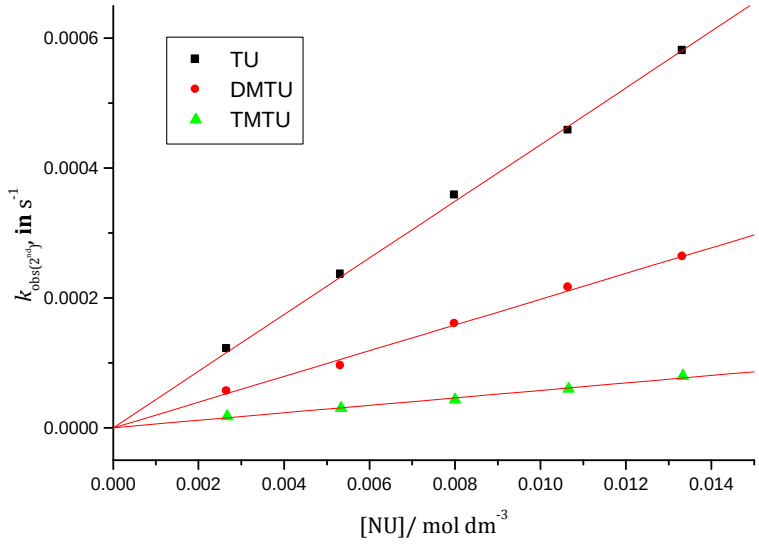

Figure S7.7: Concentration dependence of $k_{obs(2^{nd})}$, s^{-1}, for the displacement of the ammine (NH_3) ligand in **PropPt** by thiourea nucleophiles, pH =2.0, T =298 K, I = 0.1 M ($NaClO_4$, adjusted with 0.01 M $HClO_4$).

Table S7.8: Average observed rate constants, $k_{obs(1^{st})}$, for the simultaneous displacement of aqua ligands in **PropPt** at varied temperatures in the range 15 to 35 °C while maintaining nucleophile concentration at ≈ 60x [**PropPt**].

1/T, K^{-1}	**TU**		**DMTU**		**TMTU**	
	$k_{obs(1^{st})}$, s^{-1}	**ln(k_2/T)**	**$k_{obs(1^{st})}$, s^{-1}**	**ln(k_2/T)**	**$k_{obs(1^{st})}$, s^{-1}**	**ln(k_2/T)**
0.00347	0.02538	-4.5086	0.0255	-4.5037	0.002553	-6.8050
0.00341	0.03524	-4.1974	0.03631	-4.1675	0.003632	-6.4698
0.00335	0.05140	-3.8370	0.05124	-3.8400	0.005146	-6.1383
0.00330	0.06903	-3.5586	0.06890	-3.5606	0.006994	-5.8481
0.00325	0.08866	-3.3248	0.09254	-3.2819	0.009438	-5.5648

Table S7.9: Average observed rate constants, $k_{obs(2^{nd})}$, for the displacement of ammine ligand in **PropPt** at varied temperatures in the range 15 to 35 °C while maintaining nucleophile concentration at ≈ 60x [**PropPt**].

1/T, K^{-1}	**TU**		**DMTU**		**TMTU**	
	$k_{obs(2^{nd})}$, s^{-1}	**ln(k_2/T)**	**$k_{obs(2^{nd})}$, s^{-1}**	**ln(k_2/T)**	**$k_{obs(2^{nd})}$, s^{-1}**	**ln(k_2/T)**
0.00347	1.517 x 10^{-4}	-9.6281	4.420 x 10^{-5}	-10.8617	4.006 x 10^{-5}	-10.9597
0.00341	2.417 x 10^{-4}	-9.1796	6.747 x 10^{-5}	-10.4557	5.670 x 10^{-5}	-10.6297
0.00335	3.576 x 10^{-4}	-8.8050	9.738 x 10^{-5}	-10.1057	7.753 x 10^{-5}	-10.3337
0.00330	5.299 x 10^{-4}	-8.4282	1.479 x 10^{-4}	-9.7047	1.118 x 10^{-4}	-9.9847
0.00325	8.094 x 10^{-4}	-8.0210	2.080 x 10^{-4}	-9.3797	1,520 x 10^{-4}	-9.6937

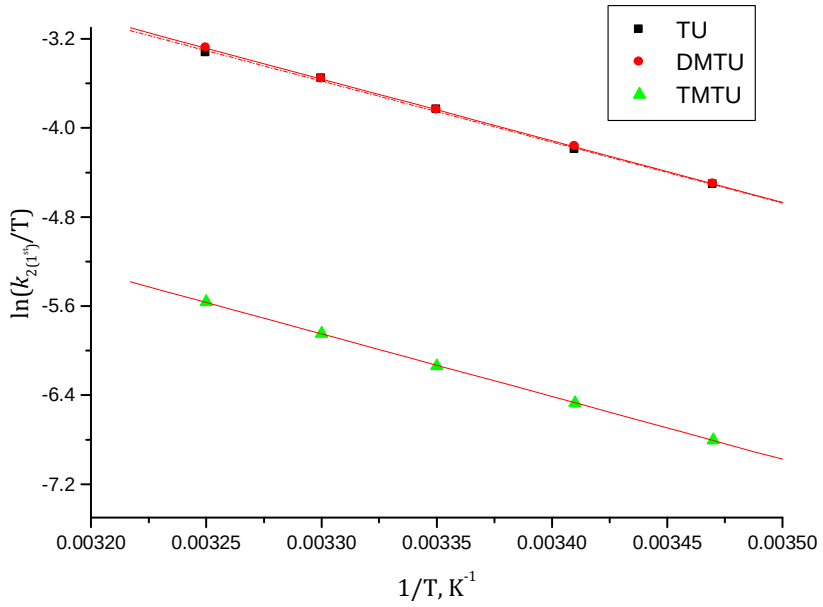

Figure S7.8: Eyring plots forthe determination of the activation enthalpies and entropies for $k_{2,1st}$ of all nucleophiles studied with **PropPt** complex.

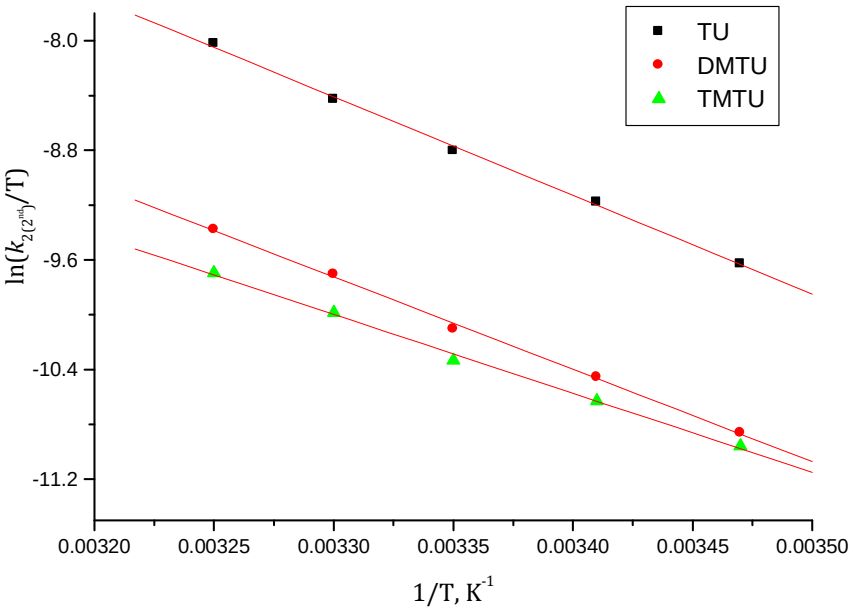

Figure S7.9: Eyring plots forthe determination of the activation enthalpies and entropies for $k_{2,2^{nd}}$ of all nucleophiles studied with **PropPt** complex.

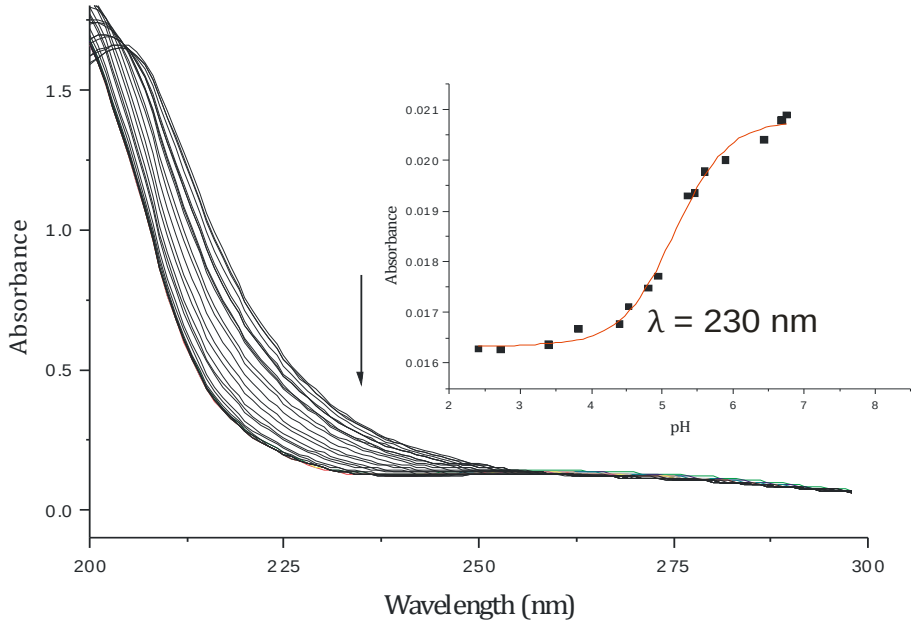

Figure S7.10: UV-Vis spectra recorded for the **PropP*t*** complex in the pH range 2-10 at 25 °C. Inset: Plot of absorbance versus pH at 230 nm.

Table S7.10: Summary of $k_{obs(1st)}$, values for simultaneous displacement of aqua ligands for **ButPt** complex with thiourea nucleophiles, pH = 2.0, T = 298 K, I = 0.1 M ($NaClO_4$, adjusted with 0.01 M $HClO_4$).

Nucleophile	$k_{obs(1st)}$, in s^{-1}		
	TU	**DMTU**	**TMTU**
0.00229	0.00935	0.00613	0.00153
0.00458	0.02027	0.01158	0.00309
0.00686	0.03140	0.01661	0.00466
0.00915	0.04238	0.02434	0.00630
0.01144	0.05428		0.00726

Table S7.11: Summary of $k_{obs(2^{nd})}$, values for displacement of ammine (NH_3) ligand for **ButPt** complex with thiourea nucleophiles, pH = 2.0, T = 298 K, I = 0.1 M ($NaClO_4$, adjusted with 0.01 M $HClO_4$).

Nucleophile	$k_{obs(2^{nd})}$, in s^{-1}		
	TU	**DMTU**	**TMTU**
0.00229	9.5494 x 10-5	3.5032 x 10-5	1.9006 x 10-5
0.00458	1.9802 x 10-4	6.7004 x 10-5	3.7380 x 10-5
0.00686	2.8605 x 10-4	1.0474 x 10-4	5.7338 x 10-5
0.00915	3.7232 x 10-4	1.3550 x 10-4	7.5472 x 10-5
0.01144	4.7298 x 10-4	1.7214 x 10-4	

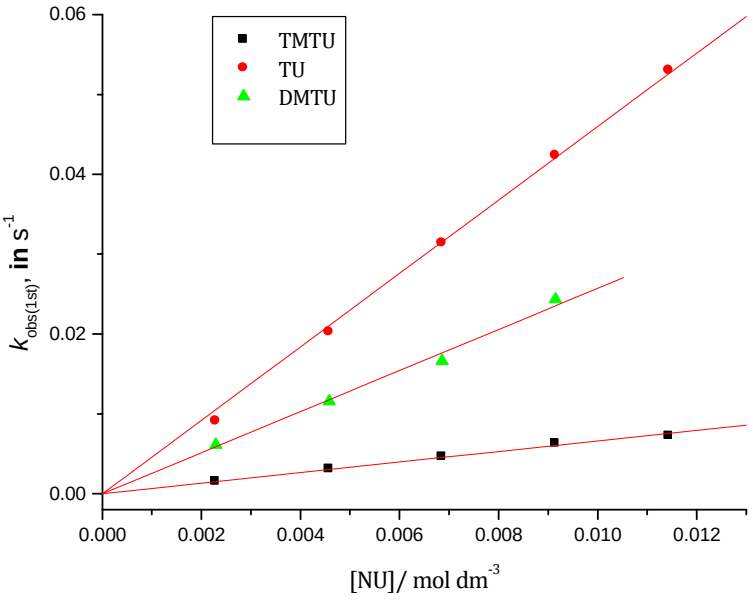

Figure S7.11: Concentration dependence of $k_{obs(1^{st})}$, s^{-1}, for the simultaneous displacement of the coordinated water molecules in **ButPt** by thiourea nucleophiles, pH =2.0, T =298 K, I = 0.1 M ($NaClO_4$, adjusted with 0.01 M $HClO_4$).

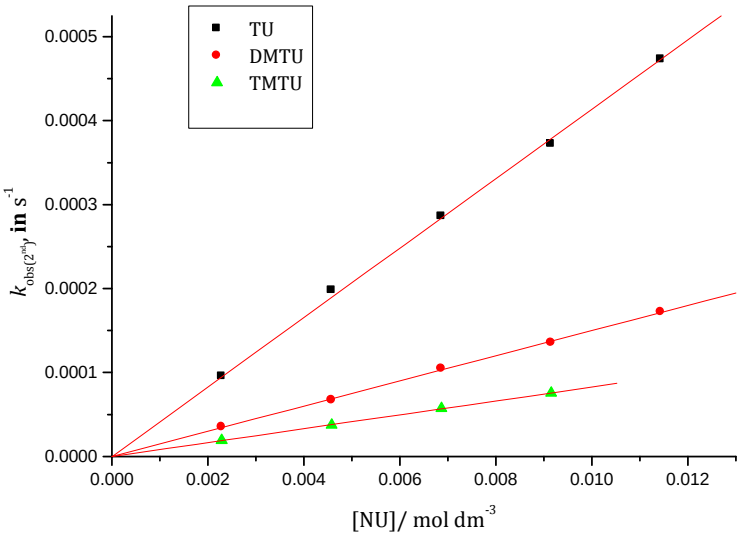

Figure S7.12: Concentration dependence of $k_{obs(2^{nd})}$, s^{-1}, for the displacement of the ammine (NH_3) ligand in **ButPt** by thiourea nucleophiles, pH =2.0, T = 298 K, I = 0.1 M ($NaClO_4$, adjusted with 0.01 M $HClO_4$).

Table S7.12: Average observed rate constants, $k_{obs(1^{st})}$, for the simultaneous substitution of aqua ligands in **ButPt** at varied temperatures in the range 15 to 35 °C while maintaining nucleophile concentration at ≈ 60x [**ButPt**].

1/T, K^{-1}	**TU**		**DMTU**		**TMTU**	
	$k_{obs(1^{st})}$, s^{-1}	**ln(k_2/T)**	**$k_{obs(1^{st})}$, s^{-1}**	**ln(k_2/T)**	**$k_{obs(1^{st})}$, s^{-1}**	**ln(k_2/T)**
0.00347	0.01224	-5.0845	0.00684	-5.6659	0.00226	-6.7739
0.00341	0.02034	-4.5939	0.0105	-5.2547	0.00300	-6.5068
0.00335	0.03140	-4.1766	0.0174	-4.7666	0.00466	-6.0844
0.00330	0.05051	-3.7179	0.0286	-4.2986	0.00615	-5.8232
0.00325	0.06943	-3.4161	0.0388	-3.9969	0.00724	-5.6768

Table S7.13: Average observed rate constants, $k_{obs(2^{nd})}$, for the displacement of ammine ligand in **ButPt** at varied temperatures in the range 15 to 35 °C while maintaining nucleophile concentration at ≈ 60x [**ButPt**].

1/T, K^{-1}	**TU**		**DMTU**		**TMTU**	
	$k_{obs(2^{nd})}$, s^{-1}	**ln(k_2/T)**	**$k_{obs(2^{nd})}$, s^{-1}**	**ln(k_2/T)**	**$k_{obs(2^{nd})}$, s^{-1}**	**ln(k_2/T)**
0.00347	7.482 x 10^{-5}	-10.1819	5.479 x 10^{-5}	-10.4935	1.450 x 10^{-5}	-11.8228
0.00341	1.092 x 10^{-4}	-9.8215	7.644 x 10^{-5}	-10.1777	2.564 x 10^{-5}	-11.2701
0.00335	1.689 x 10^{-4}	-9.4017	1.047 x 10^{-4}	-9.8796	4.170 x 10^{-5}	-10.8006
0.00330	2.404 x 10^{-4}	-9.0657	1.379 x 10^{-4}	-9.6209	6.646 x 10^{-5}	-10.3512
0.00325	3.519 x 10^{-4}	-8.7007	1.827 x 10^{-4}	-9.3561	9.532 x 10^{-5}	-10.0069

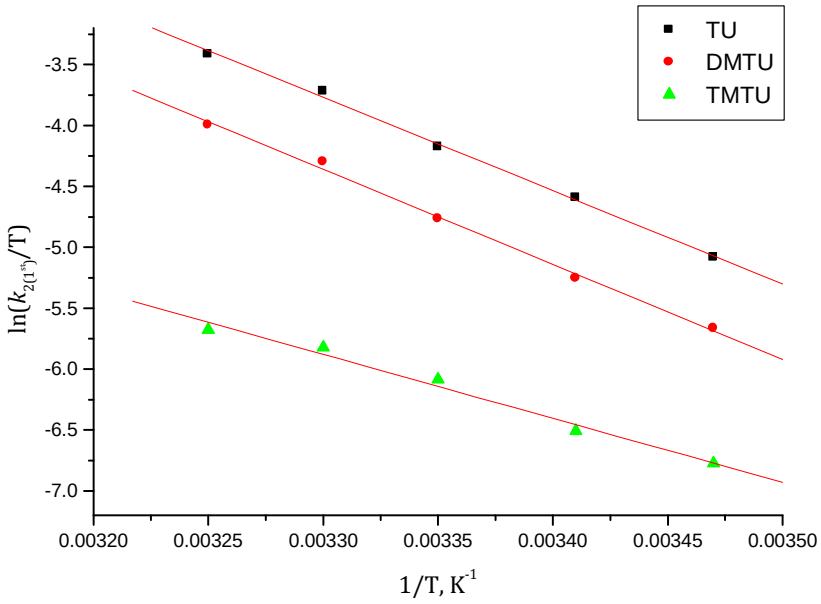

Figure S7.13: Eyring plots forthe determination of the activation enthalpies and entropies for $k_{2,1^{st}}$ of all nucleophiles studied with **ButPt** complex.

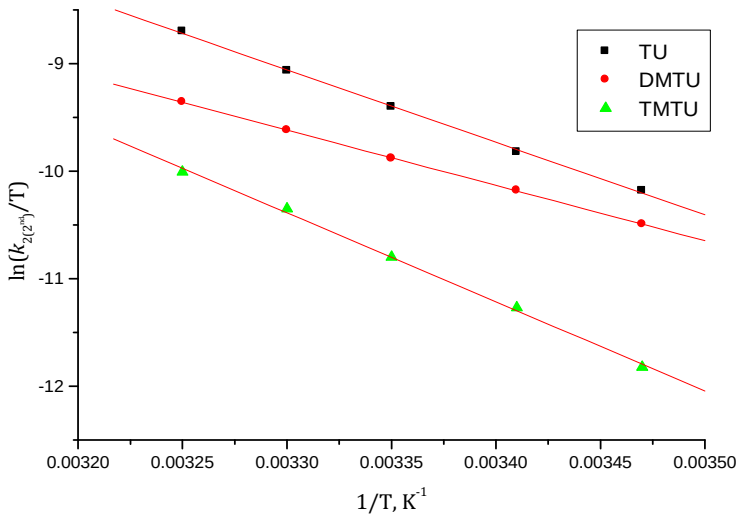

FigureS7.14: Eyring plots forthe determination of the activation enthalpies and entropies for $k_{2,2}^{nd}$ of all nucleophiles studied with **ButPt** complex.

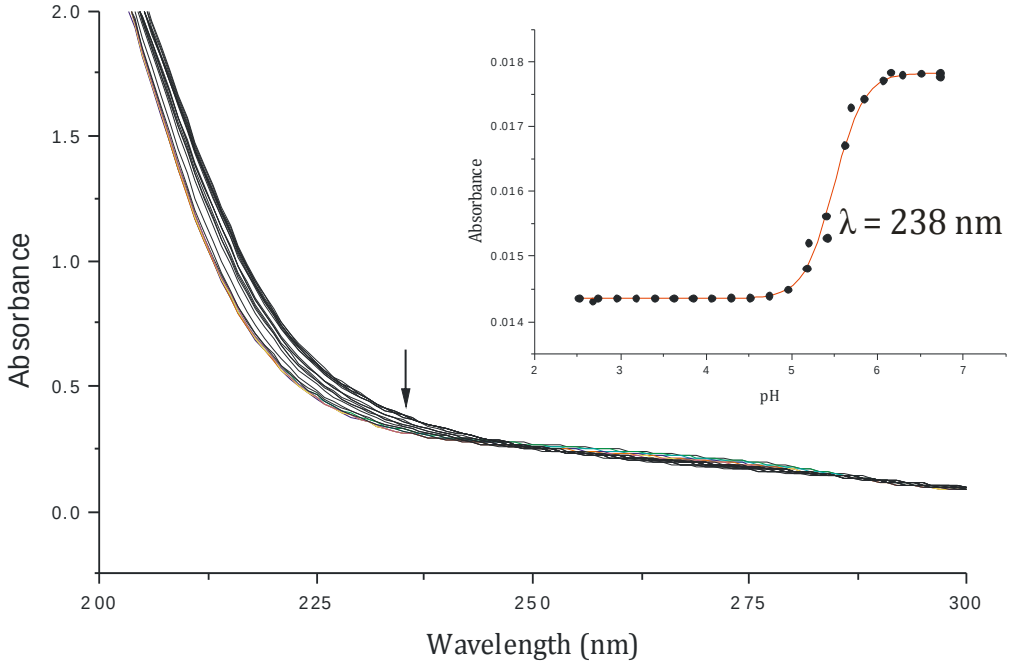

Figure S7.15: UV-Vis spectra recorded for the **ButPt** complex in the pH range 2-10 at 25 °C. Inset: Plot of absorbance versus pH at 238 nm.

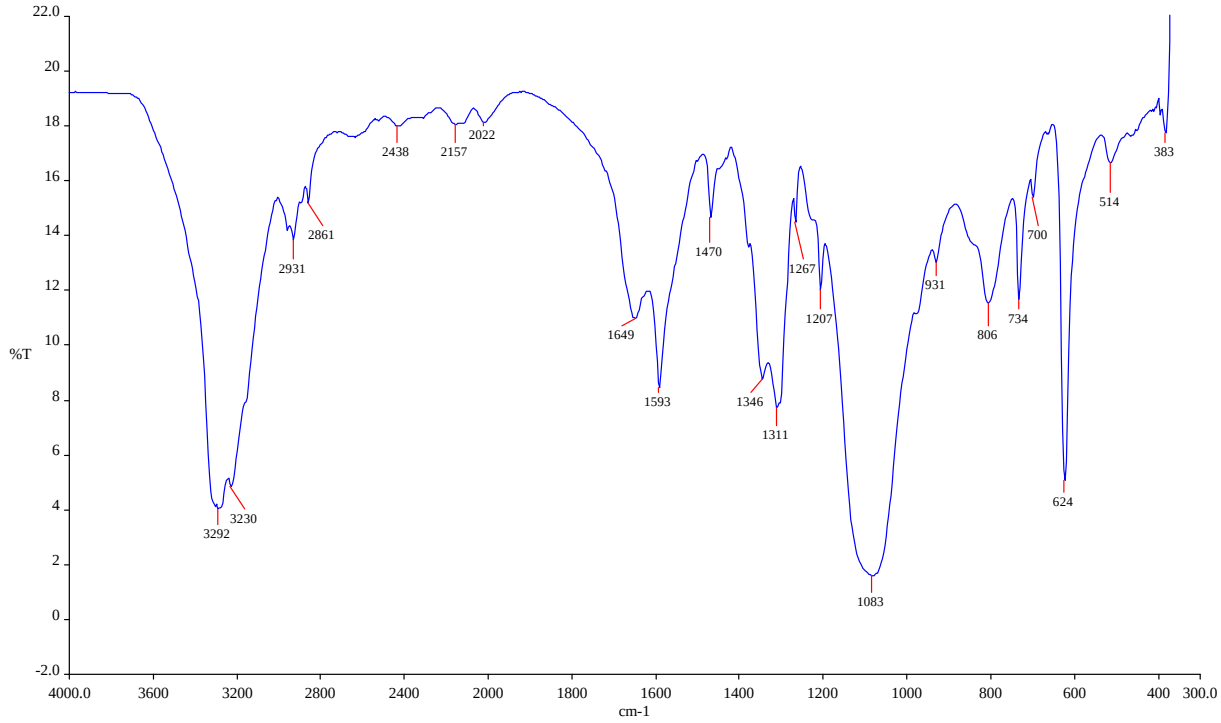

Figure S7.15: Infra-red (KBr disc) spectrum for **ButPt-Cl** complex.

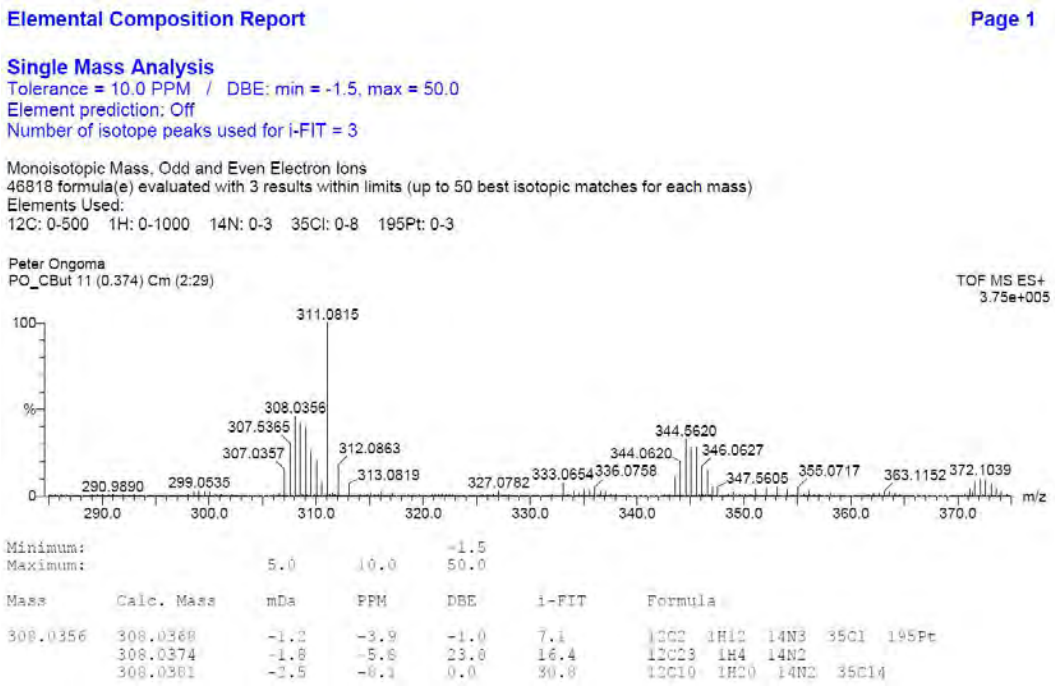

Figure S7.16: Mass spectra for **ButPt–Cl** complex (m/e, M^{2+}).

Table S7.14: Summary of $k_{obs(1^{st})}$, values for simultaneous displacement of aqua ligands for **HexPt** complex with thiourea nucleophiles, pH = 2.0, T = 298 K, I = 0.1 M ($NaClO_4$, adjusted with 0.01 M $HClO_4$).

Nucleophile	$k_{obs(1^{st})}$, in s^{-1}		
	TU	**DMTU**	**TMTU**
0.004	0.01617	0.00831	0.00310
0.008	0.03219	0.01824	0.00666
0.01199	0.04851	0.02556	0.00985
0.016	0.06417	0.03564	0.01314
0.02	0.08038	0.4123	

Table S7.15: Summary of $k_{obs(2^{nd})}$, values for displacement of ammine (NH_3) ligand for **HexPt** complex with thiourea nucleophiles, pH = 2.0, T = 298 K, I = 0.1 M ($NaClO_4$, adjusted with 0.01 M $HClO_4$).

Nucleophile	$k_{obs(2^{nd})}$, in s^{-1}		
	TU	**DMTU**	**TMTU**
0.00466	1.9050×10^{-4}	5.3492×10^{-5}	1.1197×10^{-5}
0.00932	3.7897×10^{-4}	1.0092×10^{-4}	2.0541×10^{-5}
0.01398	5.6289×10^{-4}	1.4823×10^{-4}	3.1558×10^{-5}
0.01865	7.4919×10^{-4}	1.9733×10^{-4}	4.3904×10^{-5}
0.02331	9.3180×10^{-4}	2.4301×10^{-4}	5.3042×10^{-5}

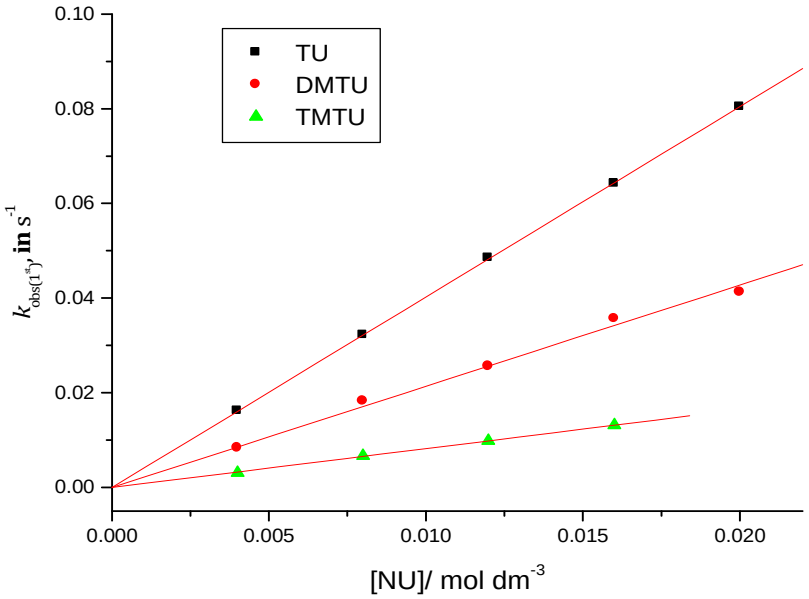

Figure S7.17: Concentration dependence of $k_{obs(1^{st})}$, s^{-1}, for the simultaneous displacement of the coordinated water molecules in **HexPt** by thiourea nucleophiles, pH =2.0, T =298 K, I = 0.1 M ($NaClO_4$, adjusted with 0.01 M $HClO_4$).

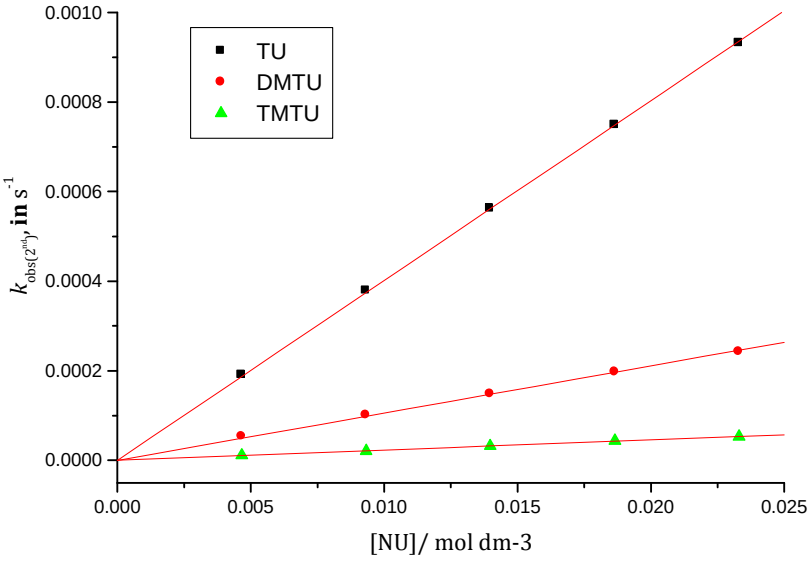

Figure S7.18: Concentration dependence of $k_{obs(2^{nd})}$, s^{-1}, for the displacement of the ammine (NH_3) ligand in HexPt by thiourea nucleophiles, pH =2.0, T = 298 K, I = 0.1 M ($NaClO_4$, adjusted with 0.01 M $HClO_4$).

Table S7.16: Average observed rate constants, $k_{obs(1^{st})}$, for the simultaneous displacement of aqua ligands in **HexPt** at varied temperatures in the range 15 to 35 °C while maintaining nucleophile concentration at ≈ 60x [**HexPt**].

1/T, K^{-1}	**TU**		**DMTU**		**TMTU**	
	$k_{obs(1^{st})}$, s^{-1}	**ln(k_2/T)**	**$k_{obs(1^{st})}$, s^{-1}**	**ln(k_2/T)**	**$k_{obs(1^{st})}$, s^{-1}**	**ln(k_2/T)**
0.00347	0.02701	-5.0040	0.01449	-5.6273	0.005154	-6.6608
0.00341	0.03642	-4.7227	0.02331	-5.1690	0.007896	-6.2514
0.00335	0.04851	-4.4530	0.03484	-4.7839	0.011452	-5.8966
0.00330	0.06134	-4.2349	0.05019	-4.4356	0.016240	-5.5639
0.00325	0.07809	-4.0099	0.07122	-4.1020	0.023000	-5.2322

Table S7.17: Average observed rate constants, $k_{obs(2^{nd})}$, for the displacement of ammine ligand in **HexPt** at varied temperatures in the range 15 to 35 °C while maintaining nucleophile concentration at ≈ 60x [**HexPt**].

1/T, K^{-1}	**TU**		**DMTU**		**TMTU**	
	$k_{obs(2^{nd})}$, s^{-1}	**ln(k_2/T)**	**$k_{obs(2^{nd})}$, s^{-1}**	**ln(k_2/T)**	**$k_{obs(2^{nd})}$, s^{-1}**	**ln(k_2/T)**
0.00347	2.528 x 10^{-4}	-9.6756	5.340 x 10^{-5}	-11.2307	1.986 x 10^{-5}	-12.2198
0.00341	4.294 x 10^{-4}	-9.1631	7.795 x 10^{-5}	-10.8695	3.349 x 10^{-5}	-11.7144
0.00335	6.919 x 10^{-4}	-8.7030	1.086 x 10^{-4}	-10.5554	5.472 x 10^{-5}	-11.2403
0.00330	1.010 x 10^{-3}	-8.3413			8.062 x 10^{-5}	-10.8694
0.00325	1.489 x 10^{-3}	-7.9699	2,248 x 10^{-4}	-9.8605	1.241 x 10^{-4}	-10.4546

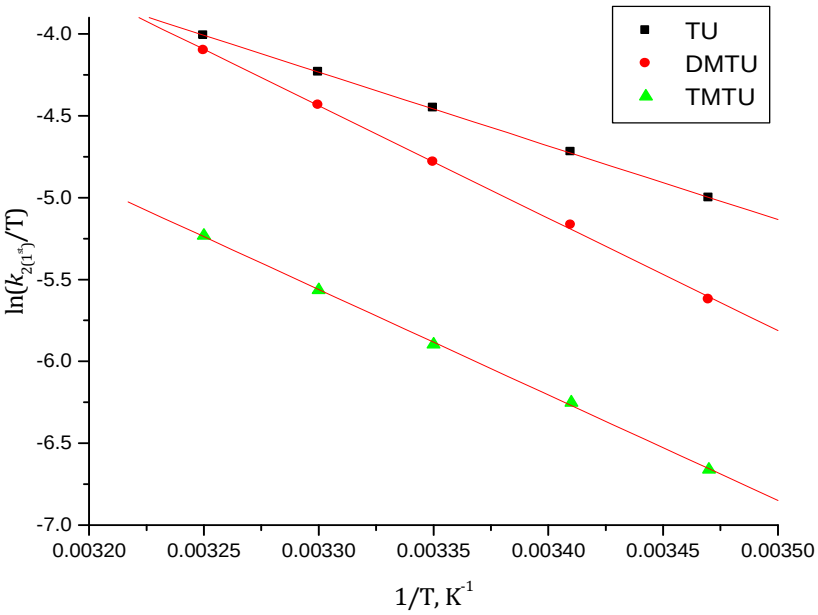

Figure S7.19: Eyring plots forthe determination of the activation enthalpies and entropies for $k_{2,1}^{st}$ of all nucleophiles studied with **HexPt** complex.

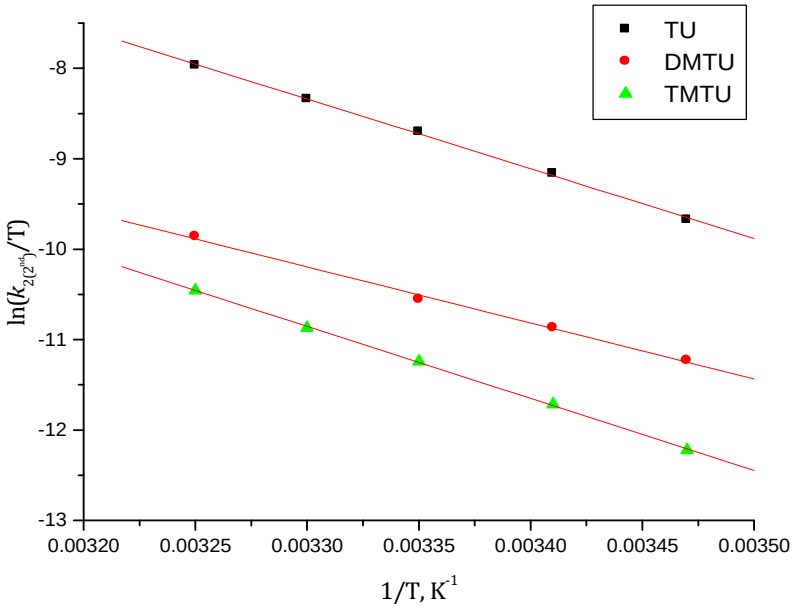

Figure S7.20: Eyring plots forthe determination of the activation enthalpies and entropies for $k_{2,2}^{nd}$ of all nucleophiles studied with **HexPt** complex.

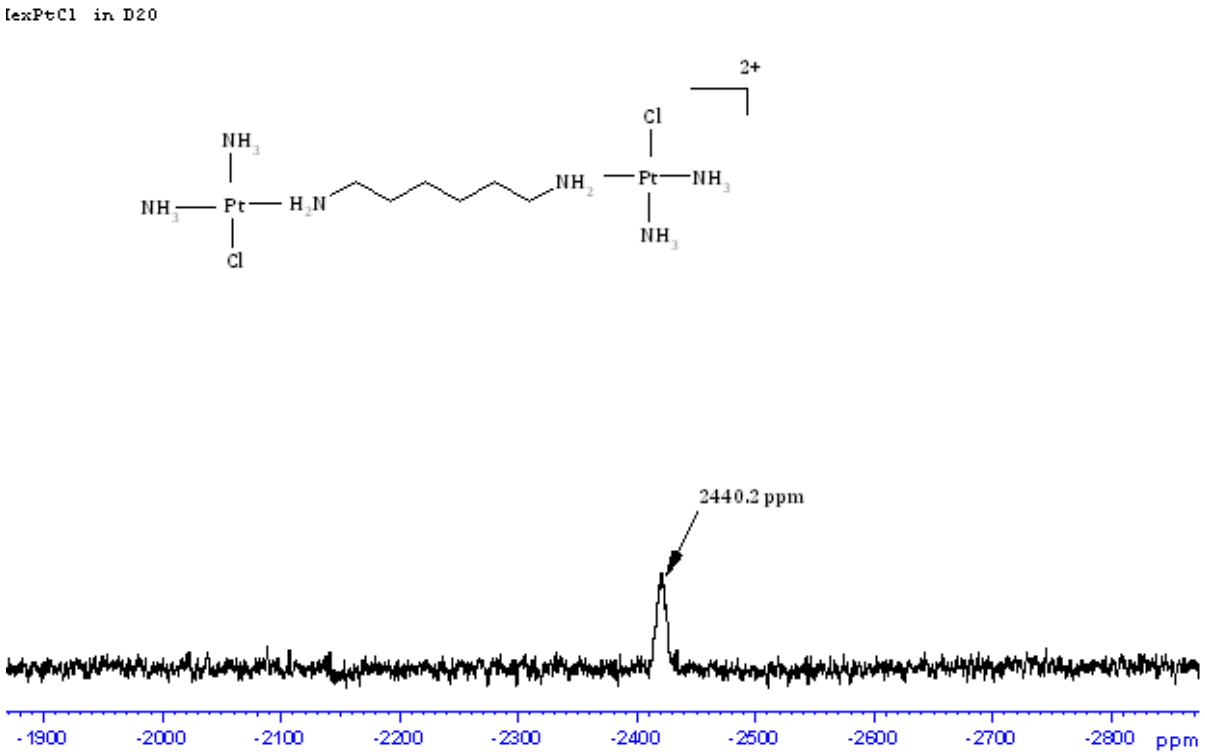

Figure S7.21: ^{195}Pt NMR for **HexPt–Cl** complex

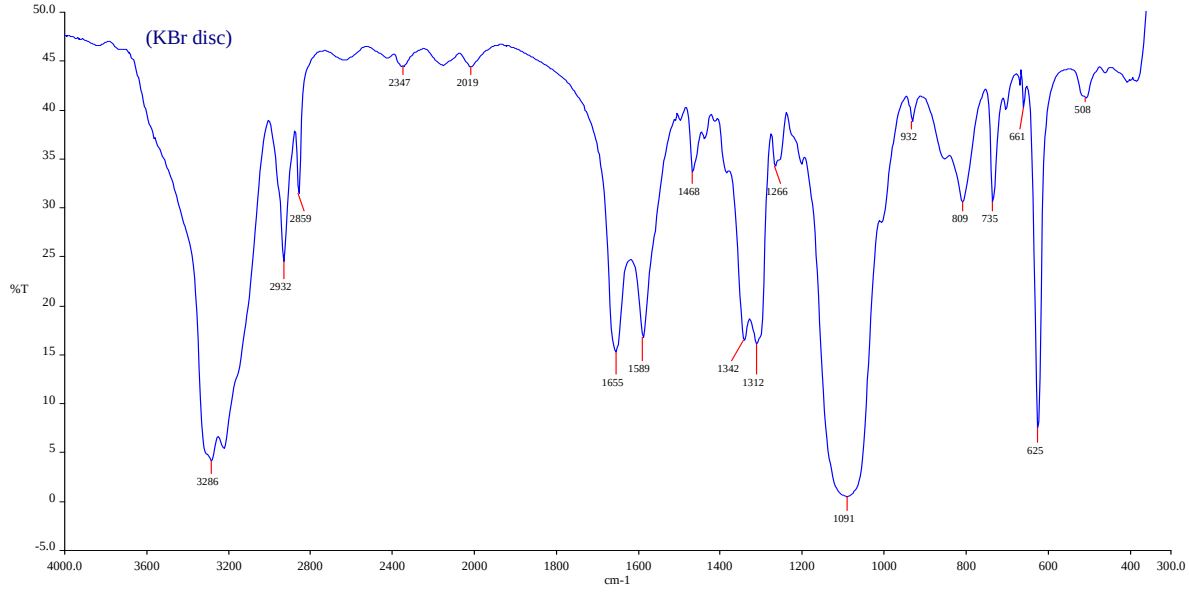

Figure S7.22: Infrared (KBr disc) spectrum for **HexPt** complex

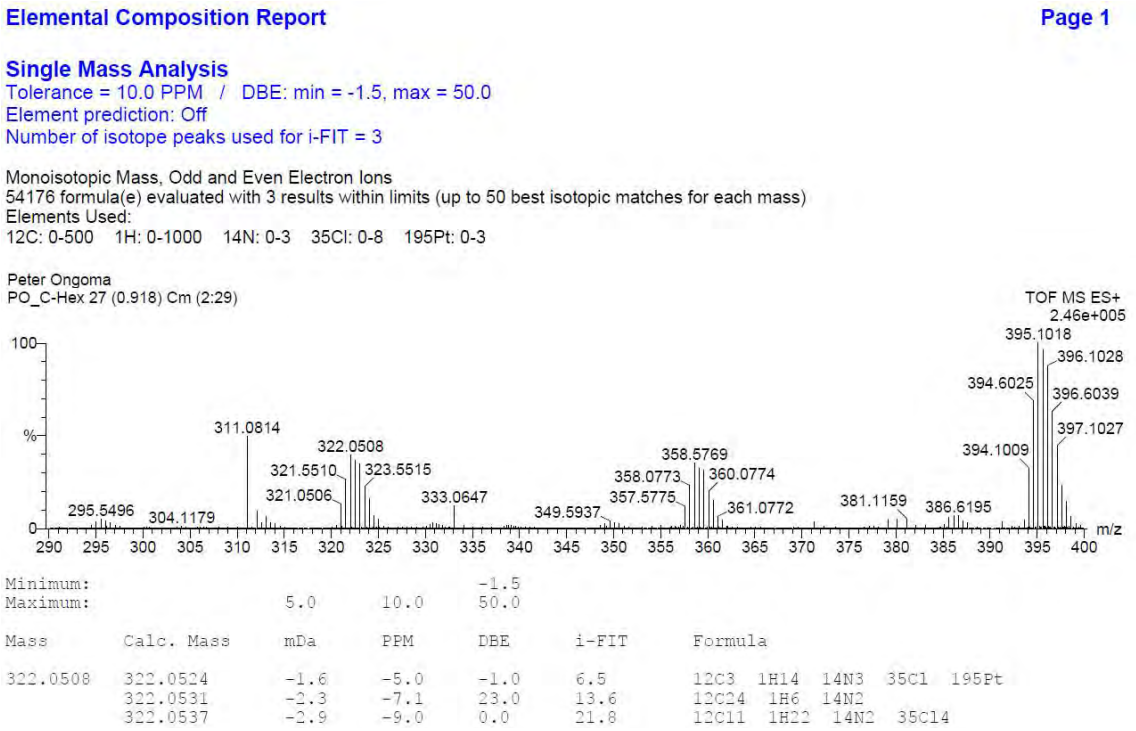

Figure S7.23: Mass spectra for **HexPt–Cl** complex (m/e, M^{2+})

Table S7.18: Summary of $k_{obs(1^{st})}$, values for simultaneous substitution of aqua ligands for **OctPt** complex with thiourea nucleophiles, pH = 2.0, T = 298 K, I = 0.1 M ($NaClO_4$, adjusted with 0.01 M $HClO_4$).

Nucleophile	$k_{obs(1^{st})}$, in s^{-1}		
	TU	**DMTU**	**TMTU**
0.00537	0.01657	0.01196	0.01020
0.01074	0.03641	0.02128	0.01163
0.01612	0.05347	0.03235	0.01328
0.02149	0.07371	0.04206	0.01728
0.02686	0.09241	0.05187	0.02004

Table S7.19: Summary of $k_{obs(2^{nd})}$, values for displacement of ammine ligands for **OctPt** complex with thiourea nucleophiles, pH = 2.0, T = 298 K, I = 0.1 M ($NaClO_4$, adjusted with 0.01 M $HClO_4$).

Nucleophile	$k_{obs(2^{nd})}$, in s^{-1}		
	TU	**DMTU**	**TMTU**
0.00537	2.3094×10^{-4}	1.0955×10^{-4}	1.3046×10^{-5}
0.01074	4.8961×10^{-4}	2.0867×10^{-4}	2.8080×10^{-5}
0.01612	7.2286×10^{-4}	3.0283×10^{-4}	4.2014×10^{-5}
0.02149	0.0010	4.1529×10^{-4}	5.4990×10^{-5}
0.02686	0.00122	5.1031×10^{-4}	

Table S7.20: Average observed rate constants, $k_{obs(1^{st})}$, for the simultaneous substitution of aqua ligands in **OctPt** at varied temperatures in the range 15 to 35 °C while maintaining nucleophile concentration at ≈ 60x [**OctPt**].

1/T, K^{-1}	**TU**		**DMTU**		**TMTU**	
	$k_{obs(1^{st})}$, s^{-1}	**ln(k_2/T)**	**$k_{obs(1^{st})}$, s^{-1}**	**ln(k_2/T)**	**$k_{obs(1^{st})}$, s^{-1}**	**ln(k_2/T)**
0.00347	0.02533	-5.2110	0.01631	-5.6512	0.005202	-6.7940
0.00341	0.03873	-4.8035	0.02436	-5.2673	0.007986	-6.3825
0.00335	0.05668	-4.4397	0.03235	-5.0007	0.011502	-6.0346
0.00330	0.07865	-4.1288	0.04613	-4.6624	0.015722	-5.7387
0.00325	0.10704	-3.8370	0.6147	-4.3916	0.022846	-5.3814

Table S21: Average observed rate constants, $k_{obs(2^{nd})}$, for the displacement of ammine ligand in **OctPt** at varied temperatures in the range 15 to 35 °C while maintaining nucleophile concentration at ≈ 60x [**OctPt**].

1/T, K^{-1}	**TU**		**DMTU**		**TMTU**	
	$k_{obs(2^{nd})}$, s^{-1}	**ln(k_2/T)**	**$k_{obs(2^{nd})}$, s^{-1}**	**ln(k_2/T)**	**$k_{obs(2^{nd})}$, s^{-1}**	**ln(k_2/T)**
0.00347	2.934 x 10^{-4}	-9.6692	1.161 x 10^{-4}	-10.5960		
0.00341	4.795 x 10^{-4}	-9.1952	1.791 x 10^{-4}	-10.1799	2.439 x 10^{-5}	-12.1740
0.00335	7.229 x 10^{-4}	-8.80171	2.758 x 10^{-4}	-9.7652	4.855 x 10^{-5}	-11.5023
0.00330	1.111 x 10^{-3}	-8.3885	3.648 x 10^{-4}	-9.5021	1.021 x 10^{-4}	-10.7756
0.00325	1.572 x 10^{-3}	-8.0575	5.251 x 10^{-4}	-9.1543	2.037 x 10^{-4}	-10.1013

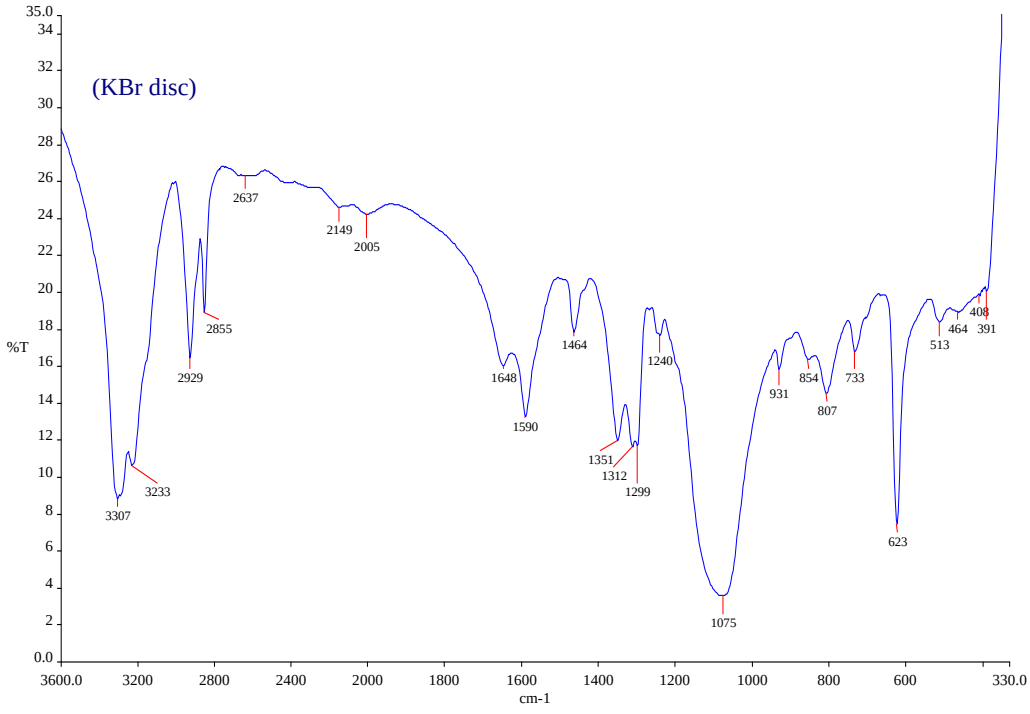

Figure S7.24: Infrared (KBr disc) spectrum for **OctPt** complex

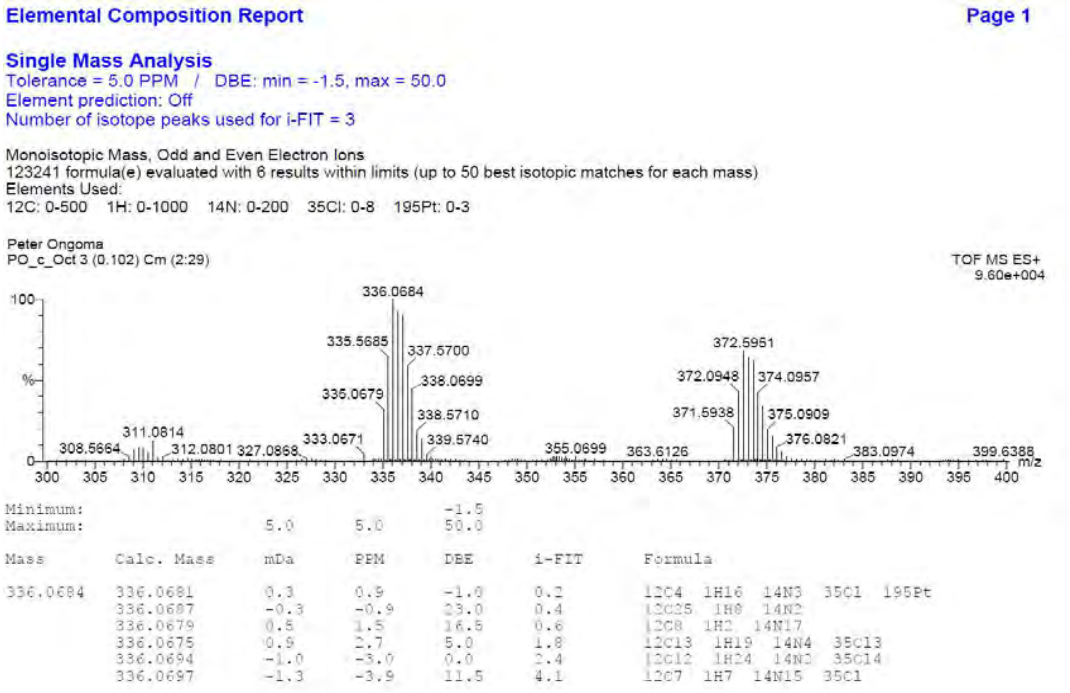

Figure S7.25: Mass spectra for **OctPt–Cl** complex (m/e, M^{2+})

Table S7.22: Summary of $k_{obs(1^{st})}$, values for simultaneous displacement of aqua ligands for **DecPt** complex with thiourea nucleophiles, pH = 2.0, T = 298 K, I = 0.1 M ($NaClO_4$, adjusted with 0.01 M $HClO_4$).

Nucleophile		$k_{obs(1^{st})}$, in s^{-1}	
	TU	**DMTU**	**TMTU**
0.004	0.01067	0.00764	0.00247
0.008	0.02211	0.01507	0.00372
0.012	0.03325	0.02204	0.00490
0.016	0.04260	0.02986	
0.02	0.05325	0.03798	0.00671

Table S7.23: Summary of $k_{obs(2^{nd})}$, values for the displacement of ammine ligand for **DecPt** complex with thiourea nucleophiles, pH = 2.0, T = 298 K, I = 0.1 M ($NaClO_4$, adjusted with 0.01 M $HClO_4$).

Nucleophile		$k_{obs(2^{nd})}$, in s^{-1}	
	TU	**DMTU**	**TMTU**
0.004	1.5397×10^{-4}	3.8955×10^{-5}	1.6433×10^{-5}
0.008	3.3925×10^{-4}	6.4793×10^{-5}	3.2068×10^{-5}
0.012	5.0926×10^{-4}	8.9079×10^{-5}	4.7073×10^{-5}
0.016	6.7317×10^{-4}	1.06525×10^{-4}	
0.02	8.4296×10^{-4}	1.3524×10^{-4}	8.1474×10^{-5}

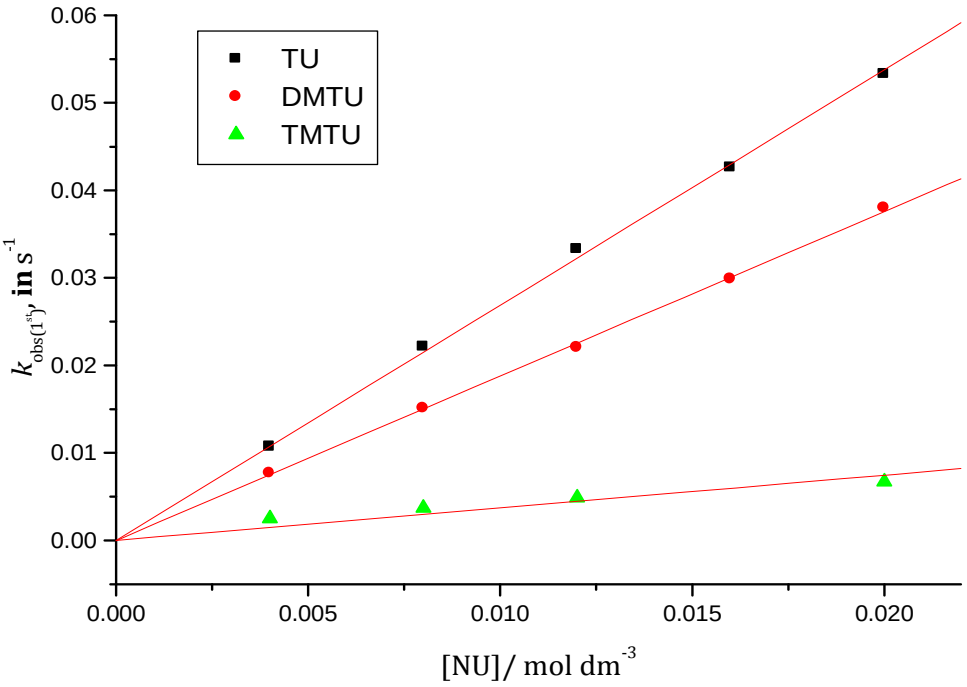

Figure S7.26 Concentration dependence of $k_{obs(1^{st})}$, s^{-1}, for the simultaneous substitution of the coordinated water molecules in **DecPt** by thiourea nucleophiles, pH =2.0, T =298 K, I = 0.1 M ($NaClO_4$, adjusted with 0.01 M $HClO_4$).

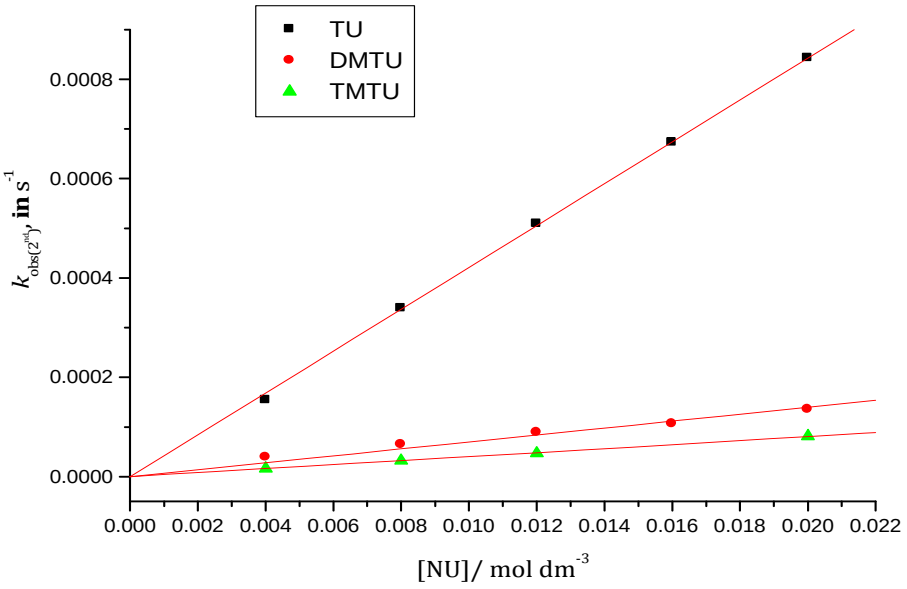

Figure S7.27: Concentration dependence of $k_{obs(2^{nd})}$, s^{-1}, for the displacement of the ammine ligand in **DecPt** by thiourea nucleophiles, pH =2.0, T =298 K, I = 0.1 M ($NaClO_4$, adjusted with 0.01 M $HClO_4$).

Table S7.24: Average observed rate constants, $k_{obs(1^{st})}$, for the simultaneous displacement of aqua ligands in **DecPt** at varied temperatures in the range 15 to 35 °C while maintaining nucleophile concentration at ≈ 60x [**DecPt**].

1/T, K^{-1}	**TU**		**DMTU**		**TMTU**	
	$k_{obs(1^{st})}$, s^{-1}	**ln(k_2/T)**	**$k_{obs(1^{st})}$, s^{-1}**	**ln(k_2/T)**	**$k_{obs(1^{st})}$, s^{-1}**	**ln(k_2/T)**
0.00347	0.01692	-5.6145	0.008528	-6.2951	0.002618	-7.1855
0.00341	0.02464	-5.2559	0.014920	-5.7575	0.003856	-6.7983
0.00335	0.03581	-4.8991	0.022037	-5.3844	0.005816	-6.4153
0.00330	0.04823	-4.6179	0.031282	-5.0508	0.008162	-6.0992
0.00325	0.06668	-4.3102	0.047719	-4.6448	0.01170	-5.7551

Table S7.25: Average observed rate constants, $k_{obs(2^{nd})}$, for the displacement of ammine ligand in **DecPt** at varied temperatures in the range 15 to 35 °C while maintaining nucleophile concentration at ≈ 60x [**DecPt**].

1/T, K^{-1}	**TU**		**DMTU**		**TMTU**	
	$k_{obs(2^{nd})}$, s^{-1}	**ln(k_2/T)**	**$k_{obs(2^{nd})}$, s^{-1}**	**ln(k_2/T)**	**$k_{obs(2^{nd})}$, s^{-1}**	**ln(k_2/T)**
0.00347	1.438 x 10^{-4}	-10.0871			3.781 x 10^{-5}	-11.4232
0.00341	2.164 x 10^{-4}	-9.6959	7.694 x 10^{-5}	-10.7298	6.608 x 10^{-5}	-10.8821
0.00335	3.174 x 10^{-4}	-9.3295	1.272 x 10^{-4}	-10.2442		
0.00330	4.492 x 10^{-4}	-8.9990	1.956 x 10^{-4}	-9.8306	1.831 x 10^{-4}	-9.8967
0.00325	6.272 x 10^{-4}	-8.6815	3.063 x 10^{-4}	-9.3984	3.023 x 10^{-4}	-9.5115

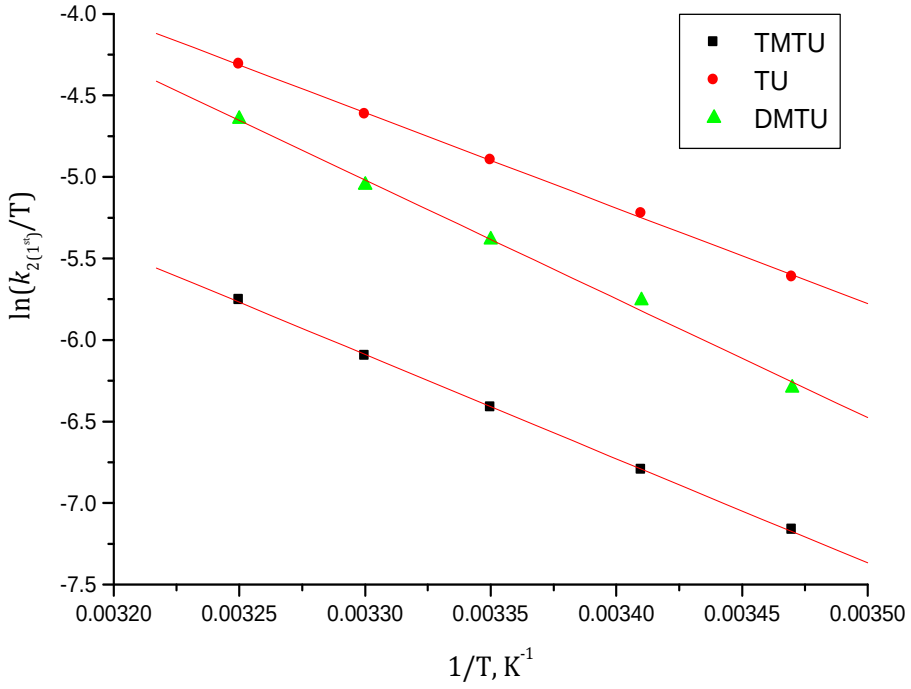

Figure S7.28: Eyring plots forthe determination of the activation enthalpies and entropies for $k_{2,1^{st}}$ of all nucleophiles studied with **DecPt** complex.

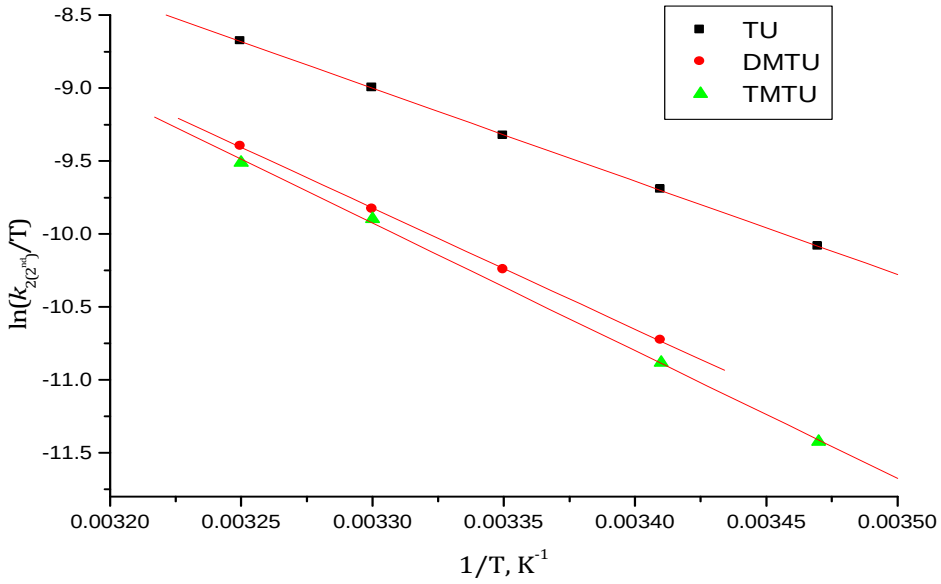

Figure S7.29: Eyring plots forthe determination of the activation enthalpies and entropies for $k_{2,2}^{nd}$ of all nucleophiles studied with **DecPt** complex.

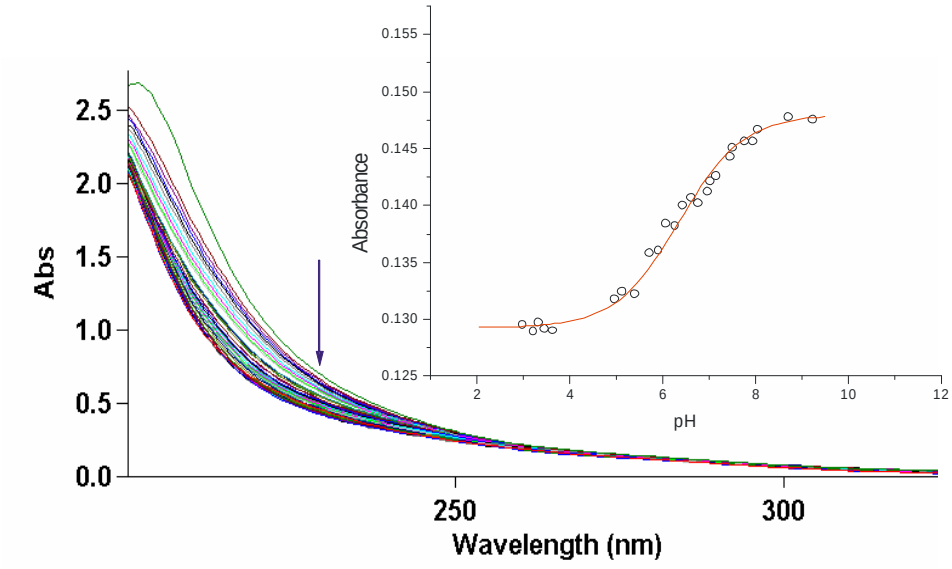

Figure S7.30: UV-Vis spectra recorded for the **DecP*t*** complex in the pH range 2-10 at 25 °C. Inset: Plot of absorbance versus pH at 261 nm.

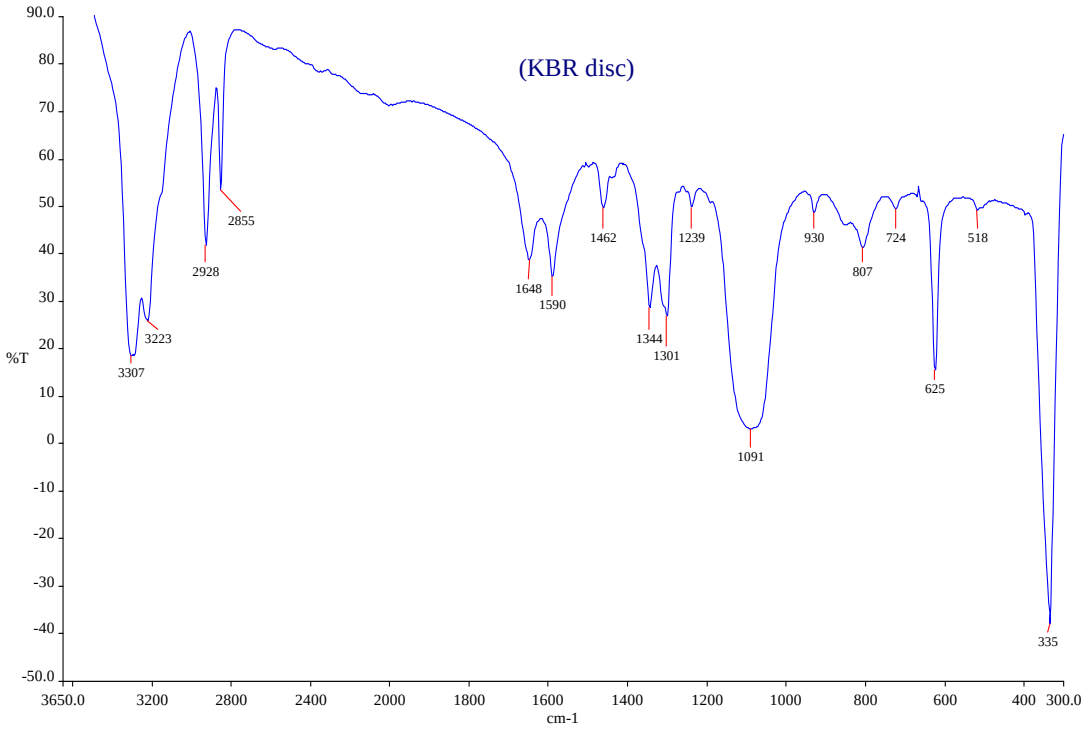

Figure S7.31: Infrared (KBr disc) spectrum for **DecPt** complex.

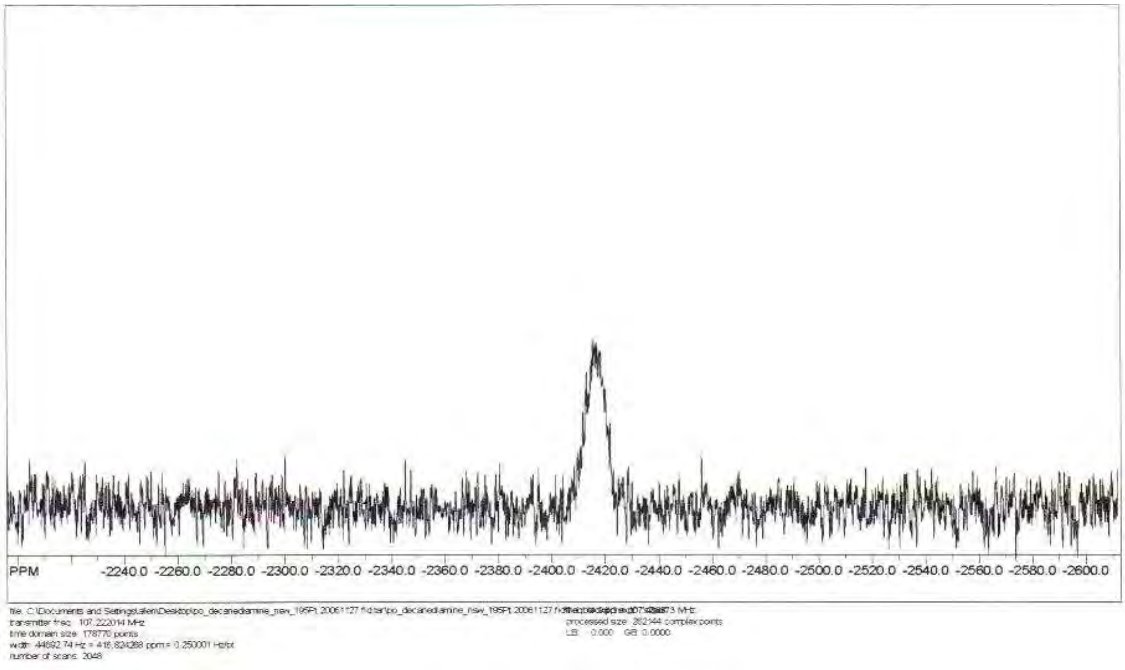

Figure S7.32: ^{195}Pt NMR spectrum for **DecPt-Cl** complex in D_2O at 30 °C.

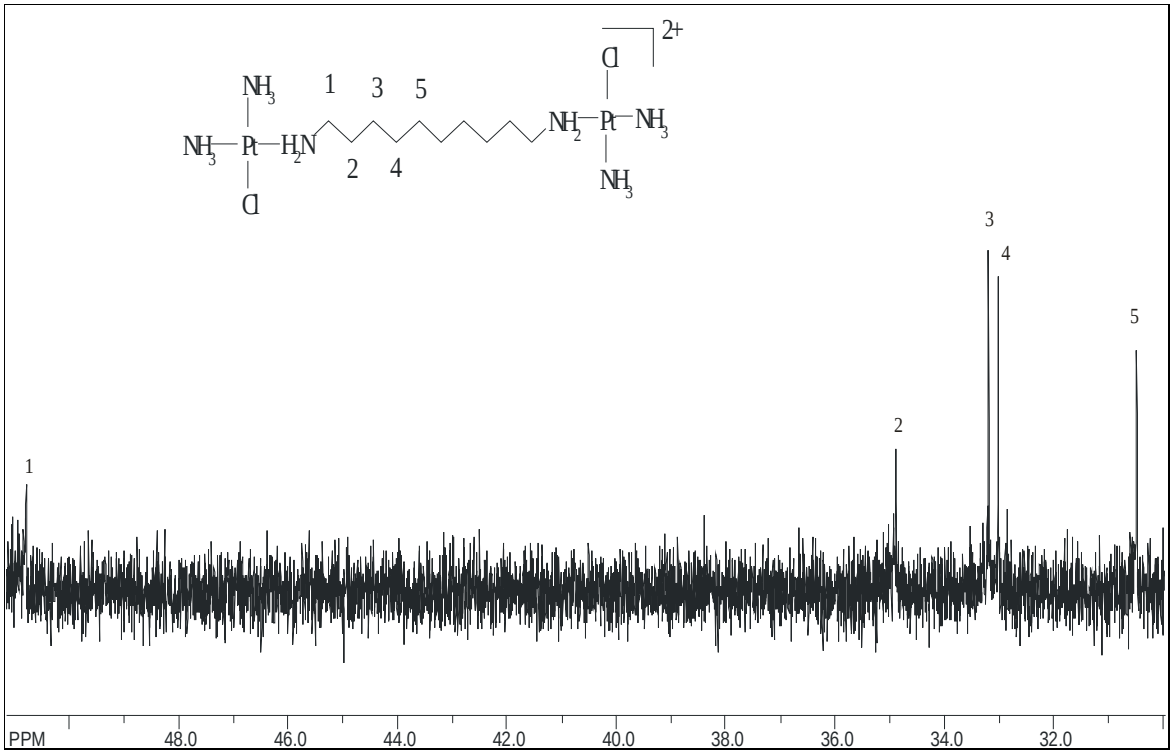

Figure 7.33: ^{13}C NMR spectra for **DecPt** complex.

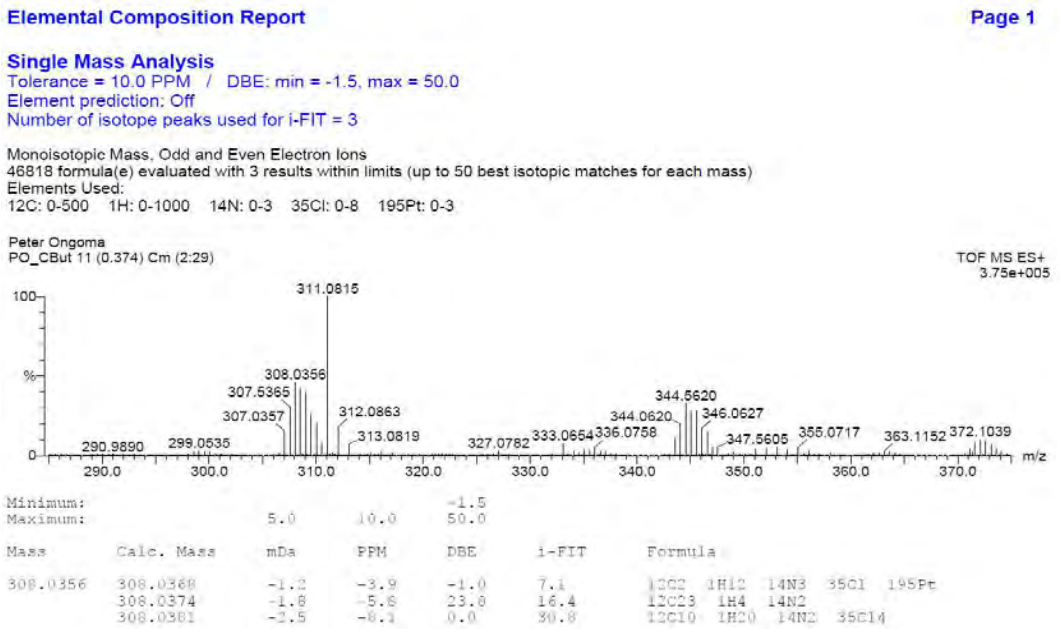

Figure S7.34: Mass spectrum for **ButPt-Cl** complex (m/e, M^{2+})

Elemental Composition Report **Page 1**

Single Mass Analysis
Tolerance = 10.0 PPM / DBE: min = -1.5, max = 50.0
Element prediction: Off
Number of isotope peaks used for i-FIT = 3

Monoisotopic Mass, Odd and Even Electron Ions
54176 formula(e) evaluated with 3 results within limits (up to 50 best isotopic matches for each mass)
Elements Used:
12C: 0-500 1H: 0-1000 14N: 0-3 35Cl: 0-8 195Pt: 0-3

Peter Ongoma
PO_C-Hex 27 (0.918) Cm (2:29)

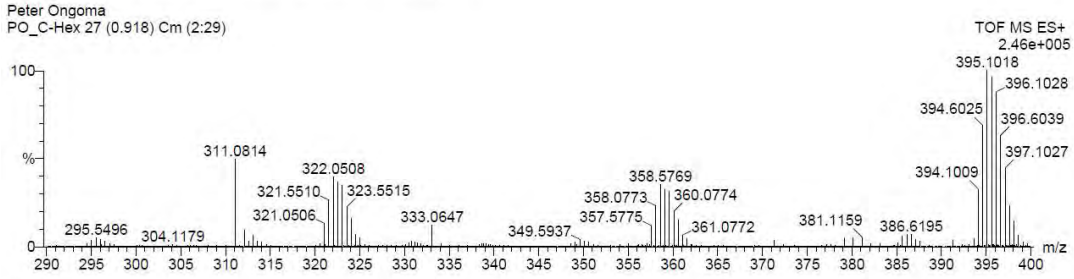

Minimum:				-1.5		
Maximum:		5.0	10.0	50.0		
Mass	Calc. Mass	mDa	PPM	DBE	i-FIT	Formula
322.0508	322.0524	-1.6	-5.0	-1.0	6.5	12C3 1H14 14N3 35Cl 195Pt
	322.0531	-2.3	-7.1	23.0	13.6	12C24 1H6 14N2
	322.0537	-2.9	-9.0	0.0	21.8	12C11 1H22 14N2 35Cl4

Figure S7.37: Mass spectrum for **HexPt-Cl** complex (m/e, M^{2+})

Elemental Composition Report **Page 1**

Single Mass Analysis
Tolerance = 5.0 PPM / DBE: min = -1.5, max = 50.0
Element prediction: Off
Number of isotope peaks used for i-FIT = 3

Monoisotopic Mass, Odd and Even Electron Ions
123241 formula(e) evaluated with 6 results within limits (up to 50 best isotopic matches for each mass)
Elements Used:
12C: 0-500 1H: 0-1000 14N: 0-200 35Cl: 0-8 195Pt: 0-3

Peter Ongoma
PO_c_Oct 3 (0.102) Cm (2:29)

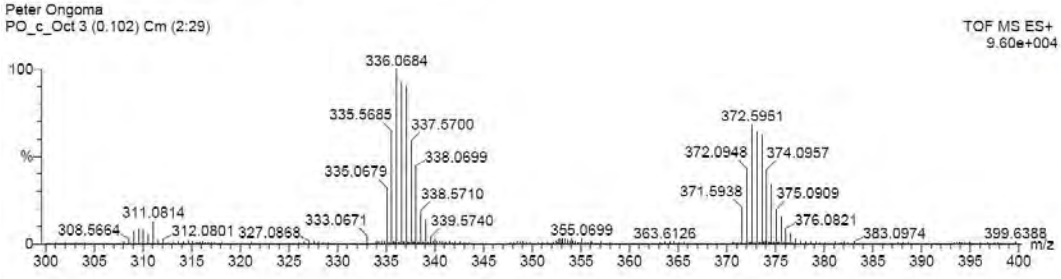

Minimum:				-1.5		
Maximum:		5.0	5.0	50.0		
Mass	Calc. Mass	mDa	PPM	DBE	i-FIT	Formula
336.0684	336.0681	0.3	0.9	-1.0	0.2	12C4 1H16 14N3 35Cl 195Pt
	336.0687	-0.3	-0.9	23.0	0.4	12C25 1H8 14N2
	336.0679	0.5	1.5	16.5	0.6	12C8 1H2 14N17
	336.0675	0.9	2.7	5.0	1.8	12C13 1H19 14N4 35Cl3
	336.0694	-1.0	-3.0	0.0	2.4	12C12 1H24 14N3 35Cl4
	336.0697	-1.3	-3.9	11.5	4.1	12C7 1H7 14N15 35Cl

Figure S7.34: Mass spectrum for **OctPt-Cl** complex (m/e, M^{2+})

Elemental Composition Report Page 1

Single Mass Analysis
Tolerance = 5.0 PPM / DBE: min = -1.5, max = 50.0
Element prediction: Off
Number of isotope peaks used for i-FIT = 3

Monoisotopic Mass, Odd and Even Electron Ions
144746 formula(e) evaluated with 6 results within limits (up to 50 best isotopic matches for each mass)
Elements Used:
12C: 0-500 1H: 0-1000 14N: 0-200 35Cl: 0-8 195Pt: 0-3

Peter Ongoma
PO_c_Dec 4 (0.136) Cm (2:28)

TOF MS ES+
1.05e+005

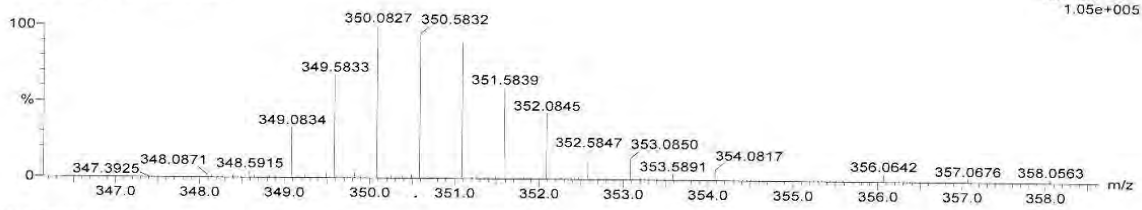

Minimum:				-1.5		
Maximum:		5.0	5.0	50.0		
Mass	Calc. Mass	mDa	PPM	DBE	i-FIT	Formula
350.0827	350.0832	-0.5	-1.4	5.0	0.6	12C14 1H21 14N4 35C13
	350.0819	0.8	2.3	4.0	1.5	12C6 1H13 14N5 195Pt
	350.0836	-0.9	-2.6	16.5	1.9	12C9 1H4 14N17
	350.0837	-1.0	-2.9	-1.0	2.4	12C5 1H18 14N3 35C1 195Pt
	350.0814	1.3	3.7	10.0	4.1	12C15 1H16 14N6 35C12
	350.0844	-1.7	-4.9	23.0	6.9	12C26 1H10 14N2

Figure S7.35: Mass spectrum for **DecPt-Cl** complex (m/e, M^{2+})

Chapter 8

Tuning Reactivity of platinum(II) complexes: *A Kinetic and Mechanistic Investigation into Substitution Behaviour of Mono- and Dinuclear Platinum(II) Complexes*

Summary

Inspired by the trend to generate new types of Pt(II) compounds with anti-cancer activity, the main aim of this study was to investigate the thermodynamic and kinetic properties of square-planar Pt(II) complexes with N-donor ligands that exhibit antitumor activity. A further aim was to determine whether the linker remains attached to the metal centre when the geometry and environment of the Pt(II) centre is *cis* to the leaving ligand in multinuclear platinum(II) compounds.

A series of complexes introduced in *Chapter 3* consists of mononuclear Pt(II) centres coordinated by tridentate N-donor ligands. The main feature of these complexes is that they are all characterised by the presence of a delocalised π-system that permits facile transfer of electrons from the metal to the ligand, while they differ by the way the fused ring system around the terpy moiety is structured. The objective was to investigate thermodynamic and kinetic properties of the complexes, mainly focusing on their dependence on the strength of π-backbonding of the spectator ligands around the Pt(II) centre. Therefore, substitution reactions with thiourea and its derivatives and anions (SCN^-, I^- Br^-) were performed with the corresponding chloro complexes at an ionic strength of 0.1 M $NaClO_4$ in presence of 10 mM LiCl to prevent solvolysis.

In comparing the reactivity of $[Pt(terpy)Cl]^+$ (**PtCl**) and **pyPhenPtCl,** (phen = phenanthroline), the extensive π-conjugation of the fused-ring system of the phen ligand, coupled with enhanced electronic communication in the aromatic system around the platinum centre, led to higher reactivity for **pyPhenPtCl** than **PtCl**. The most important feature of this work however, was elucidation of the effect of introducing the isoquinoline moiety instead of pyridine on the lability of the chloride ligand in **CH_3PhisoqPtCl**

compared to **CH_3PhPtCl**. The "unusual" decrease in reactivity of **CH_3PhisoqPtCl** is ascribed to the decrease in delocalisation of π-electron density as a result of the poor π-acceptor property of the isoquinoline ligand. The isoquinoline ligand is a net σ-donor, which slows down substitution reactions. This is supported by the Electronic absorption spectra and DFT-calculations which show that this system has the largest HOMO-LUMO energy gap. This behaviour is contrary to the *cis* σ-effect reported in other studies. The activation parameters obtained in the study supported an associative mode of substitution mechanism in all cases.

In *Chapter 4*, a series of bridged dinuclear platinum(II) complexes of the type, **[{*cis*–Pt(H_2O)(NH_3)$_2$}$_2$–μ–pzn]$^{4+}$** {where pzn = pyrazine (**pzn**), 2,3-dimthylpyrazine (**2,3pzn**), 2,5-dimethylpyrazine (**2,5pzn**) and 2,6-dimethylpyrazine (**2,6pzn**) were synthesised to investigate the influence of the rigid bridging ligand on the reactivity of the platinum(II) centres in dinuclear complexes.

The higher pK_a values for first and second deprotonation of **2,3pzn**, **2,5pzn** and **2,6pzn** compared to **pzn** are indicative of the σ-inductive effect of the methyl substituents on the pyrazine moiety that increases the electron density at the Pt(II) centre. The effect of increasing or decreasing electron density on the Pt(II) centre is also visible in the reactivity of the complexes. The reactivity of **pzn** is higher in comparison to **2,3pzn**, **2,5pzn** and **2,6pzn**. This is due to the moderate electrophilicity of the Pt(II) centre, which also experiences less steric hindrance. In addition, The DFT calculated bond angles show that the bridging pyrazine ligand lies almost perpendicular to the square-planar Pt(II) centre enabling the methyl groups on the linker ligand to effectively block the entry of the incoming nucleophile from above or below the metal centre ,slowing down the substitution process. The introduction of the methyl groups to bridging ligand also results in an increase in the separation energy of the frontier molecular orbitals (ΔE), leading to a less reactive metal centre in the ground-state.

^{1}H and ^{195}Pt NMR spectroscopy was applied to demonstrate stepwise substitution of the chloro ligands from the pyrazine bridged dichloro Pt(II) complex (**pzn**) by thiourea. A third step was observed in all the complexes and was attributed to degradation of the

dinuclear Pt(II) complexes to release the bridging ligand and form $[Pt(TU)_4]^{2+}$. This could only be achieved in presence of excess added thiourea and its derivatives. The results of temperature-dependence measurements are in agreement with expectations for d^8 square-planar Pt(II) complexes. All the values for the entropies of activation are largely negative and support an associative mode of substitution mechanism.

In *Chapter 5*, the work in chapter 4 was extended to include rigid diazine-bridged dinuclear Pt(II) complexes of the type **[{*cis*–Pt(NH$_3$)$_2$(H$_2$O)}$_2$–μ–z]$^{+4}$**, (z = diazine heterocyclic ring like pyrazine, pyrimidine, pyridazine and related benzodiazines, which differ in the relative disposition of the two Pt(II) centres. A comparison of the second order rate constants, $k_{2(1^{st}/2^{nd})}$, at 25 °C, obtained for consecutive substitution of the aqua ligands shows the reactivity of the complexes decreases as the Pt---Pt distance decreases from being *para* to each other in **pzn** to *ortho* disposition in **pdn**. This demonstrates that the steric effect increases with decreasing Pt---Pt distance among the diazine complexes.

The effect of increasing or decreasing the electron density of the Pt(II) centre is also visible in the pK_a values, which is attributed to π-resonance properties of the diazine linkers and the relative longer distances between the Pt(II) centres. In comparison the benzodiazine bridged complexes **qzn** and **pht** have better π-acceptor characteristics relative to **pmn** and **pdn**. The net result is that the Pt-metal of **qzn** is more electropositive and as such is more reactive than **pmn** as a result of the stronger π-backbonding of the diazine ring system. But the N=N bond in phthalazine (pht) ligand is strongly electron-withdrawing from the introduced aromatic ring. This makes it a net σ-inductive electron donor. Hence, the σ-donicity of the pht-bridge causes the opposite effect, by making the metal centre for **pht** more electronegative or less electrophilic than the rest of the complexes. As such it is the least reactive.

^{1}H NMR spectroscopy was applied to study the reactions of **pzn–Cl** and aqua **pdn** complexes with thiourea. The stability of the chloro complex was higher than was measured for the aqua complex. ^{1}H and ^{195}Pt NMR studies again revealed the release of linker and the formation of the corresponding PtS_4 units in the third step. At pH 2.0, this

process is accelerated by protonation of the freed terminal N atoms of the bridging ligand, which prevents re-attachment to the metal centre. All the values of the activation entropies are negative and confirm the associative character of the nucleophilic substitution mechanism.

In *Chapter 6*, thermodynamic and kinetic properties of relatively new diaqua Pt(II) complexes of the type **[{*cis*–Pt(NH$_3$)$_2$(H$_2$O)}$_2$L]$^{+4}$** (L = 4,4`-bis(pyridine)sulphide, 4,4'-bis(pyridine)disulphide or 1,2-bis(4-pyridyl)ethane) were studied for the first time. The study mainly focused on the influence of the spacer group and its effect on nucleophilic substitution reactions. The results indicate that there is electronic communication between the two platinum centres leading to two pK_a values. The thermodynamic data obtained demonstrates that the pK_a values of the coordinated aqua moieties are dependent on the nature of the linker. Clearly, higher pK_a values were obtained as the Pt---Pt separation distance becomes longer showing that the effectiveness of localised charge additions at the Pt(II) centres decreases as the distance is increased further. The pK_{a2} values of the second deprotonation step are also influenced by nature of spacer group, whereby S-based spacers are stronger σ-donors which impacts negatively on the acidity of the second coordinated water molecule. This resulted in bigger pK_{a2} values as the number of S atoms was increased.

It is also demonstrated by these investigations that the nature of the bridge has a strong influence on the reactivity of the complexes. The results of the substitution reactions with anions and thiourea nucleophiles of the corresponding diaqua complexes performed at pH 2 were explained in terms of the adopted symmetry by the different dinuclear complexes. The repulsions between the two lone pairs on S atom and the pyridine rings prevent **Pt1** to adopt a perfect C_{2v} symmetry. The DFT calculations clearly demonstrated that due to non-planarity of the ligand the structure of the **Pt1** complex is distorted. The resultant distortion imposes aerial steric hindrance at the Pt(II)) centre **Pt1** which is the reason why the reactivity of **Pt1** is about 4–7 times lower than that of the other complexes **Pt2** and **Pt3**. The magnitude of the steric hindrance imposed by the pyridyl bridge *cis* to the leaving group becomes weaker as the Pt---Pt separation distance increases, leading to the increase in rates of substitution from **Pt1** to **Pt3** and

finally **Pt2**. The order of reactivity is in agreement with that of pK_{a1} values, although observed differences in the rates of substitution are purely of steric hindrance origin. Additionally, the HOMO-LUMO energy gap is wider for **Pt3** compared to **Pt2**, suggesting a larger energy barrier and a slower substitution reaction in**Pt3**. However, the pyridyl linker is relatively weak and was released from the Pt(II) centre by thiourea and related stronger nucleophiles in the second step.

The results of temperature-dependence measurements performed with the diaqua complexes support an associative mode of activation that is characteristic of square-planar Pt(II) complexes. Because of the overall effect of charge neutralisation the values of the entropies of activation for the reaction with anions (SCN^-, Br^-) are less negative than that of thiourea and its derivatives.

In Chapter 7, the role of the α,ω-alkanediamine linker in controlling reactivity of Pt(II) complexes was investigated. In previous studies more attention has been focused on polynuclear *trans* Pt(II) complexes such as **BBR3464** that have promising anti-tumour activity. These complexes have proven to lose the bridging ligand soon after reacting with strong sulphur nucleophiles like thiourea. Investigations with thiourea and substituted thiourea on *cis* complexes of the type **[{*cis*–Pt$(NH_3)_2(H_2O)$}$_2$–μ–$NH_2(CH_2)_nNH_2$]$^{+4}$** (n = 2, 3, 4, 6, 8, 10), were performed to get detailed information on the characteristic properties of these complexes at pH 2.0.

The results of this investigation show that each of the aqua dinuclear complexes exhibited a single pK_a value. The pK_a values obtained clearly demonstrate that the σ-donor capacity of the bridging ligand increases with the elongation of aliphatic chain, resulting in higher pK_a values. This causes a reduction in the electrophilicity of the Pt(II) centre. This leads to the observed order of the second-order rate constants, k_2-values, for the simultaneous substitution of the aqua ligands, which progressively decreases from **EnPt** to **DecPt**. The corresponding diaqua complexes analysed in this study exhibited two substitution steps during the reaction with thiourea and its substituted derivatives. ^{1}H and ^{195}Pt NMR spectroscopy was applied to study the reaction of chloro **HexPt** with thiourea. This confirmed that the second reaction step, after the substitution

of water ligands, was the release of NH_3 ligand due to the *trans*-effect of the strong labilising Pt–S bond from the first substitution. This provided an additional indicator that α,ω-alkanediamine linker remained coordinated to the metal centres probably due to their *cis* geometry to the incoming thiourea nucleophiles. And the final product of substitution reactions is **$[\{cis\text{–}Pt(TU)_2NH_3\}_2\text{–}\mu\text{–}NH_2(CH_2)_nNH_2]^{+4}$**.

The current results demonstrate that the *cis*-dinuclear Pt(II) complexes with α,ω-alkanediamine linker are promising compounds for anti-tumour active drugs as they show higher stability to strong S-donor nucleophiles that are present in human cells and play an important role in biological reactions. Even if these complexes exhibited high levels of stability against the strong nucleophiles, it is expected that in presence of large amounts of the nucleophiles, they will substitute all the ligands and eventually destroy the bridging system.

In conclusion, the most striking feature of the present study is the fact that the heterocyclic amines: diazine- and dipyridine-bridged Pt(II) complexes were degraded and released the linker. Whilst the aliphatic amine linkers remained attached interact to the metal centres. Ordinarily the tendency of an electron donor to bind to metal ions decreases with decreasing basicity. Therefore, the aliphatic amine centres are strongly basic and may act as σ-electron donors, which provides the Pt(II) centres with excess electron charge density that prevents attack by excess nucleophiles at the metal centres. On the hand, one may notice that the diazine and pyridine ligands can engage in "synergic σ–/π–bonding". This type of bonding should be less dependent on the availability of σ-electrons, but here the flux of electrons is primarily directed from the metal centre to the ligand. This enhances the electrophilicity of the Pt(II) centre, allowing direct attack by the nucleophiles and eventual disintegration of the complex to release the linker as is the case in the present investigation.

A great of deal remains to be studied about the effect of bridging ligands on drug design and development and on reaction rates of multinuclear complexes. The main focus should involve drugs that comprise better:

- transport through the membranes

- prolonged survival in the cell without undue disintegration by platinophiles in the biological milieu.
- binding to the DNA
- and eventual excretion from the body with minimum side effects.

In the process, both metal coordination and hydrogen bonding will be key factors for improved stability at the molecular level.